OCS Study
BOEM 2022-047

Atlantic Deepwater Ecosystem Observatory Network (ADEON): An Integrated System for Long-term Monitoring of Ecological and Human Factors on the Outer Continental Shelf: Synthesis Report

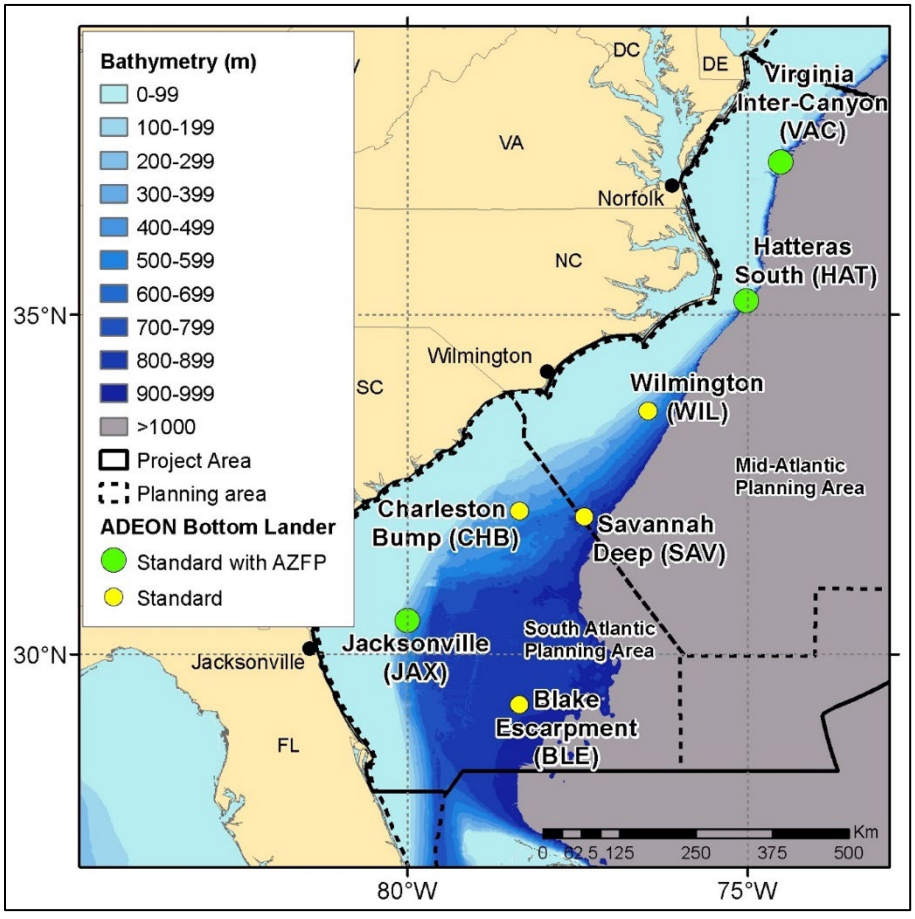

US Department of the Interior
Bureau of Ocean Energy Management
New Orleans Office

BOEM
Bureau of Ocean Energy Management

OCS Study
BOEM 2022-047

Atlantic Deepwater Ecosystem Observatory Network (ADEON): An Integrated System for Long-term Monitoring of Ecological and Human Factors on the Outer Continental Shelf: Synthesis Report

Authors

Jennifer L. Miksis-Olds
Michael Ainslie
Thomas Butkiewicz
Thomas Clay
Elliott Hazen
Kevin Heaney
Anthony Lyons
Bruce Martin
Tim Moore
Theresa Ridgeway
Joseph D. Warren

Prepared under BOEM Contract
M16PC0003
by
John Macri
University of New Hampshire
39 College Road
Durham, NH 03823

Published by

US Department of the Interior
Bureau of Ocean Energy Management
New Orleans Office

New Orleans, LA
July 2022

DISCLAIMER

This study was funded, in part, by the US Department of the Interior, National Oceanographic Partnership Program (NOPP) involving the Bureau of Ocean Energy Management (BOEM), the Office of Naval Research (ONR), and the National Oceanic and Atmospheric Administration (NOAA). Funding for ship time was provided under separate contracts by ONR, Code 32. This report has been technically reviewed by BOEM, and it has been approved for publication. The views and conclusions contained in this document are those of the authors and should not be interpreted as representing the opinions or policies of the US Government, nor does mention of trade names or commercial products constitute endorsement or recommendation for use.

REPORT AVAILABILITY

To download a PDF file of this report, go to the US Department of the Interior, Bureau of Ocean Energy Management Data and Information Systems webpage (http://www.boem.gov/Environmental-Studies-EnvData/), click on the link for the Environmental Studies Program Information System (ESPIS), and search on 2022-047. The report is also available at the National Technical Reports Library at https://ntrl.ntis.gov/NTRL/.

CITATION

Miksis-Olds, JL, Ainslie M, Butkiewicz T, Clay, T, Hazen E, Heaney K, Lyons AP, Martin B, Moore T, Ridgeway T, Warren JD. 2021. Atlantic Deepwater Ecosystem Observatory Network (ADEON): an integrated system for long-term monitoring of ecological and human factors on the Outer Continental Shelf synthesis report. New Orleans (LA): US Department of the Interior, Bureau of Ocean Energy Management. Contract No.: Report No.: OCS Study BOEM 2022-047. 320 p.

Contents

List of Figures

List of Tables

List of Abbreviations and Acronyms

Short Form	Long Form
ACF	autocorrelation function
ACI	acoustic complexity index
ADEON	Atlantic Deepwater Ecosystem Observatory Network
AEON	Atlantic Ecosystem Observatory Network
AIS	automated identification system
ALTO	autonomous long-term observatory
AMAR	autonomous multichannel acoustic recorder
AMSR-E	advanced microwave scanning radiometer-EOS
AOS	Applied Ocean Sciences
AR025	R/V *Armstrong* 025 ADEON Cruise 1 Designation
AR040	R/V *Armstrong* 040 ADEON Cruise 4 Designation
AR049	R/V *Armstrong* 049 ADEON Cruise 5 Designation
ArcGIS	Aeronautical Reconnaissance Coverage Geographic Information System
ASCAT	advanced SCATterometer
ATSR	along track scanning radiometer
AVHRR	advanced very high resolution radiometer
AVISO	Archiving, Validation and Interpretation of Satellite Oceanographic data
AZFP	acoustic zooplankton fish profiler
BLE	Blake Escarpment
BOEM	US Department of the Interior Bureau of Ocean Energy Management
BRTs	boosted regression trees
BTR	bearing-time record
CCI	Climate Change Initiative
CCMP	cross-calibrated multi-platform
CDF	cumulative density functions
CDR	Climate Data Record
CHB	Charleston Bump
CHL	chlorophyll *a* concentration
CNES	Centre national d'études spatiales (National Centre for Space Studies)
Co-PI	Co-principal Investigator
CSD	cross-spectral density
CT-DO	conductivity, temperature, and dissolved oxygen
DASCAT	daily-averaged wind and wind stress fields of ASCAT
DOI	US Department of the Interior
DPH	detection positive hours
ECMWF	European Centre for Medium-Range Weather Forecasts
eDNA	environmental DNA
EEZ	Economic Exclusion Zone
EN615	R/V *Endeavor* 615 ADEON Cruise 2 Designation
EN626	R/V *Endeavor* 626 ADEON Cruise 3 Designation
EOS	Institute for the Study of Earth Oceans and Space (at UNH), University of New Hampshire
ESA	European Space Agency
FFT	fast Fourier transform
FSAS	fine-scale acoustic surveys
FSLE	finite size Lyapunov exponent (sea surface altimetry)
G&G	geological and geophysical
GAMMs	generalized additive mixed models
GAMs	generalized additive models
GBZ	gas-bearing zooplankton
GDAL	Geospatial Data Abstraction Library
GES	NASA Goddard Earth Sciences
GESDISC	NASA Goddard Earth Sciences Data and Information Services Center
GHRSST	Group for High Resolution Sea Surface Temperature
GPM	global precipitation measurement
HARP	high-frequency acoustic recording package
HAT	Cape Hatteras
HYCOM	HYbrid Coordinate Ocean Model

Short Form	Long Form
IFREMER	Institut Français de Recherche pour l'Exploitation de la Mer
IKMT	Isaacs-Kidd midwater trawl
IMERG	Integrated Multi-satellitE Retrievals for GPM
IQOE	International Quiet Ocean Experiment
JAX	Jacksonville
JAXA	Japan Aerospace Exploration Agency
JOMOPANS	Joint Monitoring Programme for Ambient Noise in the North Sea project
JPL	Jet Propulsion Laboratory, NASA
IKMT	Isaacs Kidd midwater trawl
IOOS	International Ocean Observation System
JASCO	Joseph Arnold Scrimger Corporation
JAX	Jacksonville
JOMOPANS	Joint Monitoring Programme for Ambient Noise North Sea
LTSA	long Term Spectral Average
MAB	Mid-Atlantic Bight
MAMs	minimum adequate models
MARSS	Multivariate Autoregressive State Space Models
MARU	marine acoustic recording unit
MBON	Marine Biodiversity Observation Network
MCC	Matthews correlation coefficient
METOP	METeorological OPerational
MLD	mixed layer depth
MMD	Million Mounds ecosystem
MODIS	moderate Resolution Imaging Spectroradiometer
MSFD	Marine Strategy Framework Directive
MUR	multiscale ultrahigh resolution
NASA	National Aeronautics and Space Administration
NASC	nautical area scattering coefficient
NCEI	National Centers for Environmental Information
netCDF	Network Common Data Form
NOAA	National Oceanic and Atmospheric Administration
NOPP	National Oceanographic Partnership Program
NPP	net primary productivity
NRS	NOAA Ocean Noise Reference Station Network
NRS	non-resonant scatterers
OASIS	Ocean Acoustic Sciences and Instrumentation Services
OCS	Outer Continental Shelf
ONR	Office of Naval Research
OSCAR	Ocean Surface Current Analysis Real-time
OSU	Oklahoma State University
OTN	Ocean Tracking Network
PaCOOS	Pacific Coast Ocean Observing System
PAM	passive acoustic monitoring
PAR	photosynthetically available radiation
PI	Principal Investigator
PL	propagation loss
PO DAAC	Physical Oceanography Distributed Active Archive Center
PRECIP	daily precipitation
R2R	Rolling Deck to Repository
RCC	University of New Hampshire Research Computing Center
RS	remote sensing
RS	resonant scatterer
RTOFS	real-time ocean forecasting systems
SAB	South Atlantic Bight
SAV	Savannah
SBF	swimbladdered fish
SBU	Stony Brook University
SEL	sound exposure level
SLSTR	sea and land surface temperature radiometer
SMI	standard mapped image
SNPP	Suomi National Polar-orbiting Partnership

Short Form	Long Form
SPL	sound pressure level
SST	sea surface temperature
TKE	total kinetic energy
TNO	Nederlandse Organisatie voor Toegepast Natuurwetenschappelijk Onderzoek (Netherlands Organisation for Applied Scientific Research)
TS	target strength
TVG	time varied gain
UID	unidentified scatterers
UNH	University of New Hampshire
UNOLS	University-National Oceanographic Laboratory System
USGS	US Geological Survey
USN	US Navy
VAC	Virginia Inter-Canyon
VGPM	Vertically Generalized Production Model
VIF	variance inflation factor(s)
VIIRS	Visible Infrared Imaging Radiometer Suite
WHOI	Woods Hole Oceanographic Institution
WIL	Wilmington
WMS	Web Map Service
WSPD	surface wind speed & stress

ACKNOWLEDGMENTS

The ADEON team recognizes all the time, effort, and hard work of the captain and crew of the R/V *Armstrong*, R/V *Endeavor*, and ROV *Jason* to ensure the ADEON fieldwork was successful. Special thanks is also extended to the data team at the National Centers for Environmental Information for their partnership in evolving the archiving process for passive acoustic data.

1. Introduction

1.1 Overview

This report describes the Atlantic Deepwater Ecosystem Observatory Network (ADEON) project for the US Mid- and South Atlantic Outer Continental Shelf (OCS). ADEON generated long term measurements of the natural and human factors that describe the ecology and soundscape of the OCS. Ocean processes, marine life dynamics, and human ocean use are each inherently three-dimensional and time-dependent, and each occur at many spatial and temporal scales. No single measurement system (in situ or remote) is sufficient for describing any of the ocean state variables, and a "multi-platform, multi-variable" observational approach integrated with models was required (Seim et al., 2009). Acoustic information was combined with contextual data from space-based remote sensing, hydrographic sensors, and mobile platforms to fully comprehend how human, biologic, and natural abiotic components create the soundscape and influence ecosystem dynamics of the OCS. Measurements made within this research program serve as a baseline for pattern and trend analyses of ambient sound and the ecosystem components contributing to the OCS soundscapes.

The outputs of this study are standardized methodologies for comparing soundscapes across regions and predictive models for the soundscape and overall ecology of the southeast OCS in water depths between 100 and 1000 m. The data and models allow the public to estimate short-term and cumulative effects on the soundscape from changes in human activity, as well as ecosystem changes driven by climate change or other environmental factors. The project's public data management interface is already being used by interested parties to create value-added products so that the information is used as widely as possible. The ADEON effort went beyond basic ocean measurements and derived data products related to ecosystem components. Unique and innovative science attributes of the work scope included 1) a standardization task aimed at developing and implementing acoustic metrics and practices across ADEON components and recommending these approaches to other international monitoring programs, 2) a network design to identify the appropriate range of extrapolation for point samples, 3) ecological and soundscape modeling to predict potential influence of long-term change on the marine ecosystems, and 4) web-based tools to access and visualize multi-dimensional data streams.

1.2 Background

Ocean users and the public at large are increasingly aware of the necessity for responsible stewardship, as a result of such events as the collapse of fish stocks, increased coastal flooding during severe storms, the effects of major pollution episodes, and the increased awareness of marine charismatic megafauna in popular culture. Interest in responsible planning and management of ocean resources has sparked international research programs that are measuring baseline conditions that can be used to assess current effects and future variations, trends, and impacts. The European Union's Marine Strategy Framework Directive (MSFD) (European Commission 2010; Dekeling et al., 2014) has initiated action in Europe by requiring European member states to achieve or maintain Good Environmental Status by the year 2020, resulting in multiple national and collaborative monitoring initiatives.

US federal agencies are also taking a serious approach to assessing and managing ecosystem health and impact related to human activity. The Record of Decision issued by the Bureau of Ocean Energy Management (BOEM) in July 2014 establishes the highest practicable level of mitigation measures and

safeguards to reduce or eliminate impacts to marine life while setting a path forward for appropriate geological and geophysical (G&G) survey activities. This establishes a framework for mandatory environmental assessments that must draw upon established and validated data and tools that not only describe the baseline condition, but also model and predict future scenarios. The earliest that an oil and gas lease sale can take place in the South and Mid-Atlantic Planning Areas is 2023, if these planning areas are included as part of the BOEM's 2022–2027 5-year leasing program. Therefore, timely establishment of ADEON provided a wealth of data and products in these regions to inform potential lease sales.

Ocean sound is a national and international focus because it crosses borders unimpeded. Acoustic signals, as opposed to visual and chemical signals, can propagate long distances in the ocean and provide a means for marine life and humans to gain information about the environment and for marine animals to exchange critical information. Theory, and increasingly observations, suggest that human generated noise could be approaching levels that cause negative effects on marine life (Boyd et al., 2011). The International Quiet Ocean Experiment (IQOE) was created in 2010 in response to the growing concern about the impact of rising sound levels on the marine environment (Boyd et al., 2011). Although the majority of measurements supporting an increase in ocean sound were made in the North Pacific Ocean (Andrew et al., 2002; McDonald et al., 2006; Chapman & Price 2011), the ramifications of possible future increases are of global concern. The IQOE is developing an international program of research, observation, and modeling to better characterize ocean sound fields and to promote understanding of the effects of sound on marine life. At a national level, the National Oceanic and Atmospheric Administration (NOAA) Ocean Noise Strategy Roadmap provides a 10-year vision to improve how the US performs the science, management, public outreach and development of decision support tools that will document and preserve the soundscapes[1] and high value acoustic habitats[2] of US waters (Gedamke et al., 2016). ADEON soundscape measurements and modeling provide the baselines, methods, and visualization tools to assess how projected activity in the regional planning areas could impact regional ecosystems by integrating in situ measurements with knowledge of the oceanography, regional sound sources, and ecosystem dynamics.

1.3.1 Assessing Ecosystem Dynamics and Impacts through Sound

Previously established large scale oceanographic observatories, such as the International Ocean Observation System (IOOS) and the Pacific Coast Ocean Observation System (PaCOOS), have been heavily weighted towards physical oceanographic measurements because of the maturity and availability of physical sensors and the need to understand the physical processes driving the biological and chemical components of an ecosystem (Kite-Powell, 2009). Traditional ocean observatories using moored systems of sensors are augmented and ground-truthed by mobile sensors mounted on floats (Roemmich et al., 2009), autonomous underwater vehicles (Nicholls et al., 2008), and gliders (Johnson et al., 2009), as well as sensors carried by marine mammals (Grist et al., 2011). Acoustic observation has not, in general, been a part of many of these systems and, even when present, usually records at frequencies below those of importance to most marine organisms (Tyack et al., 2015). Passive acoustic technology can be used non-invasively to assess environmental sound levels, surface conditions, human activity, and the distribution and biodiversity of vocalizing marine life. Active acoustic technology provides a high-resolution (in both time and space) measure of biological (zooplankton and fish abundance and distribution) and physical oceanographic processes (internal waves and frontal systems) through time series of acoustic backscatter

[1] The sound present in a particular location and time, considered as a whole (Gedamke et al., 2016).

[2] Distinguishable soundscapes experienced by individual animals or assemblages of species, inclusive of both the sounds they create and those they hear (Gedamke et al., 2016).

measurements (Lavery et al., 2010). The ability to obtain passive and active acoustic measurements contemporaneously, along with ancillary data to validate and enhance interpretations, is a powerful tool facilitating insight into ocean and ecosystem dynamics.

A great deal of information related to ocean dynamics and ocean use can be gained simply by listening to the ambient sound. Information contained in soundscapes provide a means to better understand the influence of environmental parameters on local acoustic processes (Miksis-Olds et al., 2013; McWilliams & Hawkins, 2013; Staaterman et al., 2014), to assess habitat quality and health (Staaterman et al, 2014; Parks & Tyack 2014), and to better understand the impacts and risks of human contributions to the soundscape on marine life. A great number of aquatic species use sound cues contained in local soundscapes to navigate, forage, select habitat, detect predators, and communicate information related to critical life functions (e.g. migration, breeding, etc.). To evaluate the impact of anthropogenic contributions to the soundscape on marine animals, it is necessary to better understand soundscape dynamics and how animals are using or reacting to information contained within soundscapes.

Underwater soundscapes are dynamic, varying in space and time within and among habitats. Underwater soundscapes are highly influenced by local and regional conditions, but, unlike most terrestrial soundscapes, distant sources are also significant contributors because sound propagates such great distances underwater. The underwater soundscape may be composed of contributions from human activity (e.g., shipping, seismic airgun surveys), natural abiotic processes (i.e., wind, rain, ice), non-acoustic biotic factors (e.g., animal movement), and acoustic contributions from sound producing, biological sources (e.g., marine mammals, fish, and crustaceans). The soundscape can be selectively decomposed and visualized to gain a greater understanding of the sources and environmental dynamics contributing to and shaping the temporal, spatial, and spectral patterns of the acoustic environment. A feedback loop within the ADEON work scope uses measurements to refine soundscape modeling development (Figure 1).

Examination of the soundscape in its entirety provides an indicator of habitat or overall ecosystem quality and health. Indicators of habitat quality and biodiversity that were developed for terrestrial applications are now being applied to marine habitats and soundscapes (Staaterman et al., 2014; Denes et al., 2014; Parks et al., 2014). Rapid acoustic analysis of a habitat's soundscape through the calculated acoustic complexity index (ACI), acoustic entropy index, or diversity (acoustic dissimilarity index) is providing a quantitative way to assess biodiversity and compare/contrast soundscapes of different areas (Sueur et al, 2008; Staaterman et al., 2014). Sound travels further underwater than it does in air, so sound sources from afar that overlap in frequency of local or regional signals of interest often complicate interpretation of the calculated indices and limit the use of filtering techniques. Further development of soundscape derived ecosystem indicators is proposed within the ADEON data analysis and will provide a useful tool for ecosystem monitoring for a variety of applications. Acoustic indicators will be validated with *in situ* measurements and products derived from ecological modeling that integrate multiple data streams in identifying biodiversity and other ecologically relevant hotspots.

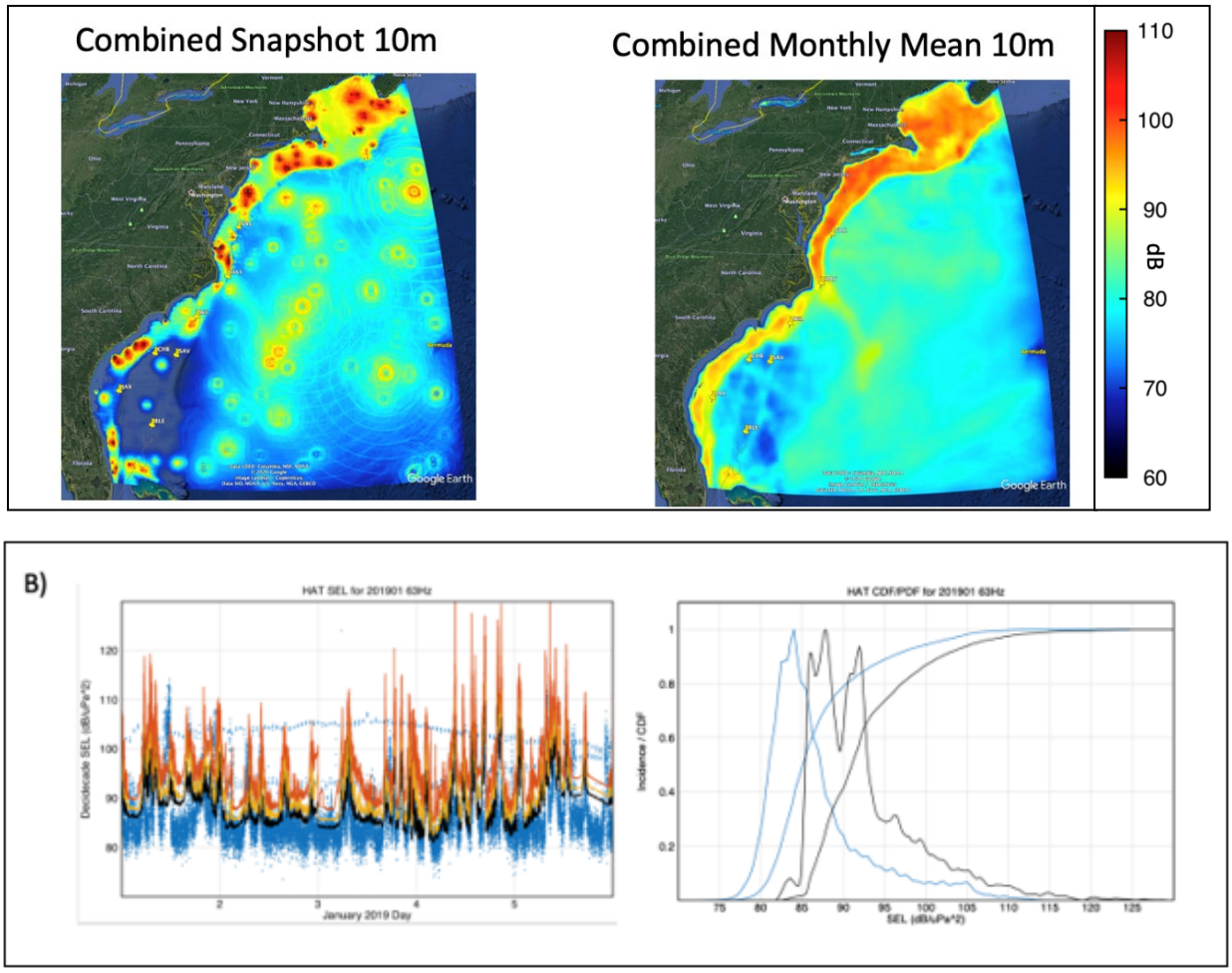

Figure 1. Examples of the Atlantic Deepwater Ecosystem Observatory Network (ADEON) soundscape modeling

(A) Models of the 20 Hz received level of combined wind and ship sources across the ADEON region showing the dependence of the propagation distance on the bathymetry. (A Left) Example snapshot of the soundscape model at 10 m. (A Right) Example of monthly mean soundscape at 10 m. (B Left) Site specific modelled sound pressure levels (SPL) levels (dB re 1 μPa^2) at Cape Hatteras (HAT). Percentiles plotted are 5th (black), 50th (yellow), 95th (red). The data is plotted as blue dots. (B Right) Histogram and cumulative density function (CDF) for the model (black) and data (blue) for the first 5 days of January 2019 at HAT.

1.3.2 Mid- and South Atlantic Outer Continental Shelf (OCS) Ecosystem

A large fraction of the region's biological production occurs near the shelf break and is supported year-round by western margin upwelling that brings nutrient–rich deep water into the euphotic zone (Lee et al., 1981). Upwelling along the Atlantic coast is both wind-driven and a result of dynamic uplift of deeper offshore nutrients that promote and sustain the region's primary productivity (Shen et al., 2000; Lentz et al., 2003). Warming of surface shelf water inhibits vertical nutrient exchange during summer, restricting upwelling to times when southwesterly winds prevail (Lee et al., 1981). In the winter, northerly winds support nutrient transfer onto the shelf from offshore waters. Mean winter values of South Atlantic Bight (SAB) pigment concentration on the outer shelf and in the Gulf Stream are about 50% greater than spring

values, confirming that winter chlorophyll production represents a significant fraction of the total year's production. (Martins & Pelegri, 2006).

Variability in the Gulf Stream and its extensions is the dominant source of short term intra-annual and annual change influencing regional production. Accelerated warming due to climate change is a significant source of inter-annual production variability. Almost 20 years of depth-averaged temperature measurements across the Mid-Atlantic Bight (MAB) indicate an increasing trend, with the most recent rate of increase being substantially larger than the overall 37-year trend (Forsyth et al., 2015). The temperature increase is not confined to surface waters, but extends throughout the water column. Additionally, the warmest anomalies have increased in intensity over the 37-year record, whereas the cold anomalies remain relatively uniform throughout the record trend (Forsyth et al., 2015). These observations indicate the establishment of ADEON is too late to accurately capture the baseline conditions and associated variability prior to the effects of recent climate change. However, measurements from ADEON will be vital in assessing the confounding factors of climate when evaluating the future impact of human activity on the regional ecosystem.

Regional primary productivity is the base of the ecosystem, supporting commercial fisheries and populations of top marine predators. The southeastern US shelf is an important nursery area for a large number of fish species which spawn offshore and are then transported into the estuarine areas as larvae (Stegmann & Yoder, 1996). The Atlantic menhaden is just one example of an important commercial fish species of the purse seine fishery that spawns offshore near the western edge of the Gulf Stream during the winter and early spring months (November–March). Thirty-four species of marine mammals take advantage of the region's high level of productivity. Six of these species are endangered (North Atlantic right, blue, fin, sei, humpback, and sperm whale). The North Atlantic right whale is considered one of the most critically endangered whales (Jefferson et al., 2008), and their critical habitat has been designated adjacent to the planning areas off the Georgia and northeast Florida coasts. Right whale movements show large excursions, including into deep water off the continental shelf (Mate et al., 1997; Baumgartner & Mate, 2005).

Five species of sea turtles (loggerhead, green, hawksbill, Kemp's ridley, and leatherback) and two offshore fishes (shortnose and Atlantic sturgeon) that inhabit the area are listed as endangered, but there are no critical habitats in the designated regions listed for sea turtle or fish species. Additionally, two "candidate" fish species (alewife and blueback herring) are undergoing a status review that has been announced in a Federal Register notice (USDOC, NMFS, 2011). The Gulf Stream, which moves through the center of the southeastern US shelf, is also used by several species of endangered marine mammals and sea turtles for various purposes, such as migration and foraging (Hoffman & Fritts, 1982). The presence of so many protected species highlights the need for both monitoring and management of the animals and their habitat. ADEON measurements provide the best available information to support the development of informed regulation that is protective yet not unnecessarily prohibitive of military and industrial activity in the region.

1.3.4 ADEON Structure

ADEON was structured into a four-phase research program: I) Network Design, Procurement, and Deployment, II) Data Acquisition and Network Maintenance, III) Data Processing, and IV) Data Integration and Visualization (Figure 2). These were complimented by overarching tasks that wove through all phases to manage data and standardize measurement, processing, and visualization metrics for the acoustic data sets. The outputs of the standardization effort allow effective comparison of acoustic results between locations and research groups. Baseline assessment of the soundscape and contributing environmental components is critical to assessing long-term patterns and trends of individual ecosystem

components and synergistic relationships, as well as providing the input parameters in support of the development of predictive models that integrate multiple data streams to determine future soundscapes and impacts resulting from environmental changes related to human activity, climate change, or other identified factors.

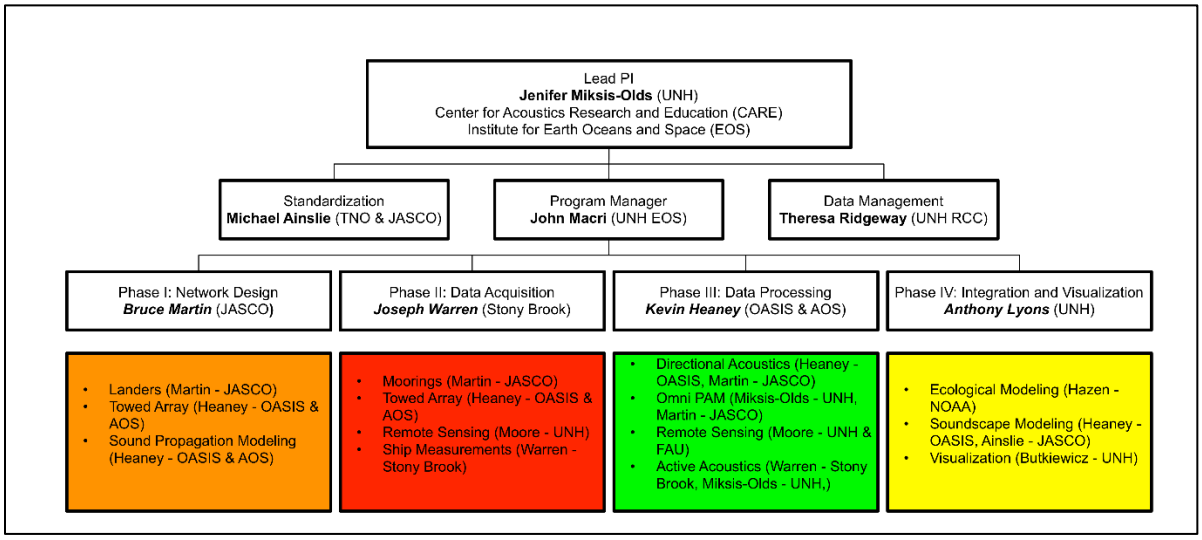

Figure 2. ADEON program structure

Four technical phases were implemented under a coordinating umbrella of program Standardization and Data Management.

The ADEON measurement network featured seven fixed ocean bottom landers (Figure 3), intensive vessel-based ecosystem sampling during deployment cruises for the landers, satellite remote sensing, and passive acoustic towed array surveys between ADEON sites. Each data set was processed separately as part of Phase III of the program, and then all data streams were integrated in Phase IV to extract new information about the ecosystem relationships.

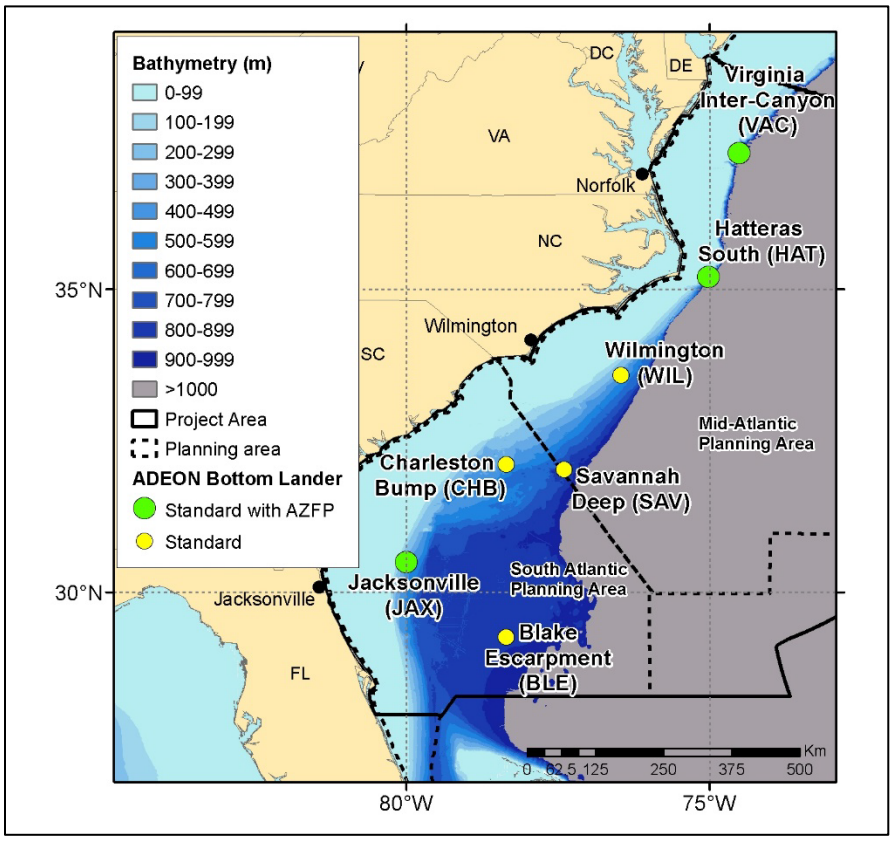

Figure 3. ADEON lander locations along the US east coast Outer Continental Shelf (OCS)

Three shallow locations (green dots) were equipped with active Acoustic Zooplankton Fish Profilers (AZFPs) in addition to passive acoustics, fish tag receivers, and physicochemical sensors. The deeper locations (yellow dots) had only passive acoustic and physiochemical sensors.

1.3 Project Objectives

The ADEON project objectives were to:

- Establish an ecosystem observation network that provides baseline monitoring and supports predictive modeling of the soundscape and its relationship to marine life and the environment of the Mid- and South Atlantic Planning Areas.
- Develop standardized measurement and processing methods and visualization metrics for comparing ADEON observations with data from other monitoring networks.
- Assess baseline soundscape and ecosystem conditions in support of predictive environmental modeling and trend analyses in the planning areas.
    1. How do soundscape and ecosystem components vary with water depth across the OCS?
    2. How do the soundscape and ecosystem components vary with latitude along the OCS?
    3. Where are the hot spots of human activity for consideration in ecosystem/habitat health impacts?
- Assess the spatial and temporal distribution of the soundscape and biological scatterers, including their expected variation and correlation with distance from the lander locations.

1. What are the environmental factors that define and constrain the horizontal range of appropriate extrapolation of observations measured at the stationary lander sites?

- Develop and apply new methods for the effective visualization of five-dimensional (5D)–time, latitude, longitude, frequency, and depth–soundscape data with interactive visual analysis tools that enable users to explore, analyze, and integrate ancillary ecosystem data streams with the 5D soundscape.
- Develop a robust data management system that archives and provides public access to multiple data streams to encourage future development of ecological models targeted at questions beyond the scope of this study.

2. Overview Phase I: Network Design

Phase I, Network Design, delivered on Atlantic Deepwater Ecosystem Observatory Network (ADEON) Objective 1: Establish an ecosystem observation network that provides baseline monitoring and supports predictive modeling of the soundscape and its relationship to marine life and the environment of the Mid- and South Atlantic Planning Areas. To satisfy all project objectives, the network design had to support characterization of the soundscape across the shelf and at multiple latitudes. The network needed to include active acoustic systems to characterize the biological scatter in the water column, and broad-area remote sensing to study the variability in environmental factors in time and space.

The Network Design was an iterative process involving all ADEON Co-Principal Investigators during which the budget for equipment and data purchase, the objectives of the project, and available knowledge about the project area were considered in order to arrive at the final design. Despite the iterative nature of design, this section presents the Network Design as three sequential sub-tasks: Selection of the monitoring sites, selection of the network components, and design or selection of the specific equipment that was employed to establish the network.

2.1 Site Selection

The goal of the observation program was supporting development of predictive models of the soundscape in the Mid and South Atlantic Planning Areas. The backbone of the measurement program was the deployment of seven autonomous observatories for a three-year study period; the budget supported including active acoustic systems for fish and zooplankton profiling at three of the sites.

The first task of Network Design was determining where to put the observatories. The over-arching consideration in choosing the sites was to sample the maximum variety of ecosystem conditions such that the soundscape and ecosystem models could be trained with sufficiently representative data that the models would be useful for future predictive applications. Factors considered during site selection were:

- Selecting lander sites with ecological relevance.
- Finding sites with a wide range of anthropogenic conditions.
- Covering the depth range of 100–1000 m.
- Including three sites < 400 m for the fish and zooplankton profilers.
- Selecting sites to support along-shelf and across-shelf comparisons of soundscapes.
- Recording both close and far from previous or concurrent projects to support analysis of soundscape portability (see Figure 4).

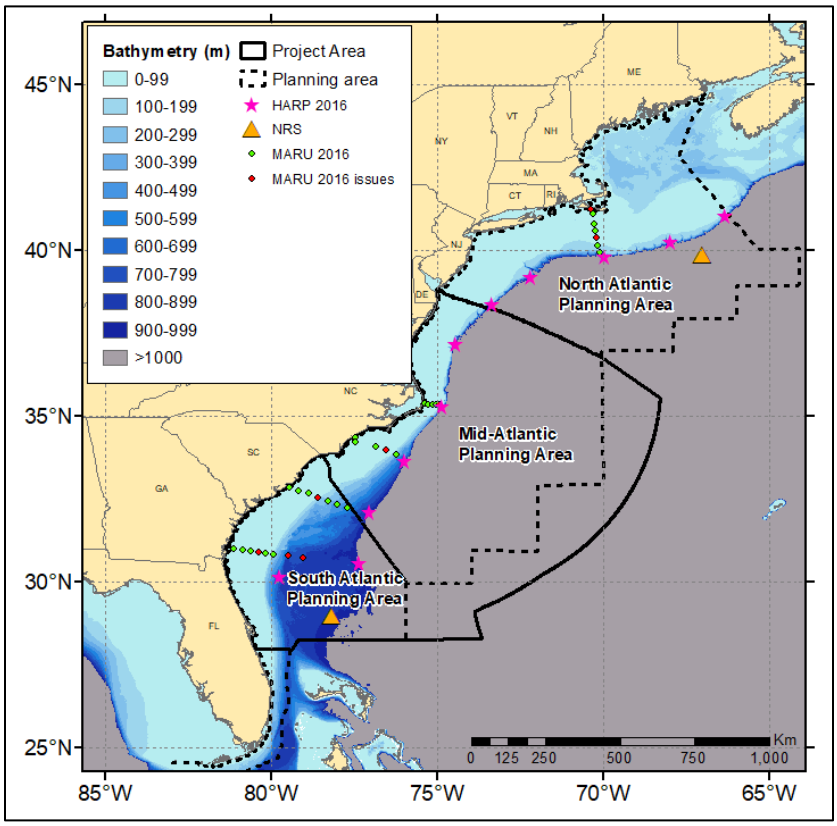

Figure 4. Map of the project area showing the locations of passive acoustic monitoring sites from previous or current projects

NRS stations are the Noise Reference Stations (National Oceanic and Atmospheric Administration [NOAA] Ocean Noise Reference Station Network [NRS] Raw Passive Acoustic Data). The High-Frequency Acoustic Recording Package (HARP) stations were deployed 2016–2019. Most of the Marine Acoustic Recording Unit (MARU) stations were deployed before 2016, with some going out until 2018; these data are mostly owned by NOAA.

Ecological relevance was assessed based on the existing knowledge of marine mammal presence, fisheries in the areas, and presence of deep-sea corals. Marine mammals are relevant to soundscape studies because the calls of some species–such as fin, blue, and humpback whales–are known to be important components of the soundscape during their mating periods (winter). Whistles and clicks from odontocetes are also important sound sources when present. The presence of marine mammals is also an indicator of the biomass and biodiversity of other marine life because they are at the apex of the food chain. A total of 32 marine mammal species may occur in the project area: 7 baleen whales, 5 beaked whales, 16 delphinids, 1 porpoise and 3 sperm or pygmy sperm whales. The expected distributions of marine mammals were assessed using the habitat density models of Roberts et al. (2016), e.g., Figure 5.

From these models and related data, it was surmised that:

- There are seasonal shifts in baleen distribution.
- Except for North Atlantic right whales in nearshore Florida and Georgia waters in winter months, and blue and Bryde's whales who occur at low densities throughout their range, peak baleen whale abundance and densities occur north of Cape Cod in summer months.

- Beaked and sperm whales occur year-round near deep, high-relief bathymetric features such as submarine canyons and slope areas north of Cape Hatteras.
- Large delphinids are most common along the shelf break from Cape Hatteras northward; lower densities south of Cape Hatteras with a broader distribution.
- Small delphinids occur at highest densities along the coast south of Cape Hatteras (bottlenose and Atlantic spotted dolphins) and along and beyond the shelf break north of Cape Hatteras.

Roberts et al. (2016) noted that the visual survey effort used to develop the models was biased towards summer months and coastal areas; year-round monitoring of deep waters would be highly informative. The previous and existing monitoring programs (Figure 4) have been targeted at two questions: mapping the movement of baleen whales in shallow waters (using the MARU lines), and understanding the presence of marine mammals, especially odontocetes, at the shelf break and canyons (using HARPs).

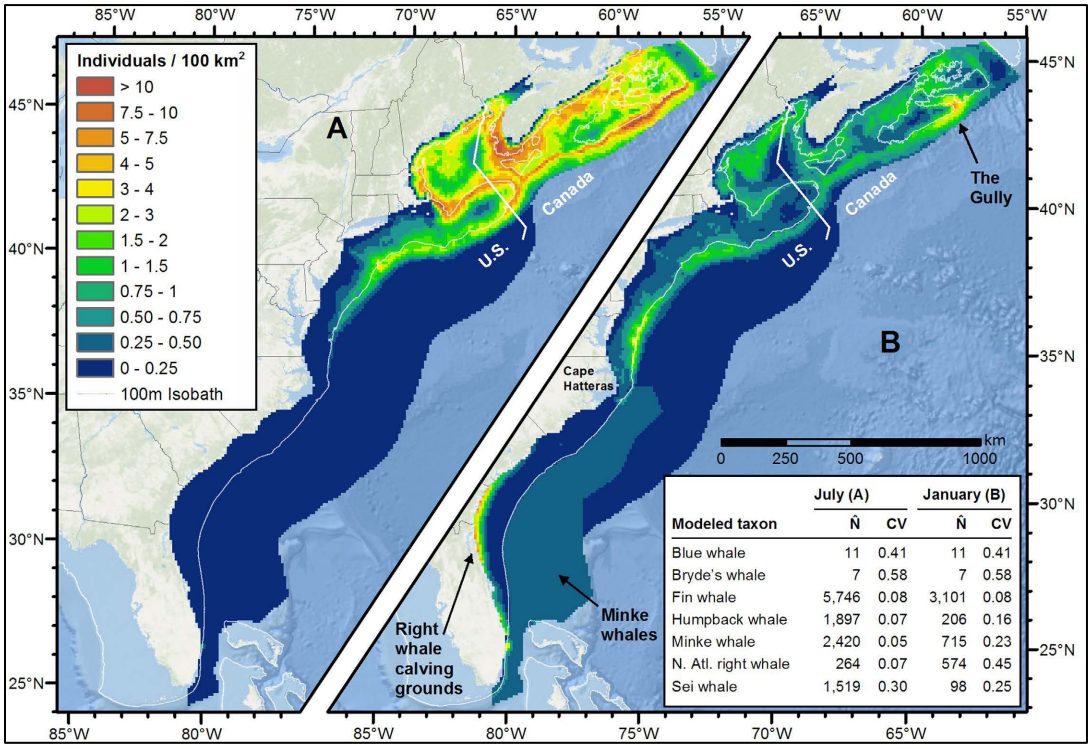

Figure 5. Distribution of mysticetes in (A) July and (B) January along the OCS and into Canadian waters (Roberts et al. 2016).

A map of known deep sea coral site and gas seeps was provided by researchers on the concurrent National Oceanographic Partnership Program (NOPP)-funded program Deep Search (Figure 6). Two ADEON locations were ultimately selected that coincided with deep-sea coral habitat.

Anthropogenic activities in the Mid and South-Atlantic Planning Areas are primarily the passage of commercial vessel traffic (e.g., Figure 7), fishing north of Cape Hatteras (Figure 8), and occasional Naval sonar exercises. During ADEON's planning there was a possibility of marine seismic airgun surveys in the project area, and therefore it was viewed as desirable to obtain baseline data in areas where surveys could occur (Figure 9).

Fisheries were assessed using the landings data for ports along the coast. It was determined that there are no significant fisheries in offshore waters south of Cape Hatteras. A new public visualization of fisheries tracks using the Living Atlas confirmed our assessment of the landings data (see Figure 8).

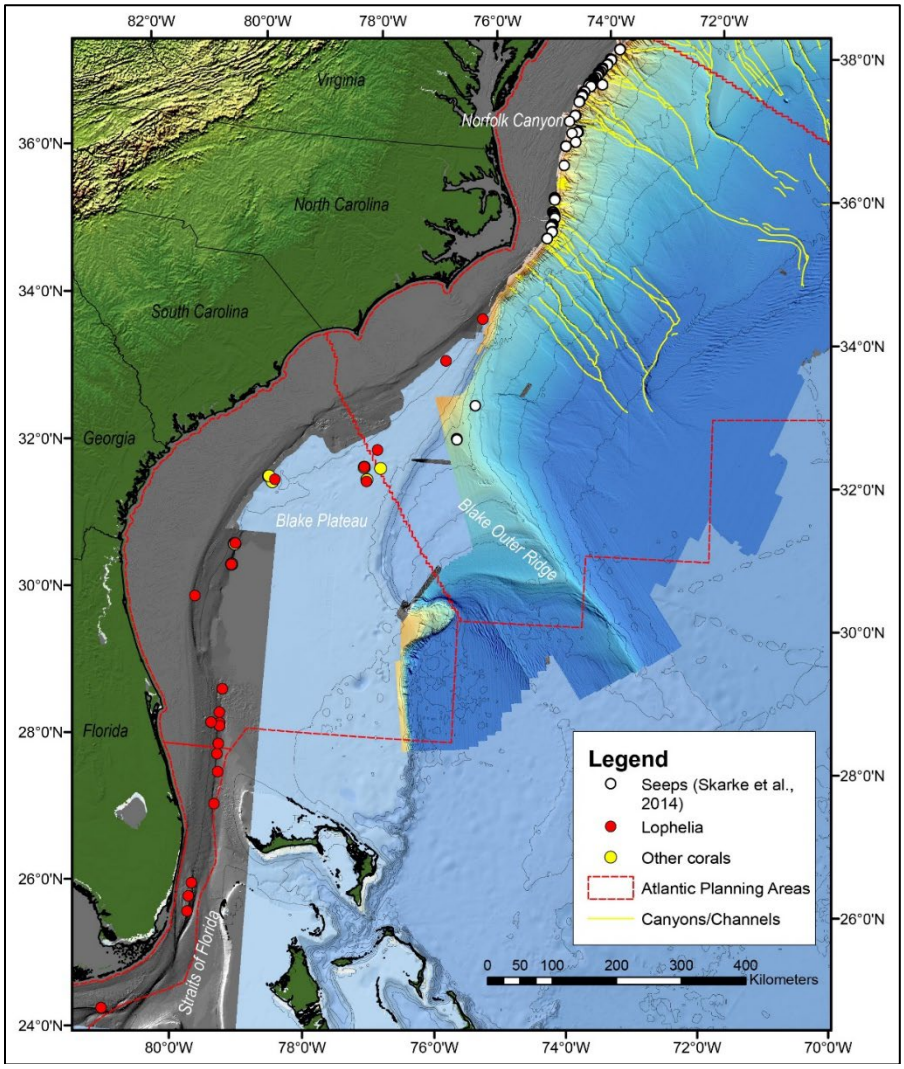

Figure 6. Map of deep sea coral sites and gas seeps provided by collaborators from the National Oceanographic Partnership Program (NOPP)-funded program, Deep Search

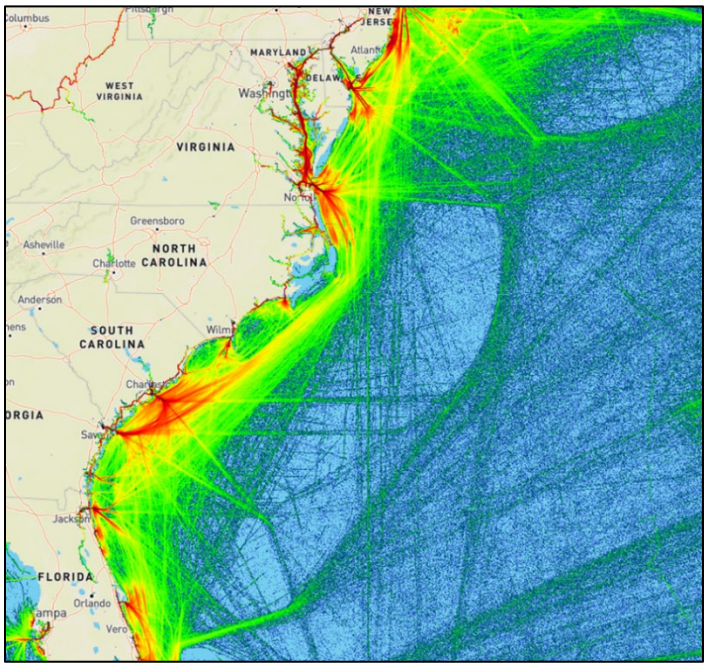

Figure 7. Density of commercial vessel traffic in the OCS as reported by the automated identification system (AIS) in 2015

(*www.marinetraffic.com*, accessed February 2017)

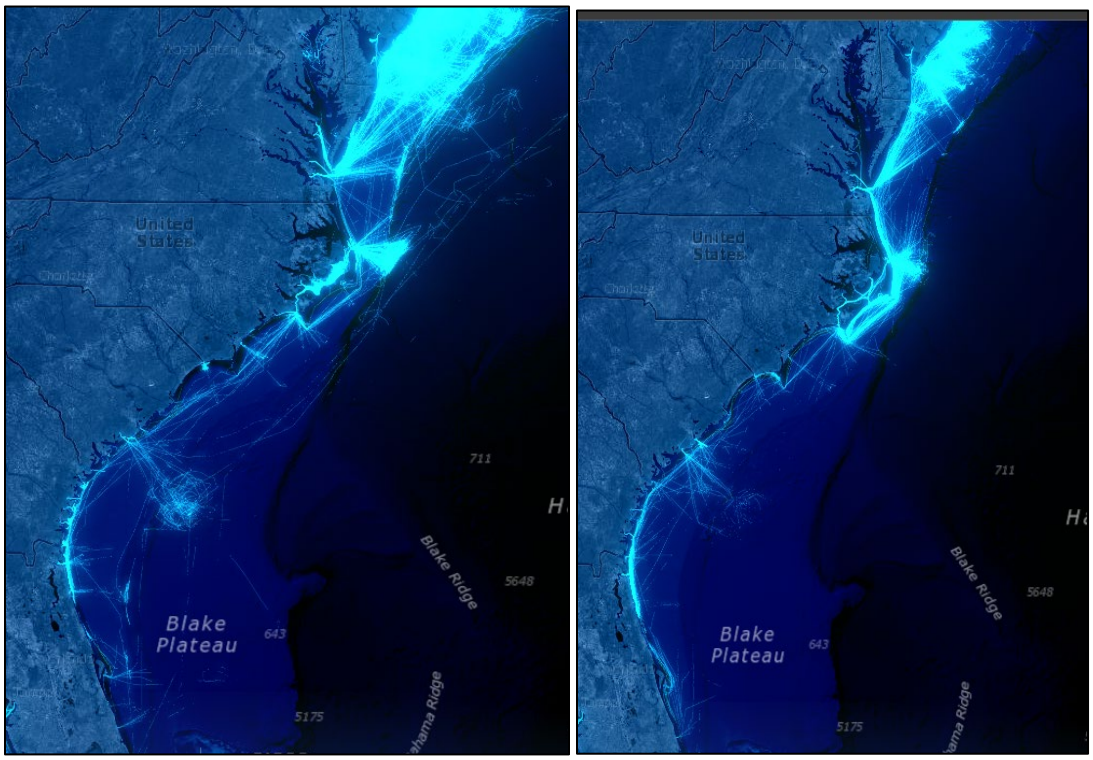

Figure 8. Fishing vessel tracks for July (left) and January (right) 2019 for the project area

(https://livingatlas.arcgis.com/vessel-traffic/#@=-81.791,31.334,6&time=201901&sublayer=Fishing, accessed 29 April 2021)

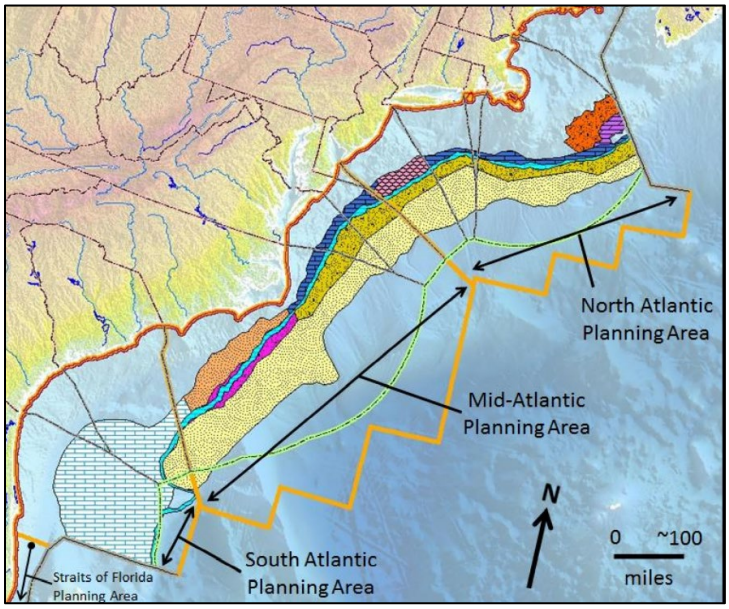

Figure 9. Geologic formations in the Atlantic Planning areas

The primary targets for oils and gas development are the thin blue feature as well as the magenta feature (BOEM OCS Report 2016-071)

The final sites were approved by the US Navy, the Bureau of Ocean Energy Management (BOEM), the National Oceanic and Atmospheric Administration (NOAA), and the Office of Protected Resources (they are shown in Figure 3). The rationale for selection of these sites is summarized in Table 1.

Table 1. Summary of rational for the selection of the seven Atlantic Deepwater Ecosystem Observatory Network (ADEON) sites

Location and Site Name	Water Depth	Rational for Placement
Virginia Inter-Canyon (VAC)	210 m	Northern soundscape with high productivity; located between two canyons on the shelf break; moderate vessel traffic and significant fishing; in the Baltimore Canyon geologic area.
Hatteras South (HAT)	290 m	Northern soundscape with high productivity; expect high vessel traffic and fishing. Near the Baltimore Canyon geologic area.
Wilmington (WIL)	460 m	Soundscape and productivity on a slope further from shelf break south of Hatteras; near traffic lanes; in Carolina Trough geologic area. In a deep-water coral area (other).
Charleston Bump (CHB)	400 m	Soundscape and productivity with moderate traffic near bathymetric features (Charleston Bump); South of Hatteras; high currents from Gulf Stream expected;
Savannah Deep (SAV)	800 m	For comparison with CHB at same latitude; light traffic; at edge of Carolina Trough area.
Jacksonville (JAX)	320 m	For comparison CHB and BLE; moderate traffic; part of the Blake Plateau area; closest to the shore shelf break. In a deep-water coral area (Lophelia).

Location and Site Name	Water Depth	Rational for Placement
Blake Escarpment (BLE)	870 m	For comparison with SAV and JAX; very light traffic. Deep water in Blake Plateau area.

2.2 Network System

As the ADEON team was finalizing the long-term monitoring sites, the types of recordings to make at the sites, and other data needed to tie the sites together in ecosystem and soundscape models was considered. One consideration was providing a rich public dataset to support analysis by researchers in the future beyond what was integral to the scientific and monitoring objectives of ADEON.

The roles of the long-term monitoring sites were providing time series of measurements for developing and validating soundscape and ecosystem models. Passive acoustic monitoring (PAM) was included in the long-term monitoring design to record the soundscape including the presence of marine mammals and the contributions of wind driven sound as well as commercial and fishing vessels. Two of the sites were near deep-water coral reefs (see Table 1) to investigate if the soundscape of these reefs is distinct from non-reef sites like tropical shallow-water reefs are distinct from other shallow water areas. A four-hydrophone volumetric array was included in the system design to measure the direction of arrival of different sound sources. The directional data can be processed to extract information on:

- The distribution of vessels and mammals in bearing around each site.
- The minimum density of vocalizing mammals based on the number of directions present.
- Interactions between mammals and human sound sources.
- The particle motion of ambient soundscapes.

To maximize the groups of marine mammals that could be detected, a sample rate of at least 256 kHz for the PAM equipment was included in the design.

It was important for the long-term measurements to also record the presence of non-vocalizing marine life. Autonomous loggers for acoustic tags that are surgically implanted in fish were included in the design to identify these species as they passed by the monitoring sites. Single beam scientific echosounders were also included in the design at three sites to record the abundance and community structure of fish and zooplankton. Multi-frequency echosounders were desired to measure the presence of animals of different size classes. The echosounder transducers were positioned on the seabed looking upwards to image the full water column where the frequency attenuation permitted.

The ADEON project area is in the Gulf Stream and in an active hurricane area. The currents and hurricane induced mixing were expected to result in variability in the water masses throughout the year. To measure the effects of these forces at the ADEON sites, conductivity, temperature, and dissolved oxygen sensors were included into the long-term monitoring design. The currents in the water column are variable with maximum daily speeds greater than 2 m/s at the top of the water column and up to 1 m/s at the seabed (see Figure 10). It is challenging to make passive acoustic measurements in these currents because flow around the hydrophones and knock-down of the mooring generating pseudo-noise (non-acoustic self-noise) greater than ambient sound levels at frequencies below 100 Hz (depending on the current speed). Since the preferred location for the echosounder was at the seabed, all of the long-term sensors were integrated into a bottom-mounted lander. Acoustic propagation modeling (see Figure 11) indicated that seabed recordings would contain sounds sources throughout the water column, and therefore the bottom-mounted lander design was implemented. The landers (see Section 2.3) were

deployed four times: Nov 2017–June 2018, Jun–Nov 2018, Nov 2018–2019 and Nov 2019–Dec 2020. University-National Oceanographic Laboratory System (UNOLS) ships Research Vessel (R/V) *Neil Armstrong* and R/V *Endeavor* were employed for these deployments, as described in Section 3.1.

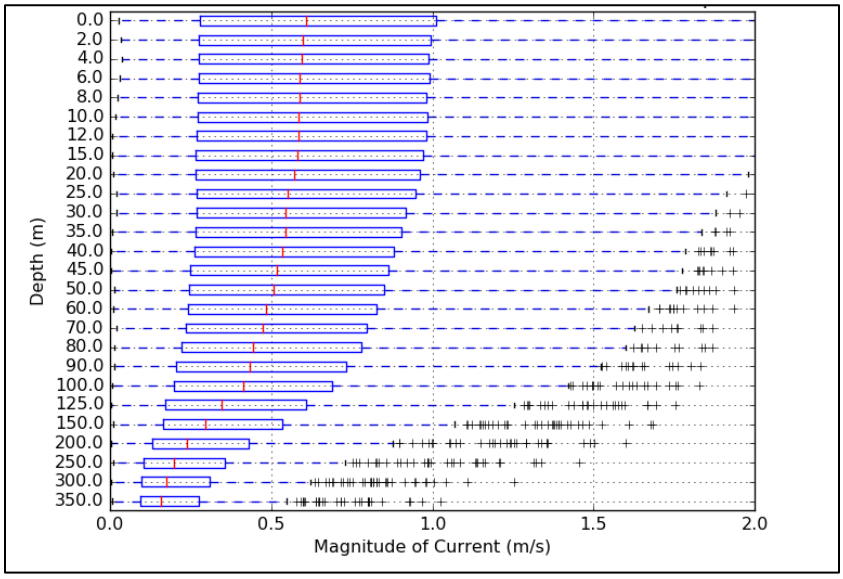

Figure 10. Box-and-whisker plot of the distribution of sub-surface current speeds generated by the HYCOM oceanographic model for all of 2015 for a site near Charleston Bump (CHB)

The edges of the boxes show the inter-quartile range of currents. The red-line is the median current. The dashed lines show the upper and lower 25% of current speeds, with outliers shown as '+' symbols.

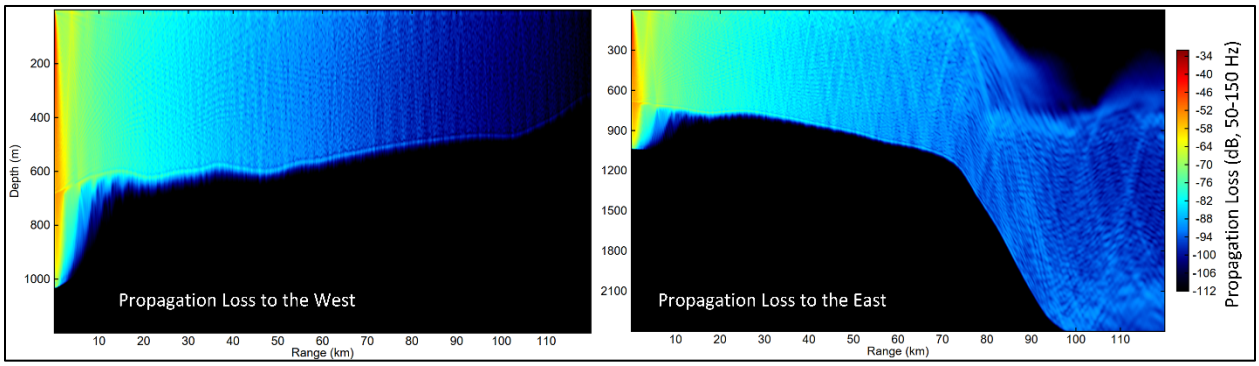

Figure 11. Propagation Loss Model for sounds from a vessel at a site near Savannah (SAV)

Left: Propagation to the West towards the continental USA. Right: Propagation loss to the east off the continental shelf.

To link the long-term measurements to environmental conditions, the network design included remote sensing of oceanic and atmospheric variables. The ADEON remote sensing team selected a robust set of satellite measurements to use as covariates in the ecosystem and soundscape data analysis. They include automated identification system (AIS) ship tracks, sea surface temperature, chlorophyll *a* concentration, net primary productivity, mixed layer depth, wind speed and direction as well as surface current speed and direction (Table 2). Remote sensing products continually improve as new algorithms evolve. The products here represent the highest level of product maturity for each variable, some of which are themselves the outputs of models such as net primary productivity and photosynthetic available radiation,

or have assimilated multiple sources of information such as sea surface temperature and ocean currents. They are now sufficiently mature to serve as the inputs for the soundscape and ecosystem models envisioned by ADEON. Automated download and archiving of the remote sensing data were established and continued throughout the three-year deployment of the autonomous observatories. The chlorophyll *a*, sea surface temperature, and wind speed data are available as layers on the Data Visualization Map (see Section 5.3). The AIS tracks of commercial vessels in the project area were provided through collaborative agreements with the US Coast Guard and Spire Inc. (see Section 3.3).

Table 2. Satellite remote sensing and derived data archived for the ADEON project area throughout the program

Parameter	Description	Data Units	Source (NASA Processing Level)*	Satellite (S) or Model (M)	Spatial Resolution	Temporal Resolution
CHL	Chlorophyll *a* concentration	mg/m^3	NASA Goddard (3)	VIIRS (S)	4.6 km²	8-day mean
SST	Sea surface temperature	°C	NASA JPL (4) Copernicus (4)	GHRSST (S) GHRSST (S)	1 km^2 0.05 degree	Daily Daily
NPP	Net primary productivity	mg Carbon/(m^2 d)	Oregon State University	VGPM (M)	12.5 km^2	8-day mean
PAR	Photosynthetically available radiation	mol /(m^2 d)	NASA Goddard (3)	VIIRS (S)	4.6 km^2	8-day mean
PRECIP	Daily precipitation	mm	NASA Goddard (3)	GPM (M)		Daily
MLD	Mixed layer depth	m	Oregon State University (4)	HYCOM (M)	12.5 km^2	8-day mean
WSPD	Surface wind speed & stress	m/s	IFREMER (3)	ASCAT (S)	0.25□	Daily
CURRENTS	Surface currents	m/s	NASA JPL	OSCAR (M)	0.25□	5 day mean

*NASA level processing hierarchy is a standard indicating the degree of transformation and processing in reference to data collected by the sensor. ADEON has collected both level-3 and level-4 data sets. Level-3 satellite products comprise single variables mapped on uniform space-time grid scales, usually with some completeness and consistency. Level-4 products refer to model output or results from analyses of lower-level data (e.g., level-3 variables) derived from multiple measurements, such primary productivity which incorporates ocean color, temperature and mixed layer depth products.

The final element of the network design was incorporating mobile measurements to tie the long-term measurements into a broader context. The main mobile data measurements were multi-beam echosounder measurements as well as horizontal and vertical net tows to determine the types of fish and zooplankton present. These measurements were performed from the UNOLS vessel that retrieved and deployed the long-term autonomous observatory landers. The fine-scale acoustic echosounder surveys (FSAS) were intended to map the spatial extent of the fish and zooplankton measured by the fixed, long-term echosounders. The net tows provided samples of animals present in the water column for groundtruthing and identifying appropriate scattering groups of the types of animals detected in the static and mobile active acoustic sensors. During daylight hours visual observers on the deployment vessel were tasked with spotting and logging the presence of marine mammal species.

The second mobile data collection platform was a towed horizontal-line array of hydrophones. The primary role of the towed array was to measure the variability in the soundscape between stations and/or between major changes in the oceanographic environment, for example coming off the shallow shelf (~100 m) to the deeper shelf (~400 m) near the Jacksnoville (JAX) station. During the network design we determined that the magnitude of the currents in the project area (Figure 10) were such that our original

proposal to use sub-surface gliders (e.g., the Teledyne Web Research Slocum gliders) was not likely to succeed. Therefore, for all but the last cruise, the towed array work was performed from a sailboat, which employed a surface autonomous vehicle. The towed array missions are described in Section 3.2.

Guided by the considerations above, the ADEON Network Design included seven long-term autonomous observatory (ALTO) landers (three with echosounders), mobile measurements from the deployment vessel and sailboat, and satellite remote sensing (and model) data (Figure 12). A mapping of data types to measurement platform is presented in Table 3. During the Network Design, the PIs had to balance the system capabilities, measurement priorities and budgets. The priority for in situ measurements were those for which an existing model was not available: the soundscape and the presence of fish and zooplankton in the water column. A significant measurement platform that was considered but was not ultimately included were surface buoys that could measure meteorological conditions as well as ocean conditions at the surface or across the water column. It was felt that NOAA and other groups were already deploying such platforms and that data at the resolution required for ADEON's models was already available through the remote sensing approach.

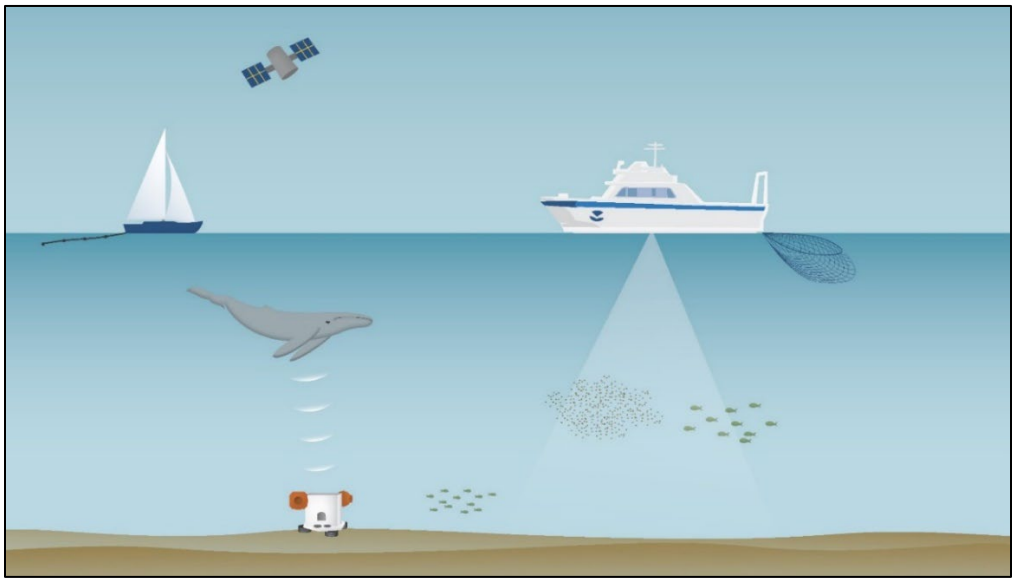

Figure 12. ADEON network design

The ADEON Network Design features autonomous long-term observatory (ALTO) bottom landers, active echosounders, visual observers and net tows from the UNOLS vessels, towed array hydrophones from sailboats and satellite-derived remote sensing.

Table 3. Data types by platform of the ADEON Network Design

Platform	Sampling Protocol	Omni Acoustics	Directional Acoustics	Active Acoustics	CTD/SST	Chlorophyll a	Dissolved Oxygen	Fish Tracking	Marine Mammal Visual.			Vessel tracking		Fish/Zooplankton Types				Wind/Wave States		
Standard Landers (4)	Continuous on duty cycle								□	□		□		□	□					
Active Acoustic Landers (3)	Continuous on duty cycle								□	□	□	□		□	□					
Sailboat	During cruises								□	□		□								
Vessel measurements	Continuous on station										□									
	Sample on Station											□	□	□					□	
	Daylight Hours															□				
Remote sensing and databases	As available											□	□				□			□

2.3 Hardware Selection

The hardware selected to implement the Network Design is described in detail in the ADEON Hardware Specification (Martin et al. 2018) and is summarized here.

2.3.1 Autonomous Long-Term Observatory (ALTO) Landers

As described in Section 2.2, a seabed mounted lander was the preferred solution for integrating and deploying the long-term monitoring sensors. The ALTO landers were designed by JASCO Applied Sciences for ADEON (Figure 13). Three trial deployments of the lander were performed by JASCO to test the ease of deployment and retrieval as well as to test the acoustic data quality.

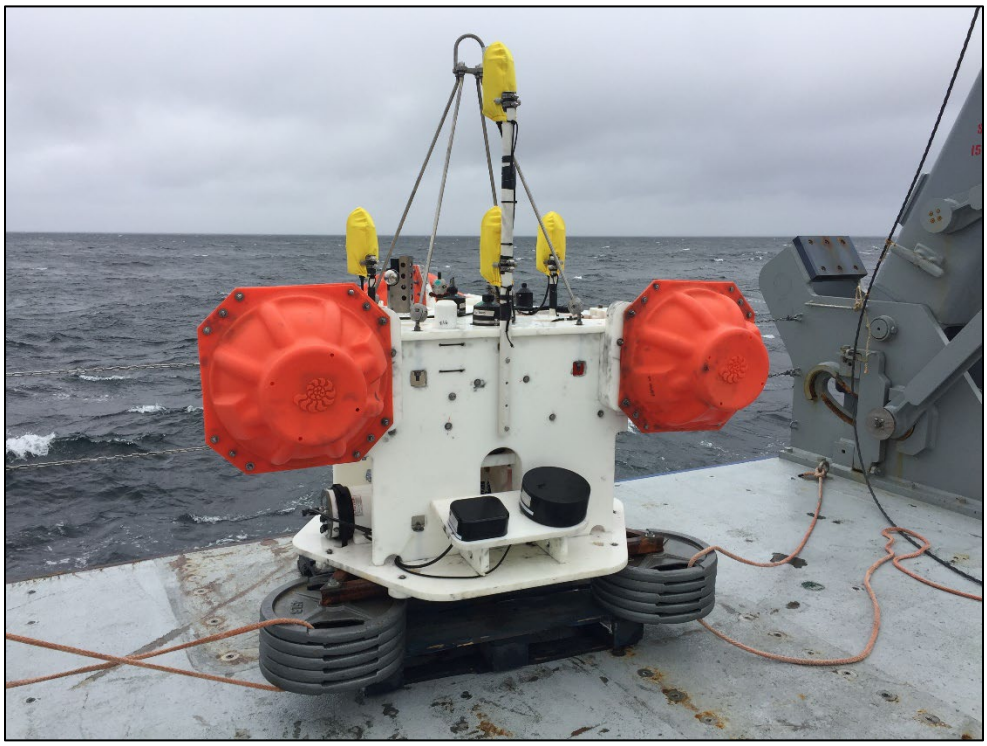

Figure 13. The ALTO lander under the A-frame on the R/V *Neil Armstrong* ready for deployment

The four yellow sleeves are the positions of the hydrophone array similar. The transducers for the four-frequency acoustic zooplankton and fish profiler (AZFP) scientific echosounder are the black objects at the bottom middle of the lander. The VEMCO fish tag logger, SBE-37 CT-DO logger, acoustic releases and Iridium satellite beacons are visible on the top deck of the lander.

The equipment on the ALTO landers were:

- Passive acoustic recorder: The passive acoustic recordings were made by autonomous multichannel acoustic recorders (AMARs) (JASCO Applied Sciences, Generation 3 for the first year and Generation 4 for the second and third years). For 27 of the 28 deployments the AMARs were equipped with four M36-V35-100 omnidirectional hydrophones; the first deployment at Virginia Inter-Canyon (VAC) had 1 M36-V35-100 and an M20-601 directional hydrophones from GeoSpectrum Technologies. The omni-directional hydrophones were arranged as an orthogonal array with a nominal spacing of 50 cm. A configuration file called '"ChannelAssociations.xml" that accompanies the raw data has the exact hydrophone locations. The duty cycles for the AMARs is shown in Table 4. Calibrations for the hydrophones are provided in the "deploymentInfo.csv" file associated with each data set.
- Acoustic zooplankton and fish profiler (AZFP): The AZFP, from ASL Environmental Sciences, collected the active acoustic data for ADEON on the bottom landers using four frequencies: 38, 125, 200, and 455 kHz. The three AZFPs available to the project were deployed at the shallowest sites: VAC, Cape Hatteras (HAT), and JAX; these are also the sites where the greatest amounts of fish and zooplankton were expected.
- Conductivity-temperature-dissolved oxygen logger: The Sea-Bird MicroCAT SBE-37 CT-DO logger was chosen to measure conductivity, temperature and dissolved oxygen because of its accuracy, reliability, and ease of integration.

- Fish-tag loggers: The VEMCO VR-2W fish-tag loggers were deployed on the bottom landers at VAC, HAT, JAX, and CHB (the remaining sites were too deep for these recorders). They were selected due to their low cost and the large number of fish tagged with the VEMCO 69 kHz tags.

Table 4. Recording configuration for the autonomous multichannel acoustic recorder (AMAR) passive acoustic recorders

Cruise 1 (Dec 17–Jun 18)			Cruise 2 (Jun 18–Nov 18)			Cruise 3 & 4 (Nov 18–Nov 20)		
Duration (sec)	Channels	Sample Rate (Hz)	Duration (sec)	Channels	Sample Rate (Hz)	Duration (sec)	Channels	Sample Rate (Hz)
300	1,2,3,4	8000	60	1	8000	60	1	512000
600	1	8000	1140	1,2,3,4	375000	540	1,2,3,4	16000
60	1	375000	60	1	8000	60	1	512000
300	N/A	SLEEP	1140	1,2,3,4	375000	540	1	16000
			60	1	8000	60	1	512000
			300	1,2,3,4	375000	540	1,2,3,4	16000
			780	N/A	SLEEP	60	1	512000
						540	1	16000
						60	1	512000
						300	1,2,3,4	16000
						60	1	512000
						780	N/A	SLEEP

The towed array hardware was different for each cruise. The systems were:

- Sail Cruise 1 (HAT–VAC): A 16-channel hydrophone array was towed behind a sailboat along the HAT-VAC line. The array was cut to 1 kHz (0.75m element spacing).
- Sail Cruise 2 and 3 (CHB-SAV-WIL [Wilmington]) A 16-channel hydrophone array was towed behind a sailboat along the HAT-VAC line. The array was cut to 1 kHz (0.75m element spacing).
- Sail Cruise 4 (JAX-CHB): A hydrophone was suspended from a small autonomous sailboat (Sub Sea Sail) platform that made the JAX-CHB transect during the storm. Single position hydrophone recordings were made at multiple ranges from CHB A continuous transect, passing across the continental shelf-break was made approaching JAX.

The equipment employed on the UNOLS vessels were:

- EK-60 and EK-80 active acoustics: The EK-80 multibeam echo sounder was fitted on the R/V *Neil Armstrong*. The ADEON team from Stony Brook University provided an EK-60 for the trips on the R/V *Endeavor* which was pole-mounted.
- Conductivity-temperature-depth: The standard oceanographic conductivity, temperature, depth (CTD) available on the UNOLS vessel used for the bottom lander service trips provided local full-water-depth CTD data for ADEON. The CTD rosette was also equipped with dissolved oxygen and fluorescence sensors to provide chlorophyll and oxygen measurements throughout the CTD cast.
- Net-tows: The ADEON project used complementary set of nets to sample zooplankton and nekton in the water column. A Bongo ring net (net diameter between 30 and 75 cm) with fine mesh (~300–500 μm) was deployed vertically in the top 100 m of the water column to capture small zooplankton. An Isaacs-Kidd (Devereux & Winsett, 1953) Midwater Trawl (IKMT) with coarser mesh (1–5 mm) targeted specific scattering layers or features in the water column that were detected using the ship-board multi-beam echo sounders.

3. Overview Phase II: Data Acquisition

3.1 University-National Oceanographic Laboratory System (UNOLS) Cruises

3.1.1 Research Cruise Summary

Five cruises (AR025, EN615, EN626, AR040, AR049) were conducted to deploy and recover the bottom landers and to collect additional data to characterize the environment and organisms at each site. Though cruise ports varied for each trip, a typical cruise track consisted of single visits to each Atlantic Deepwater Ecosystem Observatory Network (ADEON) site (e.g., Figure 14). The vessel-based sampling included: fine-scale acoustic surveys (FSASs), hydrographic (conductivity, temperature, depth [CTD]) profiles, vertical ring net hauls, midwater nekton trawls, marine mammal observations, environmental DNA (eDNA) sampling, and other data (Table 5). For some cruises, depending on weather and sea state conditions, additional acoustic surveys and net sampling were conducted to examine short-term temporal variability in the water column organisms. A full record of the activities of each cruise is contained in the individual cruise reports, so a brief summary of each cruise is provided here. Cruise operations and personnel were significantly reduced (although all objectives were met) for the final cruise (AR049, Dec 2020) due to COVID-19 pandemic regulations.

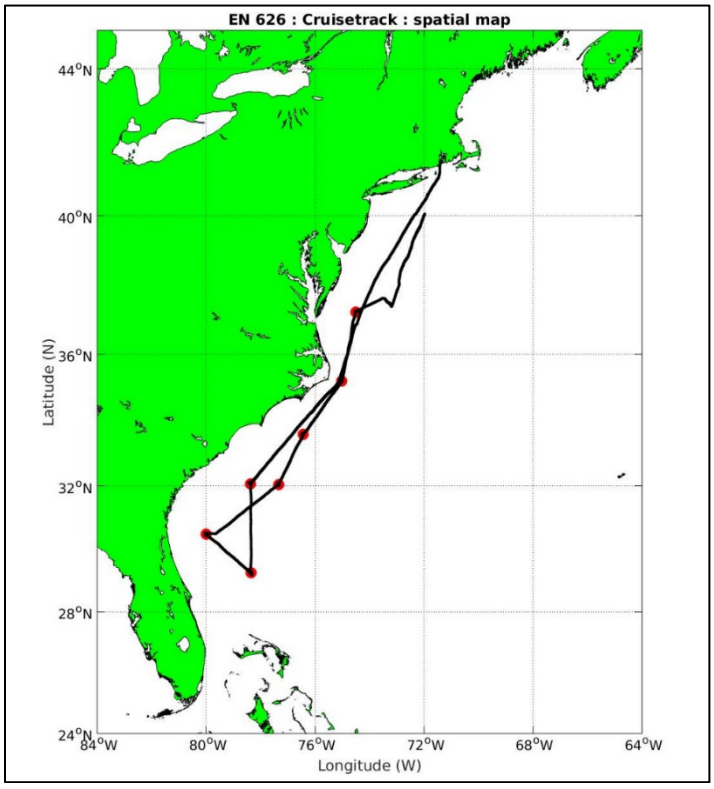

Figure 14. An example ADEON research cruise track

(R/V *Endeavor* EN626 from 31 Oct to 16 Nov 2018) departed and returned to Narragansett, Rhode Island. ADEON site locations are marked with red circles.

Additional experiments or sampling that occurred only on a subset of the cruises included: a transmission loss experiment (AR025), at sea acoustic zooplankton fish profiler (AZFP) calibration (AR025), sea surface roughness measurements (AR025), enzyme assays for microbial community analysis (EN615), water samples for Deep Search collaborators (EN615, EN626), recovery of lost vessels (AR025, AR040), recovery of a misbehaving Ocean Observatories Initiative glider (AR040), *Jason* vehicle test dives (AR049), gravimeter testing for Woods Hole Oceanographic Institution's (WHOI) Dr. Dan Fornari (AR049), and the deployment of two landers at sites for the Acoustic and Environmental Observation Network AEON project (AR049). Two of the research cruises also included an artist-at-sea (Lindsay Olson, EN615; Wendy Klemperer, AR040). Several participants in our research cruises were selected from the UNOLS volunteer program and roughly half the science team for each cruise were graduate (or in some cases undergraduate) students.

Table 5. Summary of sampling that occurred during each cruise of the ADEON project

Cruise	Site	Lander Recovered and/or Deployed	CTD casts	Ring net tows	Isaacs-Kidd midwater trawl (IKMT) net tows	Finescale Acoustic Survey	eDNA samples collected	Fish specimens preserved
AR025	VAC	Yes/Yes	15	2	6	Yes (2)	Yes	Yes
	HAT	Yes/Yes	7	1	4	Yes	Yes	Yes
	WIL	Yes/Yes	7	1	3	Yes	Yes	Yes
	SAV	Yes/Yes	4	1	3	Yes		Yes
	BLE	Yes/Yes	4	1	3	Yes		Yes
	JAX	Yes/Yes	6	1	2	Yes	Yes	Yes
	CHB	Yes/Yes	5	1	2	Yes		Yes
EN615	VAC	Yes/Yes	2	1	2	Yes (2)	Yes	Yes
	HAT	Yes/Yes	2	1	2	Yes (2)	Yes	Yes
	WIL	Yes/Yes	2	1	2	Yes	Yes	Yes
	SAV	Yes/Yes	1	1	1	Yes	Yes	Yes
	BLE	Yes/Yes	2	1	1	Yes	Yes	Yes
	JAX	Yes/Yes	2	1	1	Yes	Yes	Yes
	CHB	Yes/Yes	2	1	1	Yes	Yes	Yes
EN626	VAC	Yes/Yes	3	1	4	No	Yes	Yes
	HAT	Yes/Yes	1	0	0	No	No	No
	WIL	Yes/Yes	1	1	1	Yes	No	Yes
	SAV	Yes/Yes	1	1	1	Yes	No	Yes
	BLE	Yes/Yes	2	1	1	Yes	Yes	Yes
	JAX	Yes/Yes	1	1	2	Yes	Yes	Yes
	CHB	Yes/Yes	1	1	2	No	Yes	Yes
	MMD*	NA	0	0	1	Partial	No	No
AR040	VAC	Yes/Yes	3	1	5	Yes (3)	Yes	Yes
	HAT	Yes/Yes	2	1	3	Yes (3)	Yes	No
	WIL	Yes/Yes	1	1	2	Yes (2)	Yes	No
	SAV	Yes/Yes	1	2	2	Yes	Yes	No
	BLE	No/Yes	1	1	2	Yes	Yes	Yes
	JAX	No/No	1	1	2	Yes (2)	Yes	Yes
	CHB	Yes/Yes	1	1	1	Yes	Yes	No
AR049	HAT	Yes/No	1	1	1	Yes	No	Yes
	WIL	Yes/No	1	1	1	Yes	No	Yes
	SAV	Yes/No	1	1	1	Yes	No	Yes
	BLE	Yes/No	1	1	1	Yes	No	Yes
	JAX	Yes/No	1	1	1	Yes	No	Yes
	CHB	Yes/No	1	1	1	No	No	Yes

Cruise	Site	Lander Recovered and/or Deployed	CTD casts	Ring net tows	Isaacs-Kidd midwater trawl (IKMT) net tows	Finescale Acoustic Survey	eDNA samples collected	Fish specimens preserved
	Project Total	32/33	91	35	70	39	22	29

*MMD is Million Mounds, a Deep Search site where we were able to collect samples without impact to ADEON objectives. Sampling effort was slightly reduced during EN626 due to weather and during AR049 due to pandemic restrictions, although all objectives were still accomplished.

3.1.2 Fine Scale Acoustic Surveys

Multiple frequency acoustic backscatter data was collected from either: the R/V *Armstrong's* EK80 system (18, 38, 70, 120, and 200 kHz, Figure 15) or a pole mounted system using EK80 and EK60 echosounders on the R/V *Endeavor* (38, 70, 120, and 200 kHz). All systems were broadband with the exception of the 18 and 38 kHz on the R/V *Armstrong* and the 120 kHz on the R/V *Endeavor*. Pulse lengths were typically 1024 microseconds, and ping rate was set to maximum, except when in shallow (<150 m) water or when sea state (and thus data quality) were poor. Ping rate was then set to 0.2 to 1 Hz.

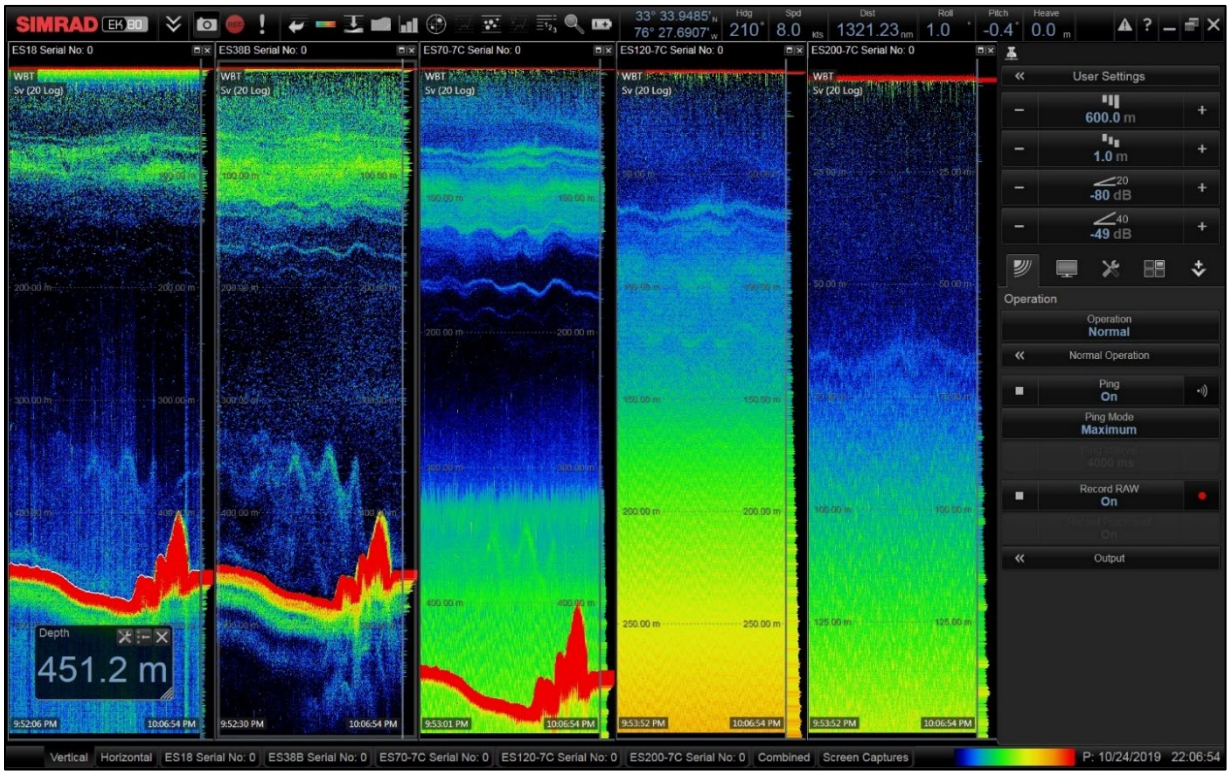

Figure 15. Example echogram from the ship's EK80 showing internal waves
Internal waves were commonly observed during the AR040 cruise as the ship transited across the continental shelf.

At each survey site, a fine-scale acoustic grid (Figure 16) was conducted at a speed of 8 kn. Survey lines were adjusted for the direction of the sea state. At a few sites, the survey grid was run multiple times, either during the day and then the night, or separated by several days or weeks.

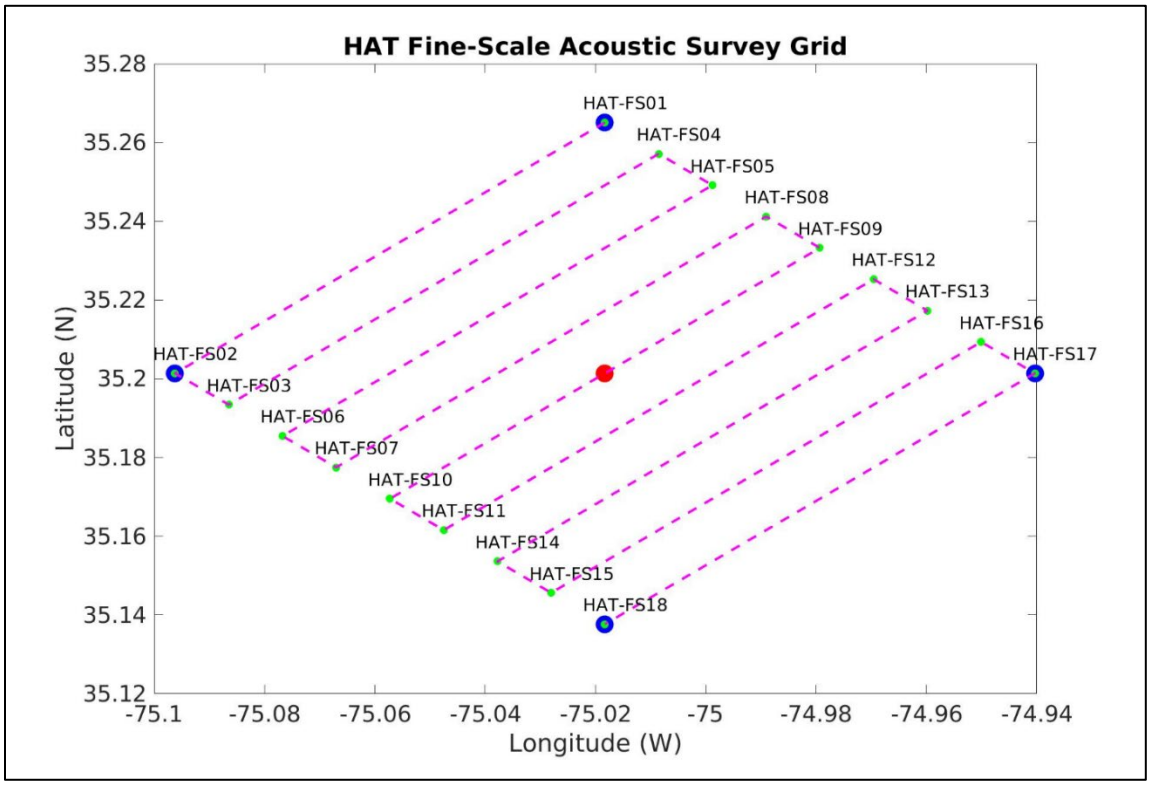

Figure 16. The grid acoustically surveyed at the Cape Hatteras (HAT) site during cruise AR040

The red dot at the center represents the location of the bottom lander. The survey grid covers an area roughly 10 km by 10 km.

3.1.3 Net and Trawl Sampling

Biological specimens were collected at each site using two different nets. A 60 cm diameter, ring-net Bongo pair (one with 1000 µm mesh, the other with 333 µm mesh) was deployed at each site (roughly at the lander location) with a vertical cast to 100 m (Figure 17). Actual net depths may be slightly less than the wire out because of surface currents causing the tow wire to be slightly off-vertical. Zooplankton and larval nekton collected in the ring net were preserved in buffered formalin solution for post-cruise identification and enumeration. Unique or interesting specimens from these tows were occasionally photographed or preserved individually.

A larger net (5 m^2 Isaacs-Kidd midwater trawl [IKMT]) was also deployed at each site (Figure 17), typically multiple times per site. One tow was done at the lander location and was targeted to sample the scattering layers observed in the water column on the echosounder display. Additional tows were conducted to sample the deep (> 750 m) scattering layers and to collect specimens from the mesopelagic region.

Figure 17. Bongo net (left) being deployed for a vertical cast to a depth of 100 m during the EN626 cruise
The IKMT (right) being deployed during the same cruise. Wire-out speeds were 20–40 meters per second, and haul-back speeds were 10 to 30 meters per second. Tow depths ranged from ~150 m to 1300 m. (Photos: Joseph Warren.)

Biological specimens from the net and trawl sampling (Figure 18) were used in onboard experiments to measure the acoustic scattering properties and characteristics of individual organisms including animal size, morphology, density and sound speed relative to seawater, and ex situ broadband target strength measurements in shipboard aquaria. A subset of organisms was sampled for biological tissue prior to formalin preservation and some individuals were frozen or preserved in ethanol for additional analyses such as stable isotope and DNA conducted by colleagues at the US Geological Survey (USGS) and Nova Southeastern University as part of our collaboration with the Deep Search project.

Figure 18. Some of the zooplankton and nekton collected by net and trawl sampling during the ADEON project

All photos taken by Joseph Warren.

3.2 Sail Cruises

In order to provide spatial sampling of the ocean soundscape at positions other than those of the fixed ADEON landers, a set of four sail cruises were conducted. On these tests, acoustic measurements were taken along transects between lander positions, including going directly over the landers. This dataset, which includes towed array measurements and single hydrophone measurements, provides the data necessary to examine spatial correlations at lags shorter than the inter-lander spacings. The sail cruises generally lasted 4–5 days and therefore do not provide significant input to the temporal correlation question. When data is taken from a horizontal line array, the directional soundscape can be evaluated by conventional beamforming of the array data. For each test, the decidecade band omni-directional levels and the bearing-time-record (BTR) of beam decidecade sound exposure level (SEL) were computed and provided to the University of New Hampshire (UNH) data server as a data product.

3.2.1 Sail Cruise 1, June 2018, Hatteras (HAT) and Virginia Canyon (VAC)

Sail Cruise 1 was conducted in June of 2018. A 16-channel hydrophone array was towed behind a sailboat along the Cape Hatteras (HAT)-Virginia Canyon (VAC) line. The chief scientist on the cruise was James Murray, of Ocean Acoustic Sciences and Instrumentation Services (OASIS) at the time. The challenge for this test was very low winds. To make way through the water, the engine was required for a portion of the experiment. These soundscape measurements are contaminated by the ship engine noise. There were measurements recorded when the engine was not on, for analysis purposes.

3.2.2 Sail Cruise 2 and 3, June 2019, Charleston Bump (CHB), Savannah Deep (SAV), Wilmington (WIL)

Sail Cruises 2 and 3 were conducted in June of 2019. The science party, led by Dr. Chris Verlinden of Applied Ocean Sciences (AOS), mobilized and sailed from Charleston, South Carolina. The first leg was Charleston Bump (CHB) to Savannah Deep (SAV). This leg constituted Cruise 2. The SAV to Wilmington (WIL) leg was then conducted for Cruise 3. The navigation from the cruise plan for the tests is shown in Figure 19. For each lander position, the propagation loss (PL) is displayed in the figure. All measurements were taken using a 16-element towed array. For this test there was sufficient wind, but there were issues with flow noise.

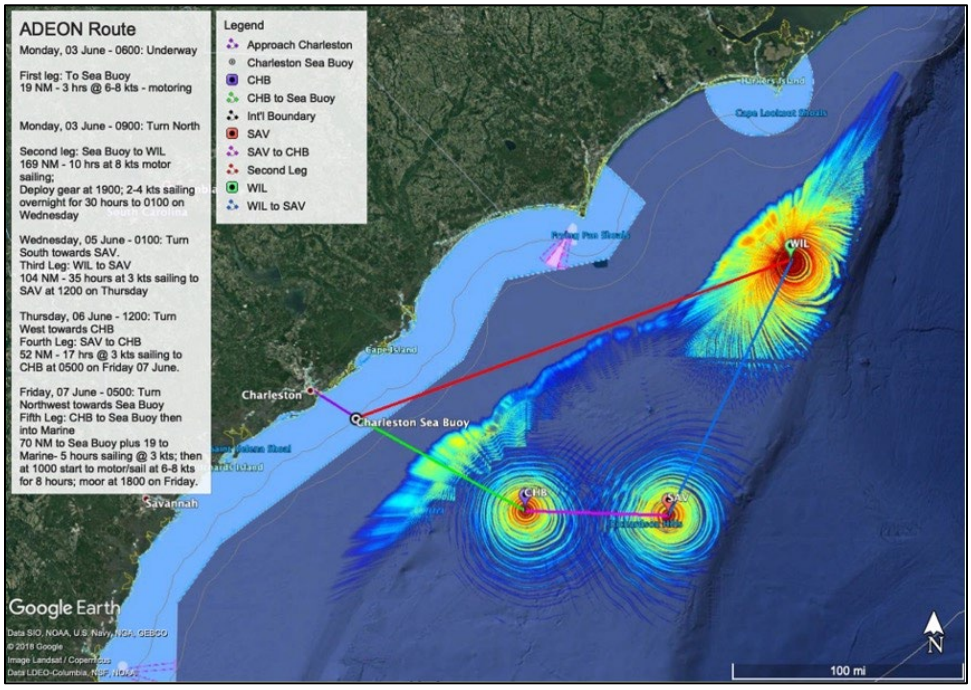

Figure 19. Sail cruise tracks from Sail Cruises 2 and 3

The propagation loss (PL) at each of the CHB, SAV, and WIL sites is shown with red colors representing the lowest loss spreading to blue where loss tapers to the range where a signal beyond the threshold a source making a sound at 20 Hz would not be recorded above ambient sound levels at the lander.

3.2.3 Sail Cruise 4, November 2020 Jacksonville (JAX)-CHB

Sail Cruise 4 was conducted in November 2020, just before the ADEON landers were recovered on AR049. The chief scientist on the cruise was Dr. Chris Verlinden of Applied Ocean Sciences. The navigation for this cruise is shown in Figure 20. This cruise was conducted in two legs due to a severe thunderstorm. During this cruise, measurements were made over and approaching the Jacksonville (JAX) lander, as well as the Charleston Bump (CHB) lander. A hydrophone was suspended from a small autonomous sailboat (Sub Sea Sail) platform that made the JAX-CHB transect during the storm (dark blue line in Figure 20). Single position hydrophone recordings were made at multiple ranges from CHB (shown as red-dots in the figure below). A continuous transect, passing across the continental shelf-break was made approaching JAX (red line in Figure 20).

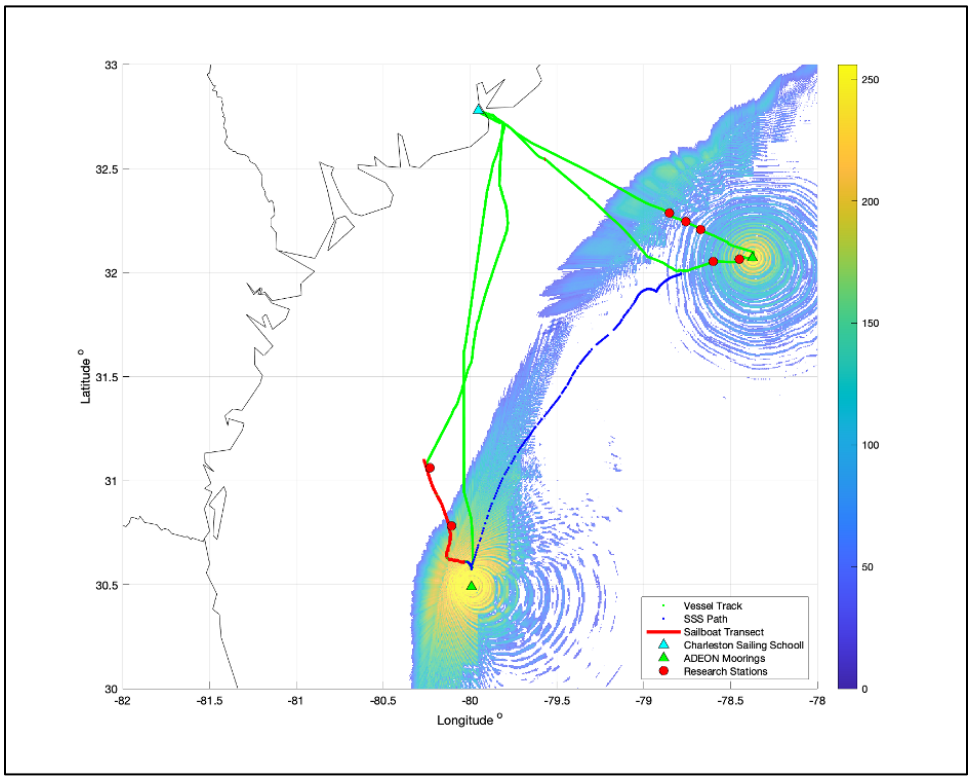

Figure 20. Sail Cruise 4 tracks

The dark blue line shows the track for the small autonomous sailboat (Sub Sea Sail) platform that made the JAX-CHB transect. Single position hydrophone recordings were made at multiple ranges from CHB (shown as red-dots). A continuous sail transect, passing across the continental shelf-break was made approaching JAX (solid red line). Propagation loss is depicted by the colors surrounding each lander site and identifies the effective range of detection at the lander for sources at different distances to the lander position.

3.3 Satellite Data

To compute the modelled soundscape, the shipping positions and wind-speeds as a function of position and time were required. Shipping location information is available through the satellite observations of automated information system (AIS) broadcasts. For 2019, the AIS dataset was purchased from SPIRE, a satellite AIS tracking company. The 2018 and 2020 datasets were obtained by request from the US Coast Guard. The data provided includes time, ship position, speed, heading, course, ship type and/or class and ship length. The wind fields for the model were obtained from the National Oceanographic and Atmospheric Administration (NOAA). The wind model, which includes satellite assimilation of data is the Cross-Calibrated Multi-Platform (CCMP) data set.

Satellite and modeled ocean datasets collected for the ADEON project study area (Table 2) were obtained from public websites, and covered a variety of spatial and temporal scales. All global data were processed to Level 3 or 4 as specified in the ADEON Data Processing Standard (Heaney et al. 2020). The global data were gridded from 1 to 25 km^2 resolution, ranging from daily to weekly time scales. There was also a near real-time Level 2 data stream originating from the National Aeronautics and Space Administration

(NASA) at higher spatial resolution (1 km^2) over the ADEON area for Chlorophyll *a* and sea surface temperature (SST). Real-Time Ocean Forecasting Systems (RTOFS) model data for the Atlantic Ocean were also being streamed and collected daily.

Global ocean data (Table 3) are in a gridded, mapped format at Level 3 or Level 4. Level 3 data are derived geophysical variables from Level 2 that have been aggregated/projected onto a defined spatial grid over a defined time period. Level 2 data consist of derived geophysical variables at the same resolution as the source Level 1 data (unprocessed satellite data). Level 4 data are model outputs or results from analyses of lower level data (e.g., variables derived from multiple measurements). Ocean net primary productivity is an example of a Level 4 product.

Table 6. Satellite product names and units for ADEON

Parameter	Processing level	Description	Units	Notes
CHL	Level 3 (NASA)[3]	Chlorophyll *a* concentration	mg /m^3	
PAR	Level 3 (NASA)	Photosynthetically available radiation	mol /(m^2 d)	NASA uses the unit einstein/(m^2 d) for this quantity. One einstein is defined loosely as the energy in a mole of photons, but ultimately PAR is the number of moles of photons per square metre of Earth's surface per day, hence our choice of unit. A PAR of 1 mol/(m^2 d) corresponds to a light energy flux spectral density of approximately 1 mW/(cm^2 □m) (Kirk, 1994; Frouin et al., 2003)
WSPD	Level 3 (IFREMER)[4]	Wind speed	m/s	
PRECIP	Level 3 (NASA)	Daily precipitation	Mm	
SST	Level 4 (NASA)[5]	Sea surface temperature	°C	Period covered: Jan. 1, 2016 through August 27, 2019
SST	Level 4 (Copernicus)[6]	Sea surface temperature	°C	Period covered: Jan. 1, 2017 through December 31, 2020
NPP	Level 4 (NASA)	Net primary productivity (C)[7]	mg / (m^2 d)	
MLD	Level 4	Mixed layer depth	m	HYbrid Coordinate Ocean Model (HYCOM) model (Oregon State University)
CURRENTS	Level 4 (NASA)	u,v surface currents vectors	m/s	

3.3.1 ADEON Sea Surface Temperature (SST) Satellite Products

There are multiple global sea surface temperature (SST) products available from a variety of sources on the internet. These products have evolved over time, favoring high spatial and temporal resolution gridded maps that blend SST observations from multiple sensors and sources.

3.3.1.1 NASA Jet Propulsion Lab Sea Surface Temperature

[3] Variables mapped on uniform space-time grid scales, usually with some completeness and consistency.
[4] Level 3 data are presented in relation to identical and standardized space-time reference scales. The data can thereby be easily compared and aggregated, including between different measurement programmes.
[5] Model output or results from analyses of lower-level data (e.g., variables derived from multiple measurements). Data availability discontinued after August 27, 2019.
[6] Model output or results from analyses of lower-level data (e.g., variables derived from multiple measurements).
[7] carbon.

ADEON used a high resolution, global blended SST product obtained from the Jet Propulsion Laboratory (JPL). The global product is from the Group for High Resolution Sea Surface Temperature (GHRSST) Level 4 sea surface temperature analysis produced as a retrospective dataset (four-day latency) and near-real-time dataset (one-day latency) at the NASA Jet Propulsion Laboratory's (JPL) Physical Oceanography Distributed Active Archive Center (PO DAAC) using wavelets as basis functions in an optimal interpolation approach on a global 0.01 degree grid. The version 4 Multiscale Ultrahigh Resolution (MUR) L4 analysis was based upon nighttime GHRSST L2P skin and subskin SST observations from several instruments including the NASA Advanced Microwave Scanning Radiometer-EOS (AMSR-E), the JAXA Advanced Microwave Scanning Radiometer 2 on GCOM-W1, the Moderate Resolution Imaging Spectroradiometers (MODIS) on the NASA Aqua and Terra platforms, the US Navy microwave WindSat radiometer, the Advanced Very High Resolution Radiometer (AVHRR) on several NOAA satellites, and in situ SST observations from the NOAA iQuam project.

3.3.1.2 Copernicus Sea Surface Temperature

Similar to the NASA JPL global product described above, the Copernicus dataset provides daily estimates of global SST based on observations from multiple satellite sensors since September 1981. The SST data provided here are based on measurements carried out by the following infrared sensors flown onboard multiple polar-orbiting satellites: the series of AVHRRs, the series of Along Track Scanning Radiometers (ATSRs), and the Sea and Land Surface Temperature Radiometer (SLSTR). ADEON is using the Level-4 processing level data. These products are available as Climate Data Records (CDRs), which have sufficient length, consistency, and continuity to be used to assess climate variability and changes. These SST CDRs are identical to those produced as part of the European Space Agency (ESA) SST Climate Change Initiative (CCI) project.

3.3.2 NASA Ocean Level-3 Standard Mapped Image (SMI) Products

The NASA standard mapping image (SMI) products were generated from binned (spatially or temporally aggregated) data products and represent data binned over the period covered by the parent product. These products include CHL and photosynthetically available radiation (PAR) for ADEON. The arithmetic mean was used in each case to obtain the values for the SMI grid points from the binned data products. Each SMI product contains one image of a geophysical parameter and is stored in one physical file. The Level 3 files for CHL and PAR are in Network Common Data Form (netCDF) format, and use a variety of international standards and conventions for metadata and file structure.

The NASA Level 3 filenames contain the date period (i.e., temporal resolution), product type: CHL or PAR, and spatial resolution. The ADEON project used the 8-day averaged fields at 4.6 km^2 pixel resolution for CHL and PAR. The NASA-NOAA Visible Infrared Imaging Radiometer Suite (VIIRS) onboard the Suomi National Polar-orbiting Partnership (SNPP) satellite was the source sensor for both CHL and PAR.

3.3.3 Net Primary Productivity (NPP)

Net primary productivity (NPP) is a Level 4 product, derived from other Level 3 and Level 4 data. The NPP product chosen for the ADEON project was the Vertically Generalized Production Model (VGPM) by Behrenfeld & Falkowski (1997), and is a commonly used algorithm for estimating oceanic NPP. The VGPM algorithm used CHL and other parameters as input fields. The NPP quantity is water column

integrated productivity per unit of ocean area, and the unit is milligrams of carbon fixed per day per unit volume.[8]

3.3.4 Mixed Layer Depth (MLD)

The mixed layer depth (MLD) product for ADEON was derived from the Hybrid Coordinate Ocean Model (HYCOM). Simplified and renamed versions of the original data files[9] were obtained from ftp servers at Oklahoma State University (OSU), served alongside with their NPP products. The OSU versions were averaged to 8-day time intervals at 4.6 km^2 resolution and based on 0.125 density contrast.

3.3.5 Precipitation Data

Daily precipitation data were obtained from NASA as a level-3 product from the Global Precipitation Measurement (GPM) mission. ADEON used products from the Integrated Multi-satellitE Retrievals for GPM (IMERG) product, which is the unified US algorithm that provides the multi-satellite precipitation product. This dataset is the GPM Level 3 IMERG *Final* Daily 10 x 10 km (GPM_3IMERGDF) derived from the half-hourly GPM_3IMERGHH. The derived result represents the final estimate of the Daily accumulated precipitation. The dataset was produced at the NASA Goddard Earth Sciences (GES) Data and Information Services Center (DISC) by simply summing the valid precipitation retrievals for the day in GPM_3IMERGHH and giving the result in (mm).

3.3.6 Altimetry Data

Altimetry "value-added" products–the Finite-Size Lyapunov Exponents or FSLE–were obtained from the AVISO web portal. These products provided the exponential rate of separation of particle trajectories initialized nearby and advected by altimetry velocities. FSLEs highlighted the transport barriers that controlled the horizontal exchange of water in and out of eddy cores, multi-mission altimetry-derived gridded backward-in-time Finite Size Lyapunov Exponents, and Orientations of associated eigenvectors.

3.3.7 Wind Speed and Stress

The Advanced SCATterometer (ASCAT) is a real aperture sensor onboard the meteorological operational (MetOp) platforms and maintained by the ESA. The prime objective of ASCAT is to measure wind speed and direction over the oceans. It is a real aperture radar (one with a physical array of sensors), operating at 5.255 GHz (C-band) and using vertically polarized antennas. With the rapid global coverage, day or night and all-weather operation, ASCAT offered a unique tool for long-term climate studies.

New gridded daily-averaged wind and wind stress fields (DASCAT) have been estimated over global oceans from ASCAT retrievals using objective methods. The analyses used standard products ASCAT L2b during the period April 2007–March 2009, and ASCAT L2b 12.5 from April 2009 to present[10]. The requested atmospheric and oceanic variables, such as sea surface temperature, air temperature, and specific air humidity, were derived from the European Centre for Medium-range Weather Forecasts (ECMWF) 6-hourly analysis. According to the ASCAT sampling scheme, the objective method allowing the determination of regular in-space and surface wind fields used ASCAT observations as well as

[8] NPP is a rate term and differs fundamentally from CHL (which is the standing stock of biomass). A more detailed description of the VGPM and model code can be found here: http://www.science.oregonstate.edu/ocean.productivity/vgpm.model.php .

[9] Available at https://hycom.org/ .

[10] See http://www.osisaf.org/biblio/docs/ss3_pm_ascat_1_8.pdf .

ECMWF analyses. The latter were considered as the temporal interpolation basis of ASCAT retrievals. The resulting fields have spatial resolutions of 0.25° in longitude and latitude. The calculation of daily estimates used ascending as well as descending available and valid retrievals. The objective method aimed to provide daily-averaged gridded wind speed, a zonal component, a meridional component, wind stress, and the corresponding components at global scale. The error associated with each parameter, related to the sampling impact and wind space and time variability, was provided as well.

3.3.8 Surface Currents

ADEON used upper ocean surface current products from the Ocean Surface Current Analysis Real-time (OSCAR) project at JPL. OSCAR contains near-surface ocean current estimates, derived using quasi-linear and steady flow momentum equations. The horizontal velocity was directly estimated from sea surface height, surface vector wind and sea surface temperature. These data were collected from the various satellites and in situ instruments. The model formulation combines geostrophic, Ekman, and Stommel shear dynamics, and a complementary term from the surface buoyancy gradient. Data are on a 1/3 degree grid with a 5 day resolution.

3.3.9 Local Real-time NASA satellite data

High-resolution satellite Level 2 imagery for the ADEON region is now available for CHL and SST products. Both products were derived from processing data from Level 1 to Level 2 using climatological ancillary datasets, thus the Level 2 products were not refined. Level 2 data were processed by NASA from the NASA-NOAA NPP VIIRS platform and NASA's MODIS-Aqua platform. Both datasets had an approximate 1 km-pixel resolution mapped to a region that spanned the US East Coast and covered the entire ADEON region (Figure 21). Image files were automatically uploaded daily from NASA ftp sites to ADEON data servers whenever there was 30 % or more satellite coverage of the defined region. This can result in multiple files per day per product, depending on the swath coverage and satellite view.

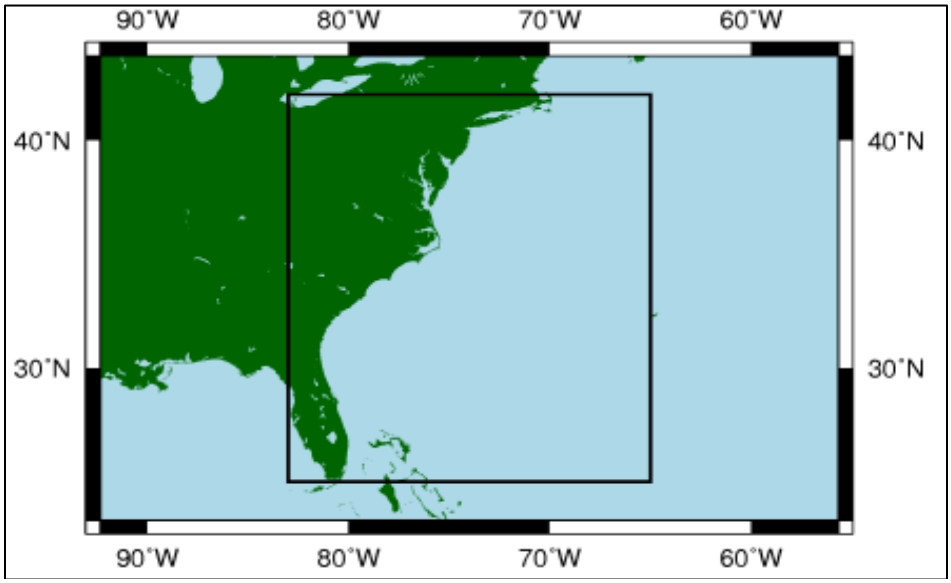

Figure 21. Defined region (black lines) for acquiring real-time NASA CHL and SST data

4. Overview Phase III: Data Processing

4.1 Passive Acoustics

4.1.1 Lander Passive Acoustics

4.1.1.1 Summary of Lander Passive Acoustic Data Collection

As discussed in Section 3.1, all landers were successfully retrieved over the four deployment periods. Three complete years of passive acoustic data were recorded from Cape Hatteras (HAT), Wilmington (WIL), Charleston Bump (CHB), Savannah (SAV), Jacksonville (JAX), and Blake Escarpment (BLE) in accordance with the duty cycle shown in Table 4.

Long-term spectral average (Figure 22) and percentile (Figure 23) figures were used to assess the data quality for each deployment. The complete set of results are contained in Appendix A. All raw data acoustic data from the landers are available through National Centers for Environmental Information (NCEI); the processed data files are all available on FigShare (see Section 8) and through the Atlantic Deepwater Ecosystem Observatory Network (ADEON) Data Portal[11].

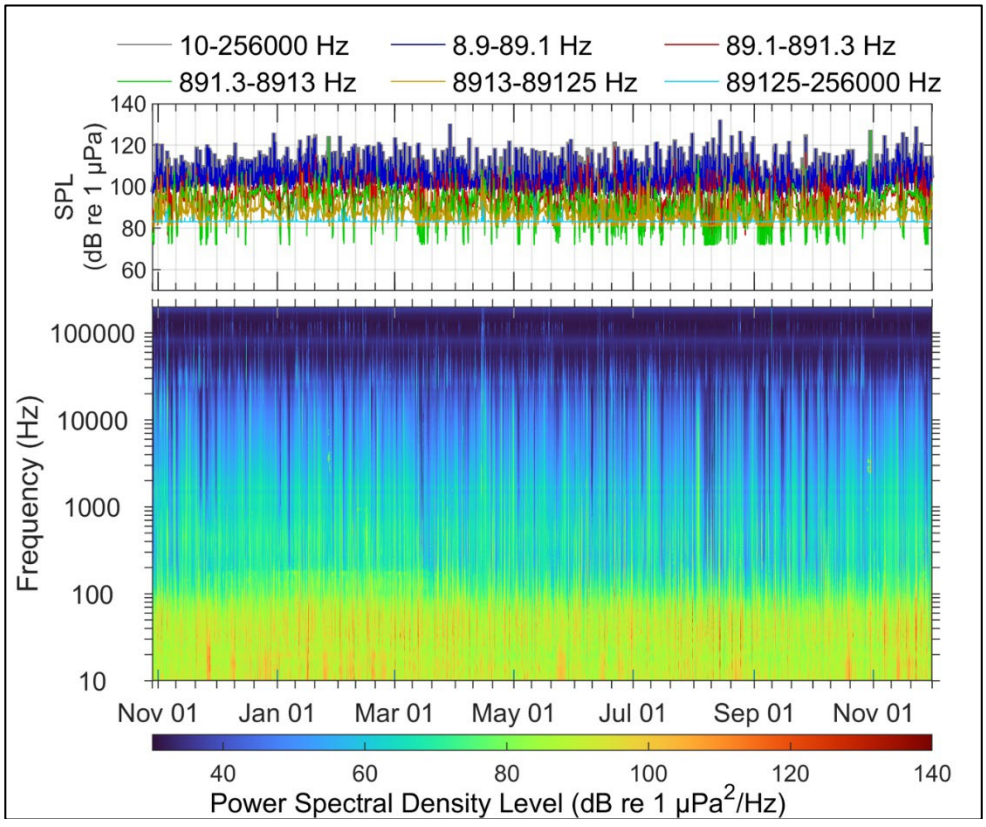

Figure 22. Summary of acoustic data collected at the Blake Escarpment (BLE) for Nov 19–Nov 20

[11] See https://adeon.unh.edu/data_portal.

The top panel shows the measured in-band sound pressure level for the ADEON decade bands and the bottom panel shows the long-term spectral average. The increase in sound levels between 100 and 200 Hz through the winter months are from minke whales.

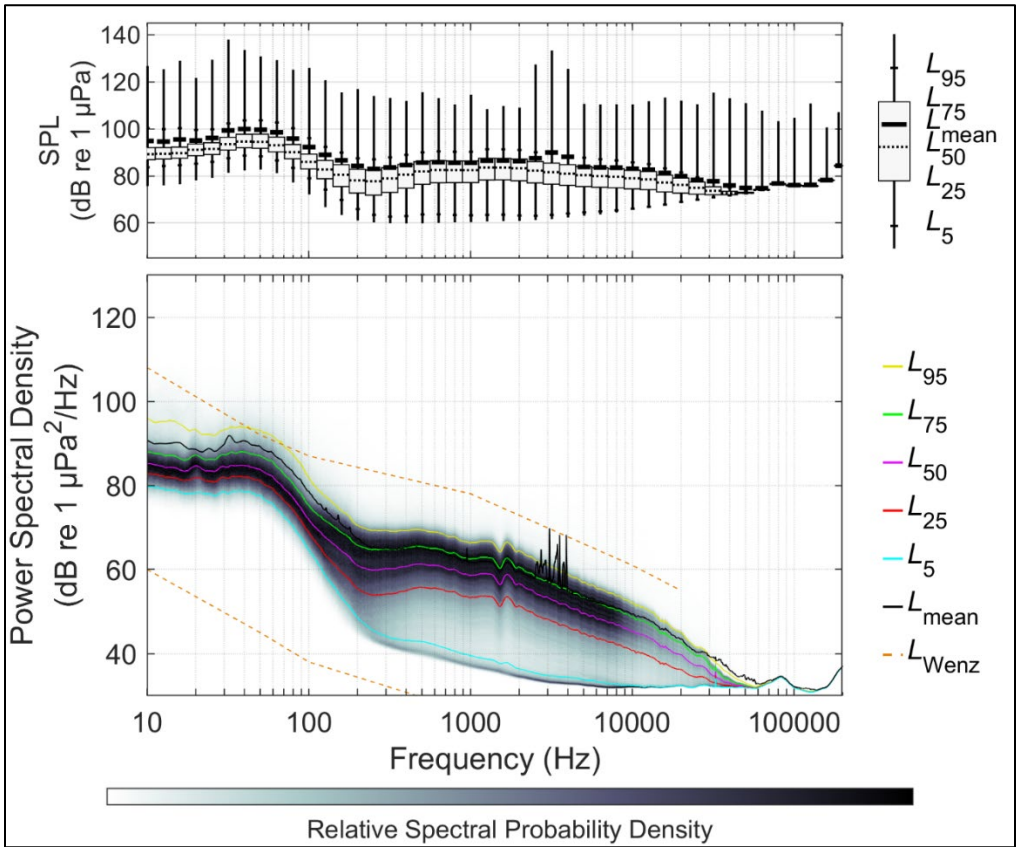

Figure 23. Distributions of spectral sound levels for the BLE data collected Nov 19–Nov 20 based on 1-min sound averages

Top: box and whisker plot of the decidecade sound pressure levels; the box represents the inter-quartile range of sound pressure levels (SPLs), the thick bar is the mean, the dashed bar is the median. The vertical lines above / below each box show the upper and lower quartile of the measured levels. The small horizontal ticks are the 5th and 95th percentile SPLs. Bottom: Percentile power spectral density and spectral probability densities, the Wenz limits of prevailing noise are shown as the dashed orange lines (Wenz, 1962).

The data from Virginia Inter-Canyon (VAC) is not complete, a total of 14 months of data identical to the data from the other sites is available (Nov 18–June 19, Jan 20–Jun 20). The issues with the other VAC data are:

- VAC-1: Nov–Dec 2017: This is four-hydrophone data from the first two weeks of the field program, no issues with the data other than that is it only two weeks long.
- VAC-2: Dec 17–May 18: This dataset features the M20 directional hydrophone with its own unique calibration issues; see Appendix B. The M20 system also ran out of battery approximately 3 weeks before the redeployment cruise. The high-sample rate channel did not record correctly during the deployment.
- Jun 18–Oct 18: The system was hit by a trawl in July 2018 and was moved approximately 2 km; the exact location is not known. The upper hydrophone mount was bent and the hydrophone position uncertain after this event.

- Nov 18–July 19: The VAC mooring was trawled up by fishing activity in early July. The fisherman notified the University of New Hampshire (UNH) and the equipment was retrieved.
- Nov 19–Jun 20: The VAC Mooring was trawled up by fishing activity in late June. The satellite beacon allowed UNH to locate and recover the equipment. The data up to 1 Jan 20 were corrupted by an unidentified noise source.

The VAC, HAT, and JAX landers had active echosounders on the landers, with their transducers angled outwards but near the hydrophones (see Figure 13). The clocks for the passive recorder and echosounder did not drift at the same rates, so there are periods where the echosounder was recorded by the passive acoustics (Figure 24). To prevent these minutes from affecting the summaries of the ambient sound levels, they were detected and removed from periods where the sum of the sound pressure levels in the 315–500 Hz decidecade bands exceeded 115 dB for at least 2 minutes. Long-term spectral average (LTSA) and percentile plots with and without this filtering are compared in Appendix A.

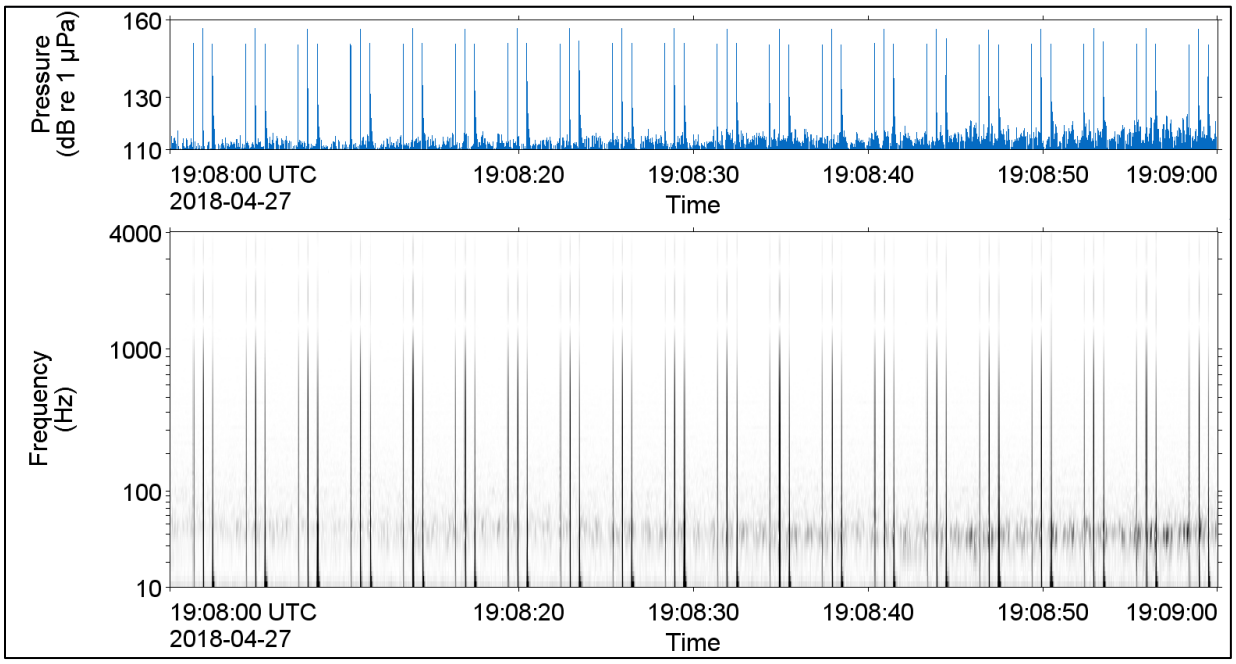

Figure 24. Example of the pings from the echosounder as recorded on one of the omnidirectional hydrophones at 8 kHz sampling rate

To remove the minutes with this data from the ambient sound level analysis we deleted minutes of data where the sound pressure level of the 315-500 Hz decidecade bands exceeded 115 dB for at least 3 minutes.

The autonomous multichannel acoustic recorders (AMARs) are optimized to minimize the power consumed and maximize recording life-times. As a result, the hydrophones were powered-off during sleep periods. When they are powered on, the capacitors in the hydrophones and at the front end of the electronics must charge, which resulted in an amplitude fluctuation in the first 2 seconds of data (Figure 25). To remove this effect from the analyzed data, the first four seconds of each recording were not processed.

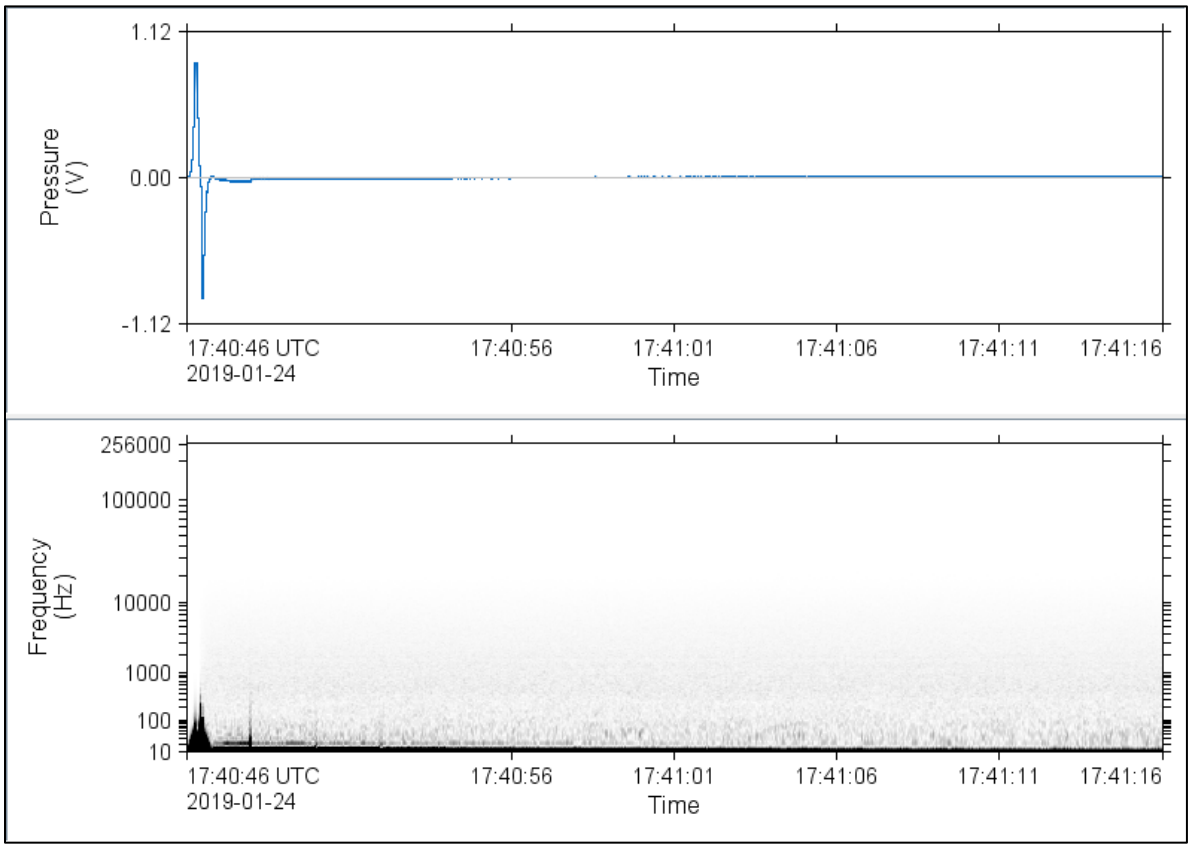

Figure 25. Example of the voltage spike when the autonomous multichannel acoustic recorder (AMAR) is first turned on after sleep

4.1.1.2 Marine Mammal Detectors

Assessing the diversity of marine mammals throughout the project area was a deliverable for ADEON. The goal of the marine mammal analysis was providing users of the ADEON data with an indication of where and when different species may be present. This section describes the automated detection and manual validation methods employed to obtain the deliverable results: hourly presence-absence data tables and number of days present per week figures. Detailed methodology can be found Appendix C.

Automated Detectors

JASCO used a combination of automated detectors and manual review by human analysts to determine the presence of sounds produced by marine mammals. First, automated detectors identified acoustic signals potentially produced by odontocetes and mysticetes (Appendices C.1 and C.2). This was followed by a manual review (validation) of automated detections within a sample of sound files for each data set (Appendix C.3). A data set consists of data recorded at a given sampling rate and station. The level of validation effort was set at 0.5% of the data, primarily based on budget available for a more extensive review. Finally, a critical review of the results of each automated detector was performed to restrict their output, where necessary, to maximize their performance metrics (Appendix C.4). Automated detector performance metrics are only presented for those species and/or vocalization types exceeding a pre-set precision (P) level (P = 75%), which ensures a level of reliability in the description of marine mammal

acoustic occurrence. When the precision was below that threshold, solely manual detections are presented.

In this report, the term “automated detector” is used to describe automated algorithms that combine detection and classification steps. An “automated detection” refers to an acoustic signal that has been automatically flagged as a sound of interest based on spectral features and subsequently classified based on similarities to several templates in a library of marine mammal signals. Acoustic files are reviewed by analysts as part of a process called manual validation or manual analysis. Manual detections refer to signals detected by an analyst.

Tonal Calls

Tonal signals are narrowband, often frequency-modulated, signals produced by many species across a range of taxa (e.g., baleen whale moans and delphinids whistles). The signals of some pinniped species, such as bearded seal trills, also have tonal components. The frequency range of baleen whale moans vary among species but is generally below 1 kHz and as low as 17 Hz in blue whales (see e.g., Parks & Tyack, 2005; Berchok et al., 2006; Dunlop et al., 2007). Delphinid tonal signals are generally more broadband and range from ~700 Hz up to 18 kHz (see e.g., Steiner, 1981; Ford, 1989; Rendell et al., 1999; Oswald et al., 2003).

The automated tonal signal detector identified continuous contours of elevated energy and classified them against a library of marine mammal signals (see Appendix C.1 for details). The suite of tonal detectors is presented in Table 7. It includes both generic detectors (e.g., low frequency (LF) Moan) and species-specific detectors targeting signals unique to a given species. Using several detectors for some species (e.g., blue, fin, and right whales) allowed some flexibility to account for the different performance of each detectors in different noise conditions. The three right whale detectors correspond to three strictness levels for the upcall template.

Table 7. List of automated detectors used to identify tonal signals produced by baleen whales and delphinids

Detector name	Species targeted	Signal targeted
Atl_BlueWhale_GL_IM	Blue whales	A-B call, tonal song note @ 17 Hz
Atl_BlueWhale_IM	Blue whales	A-B call, tonal song note @ 17 Hz
Atl_BlueWhale_IM2	Blue whales	A-B call, tonal song note @ 17 Hz
Atl_FinWhale_130	Fin whales	130-Hz song note
Atl_FinWhale_21.2	Fin whales	20-Hz pulse
Atl_FinWhale_21	Fin whales	20-Hz pulse
minkeWhalePulses	Minke whales	Pulse train
N_RightWhale_Up1	North Atlantic right whales	Upcall
N_RightWhale_Up2	North Atlantic right whales	Upcall
N_RightWhale_Up3	North Atlantic right whales	Upcall
SW	Sei whales	Broadband downsweep
WhistleLow	Pilot whale and/or killer whales	Whistle with energy between 1–10 kHz
WhistleHigh	Other delphinids	Whistle with energy between 4–20 kHz
VLFMoan	Baleen whales, FW/SW/BW	Downsweeps/upsweeps
LFMoan	Baleen whales, SW/BW/RW	Downsweeps/upsweeps
ShortLow	Baleen whales, possibly MW	Moans, pulses
MFMoanLow	Humpbacks	Moans
MFMoanHigh	Humpbacks	Moans

FW: fin whale; SW: sei whale; BW: blue whale; RW: right whale; MW: minke whale

Odontocete Echolocation Clicks

Odontocete clicks are high-frequency impulses ranging from 5 to over 150 kHz (Au et al., 1999; Møhl et al., 2000). We applied automated click detectors to all acoustic data to simplify the configuration of data processing. JASCO's click detectors are based on zero-crossings in the acoustic time series. Zero-crossings are the rapid oscillations of a click's pressure waveform above and below the signal's normal level. Zero-crossing-based features of detected events are then compared to templates of known clicks for classification (see Appendix C.2 for details).

The suite of click detectors is presented in Table 8.

Table 8. List of automated detectors used to identify clicks produced by odontocetes (narrow-band high-frequency)

Detector	Species targeted	Result nomenclature (clicks)		Result nomenclature (click trains)	Comments
DefaultClicks_HF.xml		Harbor porpoise	Porpoise:Click	Porpoise (Click Train)	HighPass Filter @ 50 kHz
			Porpoise250ksps:Click	Porpoise250ksps (Click Train)	
		Sowerby's beaked whale	Sowerbys:Click	Sowerbys (Click Train)	
		Kogiids	KSima:Click	KSima (Click Train)	
DefaultClicks_LF.xml		Sperm whale	SpermWhale:Click	SpermWhale (Click Train)	HighPass Filter @ 5 kHz
		Killer whale	KillerWhale:Click	KillerWhale (Click Train)	
DefaultClicks_MF.xml		Atlantic white-sided dolphin	AWSD_La:Click	AWSD_La (Click Train)	HighPass Filter @ 25 kHz
		Blainsville's beaked whale	Blainsvilles:Click	Blainsvilles (Click Train)	
		Cuvier's beaked whale	Cuviers:Click	Cuviers (Click Train)	
		Delphinids	Dolphin:Click	Dolphin (Click Train)	
		Gervais' beaked whale	Gervais:Click	Gervais (Click Train)	
		Northern bottlenose whale	NBW:Click	NBW (Click Train)	
		Pilot whale	PilotWhale:Click	PilotWhale (Click Train)	
		Risso's dolphin	Rissos_Gg_long:Click	Rissos_Gg_long (Click Train)	
			Rissos_Gg_Short:Click	Rissos_Gg_Short (Click Train)	
		Stenella species	StenellaSP:Click	StenellaSP (Click Train)	
		True's beaked whale	Trues:Click	Trues (Click Train)	
		Unidentified dolphin,	UDA:Click	UDA (Click Train)	

Detector	Species targeted	Result nomenclature (clicks)		Result nomenclature (click trains)	Comments
		type A			
		Unidentified dolphin, type A	UDB:Click	UDB (Click Train)	
		Unidentified beaked whale @ 51 kHz	UnknownBkW_51kHz:Click	UnknownBkW_51kHz (Click Train)	
All detectors		Unidentified odontocete	UnkClick:UnkClick		For each detector, detected clicks that cannot be classified as one of the targeted species are pooled under this category*

* In the mammalEvents.csv files compiling detections for each sound file, the counts under the UnkClick:UnkClick header include unidentified click detections for all three click detectors.

Minke Whale Pulse Trains

Minke whale pulse trains were detected using a pulse detector searching for impulsive events with specific duration and bandwidth. After the detection phase, individually detected pulses were then assembled into trains that had to match a template built using known pulse train characteristics (Risch et al. 2013, Risch et al. 2014), namely inter-pulse interval, train duration, and train length (see Appendix C.1 for details), in order to be classified as minke whale.

4.1.1.2 2 Manual Validation of Automated Detections

JASCO's suite of automated detectors are developed, trained, and tested to be as reliable and broadly applicable as possible. However, the performance of marine mammal automated detectors varies across acoustic environments (e.g., Hodge et al., 2015, Širović et al., 2015, Erbe et al., 2017, Delarue et al., 2018). Therefore, automated detector results must always be supplemented by some level of manual review to evaluate automated detector performance. Here, we manually analyzed a subset of acoustic files for the presence/absence of marine mammal acoustic signals via spectrogram review in JASCO's PAMlab software. A subset (0.5%) of acoustic data from each station and deployment (cruise) was selected via JASCO's Automated Data Selection for Validation (ADSV) algorithm (see details in Appendix C.3).

To determine the performance of the automated detectors at each station and for each cruise per acoustic file, the automated and manual results (excluding files where an analyst indicated uncertainty in species occurrence) were fed into an algorithm that calculates precision (*P*), recall (*R*), and Matthew's Correlation Coefficient (*MCC*) (see Appendix C.4 for details). *P* represents the proportion of files with detections that are true positives. A *P* value of 0.90 means that 90% of the files with automated detections truly contain the targeted signal, but it does not indicate whether all files containing acoustic signals from the species were identified. *R* represents the proportion of files containing the signal of interest that were identified by the automated detector. An *R* value of 0.90 means that 90% of files known to contain a target signal had automated detections, but it says nothing about how many files with automated detections were incorrect. An MCC is a combined measure of *P* and *R*, where an MCC of 1.00 indicates perfect performance–all events were correctly detected. The algorithm determines a per file automated detector threshold (the number of automated detections per file at and above which automated detections were considered valid) that maximizes the MCC.

Hourly Presence of Marine Mammals

The automated detection validation process produces automated detector performance metrics per file both before and after the results have been optimized, where optimization can include 'automated detection exclusion periods' and a minimum 'number of automated detections per file threshold' (Appendix B.4 and D). Each automated detector's raw output was edited to reflect the 'final' performance metrics found in Appendix D and the remaining automated detections provided as comma-separated value formatted spreadsheets with presence/absence per hour. Manual detections were provided in the same manner.

The acoustic occurrence of each species (both automated and manual results) was plotted using JASCO's Ark software as time series showing number of days with presence per week through the recording period (Appendix E). Automated detector performance metrics per file are provided and should be considered when interpreting results (Appendix D).

Processing of Directional Passive Acoustics Recordings

The automated long-term observatory (ALTO) landers included a directional sensing technology to allow for localization of sound sources or estimation of the ambient particle motion sound field. Twenty-seven of the deployments had a four- element orthogonal array of hydrophones, and one deployment, the first deployment at VAC, had an M20 directional hydrophone. The methods applied to the processing of these data and typical results are provided in Appendix B.

This section provides a summary how directional data analysis results were further interpreted to extract additional information.

Estimating the Minimum Number of Animals Present

An application of directional passive acoustic data analysis is estimating the minimum number of animals present. To test if this concept worked for long-term data from the ADEON directional arrays, the minimum number of audible minke whales at the SAV site was analyzed. Minke whale pulse trains were initially detected using an automated detected algorithm (Kiehbadroudinezhad et al., in prep). For each detected pulse train, the source direction of arrival was estimated using the beamformer described in Urazghildiiev et al. (2020) (Figure 26). The directions of arrival were aggregated into 10-degree bins. The estimated absolute minimum number of minke whales per day was the maximum number of these bins with detections in a 5-minute window (Figure 27). The actual number of animals present is likely higher since there could be more than one in each directional bin, the 1-degree bins are relatively wide at long ranges from the recorder, and not all animals present call within the sampling period.

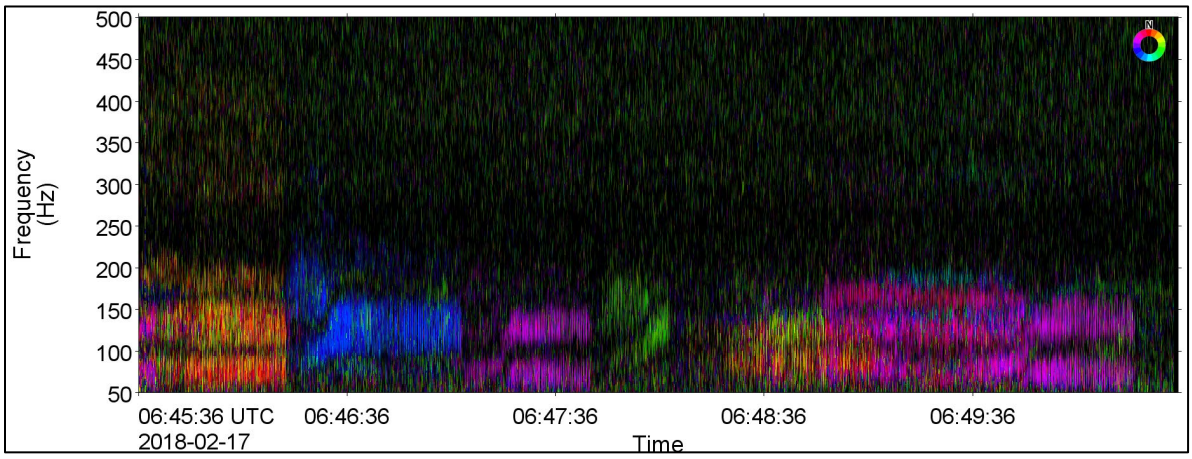

Figure 26. Directogram of at least five minke whales vocalizing at the Savannah (SAV) site on 27 Feb 2018

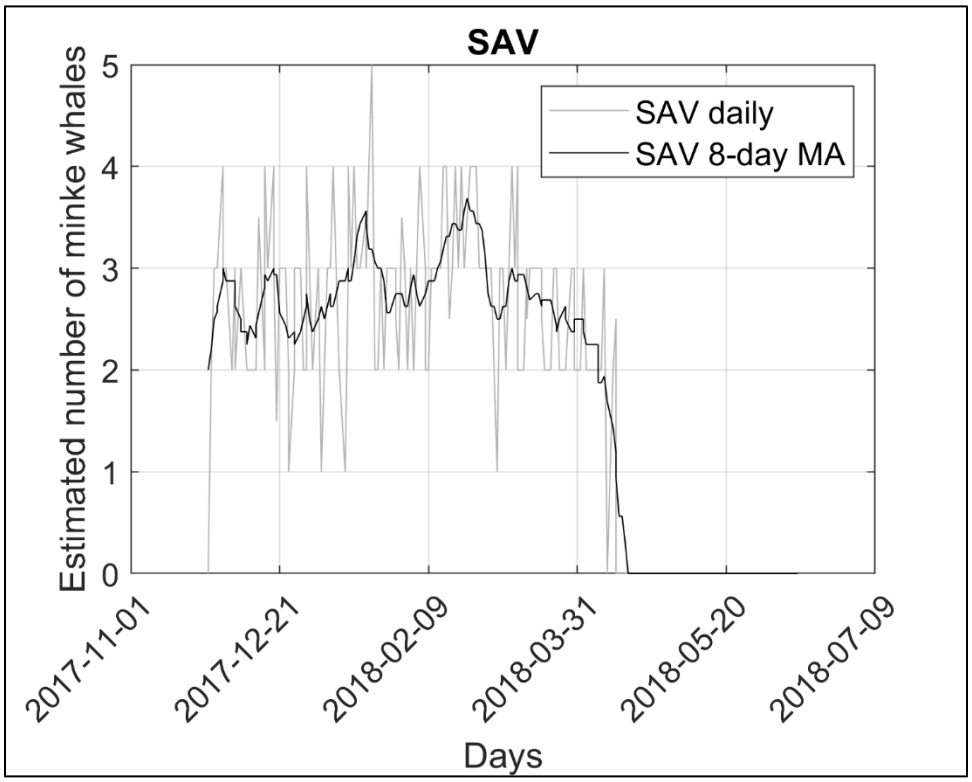

Figure 27. Estimated minimum number of minke whales per day during the first ADEON deployment at the SAV site

Tracking Vessels using the Compact Hydrophone Arrays

Recent developments in passive acoustic data analysis for tracking of vessels using the data from the compact arrays were implemented and evaluated using the ADEON data. This work was a collaboration between JASCO and a PhD student in the Electrical Engineering Department at Dalhousie University. The processing step employed were:

- Estimate the bearings of the vessel through time using an implementation of a maximum likelihood beamformer described in Urazghildiiev and Hannay (2017). This is the same algorithm employed for the minke whale work (above) and described Appendix B.
- Estimate range to the vessel through time using vertical coherence (Shajahan et al. 2020) of the two hydrophones in the vertical pair (see Figure 13). This details of the approach applied here is described in this section.
- Combine the bearings and ranges to obtain the estimated latitude and longitude of the vessel using the Haversine equations.

The coherence-range method computes the cross-spectral density (CSD) of the measured vessel sound and compares it to spatial replicas over a depth-range grid centered on the sensor location. The coherence serves to evaluate the degree of resemblance of the sound field received at pairs of sensors, and it is a representation of the squared magnitude of the phase shift between the two sound fields. The well-known generalized expression for estimating spatial coherence (Γ) in ocean ambient sound fields is:

$$\Gamma_{yz} = \frac{\overline{S_{yz}}}{\sqrt{\overline{S_{yy}S_{zz}}}}$$

where $\overline{S_{yz}}$ is the CSD between the spatially separated sensors y and z, $\overline{S_{yy}}$ and $\overline{S_{zz}}$ are the power spectral density (PSD) at each receiver, and the overbar denotes the ensemble average. These values are all frequency dependent.

Thus, Γ_{yz} is computed from the measured acoustic data at each sensor while a model that represents the acoustic propagation field is computed from the image-source method (Figure 28). The received pressure field is

$$p(r,z) = \frac{e^{ikR_1}}{R_1} - \frac{e^{ik2}}{R_2}$$

where $R_1 = \sqrt{r^2 + (z - z_s)^2}$ and $R_2 = \sqrt{r^2 + (z + z_s)^2}$ are the propagation path from the source (at z_s to each receiver at z.

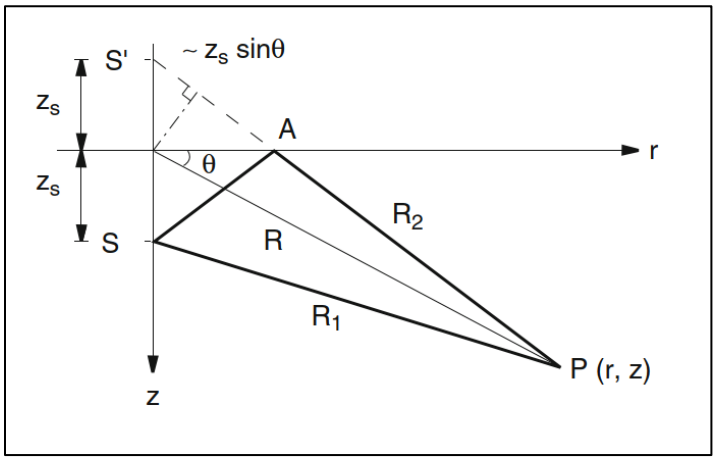

Figure 28. Sketch of the image-source model for estimated the expected signal coherence

The spatial ambiguity surface is obtained from all the possible values of range r and source depth of defined by the spatial grid

$$\hat{\mathbf{\Gamma}}_{yz}(r,z) = \begin{bmatrix} \Gamma_{yz}(r_1,z_1) & \Gamma_{yz}(r_2,z_1) & \dots & \Gamma_{yz}(r_i,z_1) \\ \Gamma_{yz}(r_1,z_2) & \Gamma_{yz}(r_2,z_2) & \dots & \Gamma_{yz}(r_1,z_2) \\ \vdots & \vdots & \ddots & \vdots \\ \Gamma_{yz}(r_1,z_j) & \Gamma_{yz}(r_2,z_j) & \dots & \Gamma_{yz}(r_i,z_j) \end{bmatrix}$$

Generally, it has been demonstrated that directional sound is more correlated when measured at vertical arrays than in horizontal arrays.

The algorithm was demonstrated using data from the passage of a vessel near the HAT mooring on 8 Jun 2019 (Figure 29). The extracted bearings are shown in Figure 30. The modeled coherence of a surface vessel with propeller depth of 3.6 m for receivers at HAT is shown in Figure 31. The measured coherence, and the range extracted by comparison of the models are shown in Figure 32 and Figure 33.

It was observed that the spatial separation of the vertical elements was not sufficient to effectively resolve the interference pattern of the vessel sound. Thus, the coherence of all three vertically offset sensors were used to estimate the vessel's range. The accuracy of the range estimation could be significantly improved by using an array with a wider aperture, however, this would then reduce the frequency range for the beamforming algorithm. An additional vertical hydrophone (2 m higher) could be considered.

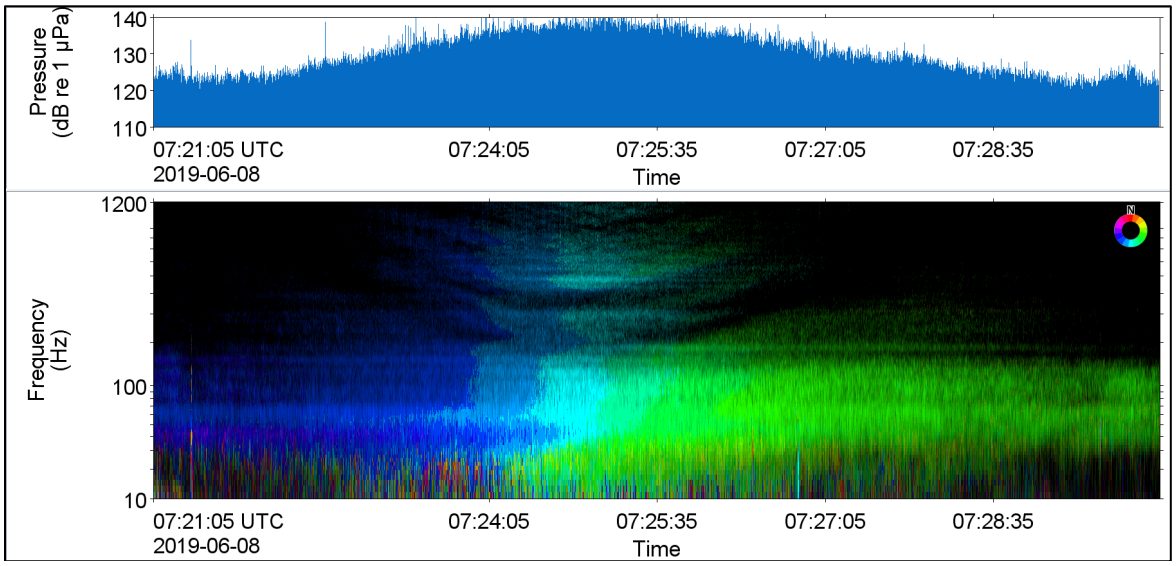

Figure 29. Directogram of the vessel passing and/or lingering at HAT on 8 June 2019

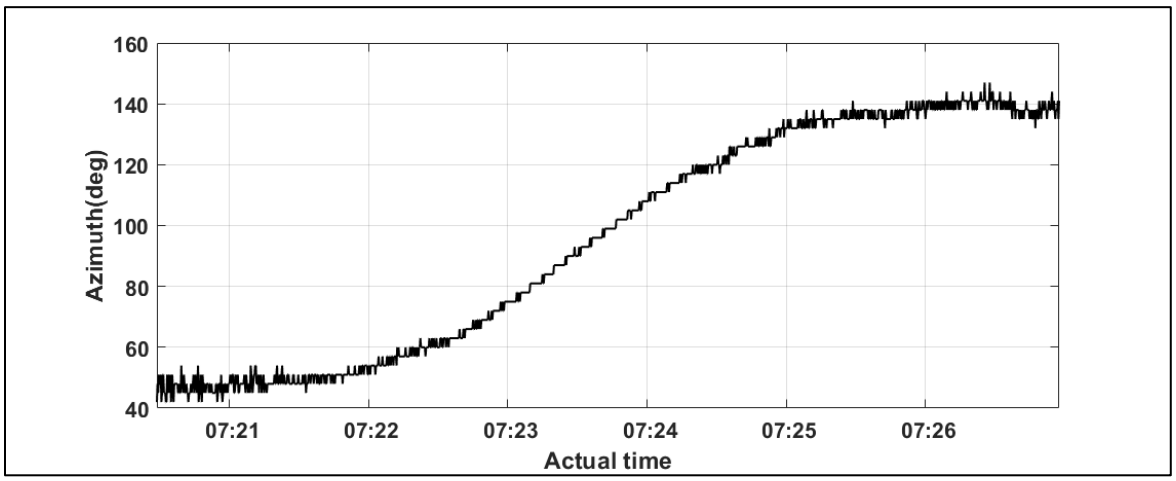

Figure 30. Extracted bearings for the vessel

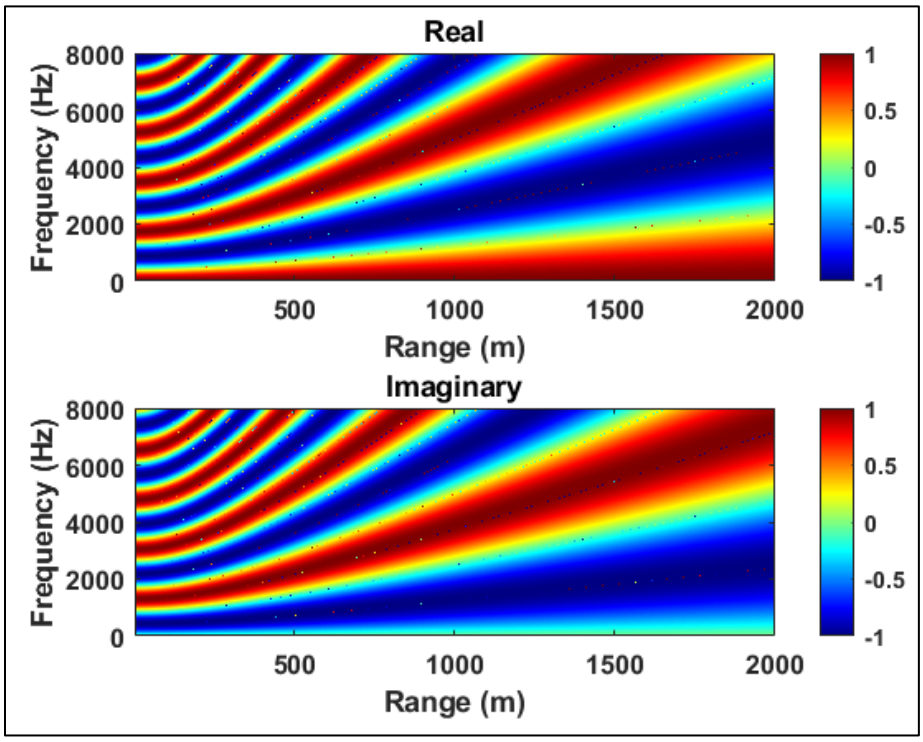

Figure 31. Modelled real and imaginary coherence for a vessel with a propeller depth of 3.6 m at HAT

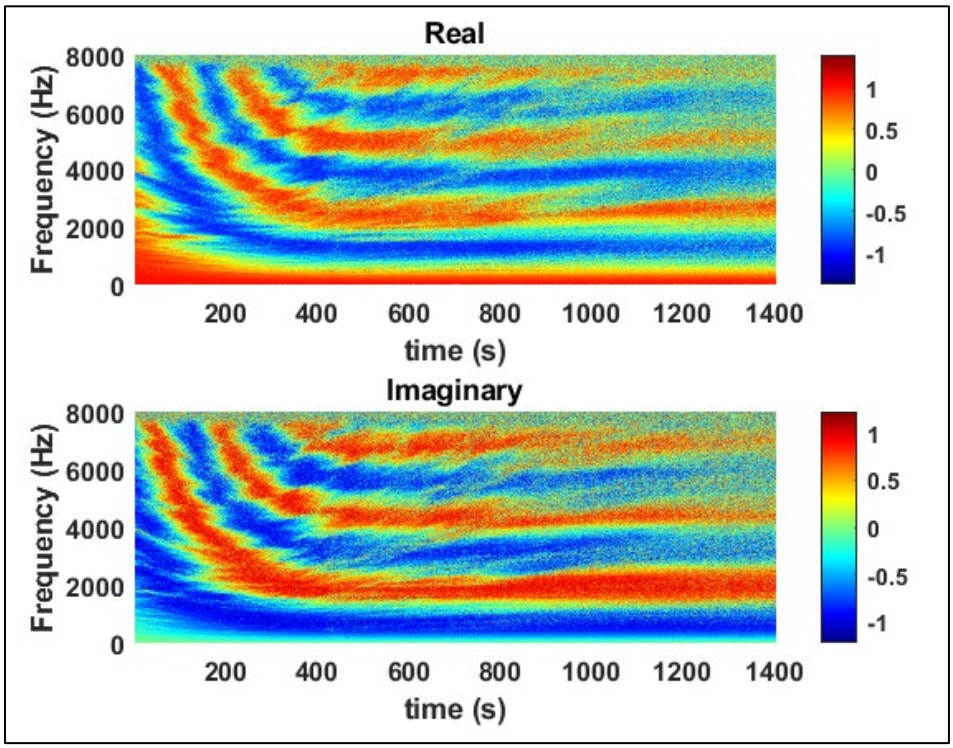

Figure 32. Measured vertical coherence for the vessel shown in

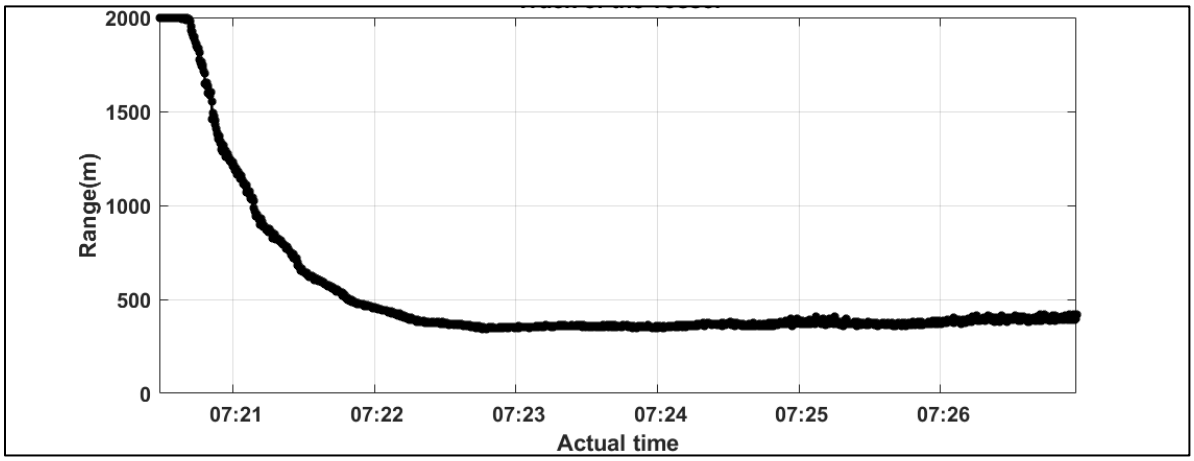

Figure 33. Range to the vessel estimated from the coherence

4.1.2 Sail Array Passive Acoustics

During the three of the four Sail Cruises a towed array was deployed. The array data was processed to generate decidecade band sound exposure level (SEL) as a function of bearing. For the single hydrophone data collected in Sail Cruise 4, the decidecade band SEL was processed. For some legs there was little wind and the data had engine noise. For others the wind was fair and there is some flow noise. Examples of the processed figures are shown below. In Figure 34, the spectrogram from a single element taken during Sail Cruise 1 is shown. The decrease in sound levels across all bands around 30 minutes is the sailboat engine being turned off. The 1000 kHz bearing-time record (BTR) is shown for a different time period and the presence of a passing surface ship is clear (Figure 35). Both figures show a very clean, usable data set, with little flow noise or any contamination (besides the engines and generator when they were on).

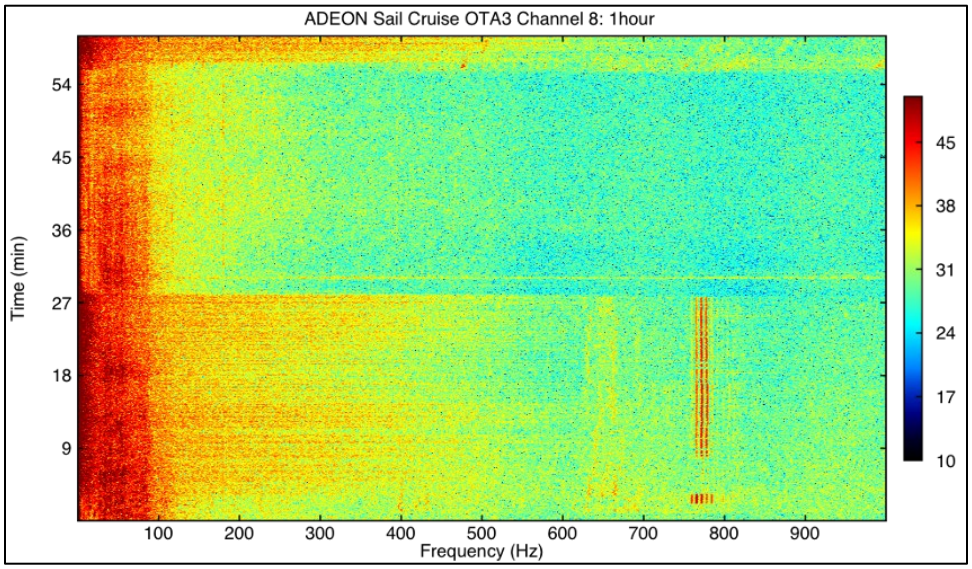

Figure 34. One hour, single element spectrogram taken during Sail Cruise 1

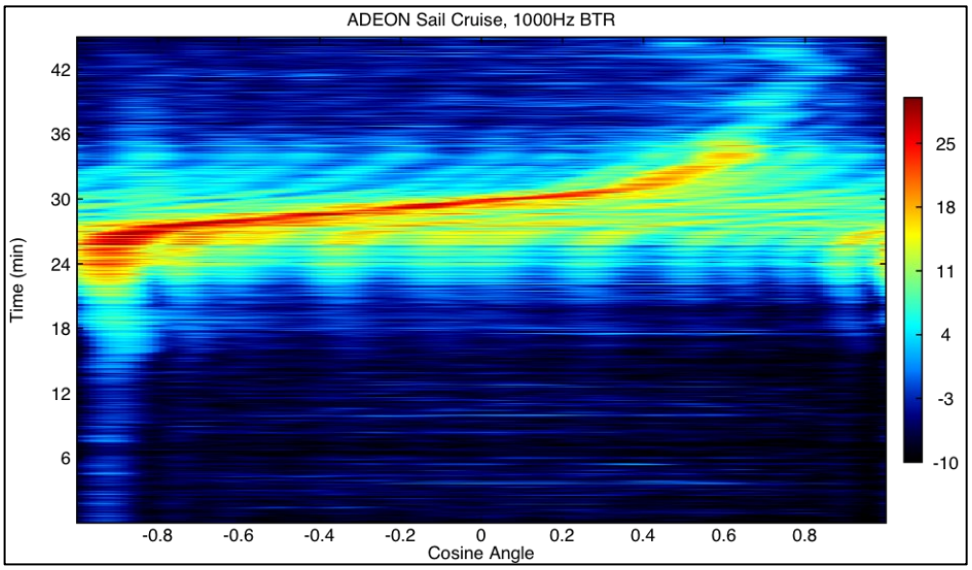

Figure 35. One hour 1000Hz bearing time record (BTR) (during a container ship closest point of approach (CPA) during Sail Cruise

4.2 Net Tows

4.2.1 Summary

Net tow data were primarily used to ground-truth the active acoustic backscatter data by providing physical specimens of organisms found at each site. Additionally, the identity and size of the net catch samples were combined with theoretical acoustic scattering models to provide parameters for processing the echosounder data into categories based on the scattering characteristics of different organisms.

As the processing of net tow samples can be very time and labor consuming, the completion of analysis of these specimens was specifically not a project deliverable. However, substantial analysis progress has been made and is nearly complete for the first four ADEON cruises. Bongo net tows are a double-net system (1000 and 333 micrometer mesh) which capture primarily zooplankton and other small organisms, whereas the Isaac-Kidd midwater trawl (IKMT) is a larger trawl which catches primarily nekton species. A subsample of organisms from the IKMT trawl were identified and measured while at sea, however taxonomic identification to the species-level was not always possible, so IKMT net samples for AR025, EN615, EN626, and AR040 were shipped to Dr. Tracey Sutton's lab at Nova Southeastern University for enumeration and identification of the fish species. A summary of net samples that have been completed is below.

Bongo net tow analysis progress includes:

- AR025 bongo net samples 14 out of 14 sample jars are complete
- EN615 bongo net samples14 out of 14 sample jars are complete
- EN626 bongo net samples12 out of 12 sample jars are complete
- AR040 bongo net samples 5 out of 14 sample jars are complete
- AR049 bongo net samples 0 out of 14 sample jars are complete

IKMT net sample analysis status:

- AR025 IKMT net samples 23 out of 23 sample jars are complete
- EN615 IKMT net samples10 out of 10 sample jars are complete
- EN626 IKMT net samples12 out of 12 sample jars are complete
- AR040 IKMT net samples17 out of 17 sample jars are complete
- AR049 IKMT net samples 0 out of 7 sample jars are complete

4.2.2 Net Tow Analyses

There are two primary data products generated from the net tow data (in addition to other datasets that use samples from these organisms): 1) An inventory of the zooplankton and nekton species assemblages at each site and how they vary (or not) across the study both spatially, temporally, or with environmental factors. 2) The net and trawl data (species counts, identifications, and length measurements) have been used in conjunction with literature values of animal lengths and acoustic scattering models to develop dB-difference filters (e.g., the difference in volume backscattering strength [Sv] at 38 and 120 kHz) for post-processing of acoustic backscatter data from multiple frequencies into backscatter variables ascribed to different taxonomic groups (e.g., small or large crustacean associated backscatter, large swim-bladdered fish and other gas-containing organism backscatter). These methods are applied to the analysis of the acoustic zooplankton fish profiler (AZFP) and fine-scale acoustic survey (FSAS) data, as well as part of a dissertation chapter by Hannah Blair. A summary of the net and trawl data is described below according to net type.

4.2.2.1 Bongo net samples

Length distributions of zooplankton were developed from 4504 animals subsampled from bongo net tows from ADEON cruises AR025, EN615, and EN626 (Figure 36, Table 9). Animals were divided into categories based on taxon, as well as body shape and composition, for the purpose of identifying target strength (TS) scattering windows. This resulted in, for example, adult decapod shrimp, zoea-form decapod larvae, and megalopa-form decapod larvae separated into three different groups. Shrimp of family Luciferidae are also their own category, due to a) their different body plan than the typical decapod shrimp, and b) the high prevalence of this family in the bongo samples. The final major groups were: siphonophore bracts, medusa-phase cnidarians, chaetognaths (arrow worms), cladocerans, ostracods, copepods, krill, amphipods, luciferid decapod shrimp, other decapod shrimp, zoea-phase decapod larvae, megalopa-phase decapod larvae, mysid shrimp, stomatopod (mantis shrimp) larvae, shelled pteropoda (with a calcium carbonate shell), pteropoda of genus *Corolla* (with a cartilaginous pseudoconch “shell”), salps, flatfish larvae, leptocephali fish larvae, and all other fish larvae. Additional minor groups (<15 individuals) included ctenophores, polychaete worms, copepodites, nauplii, heteropods, appendicularians, cephalopods, and phyllosoma larvae.

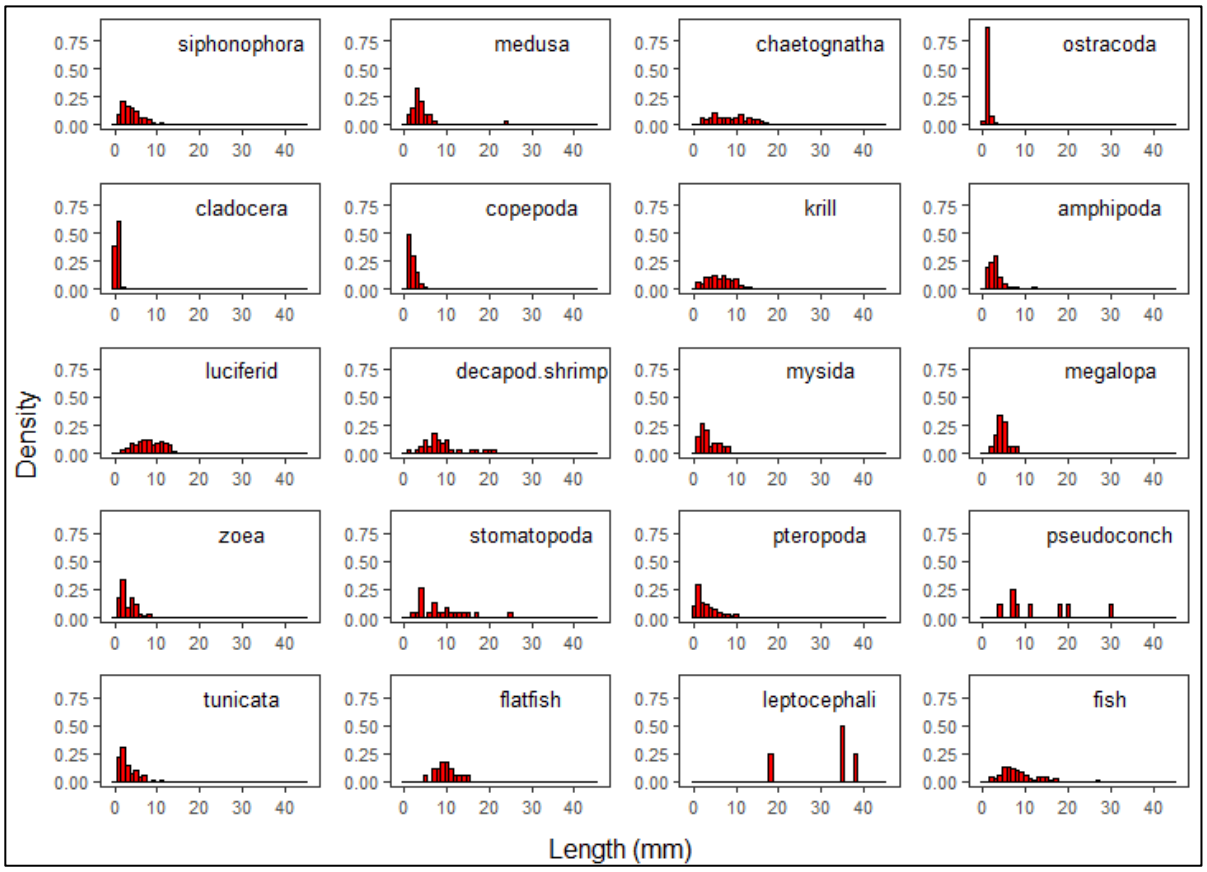

Figure 36. Length frequencies of best-represented taxonomic groups collected from bongo net tows during AR025, EN615, and EN626

Despite having fewer individuals, leptocephali fish larvae and pseudoconchs from the gastropod *Corolla* spp. were also included, as these were well represented in the IKMT tows.

Table 9. Mean and standard deviation for lengths of taxa measured from subset of animals sampled by bongo net during AR025, EN615, and EN626 cruises

General taxon	Specific taxa/taxon	Mean length (mm +/- StDev) Min–Max	N
Siphonophora (zooids/zooid colonies)	Abylidae spp. (Calycophora) Abyla schmidti (Caly) *Abyla* spp. (Caly) Abylopsis tetragona (Caly) Agalmidae spp. (Physonectae) Bassia bassensis (Caly) Ceratocymba leuckarti (Caly) Ceratocymba sagittata *Chelophyes* spp. (Caly) Diphyes chamissonis *Diphyes* spp. Enneagonum hyalinum Eudoxoides spiralis Eudoxoides spp. Halistemma rubrum (Phy) Lensia achilles Lensia hostile Lensia subtiloides *Lensia* spp. Marrus spp. Nanomia bijuga Sphaeronectes gracilis (Caly) Sphaeronectes spp. (Caly) Unidentified eudoxid-phase bracts Unidentified nectophores Unidentified physonect larvae Unidentified other zooids	4.3 (2.9) 0.6–35.0	499
Medusa-phase cnidarians	n/a	4.1 (3.8) 1.0–24.0	34
Chaetognatha	Sagitta spp. Eukronia spp.	9.2 (4.9) 1.6–27.5	377
Ostracoda	Conchoecia spp. Euconchoecia chierchiae Macroconchoecia spp. Metaconchoecia spp. Mikroconchoecia spp. Proceroecia spp. Unidentified ostracoda	1.1 (0.4) 0.4–3.2	216
Cladocera	Evadne nordmani Halocypria globosa Penilia avirostris Pseudevadne tergestina Unidentified cladocera	0.6 (0.3) 0.1–2.0	65

General taxon	Specific taxa/taxon	Mean length (mm +/- StDev) Min–Max	N
Copepoda	Acartiidae spp. Acartia spp. Acartia longiremis Aetideidae spp. Arietellus simplex Arietellus spp. Augaptilidae spp. Bathypontia spp. Calanidae spp. Calanus finmarchius Calanus spp. Calocalanus pavo Calocalanus spp. Candacia armata Candacia spp. Centropages bradyi Centropages furcatus Centropages typicus Centropages spp. Copilia lata Copilia quadrata Copilia mirabilis Corycaeus crassiusculus Corycaeus flaccus Corycaeus furcifer Corycaeus lautus Corycaeus rostrata Corycaeus speciosus Corycaeus typicus Corycaeus spp. Farranula rostrata Eucalanidae spp. Eucalanus crassus Eucalanus elongatus Euchaeta marina Euchaeta spp. Eucalanus attenuatus Eucalanus hyalinus Eucalanus spp. Euchirella spp. Lucicutia spp. Mecynocera clausi Mesaiokeras tantillus Mesaiokeras spp. Metridia spp. Miracidae spp. Metridinidae spp. Neocalanus spp. Nannocalanus minor Neocalanus tonsus Oithona atlantica Oncaeidae spp. Pachyptilus eurygnathus Pachyptilus spp. Pareucalanus sewelli Paracalanidae spp. Paracalanus parvus Paracalanus spp. Pareucalanus spp. Paraeuchaeta spp. Parvocalanus spp. Pleuromamma gracilis Pleuromamma robusta Pleuromamma xiphias Pleuromamma spp. Pontellidae spp. Pontella atlantica Pontella marplatensis Pontellina platychela Pontellopsis perspicax Pseudocalanus minutus	1.9 (0.9) 0.2–6.2	1767

General taxon	Specific taxa/taxon	Mean length (mm +/- StDev) Min–Max	N
Krill	Euphausia americana Euphausia brevis Euphausia krohni Euphausia lamelligera Euphausia mutica Euphausia pseudogibba/hemigibba complex Euphausia tenura Euphausia spp. Nematoscelis spp. Stylocheiron affine Stylocheiron carinatum Stylocheiron longicorne Stylocheiron suhmi Stylocheiron spp. Thysanoessa raschi *Thysanonessa* spp. Thysanopoda aequalis Thysanopoda astylata Thysanoessa longicaudata Thysanopoda orientalis/micropthalma complex Thysanopoda tricuspida Thysanopoda spp. Unidentified krill Unidentified krill larvae	6.2 (3.2) 1.0–17.0	223
Amphipoda	Anchylomera blossevillei Primno latreillei Phronimella elongata Hyperoche medusarum Eupronoe minuta Rhabdosoma whitei Phronima atlantica Phronima sedentaria Phronima spp. *Themisto* spp. Hyperia macrocephela Hyperia spp. *Eupronoe* spp. Eupronoe maculata Phronimopsis spinifera Thyropus sphaeroma Oxycephalus spp. *Scina* spp. Unidentified hyperiids	3.7 (4.4) 1.0–45.0	127
Decapod shrimp	Luciferidae	8.1 (3.2) 2.0–14.0	160
	Other	8.9 (4.9) 1.3–21.0	34
Mysid shrimp	Bowmaniella spp. Gnathophausia spp. Unidentified mysids	3.6 (2.1) 1.1–8.0	33
Megalopa-stage larvae	n/a	4.6 (1.4) 2.5–8.0	18
Zoea-stage larvae	n/a	3.2 (1.8) 1.0–8.0	56
Stomatopoda larvae	n/a	8.8 (5.4) 2.5–25.0	23

General taxon	Specific taxa/taxon	Mean length (mm +/- StDev) Min–Max	N
Pteropoda	Shelled pteropoda Hyalocylis striata Diacavolinia strangulata Diacavolinia spp. Diacria major *Diacria* spp. Creseis acicula Creseis chierchie Creseis virgula *Creseis* spp. Atlantidae spp. Atlanta fragilis Atlanta spp. Limacina cochlostyloide *Limacina* spp. Styliola subula *Clio* spp. Cuvierina columnella atlantica Cavoliniid juveniles Dextrally-coiled juveniles	3.2 (2.7) 0.4–11.8	146
	Pseudoconch (*Corolla* spp.)	13.2 (8.8) 4.0–30.0	8
Salps	Cyclosalpa spp. *Pegea* spp. *Ritteriella* spp. Soestia zonaria Thalia democratica Thalia spp. *Salpa* spp. Unidentified doliolids Unidentified salps	3.7 (4.1) 0.5–40.0	158
Flatfish larvae	Paralichthyidae spp. Cyclopsetta fimbriata Scophthalmus aquosus Bothus ocellatus	10 (2.6) 5.0–15.0	17
Leptocephali larvae	Ophichthidae sp. Anguilla rostrata Gymnothorax moringa Ariosoma balearicum Chilorhinus suensonii	(35.2) 11.2 18.0–49.0	5

General taxon	Specific taxa/taxon	Mean length (mm +/- StDev) Min–Max	N
Other fish larvae	Gadiformes spp. Phycidae spp. Bregmacerotidae sp. Bregmaceros sp. Clupeiformes spp. Clupeidae spp. Etrumeus teres Scorpaeniformes Scorpaenidae sp. Aulopiformes Scopelosaurus sp. Scombriformes Scombridae spp. Gempylus serpens Labriformes Labridae sp. Halichoeres sp. Xyrichtys novacula Beloniformes Cheilopogon sp. Carangiformes Carangidae sp. Caranx bartholomaei Perciformes Serranidae sp. Priacanthidae sp. Scombrolabrax heterolepis Myctophiformes Myctophidae spp. Diaphus sp. Myctophum obtusirostre Stomiiformes Phosichthyidae sp. Gonostomiformes Gonostomatidae sp. Stephanoberyciformes Scopeloberyx robustus Unidentified fish larvae	8.5 (4.4) 2.0–27.0	70

IKMT net samples

Animals from the IKMT net samples (N = 1,641 characterized individuals) represent either general groups due to either being unable to further identify animals, or the sample sizes were insufficient when separated (Figure 37, Table 10). General groups include *Thecosomata* (shelled pteropods), *Amphipoda* (various amphipods), *Euphausiacea* (krill), *Sternoptychidae* (hatchetfish and pearlsides), *Melamphaeidae* (bigscales), *Gonostomatidae* (bristlemouths, lightfish, and anglemouths), *Gempylidae* (snake mackerels), *Stomiiformes* (general mesopelagic fish), *Myctophidae* (lanternfish), *Salpidae* (salps), *Decapodiformes* (squid), and *Decapoda* (shrimp). Some animals comprised large enough sample sizes (n >= 10, or are expected to also be abundant in the bongo net samples) to be pulled out separately: *Protonogrammus martinicensis* (Roughtongue bass), *Decapterus punctatus* (round scad), *Cyclothone* sp. (bristlemouths), and *Clione* sp. (sea angels).

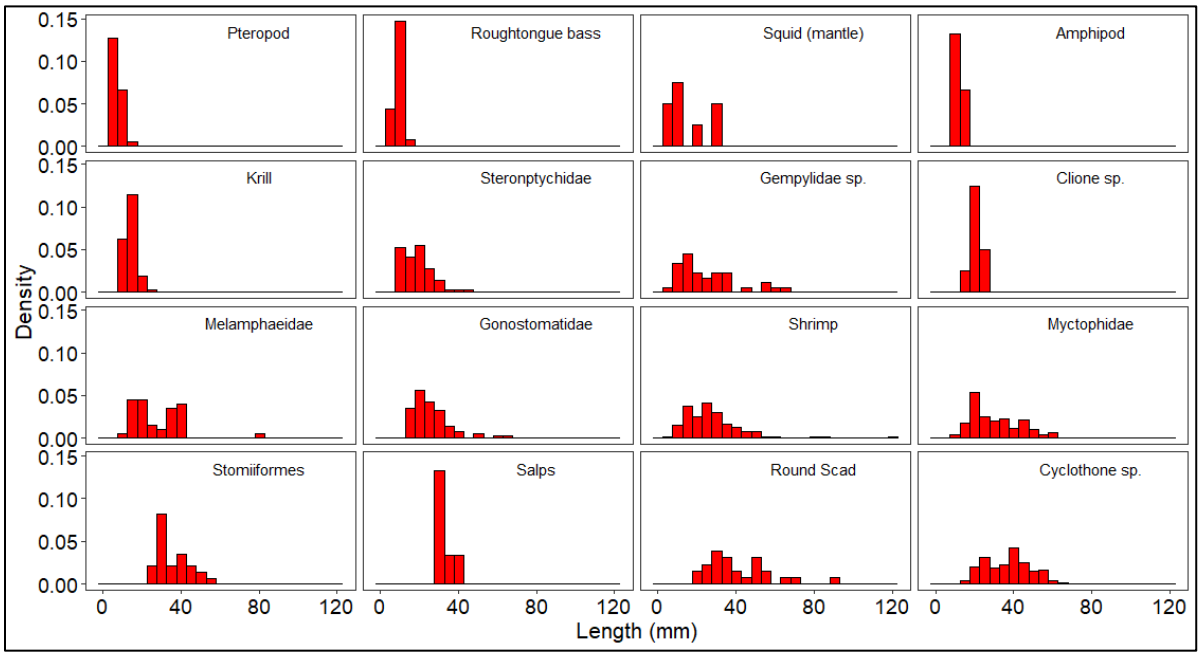

Figure 37. Length frequencies of different taxonomic groups collected from IKMT net tows during AR025, EN615, EN626, and AR040

For determining the TS of fish, two general classifications were used: swimbladdered and swimbladderless fish. In general, most of the myctophids represented here belonged to genera that mostly have swimbladders. Although some species are swimbladderless (e.g., *Myctophum asperum*), it was assumed that all myctophids measured had swimbladders. Only some adults belonging to *Melamphaidae* have swimbladders; most literature reports either regressed or lipid-filled bladders. Therefore, it was assumed that these fish were swimbladderless. Some gonostomatids are swimbladdered, but typically *Gonostoma* sp., *Margrethia* sp., and *Diplophos* sp. are swimbladderless. Fish belonging to *Chauliodontidae* (and therefore *Chauliodus* sp.), (post-larval) *Cyclothone* sp., *Gempylidae*, and (likely) *Photostomias* sp. are swimbladderless. For *Sternoptychidae*, there appears to be heavy disagreement on the presence and/or absence of swimbladders in the literature. Some species in *Argyropelecus* (e.g., *A. affinis*) and *Sternoptyx* (e.g., *S. pseudodiaphana*) contain swimbladders, as well as fish within *Maurolicus* (i.e., *M. muelleri* and *M. weitzmani*). It is unclear whether the absence/regression of swimbladders reported in the literature is due to damaged specimens, empty swimbladders that are not properly identified, simply a lack of physically dissected individuals, or some combination of the above. Therefore, it was assumed that each specimen had a swimbladder.

Table 10. Mean (and standard deviation) lengths of taxa measured from photographs of animals captured during IKMT tows aboard AR025, EN615, EN626, and AR040 cruises

General taxon	Specific taxa/taxon	Mean length (mm +/- StDev) Min-Max	N
Pteropoda	Cavolinia sp. Clio sp. C. pyramidata (possibly) Diacria sp. D. trispinosa (possibly) Limacina sp. L. helicina (possibly)	6.8 (2.5) 3.7–12.8 Note: Argonautids (paper nautilus) literature lengths are 4.3-115; however, not as abundant as pteropods in representing elastic-shelled category	39
	Clione sp.	20.6 (2.4) 16.5–23.2	8
Serranidae	Protonogrammus martinicensis	9.3 (1.8) 5.6-12.8	27
Squids	Cranchiidae Ommastrephidae Loliginidae	15.3 (10.5) 5.8–31.0 Literature size upper limits: Cranchiids: 226.7, 308 Ommastrephids: 284.6 Loliginids: 318.1	8
Amphipods	Hyperiidae Themisto sp. Caprellidae Gammaridea	11.7 (2.1) 8.5–14.3	6
Krill	Nematoscelis sp. Thysanopoda sp. Stylocheiron sp. Thysanoessa sp. Meganyctiphanes norvegica	14.1 (3.1) 7.6–29.7	502
Gempylidae	Diplospinus multistriatus (possibly)	25.1 (15.4) 6.7–65.9	35
Melamphaeidae	Melamphaes sp. Scopeloberyx sp. *Scopelogadus* sp. (possibly)	27.9 (12.9) 12.3–80.6	40
Stomiiformes	Stomiidae Chauliodus sp. Photostomias sp. *Polymetme* sp. (possibly)	41.0 (16.5) 18.5–89.4 Literature size upper limits: Chauliodus - 114 Photostomias - 115	26
	Sternoptychidae Argyripnus sp. Maurolicus weitzmani Maurolicus muelleri Sternoptyx sp. Argyropelecus hemigymnus Argyropelecus sp.	18.7 (8.7) 7.7–94.2	72
	Gonostomatidae Diplophos sp. *Margrethia* sp. (possibly) Gonostoma sp. Bonapartia pedaliota	25.6 (9.9) 12.7–63.7 Literature size upper limits: *Gonostoma* - 225, 150	74
	Cyclothone sp. (possibly mixed with some *Gonostoma* sp.)	36.9 (11.3) 16.1–64.5	247

General taxon	Specific taxa/taxon	Mean length (mm +/- StDev) Min-Max	N
Shrimp (also includes mysids)	Eusergestes arcticus Sergia robusta Janicella spinicauda Aristaeopsis edwardsiana Acanthephyra pelagica Systellaspis debilis Gnathophausia sp. Sergestes sp. *Oplophorus* sp. (possibly)	27.1 (13.6) 7.4–121.5	231
Myctophidae	Diaphus sp. D. dumerilii (possibly) Hygophum sp. Benthosema sp. Diogenichthys sp. D. atlanticus (possibly) Ceratoscopelus sp. Notoscopelus sp.	31.3 (13.6) 9.0–91.9	291
Salps	Salpa sp. Soestia zonaria	35.9 (8.2) 23.3–54.8	29
Carangidae	Decapterus punctatus	33.4 (4.4) 29.0–41.2	6

Combined Net Tow Dataset

Since several taxonomic groups were captured by both IKMT and bongo net tows (e.g., krill), overlapping taxa were combined to generate more complete length distributions that account for some of the sampling biases specific to each net tow (Table 11). All animals from overlapping taxa reported in the previous tables were summarized into one of six generalized taxonomic groups: salps, pteropods, krill, shrimp/mysids, amphipods, squid, and gas-bearing zooplankton.

Table 11. Mean (and standard deviation) lengths of taxa measured from photographs of animals captured during IKMT and bongo tows aboard AR025, EN615, EN626, and AR040 cruises

General taxon	Mean length (mm +/- StDev) Min-Max	N
Salps	8.7 (12.7) 0.5–54.8	187
Pteropods	4.6 (4.5) 0.4–12.8	193
Krill	11.6 (4.8) 1–29.7	724
Shrimp/Mysids	17.0 (13.8) 1.1–121.5	481
Amphipods	4.0 (4.6) 1.0–45	133
Squid	10.1 (9.0) 5.8–31.0	20
Gas-bearing zooplankton		n/a

4.2.3 TS Model Selection

Animals from the bongo, IKMT, and combined samples were assigned to general scattering classes (Table 12): 1) fluid-like organisms, 2) elastic-shelled organisms, 3) swimbladderless fish, 4) swimbladdered fish, 5) siphonophore pneumatophores, and 6) squid.

Table 12. Taxonomic groups were assigned to four separate scattering classes based on their backscatter characteristics and animal size

Scatterer Class	Taxa Included	TS Model	Length Categories
Fluid-like	Crustaceans: Amphipods, Chaetognaths, Copepods, Krill, Mysids, Ostracods, Shrimp, Stomatopods	Distorted Born wave approximation (DWBA, Stanton *et al.* 1998) (Fluid-sphere for radial gelatinous taxa?)	5 to 10 mm 10 to 25 mm 25 to 122 mm
	Gelatinous: *Clione* spp., *Corolla* spp., Salps, Ctenophores, Non-gas-bearing cnidarians		1 to 10 mm 10 to 55 mm
Swimbladderless fish	Cyclothone sp., Gonostomatidae, Melamphaeidae, Stomiidae	DCM (Ye 1997; Yasuma *et al.* 2006)	10 to 40 mm 40 to 225 mm
Swimbladdered fish	Gempylidae Myctophidae, Sternoptychidae	Gas-filled prolate spheroid model (Ye 1997)	7 to 30 mm 30 to 92 mm
Siphonophore pneumatophore	Physonect siphonophores	Fluid sphere (Anderson 1950)	0.1 to 0.4 mm [diameter]

These parameters were used in combination with acoustic backscatter models to produce estimates of organism TS at the relevant echosounder frequencies. The minimum and maximum size of each scatterer category was used to define dB-difference windows where the echosounder data could be "assigned" to a particularly category. Because of variations in animal size and scattering type, the scattering characteristics of categories can overlap with each other, therefore the end product of the acoustic analysis was six different scatterer categories including an unidentified group where there were multiple types of organisms that could not be differentiated (Table 13, Figure 38).

Table 13. Mean ΔMVBS windows for acoustic zooplankton fish profiler (AZFP) frequencies for narrowed-down, non-overlapping scatterer groups

Scatterer type & size		ΔMVBS 125-38 (Min, Max)
Small non-resonant scatterers (Small crustaceans, pteropods, gelatinous) *S/M*	*FLS*: 1–25 mm	+18, +21
Medium non-resonant scatterers *S* *L*	*NSBF:* 10–40 mm *FLS*: 25–55 mm	+7, +18
Large non-resonant scatterers *L* *XL*	*NSBF:* 40–225 mm *FLS*: 55–95 mm	+2, +7
Unidentified (UID)		-2, +2
Small resonant scatterers *S* *S*	*SBF:* 10–30 mm *GBZ:* 0.10–0.13 mm (radius)	-4, -2
Large resonant scatterers *L* *L*	*SBF:* 30–90 mm *GBZ:* 0.13–0.20 mm (radius)	-10, -4

Groups can be separated into resonant and non-resonant scattering groups. Non-resonant scattering groups comprised fluid-like scatterers (FLS) and nonswimbladdered (NSBF) with small and medium fluid-like scatterers combined to make three total non-resonant size groups. Resonant scattering groups

comprised swimbladdered fish (SBF) and gas-bearing zooplankton (GBZ) such as siphonophores with pneumatophores.

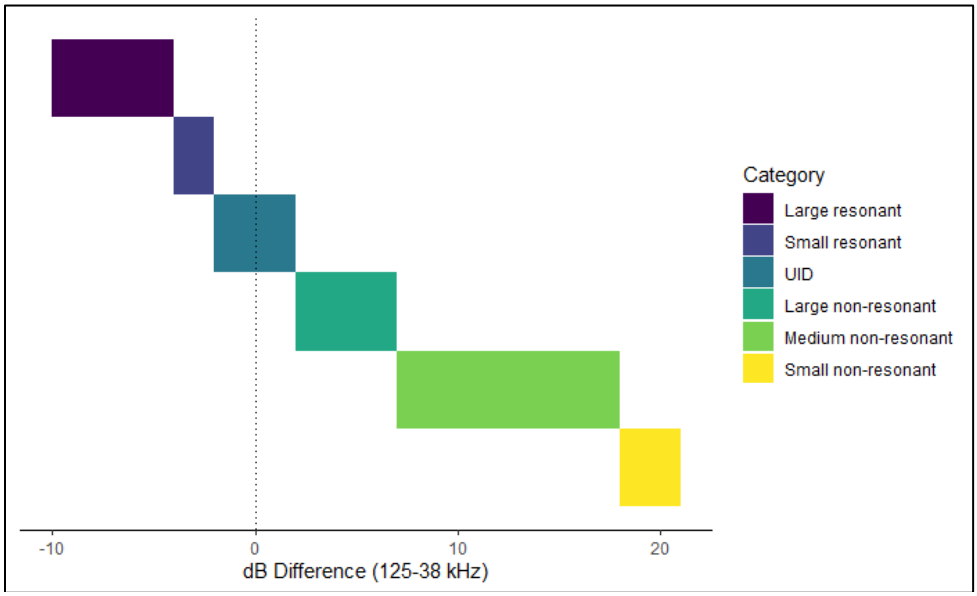

Figure 38. Non-overlapping dB difference windows for 125–38 kHz data for categories in Table 13

The UID category encompasses animals at nearly the same S_V at both frequencies, and likely includes a large amount of nautical area scattering coefficient (NASC) from bladdered and/or non-bladdered fish.

4.3 Active Acoustics

4.3.1 Active Acoustics–Lander acoustic zooplankton fish profiler (AZFP) Data

Acoustic backscatter data acquired by the lander acoustic zooplankton fish profiler (AZFP) systems at VAC, HAT, and JAX allow for the measurement of marine organism distribution, abundance, and community structure in the region surrounding the lander sites over short (daily, weekly) and long (seasonally, interannually) time scales. In addition, these data provide information on ubiquitous features (i.e., deep scattering layers) that occur throughout the study region, and more intermittent features (e.g., organisms that have a patchy distribution or move in and out of the study area). A full 3-year time series Nov 2017–Nov 2020 was produced at HAT (Figure 38). The VAC time series had several month long gaps due to the lander being trawled up by a fishing vessel in both 2019 and 2020 (Figure 39). The JAX time series started in Dec 2017 as opposed to Nov 2017 because the initial deployment of the JAX lander occurred at the very end of the first deployment cruise during the first week in Dec. 2017. The JAX lander deployed in Nov 2018 was not recovered until Nov 2020 due to a mechanical failure with the release system, so the JAX data was largely truncated by 11 months (Figure 39). A different echosounder system was deployed as a spare on the JAX lander from Jan to Nov 2020, but the substitute system did not have a 38 kHz or 125 kHz transducer to be consistent with the previous years.

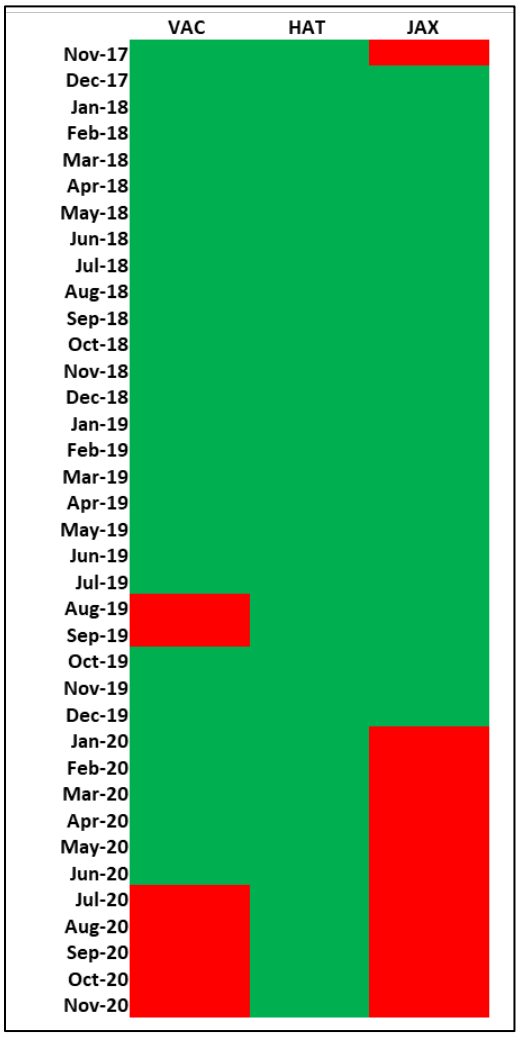

Figure 39. Acoustic backscatter time series data acquired by the AZFP system over the ADEON study period
Green indicates quality data collected. Red indicates either data absence or compromised data.

Acoustic backscatter time series were produced from the AZFP sensors at 38 kHz, 125 kHz, 200 kHz, and 455 kHz (Figure 40). The 38 kHz and 125 kHz data allowed for full water column coverage at the three ADEON sites, while the larger attenuation of the 200 kHz and 455 kHz frequencies restricted water column coverage to the deeper water column depths. Mean volume backscatter coefficient (mean S_v in units $m^2\ m^{-3}$) and NASC (NASC in units $m^2 nmi^{-2}$) were calculated at each echosounder frequency using Echoview software. Post-processing of the raw data prior to metric exports included removal of noise, surface bubble intrusions, false bottoms, lander artifacts, and acoustic crosstalk between lander instruments and frequencies.

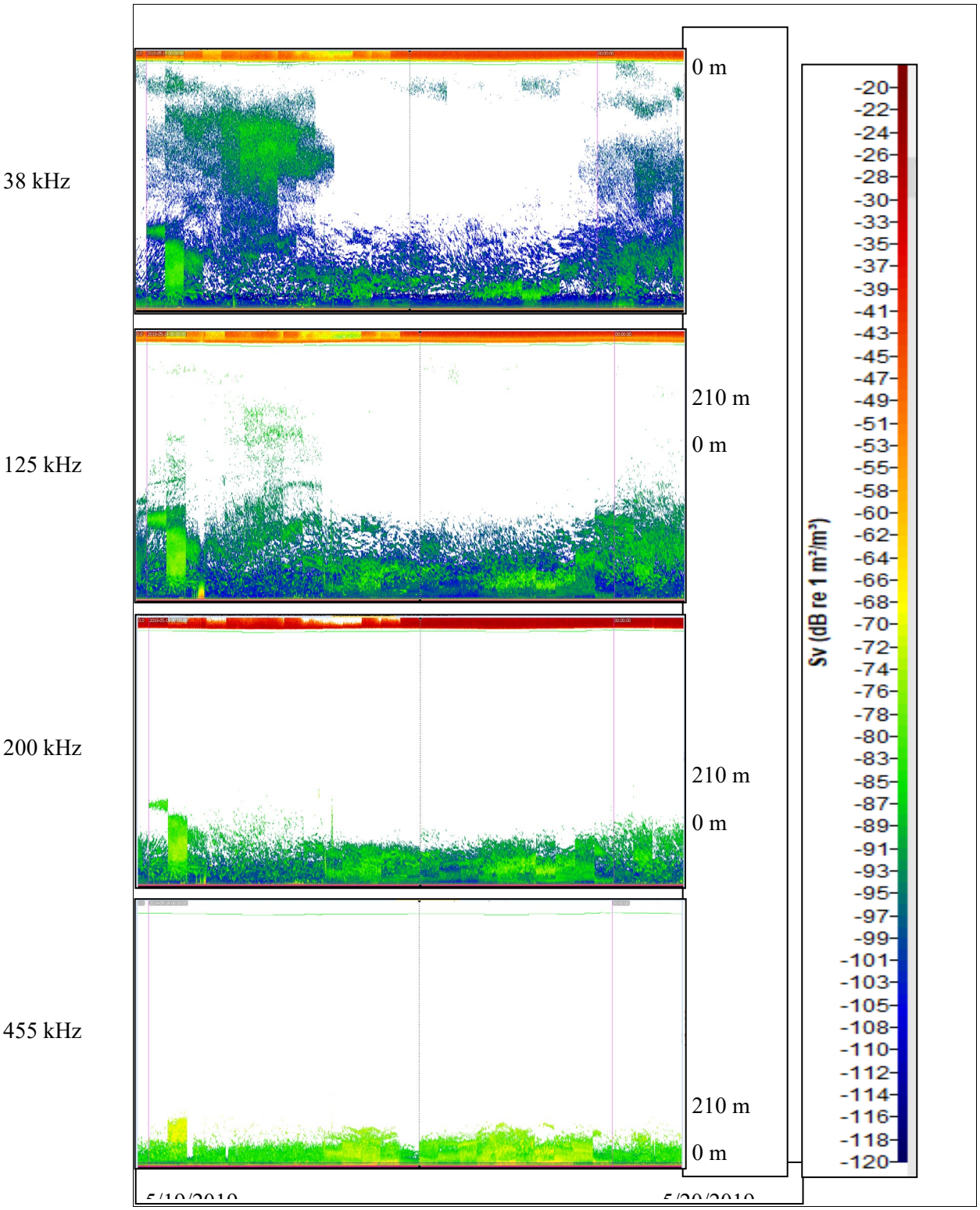

Figure 40. Four time aligned echograms from May 19, 2019 denoted by pink vertical lines

Frequencies of the echograms are labeled in each subplot. Note that the echosounder signal does not reach the surface at 455 kHz.

Full details of the AZFP data processing in terms of resolution, averaging, noise removal, filtering, and exporting are described in the ADEON Data Processing Specification (Heaney et al., 2020). A short synopsis is provided here.

Echoview Version 9 software directly read AZFP binary files and automatically input the calibration information for each frequency and unit directly into Echoview resulting in a calibrated time series. All the individual transducer calibration coefficients (contained in the configuration (.cfg) file for each instrument; ADEON Calibration and Deployment Good Practice Guide, 2017) were integrated as part of the instrument firmware and were applied to the binary data during the Echoview import process to produce fully calibrated values of S_v in Echoview. However, the AZFP binary files did not contain a time-varied gain (TVG) correction factor or frequency-dependent absorption. TVG correction and frequency-dependent absorption were applied to each dataset with a .ecs calibration file specifying STANDARD TVG and the following absorption coefficients: 0.009 dB/m at 38 kHz, 0.041 dB/m at 125 kHz, 0.056 dB/m at 200 kHz,[12] and 0.11 dB/m at 455 kHz for the ADEON region bottom conditions.

The initial processing of the Echoview files included 1) background removal via techniques outlined in De Robertis & Higginbottom (2007), and 2) a median 3 x 3 filter applied to smooth the data and remove noise interference generated either by our own ship in the region or by other passing ships. Both of these steps were accomplished within the Echoview software using the Background Noise Removal and Median Filter 3x3 operators, respectively. The parameters of the Background Noise Removal operator applied to the averaging and thresholding of ADEON AZFP data were (in the language of Echoview):

Averaging:	Thresholds:
Vertical extent (samples) = 5	Maximum noise (dB) = -90
Vertical overlap (%) =0	Minimum SNR (dB): 5

Conditioned data were exported from Echoview files to .csv files in four separate data packages (Table 14) to capture the long-term variability at selected temporal and depth scales.

Table 14. Selected data export packages from conditioned Echoview data

	Depth Averaging (m)	Time Averaging
Full Depth	200–500	24 h
Daily Partition	5	24 h
60 min Partition	5	60 min
60 min Full Depth	200–500	60 min

Community structure time series were calculated according to the six defined scattering groups and mean dB-difference windows (ΔMVBS 125-38 kHz**)** in Table 13 and Figure 38. Community structure was assessed and integrated over the full water column at hourly resolution.

[12] See http://resource.npl.co.uk/acoustics/techguides/seaabsorption/ .

4.3.2 Active Acoustics–Fine-scale Acoustic Surveys

Active acoustic data processing has produced exports of volume backscattering strength from the fine-scale acoustic surveys (FSAS) from the AR025, EN615, EN626, and AR040 cruises (in 5 m vertical, 100 m horizontal bins) which have been posted to the ADEON data portal. Five FSAS surveys were conducted on the final cruise (AR049); one is complete, one is currently in progress and three are to be finished by the end of the project period.

These data have been further processed to investigate the spatial characteristics of scattering aggregations at the ADEON sites (see section 7.2 of this report for more information).

4.3.2.1 Hydrography

The Seabird Seasoft application suite was used to convert the raw Seabird SBE-37 conductivity, temperature and dissolved-oxygen data into the final data products (Figure 41; data downloads are available as described in Section 8.3). Sensor sensitivity drift, batteries running out early, and trawling of the VAC landers resulted in the loss of some data (Figure 41).

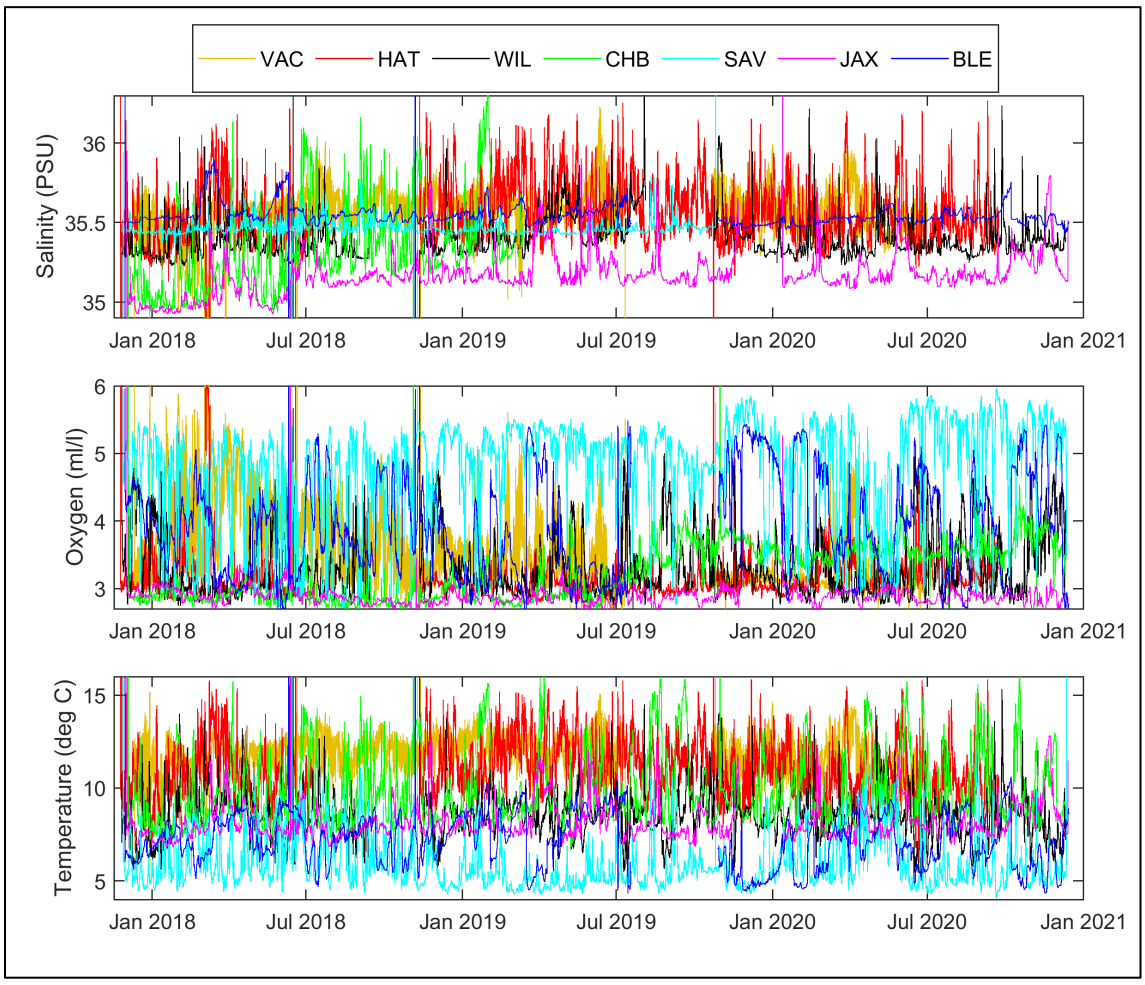

Figure 41. Summary of the conductivity, temperature, and dissolved oxygen (CT-DO) measurements made at the lander sites

Table 15. Missing conductivity, temperature, and dissolved oxygen (CT-DO) data summary ordered by Station

Station	From	To	Status
BLE	2019-07-18 13:02	2019-10-28 16:38	Recorder stopped
HAT	2018-07-10 0:33	2018-11-11 15:24	Recorder stopped
HAT	2020-09-23 4:54	2020-12-14 19:38	Recorder stopped
JAX	2019-11-22 9:04	2020-01-12 17:47	Recorder Error
VAC	2019-07-11 14:38	2019-10-22 0:54	Trawled up
VAC	2020-06-30 16:54	2020-12-14 19:38	Trawled up
WIL	2018-09-13 15:38	2018-11-11 15:24	Recorder stopped
WIL	2019-08-04 10:24	2019-10-25 18:24	Salinity Sensor out of spec
CHB	2019-03-13 7:53	2020-12-14 19:38	Salinity Sensor out of spec
SAV	2019-10-25 18:46	2020-12-11 18:52	Salinity Sensor out of spec

Fish Tag Loggers

The Ocean Tracking Network (OTN) is a global aquatic animal tracking, data management, and partnership platform headquartered at Dalhousie University in Canada. The ADEON team collaborated with this group to share data from the ADEON sites that contain VEMCO Instruments. The ADEON bottom landers are equipped with VEMCO Fish Finders which record the tag number of any tagged fish detected in the vicinity of the instrument. These fish counters are co-located with the AZPF instruments. Though ADEON has 7 acoustic listening sites, the AZFP's and the fish counters are found only at VAC, HAT, and JAX locations. Detailed information on the collections, trackers, and fish can be found at the OTN-ADEON webpage[13].

The VEMCO data presented in Table 16 is from ADEON recovery cruises EN615 (collection interval November 2017 through June 2018) and EN626 (collection interval June through November 2018). This data represents the fish detected through their tags and claimed by the "tracker" responsible for the tag. Unqualified detections are not provided by OTN as the tracker and/or owner remains unidentified. Data from AR040 and AR049 has not yet been submitted to OTN.

[13] See https://members.oceantrack.org/OTN/project?ccode=ADEON.

Table 16. Ocean Tracking Network (OTN) qualified detections of tagged fish captured by ADEON

Detections by Year	ADEON Site	Number of Detections[1]	Tracker	Family/Species of Interest
2017	HAT	2	MMFSRP	Shark
2018	HAT	53	ACT.PROJ67	Dusky Shark
	HAT	4	FACT.VIMCOB	Cobia
	HAT	110	MMFSRP	Shark
	HAT	4	Stanford U.	unknown
	HAT	2	Florida Intl. U.	Shark
	JAX	13	MMFSRP	Shark
	VAC	5	FACT.VIMCOB	Cobia
	VAC	9	Stanford U.	unknown

[1]Detections may represent a single detection or multiple detections for the same fish. Tracker abbreviations defined are: *MMFSRP*: Massachusetts Marine Fisheries Shark Research Program, *ACT.PROJ6*:Dusky Shark Habitat Use and Migration, and *FACT.VIMCOB*:Virginia Institute of Marine Science.

5. Overview Phase IV: Data Integration and Visualization

Phase IV served to integrate all data collected and processed in other phases with the overarching goals of: 1) modeling and visualizing soundscapes using known and estimated sources present during the experimental timeframe and for future scenarios; 2) establishing environmental parameters relevant to components of the ecosystem in the experimental area and timeframe and modeling the relationship of these ecosystem components with environmental parameters and with measured soundscapes; 3) visualizing soundscapes using collected data; and 4) addressing defined scientific questions which support the first three goals as outlined in detail below.

The Soundscape Modeling component focused on simulating the baseline acoustic background levels for select frequency bands for timeframes when the Atlantic Deepwater Ecosystem Observatory Network (ADEON) sensors were active. Using vessel data from the University of New Hampshire (UNH) Automated Information System (AIS) feed, wind fields from satellite remote sensing, and statistical modeling of marine mammals, simulated soundscapes were generated with the aid of a parabolic equation propagation model (Heaney & Campbell, 2016) and oceanographic parameters controlling propagation (e.g., water column temperature profiles and bottom sediment composition). Comparisons between the measured and modeled soundscapes provided confidence in the soundscape modeling component of this effort. Soundscapes for the ADEON experimental region for the duration of the measurement period were generated in standard quantities as defined in the standardization product documents produced by ADEON, producing geospatial soundscape information for visualization and for comparison with the point observations. This data is accessible for display to the public via the visualization web tools developed by the UNH Visualization team as described below.

The Ecological Modeling and Monitoring component of ADEON was centered on relating variability in top predators (e.g., marine mammals) and the broader ecosystem to oceanographic conditions via examination of patterns in marine mammal detection rates and data collected over the ADEON experimental region during times when the ADEON measurement platforms were operating. Patterns of acoustic call rates in various marine mammal species were used as the response variable for forming predictive ensemble models (e.g., generalized additive mixed models [GAMMs]) of persistent areas of high trophic transfer or biodiversity at the ADEON study site. ADEON Ecological Modeling goals were accomplished by integrating satellite oceanography, multi-tiered-trophic level data from passive and active acoustics. Additionally, higher-order data types, such as frontal persistence, were integrated into the modeling framework to identify temporal patterns of distribution and abundance that would then be used to construct a modeling framework that includes both large spatial regions and long timescales. Oceanographic drivers in the developed models were then explored to assess their predictive skill in forecasting species distribution to yield confidence in the models for serving as a tool supporting dynamic ocean management (Lewison et al., 2015; Maxwell et al., 2015).

The overarching goal of the Visualization component of ADEON was to determine ways to effectively and efficiently convey information contained in collected data or model results to downstream users such as the science community, government agencies, policy makers, and the general public. Building tools for exploring and interacting with the large, complex, multi-layered, and multi-dimensional data sets that resulted from ADEON, and developing novel ways to quickly and clearly understand the data presented were therefore critical. Properly designed visualization tools can be highly effective for revealing the complex, dynamic patterns and structures present in measurements and models (Ware et al., 2014). The visualization software developed as part of the proposed work will enable users to interactively explore and highlight subsets of environmental and modelled acoustic data in space, time, or frequency, and compare these scenarios with collected data. The tools developed also help users to quickly explore and select subsets of data that may then be requested from the Data Management repository as processed or

raw data products for separate analysis. A major part of the visualization plan revolved around the creation of a rapid, interactive web-based visualization tool(s) which will utilize existing web-based geospatial platforms and modern WebGL to create interactive visualizations that are accessible to researchers both within and outside this project.

5.1 Soundscape Modelling

A soundscape model was developed for ships and wind for the ADEON region. For frequencies below 200Hz, the acoustic propagation loss (PL) is computed from a large grid of points near the surface to the entire ocean volume, with emphasis on 10–100 m and the seafloor. Surface winds and ship positions were taken from the cross-calibrated multi-platform (CCMP) model (see Section 3.3). Ship positions and speeds were taken from satellite measurements of automated identification system (AIS). With ship and wind positions, the soundscape was computed by adding the intensity (pressure-squared) of all sources at each receiver position. The time resolution for computing the wind and/or ships and combined soundscapes is 10 min. The output products were delivered to the UNH Data server and are being displayed as part of the ADEON visualization. An example of the combined wind and ship soundscape at 63 Hz is shown below in Figure 42. The left panels show a snapshot in time (at 10 m depth–top and at the seafloor). The center panels show the mean (in pressure squared) and the rightmost panels the median. It is clear that there is more energy at the seafloor than at 10 m deep.

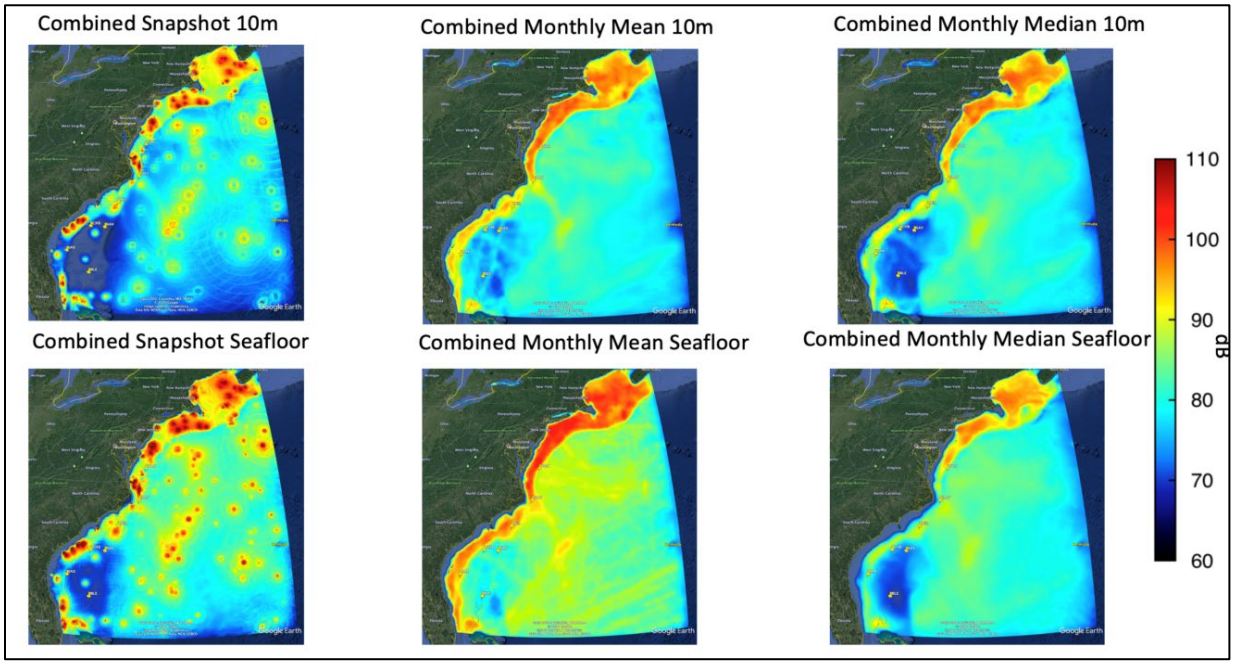

Figure 42. Maps of decidecade sound pressure level re 1 μPa^2 (dB) for wind and ships at 50 Hz on March 15, 2019, at receiver depths of 10 m and the seafloor

(Left two panels). Level of the arithmetic mean level (in dB) at 50 Hz for March, 2019, at 10 m and the seafloor (center two panels, top and bottom, respectively) and level of the median (in dB) at 50 Hz for March, 2019, at 10 m and the seafloor (center two panels, top and bottom, respectively). Temporal Observation Window = 60 s; Temporal Analysis Window = 1 mo; Spatial Observation Window = 17 km^2.

The spatial coverage of the Atlantic Outer Continental Shelf (OCS) soundscape model is significant. These model runs were computationally expensive because of the need to compute propagation loss from

everywhere (all ship/wind positions) to everywhere (all receiver positions). For the lander sites, however, there was a fixed receiver, and the propagation model can be run out in a select number of radials. This permitted a greatly expanded frequency range and incorporation of uncertainty into the model.

Multiple levels of uncertainty were incorporated in the model. The uncertainty incorporated includes oceanographic, sediment, ship source level, ship source depth and wind speed for each patch. For each site 28 realizations of the sound field were generated. The wind and ship soundscapes were computed separately for later analysis along 36 radials. The bearing information permits comparison with beamformed data provided by JASCO and provides an indication of the spatial variability of the sound field. Once the propagation modeling was complete, the soundscapes were able to be generated at any time scale of interest using the global wind field and the measured AIS. The 50Hz decidecade sound pressure level (SEL) percentiles (5, 25, 50, 75, 95) for February 1, Midnight to 1 AM at Virginia Inter-Canyon (VAC) are shown in Figure 43. This representation shows that with all the associated uncertainty there can be a 6-9 dB variation in the modeled sound field. The presence of individual ships does drive the local soundscape.

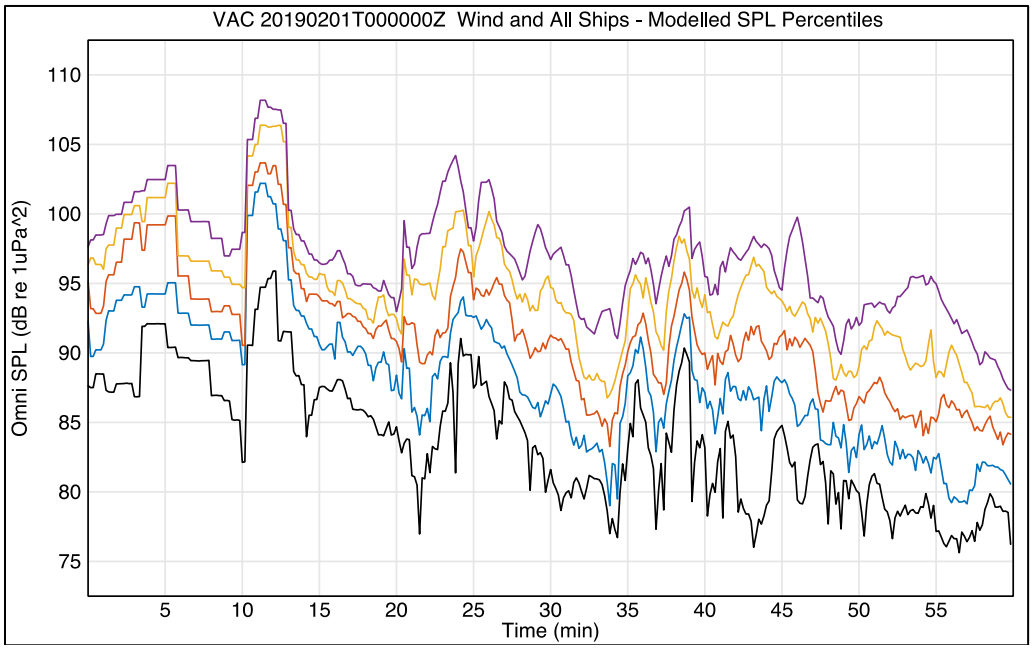

Figure 43. Ship and wind 50Hz decidecade sound pressure level (SPL) for one hour of VAC on February 1, 2019

(Plotted are the 5th, 25th, 50th, 75th and 95th percentiles.)

A small selection of the model-data comparison is shown below in Figure 44. For each plot, the measured SPL is represented by blue dots and the modelled SPL by black, yellow, red lines (for the 5th, 50th, 95th percentiles, respectively.) For the Savannah (SAV) site, the qualitative comparison is excellent except for the last day, where there were sources at 25 Hz that are not in the model. These unknown sources could be biologics. A few ships are not accounted for, but the background levels agree very well. The histogram and cumulative density functions (CDF) are in excellent agreement up to 85 dB re μPa^2. Above that, they are influenced by the loud 63 Hz event on January 5. The Wilmington (WIL) comparison in the middle panels (c–d) show agreement with many of the ships and the general shape. The background levels (times not driven by a local ship) are 5 dB lower than observed. This is likely due to the region having a softer sediment than the one used in the model. The final comparison is the Blake

Escarpment (BLE) site. At this site, there are only a few observable ships and both the model and data have them at the same times. The model results, however, are 10 dB lower than the data for both the local ships and the wind/distant ship levels. It is likely that the sediment at the BLE site is not as soft as that given by the US Navy database used in the modeling, causing the difference seen in levels. There is large variability in the model levels for BLE, due to the geo-acoustic uncertainty. The 95th percentiles of the model match the measured medians within 3 dB.

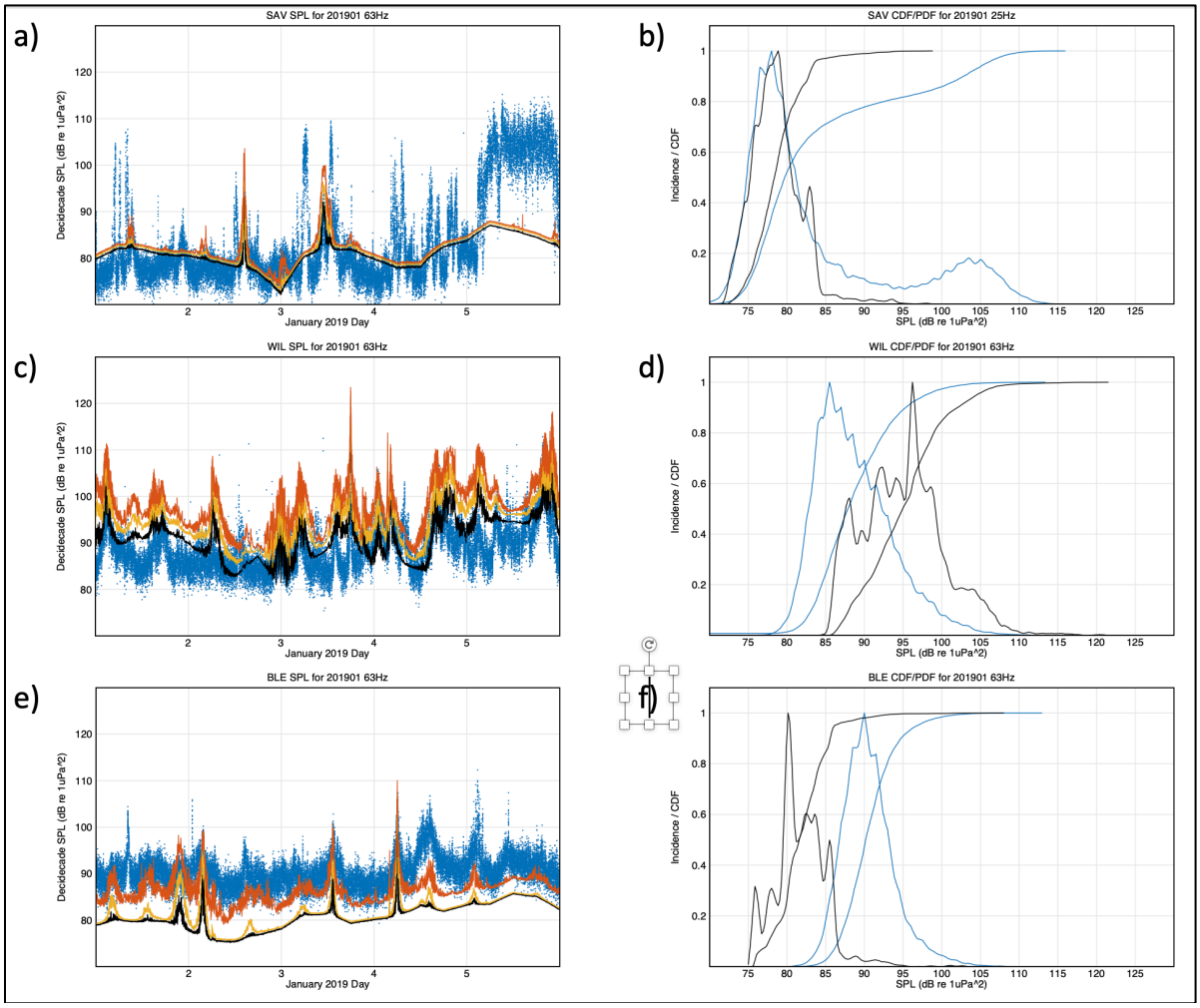

Figure 44. ADEON model-data comparison for January 1–5, 2019

All plotted values are decidecade band SPL (dB re μPa^2). a) SAV 63 Hz 5th, 25th 95th percentiles of the model (black, yellow, red) and data (blue dots). b) SAV model (black) and data (blue) histograms and cumulative density functions (CDFs) for 25 Hz. c) WIL 63 Hz 5th, 25th 95th percentiles of the model (black, yellow, red) and data (blue dots). d) WIL model (black) and data (blue) histograms and cumulative density functions (CDFs) for 63 Hz. e) BLE 63 Hz 5th, 25th 95th percentiles of the model (black, yellow, red) and data (blue dots). f) BLE model (black) and data (blue) histograms and CDFs for 25 Hz.

5.2 Soundscape Correlations

One of the stated science goals of the ADEON project was to evaluate the correlation times and distances of the ocean soundscape. Whether the sound field at one location is related to that at another location is

sensitive to bathymetry, distance from the shipping lane, whether shipping or wind dominates, and the spatial distances between the two. Note that the atmospheric spatial scales related to weather (size of high/low pressure cells in the atmosphere) are on the order of 500-1000 km.

5.2.1 Inter-lander Correlations

This work is being submitted to a scientific journal on the topic of the temporal and spatial correlations of the ocean soundscape as sampled by the ADEON hydroacoustic network. The input data is the 1-min average sound pressure level (SPL) for each lander within each decidecade band. With two magnitude time series (such as SPL), the correlation function is a measure of how related they are. Does one rise while the other does (positive correlation) or is one low while the other is high (negative correlation)? The correlation is computed as a function of the time lag between them. The normalized temporal correlation function for the 14 Hz decidecade band SPL from HAT and BLE is shown in Figure 45a. There was a positive correlation at +/- two days and a negative correlation at 0-day time lag. This implies that there is some process (likely weather) where the low frequency sources travel between HAT and BLE and take 2 days to get there. This process could be transiting ships, although this is unlikely. The monthly average correlation between CHB and the other sites at 14 Hz is shown in Figure 45c. For this month, CHB was well correlated with BLE, less so with VAC, HAT and SAV, and was negatively correlated with WIL.

The decidecade SPL as a function of frequency provides a smooth curve with information regarding the noise sources and levels. A correlation metric was developed that seeks to compare the similarity of the spectrum shape. The spectrum shape correlation for HAT and VAC for the month of April is shown in Figure 45b. This plot is at zero lag. There are periods where the spectral shapes are very similar (correlation coefficients near 1) and those as low as 0.8 or 0.85. The inter-lander comparison, averaged for the month of June 2019 between VAC and all the other landers is shown in Figure 45d.

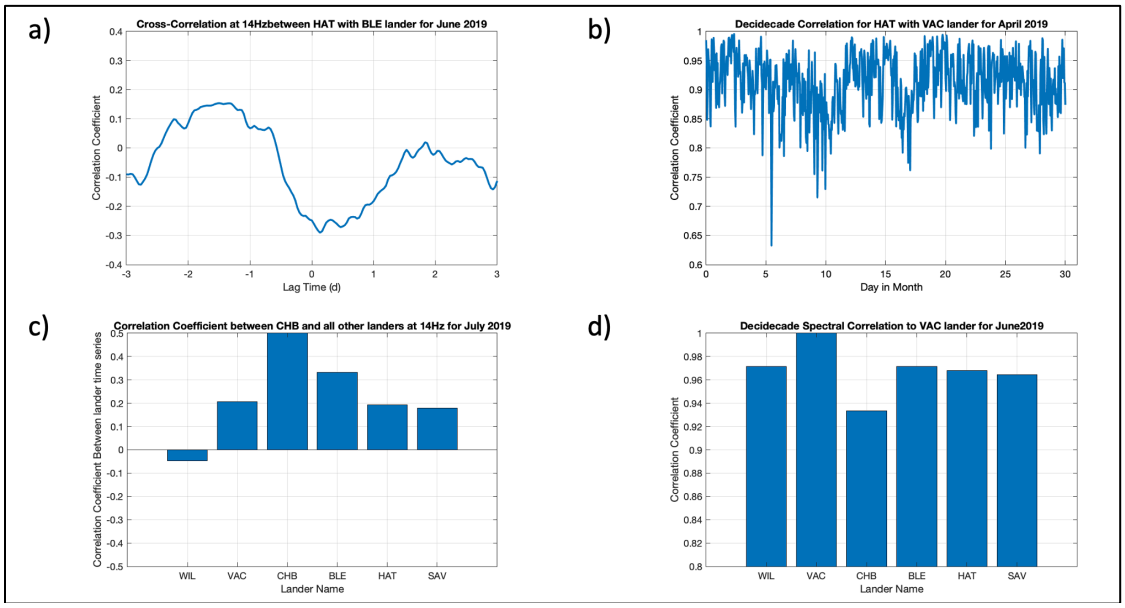

Figure 45. ADEON Lander Temporal Correlations

a) Temporal cross correlation (in days) between the 14Hz decidecade band at HAT and at BLE. (b) Correlation of the envelope of the decidecade spectra between HAT and VAC for April 2019. (c) 14 Hz decidecade band temporal correlation coefficient between CHB and the other landers. Temporal correlation is averaged across the month of July 2019. (d) Spectral shape correlation averaged over June 2019 between VAC and the other landers.

5.2.2 Sailboat Tow: Lander Correlations

To evaluate the spatial correlation at multiple ranges, and those smaller than the HAT/VAC distance, a series of sailboat towed array measurements was conducted. The final sail cruise conducted in 2020 sailed over the JAX lander (Figure 46). During this cruise, over 51 hours of usable acoustic data was recorded from a Cetacean Research hydrophone sampling at 96 kHz. This included a 23-hour south-southeasterly tow towards the JAX mooring at approximately 50m depth; a 34-hour surface transect between JAX and CHB using the same hydrophone; and 7 "research stations" where one or more 10-minute recordings were made at various depths. The data is archived on the UNH server in decidecadal band sums. The data from the 23-hour tow is described below.

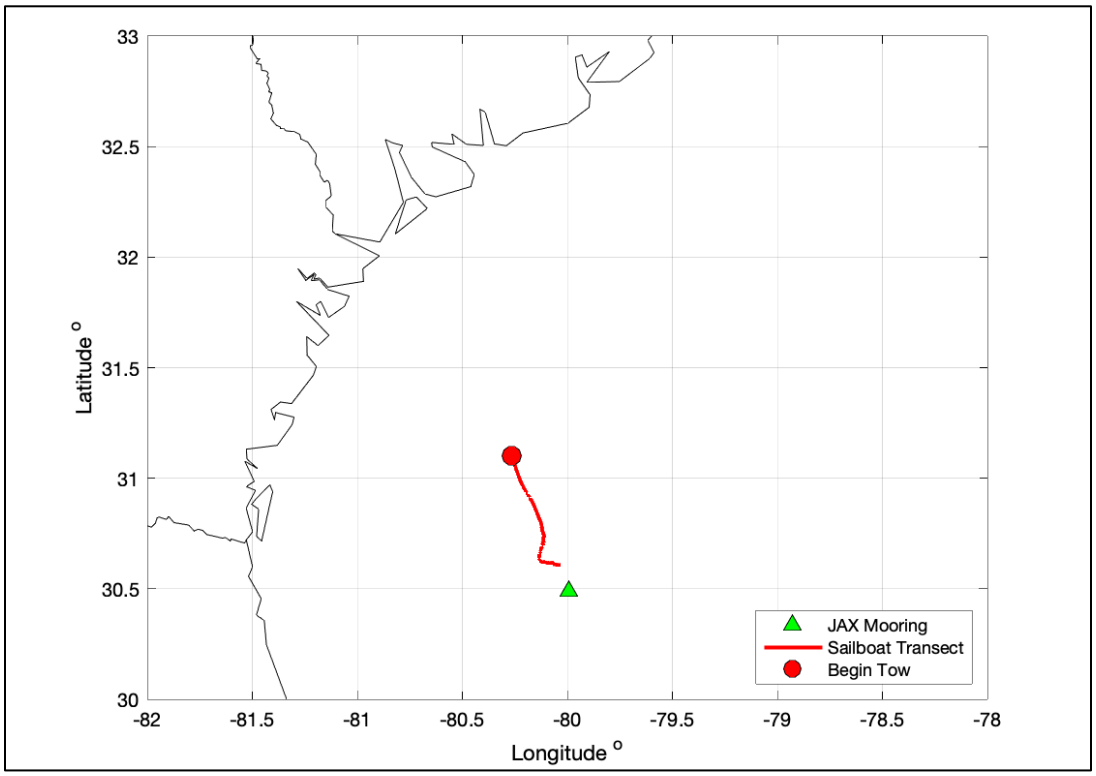

Figure 46. Navigation showing Sailboat tow and the JAX mooring

To examine the spatial correlation scales of the ambient noise field, the range of every point along the tow to the beginning point of the tow was calculated first. One way to describe spatial correlation scales of a soundscape is to plot the correlation coefficient of the noise spectra as a function of distance. Figure 47 shows this relationship during the 23-hour horizontal tow. For this figure the correlation of the sailboat soundscape with that of the sailboat measurement as it transits towards JAX, crossing the continental shelf, is plotted.

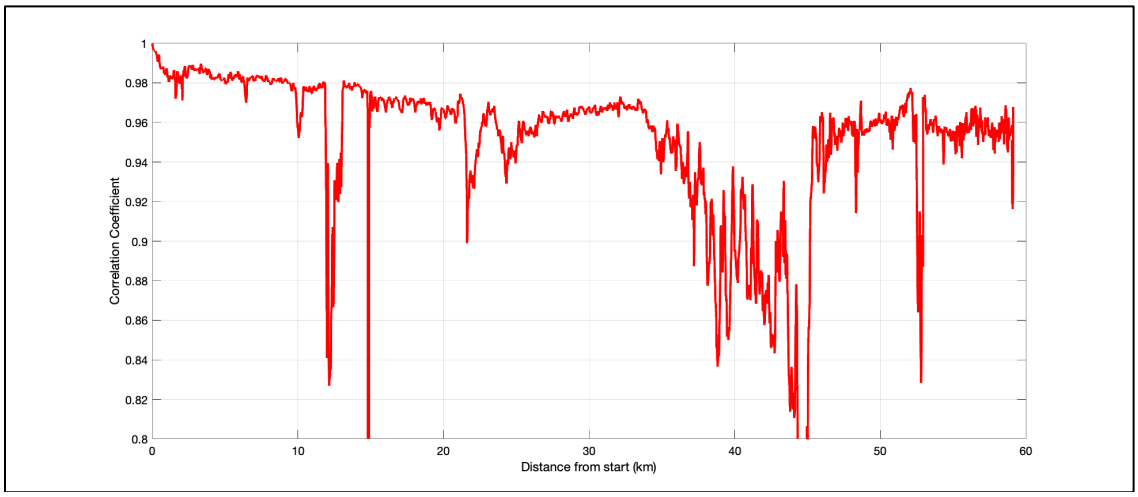

Figure 47. Correlation coefficient of acoustic spectra along 23-hour hydrophone tow towards JAX lander

5.3 Ecological Modelling

The middle of the food web is one of the often-overlooked portions of marine food webs that can tell us about how ecosystems are responding to climate variability and change. At the same time, top predators can be important indicators of ecosystem status and function, particularly when other ecosystem components are difficult to measure (Hazen et al. 2019). Previous analyses examining the distribution and spatial structure of prey communities and predators relative to environmental drivers have demonstrated strong correlations between environmental (e.g., physical, primary productivity) conditions, forage community composition, and top predators (Schroeder et al., 2014, Schroeder et al., 2019). These relationships have been critical in understanding the physical forcing of ecosystem processes, and these relationships have more recently been explored relative to biodiversity patterns (richness, diversity, evenness) as part of a National Oceanographic Partnership Program (NOPP)-funded Monterey National Marine Sanctuary Marine Biodiversity Observation Network (MBON) project (Santora et al., 2017, Santora et al., 2020, Santora et al., in review). The ecological modeling underway via MBON from physics to food to predators has been an important backdrop for our ADEON efforts.

The Ecological Modeling and Monitoring effort has gone beyond describing only the temporal abundance patterns in a study region, to also examining how variability in top predators (e.g., acoustically detected marine mammals) and the broader ecosystem relates ultimately to changing oceanographic conditions. Diversity and species-specific patterns in marine mammal detection rates have been collected and analyzed concurrent with the moored equipment. Baseline patterns of acoustic call rates were used as the response variable when developing predictive models that may be used to identify persistent areas of high trophic transfer or biodiversity at the ADEON study site. One of the ADEON Ecological Modeling objectives, how changes in abundance and distribution of the forage assemblage varies relative to warm and/or poor and cool and/or good productivity years off the US east coast remains incomplete because of a current of lack species-specific community assemblage metrics from the acoustic zooplankton fish profilers (AZFPs). Once those are complete, estimates of the acoustic complexity index (ACI) can be developed which will be compared with the ecological modeling results to gain a better understanding of the relationship between ACI and species diversity which should yield important knowledge required to further enhance the ACI as an ecological monitoring tool. For completion of ADEON Phase 4 tasks, acoustic biomass has been explored in addition to surface and at-depth measurements of physical features

coupled with acoustic detections of marine mammals to better inform the fine scale response of top predators towards understanding of ecosystems and ecosystem changes.

ADEON Ecological Modeling goals were accomplished by integrating satellite oceanography, multi-tiered-trophic level data from passive and active acoustics. A chart of the ecological modeling process is displayed in Figure 48. Ensemble models were explored that included semi-parametric (Generalized Additive Mixed Models [GAMMs]), machine learning (Boosted Regression Trees [BRTs]), and Bayesian approaches (Multivariate Autoregressive State Space Models [MARSS]). multiple biophysical data types (including frontal persistence) were processed and integrated into a common framework, exploratory analysis was performed to identify temporal patterns of distribution and abundance, and ultimately constructed a spatio-temporal modeling framework. Oceanographic drivers in a predictive model was then explored to assess the skill of this tool for species distribution forecasting capabilities which can serve as the baseline tool supporting dynamic ocean management (Lewison et al., 2015; Maxwell et al., 2015). Understanding how oceanographic structure underlies patterns of top predator biodiversity can be useful in developing adaptive management approaches, assessing risk, and ultimately predicting potential influence of long-term climate change on the marine ecosystems (Hazen et al., 2013; Maxwell et al., 2013).

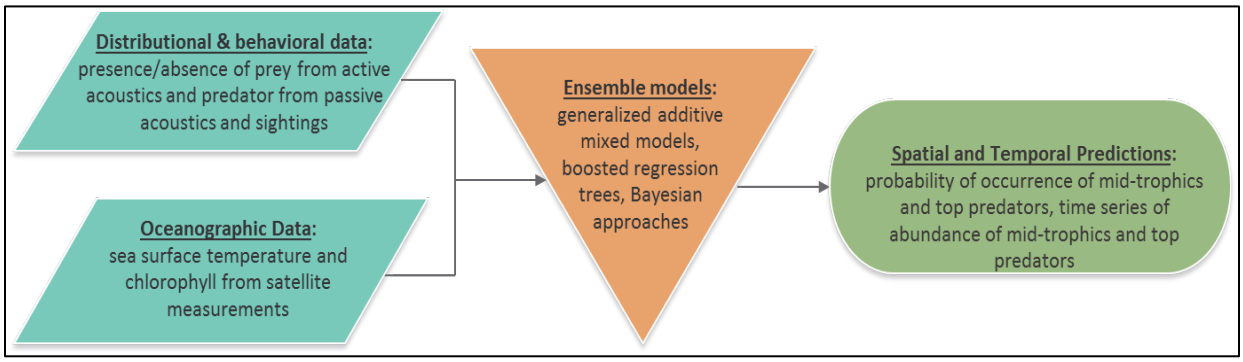

Figure 48. Ecosystem modeling framework

Two studies were carried out as part of the Ecological Modeling component of the ADEON project: 1) a shorter exploratory analysis of cetacean distributions in relation to environmental covariates from the ADEON autonomous multichannel acoustic recorder (AMAR) recordings and 2) a longer study, building on tools developed in the first study, which aimed to model regional and seasonal ecological patterns and the links between oceanography, prey and diving predators. Both of these studies are discussed below.

As part of this exploratory analysis, a workflow was developed to:

- Calculate daily occurrence and call rates of fin whales, pilot whales and delphinids at each of the seven ADEON lander sites;
- Port satellite environmental covariates from the ADEON server, and extract variables at each lander site for each day of cetacean recordings;
- Build generalized additive models relating both species occurrence and call rates to local environmental conditions;
- Create a prediction grid for a subset of the ADEON region where species distributions can reasonably be inferred;
- Create daily mapped predictions of the distributions of all cetacean species based on environmental features across this region.

Preliminary models fit to 2018 data (cruises EN615 & EN626) with an initial, reduced set of environmental covariates (sea surface temperature [SST], chlorophyll *a*, day of the year and lander site), showed strong relationships between the occurrence and calling activity of all cetacean species in 2018, and both sea surface temperature and day of the year The ability of these covariates to explain variability in both occurrence and call rate were strongest for fin whales, which likely reflects a signal of their seasonal migration along the coast. Below is output from a preliminary generalized additive model for fin whale call rate (Figure 49), as well as spatial predictions of fin whale activity for a day in fall (Figure 50). This exploratory model explains 50% of the variation in fin whale call rates across the time series and will change and improve as more covariates are added, as well as with refinement of model structure.

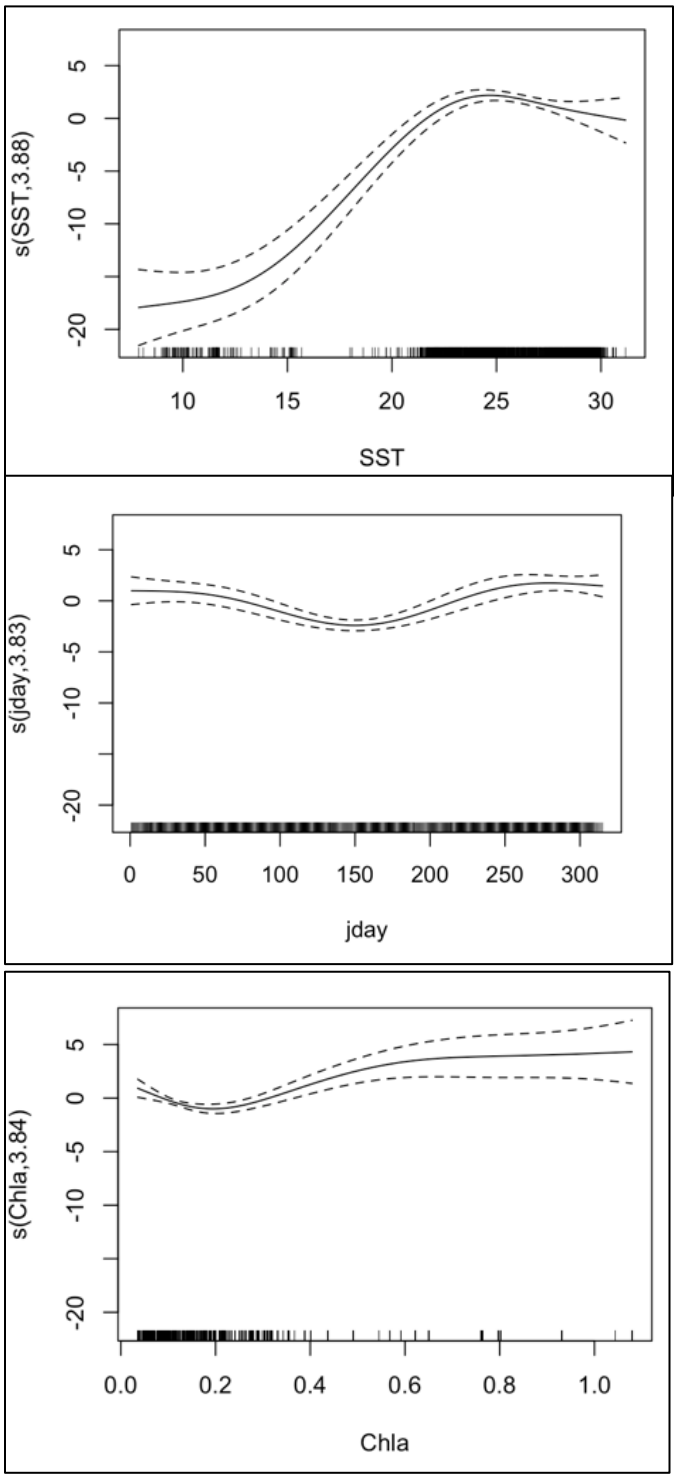

Figure 49. Preliminary generalized additive model partial plots showing smoothed responses of fin whale call rate to sea surface temperature (top plot), day of the year (middle plot), and chlorophyll *a* (bottom plot)

The generalized additive model partial plots above suggest that when accounting for the effects of site, seasonality and chlorophyll *a*, fin whale call rates increase with temperature, being highest at approximately 23ºC. This corresponds to higher call rates in fall and winter, and a slight increase in call rates at higher chlorophyll *a* values. Below is an example of a spatially-explicit daily prediction from this model for 7 September 2018, reflecting the higher relative fin whale calling activity in the north of the region near the VAC lander site during this time of the year.

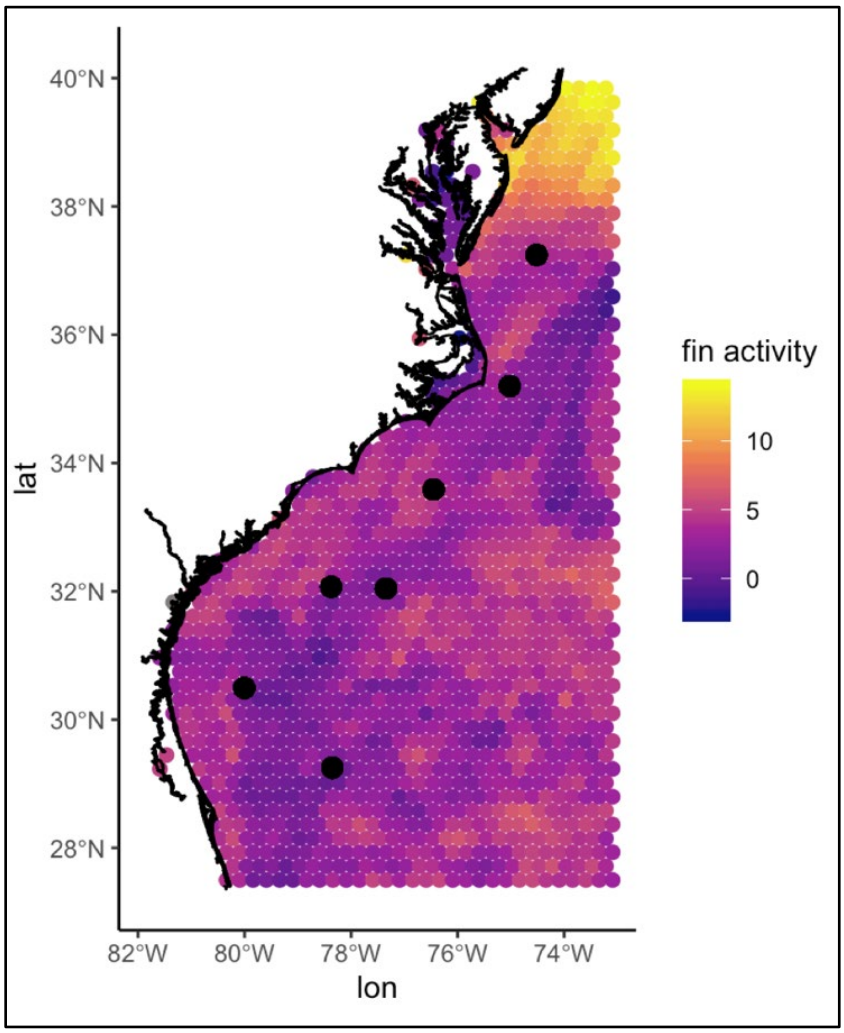

Figure 50. Example of a daily spatial prediction of relative fin whale activity on 7 September 2018 using preliminary fitted relationships from a generalized additive model

5.2.1 Modelling regional and seasonal ecological patterns

5.2.1.1 Methods

Remotely sensed and modelled oceanographic data were obtained from online databases. Through a collaboration with Dr. Peter Miller at the Plymouth Marine Lab, United Kingdom, fine-scale, daily satellite-derived front maps for the study region were also obtained. A Single-Image Edge Detection (SEID, Cayula & Cornillon, 1992) was applied to the National Aeronautics and Space Administration's (NASA) Jet Propulsion Laboratory (JPL) Multiscale Ultrahigh resolution (MUR) SST layers at a 1 km resolution to identify fronts. A detection threshold of 0.4 °C was used and the following front metrics: 1) front distance, 2) front gradient density and 3) front persistence were generated and averaged over a 7-day window, centered on each day (Scales et al., 2014; Miller et al., 2015). Front gradient density was the result of applying a Gaussian smoothing filter ($\sigma = 5$ pixels) to give a continuous distribution of frontal activity, while frontal persistence was the fraction of cloud-free observations of a pixel for which a front is detected, also smoothed to give a continuous distribution.

AZFP outputs were visually screened for anomalous values and the top and bottom 5 m of data were removed. Given that many mesopelagic species (e.g., zooplankton, fish, squid) are diel-vertical migrants, periods of the diel cycle associated with daylight and darkness in the epipelagic were separated out as the 8-hour period surrounding midday and midnight, respectively. Given the latitudes of the lander sites, these periods always occurred between sunrise and dusk, and sunset and dawn, respectively, year-round. Based on Urmy et al. (2012), three metrics were selected to characterize 1) the mean position of prey in the water column, 2) the aggregation of prey throughout the water column and 3) the total biomass of prey. Mean position was measured using the centre of mass, i.e., the average of all depths sampled weighted by their value of nautical area scattering coefficient (NASC). Aggregation was measured as the depth integral of NASC divided by the squared integral of NASC over depth and is high when small areas are much denser than the rest of the distribution. Abundance was the sum of all NASC values throughout the water column. The mean value of each metric per photoperiod (i.e., daylight and darkness) was then calculated.

For the cetacean data, only toothed whales (odontocetes) were considered, as they echolocate to navigate and find prey and so clicks are likely to be associated with foraging behaviour, unlike calls of mysticete whales that are associated with mating or communication. Data for different species were pooled based on their diving behaviour to represent four functional groups: delphinids, pilot whales, beaked whales and sperm whales which exploit different vertical niches (see Table 17). Click trains were summarized for each species group and day as the number of detection positive hours (DPH), that is, the number hours for a which a click train was detected.

Table 17. Functional species groups of toothed whales considered for analyses based on dive depths and foraging depth zones

Species group	Species included	Dive depth	Depth zone
Delphinids	Bottlenose, Atlantic white-sided, short-beaked common, Risso's, Clymene, rough-toothed and spotted dolphins	0–200 m (500–600 m for Risso's and rough-toothed)	Epi-mesopelagic
Pilot whales	Long-finned and short-finned pilot whales	20–900 m	Epi-mesopelagic
Beaked whales	True's, Gervais', Sowerby's, Cuvier's beaked whales	200–1200 m	Meso-bathypelagic
Sperm whales	-	800–1200 m	Bathypelagic

Daily prey and cetacean DPH values were linked to oceanographic data. Generalized additive models (GAMs) were used within the R package *mgcv* (Wood, 2017) to model the relationships between oceanography, metrics of prey distribution and abundance in the water column and cetacean activity for 2018 and 2019. Three sets of models were run, examining 1) the effect of oceanographic variables on prey metrics at three lander sites (HAT, JAX, and VAC), 2) the effect of oceanographic variables on cetacean activity at all seven lander sites, and 3) the combined effects of oceanographic and prey variables on cetacean activity at three lander sites (HAT, JAX, and VAC). Separate models were run for each prey metric and cetacean species group. The following covariates were considered, which are known to be important drivers of predator and prey distributions and activity in pelagic environments: chlorophyll *a* concentration, distance to 200 m isobath, total kinetic energy (i.e. current speeds), finite-size Lyapunov exponent, lander, lunar illumination, mixed layer depth, photosynthetically available radiation, sea surface temperature, front distance, front gradient density, front persistence density and wind speed. Collinearity between variables was tested using Spearman rank correlations and variance inflation factors (VIF) and correlated variables (> 0.6 Spearman correlation coefficient, VIF > 3) were removed from analyses. As frontal gradient density and frontal persistence density were highly correlated, only the latter was included in analyses. For prey models, lunar illumination was included interacting with the factor photoperiod (daylight vs darkness) to control for an effect of lunar phase only on prey behavior at night.

Prey center of mass was modelled using a Gaussian error distribution, prey abundance and aggregation were modelled using a Gamma distribution with log link, and cetacean DPH was modelled using a Poisson distribution with log link, all as a function of smoothed covariates. The number of knots was limited to 5 to prevent over-fitting. As an additional measure against overparameterization, smooths were produced using cubic regression splines with shrinkage, allowing covariates to be penalized out of the model entirely during fitting (Wood 2017). Models were constructed with all possible covariates and used a simple approach to derived minimum adequate models (MAMs), removing non-significant variables using backwards selection and likelihood ratio tests. The relative importance of covariates in MAMs was assessed by running separate models with each variable as a standalone covariate. An autoregressive term was included to account for serial autocorrelation in values and auto-correlation function (acf) plots revealed no residual serial autocorrelation in models. The developed models were then used to predict back onto original datasets from 2018 and 2019, indicating the skill of models to explain observed temporal patterns. Models are to be updated to include data from 2020, and the process of developing the approach to incorporate different landers as a random effect in generalized additive mixed models (GAMMs) will also improve upon the model selection and validation methodology to make it suitable for GAMMs.

5.2.1.2 Results

The ADEON study region encompassed the south- and mid-Atlantic Bight from north Florida to Virginia, with large latitudinal and seasonal variation in oceanography (Figures 51 and 52). The northerly sites, and in particular VAC, are characterized by lower SSTs and higher productivity (chlorophyll *a* concentration), while the more southerly and offshore sites have higher SSTs and lower productivity (Figures 51 and 52). There is also greater seasonality in the northerly sites, related to changes in SST, yet at all sites, the depth of mixed layer becomes shallower during the summer as the ocean surface warms (Figure 52). VAC has much lower SSTs than all other sites as it lies north of the Gulf Stream in the colder Labrador Current; VAC and BLE experience much weaker current speeds due their position outside the main flow of the Gulf Stream (Figures 51 and 52). Large frontal gradients form where different water masses meet, being particularly prevalent at HAT and in winter (Figures 51–53), when temperature contrasts between the warm, offshore Gulf Stream and cooler onshore Labrador Current are greatest (Figure 51). Fronts are weakest and least prevalent offshore at BLE and SAV (Figures 51 and 52).

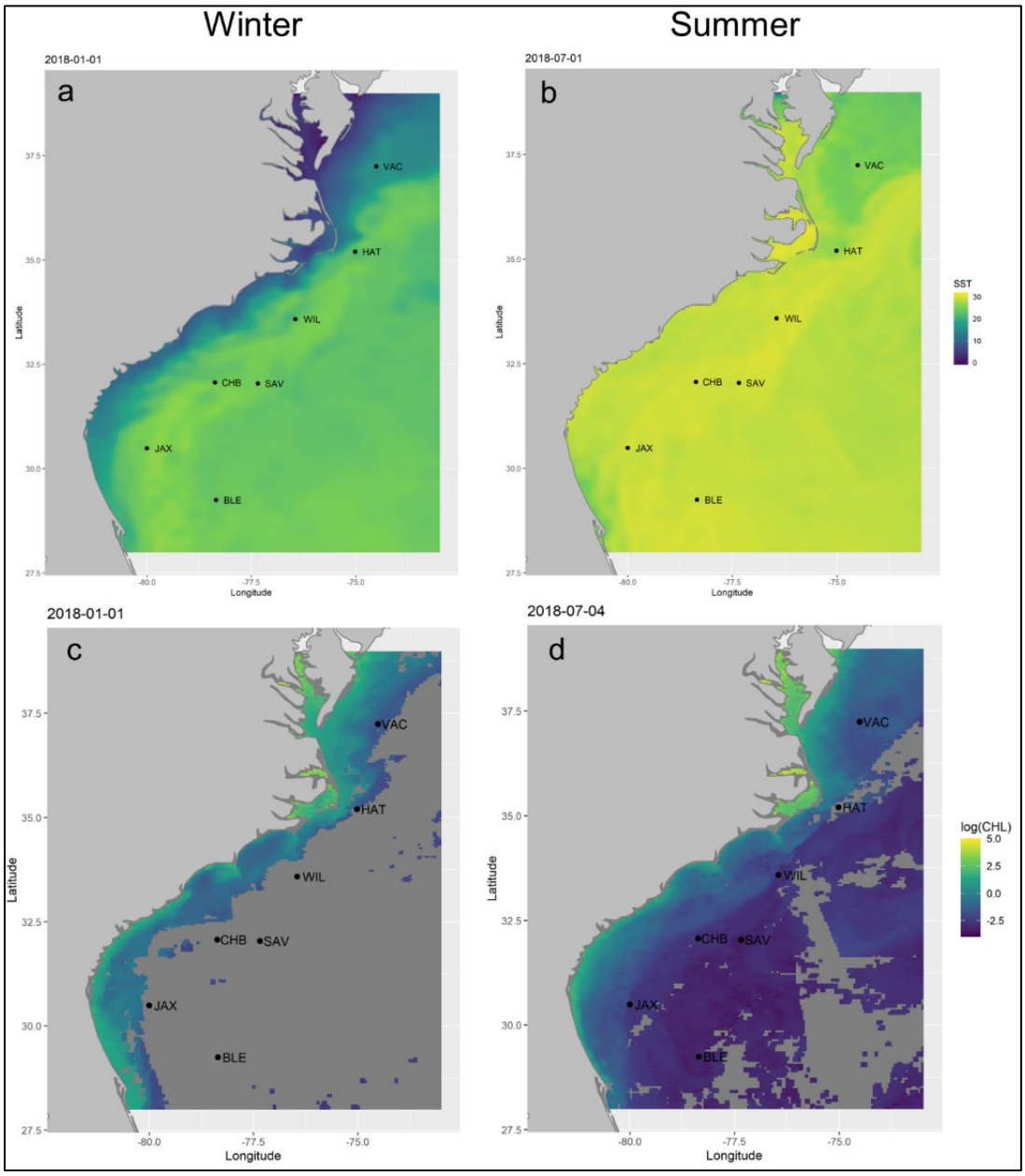
Winter
Summer
2018-01-01
a
2018-07-01
b
c
2018-01-01
2018-07-04
d
VAC
HAT
WIL
CHB
SAV
JAX
BLE
Latitude
Longitude
SST
log(CHL)

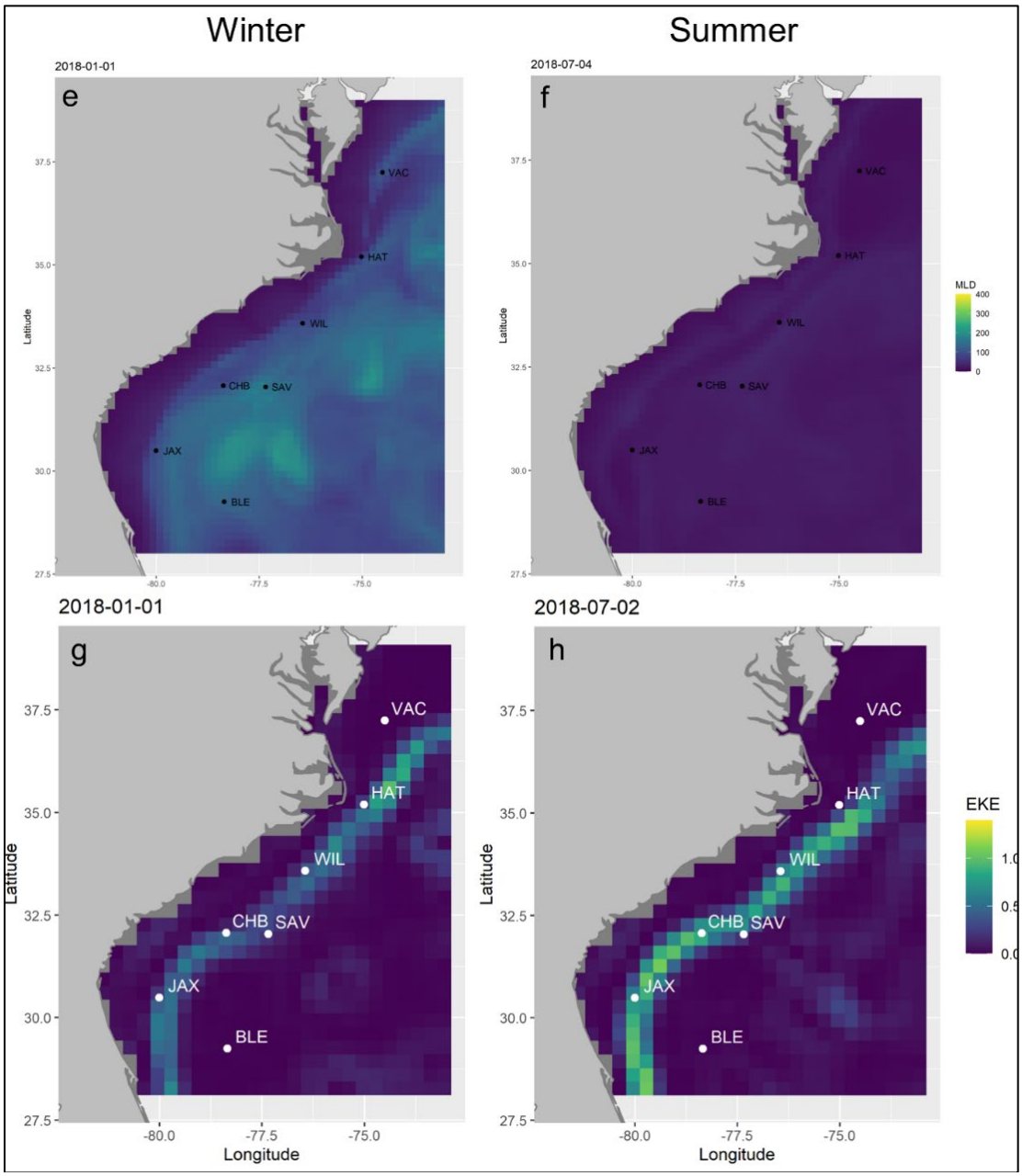
Winter
Summer
2018-01-01
e
2018-07-04
f
VAC
HAT
WIL
CHB
SAV
JAX
BLE
Latitude
MLD
400
300
200
100
0
2018-01-01
g
2018-07-02
h
EKE
Longitude
37.5
35.0
32.5
30.0
27.5
-80.0
-77.5
-75.0

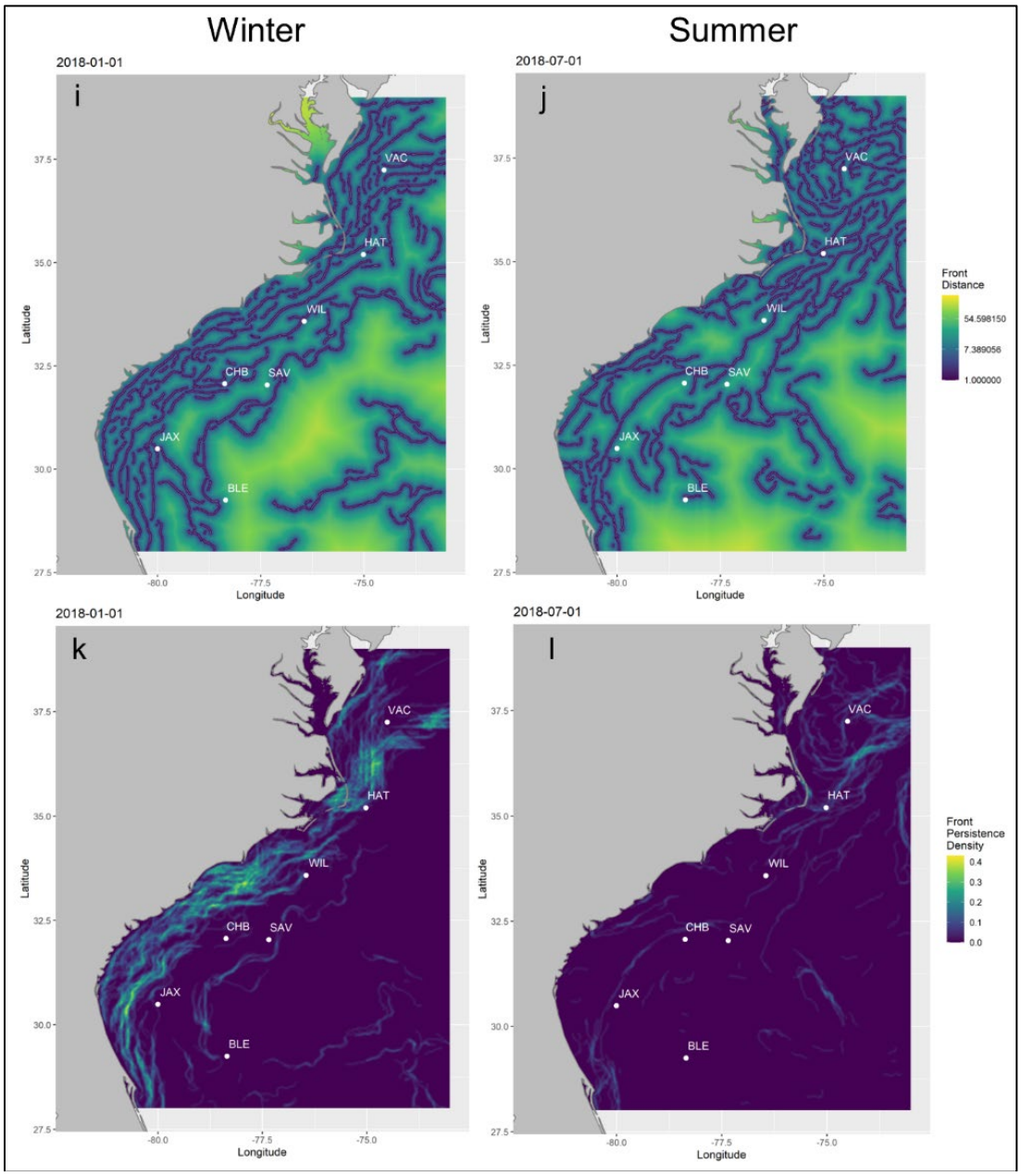

Figure 51. Maps showing key oceanographic variables for example days

Winter (date closest in time to 1 January 2018; left panels) and summer (date closest in time to 1 July 2018; right panels) are shown for the following variables: a–b) sea surface temperature (SST), c–d) chlorophyll *a* concentration (CHL), e–f) mixed layer depth (MLD), g–h) total kinetic energy (TKE), i–j) front distance and k–l) front persistence density.

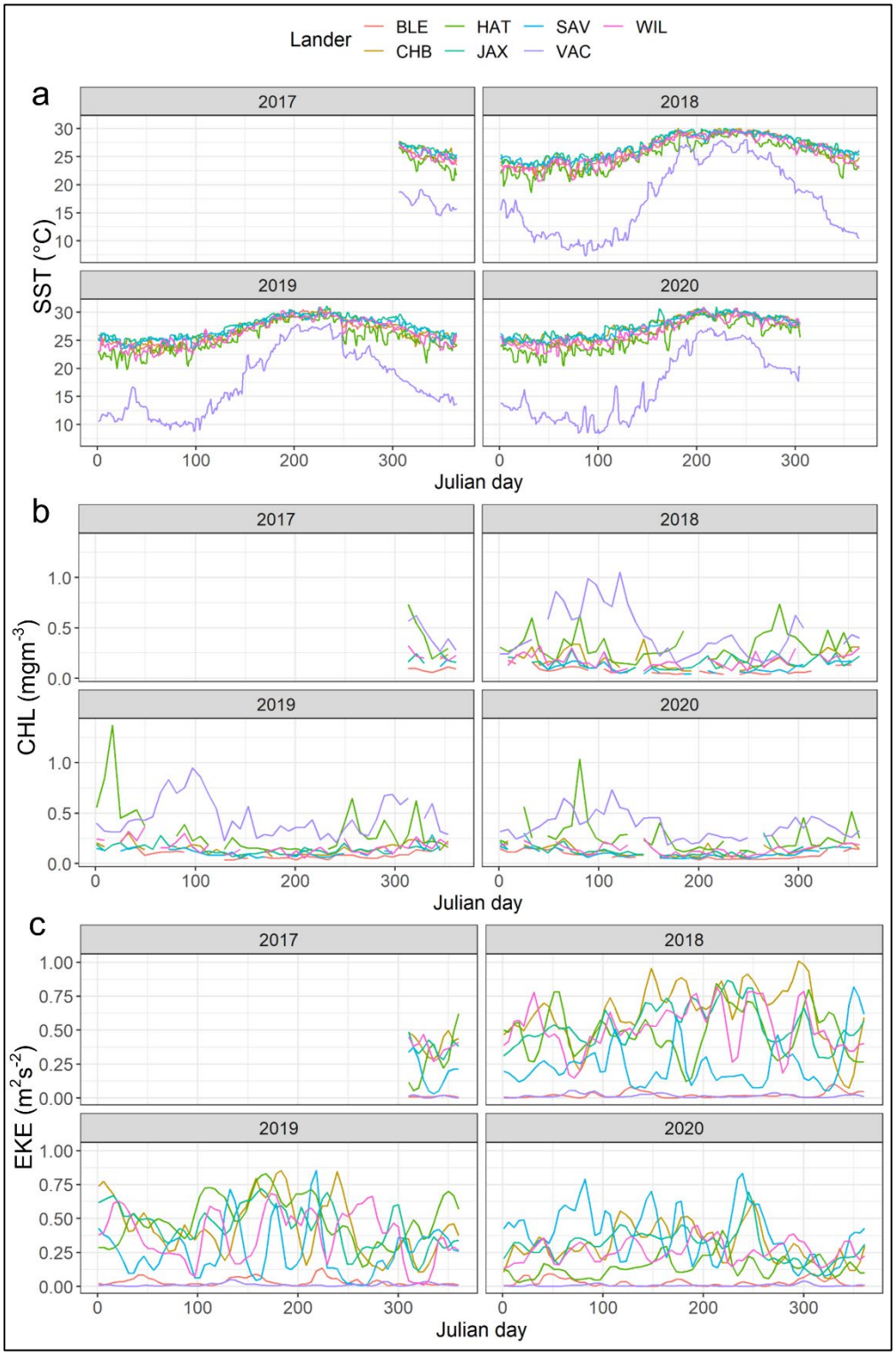
Lander
BLE
CHB
HAT
JAX
SAV
VAC
WIL
a
2017
2018
2019
2020
SST (°C)
Julian day
b
CHL (mgm-3)
c
EKE (m2s-2)

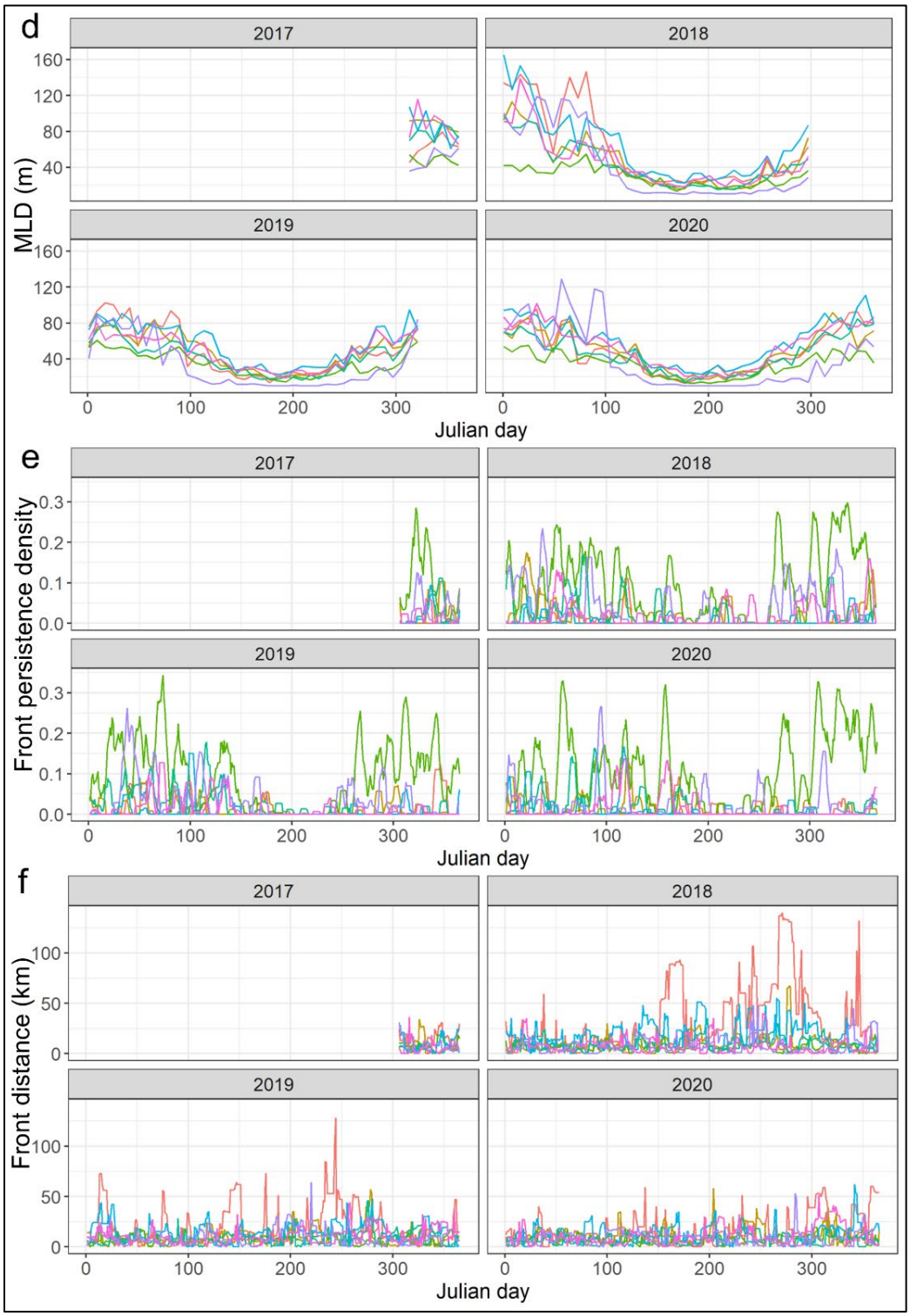

Figure 52. Time series of oceanographic variables at each lander site in each year (2017–2020)

a) sea surface temperature (SST), b) chlorophyll *a* concentration (CHL), c) total kinetic energy (TKE), d) mixed layer depth (MLD), e) front persistence density and f) front distance.

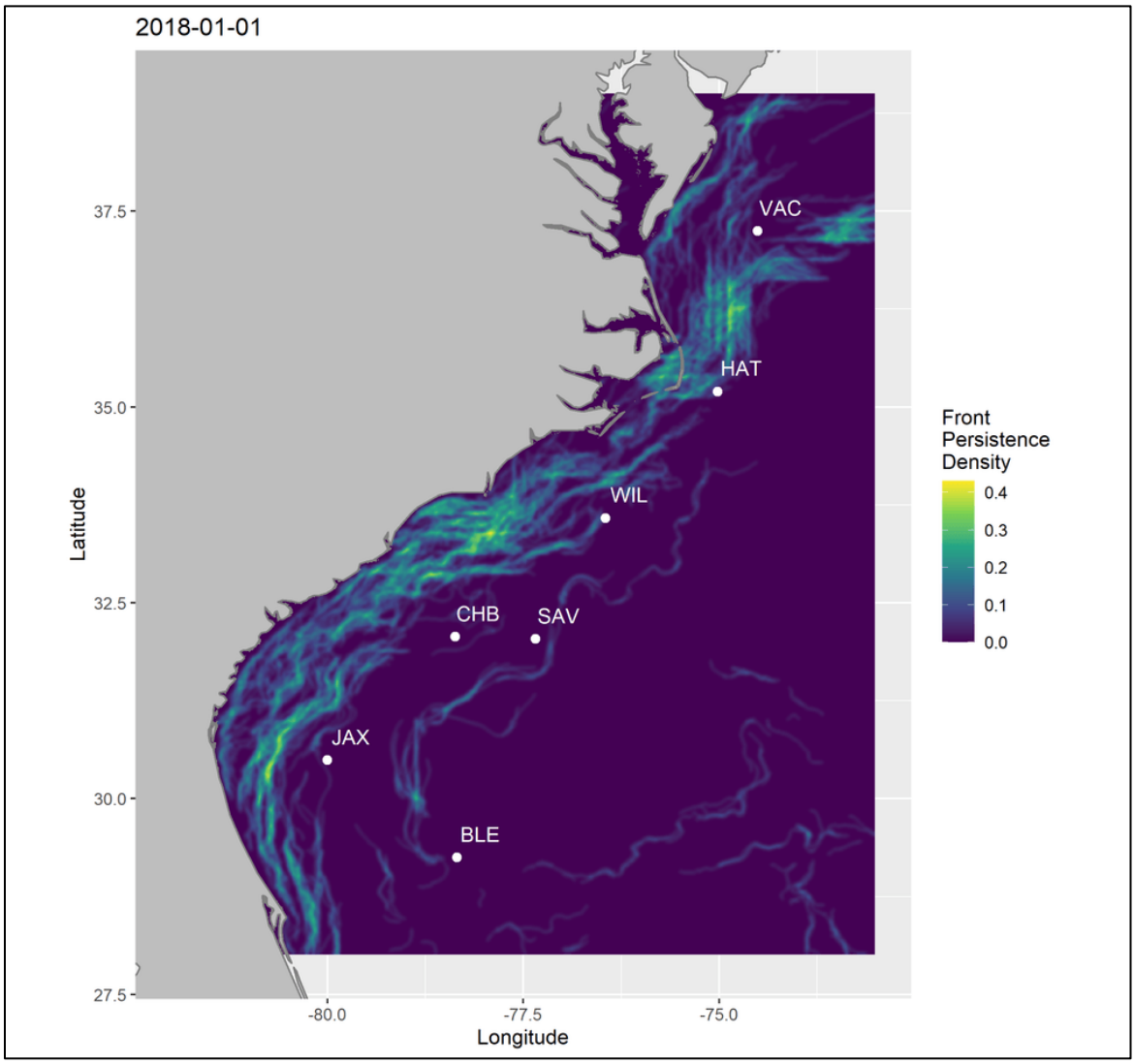

Figure 53. Daily map example of frontal persistence density for the study region

Data shown is from 1 to 31 January, highlighting the position of many of the lander sites within a dynamic region of frontal activity associated with the Gulf Stream Current, particularly during winter.

AZFP data were recorded at three lander sites: HAT, JAX, and VAC. Prey vertical distribution in the water column was generally higher during darkness than daylight, particularly at JAX (Figure 54). Prey was also highest in the water column at JAX and lowest at HAT. Prey were more aggregated at HAT and VAC than JAX and there was a clear seasonal peak in aggregation of prey at VAC in spring 2018 that was not apparent in 2019 (Figure 55). There were no obvious differences in prey abundance according to lander site and day compared to night, but substantial daily variation at all sites (Figure 56).

GAMs performed well for centre of mass and aggregation (based on deviance explained), but less so for abundance (Table 18). Lander was the most important variable for centre of mass and aggregation, but was not significant for abundance, indicating that prey biomass did not appear to vary substantially between regions. SST, total kinetic energy (TKE), and frontal distance and persistence were important variables for all metrics, while finite size Lyapunov exponent (FSLE) and mixed layer depth (MLD) were important just for centre of mass and aggregation, and chlorophyll *a* and day vs night were just important

for centre of mass and PAR just for aggregation and abundance. Surprisingly, there was no effect of lunar illumination of any metric.

Prey were distribution higher in the water column (Figure 57), were less aggregated (Figure 58) and less abundant (Figure 59) in colder waters. With decreasing distance to fronts, prey were deeper, less aggregated and moderately less abundant, and with increase frontal persistence, prey were also deeper, but more aggregated and abundant. Higher chlorophyll *a* concentration (CHL) resulted in shallower distributions. Models were able to predict seasonal patterns in prey vertical distribution and aggregation fairly well, but did not appear to capture annual variation particularly well (e.g., at HAT) nor finer-scale daily-weekly changes (Figure 60).

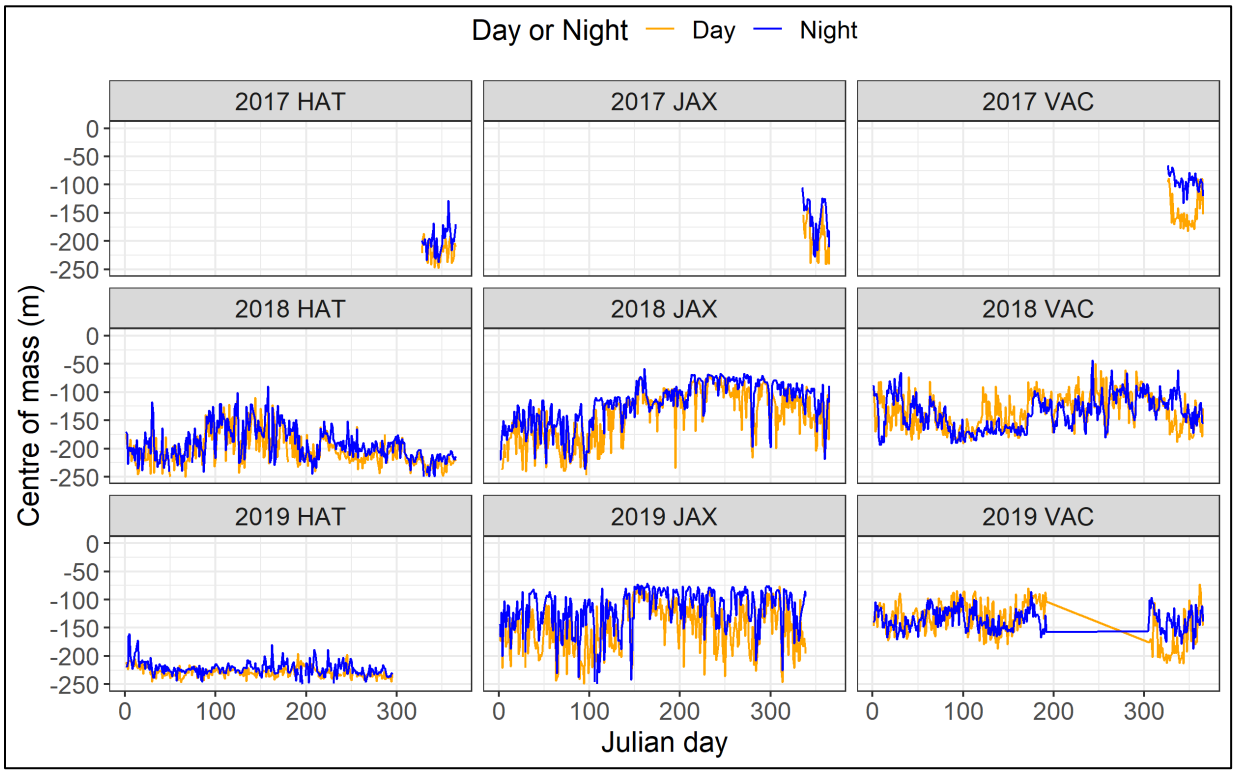

Figure 54. Daily time series of mean vertical distribution in the water column

Center of mass of prey during daylight (Day; four hours either side of midday) and darkness (Night; four hours either side of midnight) for the three lander sites (HAT, JAX, and VAC) with AZFP data in 2017–2019.

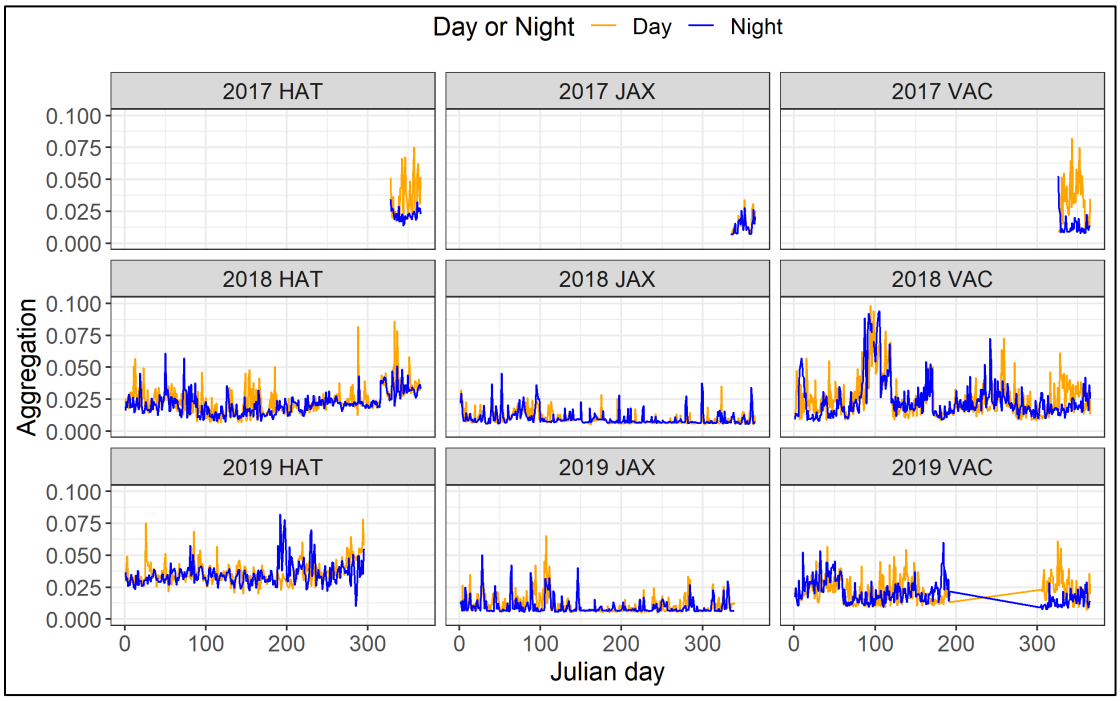

Figure 55. Daily time series of mean aggregation of prey

During daylight (Day; four hours either side of midday) and darkness (Night; four hours either side of midnight) for the three lander sites (HAT, JAX, and VAC) with AZFP data in 2017–2019

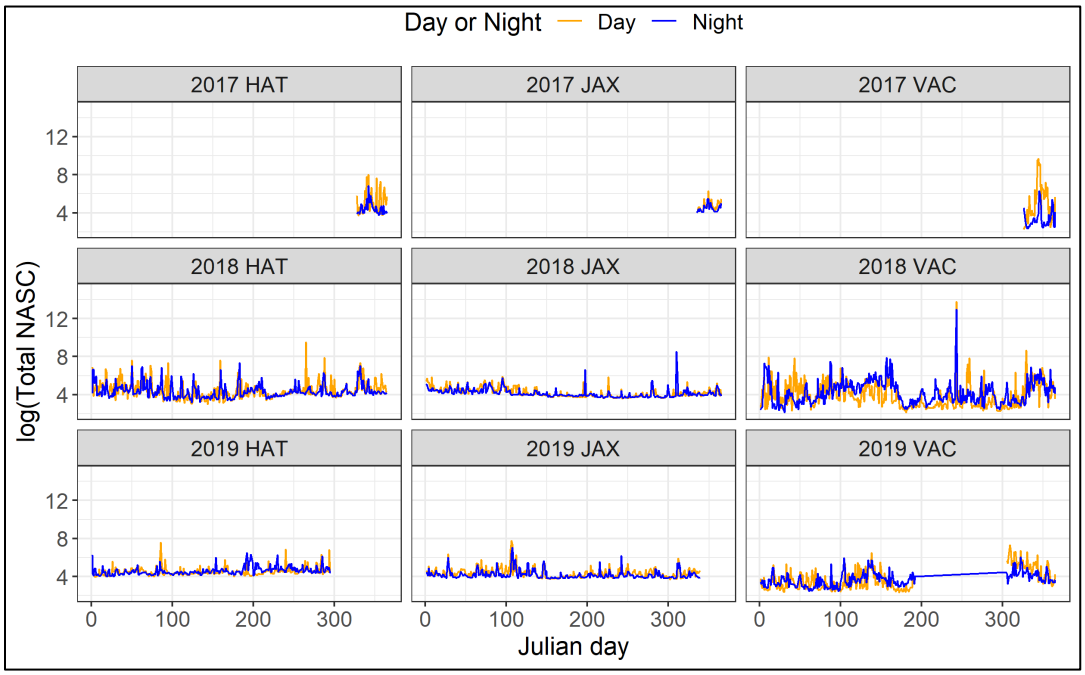

Figure 56. Daily time series of mean abundance (i.e., total NASC) of prey

During daylight (Day; four hours either side of midday) and darkness (Night; four hours either side of midnight) for the three lander sites (HAT, JAX, and VAC) with AZFP data in 2017–2019.

Table 18. Deviance explained by minimum adequate generalized additive models (GAMs) explaining the oceanographic drivers of variation in distribution and abundance of prey in the water column

Covariate	Abbreviation	Centre of mass	Aggregation	Abundance
Total		64.9	53.7	15.8
Chlorophyll *a* concentration	log.CHL_mean	6.0	-	-
Day Night	-	1.0	-	-
Distance to 200 m isobath	-	9.2	41.7	-
Total kinetic energy	sqrt.TKE_mean	12.8	4.6	2.1
Finite size Lyapunov exponent	sqrt.FSLE_mean2	8.0	7.7	-
Lander	-	53.4	46.1	-
Lunar illumination: Day Night	-	-	-	-
Mixed layer depth	log.MLD_mean	7.8	0.8	-
Photosynthetically available radiation	PAR_mean	-	2.9	4.1
Sea surface temperature	SST_mean	11.8	12.3	4.6
Front distance	log.Fdist	4.6	3.8	2.6
Front persistence density	sqrt.Fpers	17.8	8.0	5.0
Wind speed	-	-	-	-

The deviance explained by each final model is provided in bold. The deviance explained (%) by each covariate provides a relative indication of its importance and is based on standalone models with just that variable as a covariate. - = variable was not included in the minimum adequate model.

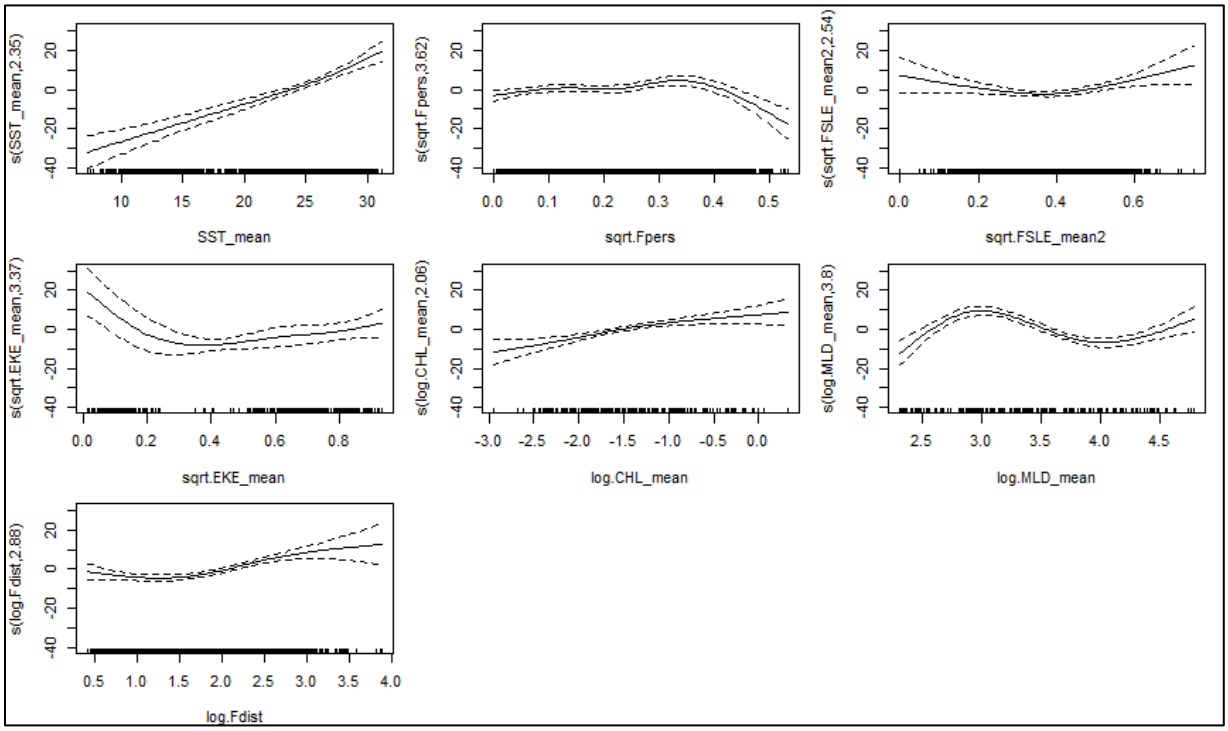

Figure 57. Partial plots for the minimum adequate generalized additive model (GAM) model explaining temporal variation in prey vertical distribution

See Table 19 for detail on covariate abbreviations.

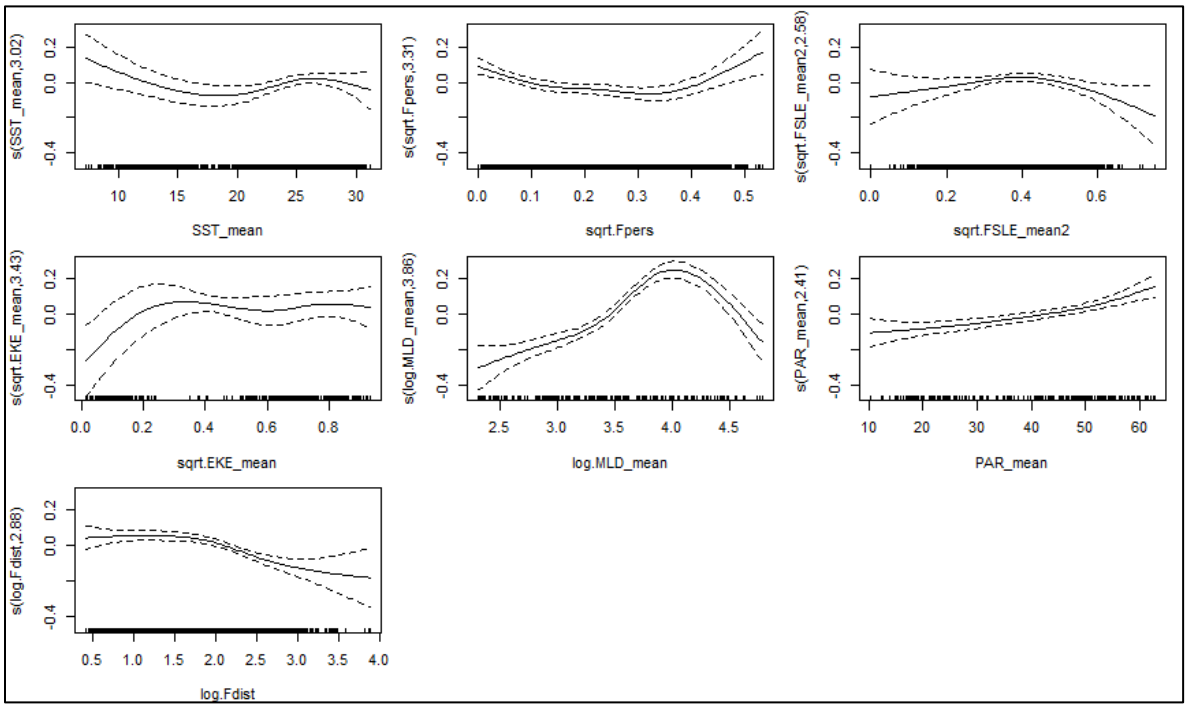

Figure 58. Partial plots for the minimum adequate GAM model explaining temporal variation in prey aggregation

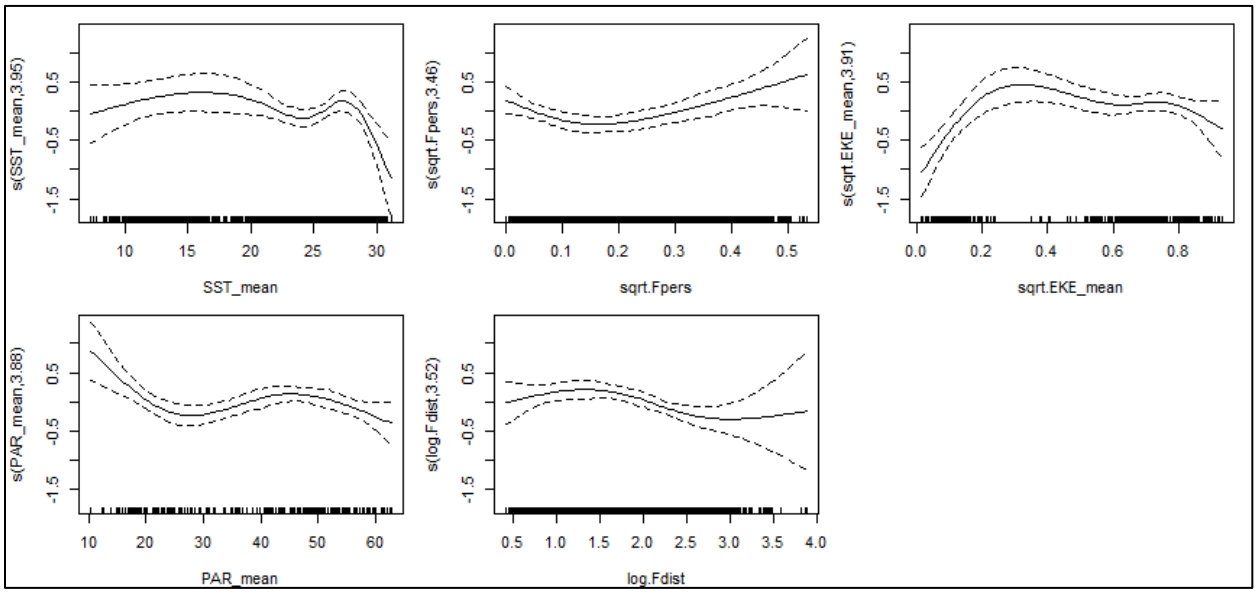

Figure 59. Partial plots for the minimum adequate GAM model explaining temporal variation in prey abundance

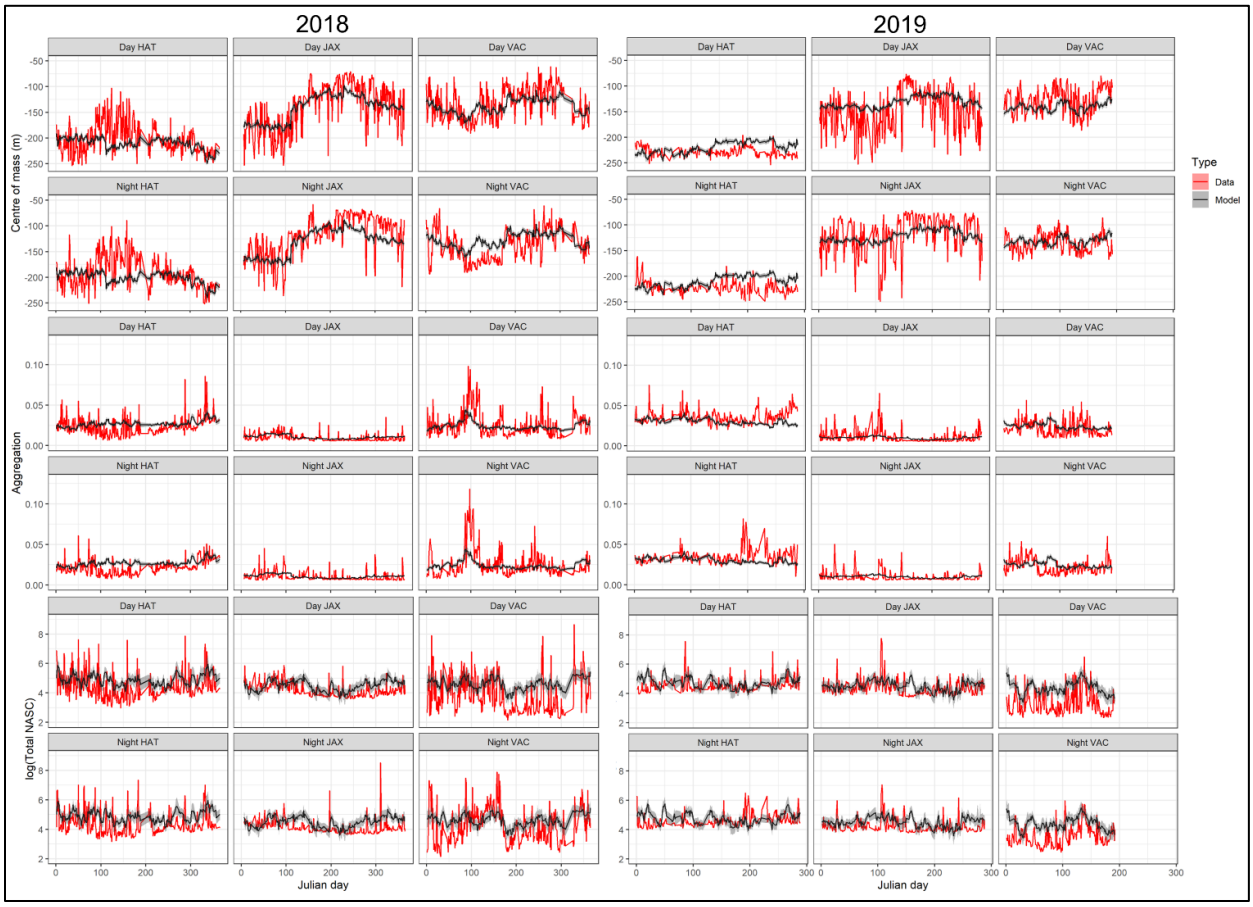

Figure 60. Predictions from minimum adequate GAMs explaining temporal variation in prey centre of mass (top two rows); prey aggregation (middle two rows) and prey abundance (bottom two rows). Plots are presented for daylight and darkness and for each lander (HAT, JAX, and VAC) in 2018 and 2019. The empirical data are shown by a red line and the mean and 95% confidence intervals of model predictions are shown by a black line with grey shading, respectively.

AMAR data were recorded at all seven lander sites. There was large variation in cetacean time spent according to species group, lander, season and year (Figure 61). Dolphin and beaked whale activity was highest at VAC increasing in late 2018 and throughout 2019. There was also year-round foraging activity of both species groups at HAT with a peak of DPH in the first months of both 2018 and 2019. They were also detected throughout the year at BLE and CHB and to a lesser extent WIL and SAV. In contrast, pilot whales were detected for shorter durations per day and more intermittently, but with a notable peak during the 2018 fall and in the first half of 2019 at VAC. Sperm whales were detected least often, but when present were recorded vocalizing in up to 8 hours per day. Like the other species, there was a notable seasonal peak in sperm whale activity in early 2019 at VAC.

The best models fit the data well for dolphins and beaked whales (deviance explained >60%) and moderately well for pilot and sperm whales (>30%) (Table 19). Lander was consistently an important variable indicating regional variation in detections for all species. Similarly, SST and front distance were important in all models. CHL and TKE were important for all groups except pilot whales, PAR for all groups except sperm whales, and front persistence for all except beaked whales. Low SSTs resulted in

increased foraging activity for dolphins (Figure 61), beaked (Figure 63) and sperm whales (Figure 64), but for pilot whales (Figure 62), moderate SSTs resulted in increased DPH. For dolphins, beaked and pilot whales, foraging activity increased when fronts were in close proximity to the lander, however there was a negligible effect for sperm whales, which responded more to increased frontal persistence. CHL and photosynthetically available radiation (PAR) had variable effects depending on the species group. Models predicted seasonal and annual patterns in DPH well for all species, particularly at VAC, however, did not capture finer-scale variability at the daily-weekly level (Figure 65).

Table 19. Deviance explained by minimum adequate GAMs explaining the oceanographic drivers of variation in the activity of cetaceans

Covariate	Abbreviation	Dolphins	Pilot whales	Beaked whales	Sperm whales
Total	-	61.7	33.4	66.2	39.6
Chlorophyll *a* concentration	log.CHL_mean	32.1	-	35.1	16.5
Distance to nearest vessel	log.Dist_ship	15.3	-	-	-
Total kinetic energy	sqrt.TKE_mean	15.9	-	21.6	17.7
Finite size Lyapunov exponent	sqrt.FSLE_mean2	13.7	-	-	13.7
Lander	-	50.0	23.4	54.6	25.5
Lunar illumination	Lunar	0.1	0.7	<0.1	-
Mixed layer depth	log.MLD_mean	-	-	4.9	1.6
Photosynthetically available radiation	PAR_mean	5.1	2.9	7.3	<0.1
Sea surface temperature	SST_mean	46.4	14.3	54.6	14.3
Front distance	log.Fdist	4.9	4.2	3.6	0.6
Front persistence density	log.Fpers	8.8	4.8	-	3.1
Wind speed	sqrt.WS_mean	0.3	1.2	0.2	2.7

The deviance explained by each final model is provided in bold. The deviance explained (%) by each covariate provides a relative indication of its importance and is based on standalone models with just that variable as a covariate. - = variable was not included in the minimum adequate model.

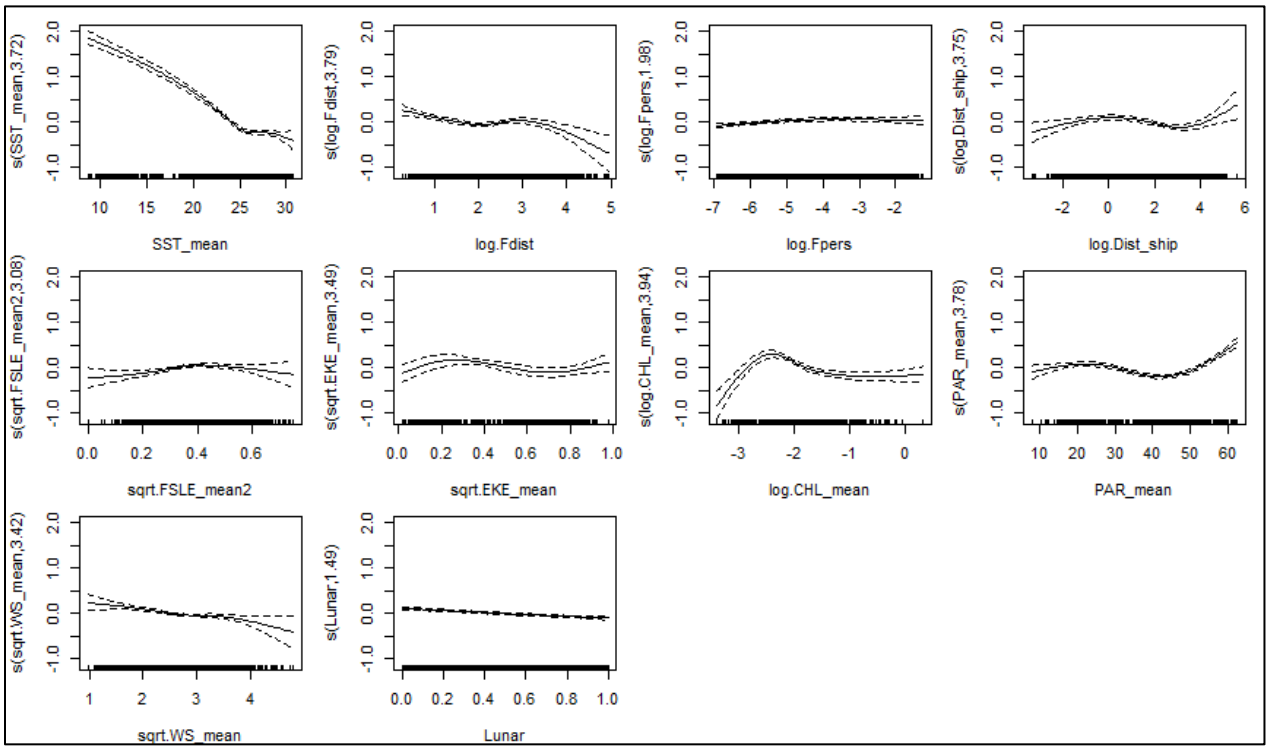

Figure 61. Partial plots for the minimum adequate GAM model explaining temporal variation in dolphin detection positive hours (DPH) in relation to oceanography

See Table 19 for detail on covariate abbreviations.

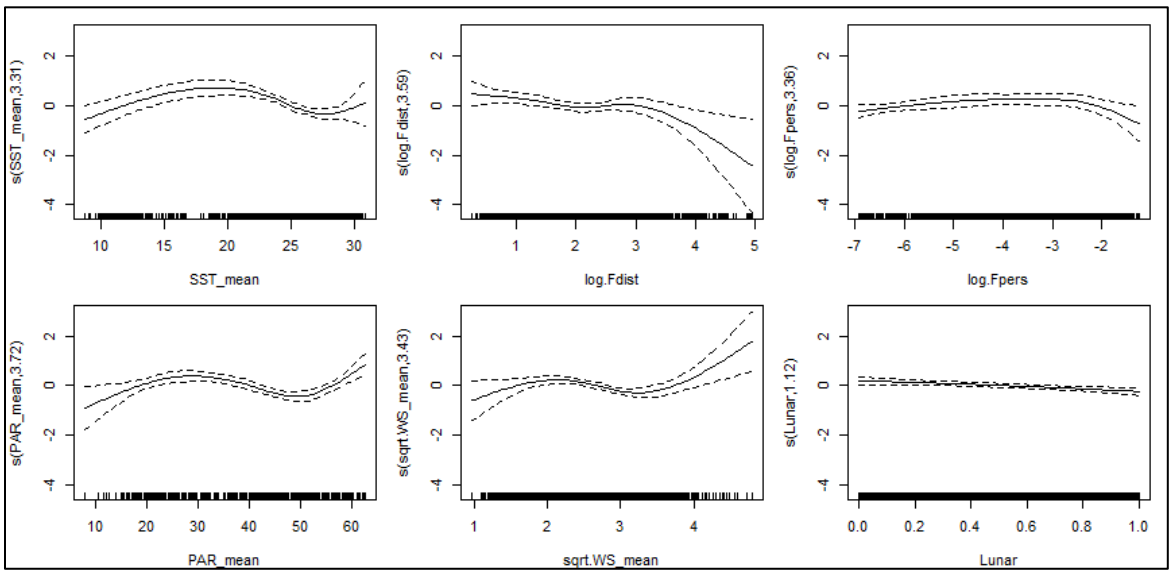

Figure 62. Partial plots for the minimum adequate GAM model explaining temporal variation in pilot whale DPH in relation to oceanography

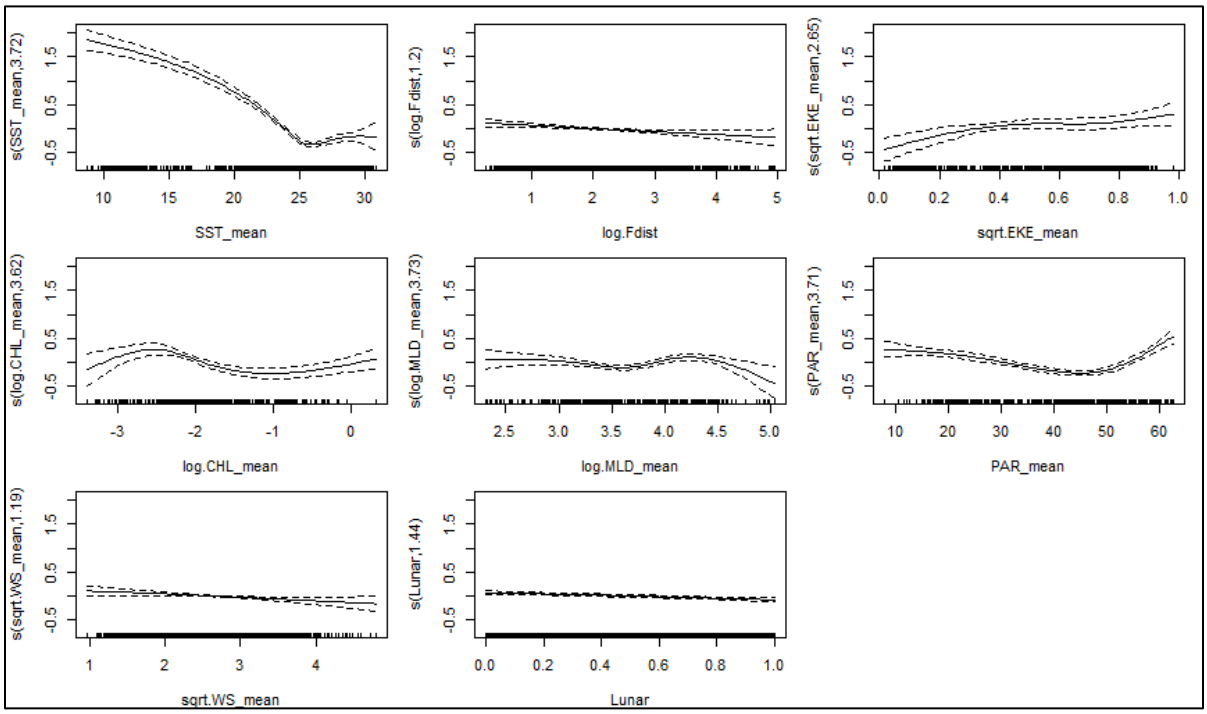

Figure 63. Partial plots for the minimum adequate GAM model explaining temporal variation in beaked whale DPH in relation to oceanography

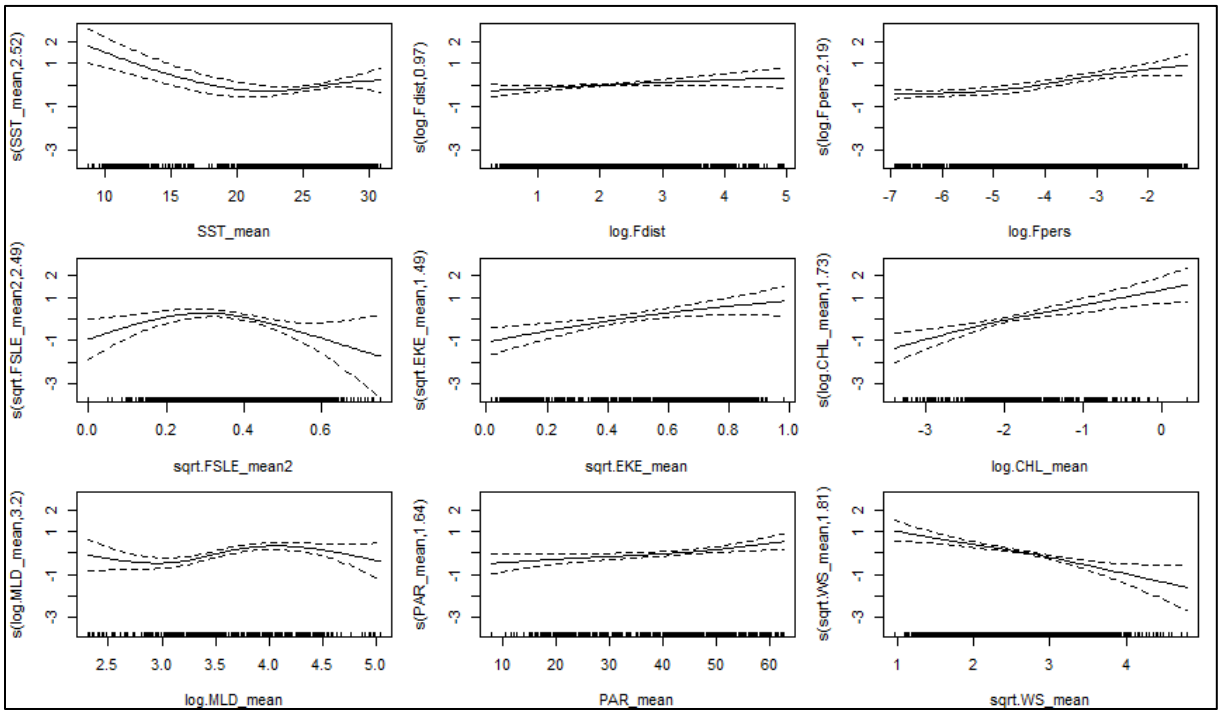

Figure 64. Partial plots for the minimum adequate GAM model explaining temporal variation in sperm whale DPH in relation to oceanography

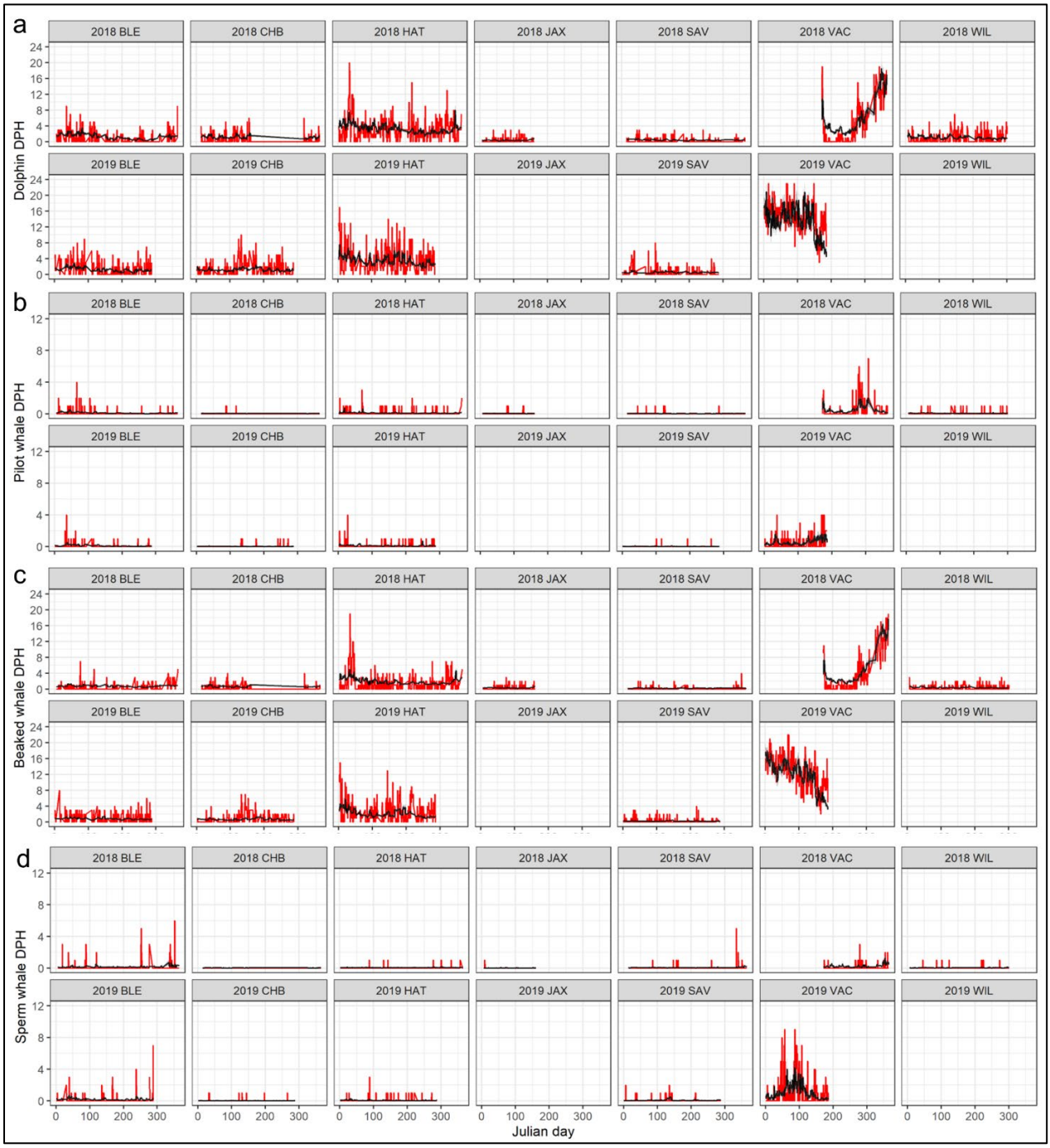

Figure 65. Predictions from minimum adequate GAMs explaining temporal variation

in a) dolphin detection positive hours (DPH), b) pilot whale DPH, c) beaked whale DPH, d) sperm whale DPH. Plots are presented for each lander (HAT, JAX, and VAC) in 2018 and 2019. The empirical data are shown by a red line and the mean and 95% confidence intervals of model predictions are shown by a black line with grey shading, respectively. Note that the y axes differ for dolphins and beaked whales and pilot and sperm whales.

GAMs looking at effect of both oceanography and prey on cetacean activity performed well and prey metrics were retained for all species except pilot whales: aggregation for dolphins, and centre of mass, aggregation and abundance for beaked and sperm whales (Table 20). The inclusion of prey metrics, however, only resulted in marginal increases (<1%) in total deviance explained relative to those models without prey included (Table 20). For dolphins, beaked and sperm whales there was a slight increase in cetacean foraging activity with increasing prey aggregation (Figures 66-68). Surprisingly, increased sperm and beaked whale activity was associated with lower prey abundance (total NASC) and shallower distribution (Figures 67 and 68).

Table 20. Deviance explained by minimum adequate GAMs determining the effect of both prey and oceanography on the activity of cetaceans

Covariate	Abbreviation	Dolphins	Pilot whales	Beaked whales	Sperm whales
Total with prey	-	67.5	36.7	71.6	55.8
Total without prey	-	67.2	-	70.8	55.8
AZFP centre of mass	CentreMass	-	-	12.2	13.6
AZFP aggregation	log.Aggregation	14.9	-	11.6	6.0
AZFP abundance	log.Abundance	-	-	12.3	17.0
Chlorophyll *a* concentration	log.CHL_mean	-	-	28.7	-
Distance to nearest vessel	Log.Dist_ship	3.7	-	5.3	-
Total kinetic energy	sqrt.TKE_mean	34.6	-	41.5	-
Finite size Lyapunov exponent	sqrt.FSLE_mean2	24.3	-	29.6	-
Lander	-	46.0	21.2	49.0	-
Lunar illumination	Lunar	<0.1	0.7	<0.1	-
Mixed layer depth	Log.MLD_mean	7.3	5.6	10.3	-
Photosynthetically available radiation	PAR_mean	8.7	5.0	12.3	0.7
Sea surface temperature	SST_mean	53.2	13.6	59.7	40.1
Front distance	Log.Fdist	2.3	5.6	2.0	3.7
Front persistence density	Log.Fpers	2.9	2.8	1.7	5.5
Wind speed	Sqrt.WS_mean	0.4	1.5	0.2	1.1

The deviance explained by each final model and by each model including just prey variables, are provided in bold. For each model including at least one prey covariate, the model was also run without prey variables and the total deviance compared between the two. The deviance explained (%) by each covariate provides a relative indication of its importance and is based on standalone models with just that variable as a covariate. - = variable was not included in the minimum adequate model.

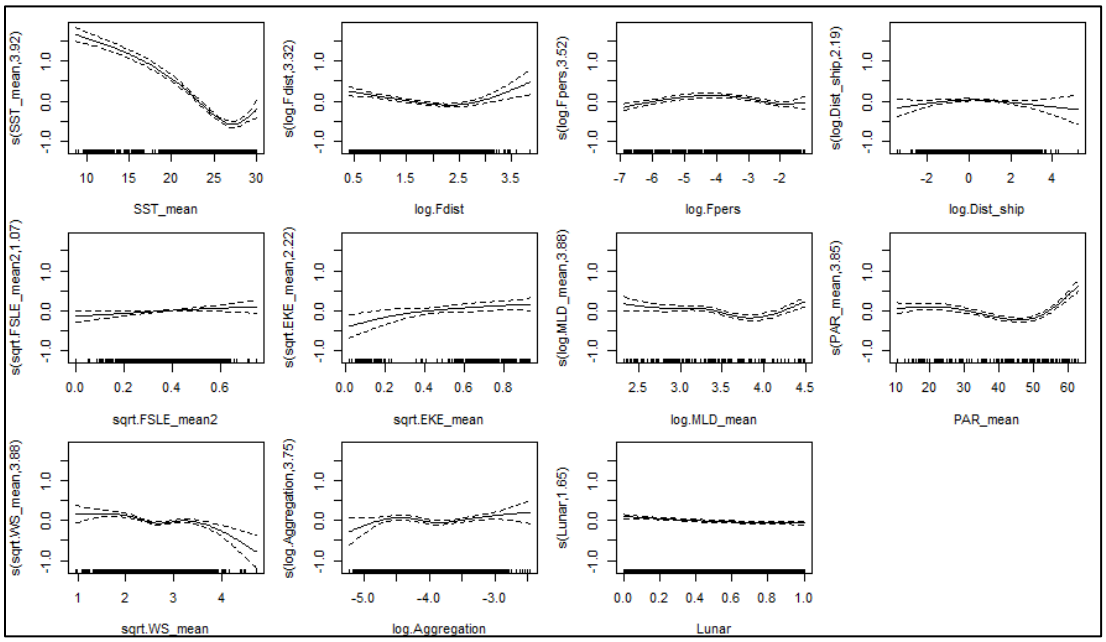

Figure 66. Partial plots for the minimum adequate GAM model explaining temporal variation in dolphin DPH in relation to oceanography and prey

See Table 20 for detail on covariate abbreviations.

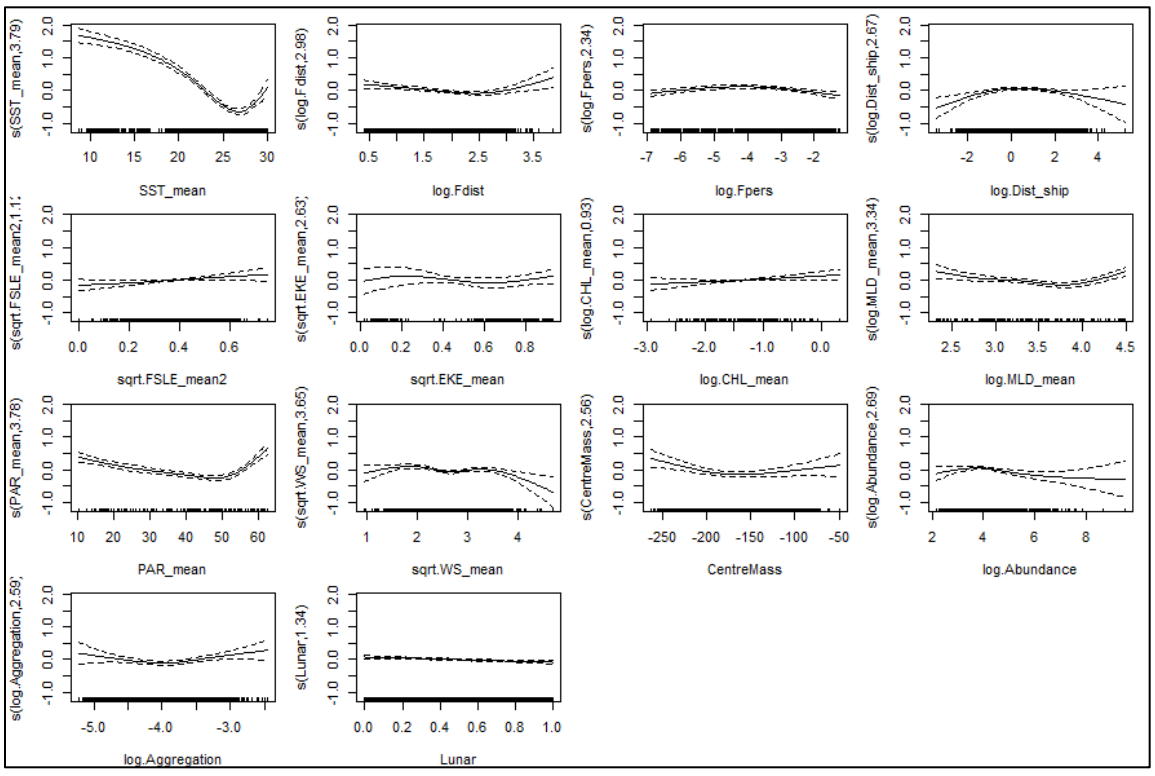

Figure 67. Partial plots for the minimum adequate GAM model explaining temporal variation in beaked whale DPH in relation to oceanography and prey

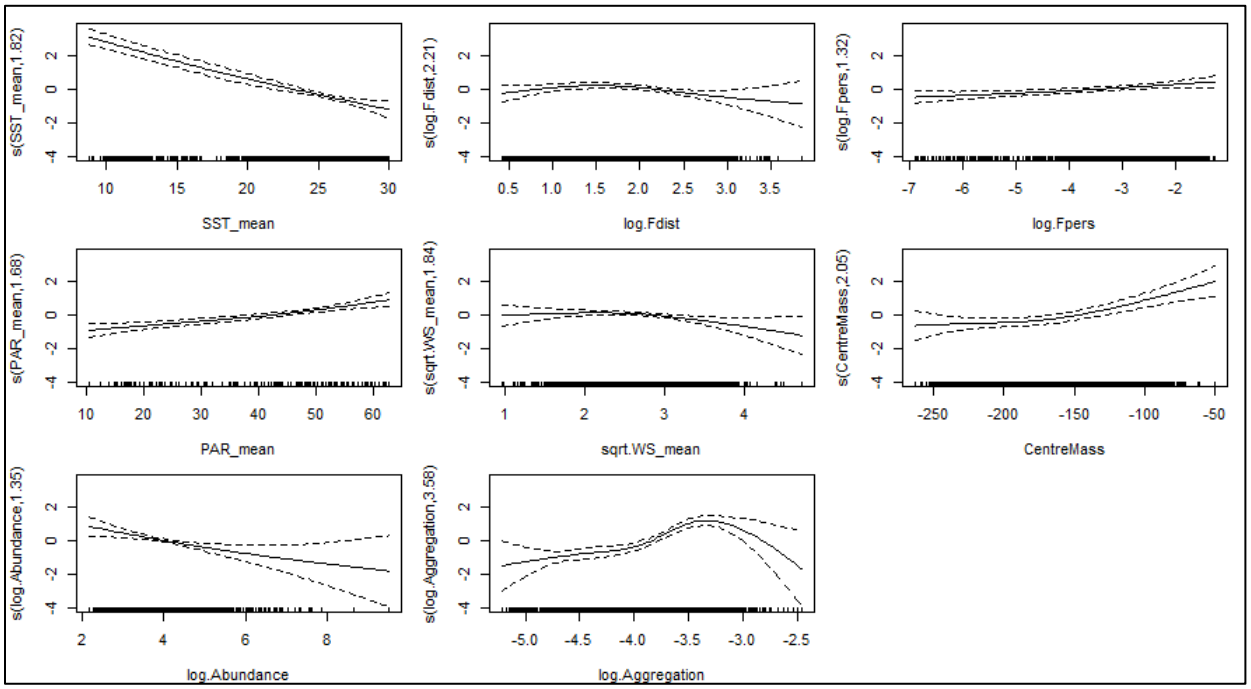

Figure 68. Partial plots for the minimum adequate GAM model explaining temporal variation in sperm whale DPH in relation to oceanography and prey

5.4 Visualization

The visualization portion of ADEON focused on the design and implementation of a web-based geospatial and acoustic visualization interface that allows anyone (researchers and the public) to easily explore the various massive datasets generated by the project to gain insight about the ecology and soundscape of the region. The massive size of the ADEON datasets (60+TB) presents many accessibility and visualization issues. It is difficult for researchers to download all of this data, due to both bandwidth and physical data storage limitations. Furthermore, finding what one is looking for in these files can be just as difficult, due to the overwhelming number and length of the recordings. Though these challenges can be overcome by researchers, they are barriers to exploration by members of the public. Beyond just the raw recordings, there are the many additional datasets produced by the project, such as the event detections based on different filters (e.g., dolphin clicks or seismic surveys) and 5D (lat/long/depth/frequency/time) modelled soundscapes of predicted sound energy levels for sound sources such as ships and surface winds. This visualization project component sought to build a single, cohesive visual interface for researchers both within and outside of the ADEON project to explore the acoustic data and the derived datasets, without having to download and store the data itself, or install any particular software.

5.4.1 Main Map Interface

Visitors to the public ADEON website can access an interactive map of the project region, which was built using the Leaflet JavaScript mapping interface (Leaflet, 2021). The map initially displays the locations of the hydrophone deployments over a bathymetric map, as shown in Figure 69. The

bathymetric map was included to show the intentional placement of the hydrophones in relation to the continental shelf. The underlying data is processed on a Linux-based server running CentOS 8 (CentOS, 2021). Mapping data is served using GeoServer (GeoServer, 2021) via Web Mapping Service for raster data (e.g., sea surface temperature), and Web Feature Service for point data (e.g., animal sighting locations). The Python-based Django web framework (Django, 2021) is used both as an interface to a PostgreSQL (PostgreSQL, 2021) database (which stores detection and supplemental data) and to serve the mapping site itself. The production website is broadly similar to this set up. The web map is built using the Leaflet JavaScript mapping library (Leaflet, 2021), enhanced with the (newly developed for this project) components for animated time sliders and environmental data legends. A sidebar interface allows users to toggle on and off the display of additional spatial datasets. This includes modeled soundscapes generated by the ADEON team, as well as environmental data layers, which provide important contextual information about the region during the times-of-interest being explored, such as the passing of a hurricane or where the Gulf Stream was bringing warmer water.

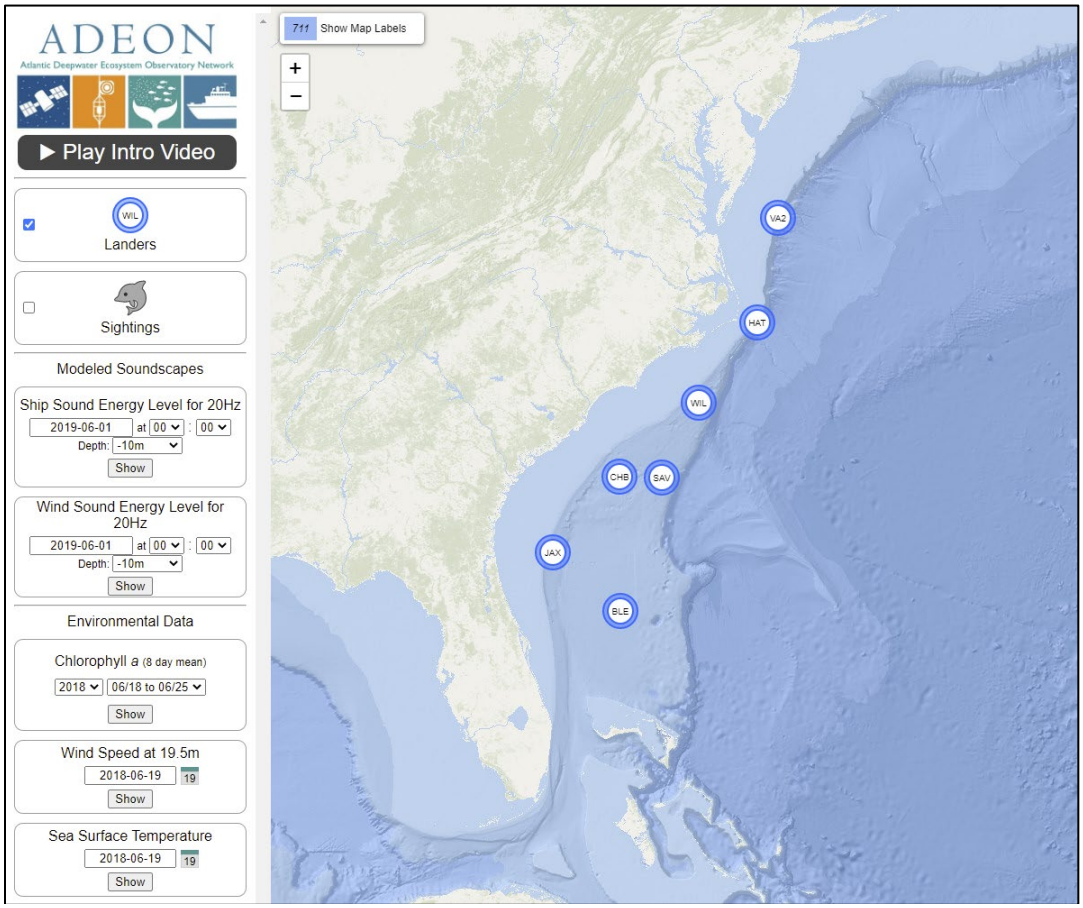

Figure 69. The initial view on the ADEON interactive map, showing hydrophone deployment locations over a hill-shaded bathymetry map of the continental shelf

Users can also choose to display marine animal sightings on the map. These are point-based records of animal sightings that occurred during the various ADEON crusies. Selecting this option will display small icons of various animals on the map where they were spotted. As shown in Figure 70, these appear mostly around the lander locations. Clicking on any of these animal icons will pop up an info panel with detailed information about that sighting event (e.g., species and time sighted).

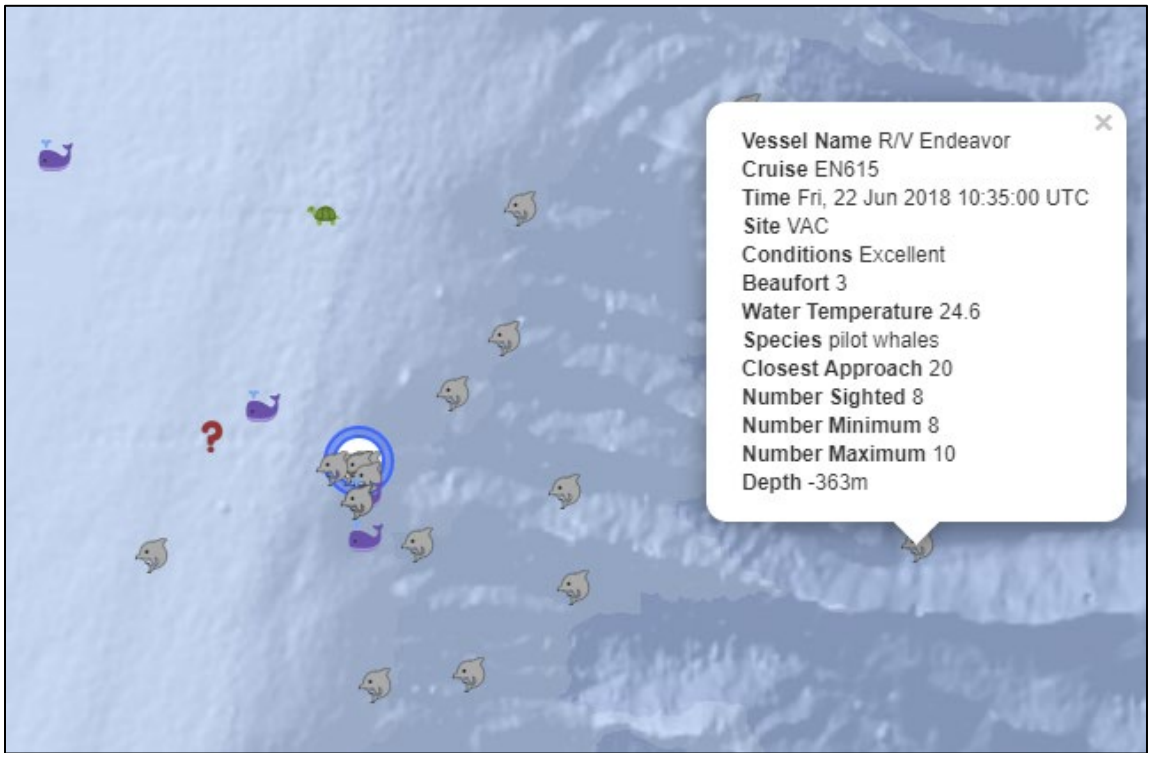

Figure 70. Marine animal sightings around the Virginia Inter-Canyon (VAC) lander site
One sighting has been selected and has an information panel above it, showing the species and other details.

5.3.2 Contextual Environmental Data Layers

Much of the sound detected at landers can be traced back to environmental factors in the surrounding sea and the atmosphere above. For example, surface winds can create high frequency sound, and the presence of high levels of chlorophyll can invigorate the food chain, attracting animals that make sounds. As such, a number of helpful layers of environmental data across the project region were provided that can help users make sense of the datasets. A chlorophyll layer, shown in Figure 71, was extracted from NASA satellite data, and shows the weekly chlorophyll concentration in the region, the presence of which could significantly affect marine mammal activity and movements. Due to limitations of cloud cover, this data layer often contains many large “holes” and regions with no data values. For display, these holes were preserved as transparent, but behind-the-scenes values were interpolated to fill the layer completely. This is done so one can pull complete time-series values for particular regions (e.g., at a lander location) for purposes of displaying contextual information in other interfaces (e.g., heat maps).

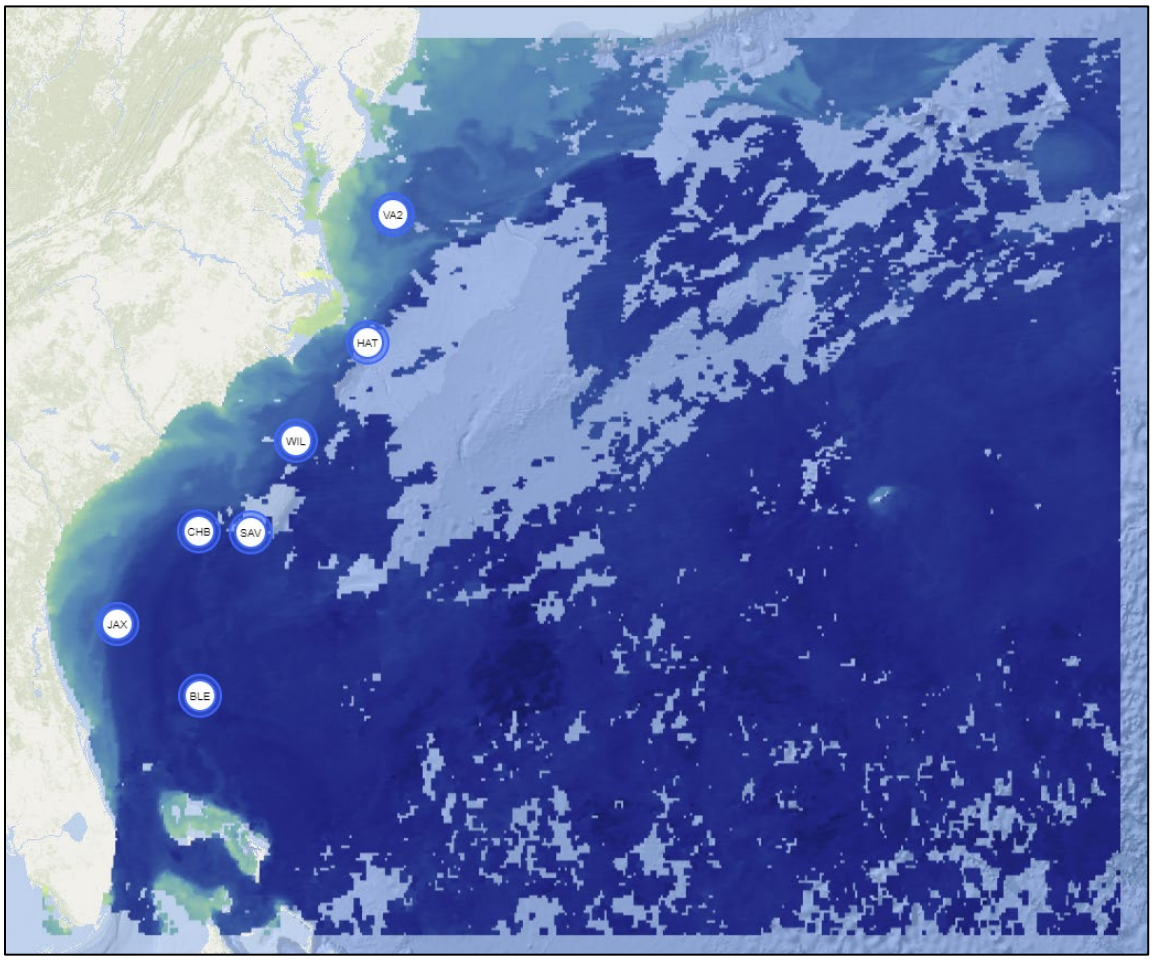

Figure 71. ADEON map displaying the chlorophyll layer

Notice the incomplete coverage (due to cloud cover) is preserved in this presentation.

A wind speed layer, shown in Figure 72, presents the near-sea surface (19.5m height) wind speed layer extracted from a larger weather model. As surface winds are a significant source of high-frequency sound, this can provide helpful contextual information as to why some regions of time and space may be noisier. For example, Figure 72 shows the passage of Hurricane Florence over a number of ADEON hydrophones in September 2018.

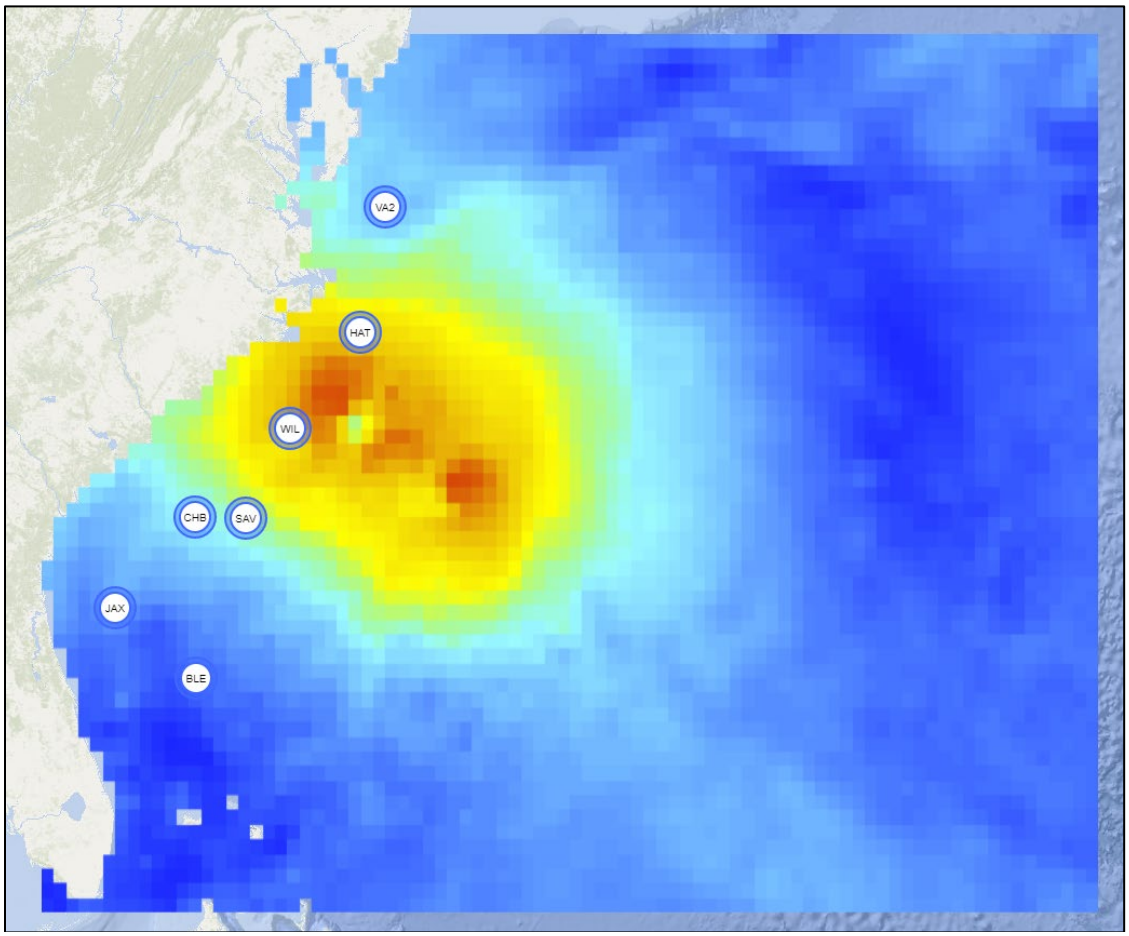

Figure 72. ADEON map displaying a wind speed layer from Sept 2018, in which Hurricane Florence passes over multiple lander locations

Finally, a sea surface temperature layer is available, as shown in Figure 73. These sea surface temperatures were extracted from the National Oceanic and Atmospheric Administration's (NOAA) Real-Time Ocean Forecasting Systems (RTOFS) model. These temperatures influence marine wildlife activity levels and migration, and so are helpful contextual data when exploring the other datasets such as event detections of marine mammal calls. This layer also clearly reveals the location of the Gulf Stream current.

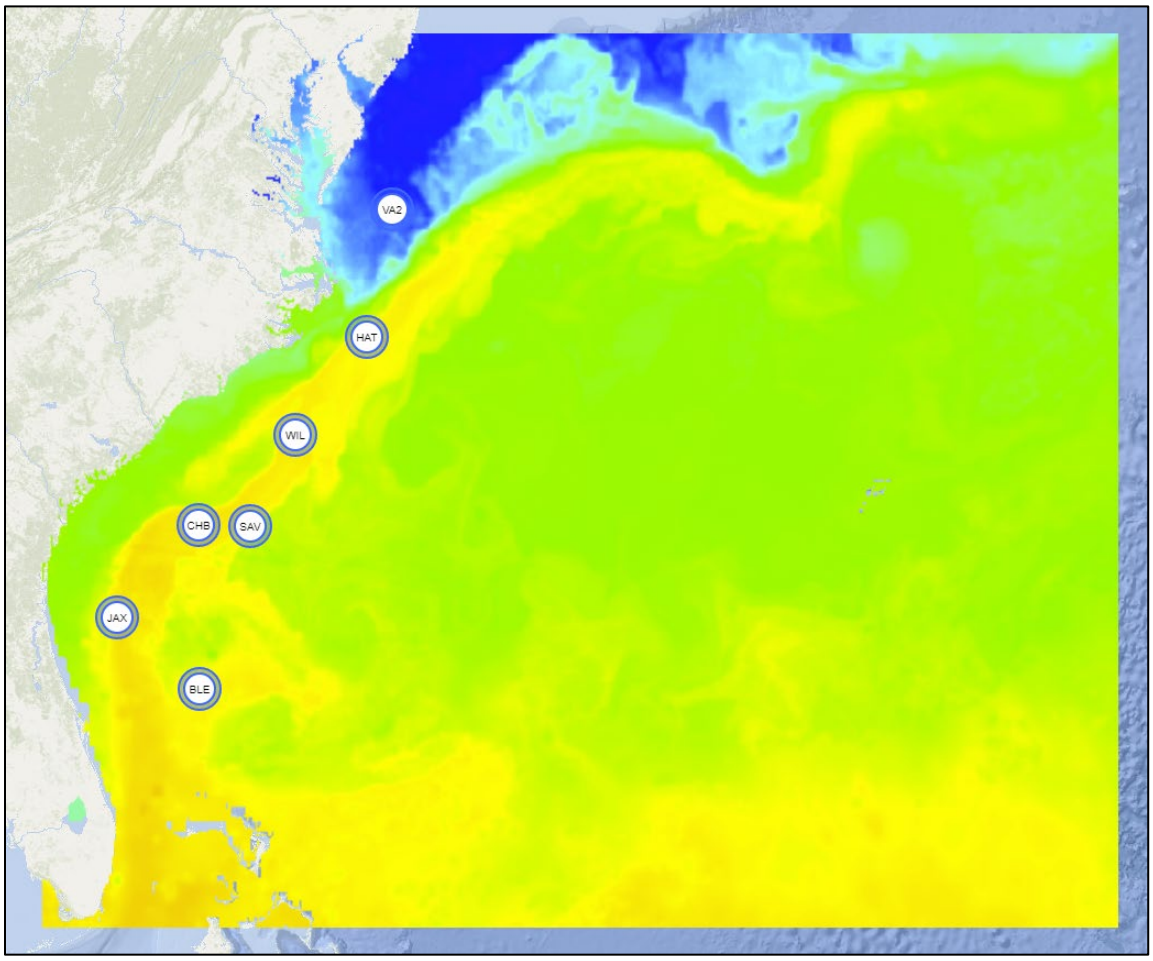

Figure 73. ADEON map showing the sea surface temperature data layer, which reveals the path of the warm Gulf Stream current over multiple lander sites, and the colder waters around the VA2 lander site

The environment datasets described above were compiled for this project by Dr. Tim Moore. Because the original sources were global datasets, they were cropped to the ADEON region using Geospatial Data Abstraction Library (GDAL) (to save storage space). Some of the source files ostensibly contained floating point decimal data, while actually containing integer data multiplied by a factor of ten (e.g., 611 instead of 6.11). In these cases, the values were converted to floating point values using the nco (NetCDF operator) utility. However, to simplify and reduce the amount of time needed to add environmental data to the production server, this step was removed in favor of integrating the 0.1 scaling factor into the code for the map legends, which was the only place where this distinction mattered for this project.

5.3.3 Modeled Soundscapes

The other main category of datasets that can be displayed on the main map is modeled soundscapes. These are 4D (lat/long/depth/time) model derived soundscapes that show the sound energy levels at particular frequencies across the ADEON project region as modelled from sound sources such as wind and ships. The wind soundscape, shown in Figure 74, displays the contribution of surface winds to ocean sound at a variety of depths and at the sea floor. The ship soundscape, shown in Figure 75, shows the modeled sound from surface ships (tracked using recorded AIS data) at different depths and at the sea floor.

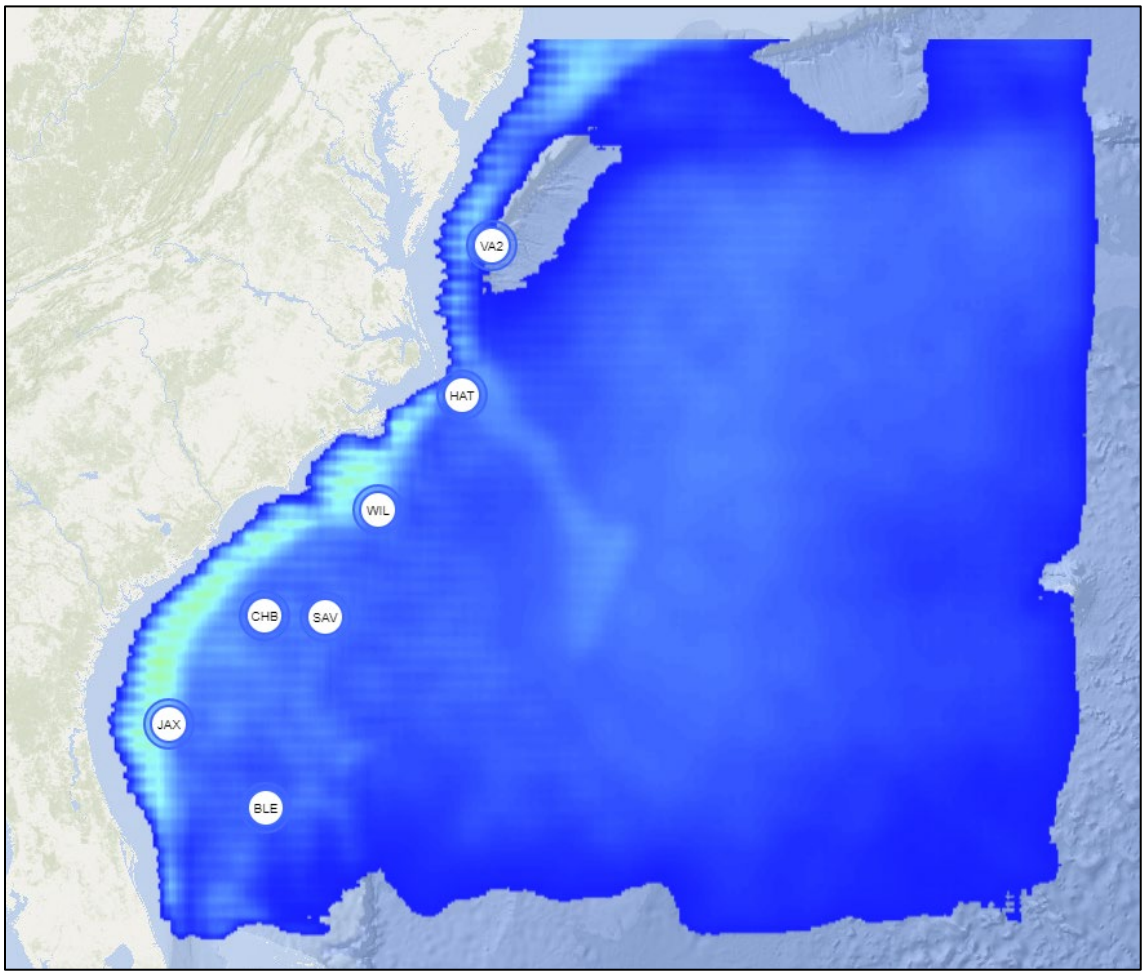

Figure 74. Modeled soundscape of wind sound in the ADEON region at a depth of 10 meters

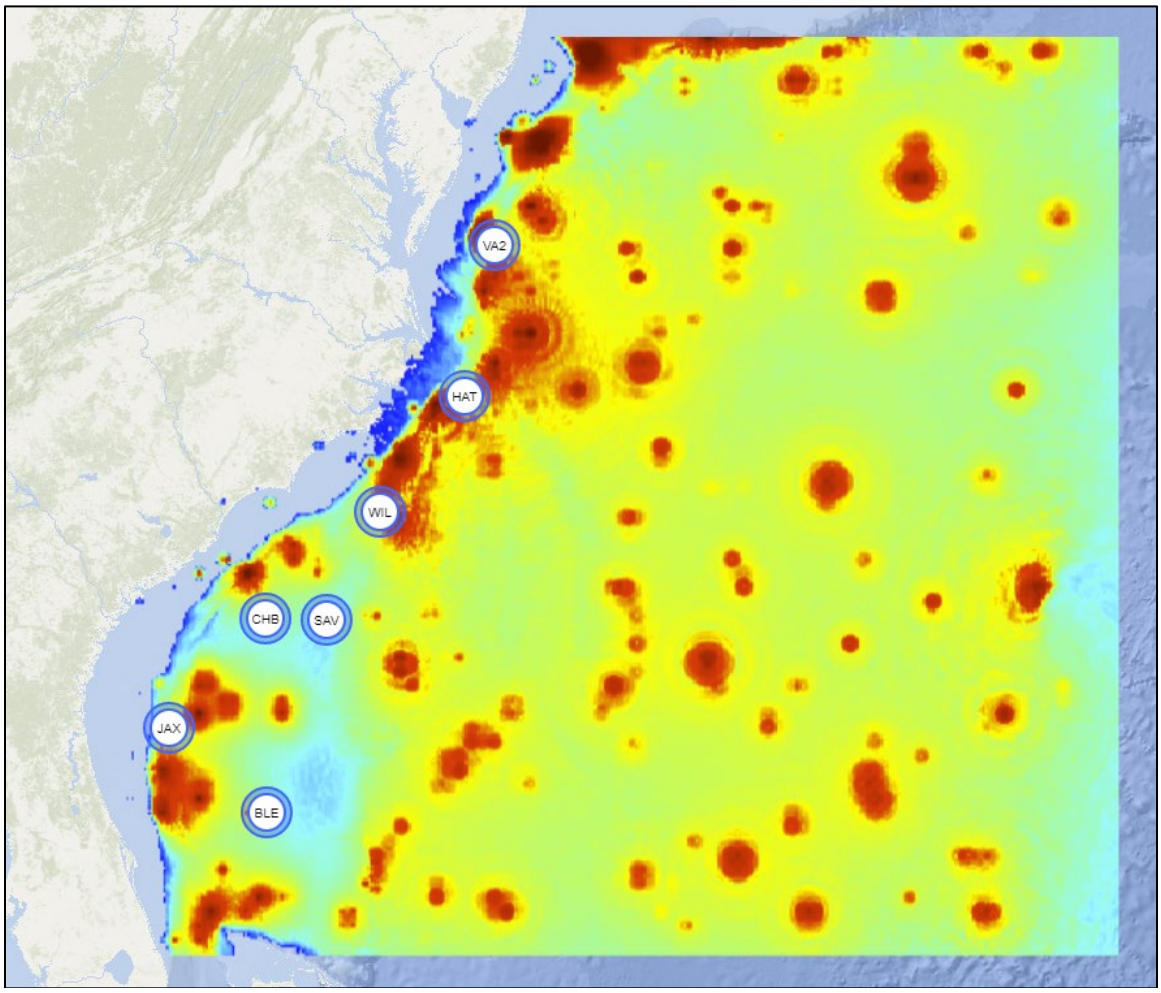

Figure 75. Modeled soundscape of ship sound (20 Hz) at the seafloor in the ADEON region

As part of this project, two custom Leaflet library components were developed. After completion, these components were then released back into the open-source software community, so that the public can reuse them in other web-based visualization projects. The first such component, shown in Figure 76, generates and displays legends for the various custom color maps (scales) used in the environmental and soundscape layers. The second component, shown in Figure 77, is a custom time-bar that is used to manipulate the time dimension of the mapping interface. It allows users to select the currently displayed time, step forward and backward through individual time steps, set time ranges for animations, and adjust the playback speed of animations.

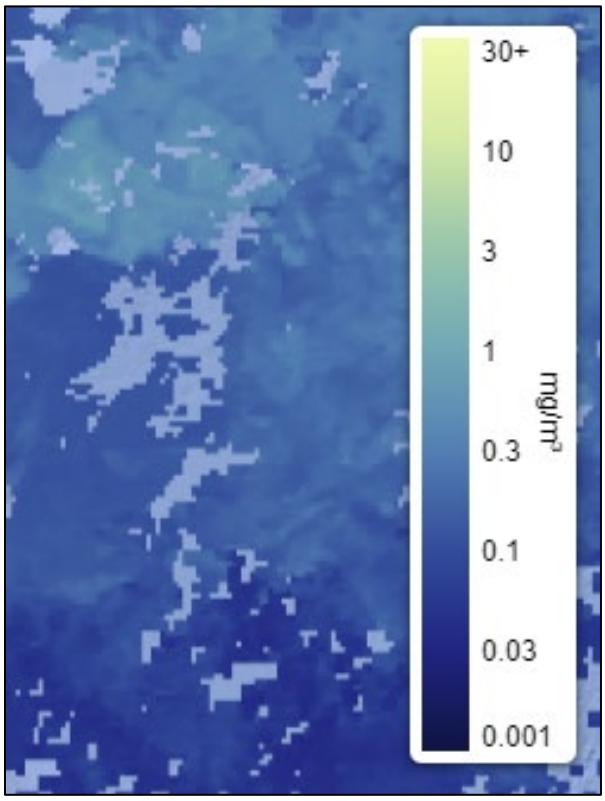

Figure 76. An example of the Leaflet component developed to provide customized color map legends

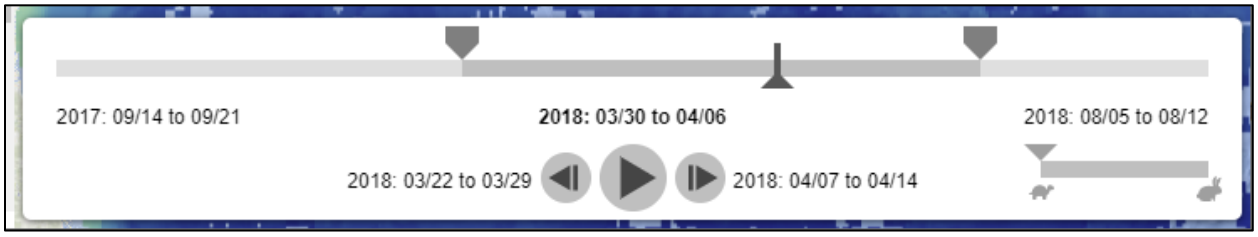

Figure 77. The time bar Leaflet component that is used to control which times are displayed, as well as the range and speed of animations

Selecting individual lander locations on the map will pop up visualization interface windows that are linked to those landers and provide multiple ways to visualize the data associated with them. As shown in Figure 78, multiple such interfaces can be opened simultaneously for multiple landers and can be rearranged to permit side-by-side comparisons between landers. These panels initially display basic information about the selected lander, and a series of tabs along the top provides access to the different visualizations available, including Heat Maps, Spectrograms, and Deviations.

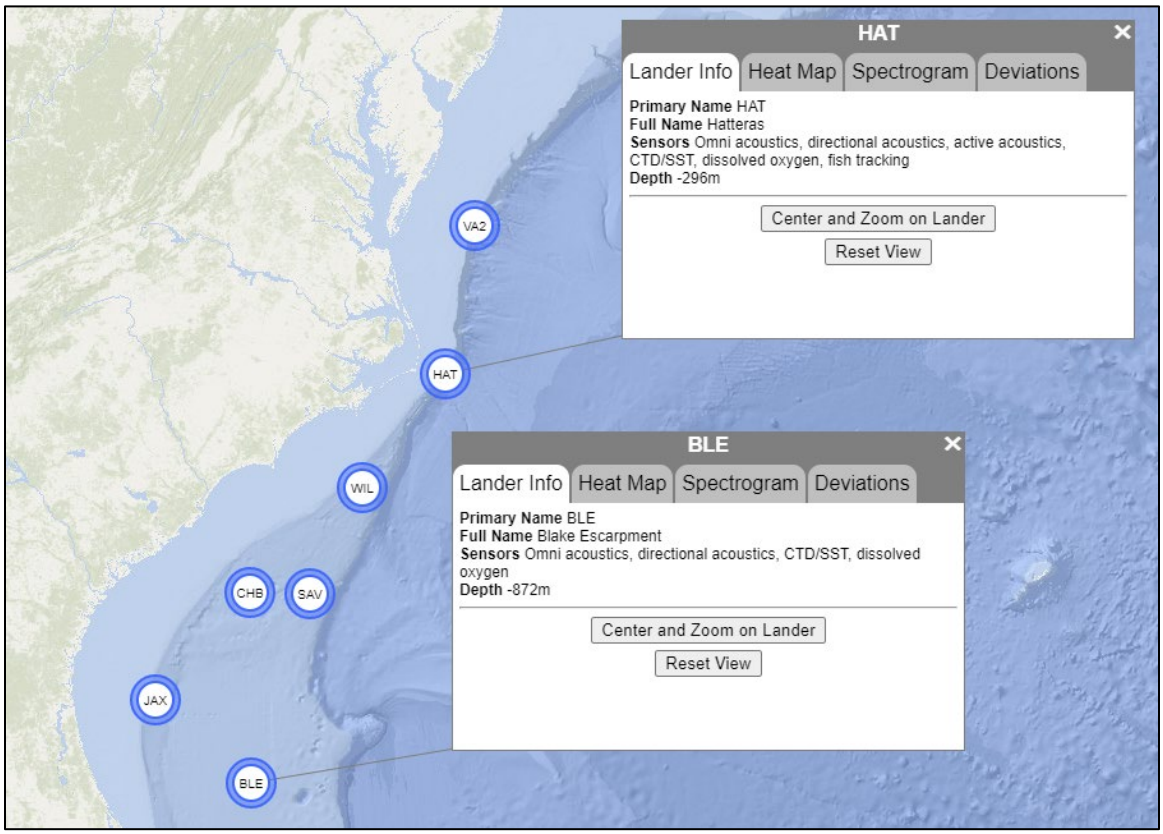

Figure 78. Example of two lander interface windows opened simultaneously
Note they are always visually linked to the associated lander locations on the map.

5.3.4 Heat Maps of Event Detections

The heat map interface, shown in Figure 79, provides an interactive visualization of the event detection datasets available for a lander location. The central heat map plot uses color intensity to indicate the number of detections that occurred within each one-hour cell. The plot is 24 cells tall, i.e., each column of cells represents a single day. While there was sufficient screen real estate to have more temporal granularity (e.g., 5 minutes/cell), this was the granularity of the datasets generated in this project.

An optional day/night indicator can be toggled on/off and can be helpful for revealing daylight-dependent animal behavior patterns, as can be seen with dolphin clicks in Figure 79. This option draws a wavy band across the plot, which indicates the hours of darkness, as calculated based on the lander's latitude and longitude. After some experimentation, it was decided that a visual style of using subtle, gray horizontal lines, behind the filled cells, was sufficient enough to provide this indication, without being distracting or imposing too much relative visual weight relative to the data cells.

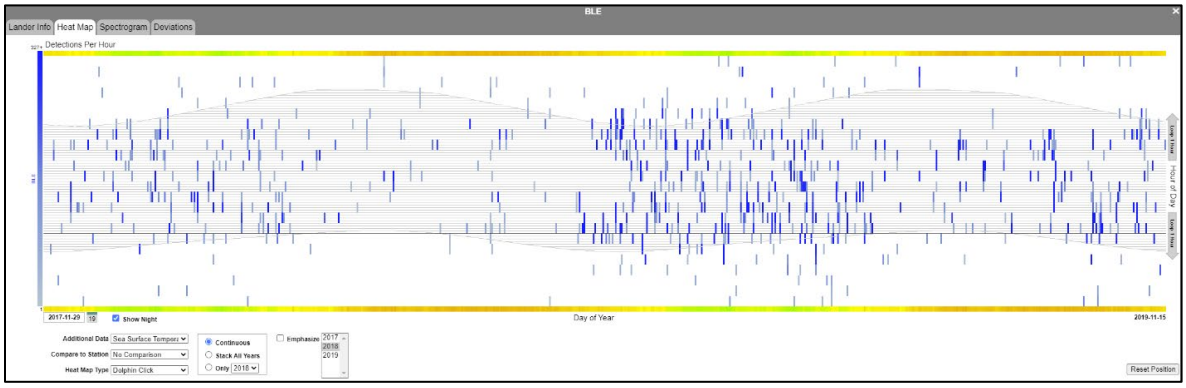

Figure 79. An example view of the heat map interface, showing a continuous plot of dolphin clicks detected around the BLE lander over a period of about two years

Notice that dolphin activity appears to correlate with the nighttime hours (line-shaded band across the plot) and cooler water temperatures (green vs orange/yellow in the colored bands above and below the plot).

The plot can be toggled between either a ‘continuous’ mode, in which the plot expands horizontally to fill the available screen space and displays all records in temporal order, or a ‘cyclic’ mode, which stacks each year of data on top of the other in a single plot 365 cells wide. The cyclic mode helps reveal patterns which repeat each year, and an ‘emphasis’ feature allows users to mouse over the year labels to indicate the contribution of each individual year to the overall stacked plot. As shown in Figure 80, this is done by de-saturating the content of cells with content from other years, thus highlighting the contribution of the selected year, while preserving the context of the other years. Arrow buttons below and to the side of the plot can be used to adjust the plot vertically and horizontally to change when wrapping occurs in terms of day of the year and time of day. This is useful because patterns can often straddle the standard, arbitrary midnight and December 31/January 1 wrapping boundaries, which can cause them to appear disconnected. By shifting the wrapping boundaries to noon and July 1, a pattern centered around winter nights would appear whole. (This is shown in Figure 80). Optional contextual data bars can be toggled on/off. These appear redundantly at both the top and bottom of the plot to indicate contextual environmental values in the lander location during the times shown in the pot. This can reveal relationships between the patterns in the plot and surrounding conditions such as temperature, wind speeds, and chlorophyll. The ability to pull in values from the modelled soundscapes and display those will be added here as well. Figures 79 and 80 show examples of contextual data bars indicating sea surface temperature.

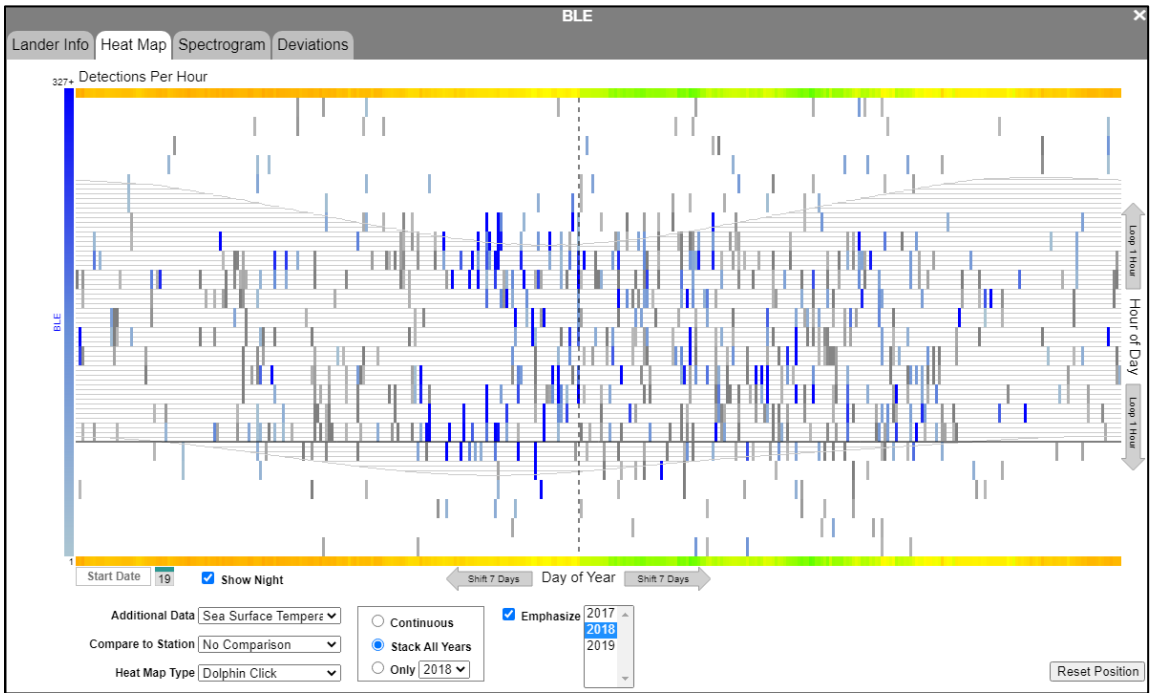

Figure 80. Example view of the heap map interface in stacked mode, showing dolphin clicks from all years (gray cells), but emphasizing those from 2018 (blue cells)

Notice the plot has been shifted to center the winter/night pattern, instead of wrapping it around the standard Dec 31–Jan 1 and midnight boundaries.

Comparisons between lander locations can also be made within this interface. By selecting a second lander location in the drop-down menu, the data from that lander will be drawn in the plot using a second color (Figure 81). One question that arises is how to display two values in a single cell that contains data from both landers. After some experimentation with mixing colors and other strategies, it was decided that cells with data from multiple landers would automatically subdivide and present the associated colors at their original intensity. This allows the viewer to visually search for a particular color and see the overall distribution of color. Though the subdivided cells add visual noise, the alternative solution of mixing colors (e.g., using purple to indicate lots of blue and red) was found to be difficult to interpret. Users can mouse-over cells in the plot to get more information about them. As shown in Figure 82, a small popup window follows the mouse cursor and displays the time that cell contains, and the number of detections in that hour period for the selected event type. If the plot is showing a comparison with another lander, mousing over subdivided cells will show the numbers of detections for both landers. Clicking on a heat map cell switches the visualization interface to the Spectrogram Viewer mode, which automatically centers its three views onto the time associated with the heat map cell that was clicked.

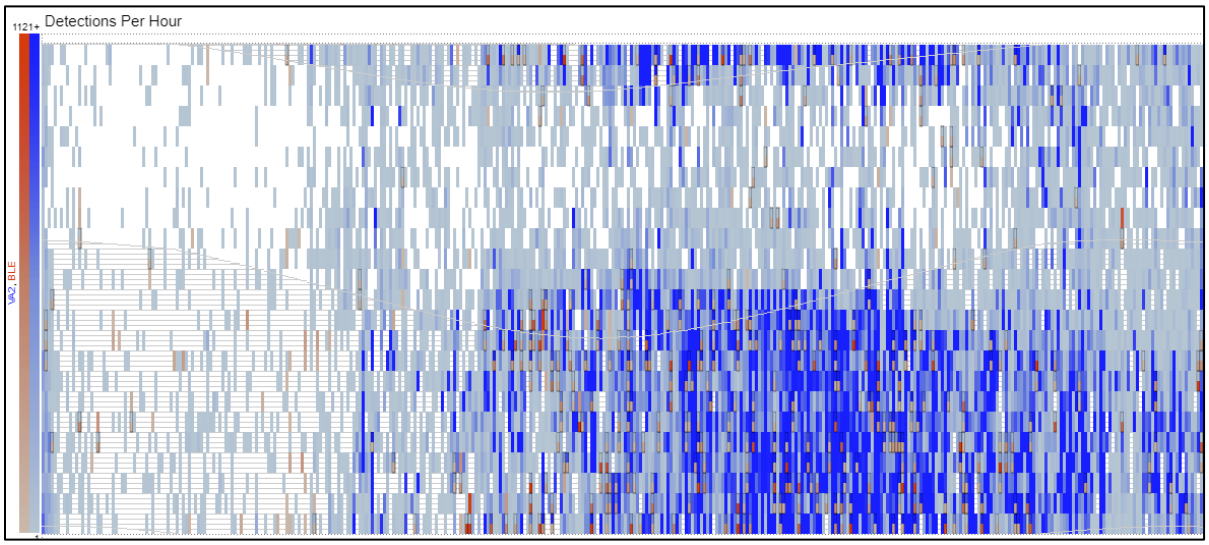

Figure 81. Example heat map comparing dolphin click detections at VA2 (blue) and BLE (red) landers

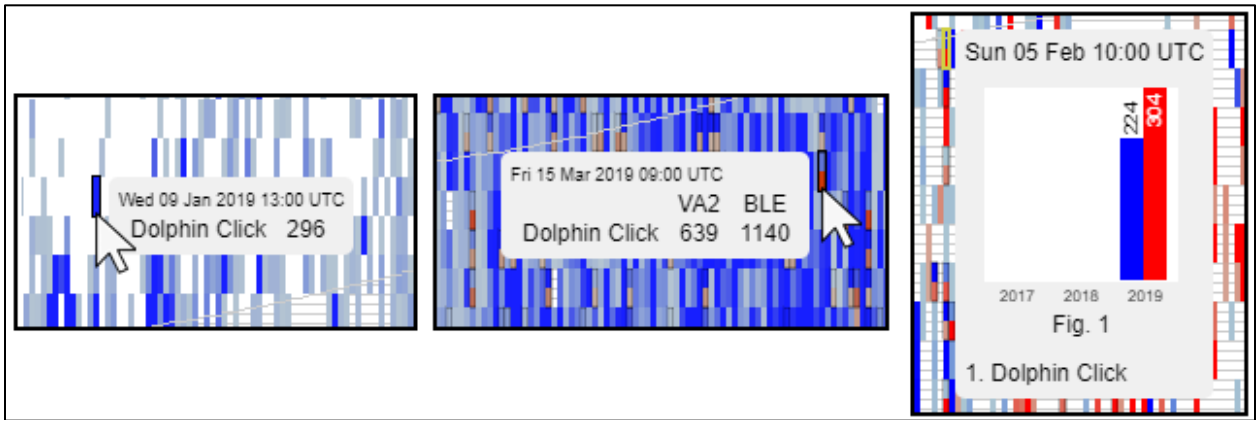

Figure 82. Small popup windows follow the mouse over the heat map, showing the time associated with each cell, as well as the number of events detected during that time

If a comparison is being made between two landers (center) the popup will show the counts for each lander. If the plot is stacking multiple years, bar graphs (right) show the distribution of events by year.

The event detection dataset from JASCO is a set of comma-separated value (CSV) files, which are read and stored in the PostgreSQL database. When this data is exported for use within the heat map, several types of data are combined for each station, including: a dictionary of JASCO fieldnames to display-names, a subset of the overall data based on this dictionary, the average value of the environmental data layer around each station (described in the next paragraph), and daily sunrise and sunset times (which are created using the Astral Python library and the lander's lat/long coordinates).

To create the environmental values (e.g., wind speed, sea surface temperature) for the contextual data bars, the values for the four closest pixels in the original data was averaged around each lander site for each environmental data layer. Initially, Web Coverage Service was used to directly retrieve these values, which were then averaged. However, this proved cumbersome to integrate into an automated export script. This was replaced by a simple WMS GetFeatureInfo request, which was found to already have the ability to get the average value of an area rather than just at a single point. Because of the sometimes-

large gaps in the chlorophyll-a data layer, additional processing was required for this data. These files were batch processed in ArcGIS, with the missing data filled in using Natural Neighbor interpolation. This specific algorithm was chosen due to its ability to produce realistic looking results, even for files with large areas of missing data. Other methods did work on files with smaller areas of missing data, but they were not able to properly process files with large areas of missing data, as often encountered with the chlorophyll data. The filled data layers were then imported into GeoServer like the rest of the layers but were not made available for display.

5.3.5 Tri-Level Spectrogram Viewer

The second visualization tab contains a multi-level spectrogram viewer that presents linked spectrograms at three different timescales, which enables rapid exploration of multiple years of raw recordings. An example view of this interface is shown in Figure 83.

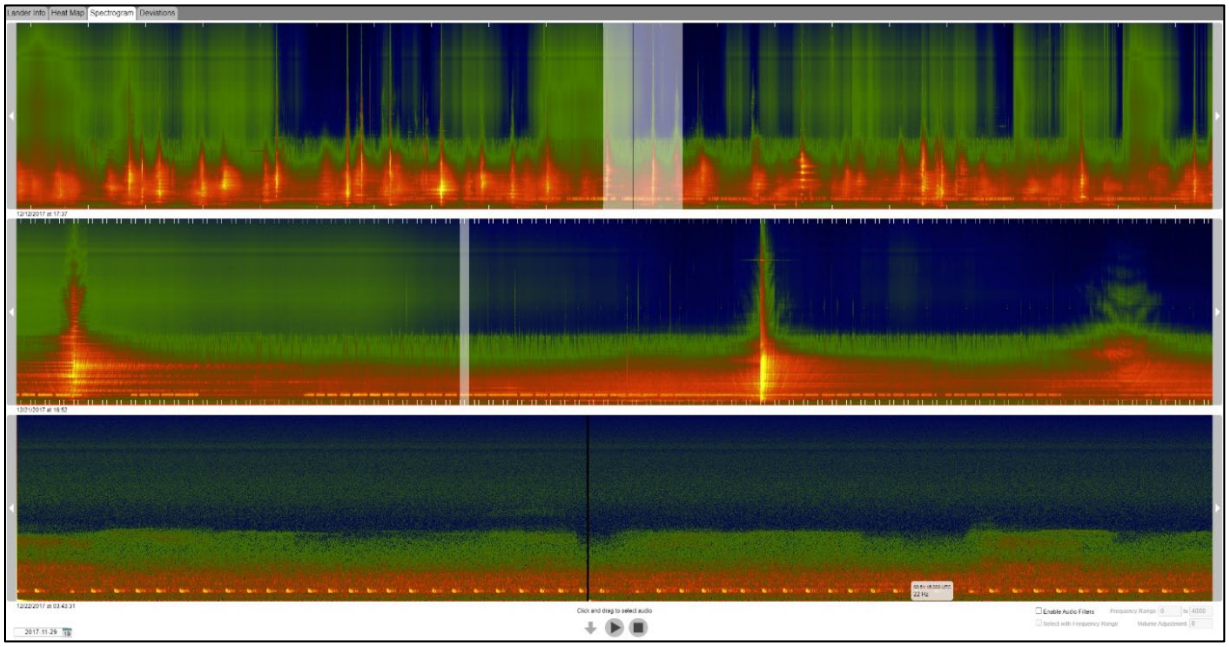

Figure 83. Example view of the spectrogram viewer on a high resolution (2560x1600) monitor

The big orange spikes seen in the top and middle levels are ships transiting the lander region, while the repeating orange blips near the bottoms of the middle and lower levels are fin whale calls.

The topmost level of spectrograms shows a few weeks on screen at a time, the middle level shows a few hours, and the bottom level shows a few minutes. (The exact amounts of time shown in each level varies based on the available screen resolution of the user's display.) All levels are linked. Users can quickly scroll through months or years of data in the top level until something catches their eye. Then, they can click on a region of interest, which centers the other two levels on that time. Likewise, clicking on a region of interest in the second level will further refine the time shown in the other levels. This multi-view, multi-resolution design facilitates exploratory analysis by letting users browse high-level overviews of the data, while being able to instantly drill-down into regions of interest to get details on demand. Instead of having to download terabytes of data, only small (~500KB–1MB) compressed image files need to be transferred from the server as needed. By pre-caching a few image files on either side of the currently active view in each level, on most broadband internet connections, scrolling is generally a seamless experience, as users do not need to wait for data to load. As can be seen in Figure 80, there are

highlighted regions in both the top and middle levels which indicate the portion of that level which is currently being shown in the level below it. A black line also follows in the upper regions to indicate the time displayed at the lowest level.

Because the recordings do not continuously/completely cover all the time (there were ~5-minute gaps between many files), it was important to indicate to users where gaps were, while not disconnecting the data visually on either side of the gap or introducing unnecessary clutter. As shown in Figure 84, our solution was to include a small black bar (right) between files with short gaps, with the bar's width equal to the missing time. However, for longer gaps, instead of a large black region that would overly-disconnect data visually, the width was limited to 100 pixels and inserted a written label indicating the total amount of missing time.

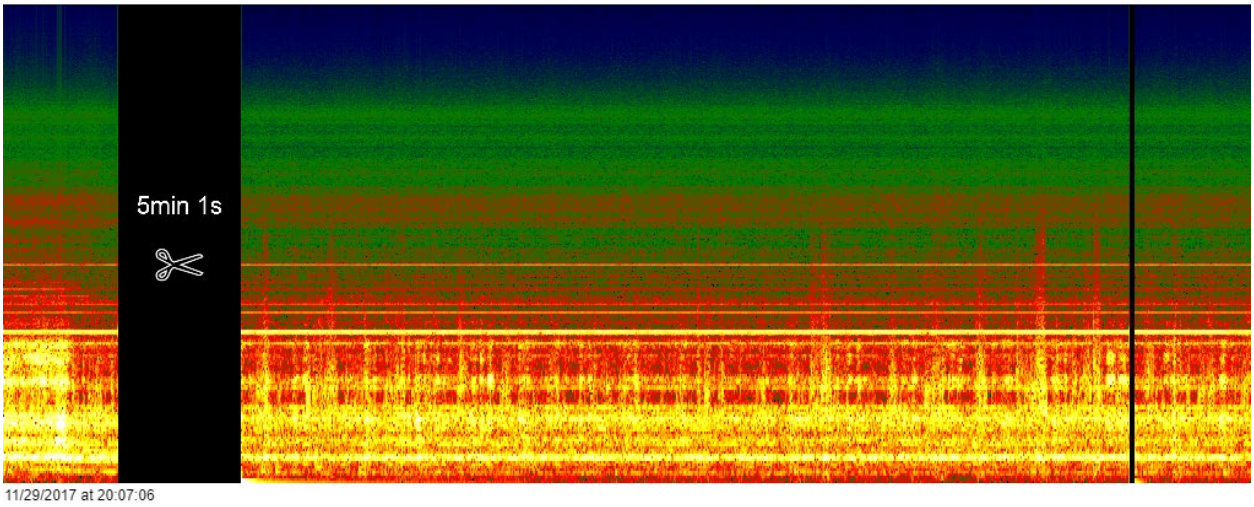

Figure 84. Lowest level of the spectrogram viewer showing three individual recording files and the gaps between them

The gap between the center file and the right file is very short, and this time is simply drawn blacked out. However, the five-minute gap between the center file and the left file would have been extremely large, and is thus condensed to a 100 pixel wide gap with a textual label indicating its actual length.

Mousing over in the bottom level shows the exact time and frequency at that point in the spectrogram. Selecting a 1D region-of-interest within the bottom spectrogram enables users to playback or download an audio clip of that particular time. By enabling the "audio filters" option, a 2D rectangular region-of-interest can be selected of a particular time and frequency range (Figure 85). This feature makes it easier to listen to a specific pattern seen in the spectrogram by removing distracting noise at other frequencies (e.g., to hear an animal vocalization drowned out by ship engine noise).

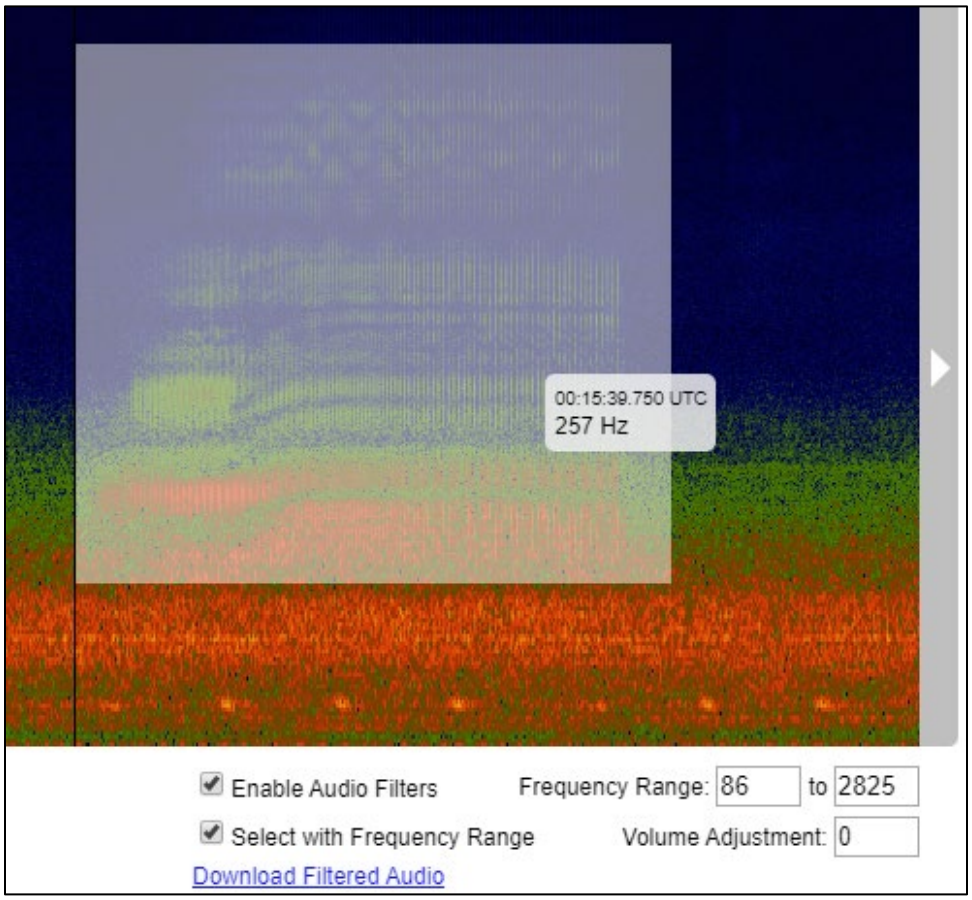

Figure 85. Selecting a region of interest in both time and frequency

After a user makes such a selection, the frequency-filtered clip can be downloaded.

The spectrogram images are generated via pre-processing with custom software written for this project. Individual .wav files are read in and a fast Fourier transform (FFT) is performed. The FFT results are then turned into a spectrogram image using a custom color map. The color map used here was designed by Colin Ware based on years of research into human visual perception issues (e.g. Ware et al., 2017). It was perceptually optimized to best reveal salient features (e.g., marine mammal sounds) and deemphasize low-level sound. As shown in Figure 86, the color scale is also compatible with several types of color-blindness: Red-Weak/Protanomaly, Green-Weak/Deuteranomaly, Blue-Weak/Tritanomaly, Blue-Blind/Tritanopia, and Blue Cone Monochromacy. However, it is not compatible with Red-Blind/Protanopia, Green-Blind/Deuteranopia, and Monochromacy/Achromatopsia.

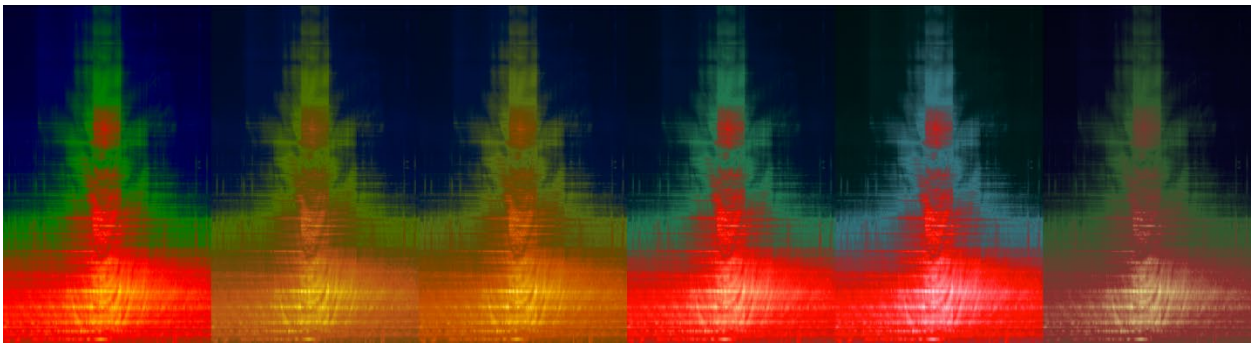

Figure 86. Coblis (Wickline, 2021) simulation of spectrogram color map appearance under different color visions

(from left to right): normal color vision, red-weak protanomaly, green-weak deuteranomaly, blue-weak tritanomaly, blue-blind tritanopia, and blue cone monochromacy.

Image compression was an important consideration for this project. The spectrogram images needed to be compressed as much as possible to save disk space on the server, reduce bandwidth costs, and most importantly, ensure that users could download spectrogram images faster than they could scroll through them (to provide a seamless experience). The high-resolution details in spectrogram images can make efficient compression challenging, and the goals was to preserve as much of this detail as possible. This necessitated the use of a lossless compression algorithm. A .png compression was explored, and the results were found to be acceptable. However, with further experimentation, it was discovered that the images could be compressed into substantially smaller files by taking advantage of various .png compression settings. A piece of open-source software called pngcrush (Randers-Pehrson, 2021) was found to be the best solution, as it tries many different combinations of settings until it finds what works best for each individual image (as the optimal algorithm/settings varies based on image content). Pngcrush also strips out all unnecessary metadata (such as color-correction data). Figure 87 shows the findings from our experimentation, with pngcrush providing the smallest file sizes.

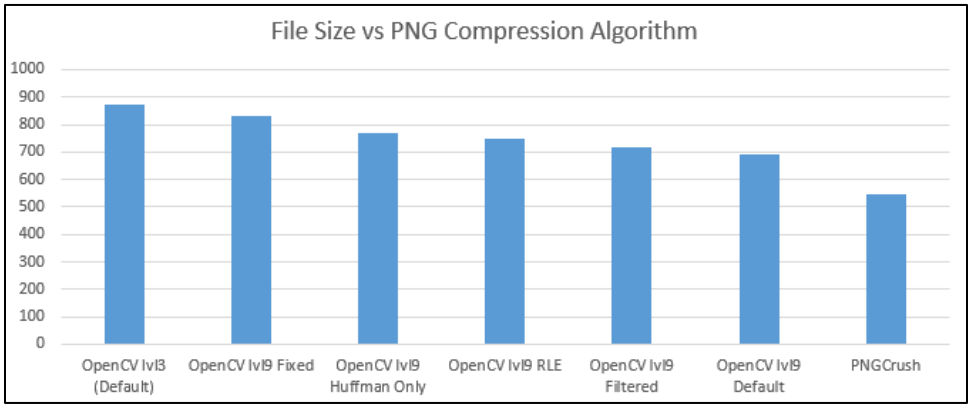

Figure 87. File sizes (in KB) for spectrogram images compressed using a variety of common png compression settings versus pngcrush, which tries many different combinations of settings, and results in the smallest file sizes

To create the second level, zoomed-out images, as .wav files are processed into full resolution (0.5 second) "lvl1" spectrogram images, they are also processed into lower resolution (15 second) spectrograms using the correct FFT calculations (versus simply squishing the full resolution images). These very narrow (~9-25 pixel wide) spectrogram images are appended horizontally into a collage until

the total image size reaches an arbitrary maximum width of 1800 pixels, at which point the collage of short spectrograms is written out as a single “lvl2” image. A “lvl2” text file is also written out with the same filename as the image. This text file contains a list of the “lvl1” source filenames and timestamps for each of the clips in the collage, as well as the length of the clip in pixels, and the start and end index of the pixels. These allow for rapid lookup of timestamps and alignment of images in linked views when the images are clicked on.

To create the top-level, most zoomed-out images, the contents of each individual recording is collapsed into a single column of pixels and added to a “lvl3” collage. Similar to the “lvl2” collages, these “lvl3” images are saved out once they reach an arbitrary size of 1200 pixels wide, along with a “lvl3” text file that contains, for each pixel column, the timestamp and source image in both the original level 1 data, and the level 2 collage. This approach was designed to be mostly agnostic to file contents and timestamps (beyond those contained in the filenames), while making integration with the web server simple, and minimizing interaction times on the website. Figure 88 shows some interesting observations discovered while exploring the ADEON dataset using the spectrogram viewer.

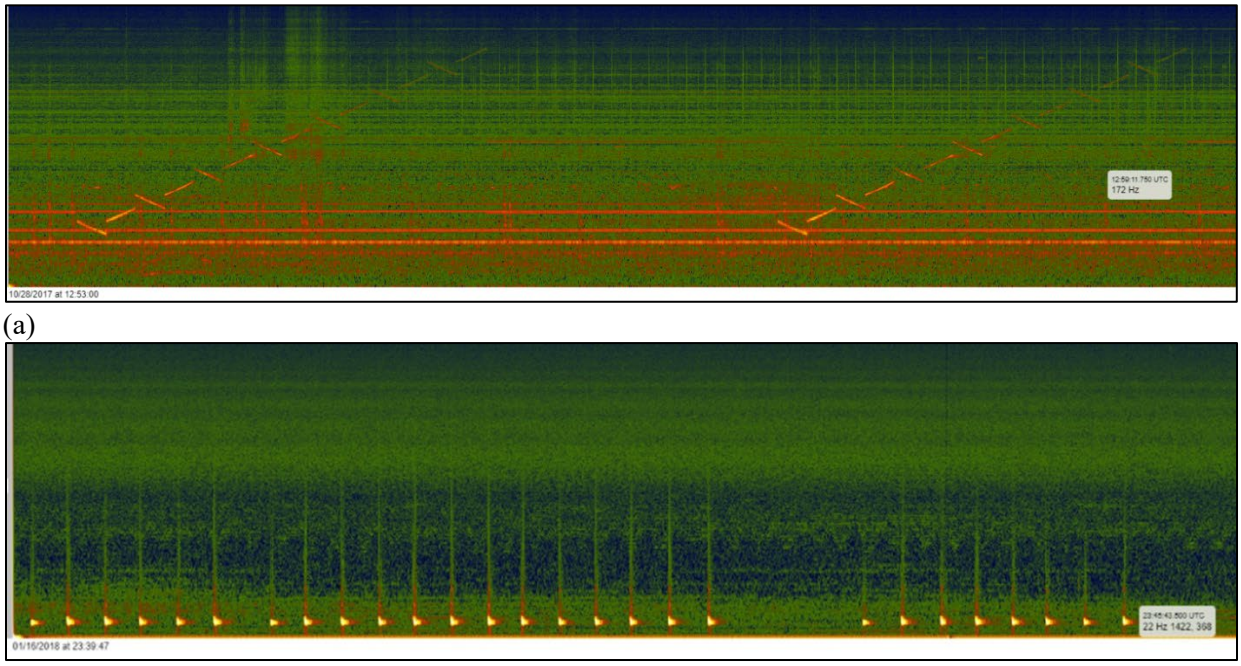

(a)

Figure 88. Interesting observations in the ADEON dataset as they appear in the spectrogram viewer

5.3.6 Deviations Viewer

The final visualization tab contains a similar tri-level viewer that presents the calculated deviations of sound levels around the lander for different frequency bins over time. Instead of showing sound levels, these plots use a diverging blue-white-red color map to reveal times when the ocean around a lander was unusually loud (or quiet) at various frequencies. An example view of this interface is shown in Figure 89. JASCO processed the ADEON recordings into CSV files containing mean sound levels across 40 decidecade frequency bins every 60 seconds. These CSV files were then processed with custom software that uses a variable-length moving window to calculate the standard deviation of sound level around each minute of each frequency bin. The values in these bins is then compared to the moving window mean

value, and the number of standard deviations away from the mean is calculated for that frequency and time. This value (standard deviations away from mean) is then used with a diverging blue-white-red color map to determine the color value for each pixel. White indicates sound levels near the mean, while blues of increasing intensity indicate sound levels at multiple standard deviations below the mean (i.e., increasingly quieter than average periods), and reds of increasing intensity indicate sound levels which are multiple standard deviations above the mean (i.e., periods that are unusually loud).

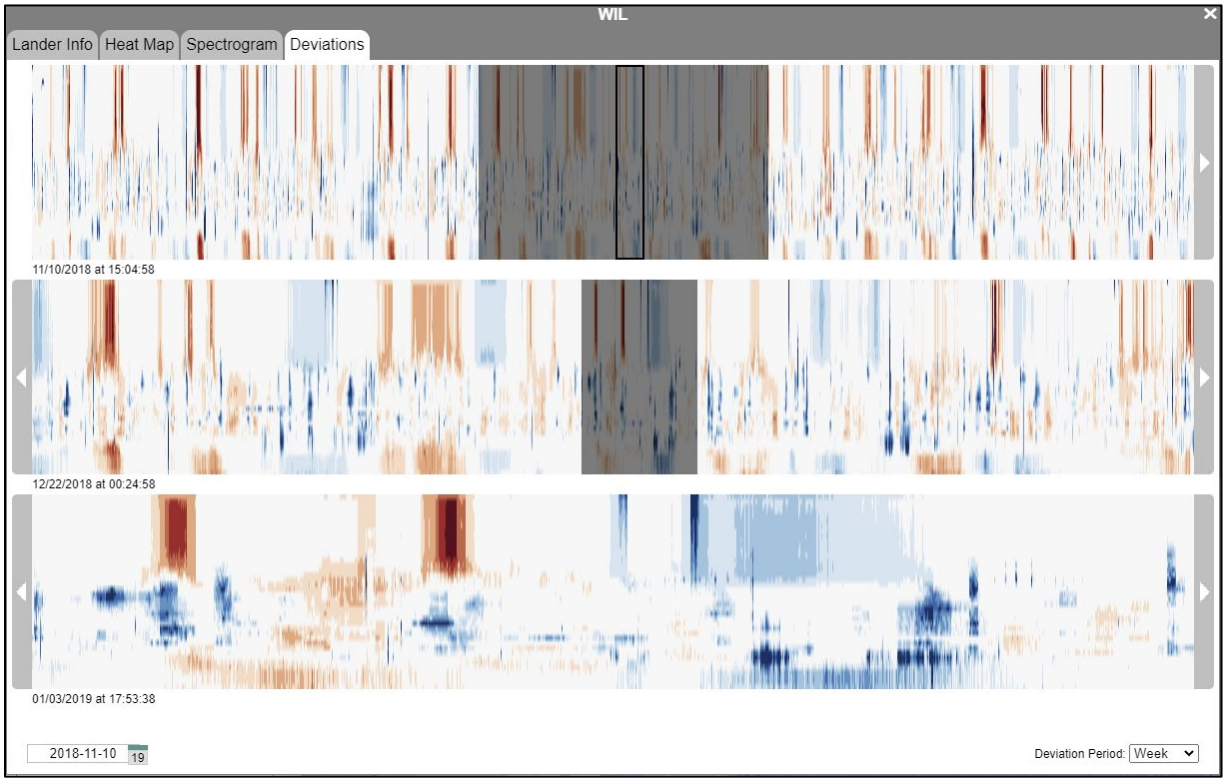

Figure 89. The Deviations Viewer

The Deviations Viewer showing time and frequency ranges that the sea around the lander was unusually quieter than normal (blue) or unusually louder than normal (red) based on a moving window of one week (with monthly and quarterly options selectable via drop-down box)

These calculations are run on the data three times, each time using different moving window sizes: weekly, monthly, and quarterly. This generates three complete sets of images, each containing three levels of images and text-based index files (same process as with the spectrograms described in the previous section). Within the web-interface, users can adjust the moving window size from weekly, monthly, or quarterly in order to suppress or highlight various factors (e.g. temperature or sensor drift). Figure 90 shows the differences in plot appearance for the same data when viewed using different window sizes.

Together, this suite of web-based visualization tools allows researchers, managers, and regulators to gain insight from the massive ADEON dataset, and can help inform future, more targeted studies into the impacts of marine sound.

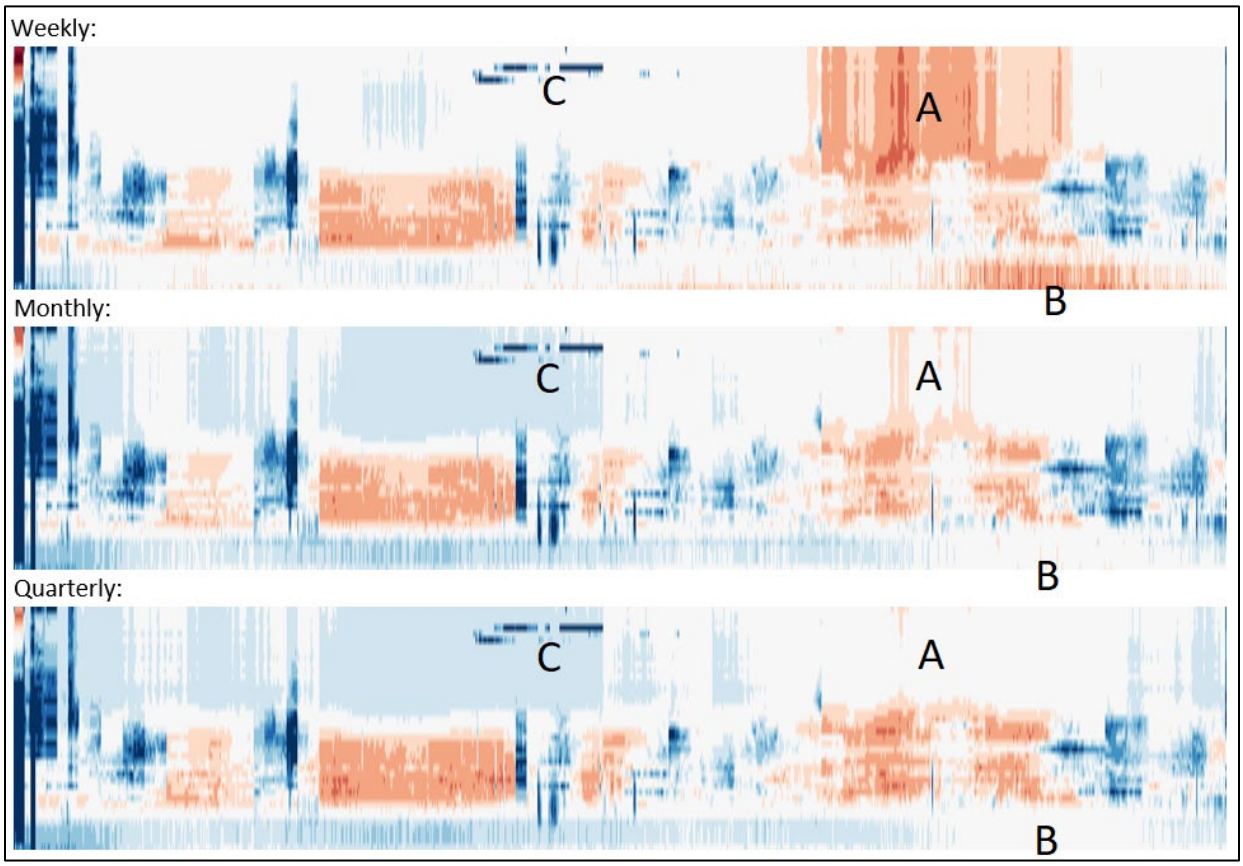

Figure 90. Deviations from mean sound level calculated using different moving window sizes

Blue is quieter than normal, red is louder. (A) and (B) show regions of high frequency (A) and low frequency (B) sound that appears unusually loud when looking at the weekly variation, but when considered over a longer time period, it appears just average. (C) shows an anomaly constrained to a narrow high frequency range, which is unusually quiet across all time ranges.

6. Standards

The Atlantic Deepwater Ecosystem Observatory Network's (ADEON's) Standardization task addresses measurements and metrics that allow for a quantitative assessment of the Mid- and South Atlantic Ocean region soundscape, with consideration of ecosystem conditions as they may be linked to extant biologic, geophysical-chemical, and/or anthropogenic processes. The overall goals of the Standardization task were to ensure compatibility between soundscapes within the ADEON project, to facilitate compatibility between other regional soundscape monitoring projects, and to facilitate compatibility between metrics used by US projects and those of the European Union's (EU's) Marine Strategy Framework Directive (MSFD). Five standardization documents (Table 21) were produced that articulate the terms and metrics used in the ADEON soundscape analysis, and provide guidance for similar regional studies. These products for the Standardization task are publicly available.

Table 21. List of products of the Standardization task

document title	available at
ADEON project dictionary: terminology standard[14]	https://doi.org/10.6084/m9.figshare.12436199.v2
ADEON underwater soundscape and modeling metadata standard[15]	https://doi.org/10.6084/m9.figshare.6792359.v2
ADEON hardware specification	https://doi.org/10.6084/m9.figshare.6809711
ADEON calibration and deployment good practice guide	https://doi.org/10.6084/m9.figshare.6793745
ADEON data processing specification	https://doi.org/10.6084/m9.figshare.12412610.v1

The objective to align with the MSFD was met by maintaining close ties with the EU project Joint Monitoring Programme for Ambient Noise in the North Sea (JOMOPANS)[16] and the International Organization for Standardization (ISO)'s underwater acoustics sub-committee (ISO TC 43/SC 3). As a result of these ties, the JOMOPANS terminology standard (Wang and Robinson, 2020) closely follows that of ADEON (Section 6.1).

The association with ISO TC 43/SC 3 has resulted in a New Work Item Proposal[17] to start a project for the development of an international standard for ambient sound measurement. The standards developed by ADEON provide a firm foundation on which this new project can build.

A summary of each of the five documents follows.

6.1 Project Dictionary

The ADEON Project Dictionary standardizes acoustical terminology for underwater soundscapes. This document, used together with ISO 18405:2017, the international standard for underwater acoustical terminology, facilitates effective communication by providing standardized terms and their definitions for soundscape measurement, modelling, and reporting. It introduces appropriate mathematical symbols and

[14] Also available as BOEM report, in process.

[15] Also available as BOEM report, in process.

[16] See https://northsearegion.eu/jomopans.

[17] ISO/NP 7605, balloted at the time of writing.

conventions, and defines acoustical terminology appropriate for soundscape description, including source properties, quantities associated with propagation and scattering, and statistical measures of the sound field. The ADEON terminology standard further defines quantities used for specification of hardware, especially echo sounders, and quantities associated with the dynamic range of an acquisition system. The standard specifies requirements for reporting soundscapes and defines selected non-acoustical terminology, such as units of distance and time, and data processing levels used by ADEON.

6.2 Soundscapes and Modelling Metadata

The ADEON Underwater Soundscape and Modeling Metadata Standard clarifies the meaning of "soundscape" for the ADEON project, lists quantitative and qualitative soundscape metrics, and states requirements for reporting soundscape products. This document facilitates direct comparisons between soundscapes reported by different ambient sound monitoring projects, nationally and internationally. It specifies a minimum metadata standard for measured and predicted Outer Continental Shelf (OCS) soundscapes in the US Economic Exclusion Zone (EEZ). Adherence to this standard permits an assessment of changes of the soundscape over that time. Soundscape monitoring comprises both measurement and modeling components, and these components differ in their temporal and spatial resolution. By their nature, measurements typically have a high temporal resolution and low spatial resolution, whereas model predictions by comparison can have a high spatial resolution but typically low temporal resolution. The accuracy and precision of measurements are limited by the characteristics of the equipment used, on the way the equipment is deployed and used, and on how the measured data are processed–initial ignorance of the soundscape does not affect our ability to measure it. Prediction of soundscapes is possible by combining available information about underwater sound sources with advanced acoustic propagation models, but the accuracy and precision of model predictions are fundamentally limited by our knowledge of the properties of all sources that contribute to the soundscape. The question then arises of how much information is needed about the presence or absence of any given sound source, and if present the temporal, spatial and spectral distribution of that source.

6.3 Hardware

The ADEON Hardware Specification describes the equipment and its configuration used for ADEON data collection. It provides an overview of the hardware selected, describes the generic structure of autonomous acoustic recorders and performance trade-offs, and describes active acoustic echo sounders for biologic measurements.

6.4 Calibration and Deployment Guide

The ADEON Calibration and Deployment Good Practice Guide provides information to future field scientists who wish to deploy instruments similar to those used in the ADEON project. Though the scope of these descriptions is limited to the specific instruments used in the ADEON project, the information is intended to be of general use, regardless of the system manufacturer.

This document discusses the deployment and calibration of passive acoustic systems, active acoustic echo sounders, and hydrographic sensors. It describes propagation loss experimental procedures and the use of a horizontal line array, and details the use of net or trawl gear to collect ground truthing data about the zooplankton and fish occurring in the water column.

6.5 Data Processing

The ADEON Data Processing Specification specifies data analysis steps used to produce data made available to the public from raw data and documents detailed processing for soundscape metrics. Each system records machine readable raw data (Level 0 processing[18]) that are first calibrated (L1 processing) and then further processed, typically involving error checking, spectral processing, and averaging (L2 processing). An example of this processing stream is the generation of soundscape percentiles from the hydrophone data collected on the bottom-lander omni-directional hydrophones. The acoustic time series, digitized from the voltage changes of the hydrophone are the raw Level 0 data. After calibration to sound pressure (L1 time series), the data are band-passed to generate a filtered time-series. The filtered data are then processed for quantitative soundscape metrics (Level 2) such as the level in decidecade bands or the peak sound pressure level. Event detection and classification of signals as marine mammals and ships are Level 3 data. Satellite data products used by ADEON are generally received after Level 3 (or Level 4) processing.

[18] See the ADEON Project Dictionary (Table A-4) for definitions of Level 0 to Level 5 processing.

7. Synthesis of Study Results

7.1 Passive Acoustic Correlation

During the December 2020 cruise, over 51 hours of usable acoustic data were recorded from a Cetacean Research hydrophone, sampling at 96 kHz. This included a 23-hour south-southeasterly tow towards the Jacksonville (JAX) mooring at approximately 50m depth (Figures 46 and 91); a 34-hour surface transect between JAX and Charleston Bump (CHB) using the same hydrophone; and 7 "research stations" where one or more 10-minute recordings were made at various depths.

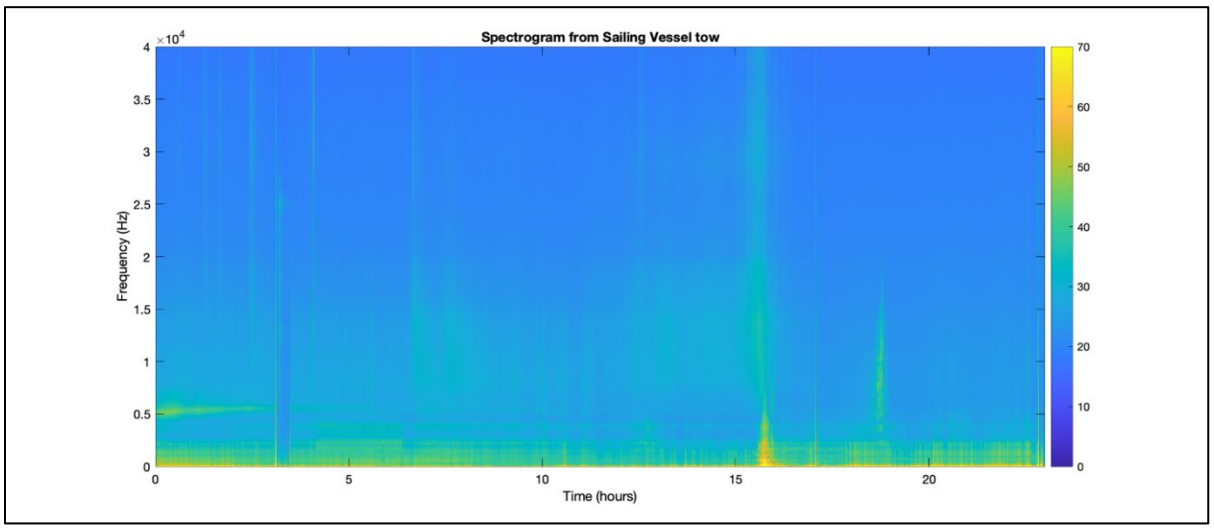

Figure 91. Spectrogram of data from 23-hour hydrophone tow towards JAX mooring

To examine the spatial correlation scales of the ambient sound field, the range of every point along the tow to the beginning point of the tow was first calculated (Figure 63).

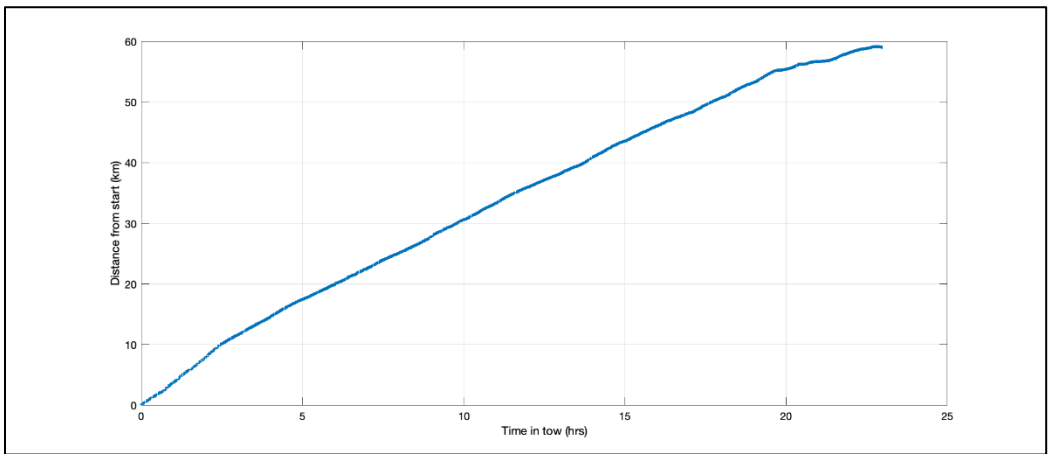

Figure 92. Distance from starting point during the 23-hour hydrophone tow towards JAX mooring

One way to describe spatial correlation scales of a soundscape is to plot the correlation coefficient of the sound spectra as a function of distance. Figure 64 shows this relationship during the 23-hour horizontal tow.

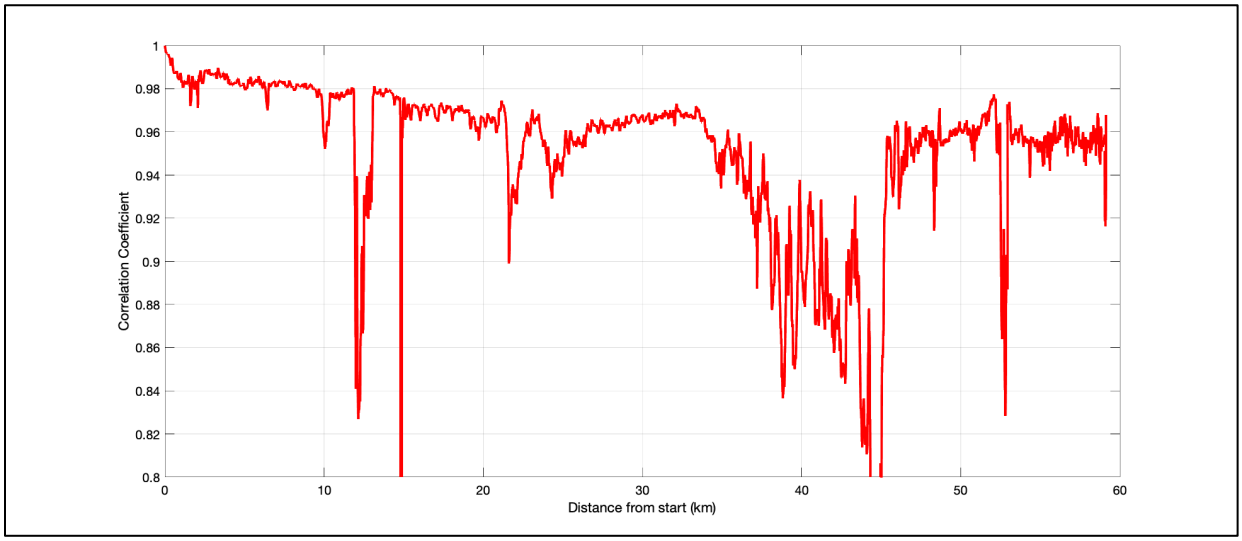

Figure 93 Spatial correlation coefficient of acoustic spectra along 23-hour hydrophone tow towards JAX mooring

The correlation is more pronounced when decidecadal bands are correlated instead of the linear spectra as the variability in noise tends to be logarithmic in nature. The average decidecadal band sums for the towed hydrophone and the JAX lander for the same 23-hour period are shown in Figure 65. The shapes are similar, and the difference can likely be attributed to the fact that the towed sensor was in shallow water, near the surface, while the lander was on the bottom. The towed sensor recorded data at distances ranging from 10 to 70 km from the lander.

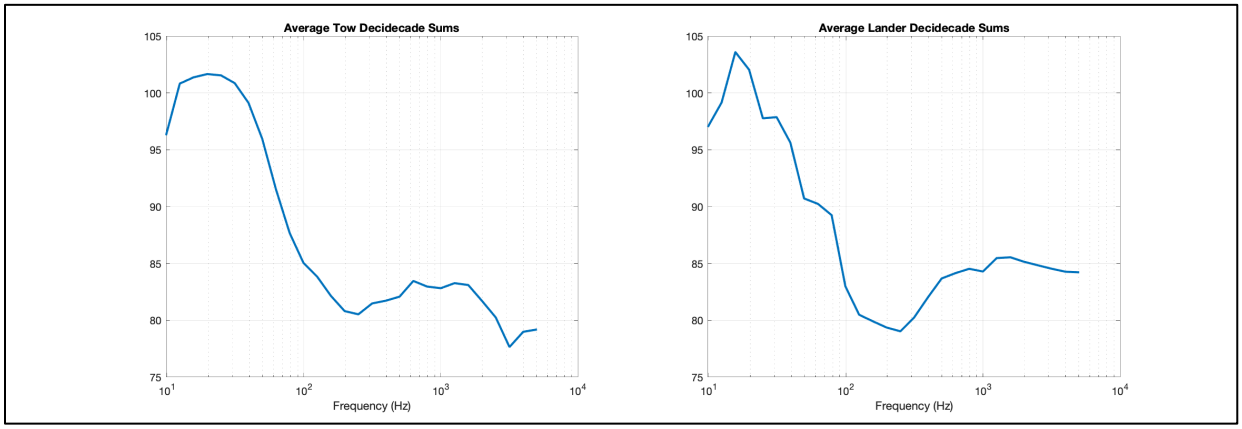

Figure 94. Average decidecadal bands for lander and tow for the two- hour period

When these decidecadal sums are compared instead of the linear spectra, and both datasets are demeaned using a representative average spectra for the area (average of all the recordings during the sea test for each sensor respectively), the correlation along the two becomes more pronounced (Figure 66).

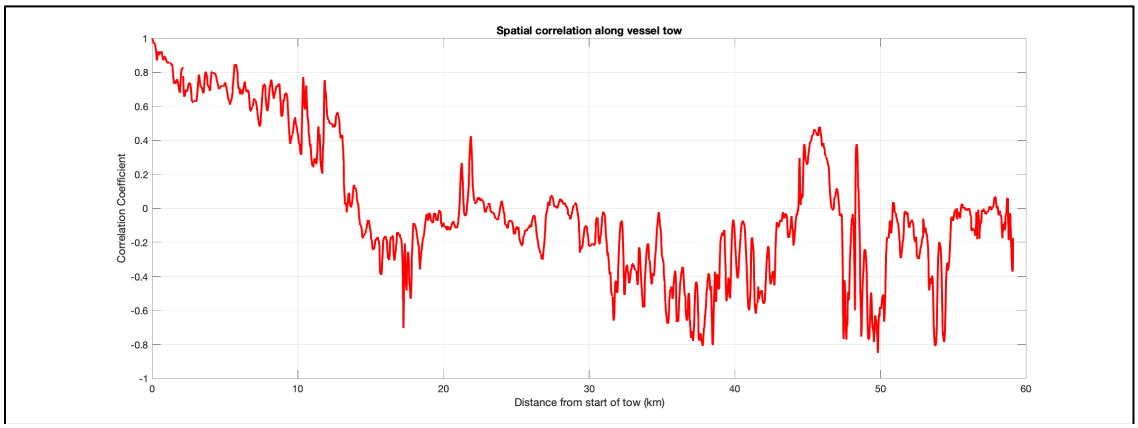

Figure 95. Spatial correlation coefficient of decidecadal spectra along the tow

This same method can be used to examine temporal correlation scales at a single point. Figure 67 shows the autocorrelation, or the correlation coefficient of the demeaned decidecadal bands on the JAX lander for the 23-hour period, compared to the spectra at the beginning of the period. There is a 6-minute moving average applied to each decidecade band.

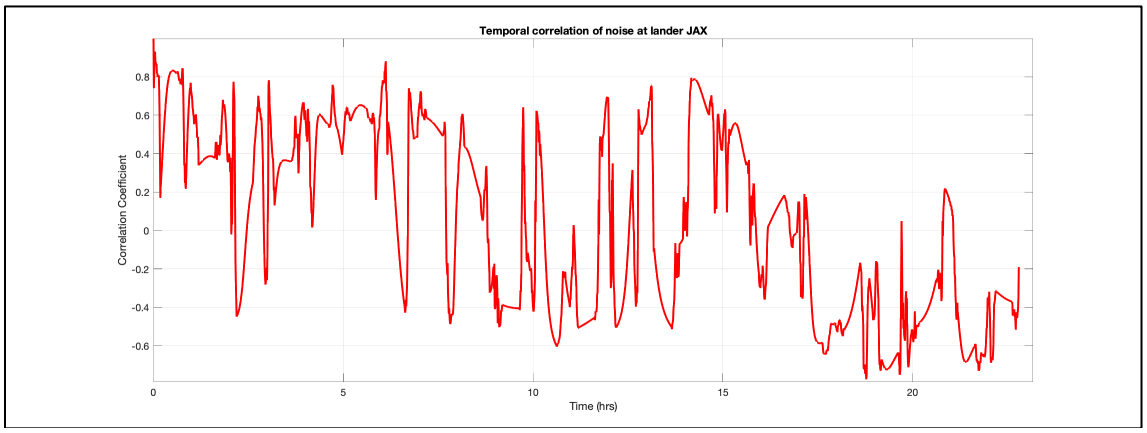

Figure 96. Temporal correlation coefficient of decidecadal spectra at the JAX lander

Next, the correlation coefficient between the lander and the towed hydrophone decidecade spectra was computed as a function of the distance from the JAX mooring (Figure 68). This is a comparison of the 6-minute moving average, demeaned, decidecade bands on the towed hydrophone, and the lander at the same moment in time, along the entire tow.

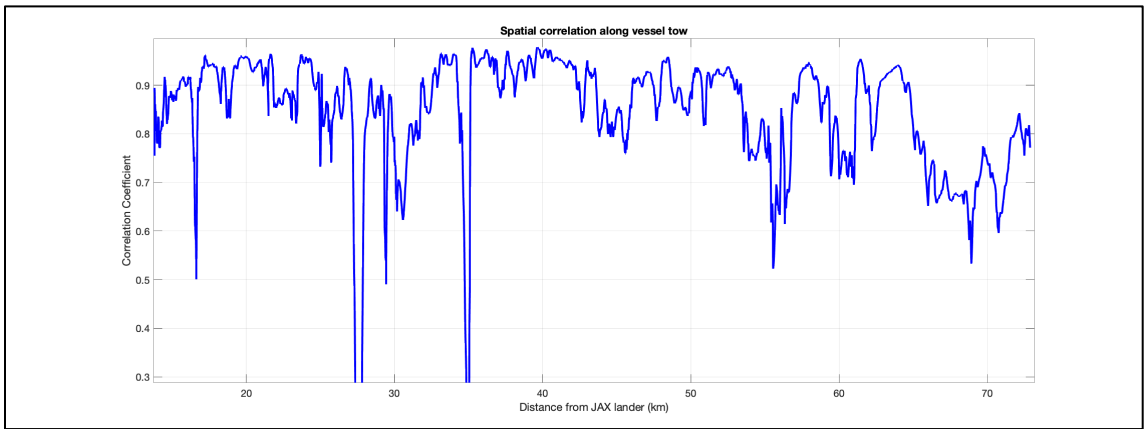

Figure 97. Spatial correlation coefficient of decidecadal spectra from the towed sensor and the JAX lander

The Figure 69 correlation plot is noisier than the autocorrelations, but there is a clear downward trend as the towed sensor gets further away from the lander. The correlation coefficient between the demeaned decidecadal spectra ranges from 0.95 near the lander, to 0.75 further away from the lander. Part of the noise in this dataset could be derived from variability in the flow noise dominating the low frequency bands on the towed sensor. This noise will naturally be uncorrelated with the ambient sound on the lander. Additionally, especially at lower frequencies, differences between sensors at the surface and sensors on the seafloor would be expected. A good way to isolate some of these differences is to look at each decidecade band individually.

7.2 Active Acoustic Correlation

The fine scale acoustic survey (FSAS) data from the first four cruises have been used to investigate the spatial characteristics of scattering aggregations at the Atlantic Deepwater Ecosystem Observatory Network (ADEON) sites and the results of this work have been accepted for publication in the peer-reviewed journal Marine Ecology Progress Series (Blair et al., 2021).

Spatial variability of epi- and mesopelagic 38 kHz backscatter from nekton and macrozooplankton across the southeastern US shelf break

Hannah B. Blair, Jennifer L. Miksis-Olds, Joseph D. Warren**Corresponding author

ABSTRACT: Acoustic echosounders collect detailed information on the location of patchily-distributed pelagic organisms over varying spatial scales. This study measured the spatial variability of epi- and mesopelagic 38 kHz backscatter along the US Mid- and South Atlantic continental shelf and slope. We used variogram analysis to estimate the horizontal spatial structure of backscatter measurements, examined whether environmental variables might affect these estimates, and assessed potential impacts of acoustic survey design. Backscatter data were collected during ship-based surveys (50 to 100 km2) at seven sites during four cruises from November 2017–2019. Average patch size estimates were consistently between 2 and 4 km among locations. Modeled variogram range varied significantly with the depth of the backscatter layer, but linear effect sizes were negligible (<1 m). Chlorophyll a (chl-a) concentration had a significant positive effect on range (95 m), suggesting patch sizes are slightly larger in the epipelagic where chl-a concentration is higher. Incorporating variogram parameters of range, sill, and nugget produced some clustering of spatial correlation parameters with scattering layer depth, particularly for the deepest sites assessed (700–900 m deep). Spatial characteristics of a given location

were not significantly different between surveys of the same size, but sometimes differed with smaller (25% of area) survey sizes. These results offer insight into nekton and macrozooplankton backscatter patterns in important shelf break and slope systems across horizontal and vertical dimensions, and provide needed information for monitoring fine- to mesoscale offshore marine habitat areas.

7.3 Soundscape Summary

One of the objectives of ADEON was to gain an understanding of how the soundscape varies with latitude and distance from shore in the OCS. The soundscape at a location is the sum of all sources that contribute to the sound field at that location (Jennings & Cain, 2013). Because the weather changes and sources like mammals or vessels move, the soundscape changes over short time scales (minutes), but also over days and seasons. The ADEON project included a 3-year measurement program with seven recording locations, where vessels, marine mammals (especially fin and minke whales, see Section 7.5 and Appendix E), and weather contributed to the soundscape.

As an overview of the range of soundscapes recorded during ADEON, Figure 98 provides two examples of the long-term soundscape results for the 2018-2019 deployment. The top two figures are the long-term spectral average (LTSA) and percentile plots from the highest energy station in ADEON - VAC (which was trawled by a fisher in early July 2019). The bottom two figures are from the quietest station – SAV. At VAC, there are a large number of vessel passages which appear as the red vertical marks in the band of 20-100 Hz of in the LTSA and the rounded bump that peaks at 50 Hz in the percentile plot.. VAC also has substantial fin whale presence in the winter months which created the horizontal line at 20 Hz in the LTSA, and the spike at 20 Hz in the percentile plot. Odontocetes were present daily at VAC (see Section 7.5.1) which can be seen as the regular period of light blue sound energy above 20 kHz. In contrast, SAV does not have the ‘fingerprint’ of passing vessels, although there are periods of flow noise below 50 Hz which create the ‘smudge’ of sound energy in the percentile plot and relatively long periods of red vertical strips in the LTSA. Fin whales were only faintly heard at SAV. Odontocetes were rare and as a result there is a dark blue region of no sound above 20 kHz. A notable acoustic source at SAV was the presence of minke whales in the winter months which elevated sound levels in the 80-200 Hz frequency band (see Section 7.5.2).

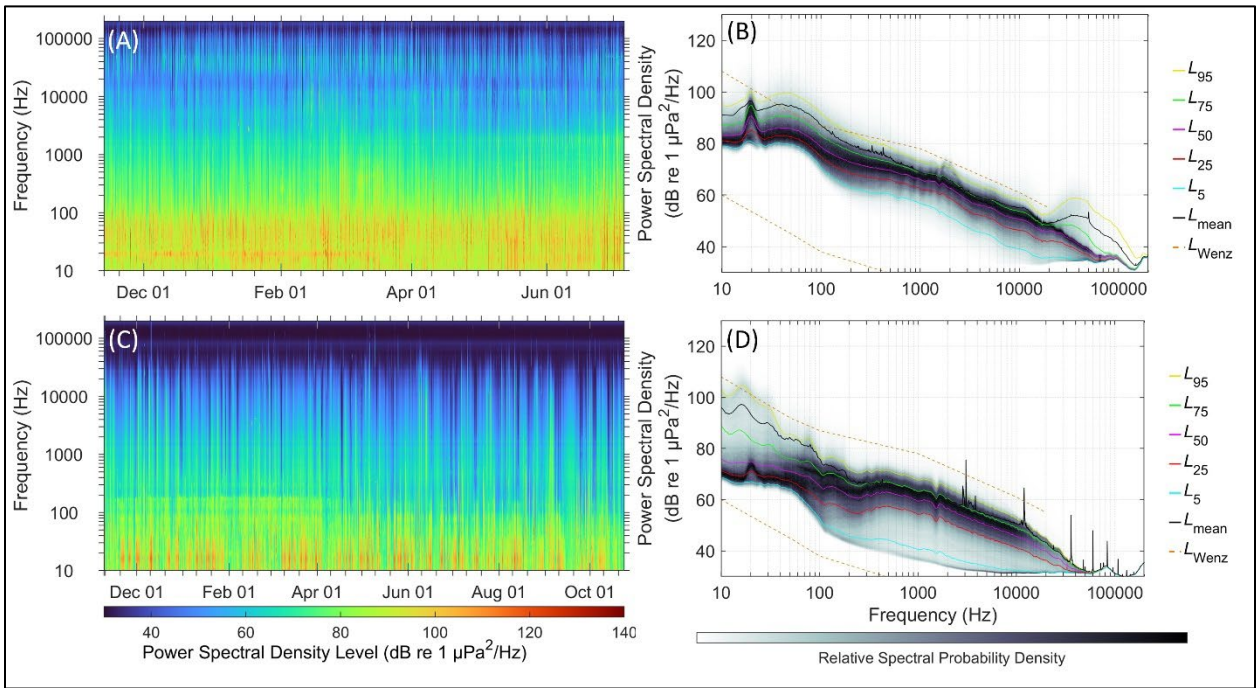

Figure 98. Summary of the data from VAC (A, B) and SAV (C, D) for Nov 18–Nov 19 (VAC was trawled up in Jul 19)

A) and C) are the long-term spectral averages, B) and D) show the percentiles of the power spectral densities and relative spectral probability densities.

The differences between stations were greatest at low frequency and decreased at high frequencies. The median power spectral density for the Nov 2019–Nov 2020 deployment (Figure 99) allows a comparison of the differences between stations. The greatest differences were 16 dB between SAV and VAC at 50 Hz, and decreased to ~ 6dB between all stations for frequencies above 600 Hz. At 60 kHz all stations have almost identical median noise profiles that are determined by the electronic and hydrophone noise floors.

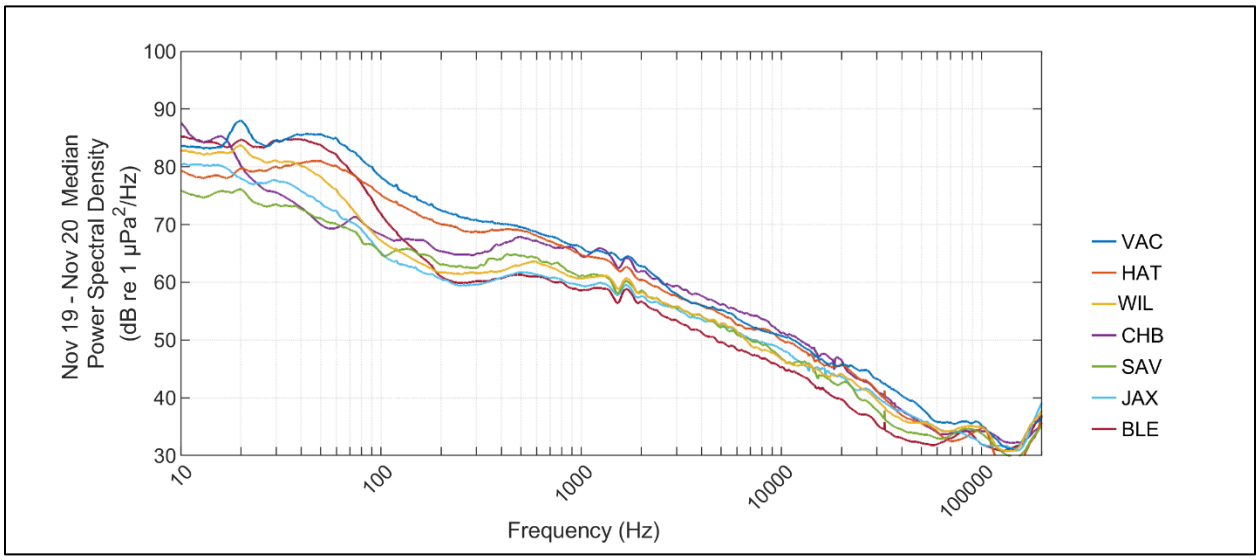

Figure 99. Median power spectral density for the ADEON data from Nov 18–Nov 19 from the high frequency channels (512 kHz, 5 minutes / hour recording)

To further study long term trends in the soundscape, the ADEON team chose four decidecade bands to compare and contrast in time and location. The 20 Hz band was chosen because fin whales are a well-known source that can be dominant throughout the winter in northern latitudes at this frequency. This band has some sound contribution from vessels, as well as flow and motion induced non-acoustic noise. Large vessels have the peak of their cavitation spectrum in the 50-60 Hz range, while smaller vessels are in the 100-200 Hz range. With this in mind, 80 Hz was also chosen as the representative band for vessels. The 80 Hz band is also part of the minke whale pulse train spectrum, which was found to be an important source throughout the winter further south in the project area (see Section 7.5). The wind driven noise spectrum peaks at 630 Hz, but this band also has contributions from shipping, which makes it an interesting frequency for analysis. Finally, we chose 3150 Hz as a band that is dominated by wind noise, but at a lower amplitude than at 630 Hz.

To compare across time and location, the 1-minute decidecade sound pressure levels were analyzed to compute the empirical probability density functions (EPDF). The EPDFs present the probability of different sound pressure levels occurring based on the measured data. The bands are compared for each month by station in Figure 100, and for each station by month in Figure 101. The SPL that is most likely to occur (highest probability) is referred to as the mode of the EPDF.

The lower frequency bands had more variability between stations and over time than the higher frequency bands. The low frequencies at CHB have a very flat EPDF due to flow noise levels from the Gulf Stream affecting the results up to ~100 Hz (see Appendix A). All other stations expect JAX show a separation between the winter and summer months at 20 Hz which is attributed to fin whale chorusing. This effect decreases with latitude. A similar shift in the 80 Hz band can be seen at SAV, JAX, WIL and BLE, the four stations with the highest occurrence of minke whale chorusing (see Section 7.5 and Appendix E). The two stations closest to heavy shipping lanes, VAC and HAT, have the highest mode SPLs and greater probabilities of high SPLs than the other stations. BLE, which is also close to shipping, has an elevated mode SPL but does not have the same probability of high SPLs as VAC and HAT. WIL and SAV had substantially lower mode SPLs at 80 Hz than the other stations.

At the frequencies influenced mostly by wind (630 and 3150 Hz), the EPDFs are more affected by season than by location. All stations showed a distinct separation between the summer and winter seasons which is attributed to increased wind speeds in winter. The stations had higher mode SPLs in winter as well as a greater probability of low SPLs in summer and high SPLs in winter. In the high frequency bands there is a trend of lower sound levels at lower latitudes, with JAX and BLE consistently having the lowest mode SPLs in each month.

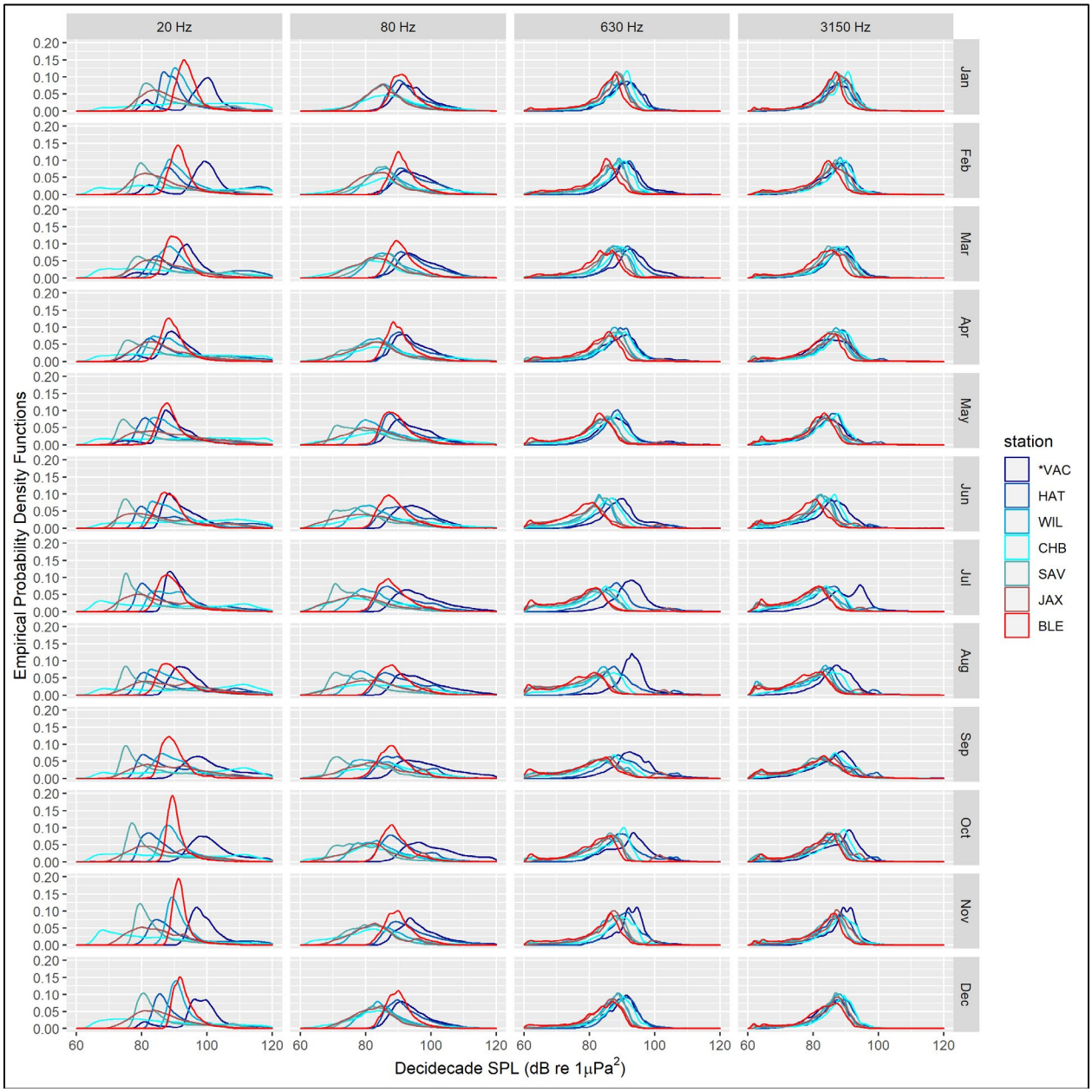

Figure 100. Comparison of the empirical probability density functions for the 20, 80, 630 and 3150 Hz decidecade bands for each month

The color of the curves represents the locations, which are plotted from north to south and west to east (on shore to offshore). *VAC data were missing for parts of May–Dec in most years, see Section 4.1.1.1.

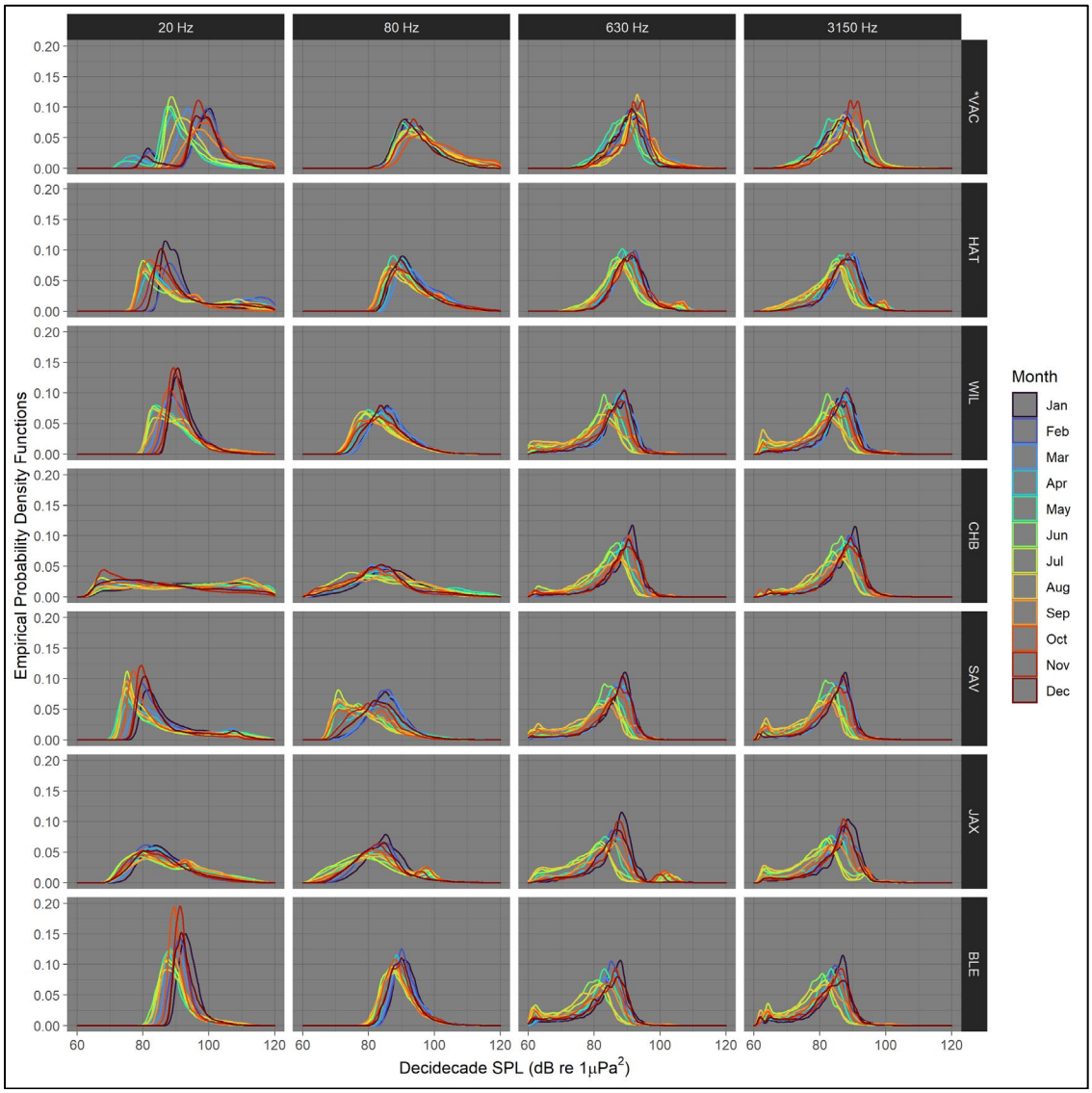

Figure 101. Comparison of the empirical probability density functions for the 20, 80, 630 and 3150 Hz decidecades for each station

Stations are plotted from north to south and west to east (on shore to offshore). The color of the curves represents the month of the year. *VAC data were missing for parts of May–Dec in most years, see Section 4.1.1.1.

Acoustic vessel detection was performed on the ADEON data as described in Martin (2013). Acoustic detection relies on the sound pressure level in the frequency band of 36-355 Hz (40-315 Hz decidecade bands) increasing by at least 3 dB compared to the 12-hour average levels. As a result, the number of vessels that are detectable per day depends on the number of vessels present as well as the average sound levels. When many vessels are present, the sound levels increase, and the only vessels that are detectable will be ones that pass close to the recording location and are able to increase the sound levels. At the ADEON sites the average number of vessels per day that were acoustically detected ranged from 2 to 10 (Figure 102). At each site more vessels were detected when the average daily sound pressure level in the

detection frequency band was lower. The two northern stations (VAC, HAT) had the highest daily number of detections, and the highest sound levels.

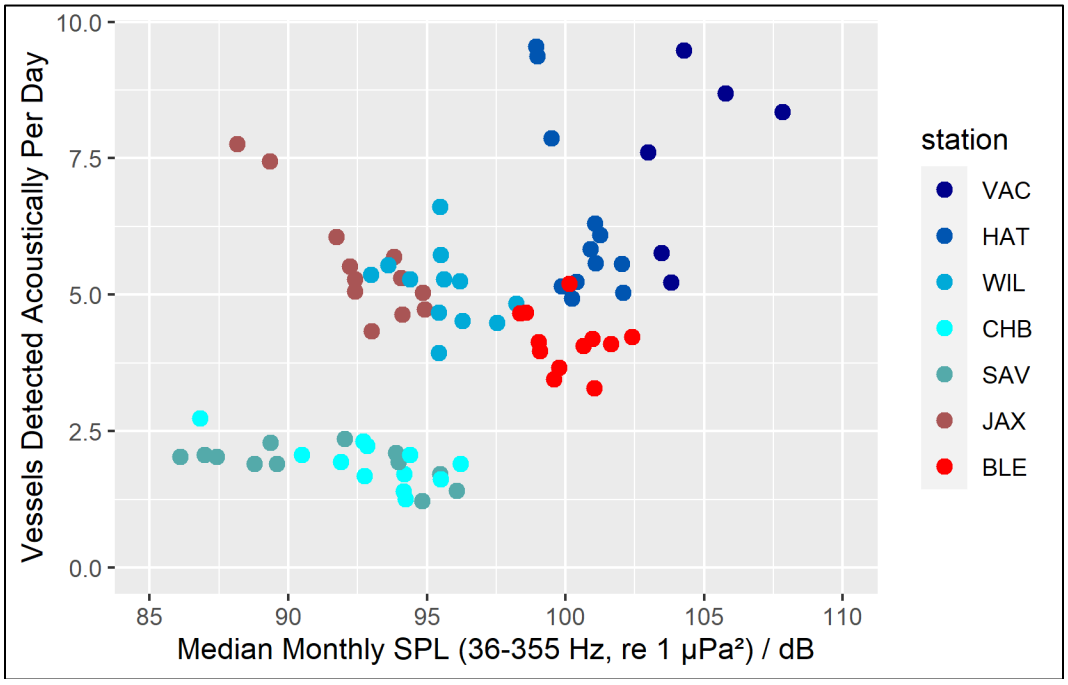

Figure 102. Monthly average vessels detected per day vs average for the Nov 2019–Nov 2020

For each station, more vessels are detected when the sound levels are lower.

Thus, ADEON demonstrated that for the OCS the soundscape is determined by local and seasonal effects:

- Fin and minke whales have substantial effects on the soundscapes in the winter months, with fin whales to the north of the area, and minke whales to the south.
- Proximity to vessel traffic increases the SPLs at low frequencies.
- There is a seasonal and latitudinal difference in high frequency SPLs.

7.4 Backscatter Summary

The acoustic backscatter time series from the lander acoustic zooplankton fish profiler (AZFP) systems at JAX, HAT, and VAC provided the opportunity to look at water column biomass and community structure as a function of both latitude and oceanographic features. All three AZFP equipped landers were within approximately 100 m depth or each other from JAX in the south to VAC in the north (Figure 103). JAX and HAT were in similar oceanographic conditions in relation to the Gulf Stream current; both locations were located on the western boundary (Figure 103). The VAC site was location in a cooler water mass west of the Gulf Stream. Temperature is often a large driver of production, and surface temperatures were again similar between HAT and JAX in terms of level and variability (Figure 104). VAC had a larger seasonal dynamic range with minimum temperatures approximately 15°C cooler than either HAT or JAX. Bottom temperatures showed little to no seasonal trend at any of the three locations. By contrast to the sea surface temperature (SST) at JAX being the warmest, JAX had the coolest bottom temperatures most likely due to the slightly deeper depth (Figure 104). VAC and HAT had a much more variability in bottom temperature compared to JAX. How the different oceanographic conditions manifested in the

temporal zooplankton and fish abundance and community structure was the focus of the AZFP acoustic backscatter analysis.

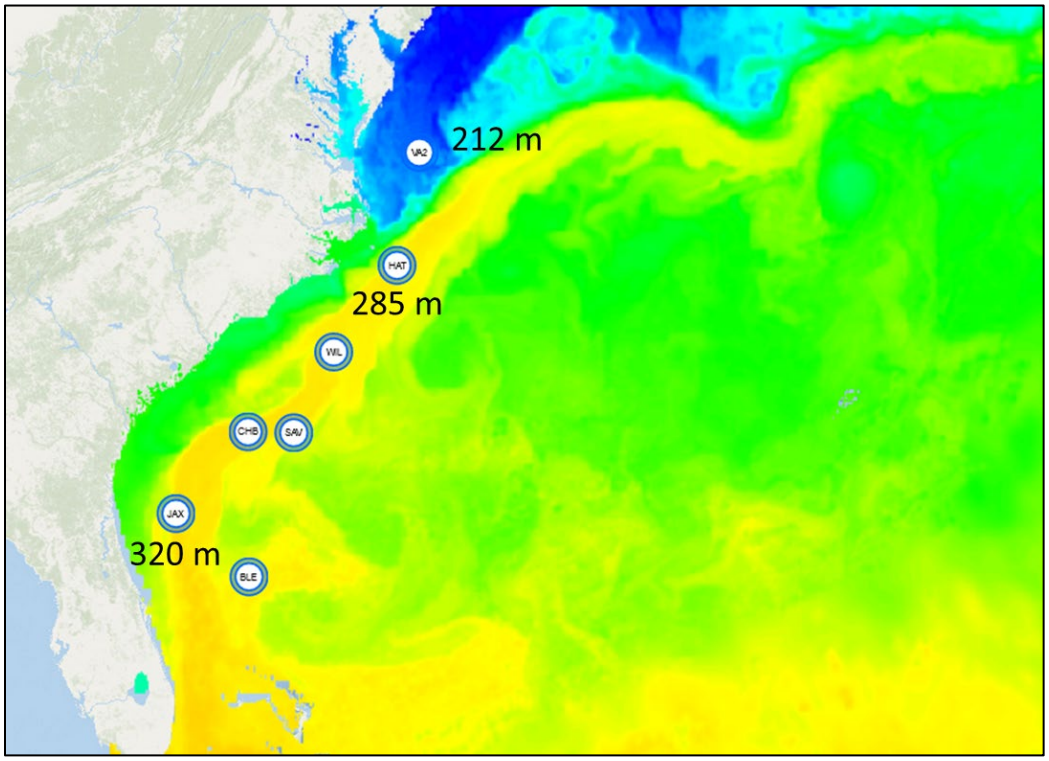

Figure 103. Location and depth of the three ADEON landers equipped with AZFP echosounder systems: VAC, HAT, and JAX

JAX and HAT are on the western boundary of the Gulf Stream, whereas the VAC site was located in a cooler water mass outside the Gulf Stream.

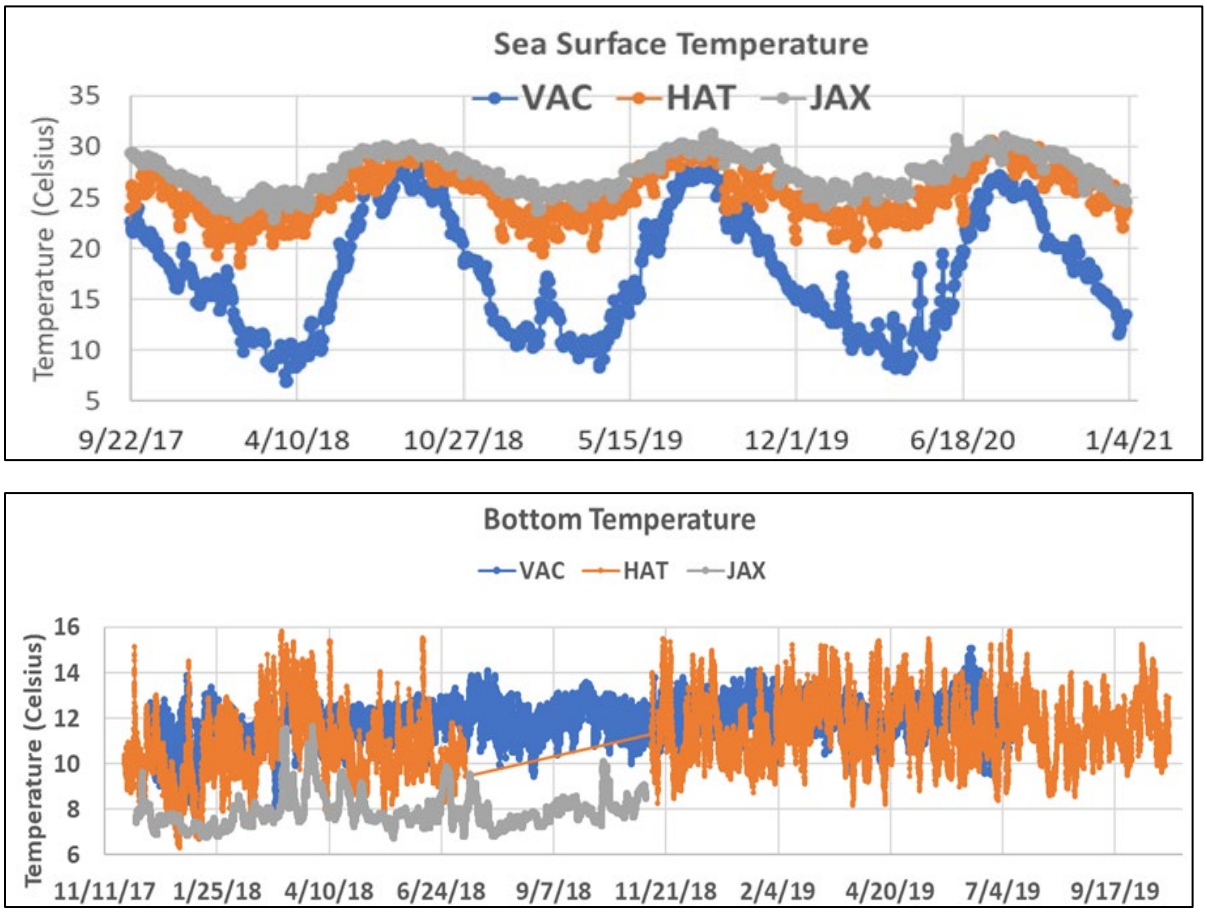

Figure 104. (Top) SST satellite time series at the VAC, HAT, and JAX lander locations. (Bottom) Bottom temperature time series acquired by the lander CTD system on each of the ADEON landers

The time series of hourly nautical area scattering coefficient (NASC) integrations over the water column showed a general pattern of seasonal blooms in the fall and spring (Figure 105). Lowest levels of biomass in the water column was observed in the summer, and period of the largest variability was observed in the winter season. Water column abundance at the JAX locations was less than at either HAT or VAC with JAX also having the least amount of yearly variation (Figure 105 and Table 22). VAC had the highest levels of biomass imaged by the 125 kHz, 200 kHz, and 455 kHz frequencies. HAT had the highest biomass values imaged in the 38 kHz backscatter.

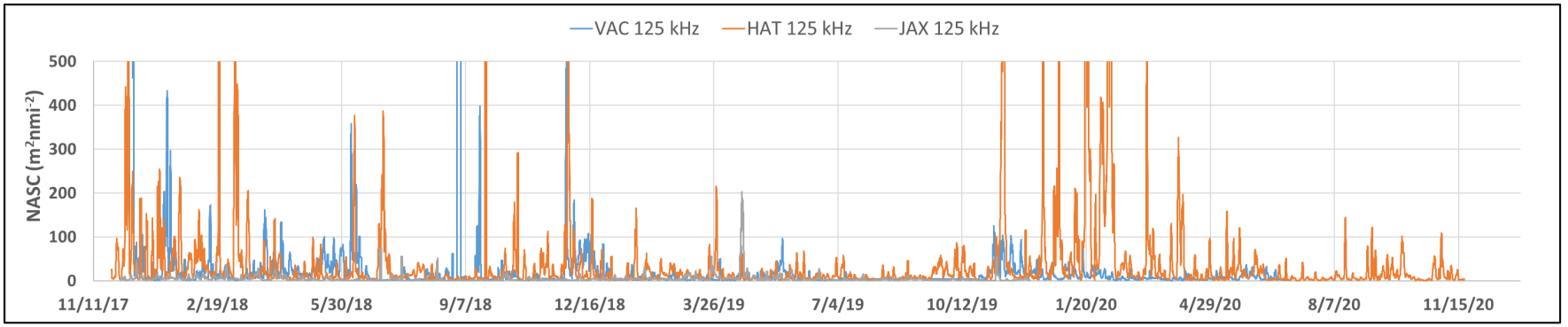

Figure 105. Full NASC times series at 125 kHz for the duration of the ADEON program

Table 22. Median Sv (dB re 1 m^2m^{-3}) /NASC (m^2nmi^{-2}) values over the Full duration of the ADEON project and individual years.

		Full	Dec 17–18	Dec 18–19	Dec 19–20	Inter-annual Variability*		
38 kHz	VAC	-94 / 3.5	-94 / 3.7	-94 / 3.3	-95 / 3.4	Low		
	HAT	-91 / 9.2	-91 / 8.4	-90 / 12.6	-96 / 3.14	High		
	JAX	-96 / 3.0	-96 / 2.9	-96 / 3.2		Low		
125 kHz	VAC	-87 / 17.5	-83 / 41.2	-90 / 7.6	-88 / 13.5	High		
	HAT	-92 / 6.6	-92 / 7.8	-93 / 5.8	-92 / 6.5	Low		
	JAX	-98 / 2.0	-98 / 1.8	-97 / 2.4		Low		
200 kHz	VAC	-95 / 2.8	-95 / 2.7	-96 / 2.1	-94 / 3.8	Low		
	HAT	-100 / 1.1	-100 / 1.2	-100 / 1.1	-101 / 1.0	Low		
	JAX	-107 / 0.3	-103 / 0.6	-108 / 0.2		Moderate		
455 kHz	VAC	-89 / 9.6	-90 / 8.4	-90 / 9.4	-89 / 11.1	Low		
	HAT	-96 / 2.4	-95 / 3.5	-97 / 2.3	-99 / 1.5	Moderate		
	JAX	-108 / 0.2	-108 / 0.2	-108 / 0.2		Low		

*Inter-annual variability was assessed as Low when Sv varied less than 3 dB between all years, Moderate was Sv varied 3 - <6 dB between all years and High when Sv varied > 6 dB between all years.

A community structure time series over the duration of the ADEON program was constructed for 5 scattering groups: small non-resonant scatterers (NRS), medium NRS, large NRS, small resonant scatterers (RS), large RS, and unidentified scatterers (UID) (Figures 106–108). The animal groups and lengths comprising each scattering group are defined in Table 13 and Figure 38. Over the course of the study, there was very little small NRS biomass registered in the time series at any location, so this category was not included in further analyses. The UID time series aligned with other of the defined categories, but which category was site and year dependent and requires additional analyses. For this reason, the UID is not reflected in Figures 106–108.

Results from 2017-2019 indicate that VAC was dominated by Large NRS throughout the time series with contributions from Medium NRS and Large RS. HAT was very similar to VAC during the first half of the year with Large NRS dominating the time series. The dominant community structure at HAT shifted during the late 2018 summer from Large NRS to Large RS. JAX showed low levels of any scattering group for a majority of the year, the exception being for 2 months in summer 2018 when Large and Small RS groups dominated the water column.

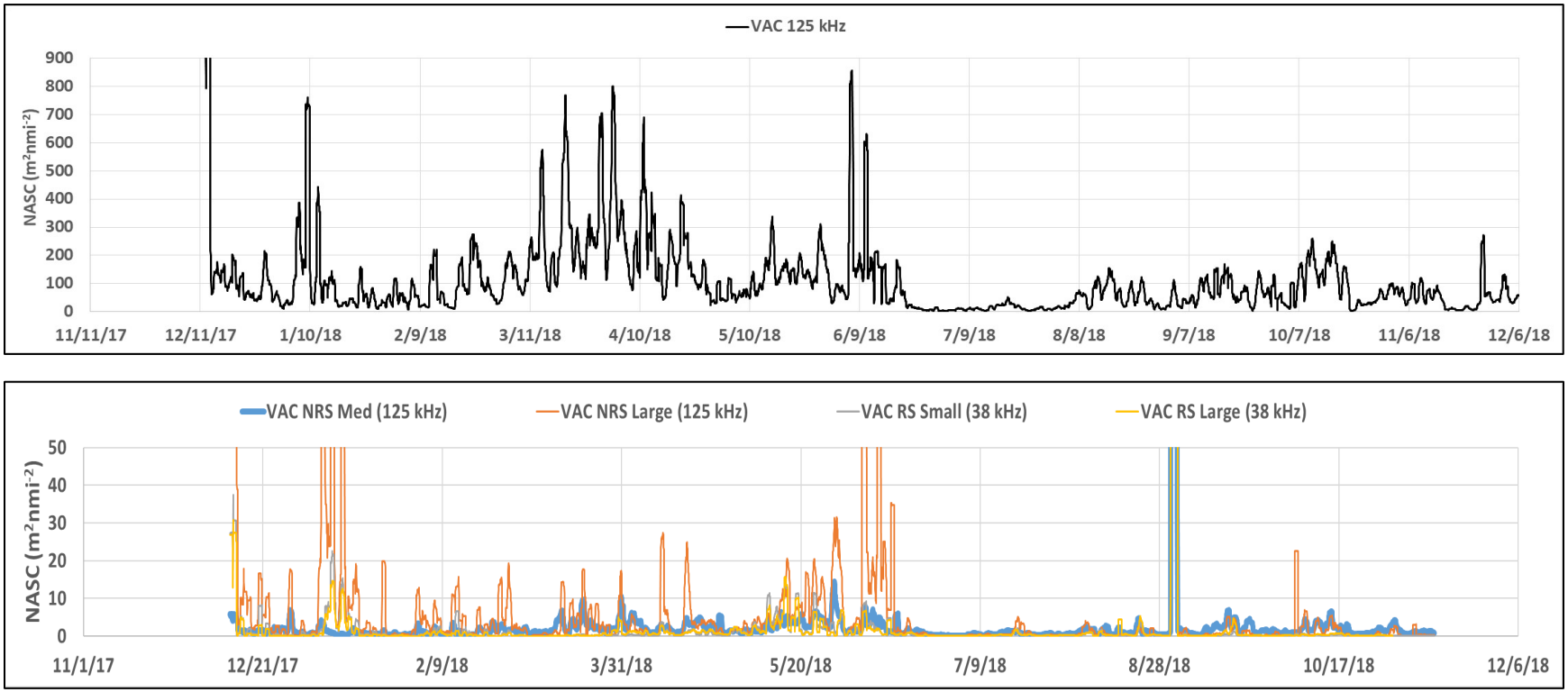

Figure 106. Virginia Inter-Canyon (VAC) one year time series of nautical area scattering coefficient (NASC) time aligned with community structure

Top: Hourly full water column integrated VAC 125 kHz NASC time series smoothed with a 24 point moving average. Bottom: Time aligned VAC community structure NASC time series where the NRS Medium and NRS Large were exported from the 125 kHz data, and the RS Small and RS Large were exported from the 38 kHz data.

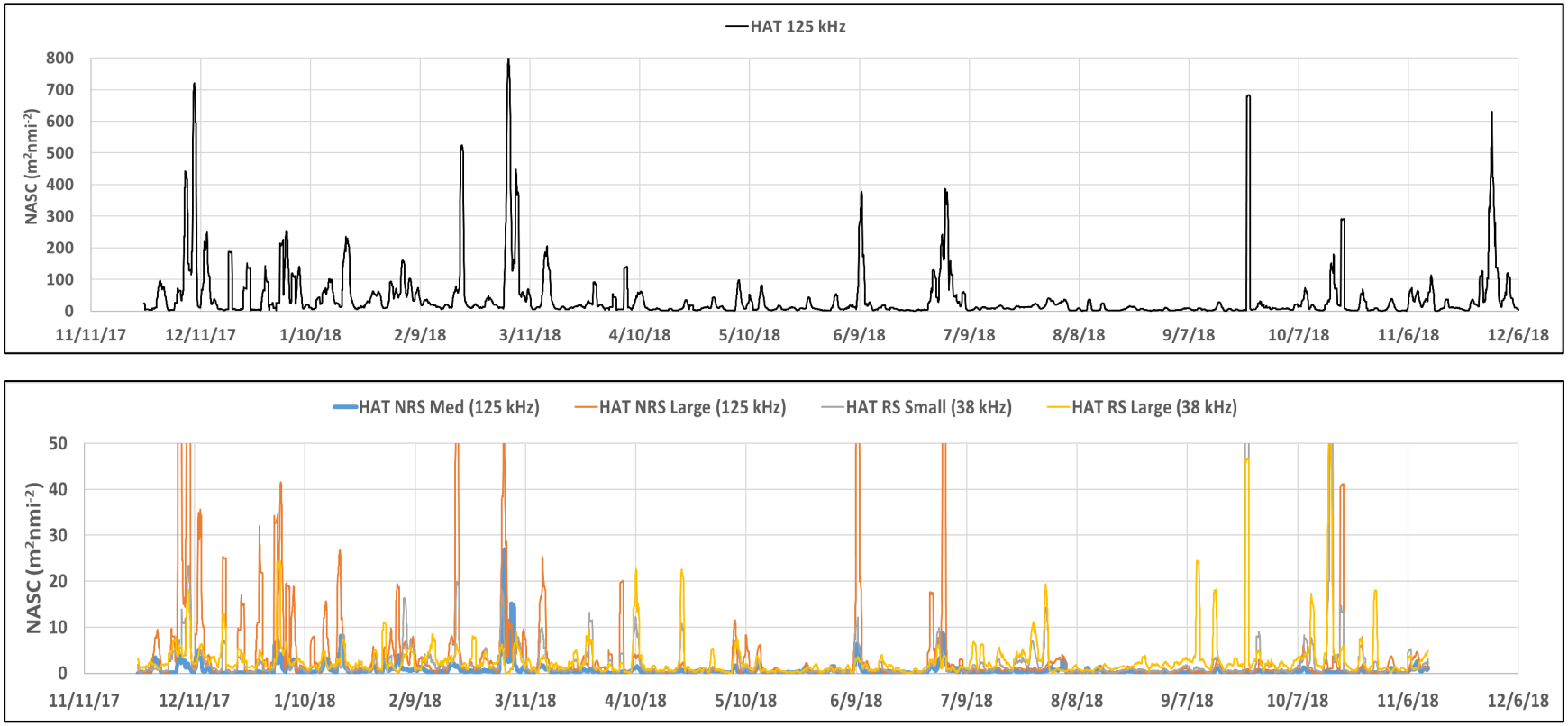

Figure 107. Cape Hatteras (HAT) one year time series of nautical area scattering coefficient (NASC) time aligned with community structure

Top: Hourly full water column integrated HAT 125 kHz NASC time series smoothed with a 24 point moving average. Bottom: Time aligned HAT community structure NASC time series where the NRS Medium and NRS Large were exported from the 125 kHz data, and the RS Small and RS Large were exported from the 38 kHz data.

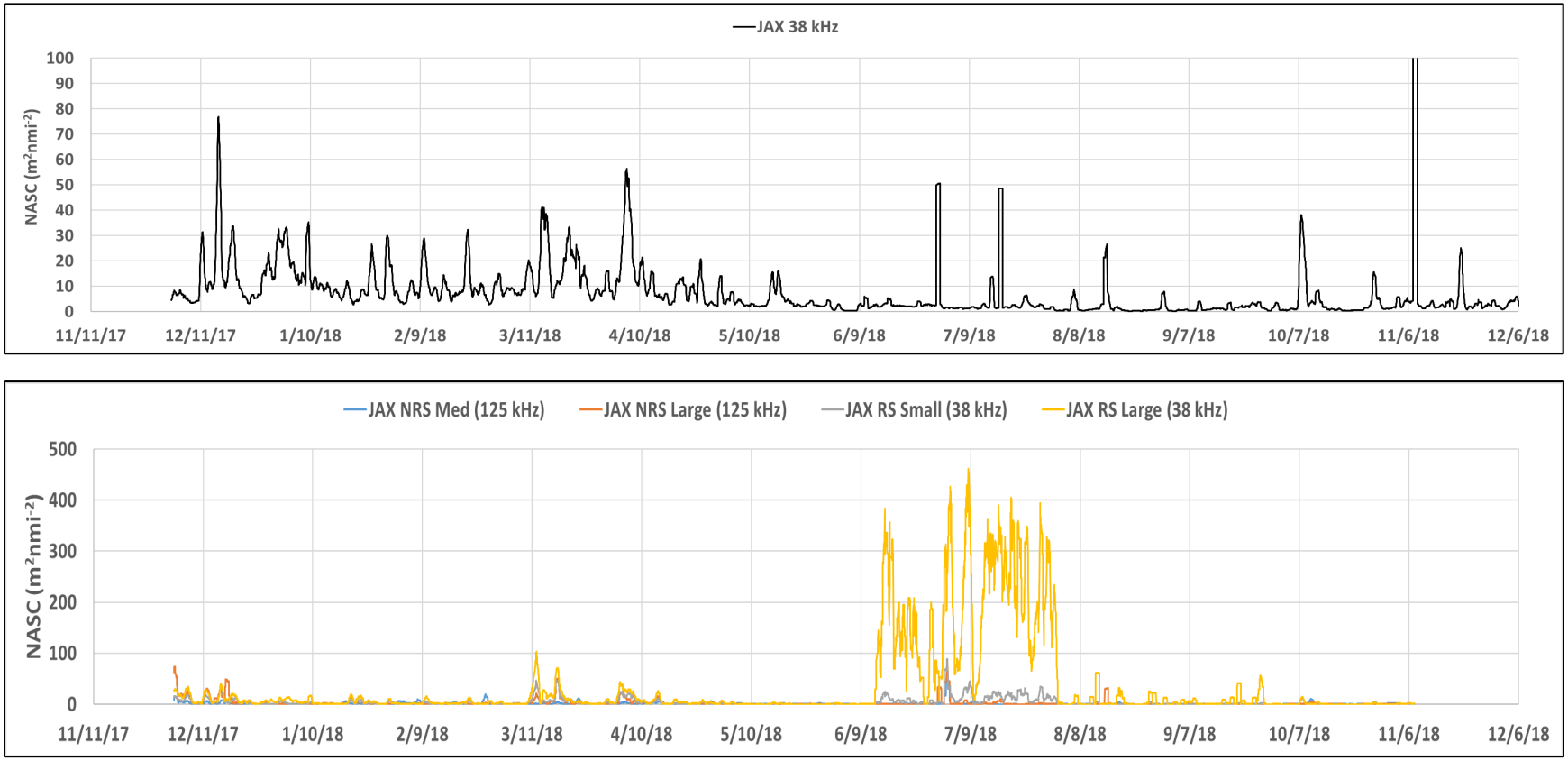

Figure 108. Jacksonville (JAX) one year time series of NASC time aligned with community structure

Top: Hourly full water column integrated JAX 125 kHz NASC time series smoothed with a 24 point moving average. Bottom: Time aligned JAX community structure NASC time series where the NRS Medium and NRS Large were exported from the 125 kHz data, and the RS Small and RS Large were exported from the 38 kHz data.

7.5 Marine Mammal Summary

7.5.1 Marine Mammal Biodiversity Summary by Site

Appendix E describes the presence of each species or group of marine mammals detected in the ADEON data. This section provides a summary of the marine mammal diversity and a discussion of the limitations of the analysis performed.

The acoustic marine mammal results presented in this report can be used to describe the relative occurrence trends of species across the study area. However, many factors influence the detectability of marine mammal acoustic signals and these should be considered when interpreting the results. An absence of detections does not necessarily indicate absence of animals; that can be due to lack of vocalizations by individuals near the acoustic recorders, masking of signals by environmental or anthropogenic noise sources, or a combination of these factors. Different sound propagation environments (influenced by anthropogenic activity, season, weather, etc.) will affect the detection range of a given signal and therefore influence whether signals are detected. Furthermore, some species change their vocal repertoire seasonally making it challenging to interpret true changes in seasonal occurrence via acoustics alone. Some acoustic signals cannot be reliably differentiated across species, therefore, in some instances, species groups can be identified but not separate species.

The method employed to analyze large acoustic data sets can also influence occurrence results and the strengths and shortcomings of any method employed should be considered. Reliable identification of marine mammal vocalizations in acoustic data by human analysts (manual analysis) via spectrograms is considered the gold standard in PAM analysis and is often the closest researchers can get to truth data. Though manual acoustic data analysis is considered reliable, it is extremely time consuming, can be challenging, requires expert analysts, and is subject to human error and bias with performance across analysts varying (Leroy et al., 2018). A second method commonly employed to identify marine mammal signals in acoustic data is the implementation of automated detector-classifier algorithms (henceforth referred to as automated detectors). Automated detectors have the benefit of being consistent and efficient. However, the performance of such systems can be variable and require some level of human validation as was argued in Kowarski & Moors-Murphy (2020).

Given the size of the present data set (both spatially and temporally), and the limited time allocated to identifying marine mammal occurrence, a combination of automated and manual detection techniques was employed with a suite of automated detectors applied to the data and 0.5% of the data subsequently selected for manual validation (Kowarski et al., 2021). It is important to note that with such limited data manually reviewed, very rare species may have been missed or their occurrence underestimated, especially where automated detector performance was low. The performance of each automated detector was determined (see performance metrics in Appendix C), and only automated results deemed reliable were provided for each acoustic signal type in Appendix C. If ever the 0.5% subset of data manually analyzed was not sufficiently large to capture the full range of acoustic environments in the full data set, the resulting automated detector performance metrics may be inaccurate and therefore should be taken as an estimate.

More fine-scale marine mammal acoustic occurrence results by species and vocalization type can be found in Appendix E, but overall occurrence for all species by month is summarized in Figure 109 and is based solely on manual analysis, therefore marine mammal presence discussed here has been validated and can be considered reliable. Indeed, the few inevitable human errors at the acoustic file level during

manual analysis are not expected to influence the broad-scale monthly occurrence trends presented in Figure 109.

In total, six mysticete, and at least eight odontocete species occurred during the monitoring period. Mysticete species include blue, fin, humpback, minke, right, and sei whales with minke and fin whales being the most common (Figure 109). Odontocete species acoustically confirmed or suspected to be present included Kogia sp., Cuvier's beaked whales, Gervais' and True's beaked whales (considered together due to overlapping repertoire), Blainville's beaked whales, sperm whales, and delphinid sp. which include small dolphins as well as killer and pilot whales (Figure 109). It was not uncommon to have five or more species present in the sane month at a given station with species diversity increasing in the winter months when more mysticete species were acoustically present (Figure 109).

Mysticete whale acoustic occurrence in the recording area was largely seasonal (most occurring between fall and spring), reflecting both their migratory patterns (broadscale southern movement during winter and northern movement during summer) and, perhaps more so, changes in their vocal repertoire. For some well-studied species like the humpback whale, changes in vocal repertoire, and therefore acoustic occurrence, are well documented with males producing songs in the western north Atlantic during their breeding season from as early as September to as late as May (with rare song occurrence in summer months) (Stanistreet et al., 2013; Kowarski et al., 2019). Similarly, both blue and fin whales sing from the fall to the spring, a behavior believed to be undertaken by males for the purpose of reproductive success, much like the humpback whales (Mellinger & Clark, 2003; Delarue et al., 2009; Delarue et al., 2018). While yet to be confirmed, it has also been proposed that sei and minke (and potentially even right) whales have a seasonal level to their vocal repertoire that is likely driven by males, and such trends are apparent in Figure 102 (Risch et al., 2019, Nieukirk et al., 2020). North Atlantic right whales were only identified on one occasion and it is unclear if this is an underestimate resulting from limited manual review. Some mysticete species were more prevalent at northern stations such as the fin, blue, and humpback whales, while sei and minke whales were more dominant at the more southern stations (Figure 109).

Sperm whales were sporadically acoustically present throughout the recording period at all stations (Figure 109), though this is believed to be an underestimate in the true occurrence of the species due to a largely ineffective automated detector (see Sections D.12 and E.10). Dwarf and/or pygmy sperm whales (Kogia sp.) were absent from VAC and HAT and became increasingly common at the more southern stations, with a near-monthly presence at BLE (Figure 109).

Beaked whale clicks were detected in the acoustic data in all months of the year at SAV and BLE as well as in two instances at WIL (see Section E.1). Blainville's beaked whales, Cuvier's beaked whales, and a click type that belongs to Gervais and/or True's beaked whales were identified in the acoustic data (Figure 109). All beaked whale clicks at SAV were believed to be Gervais/True's beaked whales, the majority of detections at BLE were believed to be Blainsville's beaked whales, and Cuvier's beaked whales were suspected in three months at BLE (Figure 109).

Delphinids were by far the most acoustically prolific group of species in the recordings (Figure 109), occurring across essentially all months at all stations. The majority of delphinid clicks and dolphin whistles (see Dolphins in Figure 109) are likely produced by small dolphin species such as the Atlantic spotted, bottlenose, clymene, Fraser's, pantropical spotted, and/or Risso's dolphins. However, due to overlapping repertoires, some larger delphinids including false killer, killer, long-finned pilot, and short-finned pilot whale vocalizations are likely captured within the 'Dolphins' category (see Appendix E.3). Effort was made to differentiate pilot and killer whale whistles from small dolphin tonals, though some level of error is expected given the overlapping repertoires (see Appendix E.3). Pilot whale whistles

occurred sporadically through the recordings at all stations while killer whale whistles were more rare (Figure 109). With such overlapping repertoires, it is difficult to know to what extent these species were underestimated.

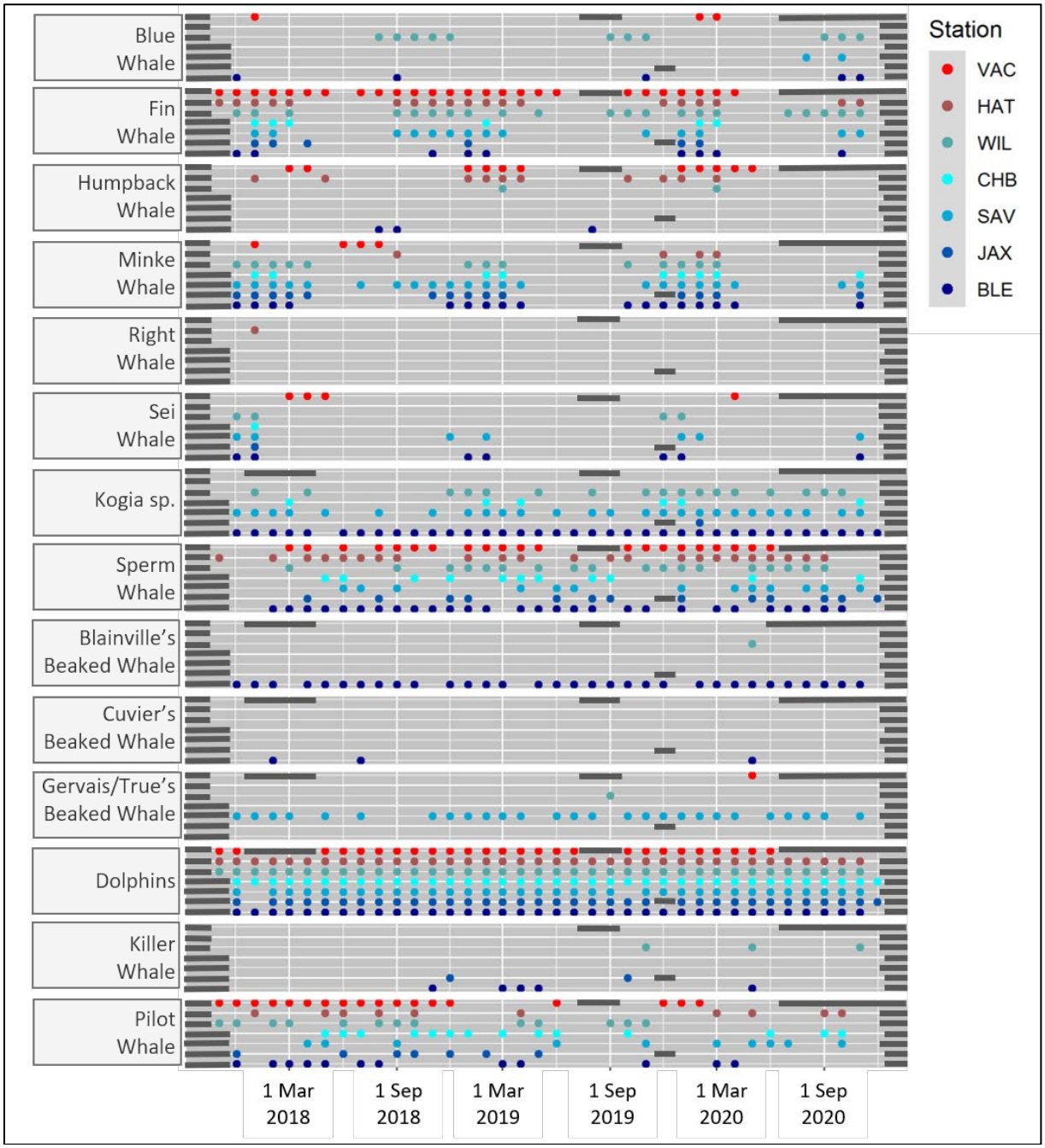

Figure 109. Presence of marine mammals by month and station for the ADEON project

The species is shown in the left-hand tab of each sub-figure. Kogia sp. may also include instances of harbor porpoise clicks. Some instances of pilot and killer whale vocalizations are likely captured across each other and within Dolphins due to the difficulty in discriminating between these species. Horizontal dark lines indicate periods where no acoustic data was collected. See Appendix E.3 for detailed species and vocalization occurrence results.

7.5.2 Relative Abundance of Minke Whales

Passive acoustic monitoring (PAM) as an indirect observation method is effective for monitoring marine mammal populations (Marques et al., 2013). Even though PAM devices can monitor a large area from a single site, the size of the monitored area will fluctuate over time due to the proximity of human activities, changing wind-driven ambient sound levels and/or changes in vocal behavior (Tyack, 2008; Carey & Evans, 2011; Pine et al., 2018). Abundance or density estimation methods based on PAM data need to account for these effects.

Abundance estimation methods may provide estimates of population size (absolute abundance) or indices (relative abundance) (Eberhardt & Simmons, 1987; Chen et al., 2004). Because it is often difficult or impractical to estimate absolute abundance, relative abundance indices are more commonly used (Dice, 1941; Nichols & Pollock, 1983; Chen et al., 2004; Hopkins & Kennedy, 2004).

In recent years, counts of animal vocalizations in PAM recordings have been used to estimate animal density using a canonical density estimator equation (Mellinger et al., 2007; Marques et al., 2009; Kusel et al., 2011; Martin et al., 2013; Hildebrand et al., 2019):

$$\widehat{\boldsymbol{D}} = \frac{\boldsymbol{n_c}\,(\boldsymbol{1}-\hat{\boldsymbol{c}})}{\boldsymbol{k\pi w^2 \widehat{P} T \hat{r}}} \qquad 1$$

In this approach, the estimated density of marine mammals ($\widehat{D}$) is calculated from the number of vocalizations (n_c) corrected by the estimated average proportion of false positives ($\hat{c}$), divided by the number of sensors (k), study time (T), the estimated mean probability of detecting the vocalization in the area surveyed by each sensor ($\widehat{P}$), the area surveyed (πw^2 where w is the area's radius), and the estimated vocalization production rate ($\hat{r}$).

Equation 1 includes factors that represent the probability of detecting vocalizations as a function of distance ($\widehat{P}$). Due to complexity and cost to estimate this parameter, $\widehat{P}$ as a function of distance is generally estimated once and treated as fixed for a full data set (Marques et al., 2010; Martin et al., 2013).

In the method proposed in Kiehbadroudinezhad et al. (in prep) which was developed using ADEON data, the elements of $\widehat{P}$ that represent the probability of missed detections are combined with $\hat{c}$. The remaining elements of $\widehat{P}$ are replaced with a detectability coefficient (Ω) that accounts for noise and acoustic propagation conditions. The proposed equation for the relative abundance index $\hat{A}$ is:

$$\hat{A} = \Omega \frac{n_{ca}\,(1 - PFP + PFN)}{T\hat{r}} \qquad 2$$

where Ω is the detectability coefficient, n_{ca} is the total number of pulse trains obtained from the automated detection algorithm, T is the study time, $\hat{r}$ is the estimated vocalization production rate,

PFP is the proportion of false positives, and PFN is the proportion of false negatives.

Figure 110 presents the result of applying the relative abundance index to all seven ADEON stations for both years. Temporally, the result shows the minke whales present from winter to mid-spring. This agrees with the known wintering of minke whales in southern waters (Risch et al. 2014).

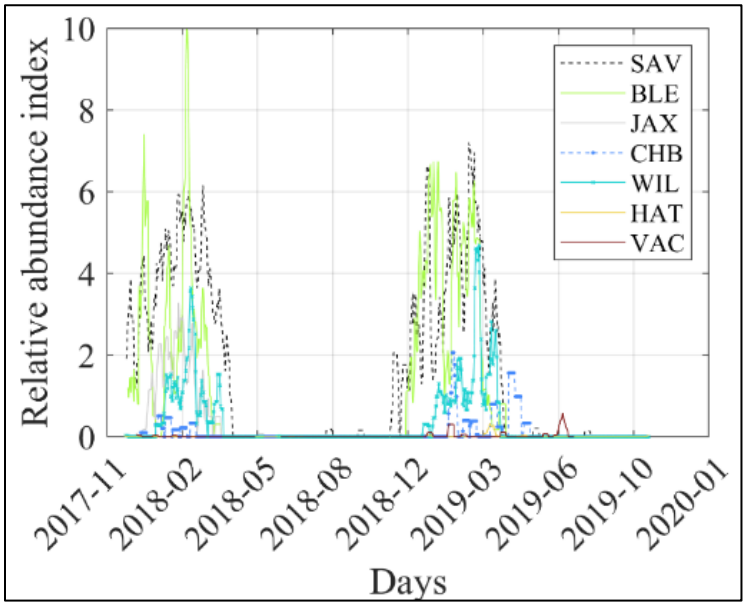

Figure 110. An 8-day moving average for relative abundance index of audible minke whales for 2 years at the seven stations using Equation 2

To be published in Kiehbadroudinezhad et al. (in prep).

To summarize the results and provide a spatial and temporal interpretation, the relative abundance index was summed by month per year and the average of two years was calculated and plotted as variable sized bubbles by station (Figure 111). Minke whales are present in deep waters of the OCS from December through April and have a peak concentration near the site offshore of Savannah Georgia (SAV) in both years. They also show a high concentration at Blake Escarpment (BLE) station and are present at JAX, CHB, and Wilmington (WIL). They were rarely present at HAT and VAC. The results also indicate a northward migration starting in February through April.

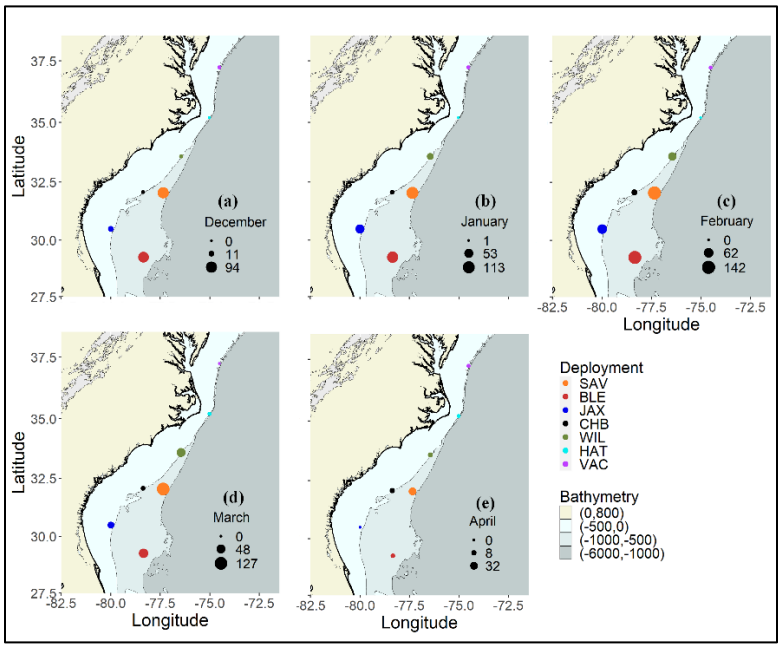

Figure 111. The relative minke whale abundance index at the ADEON sites

Relative minke whale abundance index at the ADEON sites in a) December, b) January, c) February, d) March, and e) April. The maximum relative abundance index values were 94, 113, 142, 127, and 32 for December, January, February, March, and April, respectively. The minimum value of 0 represents the absence of minke whales in March, April, and February at VAC, JAX, and HAT, respectively. The best available minke whales density results from (Roberts et al. 2016) were 731, 715, 691, 750, 1498 in December, January, February, March, and April, respectively, at the East Coast The peak concentrations were towards south at the ADEON sites in December–March and was towards north in April. To be published in Kiehbadroudinezhad et al. (in prep).

7.6 Ecological Modeling

Based on the ADEON ecological modelling effort to date, several main conclusions can be drawn regarding regional and seasonal ecological patterns. Dynamic oceanographic variables explained seasonal and regional patterns in cetacean activity and prey distribution in the water column well but explained prey abundance with moderate success due to the high variability associated with NASC values estimated via the AZFP active acoustic data. Sea surface temperature (SST), front metrics and current speeds were the most important predictors of prey vertical distribution and biomass. Prey were shallower and more aggregated in warmer waters and contrary to expectations, were deeper in association with more persistent fronts and faster current speeds. SST, chlorophyll, current speeds and, to a lesser extent, frontal metrics were important predictors of cetacean activity. Likelihood of occurrence of all species of cetaceans was highest in cooler waters (<20 °C), in areas of moderate productivity and with decreasing distance from sea surface fronts. Responses varied according to cetacean group, and frontal metrics were more important predictors of activity for epi-to-mesopelagic species (dolphins, pilot whales) than meso-bathypelagic species (beaked, sperm whales), indicating that species foraging closer to surface are more responsive to physical processes at/near the sea surface. Prey metrics were significantly correlated with cetacean activity (except for pilot whales), but only marginally increased model performance compared to

models just retaining oceanographic variables. Cetacean activity generally increased with prey aggregation. Future work will disentangle the effect of different prey communities on cetacean activity.

8. Outreach and Partnerships

8.1 Data Management and Access

8.1.1 NOAA's National Centers for Environmental Information

The National Oceanic and Atmospheric Administration's (NOAA's) National Centers for Environmental Information (NCEI-Boulder) was chosen for the Atlantic Deepwater Ecosystem Observatory Network (ADEON) data collection archive because it serves the ocean passive and active acoustics data domain. The NCEI archive provides an online searchable map of raw data (Figure 112) collected at specific sites within the world's oceans. This public data is searchable by Organization, Agency, Ship, or Instrument. The ADEON dataset types, acoustic zooplankton fish profiler (AZFP) (active acoustics) and autonomous multichannel acoustic recorder (AMAR) (passive acoustics), were the first of their kind to be housed at NCEI.

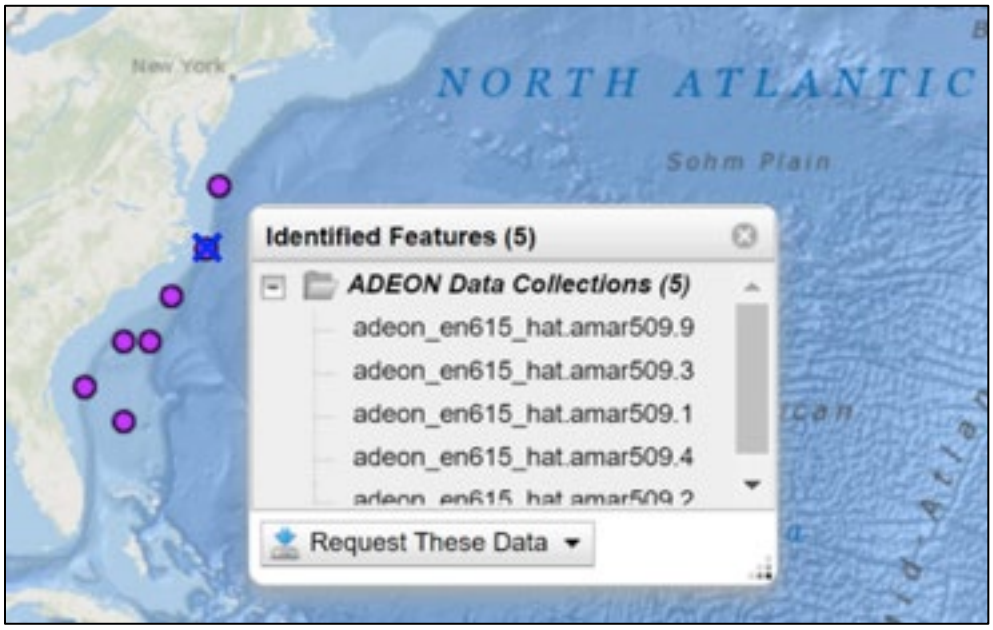

Figure 112. ADEON data served out of National Centers for Environmental Information (NCEI) archive

The NCEI data software (one for active acoustics and one for passive) that packages raw data for archiving at the facility was sent to the data management team at the University of New Hampshire (UNH) Research Computing Center (RCC). The software operates on a Microsoft® Windows computer but given the magnitude of data files to be archived (8 to 10 TB), RCC had to adapt the NCEI source code to run on a high capacity, fast compute, Linux-based server.

The adapted code testing included the software assisted International Organization for Standardization (ISO) 19-115 metadata standardization generator that bundles metadata with the dataset. After supplying NCEI with a full packet, a review of the dataset and metadata was performed by NCEI and RCC for accuracy and compliance. This work ensured that ADEON data sent to NCEI transferred with quality, accuracy, and in compliance with ISO 19-115. Because of this fruitful collaboration, the first of ADEON's raw data was served out to the public two years ahead of the contract deliverable date. The success of this collaboration is highlighted in a correspondence from a colleague at NCEI:

“The ADEON team are a pleasure to work with and have set a new standard for science teams sending data to NCEI for archiving. They reached out to NCEI long before data started flowing to learn what was needed to archive their data with NCEI and have worked closely with us to develop a smooth pipeline for data submission. The ADEON team shows particular dedication to providing the rich metadata necessary for long-term data preservation and usability. They are also the driving force behind utilizing high-capacity network connections to transfer large data volumes to NCEI. The partnership with the ADEON team has even led to external funding proposals to develop new tools tailored to large data submissions to NCEI.” Charles Anderson, NCEI.

The ADEON data collection at NCEI can be accessed by clicking on the ADEON data portal links or directly via the NCEI links.[19]

8.1.2 The Ocean Tracking Network (OTN)

The Ocean Tracking Network (OTN) is a global aquatic animal tracking, data management, and partnership platform headquartered at Dalhousie University in Canada. The ADEON team collaborated with this group to share data from the ADEON sites that contain VEMCO Instruments (Figure 113). ADEON bottom landers equipped with VEMCO Fish Finders record the tag number of any tagged fish that passes through its vicinity. The fish counters are co-located with the AZPF instruments. Though ADEON has seven acoustic listening sites, the AZFP’s and the fish counters are found only at Virginia Inter-Canyon (VAC), Cape Hatteras (HAT), and Jacksonvlle (JAX) locations. ADEON data can be found on OTN[20].

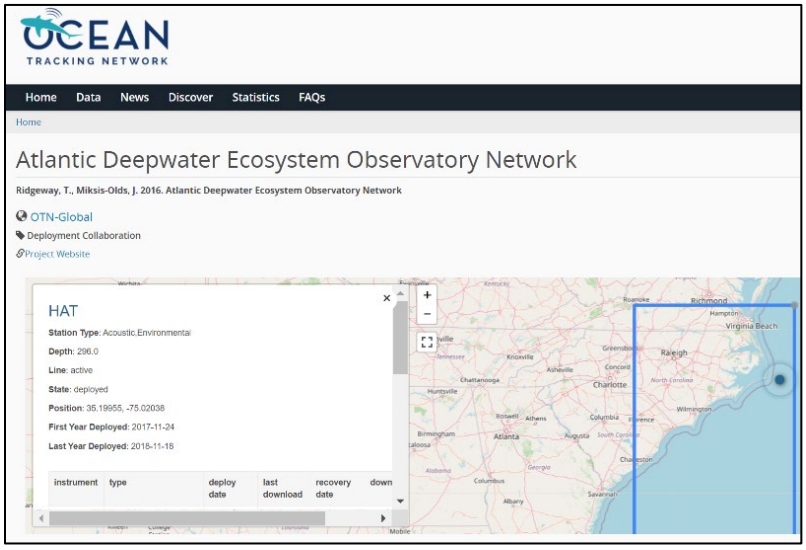

Figure 113. ADEON "Fish Tag" data shared on the Ocean Tracking Network (OTN) online map

[19] See https://www.ngdc.noaa.gov/maps/water_column_sonar/index.html and https://maps.ngdc.noaa.gov/viewers/passive_acoustic/ .
[20] See https://members.oceantrack.org/OTN/project?ccode=ADEON .

8.2 Art at Sea

Acoustics, though an exciting interdisciplinary technical field, is often not easily appreciated by the general public. Art, in all of its forms, is designed to reach every part of society. The motivation for developing partnerships with the fine arts community was to foster relationships where acoustics can be celebrated and captured through art, making it more assessable to the general public. Science artist, Lindsay Olson, joined the science crew of the second ADEON cruise EN615. Lindsay participated in all aspects of safety and science while onboard, in addition to devoting time to cultivating artistic ideas (Figure 114).

Figure 114. Artist Lindsay Olson (right) participating in a fire hose safety drill aboard the RV *Endeavor*. (Photo credit: Jennifer Miksis-Olds).

Lindsay is a textile artist and produced two tapestries as a direct result of her participation in ADEON. The first piece illustrates passive acoustics and gracefully weaves together the beauty, utility, and math of passive acoustics. The wave equation and other relevant equations governing the behavior of acoustic energy in the ocean are handstitched throughout the piece (Figure 115). The second work was focused on active acoustics and captures the daily migration of zooplankton as images by an echosounder (Figure 116). In October 2019, the UNH Center for Acoustics Research and Education and the UNH Museum of Art co-sponsored a community seminar titled “Sounds in the Sea: The Art and Science of the Ocean” that was jointly given by Artist Lindsay Olson and ADEON Lead-PI Jennifer Miksis-Olds. Lindsay’s art has been on display at UNH, invited to the Smithsonian, and featured in many other seminars and popular articles.[21] .

[21] See https://www.lindsayolsonart.com/portfolio/soundinthesea .

Figure 115. Passive acoustic tapestry artwork depicting embroidered equations governing ocean sound (Photo credit: Lindsay Olson.)

Figure 116. Active acoustic tapestry artwork depicting zooplankton daily migration

The mathematic equations specific to the sonar equation are embroidered throughout the work. (Photo credit: Lindsay Olson.)

Artist Wendy Klemperer joined the fourth ADEON cruise AR040. Wendy is a watercolor artist and sculptor. Wendy produced many water colors and portrait drawings throughout the cruise. She was able to share her art and passion with the science and ship crew during an onboard art show (Figure 117). The UNH Center for Acoustics Research and Education and the UNH Museum of Art co-sponsored a full gallery show during the Fall of 2021.

Figure 117. Artist Wendy Klemperer.
At work (left) and during the onboard art show (right). (Photo credit: Jennifer Miksis-Olds.)

8.3 Web Presence

The ADEON project hosted a well visited website[22] (Figure 118). This site delivers information to the public about the project through: 1) a cruise blog where topics provide a glimpse (and photographs) of the science being done, 2) a news and events column, 3) a cruise page with reports, network maps, and lander deployment videos, 4) a dynamic data visualization and mapping mini site which includes the opportunity to download raw data snippets of selected sound recording files, 5) a visual gallery of cruise tracks and activities, and 6) an audio gallery where visitors can run animated visualizations while listening to sounds (e.g. whales calls, dolphin clicks, ship sound) collected from the ADEON network ocean bottom landers by clicking on spectrograms (Figure 119). The location of each recording is identified by animal, seismic, or human-produced sounds along with the location of where the recording was captured.

[22] See ADEON Website and Data Portal - https://adeon.unh.edu/ .

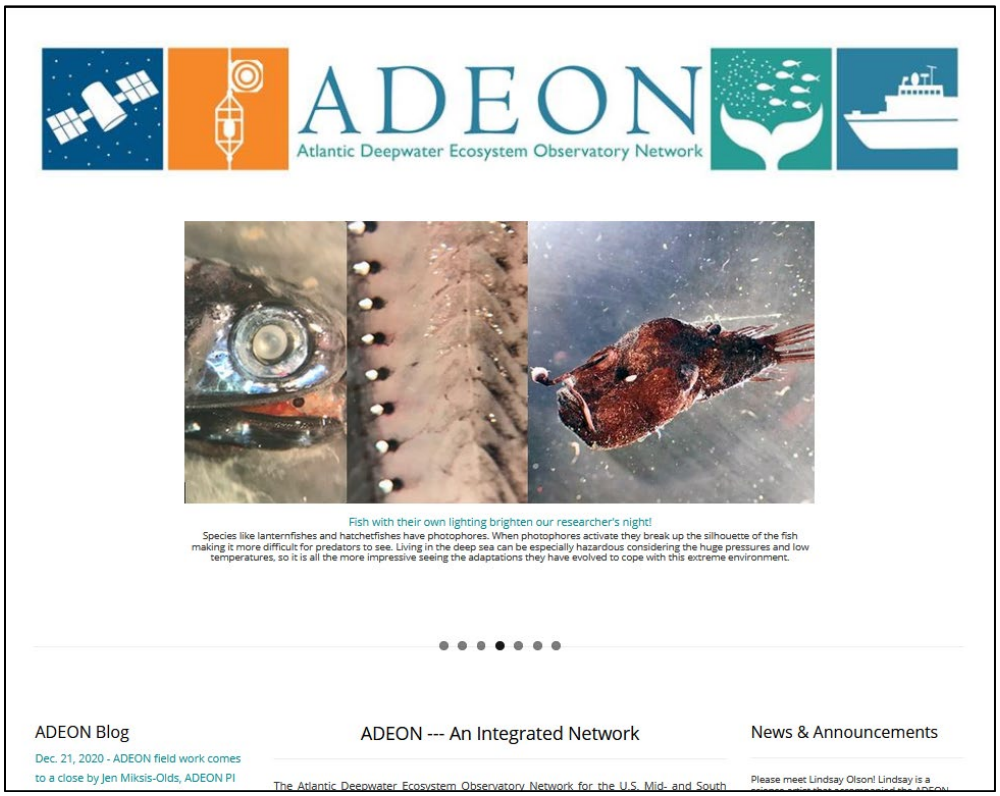

Figure 118. Screen shot of the ADEON website home page

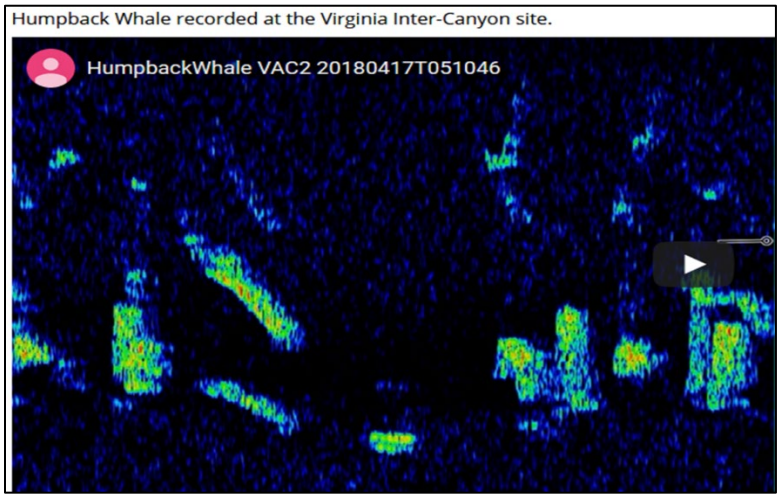

Figure 119. Soundscape spectrogram in the ADEON Audio Gallery

On the “Data & Standards” page, visitors can access and download the information provided in the ADEON Standardization Library and the Data Portal. The library contains all the ADEON Standards products: Soundscape Standardization document, the Project Dictionary, the Calibration and Deployment Good Practice Guide, the Hardware Specification, and the Data Processing Specification. The ADEON data portal provides visitors with access to raw data files and data products. Files are served from ADEON’s server, Figshare.com, or NCEI.

NOAA’s NCEI-Boulder was chosen for the ADEON raw data collection archive because it serves the ocean passive and active acoustics data domain. The NCEI archive provides an online searchable map of raw data (Figure 112) collected at specific sites within the world’s oceans. This public data is searchable by Organization, Agency, Ship, or Instrument. The ADEON dataset types, AZFP (active acoustics) and AMAR (passive acoustics), were the first of their kind to be housed at NCEI. The ADEON data collection at NCEI can be accessed by clicking on the ADEON website data portal links or directly via the NCEI links[23].

FIGSHARE is a global, online repository where research outputs can be made publicly available in a citable, shareable, and discoverable manner. It was selected for archiving ADEON produced data, model videos, and documentation. Each item placed in this collection is assigned a unique digital object identifier (DOI). As shown in the Figure 120, when a Figshare search on “ADEON” is performed, the collection contents and DOIs are listed. If data is used or referenced by others, the ADEON project and researchers must be cited using the citation that is provided with the data or file set. ADEON data is shared under a Creative Commons CC (by attribution) BY 4.0 license.

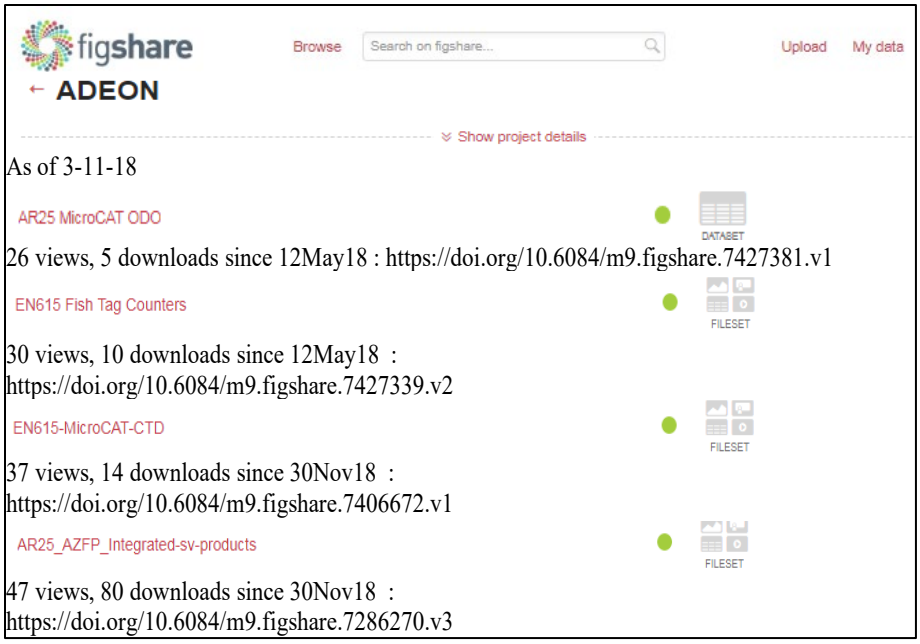

Figure 120. Figshare sample of ADEON collection search

[23] See https://www.ngdc.noaa.gov/maps/water_column_sonar/index.html and https://maps.ngdc.noaa.gov/viewers/passive_acoustic/ .

The ADEON Data Portal serves information to the public by Research Cruise and then by the method of data measurement. ADEON data is collected from instruments: 1) making measurements while underway during the deployment, harvesting, and redeployment of our bottom-landers (e.g. EK80, ES60, CTD, net tows, and marine mammal observations) along with various "Ship Data" collected as part of the vessel's participation in the Rolling Deck to Repository (R2R) project; and 2) the bottom-lander platform instrumentation (e,g, AMAR, AZFP, conductivity, temperature, depth [CTD], Fish Tag Counter) that collect data for 6–12 months at a fixed location. The portal provides access to both level 0–1 (raw) data and level 2+ (produced) data. Visitors can use the portal table (e.g., Figure 121) to obtain data access by clicking on the links in the rows below each cruise name and date.

Data and Products	Data File Type	Cruise AR25 Nov-Dec 2017	Cruise EN615 Jun-18	Cruise EN626 Nov-18	Cruise AR040 Nov-19	Cruise AR049 Dec-20
Cruise Report - describes work performed and data collected.	.pdf	CruiseReport_AR25	CruiseReport_EN615	CruiseReport_EN626	CruiseReport_AR040	CruiseReport_AR049
Marine Mammal Observation Database (MMO)	.xlsx	MMO_AR25	MMO_EN615	MMO_EN626	MMO_AR040	no data this cruise
Acoustic Zooplankton Fish Profiler (AZFP)						
Calibrated sv matrices	.csv	coming soon via NCEI	coming soon via NCEI	coming soon via NCEI	coming soon via NCEI	coming soon via NCEI
Integrated sv products	.csv	AZFP_sv_AR25	AZFP_sv_EN615	AZFP_sv_EN626	AZFP_sv_AR040	AZFP_sv_AR049
Vessel-based Fine Scale Acoustic Surveys (FSAS)						
Echosounder data (e.g. EK80, ES60)	.raw	R2R_AR25	EN615 EchoSound(NCEI)	coming soon via NCEI	R2R_AR040	R2R_AR049
FSAS binned into cells of 100m horizontal and 5m vertical	.csv	FSAS_AR25	FSAS_EN615	FSAS_EN626	FSAS_AR040	FSAS_AR049
JASCO Autonomous Multichannel Acoustic Recorder (AMAR)						
Raw .wav files	.wav	coming soon via NCEI	AMAR EN615 (NCEI)	coming soon via NCEI	coming soon via NCEI	coming soon via NCEI
AMAR Products		AMAR L2 AR025	AMAR L2 EN615	AMAR L2 EN626	AMAR L2 AR040	AMAR L2 AR049
MicroCAT CTD	.xlsx	C-T-ODO_AR25	C-T-ODO_EN615	C-T-ODO_EN626	C-T-ODO_AR040	C-T-ODO_AR049
Vemco Fish Finder	.csv	n/a	Tag Counts_EN615	Tag Counts_EN626	Tag Counts_AR040	Tag Counts_AR049
Rolling Deck to Repository (R2R) - underway data.	varied	R2R_AR25	R2R_EN615	R2R_EN626	R2R_AR040	R2R_AR049

Figure 121. ADEON Data Portal Table Schema

The UNH Research Computing Center uses AWStats to monitor ADEON's website activity. Figure 122 below, demonstrates when the site experienced additional visitors during cruise time. ADEON cruises provided daily blogging [including photos] on research activities and findings. Figure 123 provides download rates for ADEON documents. The totals do not include rates at ADEON's Figshare archive[24]. The Soundscape Standardization document has been downloaded more than any other document[25]. Over the duration of the project, this document was downloaded at an average of 50 per month.

[24] See Figshare.com/ADEON .

[25] See https://doi.org/10.6084/m9.figshare.6792359.v3

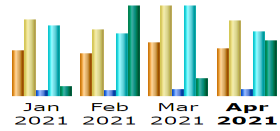

Month	Unique visitors	Number of visits	Pages	Hits
Jan 2021	411	688	1,680	21,665
Feb 2021	383	605	1,726	19,410
Mar 2021	484	813	2,039	27,783
Apr 2021	427	683	2,035	19,968

Project End September 2021

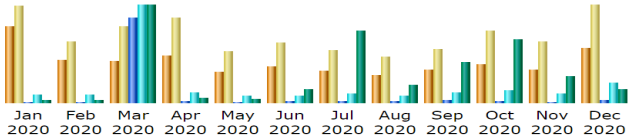

Unique visitors	Number of visits	Pages	Hits
5,275	8,676	245,680	507,145

December 2020: Cruise 5, AR049

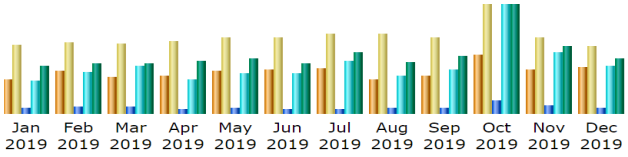

Unique visitors	Number of visits	Pages	Hits
5,336	9,843	27,866	215,979

November 2019: Cruise 4, AR040

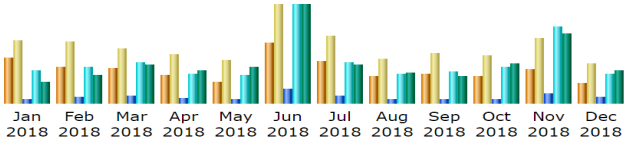

Unique visitors	Number of visits	Pages	Hits
8,025	13,623	45,213	307,524

2018: Cruises 2&3, EN615 June, EN626 Nov.

Project Start October 2017

Unique visitors	Number of visits	Pages	Hits
2,254	3,350	14,527	139,232

Nov/Dec 2017: Cruise 1, AR025

Figure 122. ADEON website statistics

Unique Visitor: a unique visitor is a person or computer that has made at least 1 hit on 1 page of the site. If a user makes several visits during a single month, it is counted only once. *Visits*: the number of visits made by all visitors. All "pages" are included per visit; expect multiple pages per visit and multiple visits per unique visitor. Pages: the number of "pages" viewed by visitors. *Hits*: files requested from the server (including files that are "Pages"). Please note, website analytics are complicated; values should be used only to visualize general use and downloading trends.

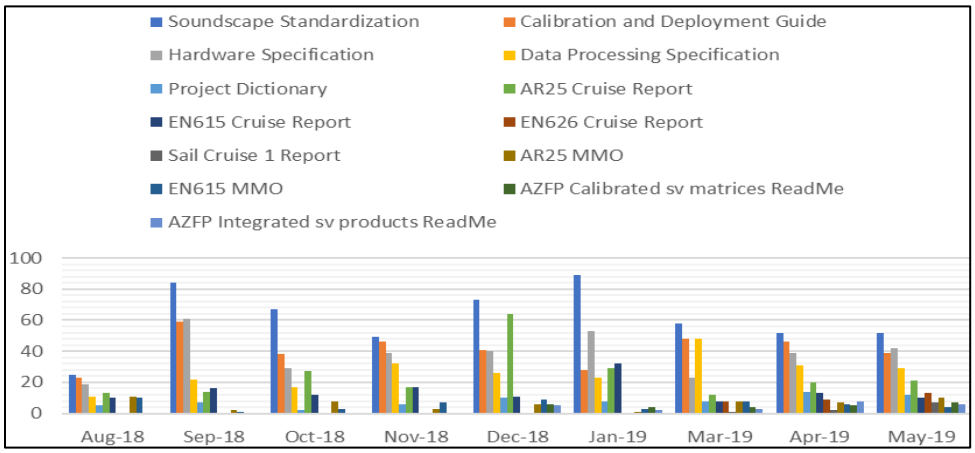

Figure 123. ADEON's website documentation download rates from 2018–2019

References

Agafonkin V, Leaflet, https://leafletjs.com/, July 2021.

Ainslie MA, Miksis-Olds JL, Martin B, Heaney K, de Jong CAF, et al. 2018. ADEON underwater soundscape and modeling metadata standard. Version 1.0. Durham (NH): University of New Hampshire. Contract No. M16PC00003.

Ainslie MA, de Jong CAF, Martin SB, Miksis-Olds JL, Warren JD et al. 2020. ADEON project dictionary: terminology standard. Document 02075, Version 1.0. Durham (NH): University of New Hampshire. Contract No. M16PC00003. https://doi.org/10.6084/m9.figshare.12436199.v2

Anderson VC. 1950. Sound scattering from a fluid sphere. J Acoust Soc Am. 22(4):426-431.

Andrew RK, Howe BM, Mercer JA, Dzieciuch MA. 2002. Ocean ambient sounds: comparing the 1960's with the 1990's for a receiver off the California coast. Acoust Res Lett Online. 3(2):65-70.

Aschettino JM, Engelhaupt DT, Engelhaupt AG, DiMatteo A, Pusser T et al. 2020. Satellite telemetry reveals spatial overlap between vessel high-traffic areas and humpback whales (*Megaptera novaeangliae*) near the mouth of the Chesapeake Bay. Front Mar Sci. 7: 121. https://doi.org/10.3389/fmars.2020.00121.

Au WWL, Kastelein RA, Rippe T, Schooneman NM. 1999. Transmission beam pattern and echolocation signals of a harbor porpoise (Phocoena phocoena). J Acoust Soc Am. 106(6):3699-3705. https://doi.org/10.1121/1.428221.

Azzolin M, Papale E, Lammers MO, Gannier A, Giacoma, C. 2013. Geographic variation of whistles of the striped dolphin (*Stenella coeruleoalba*) within the Mediterranean Sea. J Acoust Soc Am. 134: 694-705. https://doi.org/10.1121/1.4808329.

Baumann-Pickering S, McDonald MA, Simonis AE, Berga AS, Merkens KPB, et al. 2013. Species-specific beaked whale echolocation signals. J Acoust Soc Am. 134(3): 2293-2301. https://doi.org/10.1121/1.4817832.

Baumgartner MF, Fratantoni DM. 2008. Diel periodicity in both sei whale vocalization rates and the vertical migration of their copepod prey observed from ocean gliders. Limnol Oceanogr. 53(5): 2197-2209. https://doi.org/10.4319/lo.2008.53.5_part_2.2197.

Berchok CL, Bradley DL, Gabrielson TB. 2006. St. Lawrence blue whale vocalizations revisited: characterization of calls detected from 1998 to 2001. J Acoust Soc Am. 120(4):2340-2354. [accessed 4 June 2021]; https://doi.org/10.1121/1.2335676

Blair HB, Miksis-Olds JL, Warren JD. 2021. Spatial variability of epi-and mesopelagic 38 kHz backscatter from nekton and macrozooplankton across the southeastern US shelf break. Mar Ecol Prog. 669:33-50.

Boyd I, Frisk G, Urban E, Tyack P, Ausubel J, et al. 2011. An international quiet ocean experiment. Oceanography. 24:174-181.

Carey WM, Evans RB, eds. 2011. Ocean ambient noise: measurement and theory. Underwater Acoustics Series. New York (NY): Springer. [accessed 4 June 2021]; https://doi.org/10.1007/978-1-4419-7832-5

Cayula J, Cornillon P. 1992. Edge detection algorithm for SST images. J Atmos Oceanic Technol. 9(1):67-80.

Chapman NR, Price A. 2011. Low frequency deep ocean ambient noise trend in the Northeast Pacific Ocean. J Acoust Soc Am. 129: EL161-EL165.

Chen J, Thompson ME, Wu C. 2004. Estimation of fish abundance indices based on scientific research trawl surveys. Biometrics. 60(1):116-23.

D'Spain GL, Hodgkiss WS, Edmonds GL. 1991. Energetics of the deep ocean's infrasonic sound field. J Acoust Soc Am. 89(3): 1134-1158. [accessed 4 June 2021]; https://doi.org/10.1121/1.400677.

Davis GE, Baumgartner MF, Corkeron PJ, Bell J, Berchok C et al. 2020. Exploring movement patterns and changing distributions of baleen whales in the western North Atlantic using a decade of passive acoustic data. Glob Change Biol.: 1-30. https://doi.org/10.1111/gcb.15191.

Davis GE. 2020. Using Passive Acoustic Data to track changes in baleen whale distribution throughout the Western North Atlantic Ocean [dissertation]. Boston (MA): University of Massachusetts Boston.

DeAngelis AI, Stanistreet JE, Baumann-Pickering S, Cholewiak DM. 2018. A description of echolocation clicks recorded in the presence of True's beaked whale (*Mesoplodon mirus*). J Acoust Soc Am. 144(5): 2691-2700. https://doi.org/10.1121/1.5067379.

De Robertis A, Higginbottom I. 2007. A post-processing technique to estimate the signal-to-noise ratio and remove echosounder background noise. ICES J Mar Sci. 64(6):1282-1291.

Dekeling RPA, Tasker ML, Van der Graaf AJ, Ainslie MA, Andersson M.H. et al. 2014. Monitoring guidance for underwater noise in European Seas, part II: monitoring guidance specifications, JRC Scientific and Policy Report EUR 26555 EN, Luxemburg (BE): Publications Office of the European Union.

Delarue JJ-Y, Kowarski KA, Maxner EE, MacDonnell JT, Martin SB. 2018. Acoustic Monitoring Along Canada's East Coast: August 2015 to July 2017. Document Number 01279, Environmental Studies Research Funds Report Number 215, Version 1.0. Technical report by JASCO Applied Sciences for Environmental Studies Research Fund, Dartmouth, NS, Canada. 120 pp + appendices.

Delarue JJ-Y, Todd SK, Van Parijs SM, Di Iorio L. 2009. Geographic variation in Northwest Atlantic fin whale (*Balaenoptera physalus*) song: Implications for stock structure assessment. J Acoust Soc Am. 125(3): 1774-82. https://doi.org/10.1121/1.3068454.

Dice LR. 1941. Methods for estimating populations of mammals. J Wildl Manage. 5(4): 398–407. [accessed 4 June 2021]; https://www.jstor.org/stable/pdf/3795684.pdf

Django. 2021. Django Software Foundation, https://www.djangoproject.com/, July 2021.

[DoN] Department of the Navy (US). 2016. Marine Species Monitoring Report for the U.S. Navy's Atlantic Fleet Training and Testing (AFTT) – 2015 Annual Report. Report by US Fleet Forces Command, Norfolk, Virginia.

Dunlop RA, Noad MJ, Cato DH, Stokes D. 2007. The social vocalization repertoire of east Australian migrating humpback whales (*Megaptera novaeangliae*). J Acoust Soc Am. 122(5):2893-2905. [accessed 4 June 2021]; https://doi.org/10.1121/1.2783115

Eberhardt LL, Simmons MA. 1987. Calibrating population indices by double sampling. J Wildl Manage. 51(3):665–675. [accessed 4 June 2021]; https://doi.org/10.2307/3801286

Erbs, F., S.H. Elwen, and T. Gridley. 2017. Automatic classification of whistles from coastal dolphins of the southern African subregion. J Acoust Soc Am. 141(4): 2489-2500. https://doi.org/10.1121/1.4978000.

Eskesen IG, Wahlberg M, Simon M, Larsen ON. 2011. Comparison of echolocation clicks from geographically sympatric killer whales and long-finned pilot whales. J. Acoust. Soc. Am. 130(1): 9-12. https://doi.org/10.1121/1.3583499.

European Commission. 2010. European Commission (2010) Commission Decision of 1 September 2010 on criteria and methodological standards on good environmental status of marine waters (notified under document C(2010) 5956). Official Journal of the European Union. L(232): 14–24. [accessed 4 June 2021]; http://dx.doi.org/10.25607/OBP-820

Filatova OA, Miller PJO, Yurk H, Samarra FIP, Hoyt E. et al. 2015. Killer whale call frequency is similar across the oceans, but varies across sympatric ecotypes. J. Acoust. Soc. Am. 138(1): 251-257. https://doi.org/10.1121/1.4922704.

Ford JKB. 1989. Acoustic behaviour of resident killer whales (Orcinus orca) off Vancouver Island, British Columbia. Can J Zool. 67(3):727-745. [accessed 4 June 2021]; https://doi.org/10.1139/z89-105.

Freedman D, Diaconis P. 1981. On the histogram as a density estimator: L_2 theory. Zeitschrift für Wahrscheinlichkeitstheorie und Verwandte Gebiete. 57(4):453-476. [accessed 4 June 2021]; https://doi.org/10.1007/BF01025868

Garcia HA, Zhu C, Schinault ME, Kaplan AI, Handegard NO et al. 2018. Temporal–spatial, spectral, and source level distributions of fin whale vocalizations in the Norwegian Sea observed with a coherent hydrophone array. ICES J. Mar. Sci.: fsy127. https://doi.org/10.1093/icesjms/fsy127.

Gassmann M, Wiggins SM, Hildebrand JA. 2015. Three-dimensional tracking of Cuvier's beaked whales' echolocation sounds using nested hydrophone arrays. J. Acoust. Soc. Am. 138(4): 2483-2494. https://doi.org/10.1121/1.4927417.

Gedamke J, Harrison J, Hatch L, et al. 2016. Ocean noise strategy framework roadmap. 144 p. Washington (DC): National Oceanic and Atmospheric Administration. [accessed 4 June 2021]; http://cetsound.noaa.gov/road-map

GeoServer, Open Source Geospatial Foundation, http://geoserver.org/, July 2021.

Gillespie D, Dunn C, Gordon J, Claridge D, Embling CB, Boyd I. 2009. Field recordings of Gervais' beaked whales *Mesoplodon europaeus* from the Bahamas. *J. Acoust. Soc. Am. 125*(5): 3428-3433. https://doi.org/10.1121/1.3110832.

Hamran ET. 2014. Distribution and vocal behavior of Atlantic white-sided dolphins (Lagenorhynchus acutus) in northern Norway. MSc Thesis. University of Nordland. http://hdl.handle.net/11250/282365.

Hayes SA, Josephson E, Maze-Foley K, Rosel PE. 2020. U.S. Atlantic and Gulf of Mexico Marine Mammal Stock Assessments - 2019. US Department of Commerce. US Department of Commerce. NOAA Technical Memorandum NMFS-NE-264, Woods Hole, MA, USA. 479 p. https://media.fisheries.noaa.gov/dam-migration/2019_sars_atlantic_508.pdf.

Hazen EL, Suryan RM, Santora JA, Bograd SJ, WatanukiY, et al. 2013. Scales and mechanisms of marine hotspot formation. Mar Ecol Prog Ser. 487:177-183.

Hazen EL, Abrahms B, Brodie S, Carroll G, Jacox MG, et al. 2019. Marine top predators as climate and ecosystem sentinels. Front Ecol Environ. 17(10):565-574.

Heaney KD, Campbell RL. Three-dimensional parabolic equation modeling of mesoscale eddy deflection. J Acoust Soc Am. 2016. 139(2):918-926.

Heaney K, Martin B, Miksis-Olds J, Ainslie M, Moore T. et al. 2020. ADEON Data Processing Specification, Version 1.0 FINAL. Durham (NH): University of New Hampshire. Contract No. M16PC00003.. https://doi.org/10.6084/m9.figshare.12412610.v1

Hildebrand JA, Baumann-Pickering S, Frasier KE, Trickey JS, Merkens KP et al. 2015. Passive acoustic monitoring of beaked whale densities in the Gulf of Mexico. Sci. Rep. 5: 16343. https://doi.org/10.1038/srep16343.

Hildebrand JA, Frasier KE, Baumann-Pickering S, Wiggins SM, Merkens KP et al. 2019. Assessing Seasonality and Density From Passive Acoustic Monitoring of Signals Presumed to be From Pygmy and Dwarf Sperm Whales in the Gulf of Mexico. Front. Mar. Sci 6. https://doi.org/10.3389/fmars.2019.00066.

Hodge KB, Muirhead CA, Morano JL, Clark CW, Rice,AN. 2015. North Atlantic right whale occurrence near wind energy areas along the mid-Atlantic US coast: Implications for management. Endanger. Species Res. 28(3): 225-234. https://doi.org/10.3354/esr00683.

Hodge LEW, Baumann-Pickering S, Hildebrand JA, Bell JT, Cummings EW et al. 2018. Heard but not seen: Occurrence of *Kogia* spp. along the western North Atlantic shelf break [Note]. Mar. Mamm. Sci. 34(4): 1141-1153. https://doi.org/10.1111/mms.12498.

Hopkins H, Kennedy ML. 2004. An assessment of indices of relative and absolute abundance for monitoring populations of small mammals. Wildl Soc Bull. 32(4):1289-1296.

Jennings P, Cain R. 2013. A framework for improving urban soundscapes. Appl. Acoust. 74(2): 293-299. https://doi.org/10.1016/j.apacoust.2011.12.003.

Johnson M, Madsen PT, Zimmer WMX, Aguilar de Soto N, Tyack PL. 2006. Foraging Blainville's beaked whales (*Mesoplodon densirostris*) produce distinct click types matched to different phases of echolocation. J. Exp. Biol. 209 (24): 5038-5050. https://doi.org/10.1242/jeb.02596.

Killebrew DA, Mercado E, III, Herman LM, Pack AA. 2001. Sound production of a neonate bottlenose dolphin. Aquat. Mamm. 27(1): 34-44.

Kite-Powell HL. 2009. Economic considerations in the design of ocean observing systems. Oceanography. 22:44-49.

Kowarski KA, Delarue JJ-Y, Gaudet BJ, Martin SB. 2021. Automatic data selection for validation: A method to determine cetacean occurrence in large acoustic data sets. JASA Express Lett 1: 051201. https://doi.org/10.1121/10.0004851.

Kowarski KA, Delarue JJ-Y, Martin B, O'Brien J, Meade R, Ó Cadhla O, Berrow SD. 2018. Signals from the deep: Spatial and temporal acoustic occurrence of beaked whales off western Ireland. PLOS ONE 13(6). https://doi.org/10.1371/journal.pone.0199431.

Kowarski KA, Moors-Murphy H, Maxner EE, Cerchio S. 2019. Western North Atlantic humpback whale fall and spring acoustic repertoire: Insight into onset and cessation of singing behavior. J. Acoust. Soc. Am. 145(4): 2305-2316. https://doi.org/10.1121/1.5095404.

Kowarski KA, Moors-Murphy H. 2020. A review of big data analysis methods for baleen whale passive acoustic monitoring. Mar. Mamm. Sci. (Early View). https://doi.org/10.1111/mms.12758.

Küsel ET, Mellinger DK, Thomas L, Marques TA, Moretti D, Ward J. 2011. Cetacean population density estimation from single fixed sensors using passive acoustics. J. Acoust. Soc. Am. 129(6): 3610-3622. https://doi.org/10.1121/1.3583504.

Lavery AC, Chu D, Moum J. 2010. Measurements of acoustic scattering from zooplankton and oceanic microstructure using a broadband echosounder. ICES J Mar Sci. 67(2):379-394.

Leroy EC, Thomisch K, Royer J-Y, Boebel O, Van Opzeeland I. 2018. On the reliability of acoustic annotations and automatic detections of Antarctic blue whale calls under different acoustic conditions. J. Acoust. Soc. Am. 144(2): 740-754. https://doi.org/10.1121/1.5049803.

Lesage V, Gavrilchuk K, Andrews RD, Sears R. 2017. Foraging areas, migratory movements and winter destinations of blue whales from the western North Atlantic. Endanger. Species Res. 34: 27-43. https://doi.org/10.3354/esr00838.

Lewison R, Hobday AJ, Maxwell S, Hazen E, Hartog JR, et al. 2015. Dynamic ocean management: identifying the critical ingredients of dynamic approaches to ocean resource management. BioScience. 65(5):486-498.

Macleod CD, Perrin WF, Pitman R, Barlow JP, Ballance L, D'Amico A et al. 2005. Known and inferred distributions of beaked whale species (Cetacea: Ziphiidae). J. Cetacean Res. Manage. 7(3): 271-286.

Madsen PT, Carder DA, Bedholm K, Ridgway SH. 2005. Porpoise clicks from a sperm whale nose - Convergent evolution of 130 kHz pulses in toothed whale sonars? Bioacoustic*s* 15(2): 195-206. https://doi.org/10.1080/09524622.2005.9753547.

Madsen PT, Payne R, Kristiansen NU, Wahlberg M, Kerr I, Møhl B. 2002. Sperm whale sound production studied with ultrasound time/depth-recording tags. *J. Exp. Biol.* 205(13): 1899-1906. https://doi.org/10.1242/jeb.205.13.1899.

Marques TA, Thomas L, Ward J, DiMarzio N, Tyack PL. 2009. Estimating cetacean population density using fixed passive acoustic sensors: an example with Blainville's beaked whales. J Acoust Soc Am. 125(4):1982-94. [accessed 4 June 2021]; DOI: 10.1121/1.3089590

Marques TA, Thomas L, Martin SW, Mellinger DK, Jarvis S, Morrissey RP, Ciminello C-A, DiMarzio N. 2010. Spatially explicit capture–recapture methods to estimate minke whale density from data collected at bottom-mounted hydrophones. J Ornith. 152:445-455. [accessed 4 June 2021]; https://doi.org/10.1007/s10336-010-0535-7

Marques TA, Thomas L, Martin SW, Mellinger DK, Ward JA, et al. 2013. Estimating animal population density using passive acoustics. Biol Rev. 88(2):287-309. [accessed 4 June 20210]; DOI: 10.1111/brv.12001

Marten K. 2000. Ultrasonic analysis of pygmy sperm whale (*Kogia breviceps*) and Hubb's beaked whale (*Mesoplodon carlhubbsi*) clicks. Aquat. Mamm. 26(1): 45-48.

https://www.aquaticmammalsjournal.org/share/AquaticMammalsIssueArchives/2000/AquaticMammals_26-01/26-01_Marten.pdf.

Martin B. 2013. Computing cumulative sound exposure levels from anthropogenic sources in large data sets. Proceedings of Meetings on Acoustics 19(1): 9. https://doi.org/10.1121/1.4800967.

Martin B, Hillis CA, Miksis-Olds J, Ainslie MA, Warren J. et al. 2018. ADEON Hardware Specification. Document 01412, Version 2.3. Durham (NH): University of New Hampshire. Contract No. M16PC00003.. https://doi.org/10.6084/m9.figshare.6809711

Martin SW, Marques TA, Thomas L, Morrissey RP, Jarvis S, et al. 2013. Estimating minke whale *(Balaenoptera acutorostrata*) boing sound density using passive acoustic sensors. Mar Mammal Sci. 29(1):142-158. [accessed 4 June 20210]; https://doi.org/10.1111/j.1748-7692.2011.00561.x

Maxwell SM, Hazen E, Bograd SJ, Halpern BS, Breed GA, et al. 2013. Cumulative human impacts on marine predators. Nat Commun. 4(1): 1-9.

Maxwell SM, Hazen EL, Lewison RL, Dunn DC, Bailey H, et al. 2015. Dynamic ocean management: Defining and conceptualizing real-time management of the ocean. Mar Pol. 58:42-50.

McDonald MA, Hildebrand JA, Wiggins SM. 2006. Increases in deep ocean ambient noise in the Northwest Pacific west of San Nicolas Island, California. J Acoust Soc Am. 120:711-717.

Mellinger DK, Clark CW. 2003. Blue whale (*Balaenoptera musculus*) sounds from the North Atlantic. J. Acoust. Soc. Am. 114(2): 1108-1119. https://doi.org/10.1121/1.1593066.

Mellinger D, Stafford K, Moore S, Dziak R, Matsumoto H. 2007. An overview of fixed passive acoustic observation methods for cetaceans. Oceanography. 20(4):36-45.

Miksis-Olds JL, Harris DV, Heaney KD. 2019. Comparison of estimated 20-Hz pulse fin whale source levels from the tropical Pacific and Eastern North Atlantic Oceans to other recorded populations. J. Acoust. Soc. Am. 146(4): 2373-2384. https://doi.org/10.1121/1.5126692.

Miksis-Olds JL, Martin SB, Tyack PL. 2018. Exploring the ocean through soundscapes. Acoust Today. 14(1):26-34. [accessed 4 June 2021]; https://acousticstoday.org/wp-content/uploads/2018/03/Exploring-the-Ocean-Through-Soundscapes.pdf

Miksis-Olds JL, Stabeno PJ, Napp JM, Pinchuk AI, Nystuen JA, et al. 2013. Ecosystem response to a temporary sea ice retreat in the Bering Sea. Prog Oceanogr. 111: 38-51. [accessed 4 June 2021]; https://doi.org/10.1016/j.pocean.2012.10.010

Miller PI, Scales KL, Ingram SN, Southall EJ, Sims DW. 2015. Basking sharks and oceanographic fronts: quantifying associations in the north-east Atlantic. Funct Ecol. 29:1099-1109.

Møhl B, Wahlberg M, Madsen PT, Miller LA, Surlykke A. 2000. Sperm whale clicks: directionality and source level revisited. J Acoust Soc Am. 107(1):638-648. [accessed 4 June 2021]; https://doi.org/10.1121/1.428329.

Moore PWB, Dankiewicz LA, Houser DS. 2008. Beamwidth control and angular target detection in an echolocating bottlenose dolphin (*Tursiops truncatus*). J. Acoust. Soc. Am. 124(5): 3324-3332. https://doi.org/10.1121/1.2980453.

Nemiroff L, Whitehead H. 2009. Structural characteristics of pulsed calls of long-finned pilot whales *Globicephala melas*. Bioacoustics 19(1-2): 67-92. https://doi.org/10.1080/09524622.2009.9753615.

Nicholls KW, Abrahamsen EP, Heywood KJ, Stansfield K, Osterhus S. 2008. High-latitude oceanography using the Autosub autonomous underwater vehicle. Limnol Oceanogr. 53:2309-2320.

Nichols JD, Pollock KH. 1983. Estimation methodology in contemporary small mammal capture-recapture studies. J Mammal. 64(2):253-260.

Nieukirk SL, Mellinger DK, Dziak RP, Matsumoto H, Klinck H. 2020. Multi-year occurrence of sei whale calls in North Atlantic polar waters. J. Acoust. Soc. Am. 147(3): 1842-1850. https://doi.org/10.1121/10.0000931.

Oswald JN, Barlow JP, Norris TF. 2003. Acoustic identification of nine delphinid species in the eastern tropical Pacific Ocean. Mar Mammal Sci. 19(1):20-37. [accessed 4 June 2021]; https://doi.org/10.1111/j.1748-7692.2003.tb01090.x

Parks SE, Cusano DA, Van Parijs SM, Nowacek DP. 2019. North Atlantic right whale (*Eubalaena glacialis*) acoustic behavior on the calving grounds. J. Acoust. Soc. Am. 146(1): EL15-EL21. https://doi.org/10.1121/1.4824682.

Parks SE, Tyack PL. 2005. Sound production by North Atlantic right whales (Eubalaena glacialis) in surface active groups. J Acoust Soc Am. 117(5):3297-3306. [accessed 4 June 2021]; https://doi.org/10.1121/1.1882946

Payne RS, McVay S. 1971. Songs of humpback whales. Science 173(3997): 585-597. https://doi.org/10.1126/science.173.3997.585.

Pine MK, Hannay DE, Insley SJ, Halliday WD, Juanes F. 2018. Assessing vessel slowdown for reducing auditory masking for marine mammals and fish of the western Canadian Arctic. Mar Pollut Bull 135:290-302. https://www.ncbi.nlm.nih.gov/pubmed/30301040.

PostgreSQL, PostgreSQL Global Development Group, https://www.postgresql.org/, July 2021.

Rafter MA, Trickey JS, Rice AC, Merrifield M, Thayre BJ, O'Neill E. et al. 2020a. Passive Acoustic Monitoring for Marine Mammals offshore of Cape Hatteras June 2018 – September 2019. Report by Marine Physical Laboratory (MPL) and Duke University Marine Laboratory, Nicolas School of the Environment for the Naval Facilities Engineering Command (NAVFAC) Atlantic. MPL Technical Memorandum 647. 39 p. http://www.cetus.ucsd.edu/docs/reports/MPLTM647-2020.pdf.

Rafter MA, Trickey JS, Rice AC, Merrifield M, Thayre BJ, O'Neill E, et al. 2020b. Passive Acoustic Monitoring for Marine Mammals Near Norfolk Canyon June 2018 – May 2019. Report by Marine Physical Laboratory (MPL) and Duke University Marine Laboratory, Nicolas School of the Environment for the Naval Facilities Engineering Command (NAVFAC) Atlantic. MPL Technical Memorandum 648. 40 p. https://www.navymarinespeciesmonitoring.us/files/6115/9363/8923/MPLTM648-2020_NFC.pdf.

Randers-Pehrson G, pngcrush, https://pmt.sourceforge.io/pngcrush/, July 2021.

Rendell LE, Matthews JN, Gill A, Gordon JCD, MacDonald DW. 1999. Quantitative analysis of tonal calls from five odontocete species, examining interspecific and intraspecific variation. J Zool. 249(4):403-410. [accessed 4 June 2021]; https://doi.org/10.1111/j.1469-7998.1999.tb01209.x

Risch D, Clark CW, Dugan PJ, Popescu M, Siebert U, et al. 2013. Minke whale acoustic behavior and multi-year seasonal and diel vocalization patterns in Massachusetts Bay, USA. Mar Ecol Prog Ser. 489:279-295. [accessed 4 June 2021]; https://doi.org/10.3354/meps10426

Risch D, Siebert U, Van Parijs SM. 2014. Individual calling behaviour and movements of North Atlantic minke whales (*Balaenoptera acutorostrata*). Behaviour. 151(9):1335-1360. [accessed 4 June 2021]; https://doi.org/10.1163/1568539X-00003187

Risch D, Wilson SC, Hoogerwerf M, van Geel NCF, Edwards EWJ, Brookes KL. 2019. Seasonal and diel acoustic presence of North Atlantic minke whales in the North Sea. Sci. Rep. 9: 3571. https://doi.org/10.1038/s41598-019-39752-8.

Roberts JJ, Best BD, Mannocci L, Fujioka E, Halpin PN, , et al. 2016. Habitat-based cetacean density models for the U.S. Atlantic and Gulf of Mexico. Sci Rep. 6: 22615. [accessed 4 June 2021]; DOI: 10.1038/srep22615

Roemmich D, Johnson GC, Riser S, Davis R, Gilson J, et al. 2009. The ARGO program observing the global ocean with profiling floats. Oceanography. 22:34-43.

Santora J, Hazen EL, Schroeder ID, Bograd SJ, Sakuma KM, et al. 2017. Impacts of ocean climate variability on biodiversity of pelagic forage species in an upwelling ecosystem. Mar Ecol Prog Ser. 580:205-220.

Santora JA, Mantua NJ, Schroeder ID, Field JC, Hazen EL, et al. 2020. Habitat compression and ecosystem shifts as potential links between marine heatwave and record whale entanglements. Nat Commun. 11(1):1-12.

Santora JA, Schroeder ID, Bograd SJ, Chavez F, Cimino M, et al. In review. Pelagic biodiversity, ecosystem function and services: an integrated observing and modeling approach. Oceanography.

Scales KL, Miller PI, Embling CB, Ingram SN, Pirotta E, et al. 2014. Mesoscale fronts as foraging habitats: composite front mapping reveals oceanographic drivers of habitat use for a pelagic seabird. J R Soc, Interface.11:20140679. [accessed 4 June 2021]; https://doi.org/10.1098/rsif.2014.0679

Schroeder ID, Santora JA, Moore AM, Edwards CA, Fiechter J, et al. 2014. Application of a data-assimilative regional ocean modeling system for assessing California Current System ocean conditions, krill, and juvenile rockfish interannual variability. Geophys Res Lett. 41(16):5942-5950.

Schroeder ID, Santora JA, Bograd SJ, Hazen EL, Sakuma KM, et al 2019. Source water variability as a driver of rockfish recruitment in the California current ecosystem: implications for climate change and fisheries management. Can J Fish Aquat Sci. 76(6):950-960.

Seim HE, Fletcher M, Mooers CNK, Nelson JR, Weisberg RH. 2009. Towards a regional coastal ocean observing system: an initial design for the Southeast Coastal Ocean Observing Regional Association. J Mar Syst. 77:261-277.

Shajahan N, Barclay DR, Lin Y-T. 2020. Quantifying the contribution of ship noise to the underwater sound field. J Acoust Soc Am. 148(6):3863-3872. [accessed 4 June 2021]; https://doi.org/10.1121/10.0002922.

Simões Amorim TO, Rezende de Castro F, Rodrigues Moron J, Ribeiro Duque B, Couto Di Tullio J, Resende Secchi E, Andriolo A. 2019. Integrative bioacoustics discrimination of eight delphinid species in the western South Atlantic Ocean. PLOS ONE 14(6). https://doi.org/10.1371/journal.pone.0217977.

Širović A, Rice A, Chou E, Hildebrand JA, Wiggins SM, Roch MA. 2015. Seven years of blue and fin whale call abundance in the Southern California Bight. Endanger. Species Res. 28(1): 61-76. https://doi.org/10.3354/esr00676.

Smith AB, Kloepper LN, Yang W-C, Huang W-H Jen, I-F, Rideout BP, Nachtigall PE. 2016. Transmission beam characteristics of a Risso's dolphin (*Grampus griseus*). J. Acoust. Soc. Am. 139(1): 53-62. https://doi.org/10.1121/1.4937752.

Soldevilla MS, Henderson EE, Campbell GS, Wiggins SM, Hildebrand JA, Roch MA. 2008. Classification of Risso's and Pacific white-sided dolphins using spectral properties of echolocation clicks. *J. Acoust. Soc. Am.* 124(1): 609-624. https://doi.org/10.1121/1.2932059.

Stanistreet JE, Nowacek DP, Baumann-Pickering S, Bell JT, Cholewiak DM, Hildebrand JA, Hodge LEW et al. 2017. Using passive acoustic monitoring to document the distribution of beaked whale species in the western North Atlantic Ocean. Can. J. Fish. Aquat. Sci. 74(12): 2098-2109. https://doi.org/10.1139/cjfas-2016-0503.

Stanistreet JE, Risch D, Van Parijs SM. 2013. Passive acoustic tracking of singing humpback whales (*Megaptera novaeangliae*) on a Northwest Atlantic feeding ground. PLOS ONE 8(4). https://doi.org/10.1371/journal.pone.0061263.

Stanton TK, Chu D, Wiebe PH. 1998. Sound scattering by several zooplankton groups. II. Scattering models. J Acoust Soc Am. 103(1):236-253.

Staudinger MD, McAlarney RJ, McLellan WA, Pabst AD. 2014. Foraging ecology and niche overlap in pygmy (*Kogia breviceps*) and dwarf (*Kogia sima*) sperm whales from waters of the U.S. mid-Atlantic coast. Mar. Mamm. Sci. 30(2): 626-655. https://doi.org/10.1111/mms.12064.

Steiner WW. 1981. Species-specific differences in pure tonal whistle vocalizations of five western North Atlantic dolphin species. Behav Ecol Sociobiol. 9(4):241-246. [accessed 4 June 2021]; https://www.jstor.org/stable/4599442

Thode AM, Sakai T, Michalec J, Rankin S, Soldevilla MS, et al. 2019. Displaying bioacoustic directional information from sonobuoys using “azigrams”. J Acoust Soc Am. 146(1):95-102. [accessed 4 June 2021]; https://doi.org/10.1121/1.5114810 .

Tyack PL. 2008. Implications for marine mammals of large-scale changes in the marine acoustic environment. J Mammal. 89(3):549-558. [accessed 4 June 2021]; https://doi.org/10.1644/07-MAMM-S-307R.1.

Tyack PL, Frisk G, Boyd I, Urban E, Seeyave S, eds. 2015. International Quiet Ocean Experiment science plan. 111 p. Scientific Committee on Oceanic Research, and Partnership for Observation of the Global Oceans. [accessed 21 June 2021]; https://www.scor-int.org/IQOE/IQOE_Science_Plan-Final.pdf

Urazghildiiev IR, Hannay DE. 2017. Maximum likelihood estimators and Cramér–Rao bound for estimating azimuth and elevation angles using compact arrays. J Acoust Soc Am. 141(4):2548-2555. [accessed 4 June 2021]; https://doi.org/10.1121/1.4979792 .

Urmy SS, Horne JK, Barbee DH. 2012. Measuring the vertical distributional variability of pelagic fauna in Monterey Bay. ICES J Mar Sci. 69:184–196. [accessed 4 June 2021]; DOI:10.1093/icesjms/fsr205

Van Cise AM, Mahaffy SD, Baird RW, Mooney TA, Barlow JP. 2018. Song of my people: Dialect differences among sympatric social groups of short-finned pilot whales in Hawai'i. Behav. Ecol. Sociobiol. 72(12). https://doi.org/10.1007/s00265-018-2596-1.

Wang L, Robinson S. 2020. JOMOPANS standard: Terminology for ambient noise monitoring. Version 2.0, March 2020 2020. [Online]. Available: https://northsearegion.eu/media/13062/jomopans_wp3-standard-terminology_version_-2.pdf

Ware C, Kelley JG, Pilar DHF. 2014. Improving the display of wind patterns and ocean currents. Bull Am Meteorol Soc. 95:1-9.

Ware C, Turton TL, Samsel F, Bujack R, Rogers DH, Evaluating the Perceptual Uniformity of Color Sequences for Feature Discrimination, EuroVis Workshop on Reproducibility, Verification, and Validation in Visualization, 2017.

Warren JD, Ainslie MA, Miksis-Olds JL, Martin B, Heaney KD. 2018. ADEON Calibration and Deployment Good Practice Guide. Version 1.0. (NH): University of New Hampshire. Contract No. M16PC00003. https://doi.org/10.6084/m9.figshare.6793745

Wenz GM. 1962. Acoustic ambient noise in the ocean: spectra and sources. J Acoust Soc Am. 34(12):1936-1956. [accessed 4 June 2021]; https://doi.org/10.1121/1.1909155.

Wickline M, Human-Computer Interaction Resource Network, Coblis Color Blindness Simulator, https://www.color-blindness.com/coblis-color-blindness-simulator/, July 2021.

Wood SN. 2017. Generalized additive models: an introduction with R. 2nd ed. 496 p. Boca Raton (FL): Taylor & Francis Group, CRC Press.

Yasuma H, Takao Y, Sawada K, Miyashita K, Aoki I. 2006. Target strength of the lanternfish, Stenobrachius leucopsarus (family Myctophidae), a fish without an airbladder, measured in the Bering Sea. ICES J Mar Sci. 63(4):683-692.

Ye Z. 1997. A novel approach to sound scattering by cylinders of finite length. J Acoust Soc Am. 102(2):877-884.

Yeatman P, Amstrong BA. 2011. Particle velocity measurements. Proceedings of the Institute of Acoustics. Volume 33(5):1-5.

Zimmer WMX, Johnson MP, Madsen PT, Tyack PL. 2005. Echolocation clicks of free-ranging Cuvier's beaked whales (*Ziphius cavirostris*). J. Acoust. Soc. Am. 117(6): 3919-3927. https://doi.org/10.1121/1.1910225.

Appendix A. Ambient Noise Summary: Long-term Spectral Averages and Percentile Distributions.

Certain stations, notably HAT, JAX, and VAC were deployed with a collocated echosounder for AZFP observations. As this contaminated the soundscape it had to be removed in post processing. Echosounder removal was accomplished by calculating the rms SPL value in the echosounder operating band and discarding all data in that timestep if it exceeded the cutoff threshold.

A.1 Cruise AR25: Data from Nov 2017 – Dec 2017

Cruise AR25 deployed the landers at all stations, and retrieved and redeployed a lander at VAC, referred to as VAC-1.

A.1.1 VAC-1

VAC-1 was the first lander deployed during cruise AR25 as the vessel transited north to south. It was retrieved in Dec 2017 on the return leg of the cruise and replaced with VAC-2. The data from VAC-1 allowed the ADEON team to test and tune the data analysis and management software before the first full set of data was recovered in June 2018. The long-term spectral average data and percentile data for the high-frequency sampling rate of this lander's PAM recording are shown in Figure 124 and Figure 125 respectively. The active echosounder energy overlapped with the high-frequency PAM data for the time period shown. Figure 126 and Figure 127 show the removal of the echosounder signal from the long-term spectral average and power spectral densities, respectively. They show an increase in energy around 20 Hz which indicates the presence of fin whale 20 Hz sound from November to December at this station. Frequent bursts of energy above 25 kHz are from odontocete echolocation clicks which are more common at night than during the day.

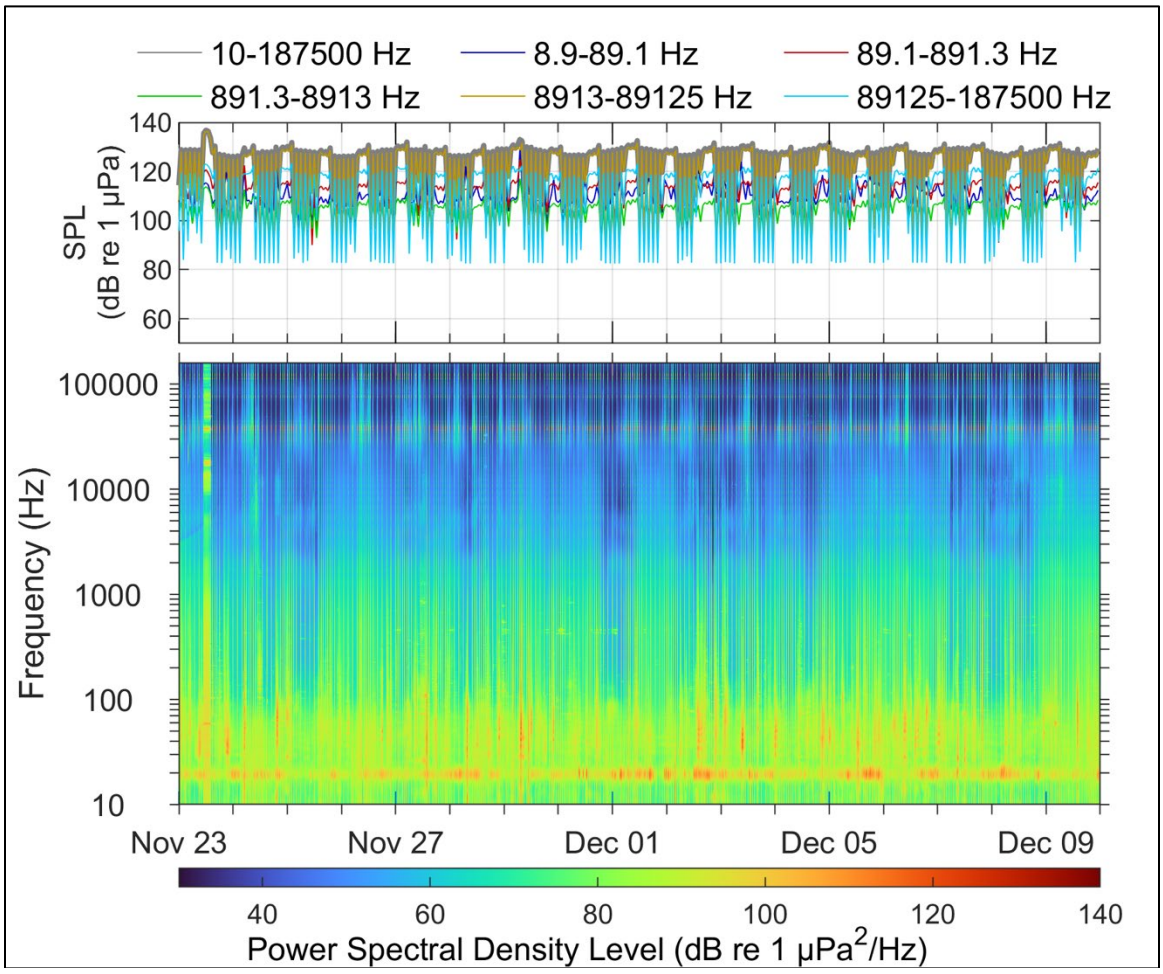

Figure 124. Long-Term Spectral Average and decade band SPL summary of acoustic data collected at VAC for the data collected 23 Nov 17–10 Dec 17

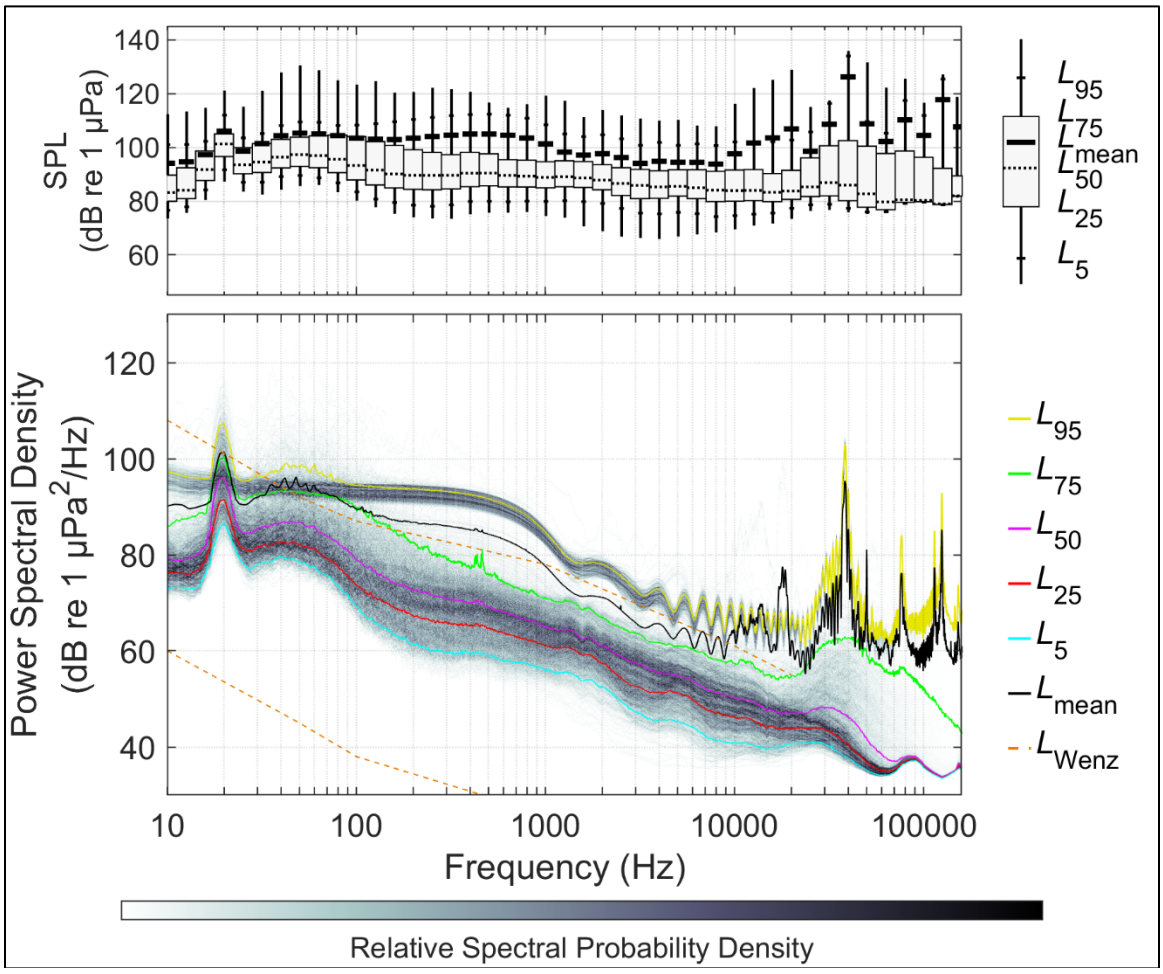

Figure 125. Distributions of decidecade SPL and power spectral densities at VAC in the data collected 23 Nov 17–10 Dec 17

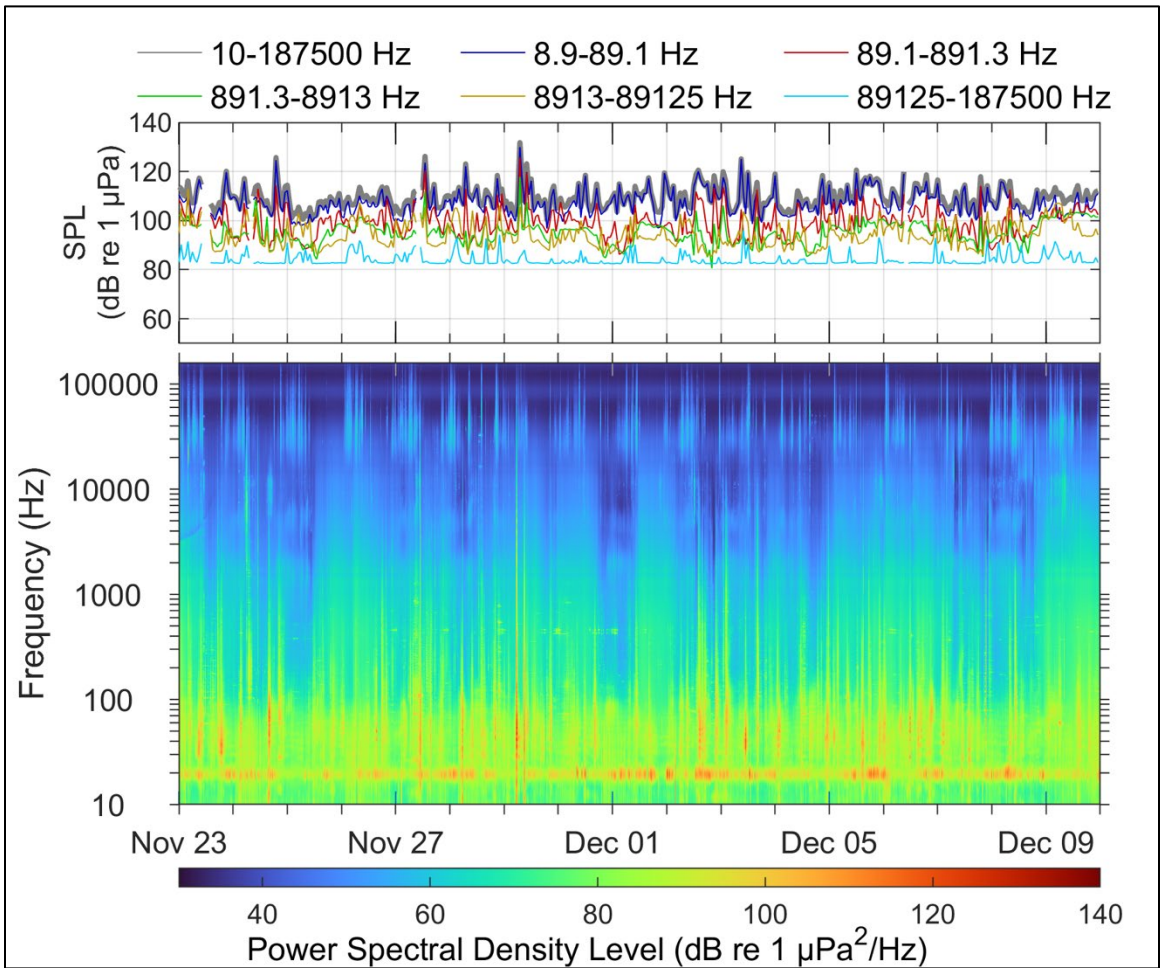

Figure 126. Long-Term Spectral Average and decade band SPL summary of acoustic data collected at VAC for the data collected 23 Nov 17 – 10 Dec 17, processed to remove the echosounder

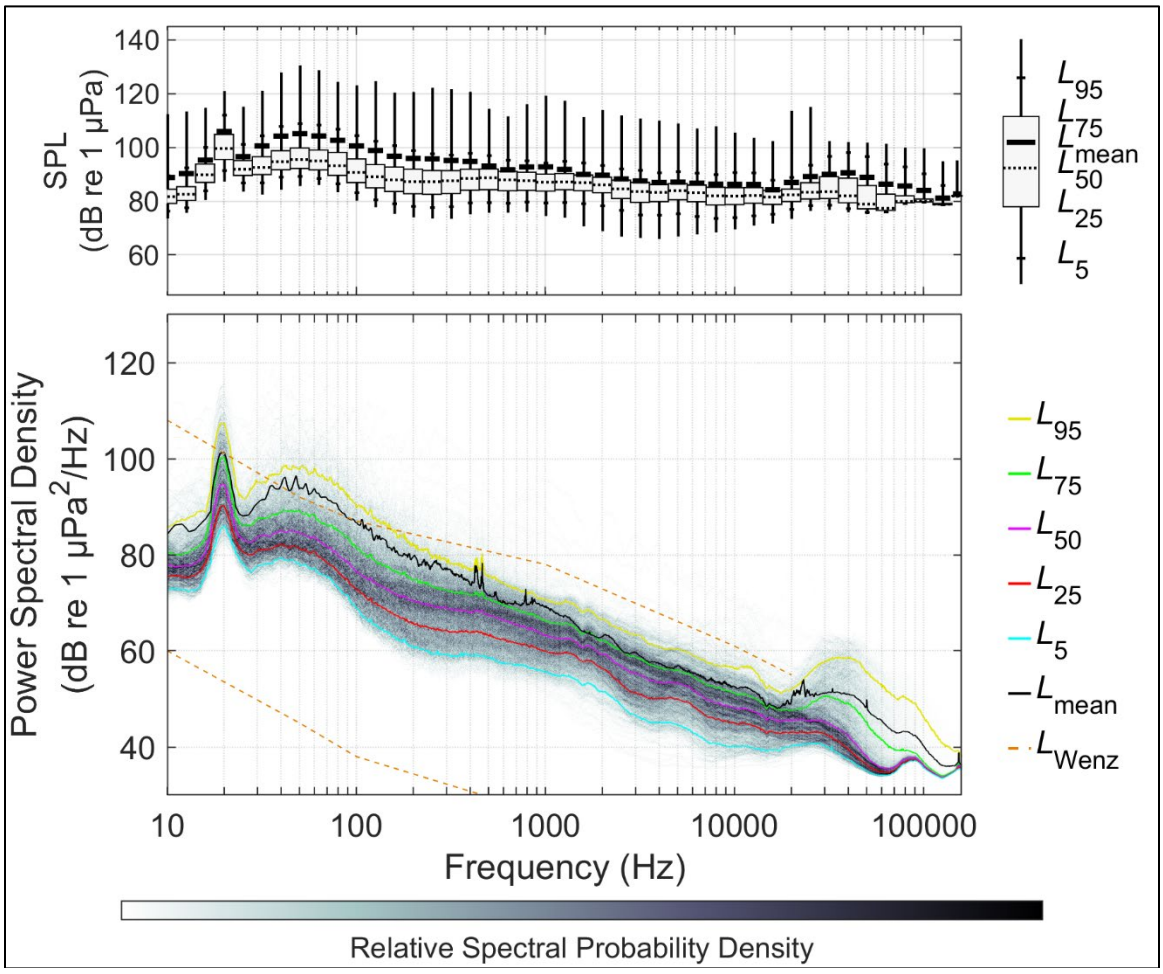

Figure 127. Distributions of decidecade SPL and power spectral densities at VAC in the data collected 23 Nov 17–10 Dec 17, processed to remove the echosounder

A.2 Cruise EN615: Data from Nov 2017 – June 2018

Cruise EN615 retrieved and redeployed the landers at all stations, providing an opportunity for data download, lander refurbishment, and battery replacement.

A.2.1 BLE

The long-term spectral average data and percentile data for the high-frequency sampling rate (375 kHz) at BLE for the period of 30 Nov 17 – 09 Jun 18 are in Figure 128 and Figure 129 respectively. Constant vessel traffic in the general area of BLE increased the sound level below 100 Hz. The broadband noise level below 20 kHz is due to wind noise and the constant energy line around 70 kHz is a recorder artefact. The elevation in sound energy from 100-200 Hz in the winter months is from minke whales.

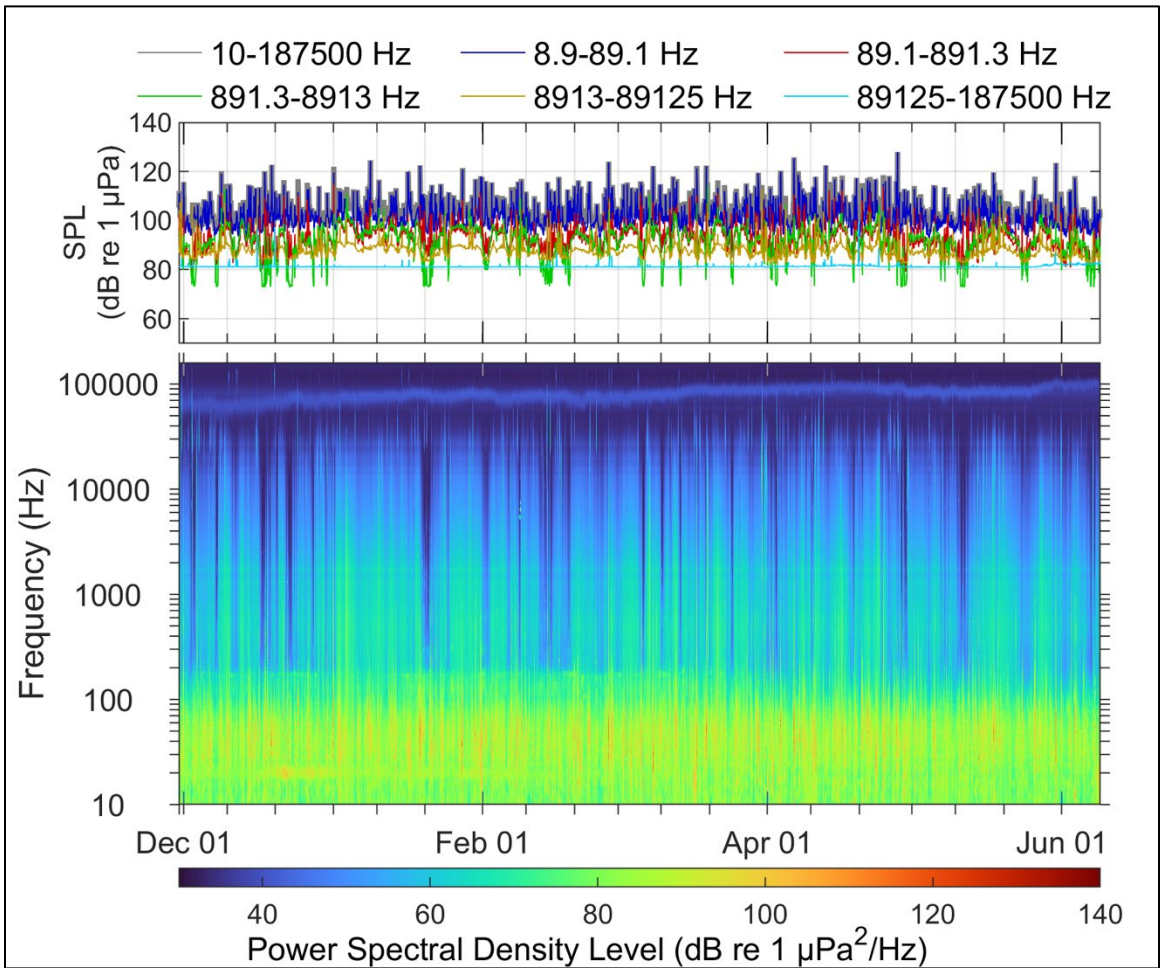

Figure 128. Long-Term Spectral Average and decade band SPL summary of acoustic data collected at BLE for the data collected 30 Nov 17–09 Jun 18

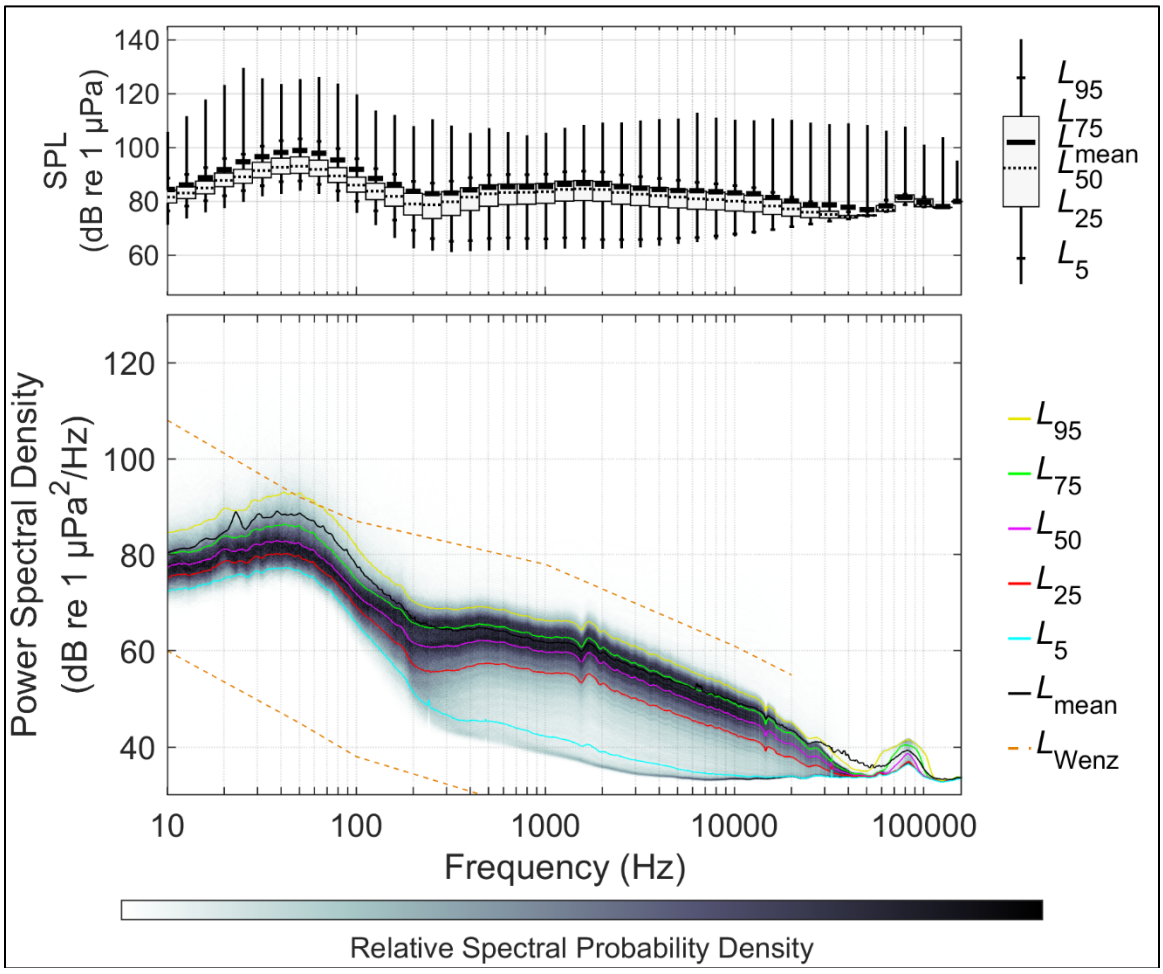

Figure 129. Distributions of decidecade SPL and power spectral densities at BLE in the data collected 30 Nov 17–09 Jun 18

A.2.2 CHB

The long-term spectral average data and percentile data for the high-frequency sampling rate (375 kHz) at CHB for the period of 04 Dec 17 – 12 Jun 18 are in Figure 130 and Figure 131 respectively. As these figures show, the increase in the noise level below 100 Hz in the spectral figure, during winter and fall illustrates the increase in the flow noise or strong currents. There is also broadband sound level increase due to wind which occurs below 20 kHz.

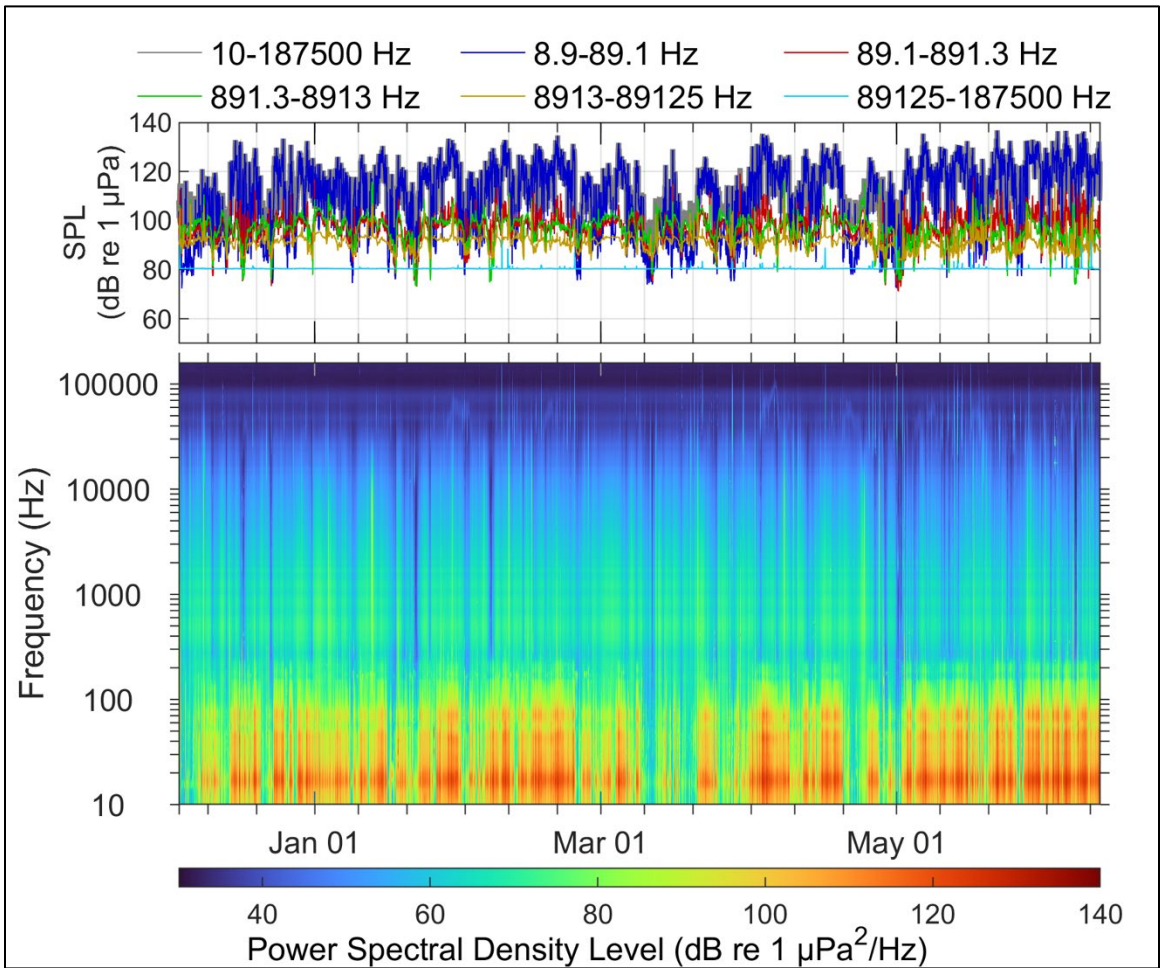

Figure 130. Long-Term Spectral Average and decade band SPL summary of acoustic data collected at CHB for the data collected 04 Dec 17–12 Jun 18

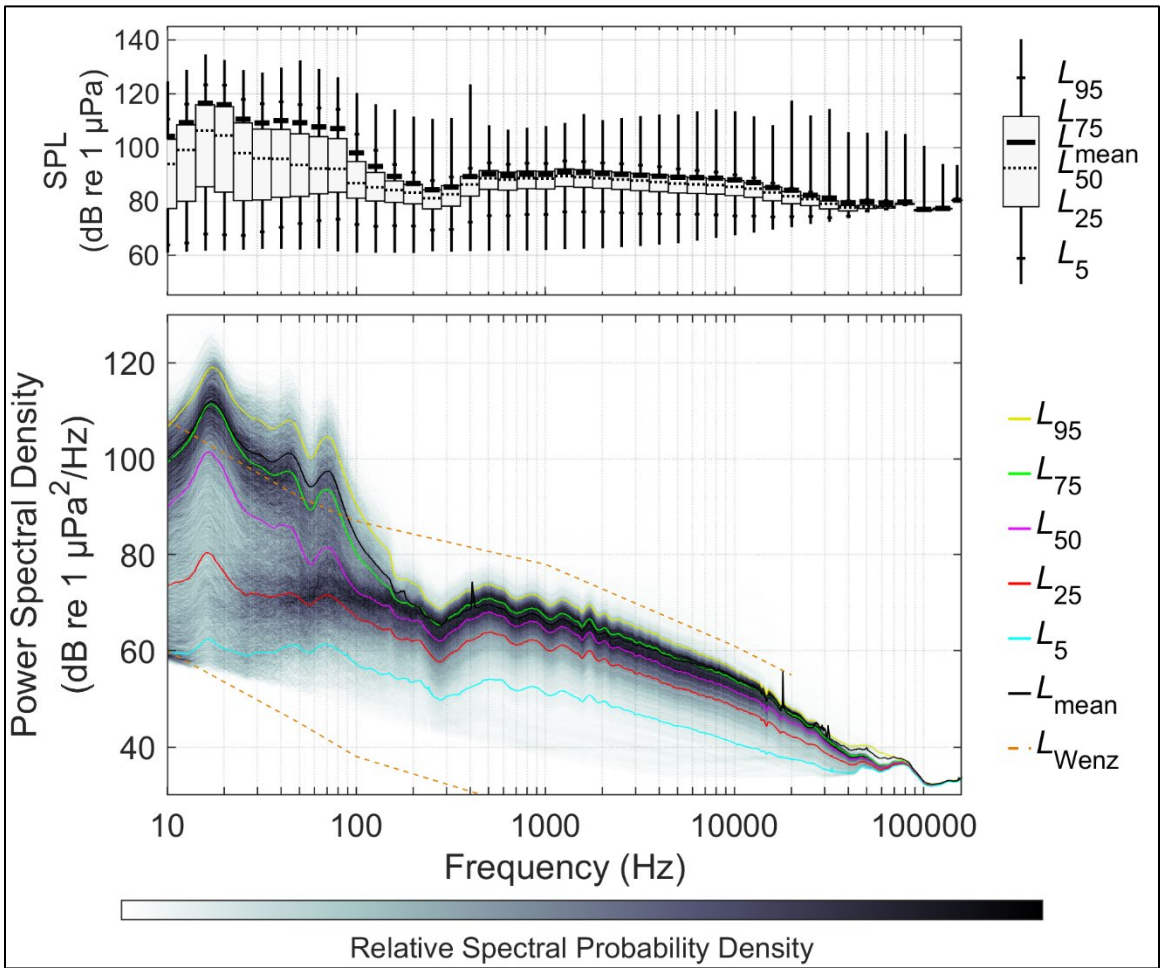

Figure 131. Distributions of spectral sound levels for the CHB data collected 04 Dec 17–12 Jun 18 based on 1-min sound averages

A.2.3 HAT

The long-term spectral average data and percentile data for the high-frequency sampling rate (375 kHz) at HAT for the period of 25 Nov 17 – 17 Jun 18 are in Figure 132 and Figure 133 respectively. The energy increase below 1000 Hz is predominantly due to nearby vessel traffic and some flow noise. The constant energy line around 40 kHz is attributed to the echosounder noise. Figure 134 and Figure 135 show the removal of the echosounder signal from the long-term spectral average and power spectral densities, respectively.

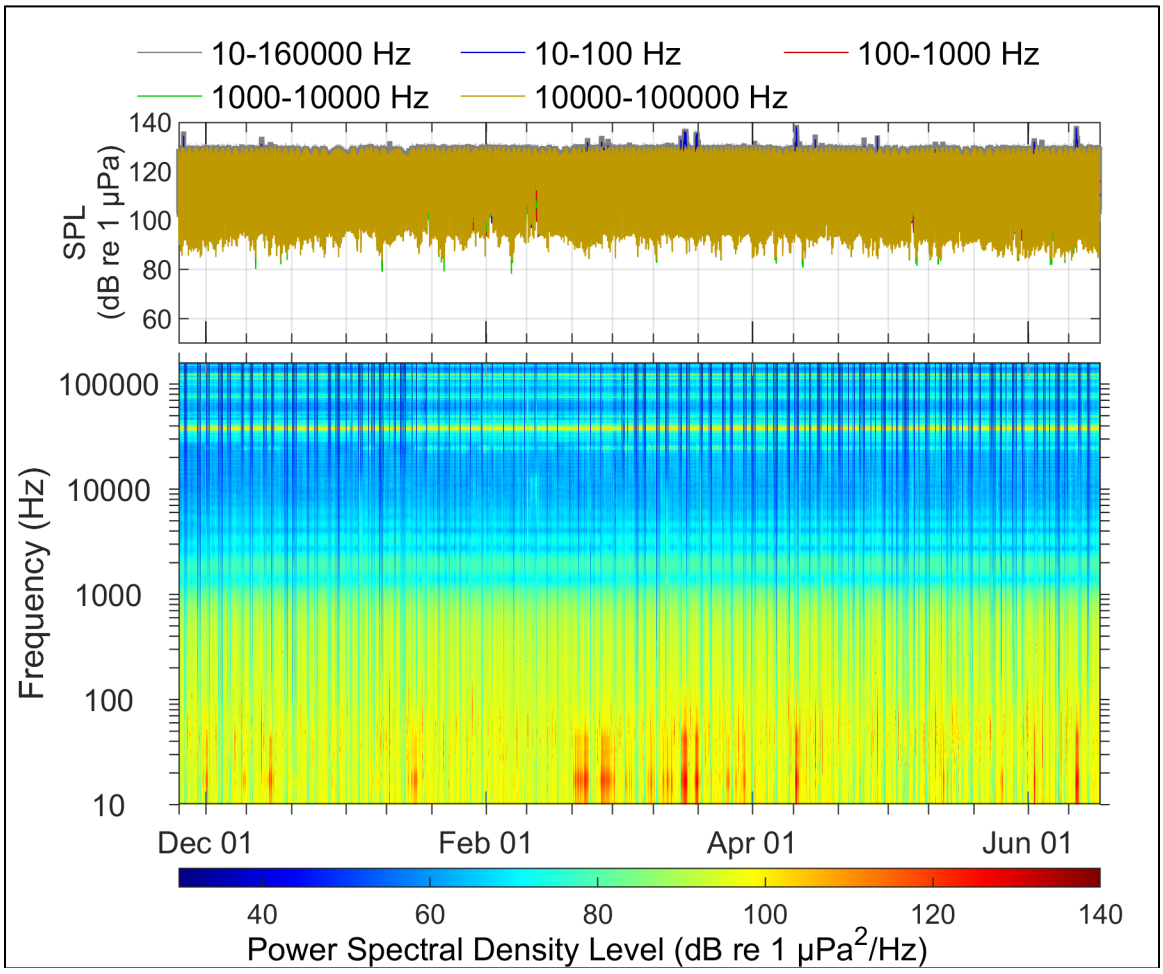

Figure 132. Long-Term Spectral Average and decade band SPL summary of acoustic data collected at HAT for the data collected 25 Nov 17–17 Jun 18

Note, bands were changed during Echosounder removal process.

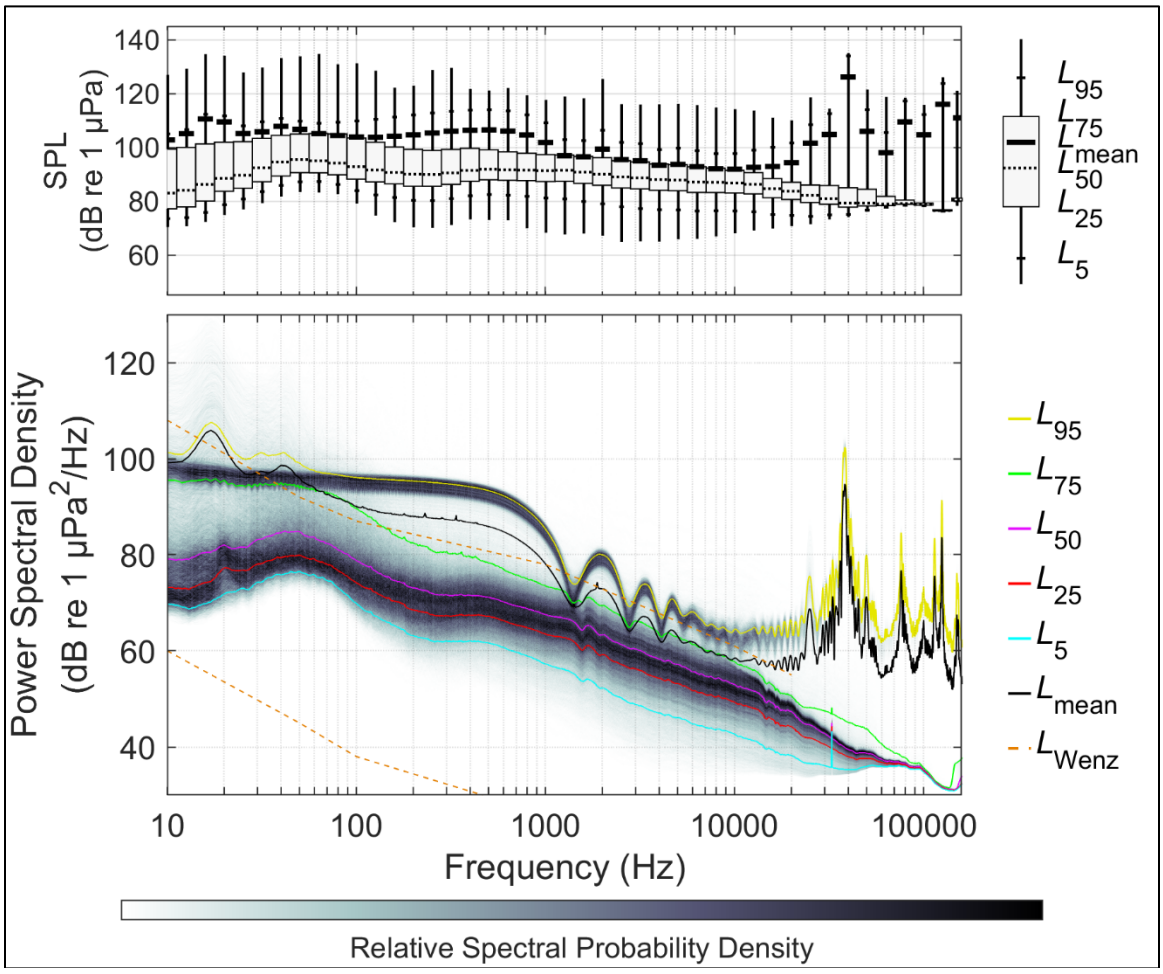

Figure 133. Distributions of spectral sound levels for the HAT data collected 25 Nov 17–17 Jun 18 based on 1-min sound averages

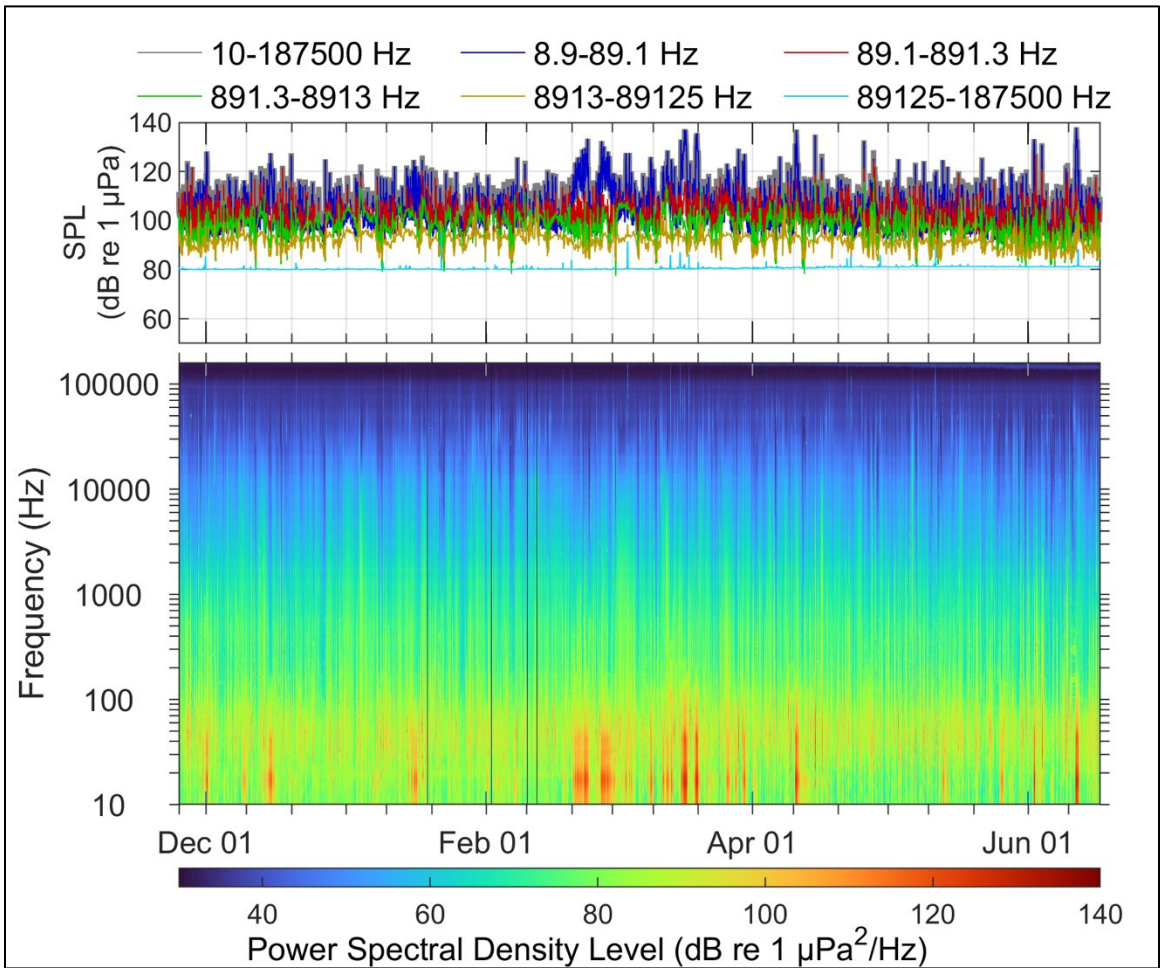

Figure 134. Long-Term Spectral Average and decade band SPL summary of acoustic data collected at HAT for the data collected 25 Nov 17–17 Jun 18, processed to remove the echosounder

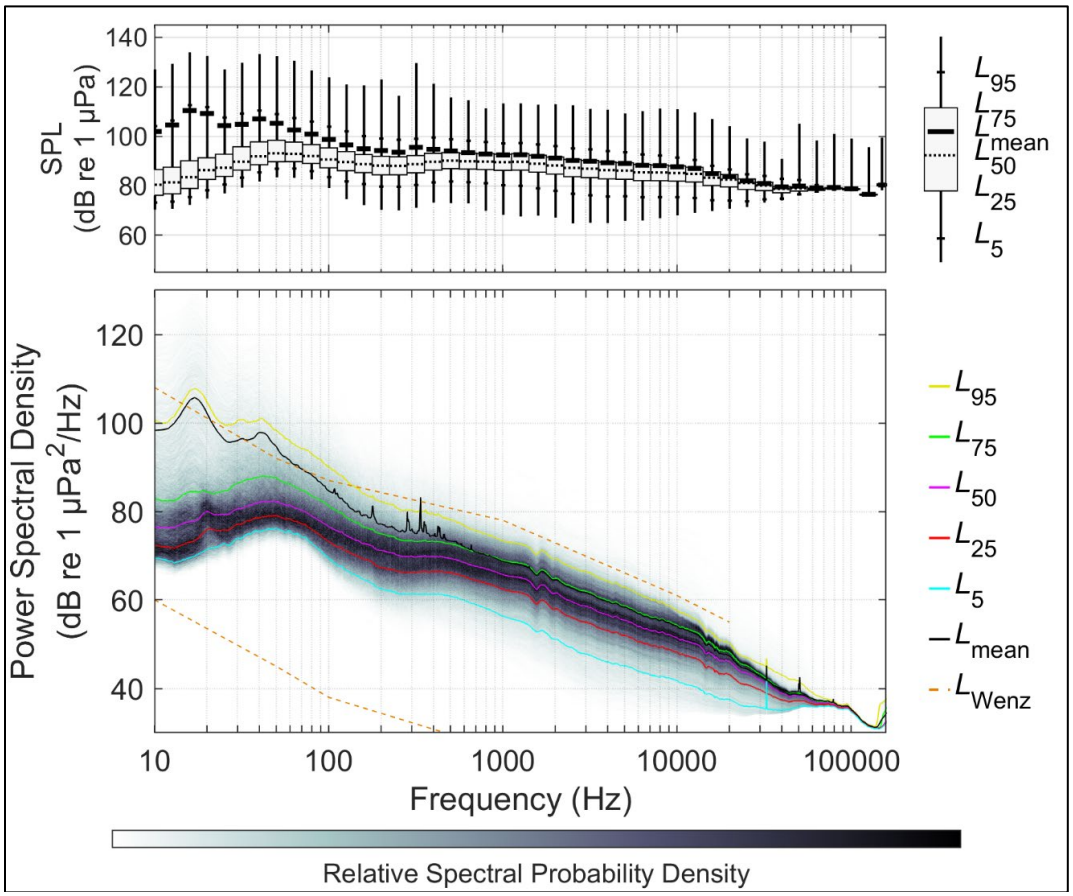

Figure 135. Distributions of spectral sound levels for the HAT data collected 25 Nov 17–17 Jun 18 based on 1-min sound averages, processed to remove the echosounder

A.2.4 JAX

The long-term spectral average data and percentile data for the high-frequency sampling rate (375 kHz) at JAX for the period of 02 Dec 17 – 12 Jun 18 are in Figure 136 and Figure 137 respectively. As it has been shown in the figures, the energy increase below 1000 Hz is due to two sources: nearby vessel traffic and flow noise. However, the constant energy line around 40 kHz is due to the echosounder noise. Figure 138 and Figure 139 show the removal of the echosounder signal from the long-term spectral average and power spectral densities, respectively. The elevation in sound energy from 100-200 Hz in the winter months is from minke whales.

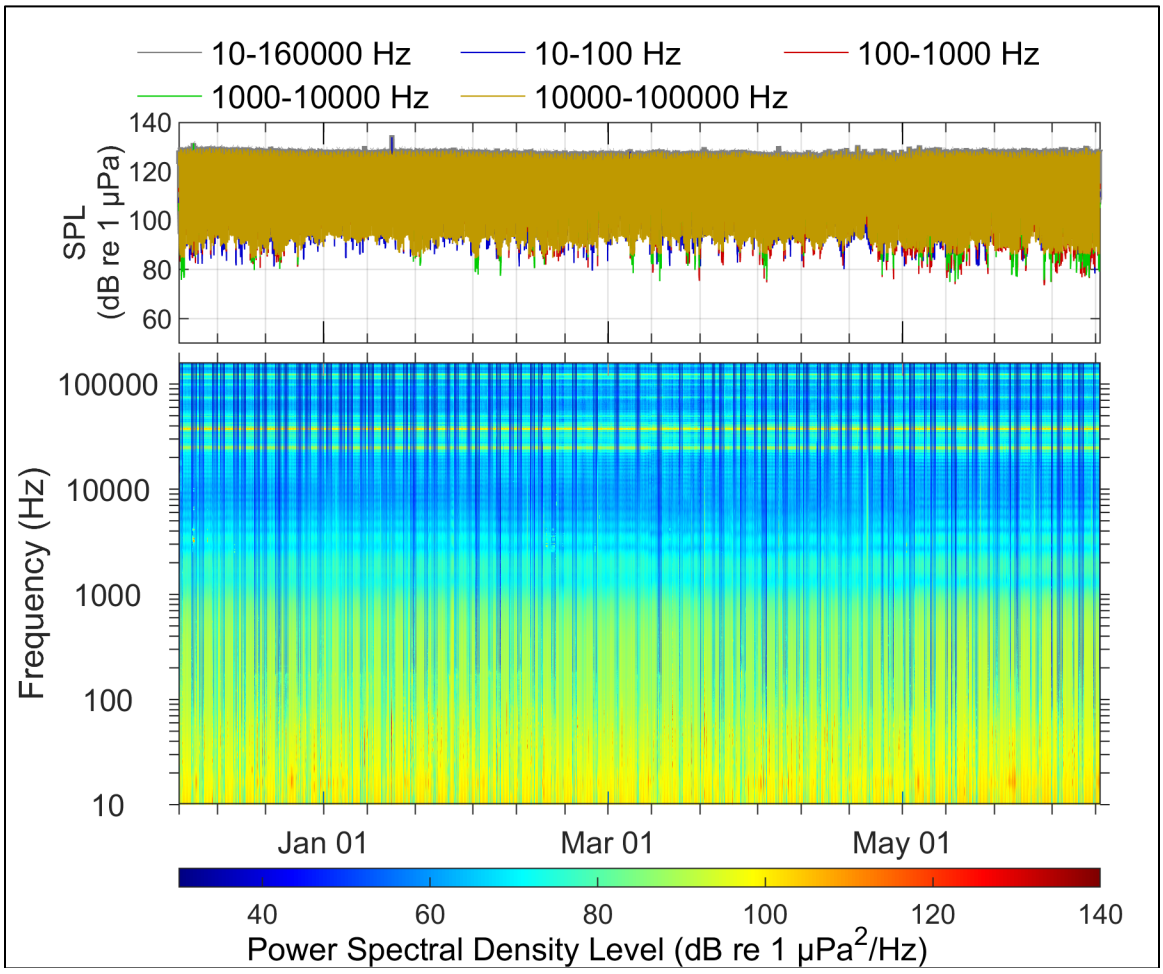

Figure 136. Long-Term Spectral Average and decade band SPL summary of acoustic data collected at JAX for the data collected 02 Dec 17–12 Jun 18

Note bands were changed during echosounder removal process.

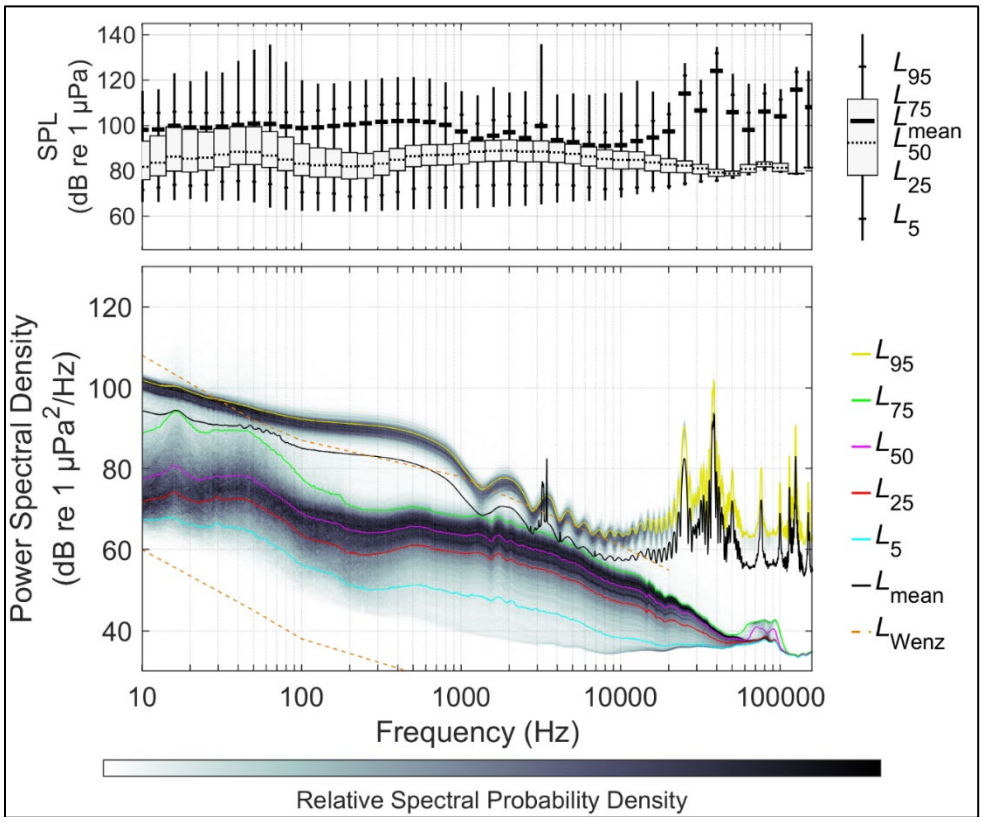

Figure 137. Distributions of spectral sound levels for the JAX data collected 02 Dec 17–12 Jun 18 based on 1-min sound averages

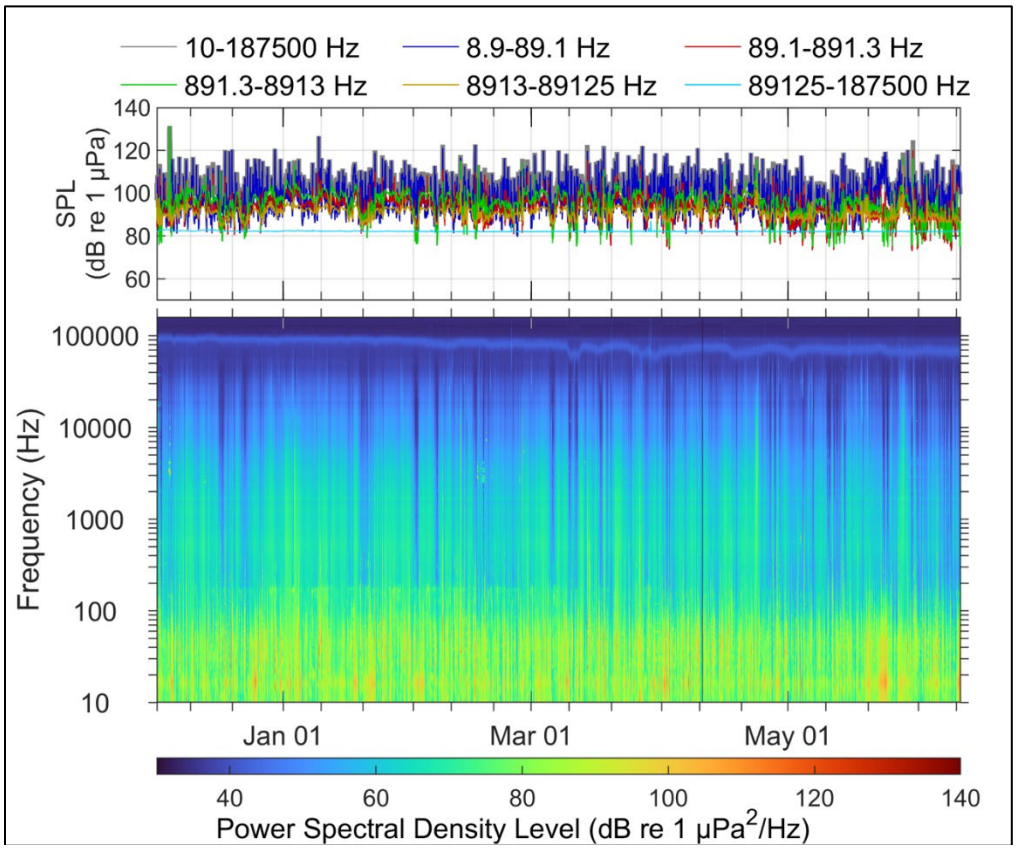

Figure 138. Long-Term Spectral Average and decade band SPL summary of acoustic data collected at JAX for the data collected 02 Dec 17–12 Jun 18, processed to remove echosounder

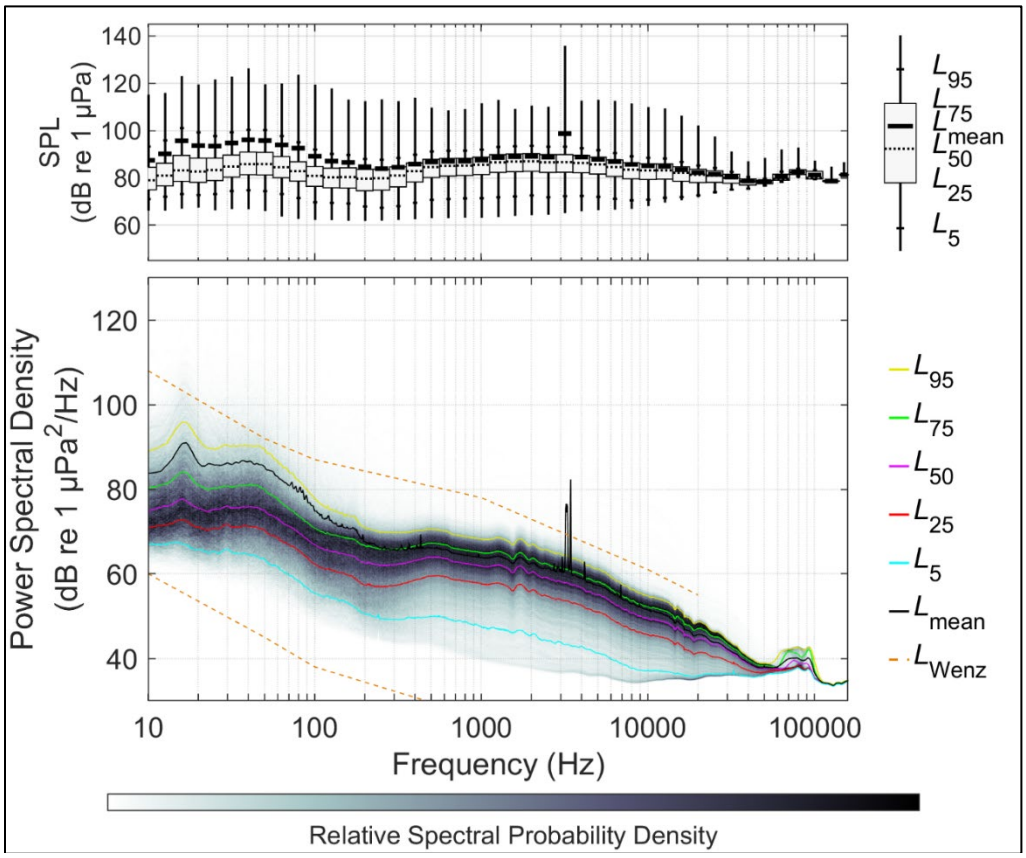

Figure 139. Distributions of spectral sound levels for the JAX data collected 02 Dec 17–12 Jun 18 based on 1-min sound averages, processed to remove echosounder

A.2.5 SAV

The long-term spectral average data and percentile data for the high-frequency sampling rate (375 kHz) at SAV for the period of 28 Nov 17 – 13 Jun 18 are in Figure 140 and Figure 141 respectively. The elevation in sound energy from 100-200 Hz in the winter months is from minke whales.

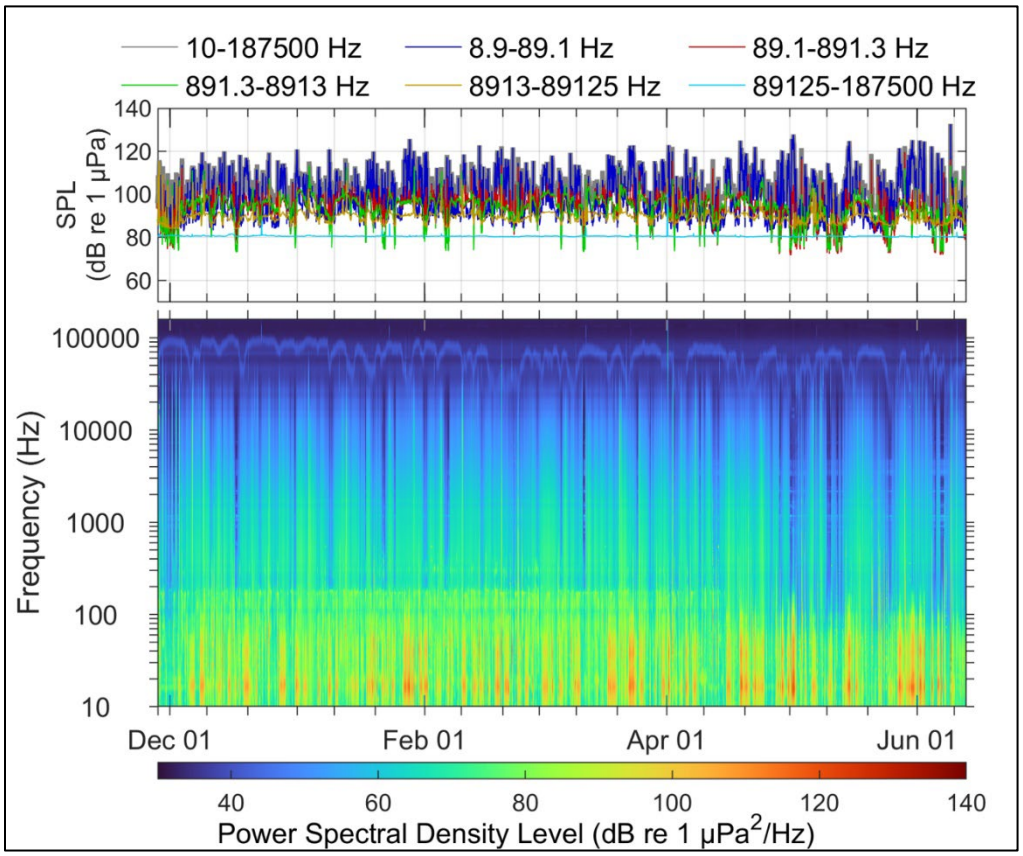

Figure 140. Long-Term Spectral Average and decade band SPL summary of acoustic data collected at SAV for the data collected 28 Nov 17–13 Jun 18

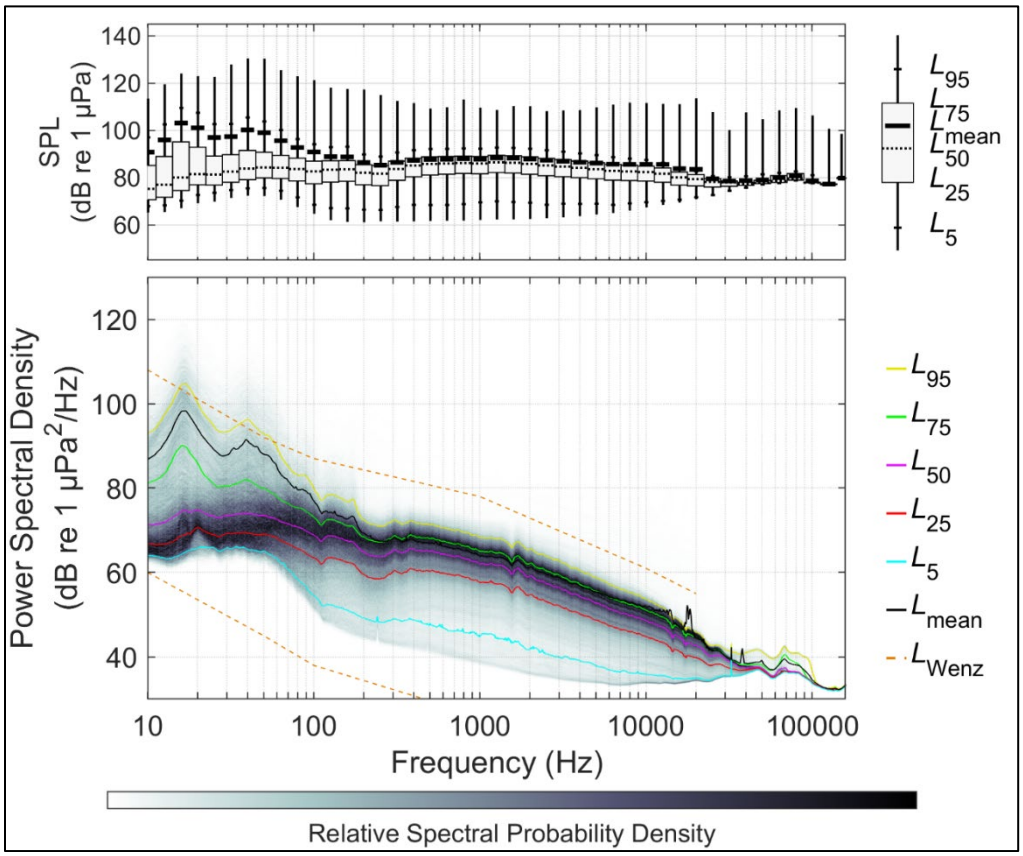

Figure 141. Distributions of spectral sound levels for the SAV data collected 28 Nov 17–13 Jun 18 based on 1-min sound averages

A.2.6 VAC-2

The long-term spectral average data and percentile data for the low-frequency sampling rate (8 kHz on the M20 directional hydrophone) at VAC-2 for the period of 11 Dec 17 – 19 Jun 18 are in Figure 142 and Figure 143 respectively. Fin whale chorusing at 20 Hz is faintly visible in this data during the winter months.

The lander redeployed at VAC for Dec 17 – Jun 18 did not record correctly on the high frequency channel. The data from the M20 omnidirectional hydrophone is shown here instead. The batteries on this recorder ran out in late May 2018.

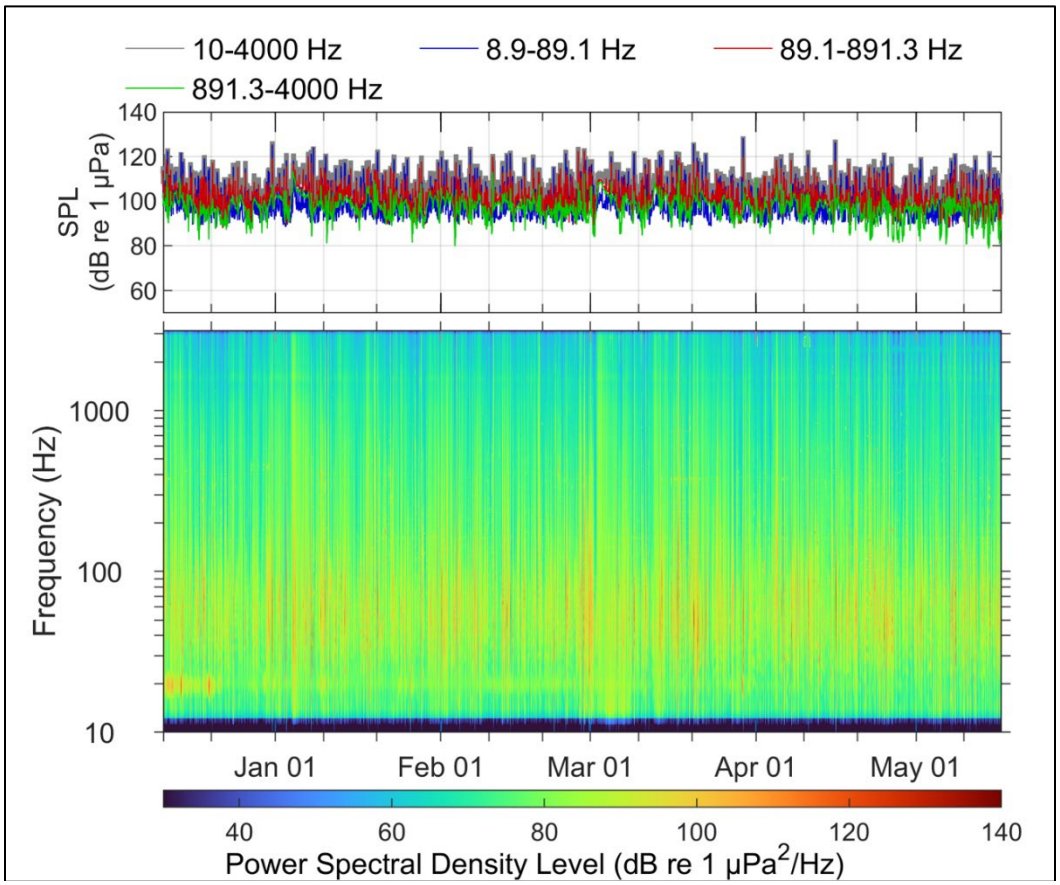

Figure 142. Long-Term Spectral Average and decade band SPL summary of acoustic data collected at VAC for the data collected 11 Dec 17–19 Jun 18

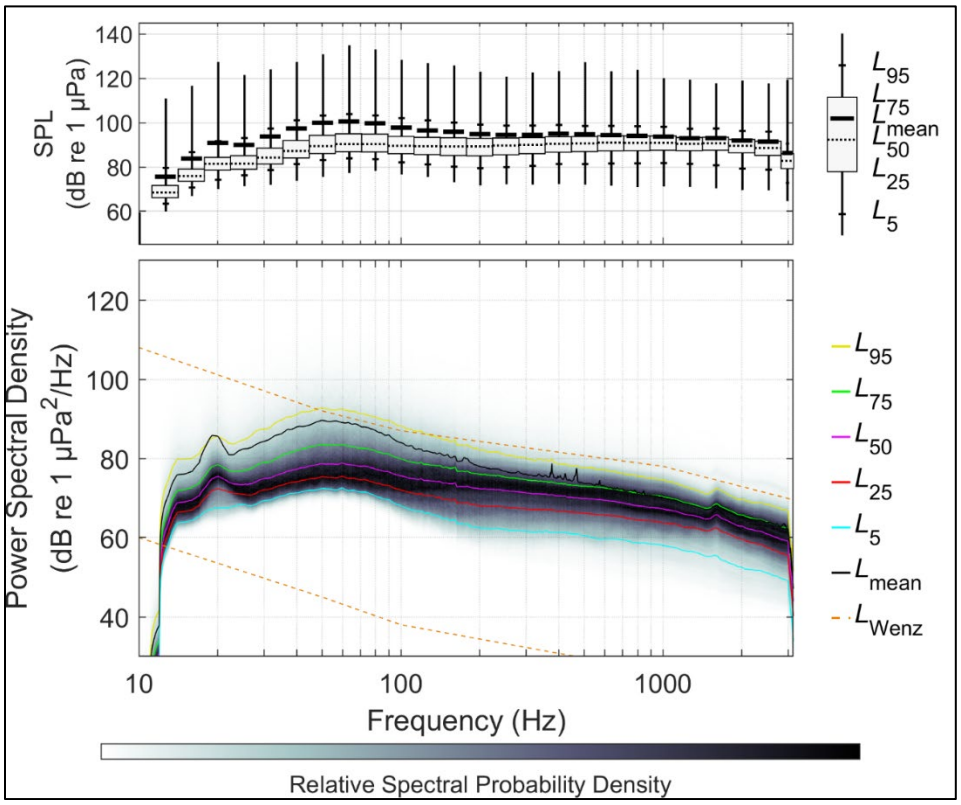

Figure 143. Distributions of spectral sound levels for the VAC data collected 11 Dec 17–19 Jun 18 based on 1-min sound averages

A.2.7 WIL

The long-term spectral average data and percentile data for the high-frequency sampling rate (375 kHz) at WIL for the period of 26 Nov 17 – 14 Jun 18 are in Figure 144 and Figure 145, respectively. The elevation in sound energy from 100-200 Hz in the winter months is from minke whales.

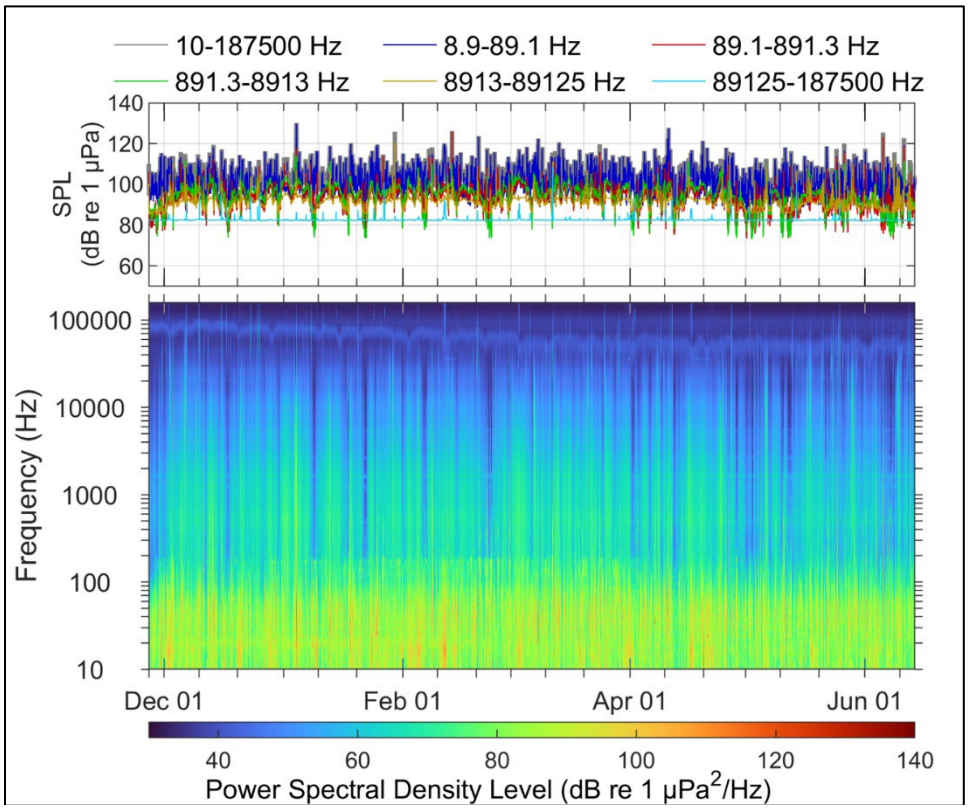

Figure 144. Long-Term Spectral Average and decade band SPL summary of acoustic data collected at WIL for the data collected 26 Nov 17–14 Jun 18

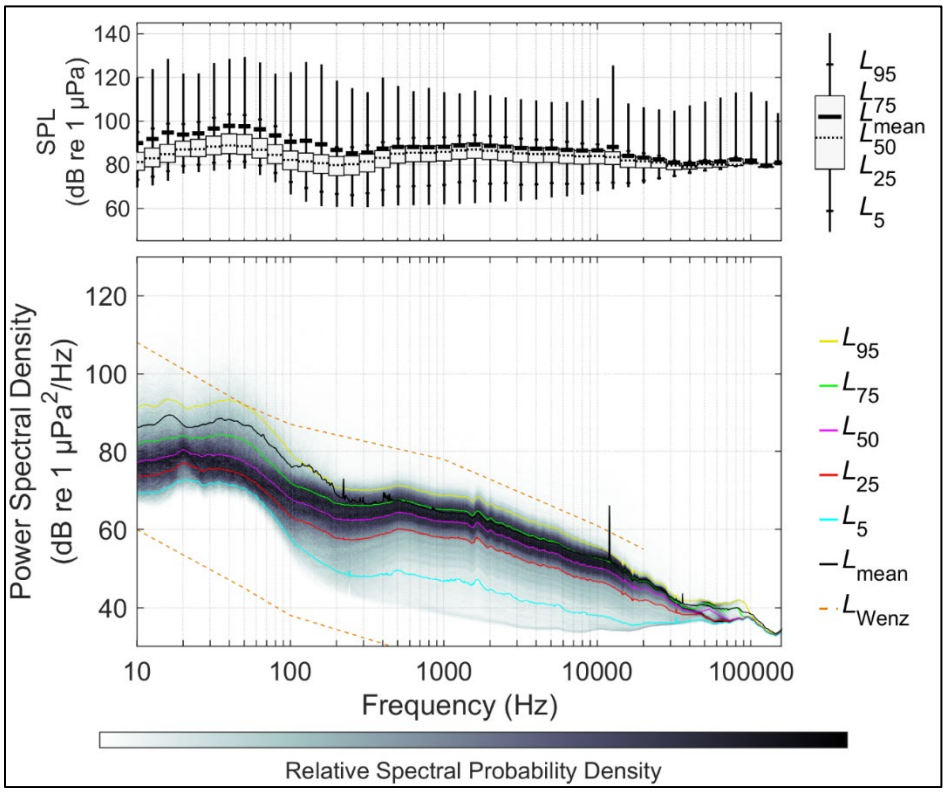

Figure 145. Distributions of spectral sound levels for the WIL data collected 26 Nov 17–14 Jun 18 based on 1-min sound averages

A.3 Cruise EN626: Data for Jun 2018–Nov 2018

Cruise EN626 retrieved and redeployed the landers at all stations, providing an opportunity for data download, lander refurbishment, and battery replacement. Short-term, broad band energy increases can be attributed to hurricanes Beryl (formed 4 Jul), Chris (formed 6 Jul), Florence (formed 31 Aug), Helene (formed 21 Sept), Isaac (formed 7 Sept), Leslie (formed 23 Sept), Michael (formed 7 Oct), and Oscar (formed 26 Oct).

A.3.1 BLE

The long-term spectral average data and percentile data for the high-frequency sampling rate (375 kHz) at BLE for the period of 11 Jun 18 – 05 Nov 18 are in Figure 146 and Figure 147 respectively. Increases in wind noise in the 100 – 10000 Hz band are associated with changes in wind speed, especially during hurricanes.

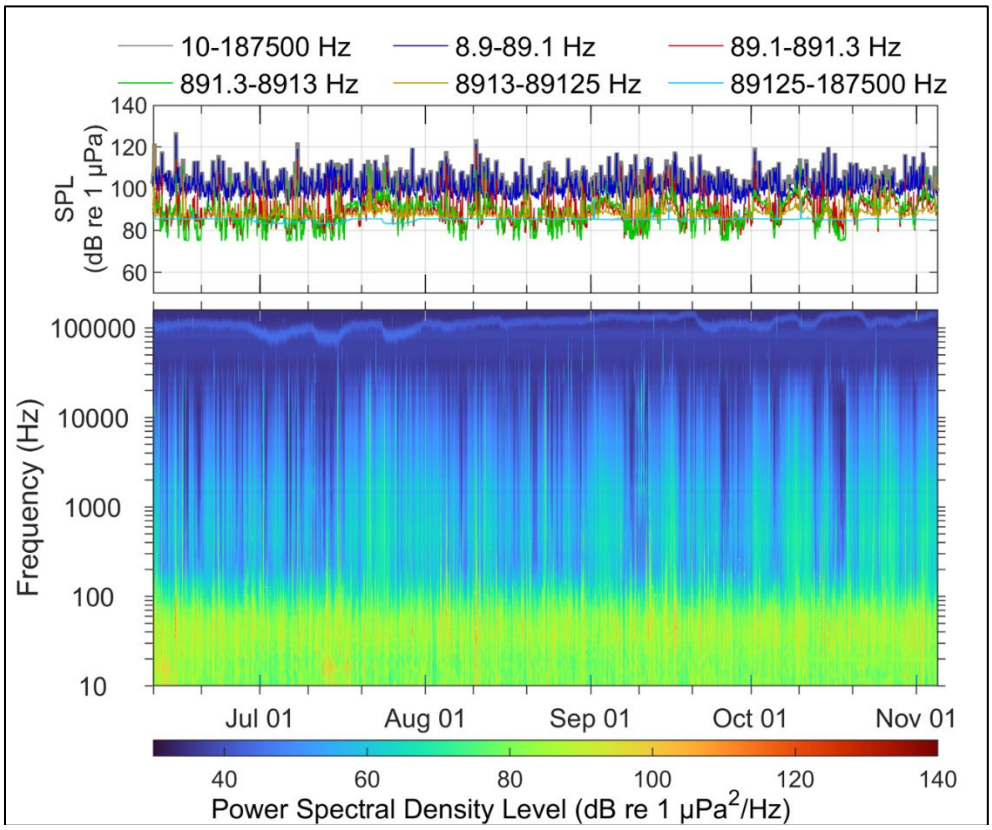

Figure 146. Long-Term Spectral Average and decade band SPL summary of acoustic data collected at BLE for the data collected 11 Jun 18–05 Nov 18.

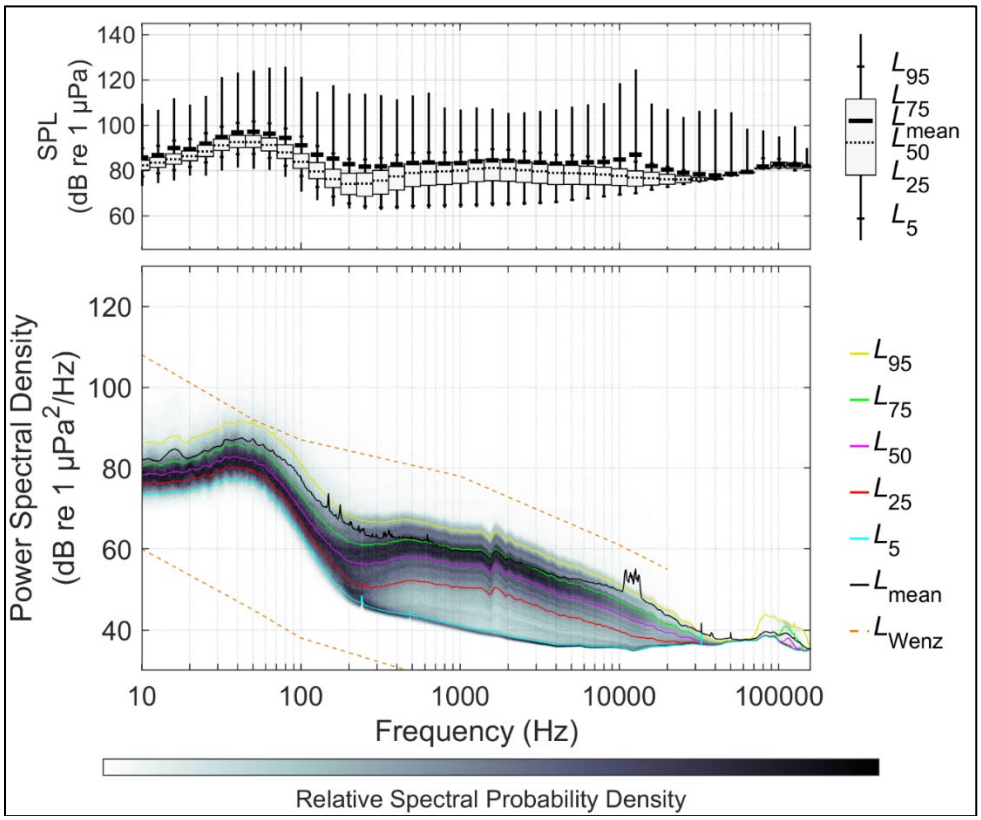

Figure 147. Distributions of spectral sound levels for the BLE data collected 11 Jun 18–05 Nov 18 based on 1-min sound averages

A.3.2 CHB

The long-term spectral average data and percentile data for the high-frequency sampling rate (375 kHz) at CHB for the period of 14 Jun 18 – 03 Nov 18 are in Figure 148 and Figure 149, respectively. This station is substantially affected by flow noise for frequencies below 100 Hz.

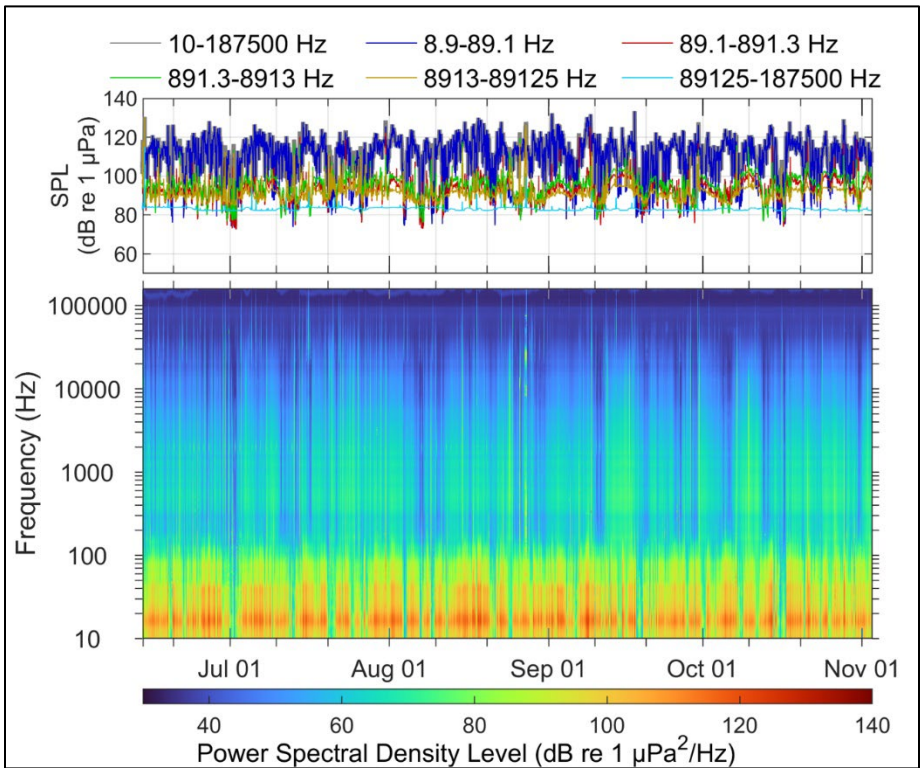

Figure 148. Long-Term Spectral Average and decade band SPL summary of acoustic data collected at CHB for the data collected 14 Jun 18–03 Nov 18

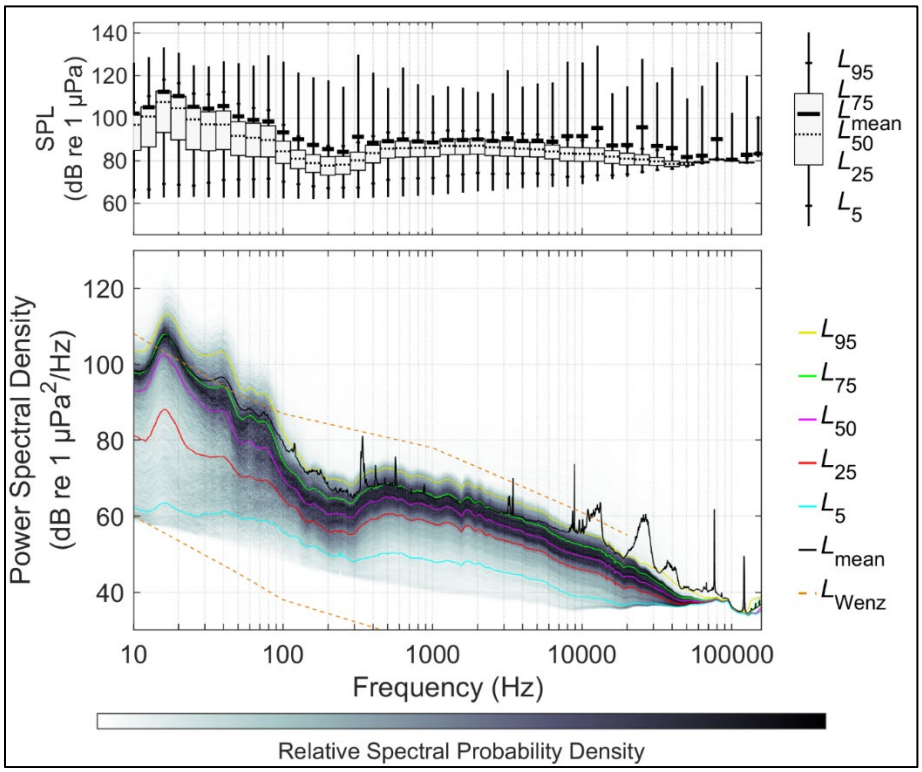

Figure 149. Distributions of spectral sound levels for the CHB data collected 14 Jun 18–03 Nov 18 based on 1-min sound averages

A.3.3 HAT

The long-term spectral average data and percentile data for the high-frequency sampling rate (375 kHz) at HAT for the period of 19 Jun 18 – 10 Nov 18 are in Figure 150 and Figure 151 respectively. The energy increase in the sound level for frequencies below 100 Hz is due to the strong flow noise. The constant energy line also shows the presence of the sound of echosounder after August. Figure 152 and Figure 153 show the removal of the echosounder signal from the long-term spectral average and power spectral densities, respectively.

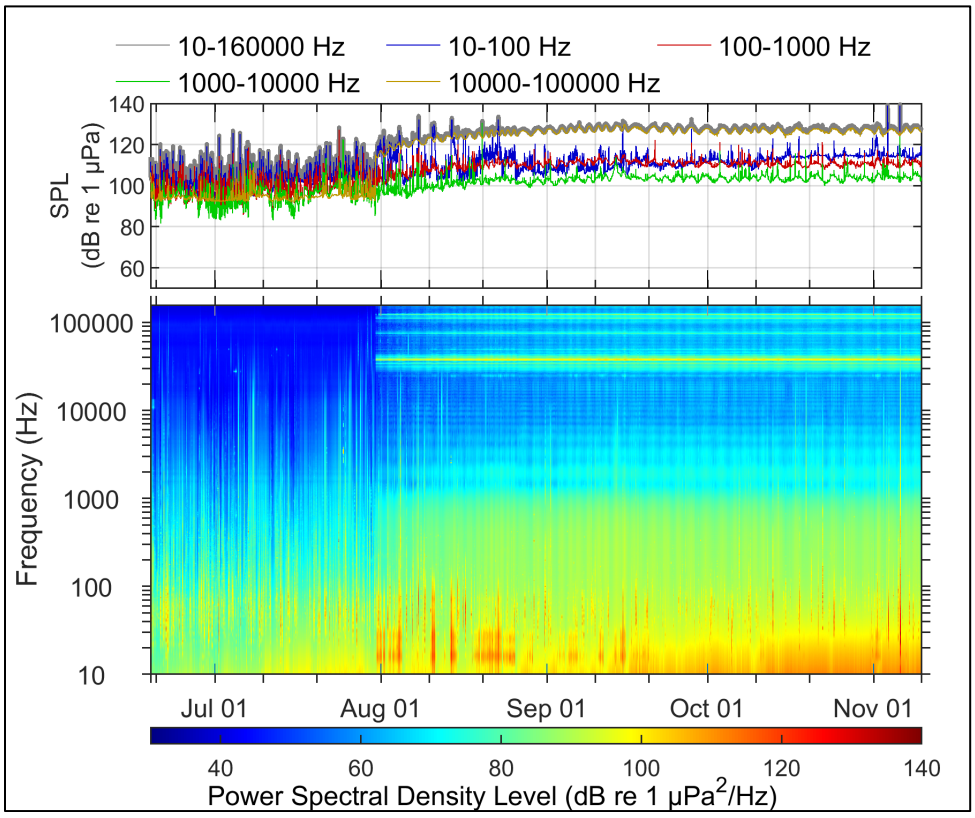

Figure 150. Long-Term Spectral Average and decade band SPL summary of acoustic data collected at HAT for the data collected 19 Jun 18–10 Nov 18

Note, bands were changed during echosounder removal process.

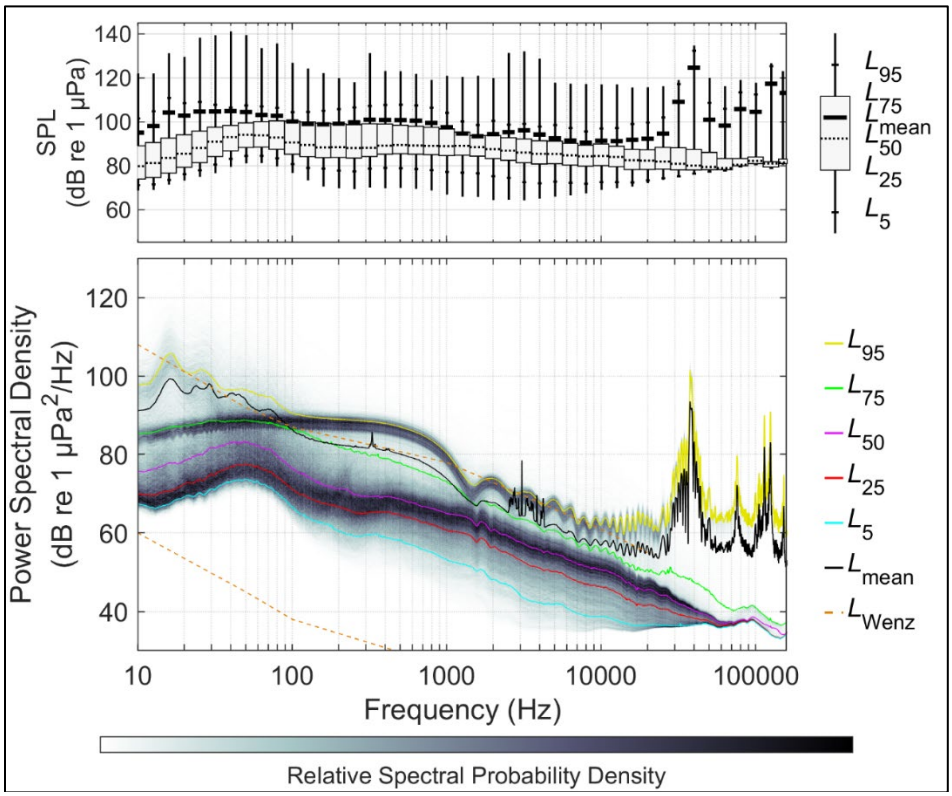

Figure 151. Distributions of spectral sound levels for the HAT data collected 19 Jun 18–10 Nov 18 based on 1-min sound averages

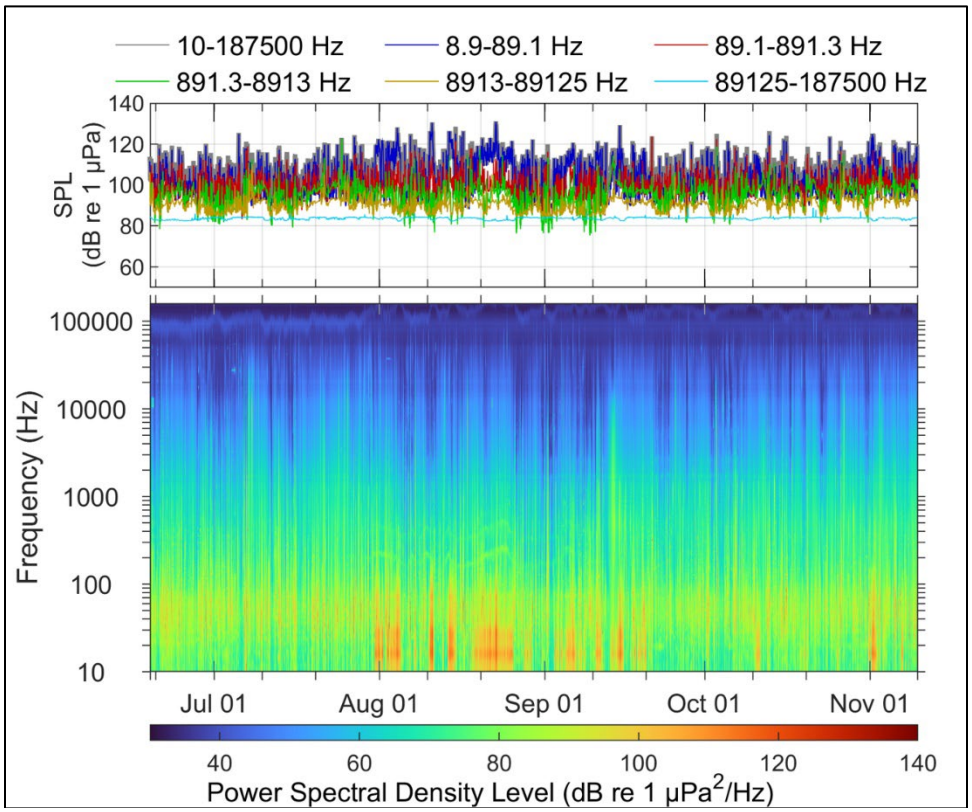

Figure 152. Long-Term Spectral Average and decade band SPL summary of acoustic data collected at HAT for the data collected 19 Jun 18–10 Nov 18, processed to remove the echosounder signature

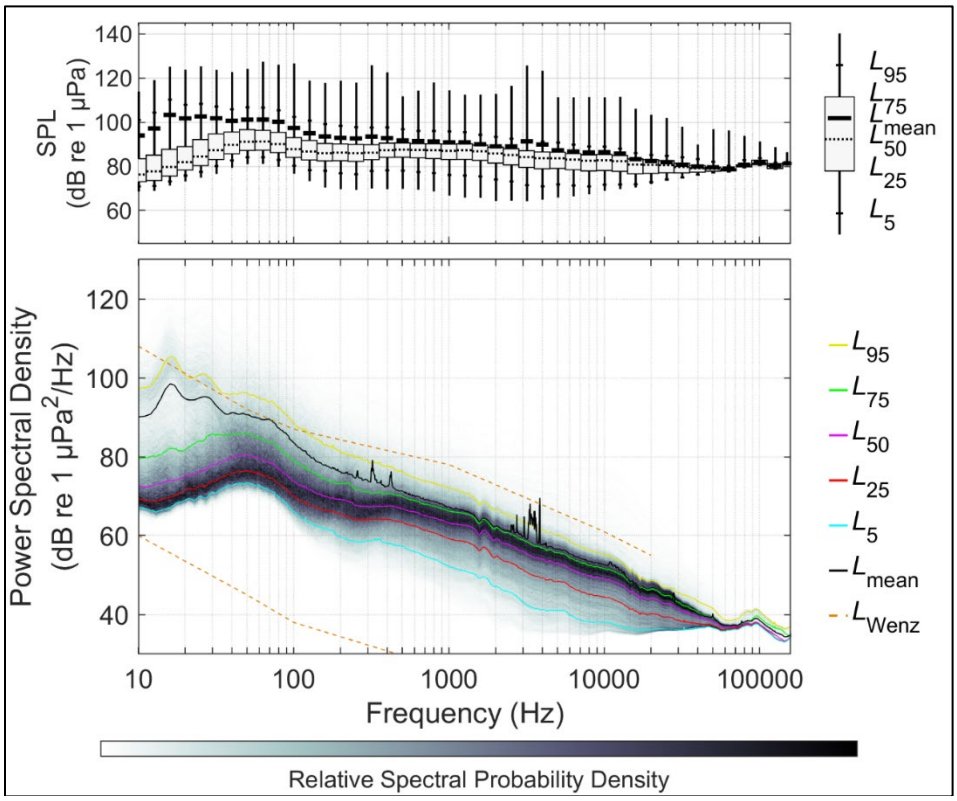

Figure 153. Distributions of spectral sound levels for the HAT data collected 19 Jun 18–10 Nov 18 based on 1-min sound averages, processed to remove the echosounder signature

A.3.4 JAX

The long-term spectral average data and percentile data for the high-frequency sampling rate (375 kHz) at JAX for the period of 13 Jun 18 – 06 Nov 18 are in Figure 154 and Figure 155 respectively. In the spectral figure, the sound level increase below 100 Hz indicates high levels of shipping. The echosounder is visible as the constant energy lines with a peak around 30kHz, appearing after late July. Figure 156 and Figure 157 show the removal of the echosounder signal from the long-term spectral average and power spectral densities, respectively. Increases in wind noise in the 100 – 10000 Hz band are associated with changes in wind speed, especially during hurricanes.

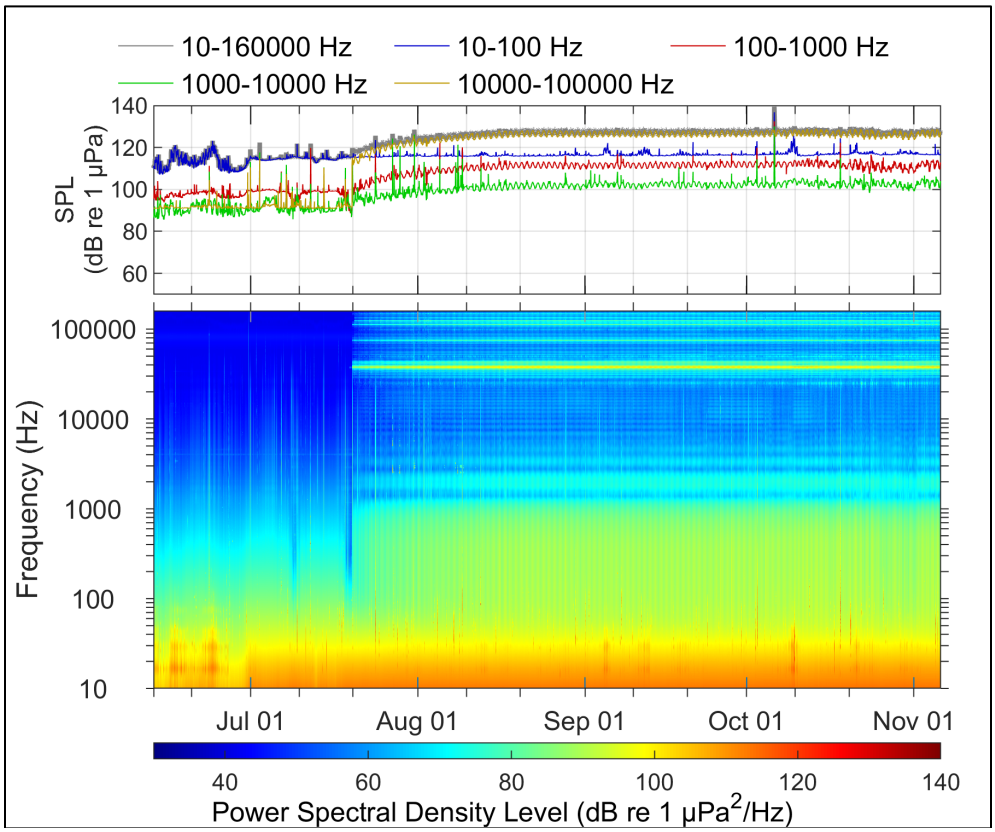

Figure 154. Long-Term Spectral Average and decade band SPL summary of acoustic data collected at BLE for the data collected 13 Jun 18–06 Nov 18

Note, bands were changed during the echosounder removal process.

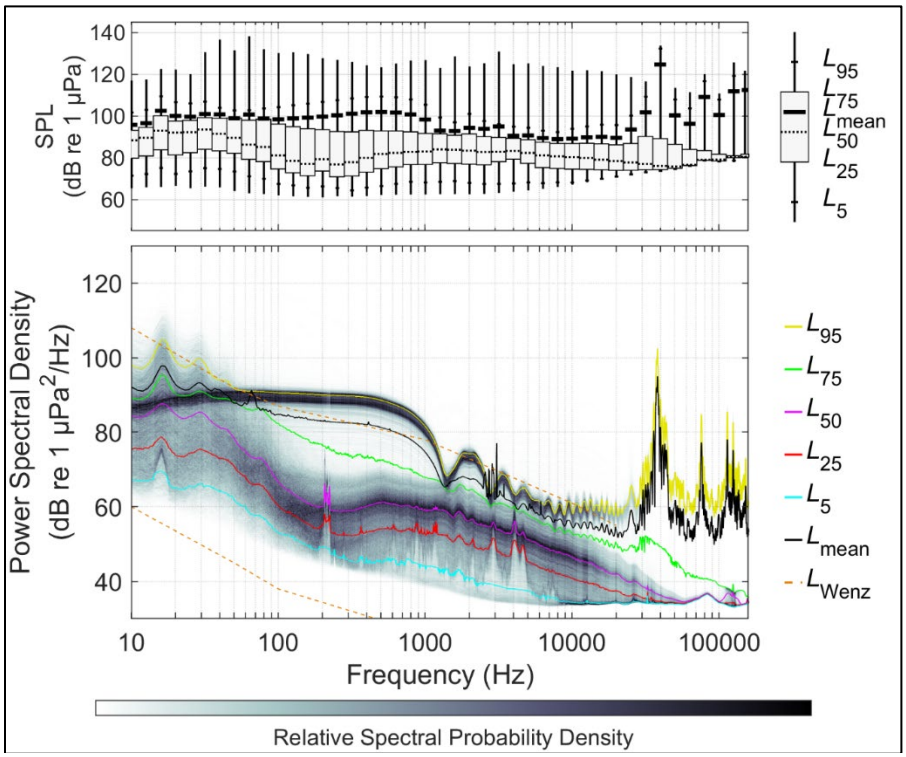

Figure 155. Distributions of spectral sound levels for the JAX data collected 13 Jun 18–06 Nov 18 based on 1-min sound averages

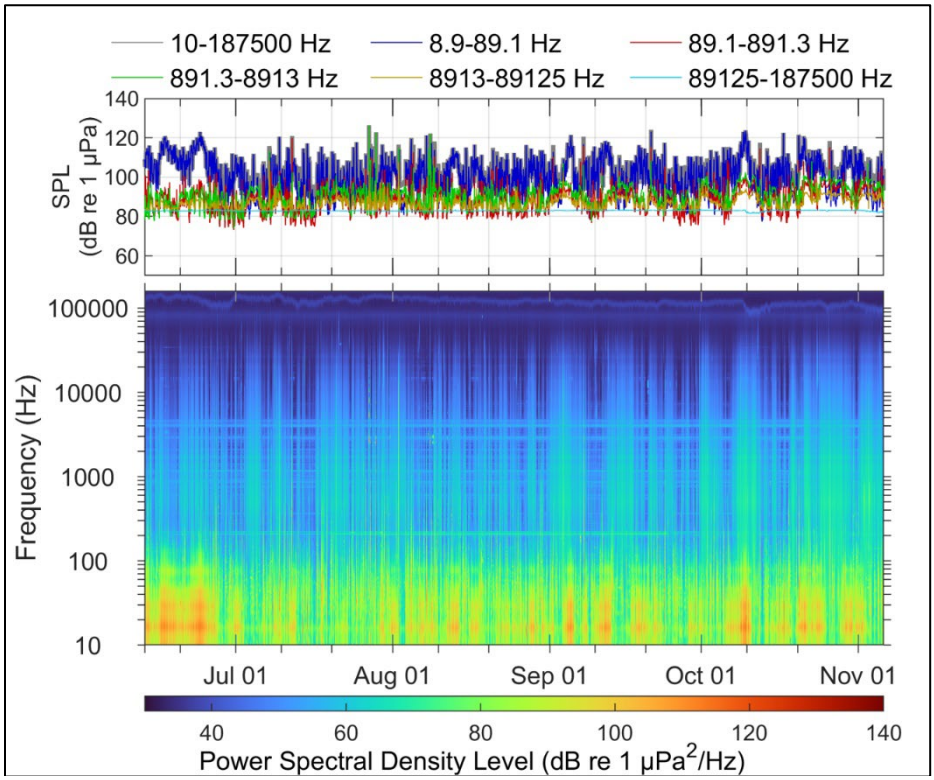

Figure 156. Long-Term Spectral Average and decade band SPL summary of acoustic data collected at BLE for the data collected 13 Jun 18–06 Nov 18, processed to remove the echosounder signature

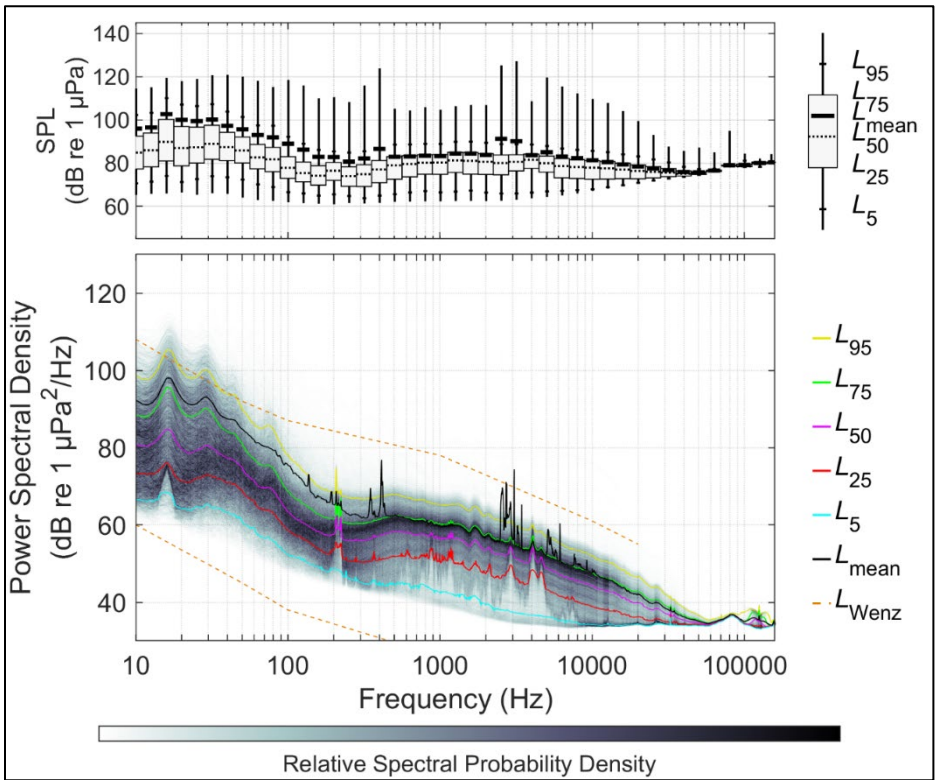

Figure 157. Distributions of spectral sound levels for the JAX data collected 13 Jun 18–06 Nov 18 based on 1-min sound averages, processed to remove the echosounder signature

A.3.5 SAV

The long-term spectral average data and percentile data for the high-frequency sampling rate (375 kHz) at SAV for the period of 15 Jun 18 – 07 Nov 18 are in Figure 158 and Figure 159, respectively. Wind noise is the major sources of noise in SAV during July to October in frequencies above 100 Hz as is apparent in the spectrogram figure. The energy increase in mid-September is also attributable to rain from hurricane events in the region, likely Issac.

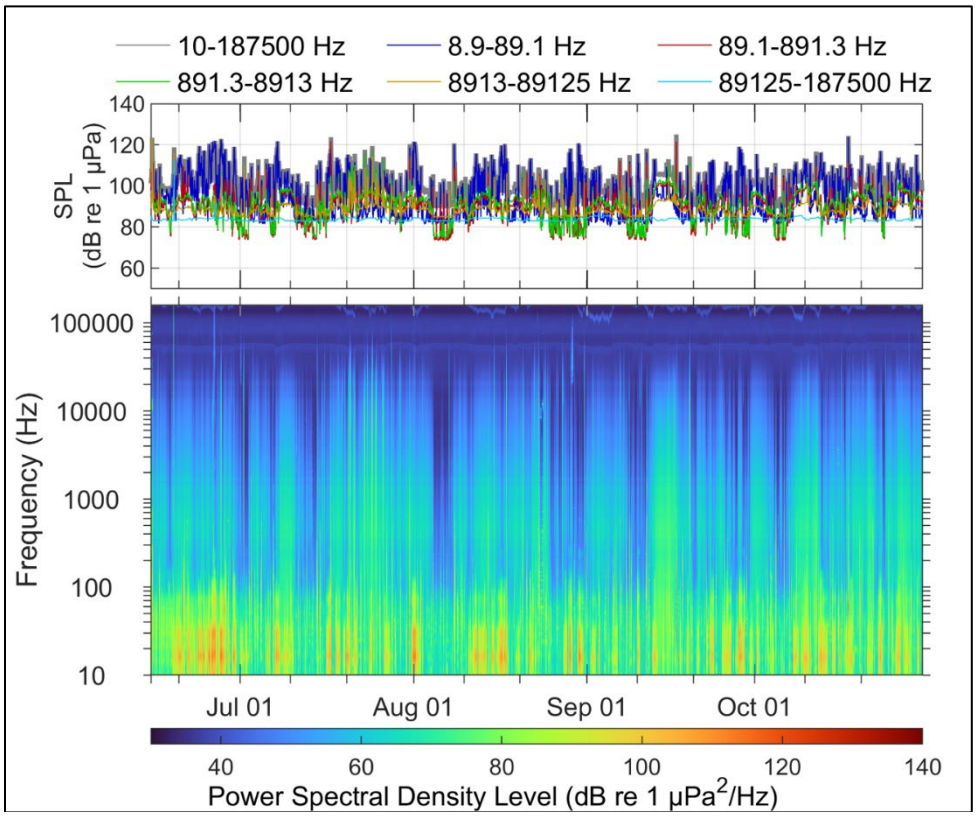

Figure 158. Long-Term Spectral Average and decade band SPL summary of acoustic data collected at SAV for the data collected 15 Jun 18–07 Nov 18

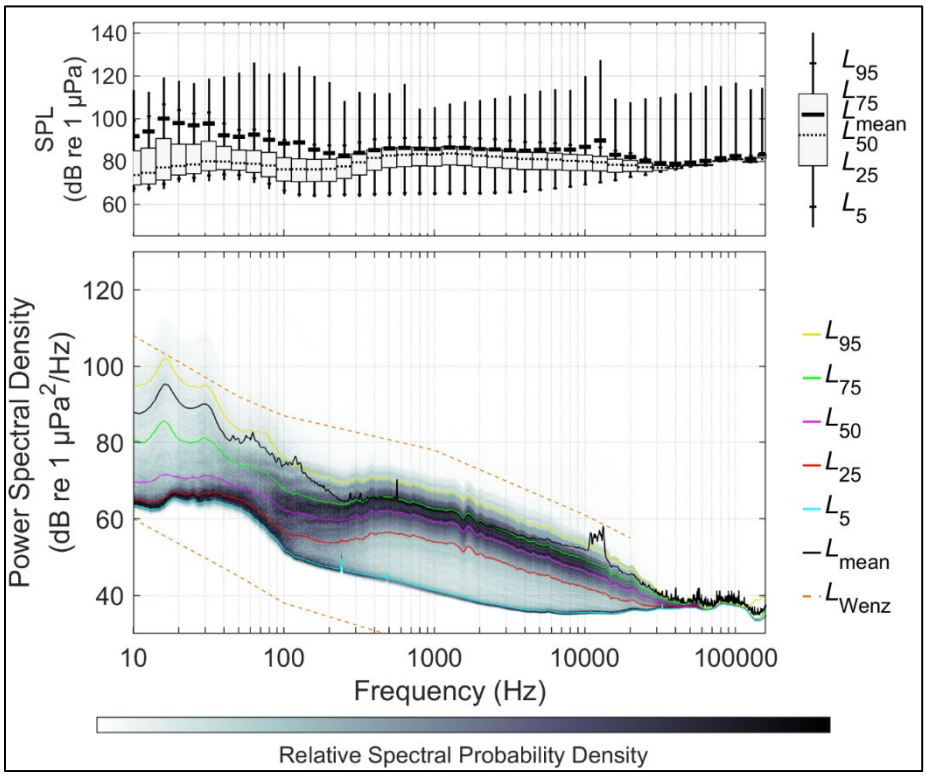

Figure 159. Distributions of spectral sound levels for the SAV data collected 15 Jun 18–07 Nov 18 based on 1-min sound averages

A.3.6 VAC

The long-term spectral average data and percentile data for the high-frequency sampling rate (375 kHz) at VAC for the period of 21 Jun 18 – 11 Nov 18 are in Figure 160 and Figure 161, respectively. In the spectral figure, the energy increase in frequencies below 100 Hz is attributable shipping in the region. The constant energy line around 30 kHz, beginning in early august, represents the echosounder beginning its sampling process. The peak at 20Hz is attributable to fin whale calls. Figure 162 and Figure 163 show the removal of the echosounder signal from the long-term spectral average and power spectral densities, respectively.

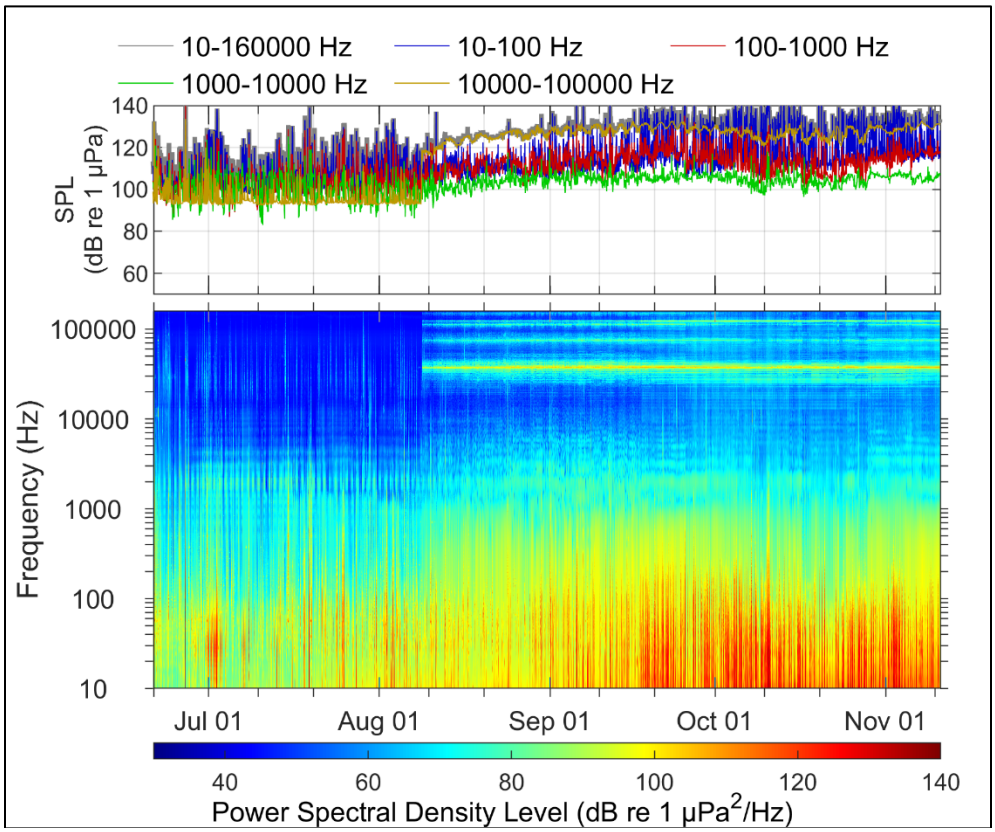

Figure 160. Long-Term Spectral Average and decade band SPL summary of acoustic data collected at VAC for the data collected 21 Jun 18–11 Nov 18

Note, bands were changed during the echosounder removal process.

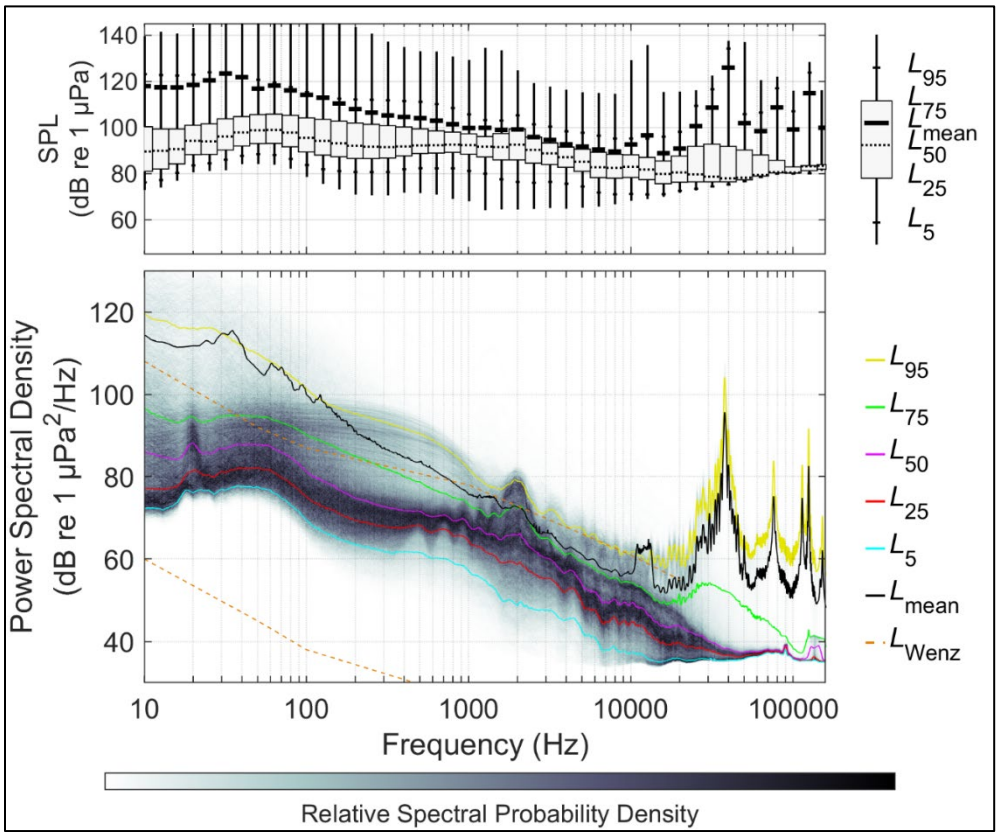

Figure 161. Distributions of spectral sound levels for the VAC data collected 21 Jun 18–11 Nov 18 based on 1-min sound averages

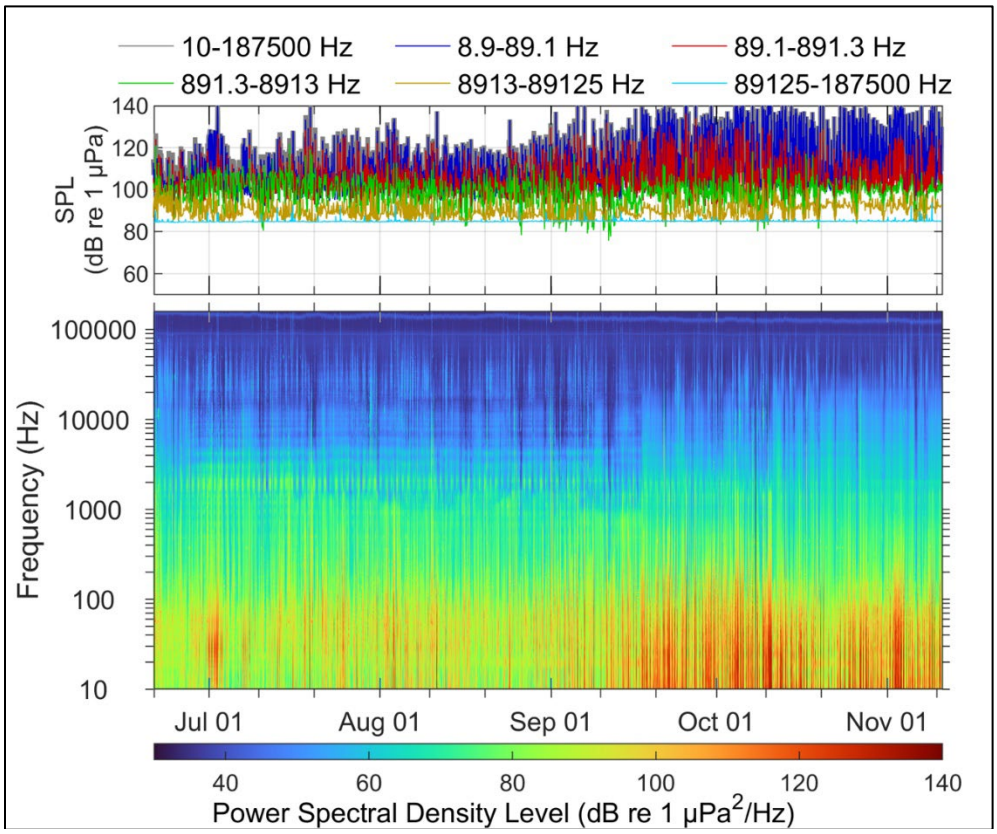

Figure 162. Long-Term Spectral Average and decade band SPL summary of acoustic data collected at VAC for the data collected 21 Jun 18–11 Nov 18, processed to remove the echosounder signature

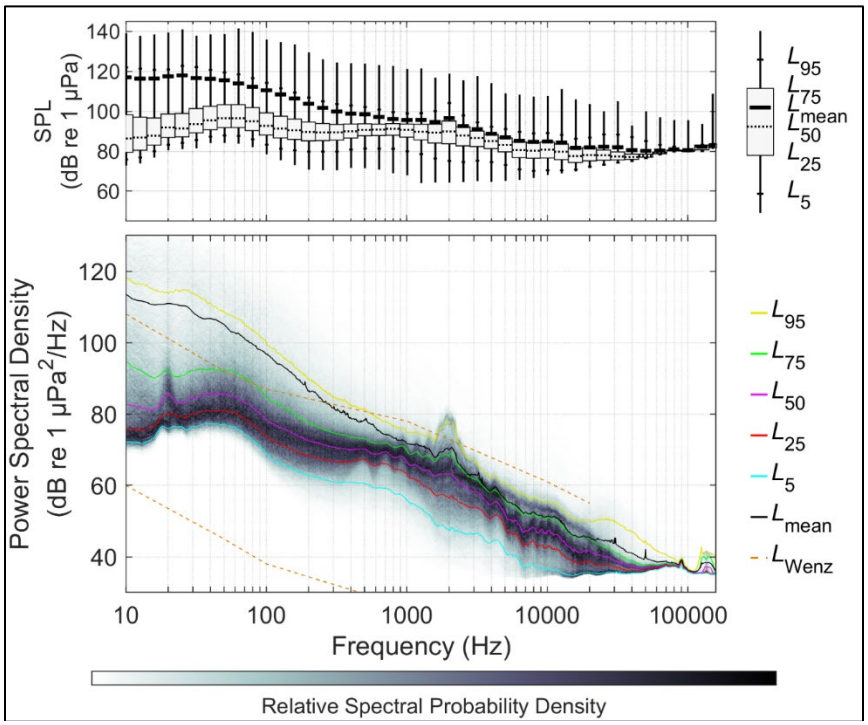

Figure 163. Distributions of spectral sound levels for the VAC data collected 21 Jun 18–11 Nov 18 based on 1-min sound averages, processed to remove the echosounder signature

A.3.7 WIL

The long-term spectral average data and percentile data for the high-frequency sampling rate (375 kHz) at WIL for the period of 06 Jun 18 – 09 Nov 18 are in Figure 164 and Figure 165, respectively. According to these figures, the major sources of noise in this station are in the frequencies below 20 Hz and 100 Hz which are due to flow and wind noise, respectively. Hurricane is also another source of noise at mid-September which increased the energy level over a broad frequency band above approximately 100 Hz.

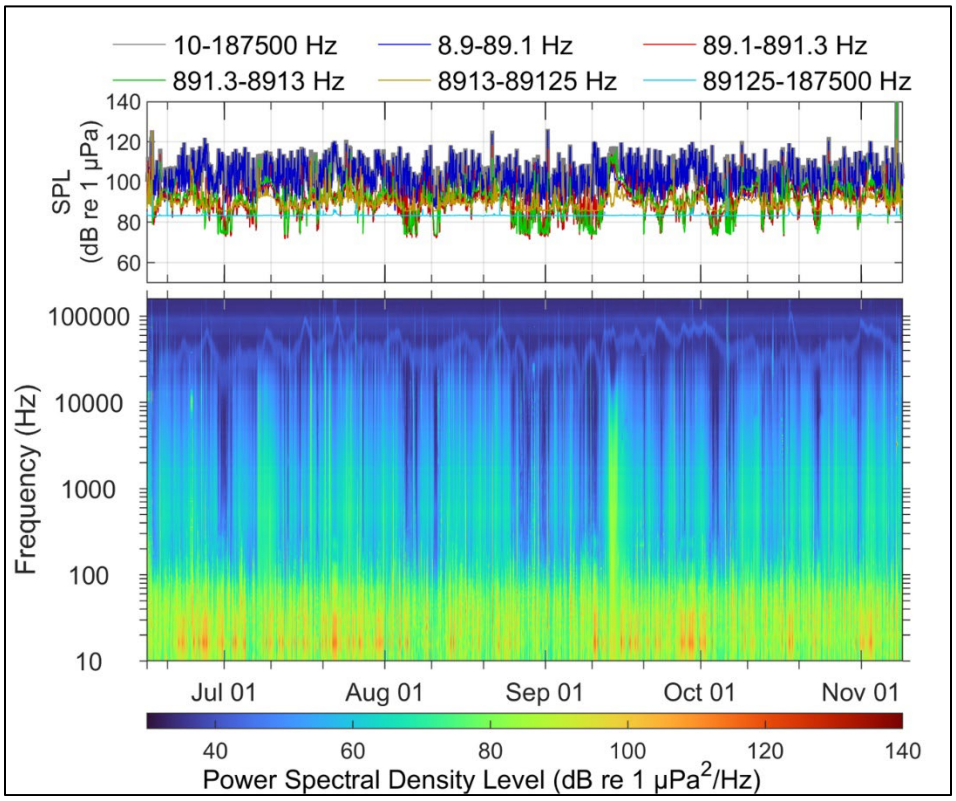

Figure 164. Long-Term Spectral Average and decade band SPL summary of acoustic data collected at WIL for the data collected 16 Jun 18–09 Nov 18

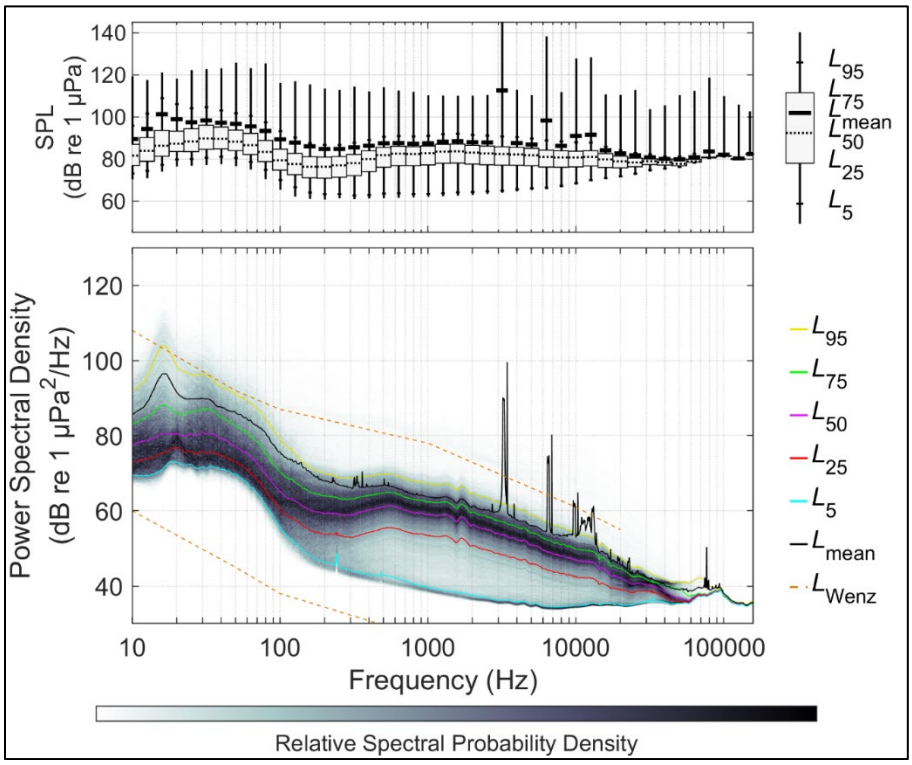

Figure 165. Distributions of spectral sound levels for the WIL data collected 16 Jun 18–09 Nov 18 based on 1-min sound averages

A.4 Cruise AR40: Data From Nov 2018–Nov 2019

Cruise AR040 retrieved and redeployed the landers at all stations, providing an opportunity for data download, lander refurbishment, and battery replacement. Named storms during the 2019 hurricane season in the study area were Barry (formed 11 Jul), Dorian (formed 24 Aug), Humberto (formed 13 Sept), Jerry (formed 17 Sept), Lorenzo (formed 23 Sept), and Pablo (formed 25 Oct). VAC was retrieved prematurely after becoming entangled in trawling gear.

A.4.1 BLE

The long-term spectral average data and percentile data for the high-frequency sampling rate (512 kHz) at BLE for the period of 06 Nov 18 – 15 Nov 19 are in Figure 166 and Figure 167, respectively. In the spectral figure, the dominant sources of noise are flow noise and wind noise for the frequencies below 100 Hz. There is evidence of hurricanes increasing the spectral energy level in mid-September. Moreover, the broadband energy increase on October 27 shows that the deployments are out of water. Increased sound levels between 100-200 Hz in the winter months is from minke whales.

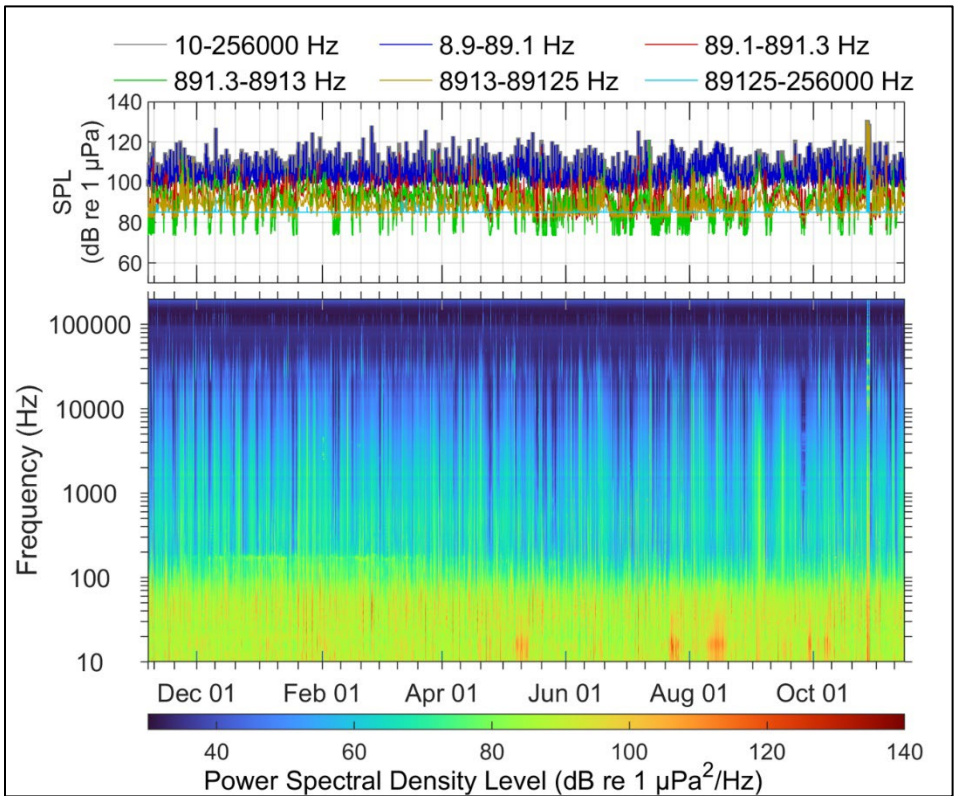

Figure 166. Long-Term Spectral Average and decade band SPL summary of acoustic data collected at BLE for the data collected 06 Nov 18–15 Nov 19

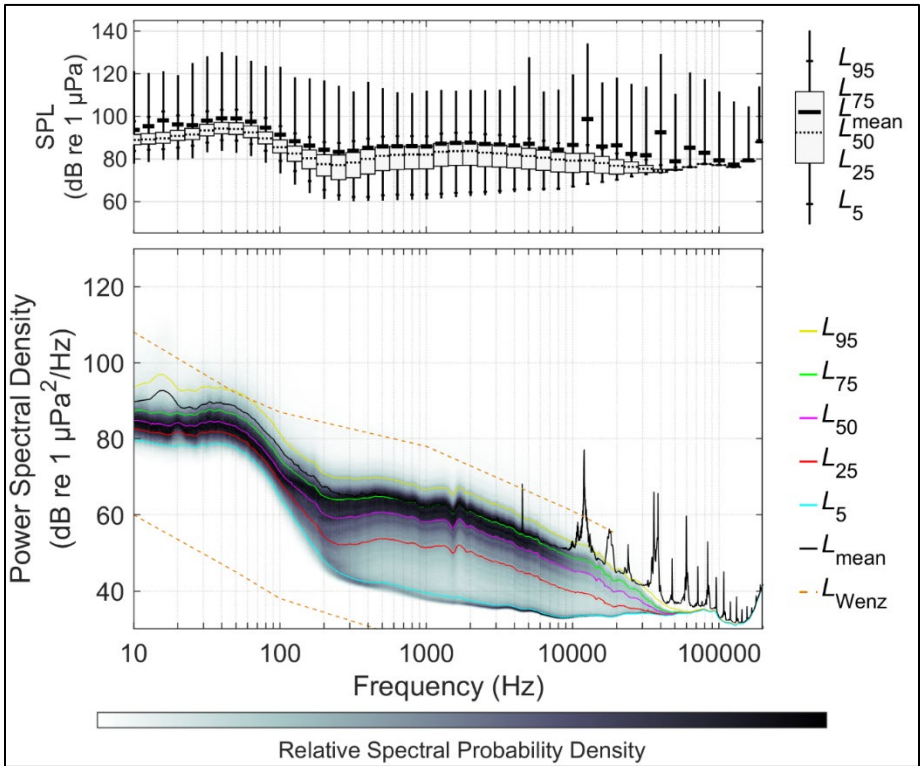

Figure 167. Distributions of spectral sound levels for the BLE data collected 06 Nov 18–15 Nov 19 based on 1-min sound averages

A.4.2 CHB

The long-term spectral average data and percentile data for the high-frequency sampling rate (512 kHz) at CHB between 05 Nov 18 – 29 Oct 19 are in Figure 168 and Figure 169, respectively. Strong currents and associated flow noise are implicated in the higher spectral levels under 100 Hz. There is also broadband sound level increase due to wind below 20 kHz.

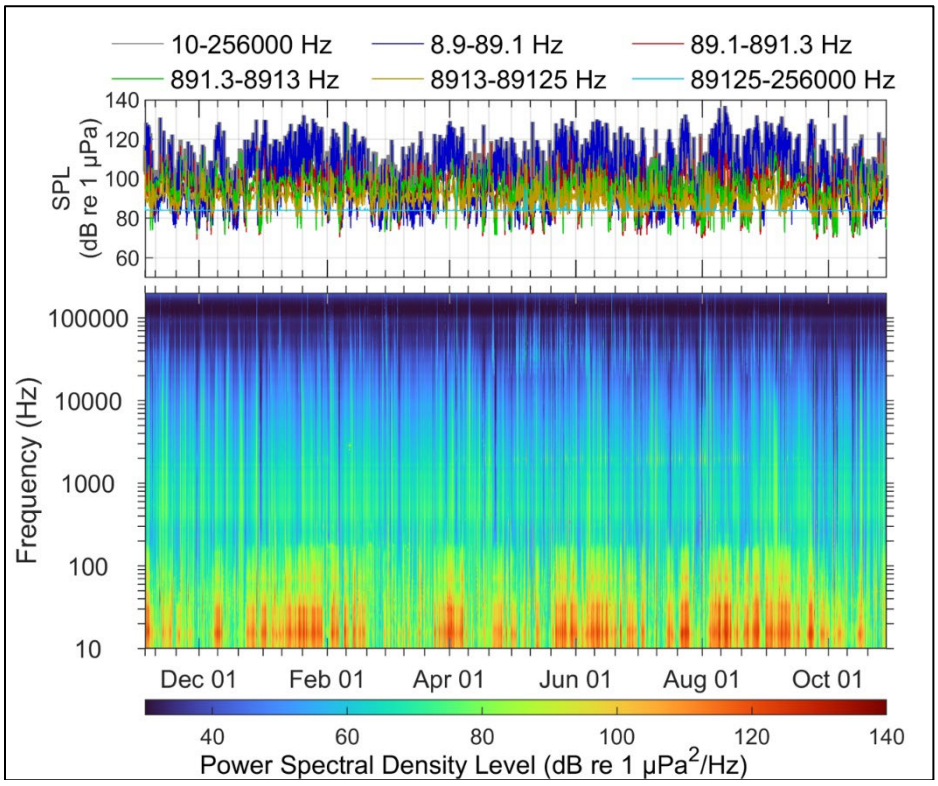

Figure 168. Long-Term Spectral Average and decade band SPL summary of acoustic data collected at CHB for the data collected 05 Nov 18–29 Oct 19

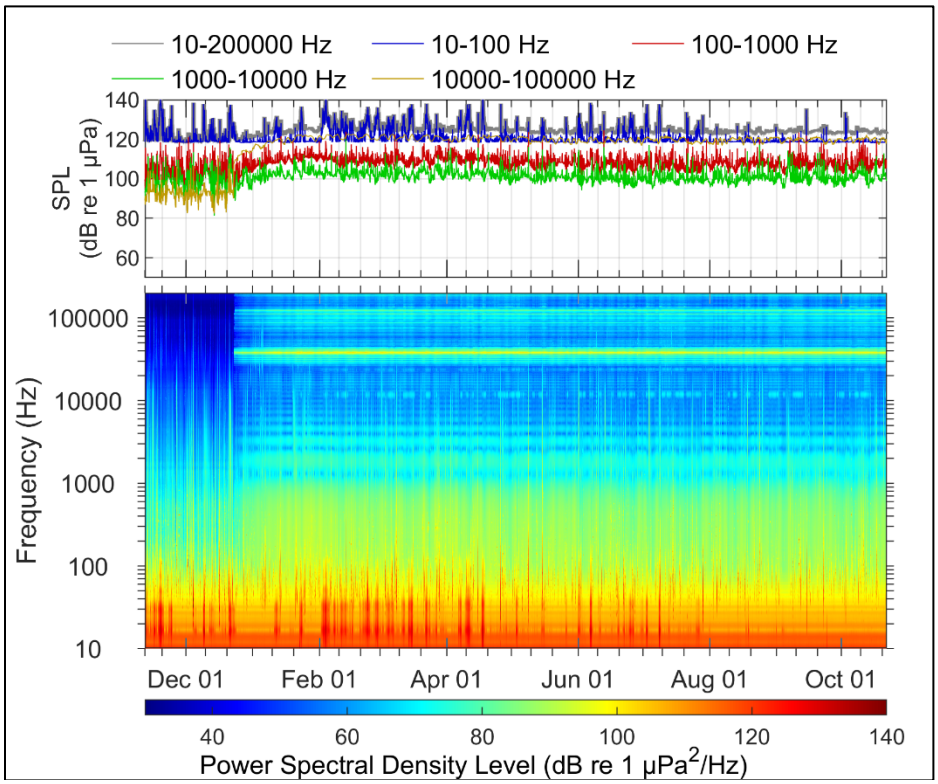

Figure 169. Distributions of spectral sound levels for the CHB data collected 05 Nov 18–29 Oct 19 based on 1-min sound averages.

A.4.3 HAT

The long-term spectral average data and percentile data for the high-frequency sampling rate (512 kHz) at HAT between 12 Nov 18–22 Oct 19 are presented in Figure 170 and Figure 171, respectively. Flow noise is the main cause of elevated energy below 100 Hz. The constant energy line around 30 kHz represents the activation of the onboard echosounder. Figure 172 and Figure 173 show the removal of the echosounder signal from the long-term spectral average and power spectral densities, respectively. Fin whale calls are attributed to the increase in energy at 20Hz.

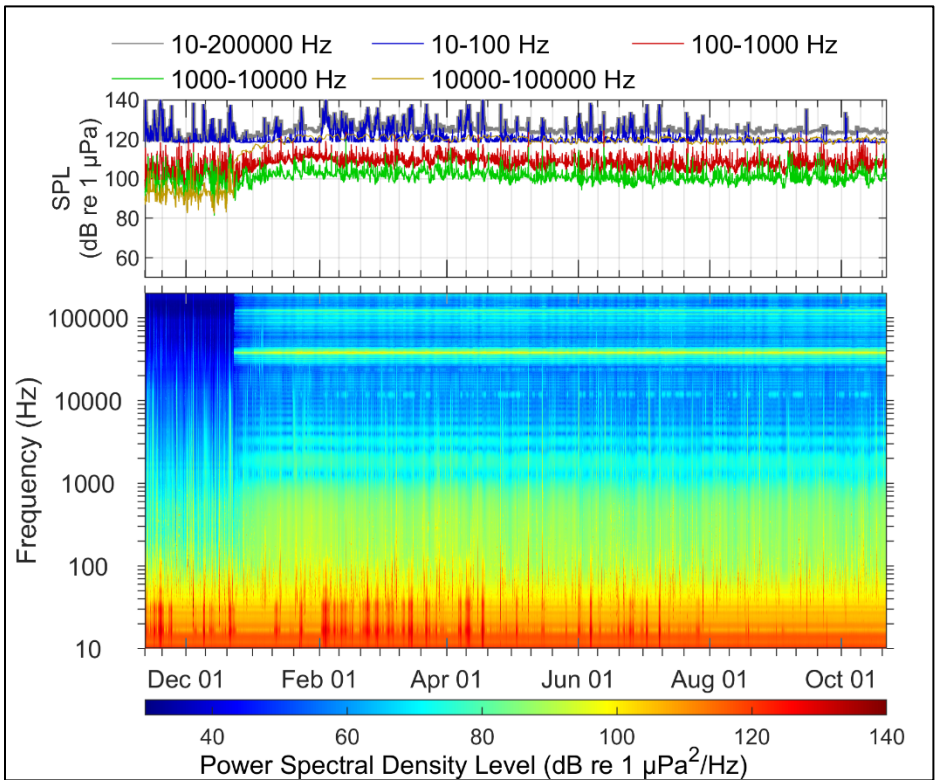

Figure 170. Long-Term Spectral Average and decade band SPL summary of acoustic data collected at HAT for the data collected 12 Nov 18–22 Oct 19

Note, bands were changed during echosounder removal process.

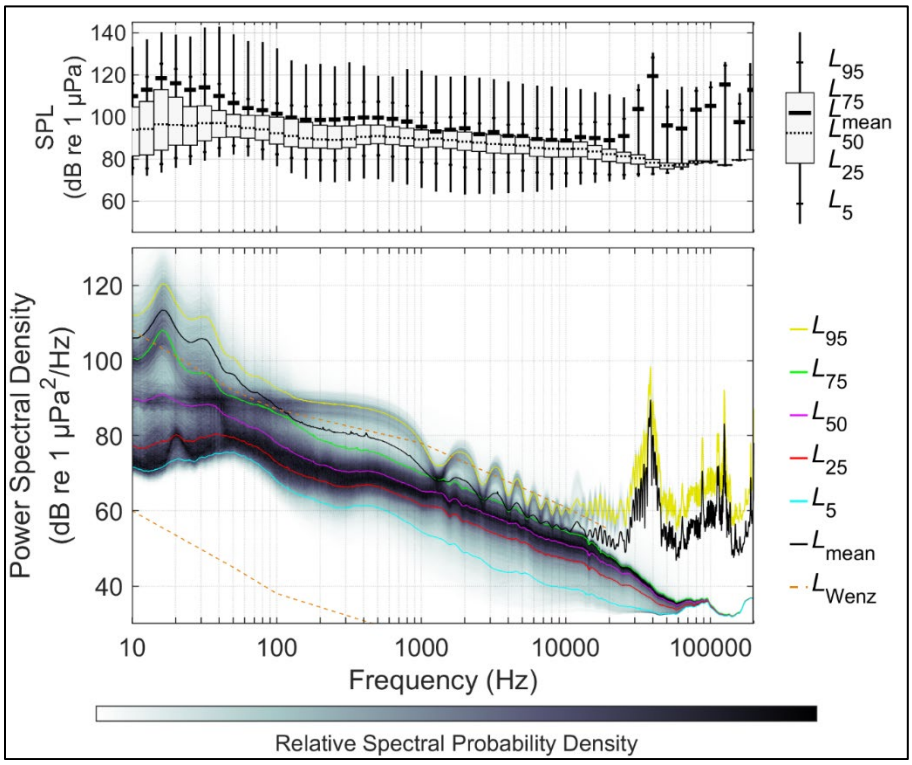

Figure 171. Distributions of spectral sound levels for the HAT data collected 12 Nov 18–22 Oct 19 based on 1-min sound averages

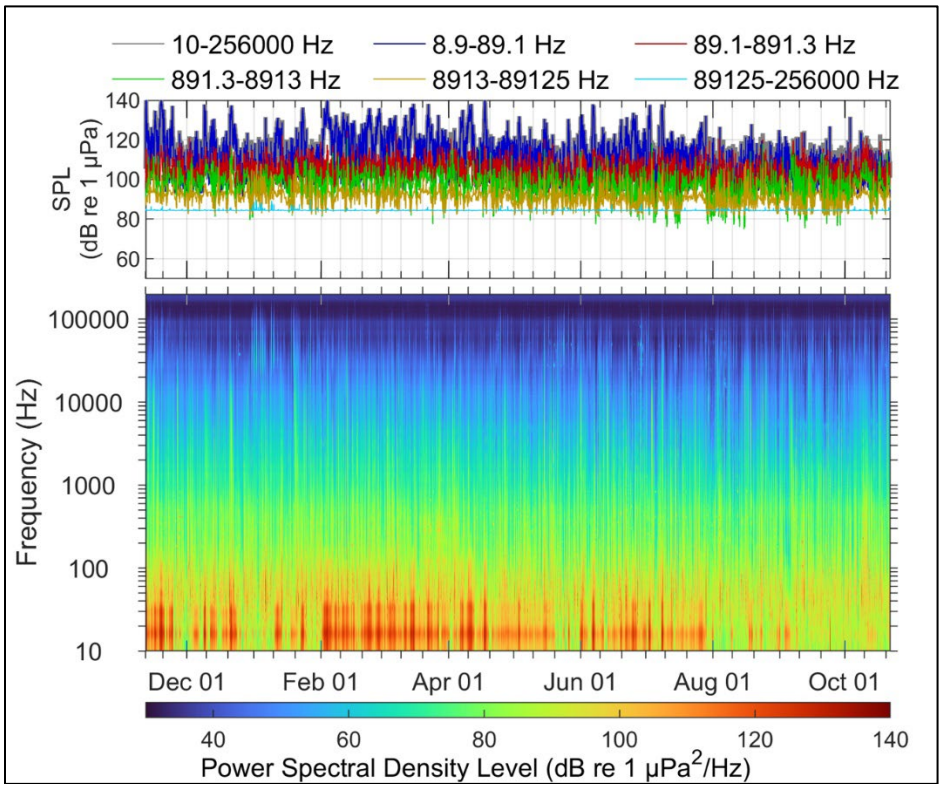

Figure 172. Long-Term Spectral Average and decade band SPL summary of acoustic data collected at HAT for the data collected 12 Nov 18–22 Oct 19, processed to remove the echosounder signature

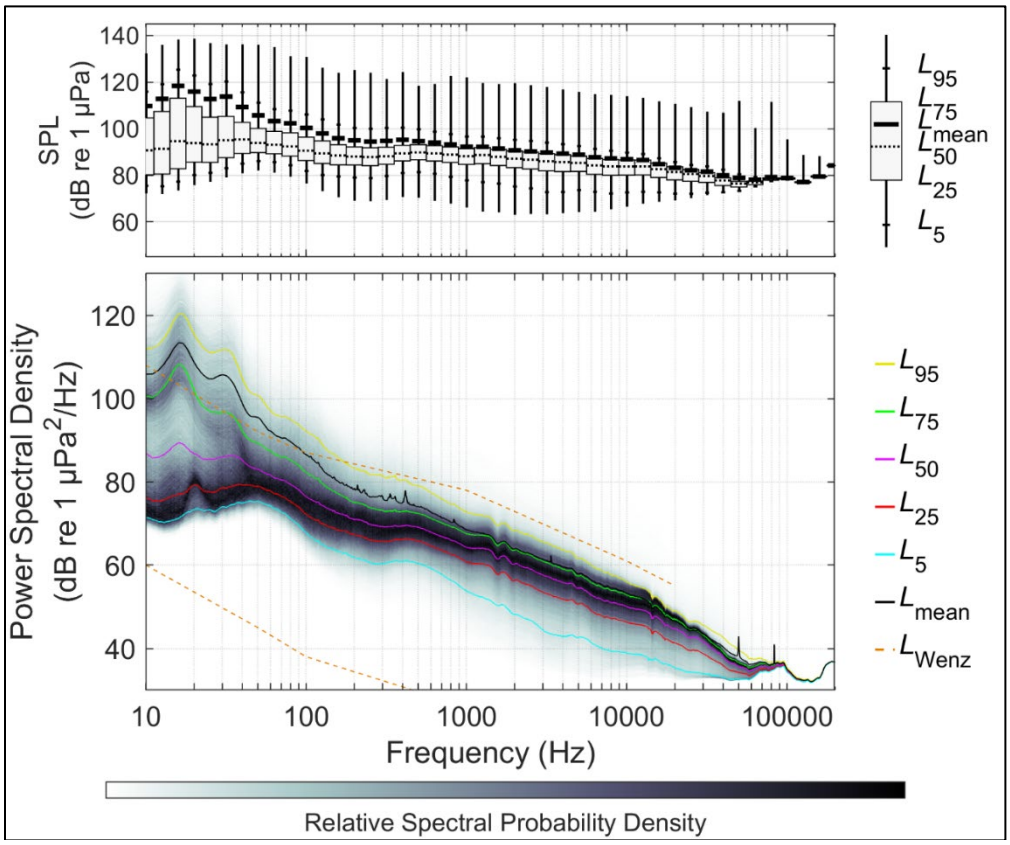

Figure 173. Distributions of spectral sound levels for the HAT data collected 12 Nov 18–22 Oct 19 based on 1-min sound averages, processed to remove the echosounder signature

A.4.4 JAX

The long-term spectral average data and percentile data for the high-frequency sampling rate (512 kHz) at JAX between 8 Nov 18–15 Nov 19 are in Figure 174 and Figure 175, respectively, after the echosounder signature had been removed from the records. In the spectral figure below, shipping is the main cause of energy increase for the frequencies below 100 Hz. The elevation in sound energy from 100-200 Hz in the winter months is from minke whales.

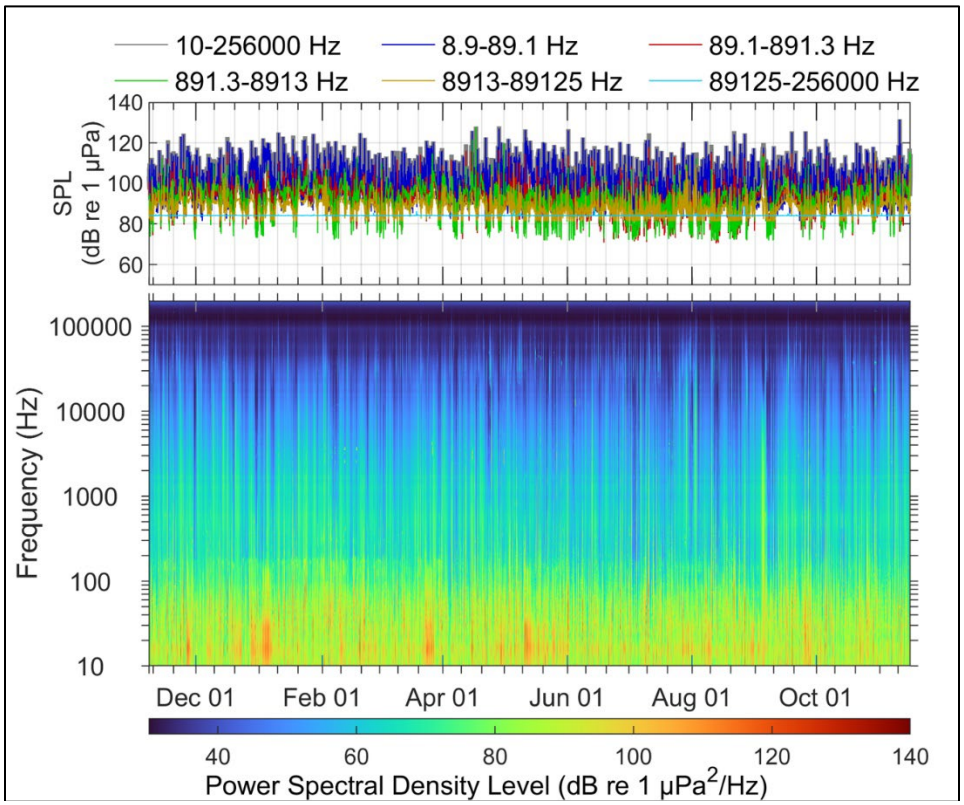

Figure 174. Long-Term Spectral Average and decade band SPL summary of acoustic data collected at JAX for the data collected 8 Nov 18–15 Nov 19, processed to remove the echosounder signature

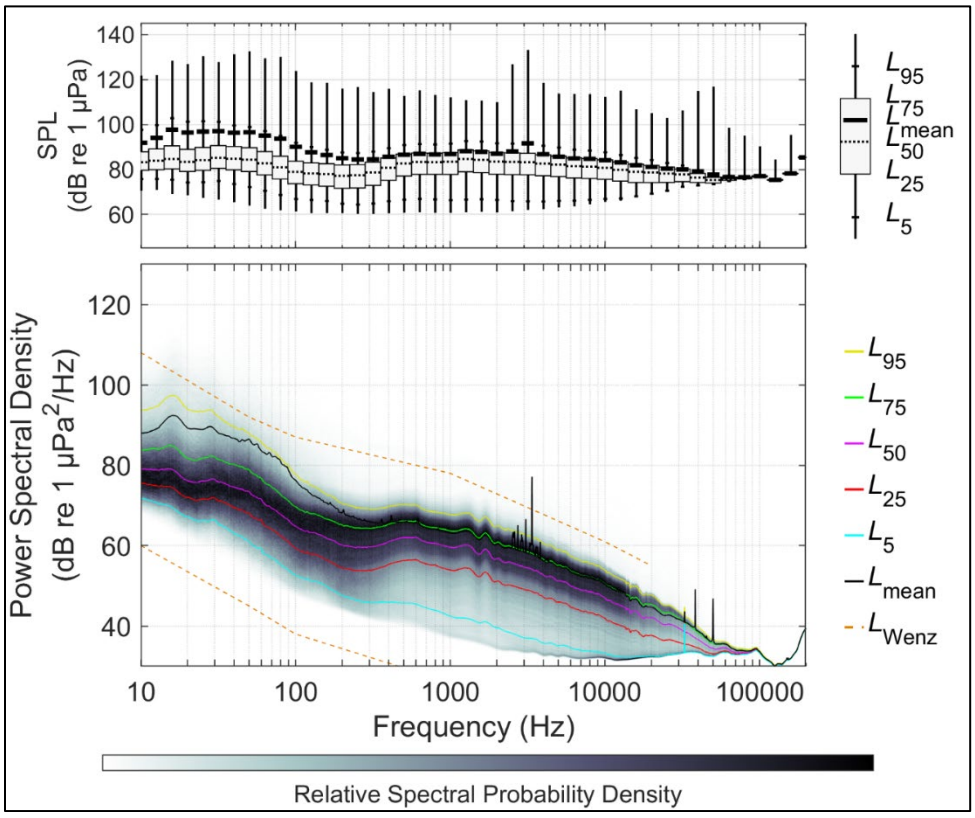

Figure 175. Distributions of spectral sound levels for the HAT data collected 8 Nov 18–15 Nov 19 based on 1-min sound averages, processed to remove the echosounder signature.

A.4.5 SAV

The long-term spectral average data and percentile data for the high-frequency sampling rate (512 kHz) at SAV between 08 Nov 18 – 24 Oct 19 are in Figure 176 and Figure 177, respectively. Fin whale calls are attributed to the spectral peak at 20 Hz, while minke whales contribute to the 80-200Hz band between December and April. Wind events are implicated in raising the spectral level between 630 and 10000 Hz.

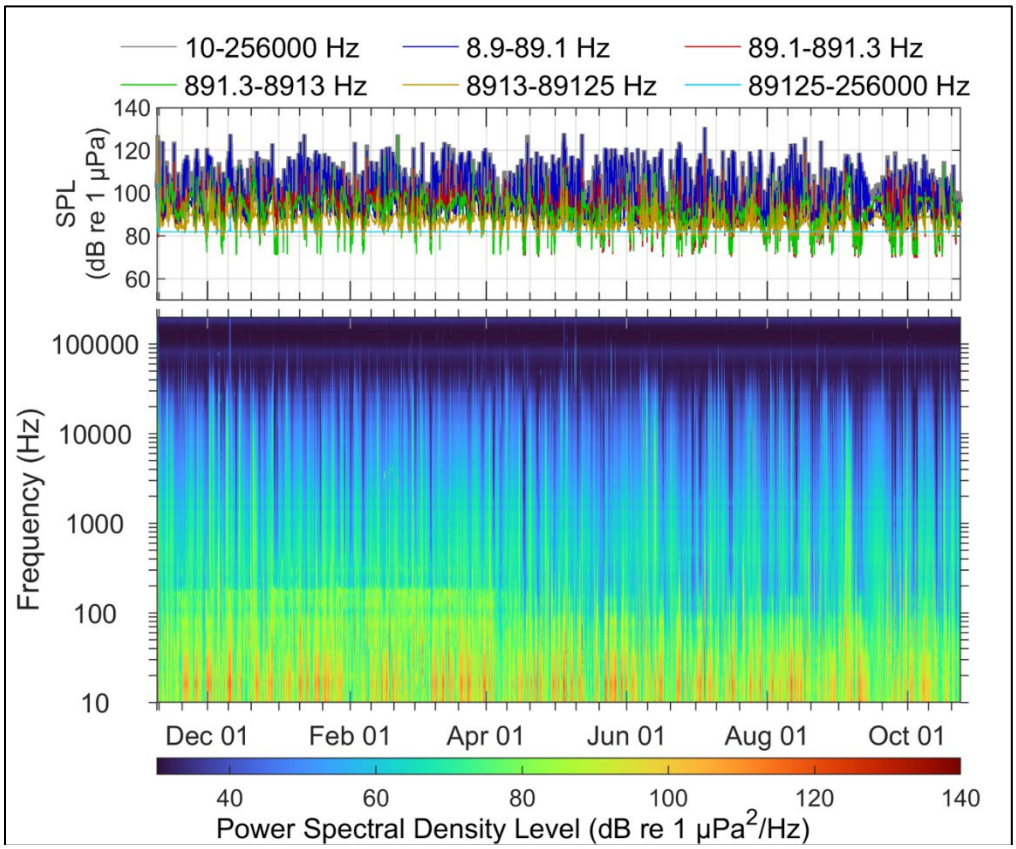

Figure 176. Long-Term Spectral Average and decade band SPL summary of acoustic data collected at SAV for the data collected 08 Nov 18–24 Oct 19.

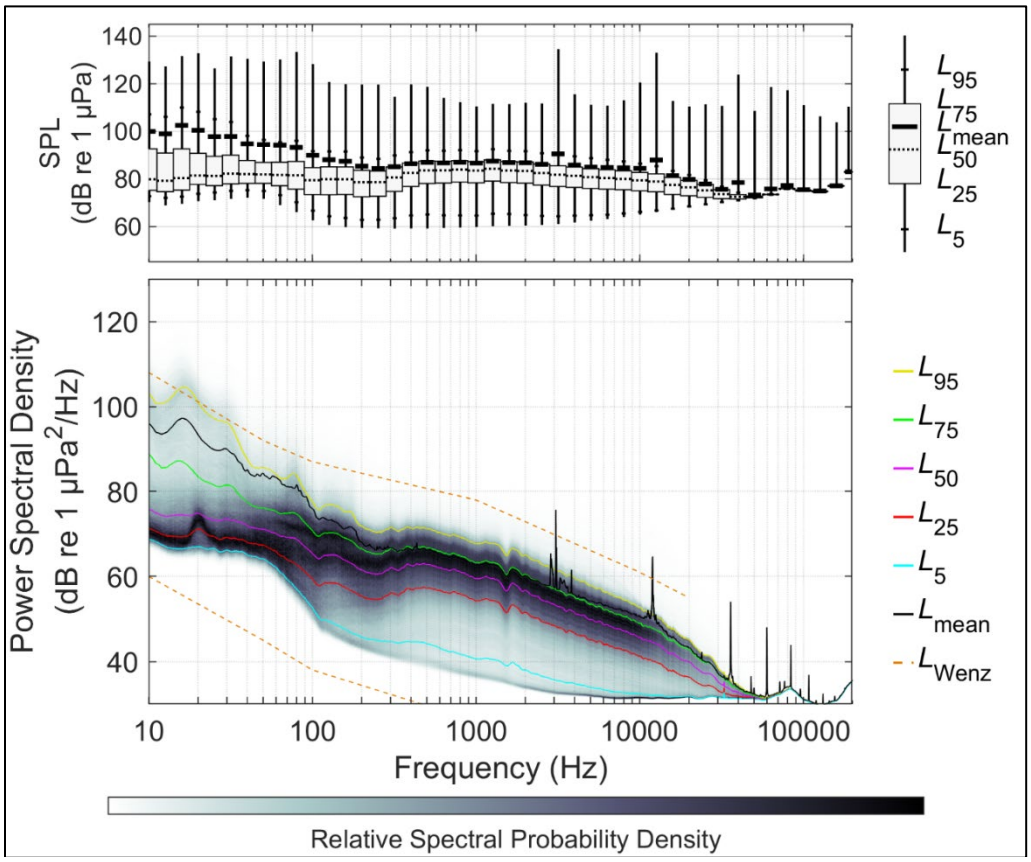

Figure 177. Distributions of spectral sound levels for the SAV data collected 08 Nov 18–24 Oct 19 based on 1-min sound averages.

A.4.6 VAC

The long-term spectral average data and percentile data for the high-frequency sampling rate (512 kHz) at VAC between 13 Nov 18 – 06 Jul 19 are in Figure 178 and Figure 179, respectively. From December to March, Figure 171 highlights fin whale calling in the 20 Hz band. The energy at 2 kHz from February to July is attributable to vessel engines, while the broadband noise increase below 10 kHz is due to the noise emitted by the passing vessel traffic. Figure 180 and Figure 181 show the removal of the echosounder signal from the long-term spectral average and power spectral densities, respectively.

After the data recovery in June 2018, VAC-2 was retrieved prematurely after becoming entangled in trawling gear in early July.

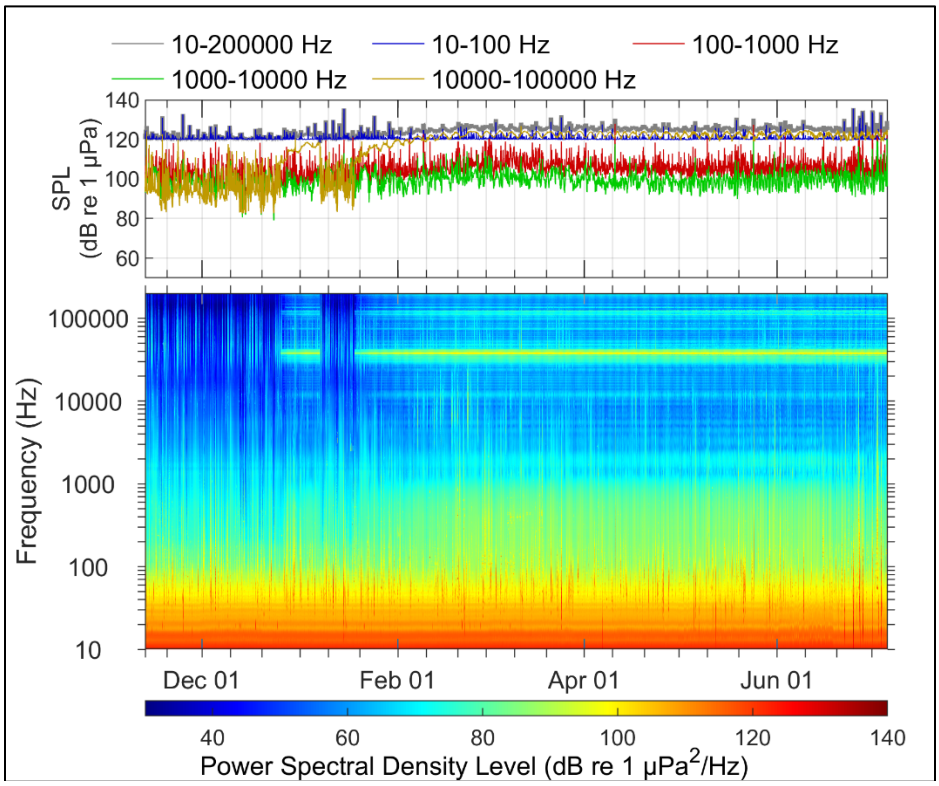

Figure 178. Long-Term Spectral Average and decade band SPL summary of acoustic data collected at VAC for the data collected 13 Nov 18–06 Jul 19

Note, bands were changed during echosounder removal process.

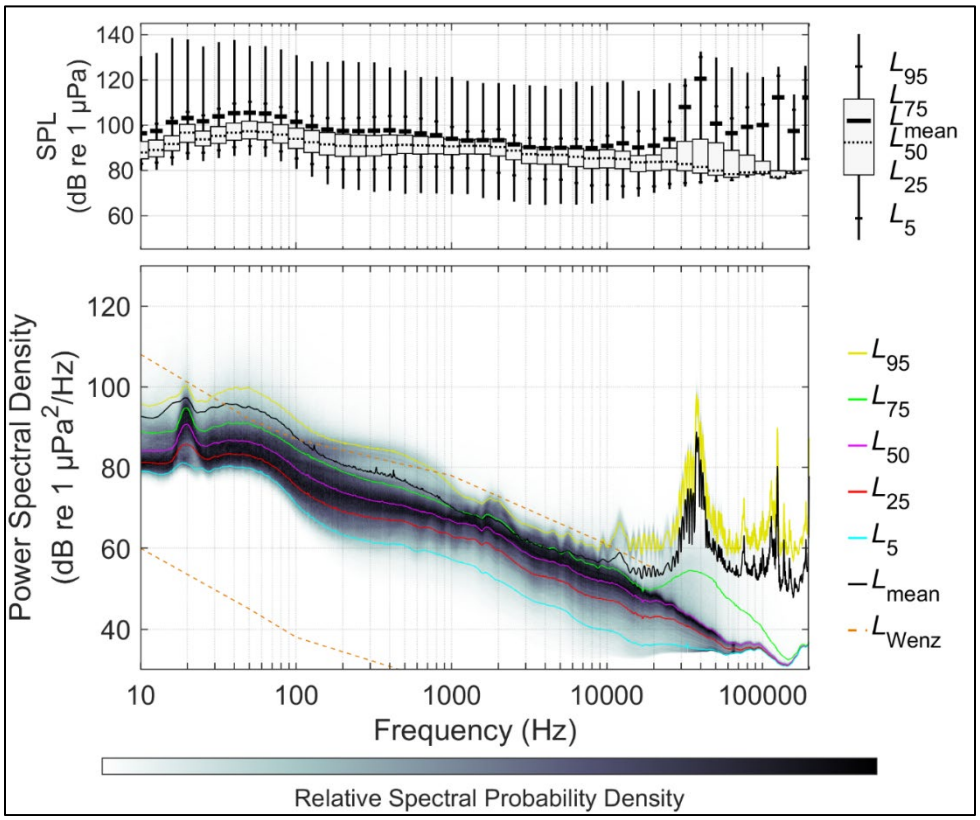

Figure 179. Distributions of spectral sound levels for the VAC data collected 13 Nov 18–06 Jul 19 based on 1-min sound averages

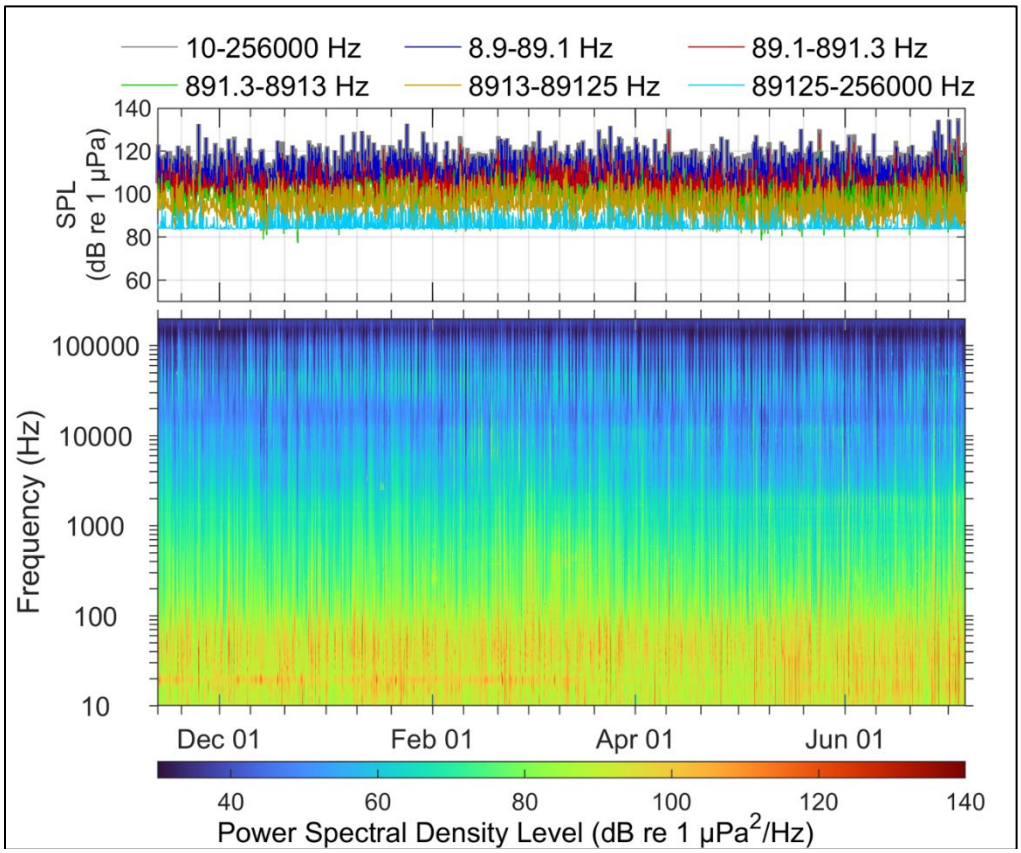

Figure 180. Long-Term Spectral Average and decade band SPL summary of acoustic data collected at VAC for the data collected 13 Nov 18–06 Jul 19, processed to remove the echosounder signature

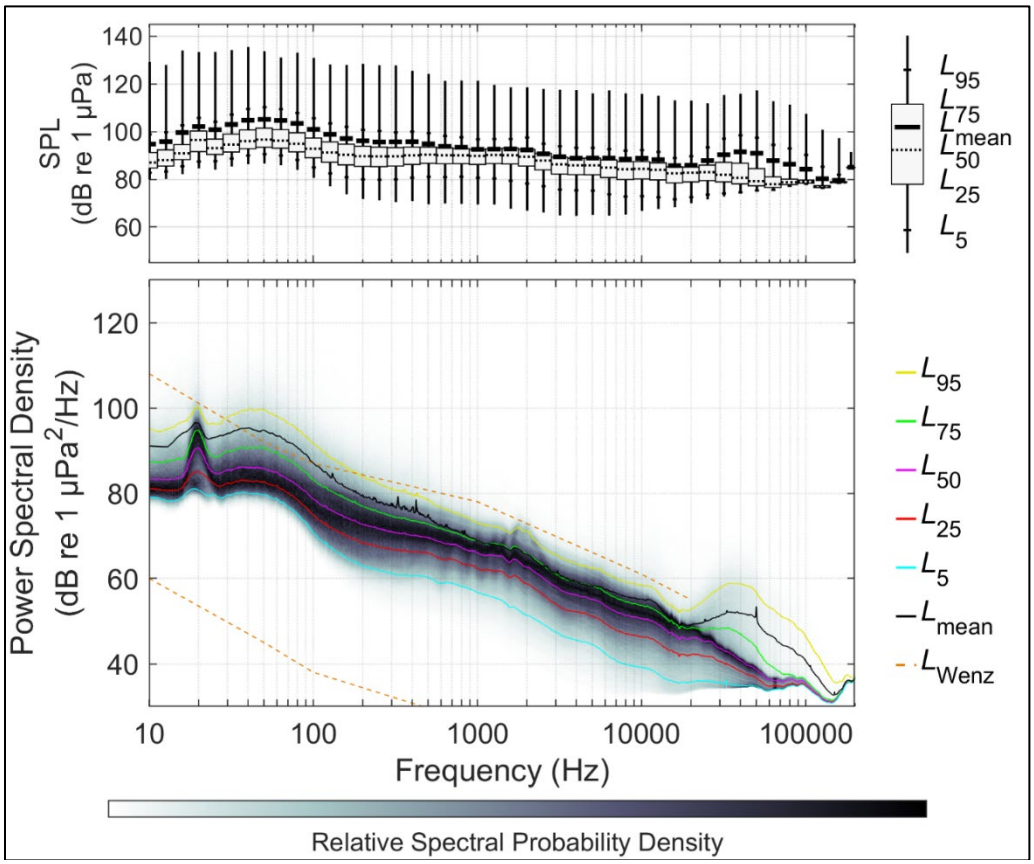

Figure 181. Distributions of spectral sound levels for the VAC data collected 13 Nov 18–06 Jul 19 based on 1-min sound averages, processed to remove the echosounder signature

A.4.7 WIL

The long-term spectral average data and percentile data for the high-frequency sampling rate (512 kHz) at WIL between 11 Nov 18–23 Oct 19 are in Figure 182 and Figure 183, respectively. As is apparent in the figures below, the main source of noise is wind for the frequencies below 20 kHz. Fin whales are attributed to the 20 Hz spectral peak.

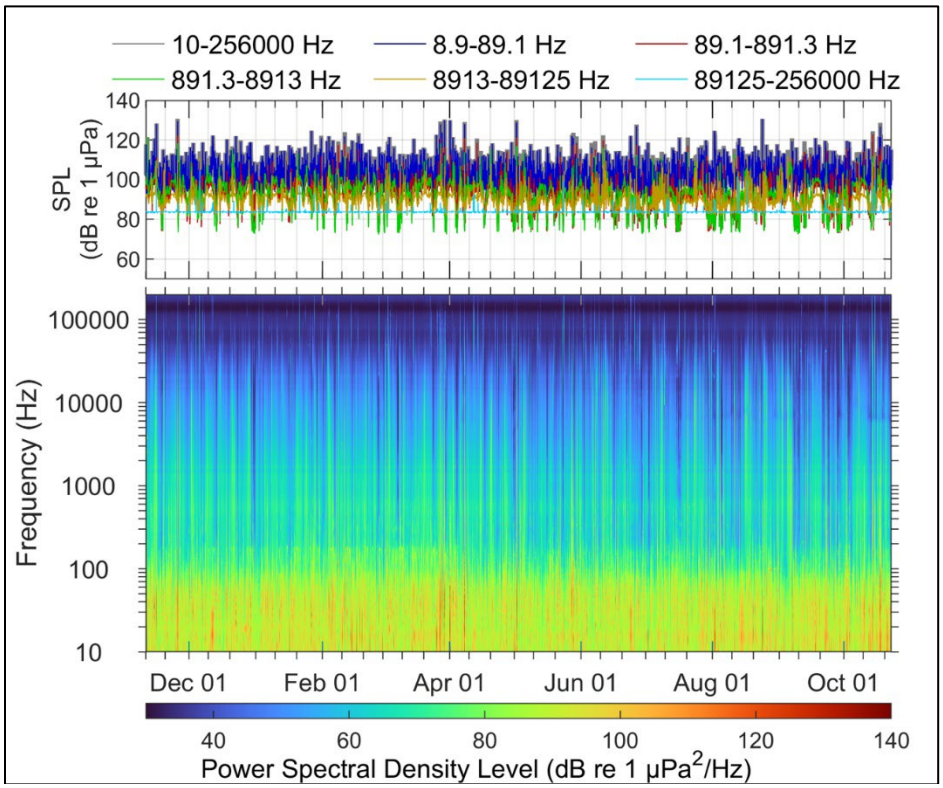

Figure 182. Long-Term Spectral Average and decade band SPL summary of acoustic data collected at WIL for the data collected 11 Nov 18–23 Oct 19

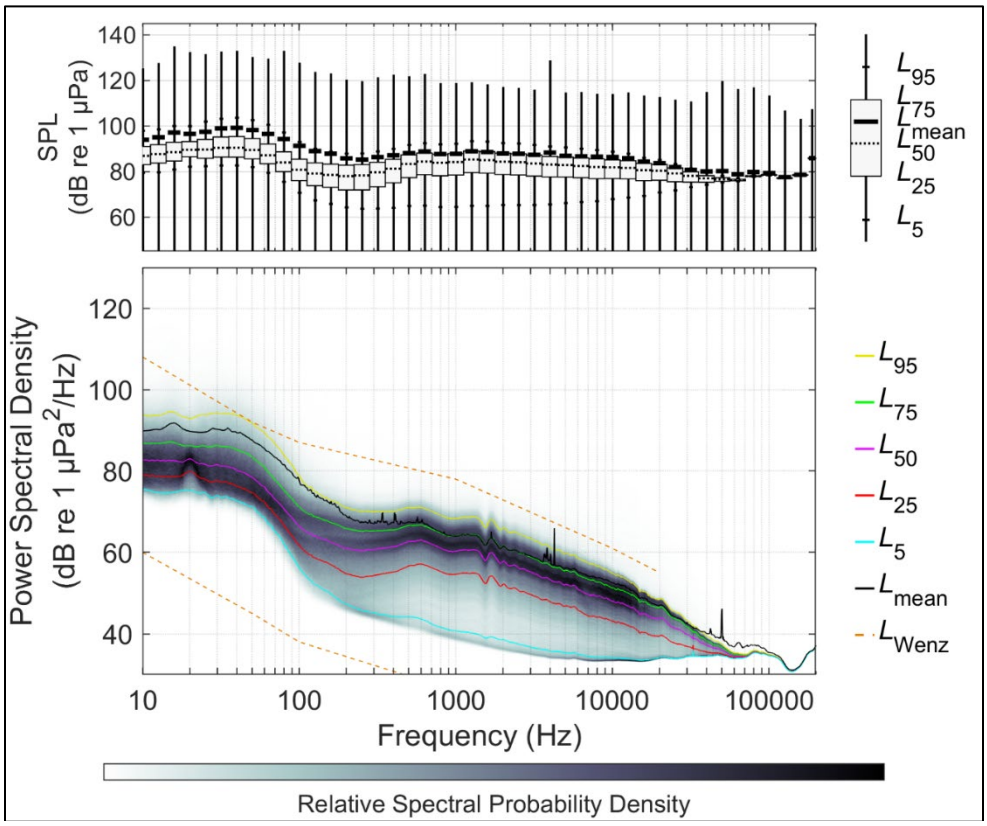

Figure 183. Distributions of spectral sound levels for the WIL data collected 11 Nov 18–23 Oct 19 based on 1-min sound averages

A.5 Cruise AR49: Data from Nov 2019 – Nov 2020

Cruise AR49 retrieved and redeployed the landers at all stations, providing an opportunity for data download, lander refurbishment, and battery replacement. Named storms in the 2020 hurricane season in the study area were Hanna (formed 23 July), Isaias (formed 30 July), Laura (formed 20 Aug), Marco (formed 21 Aug), Nana (formed 1 Sep), Paulette (formed 7 Sept), Sally (formed 11 Sept), Teddy (formed 12 Sept), Gamma (formed 2 Oct), Delta (formed 4 Oct), Epsilon (formed 19 Oct), Zeta (formed 24 Oct), Eta (formed Oct 31) , and Iota (formed 13 Nov).

A.5.1 BLE

The long-term spectral average data and percentile data for the high-frequency sampling rate (512 kHz) at BLE for the period of 29 Oct 19 – 01 Dec 20 are in Figure 184 and Figure 185, respectively. Increased energy below 100 Hz illustrates the presence of Shipping and some flow noise. There is also broadband sound level increase due to wind which is below 20 kHz. The increase in sound energy from 100-200 Hz in the winter months is attributed to minke whales.

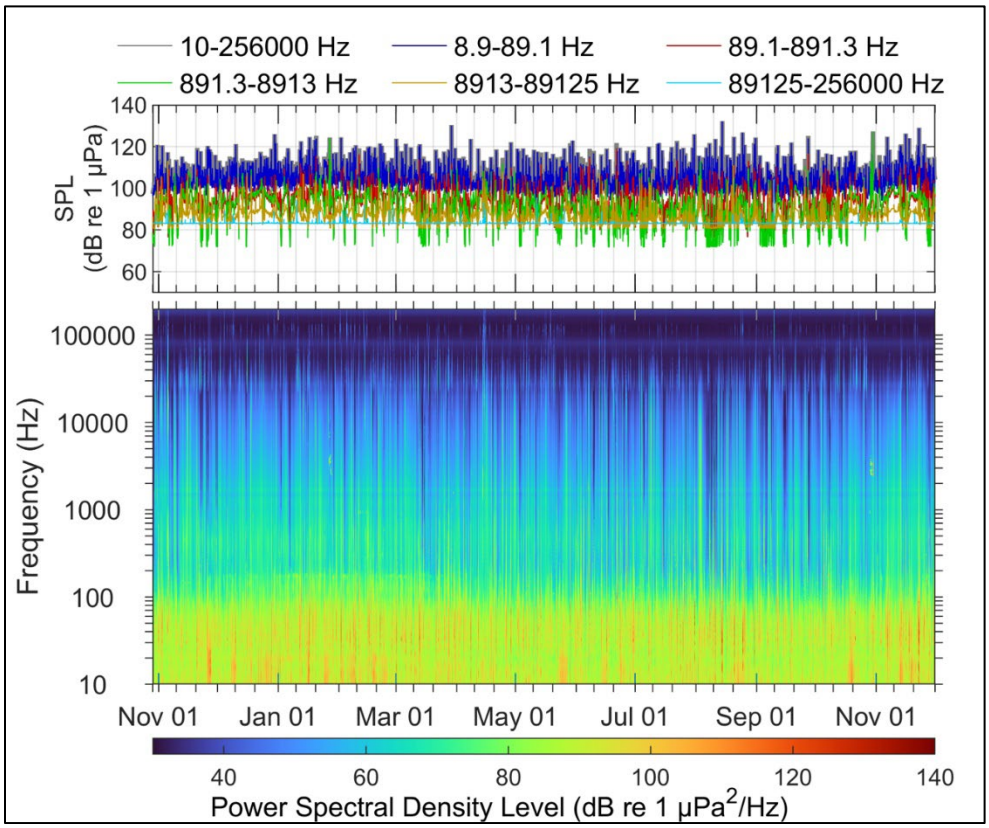

Figure 184. Long-Term Spectral Average and decade band SPL summary of acoustic data collected at BLE for the data collected 29 Oct 19–01 Dec 20

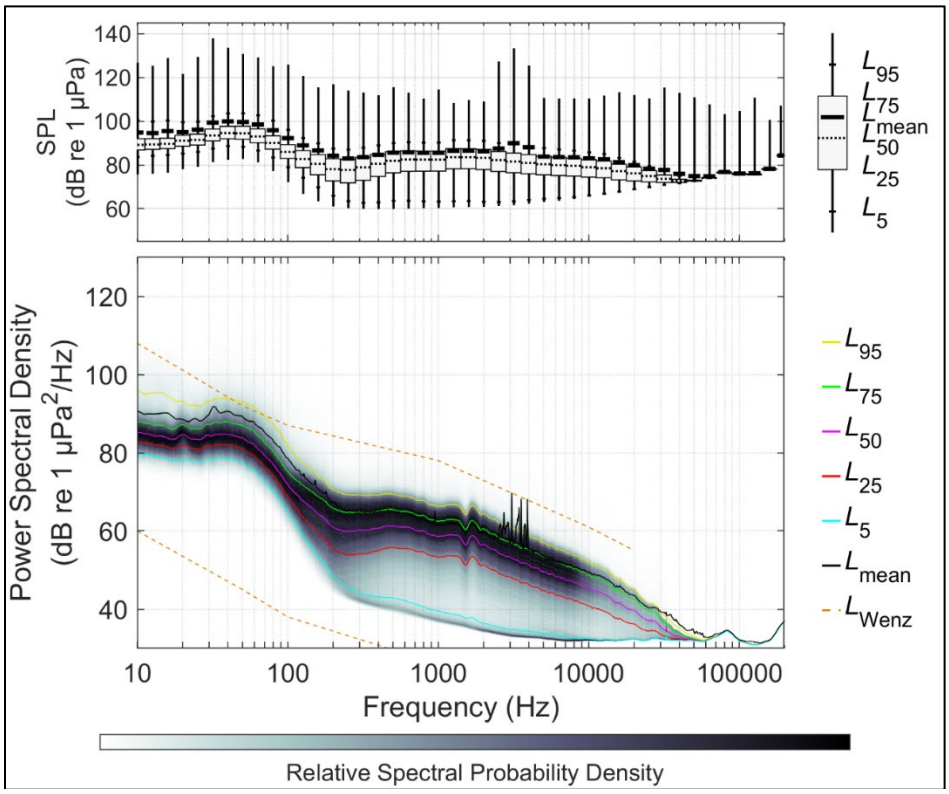

Figure 185. Distributions of spectral sound levels for the BLE data collected 29 Oct 19–01 Dec 20 based on 1-min sound averages

A.5.2 CHB

The long-term spectral average data and percentile data for the high-frequency sampling rate (512 kHz) at CHB between 01 Dec 19–03 Dec 20 are in Figure 186 and Figure 187, respectively. Flow noise is attributable to higher spectral levels below 100 Hz, while below 20 kHz, wind and other weather systems are driving the soundscape.

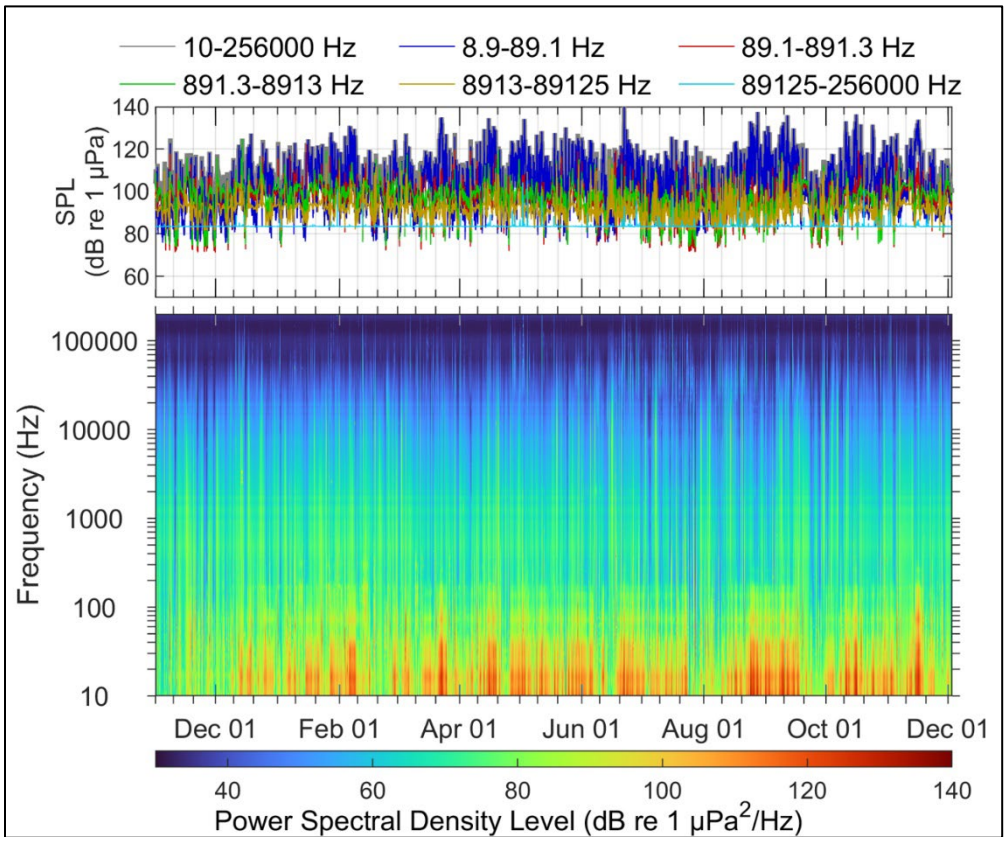

Figure 186. Long-Term Spectral Average and decade band SPL summary of acoustic data collected at CHB for the data collected 01 Dec 19–03 Dec 20

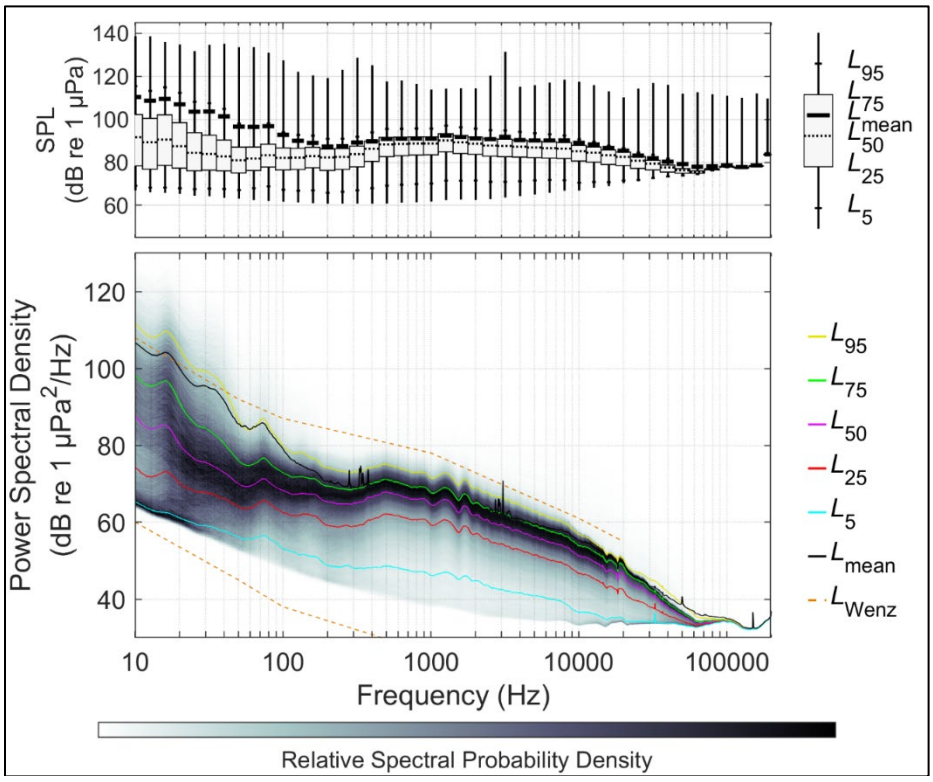

Figure 187. Distributions of spectral sound levels for the CHB data collected 01 Dec 19–03 Dec 20 based on 1-min sound averages.

A.5.3 HAT

The long-term spectral average data and percentile data for the high-frequency sampling rate (512 kHz) at HAT for the period of 24 Oct 19–26 Nov 20 are in Figure 188 and Figure 189, respectively. There are four general sources of noise shown in the spectral figure below: strong flow noise, wind noise, nearby ship noise, and the onboard echosounder causing increased energy at 30 kHz. Figure 190 and Figure 191 show the removal of the echosounder signal from the long-term spectral average and power spectral densities, respectively.

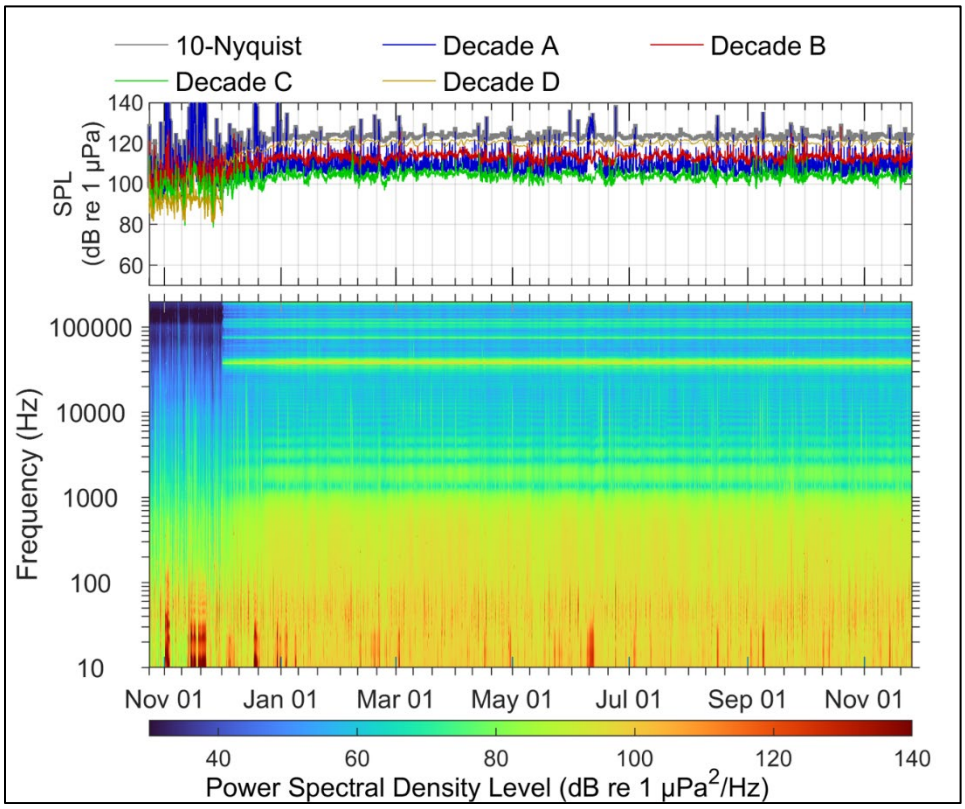

Figure 188. Long-Term Spectral Average and decade band SPL summary of acoustic data collected at HAT for the data collected 24 Oct 19–26 Nov 20. Note, bands were changed during echosounder removal process

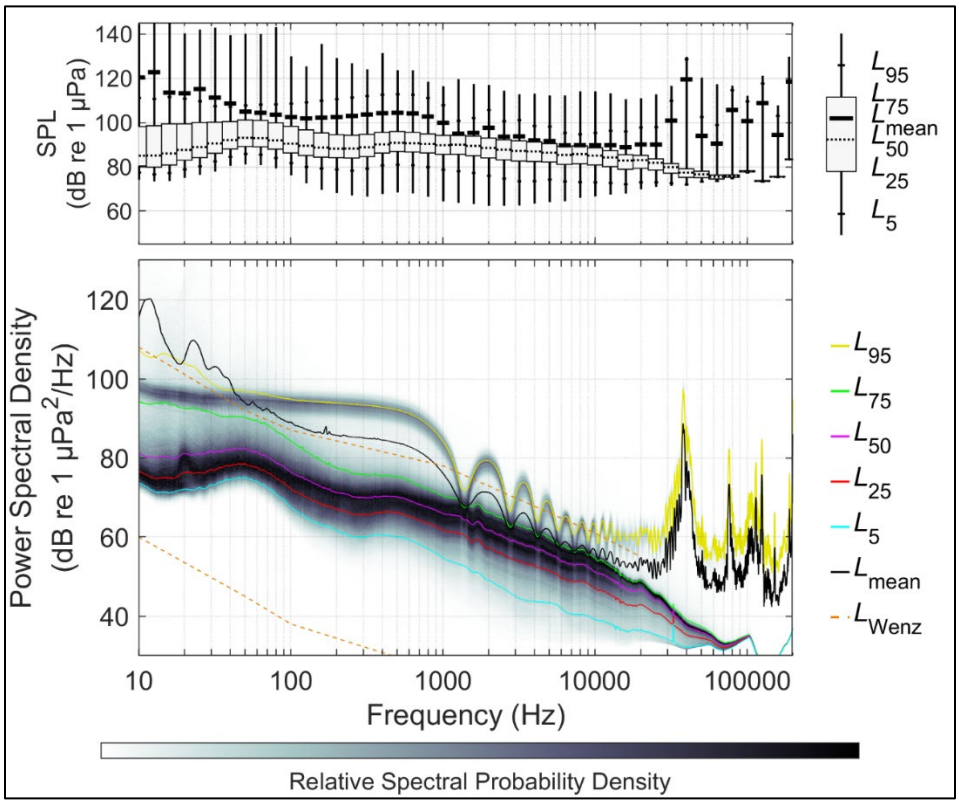

Figure 189. Distributions of spectral sound levels for the HAT data collected 24 Oct 19–26 Nov 20 based on 1-min sound averages

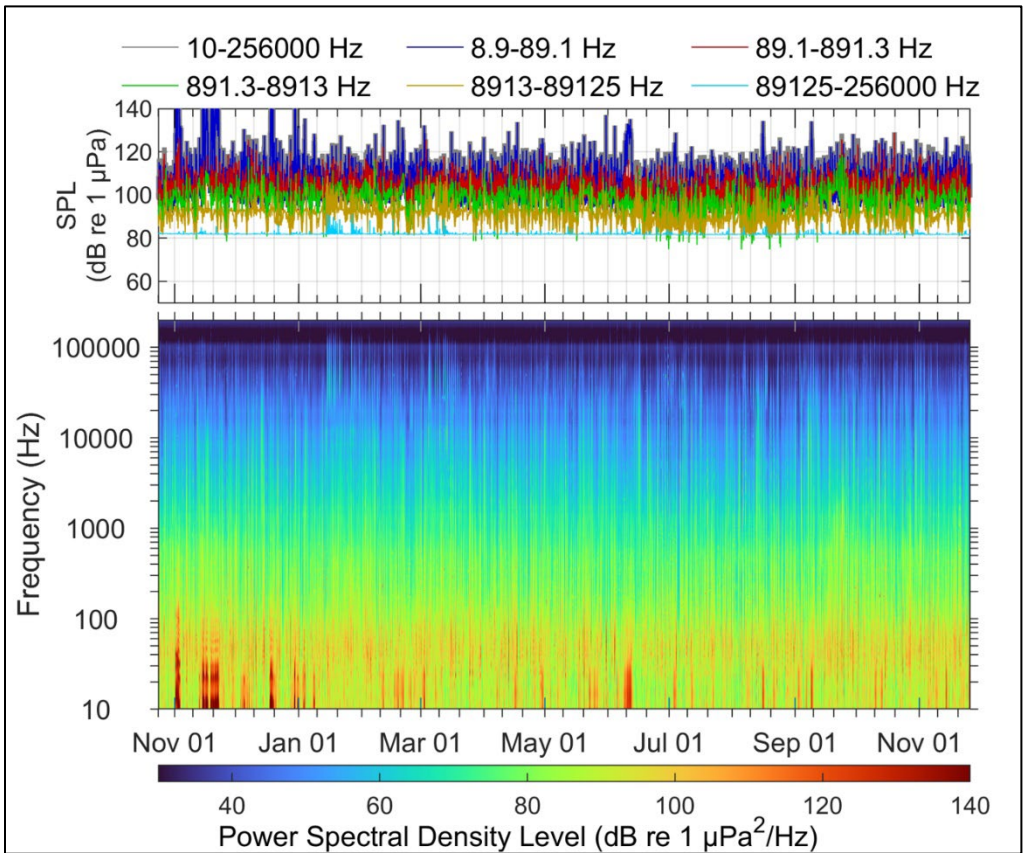

Figure 190. Long-Term Spectral Average and decade band SPL summary of acoustic data collected at HAT for the data collected 24 Oct 19–26 Nov 20, processed to remove the echosounder signature

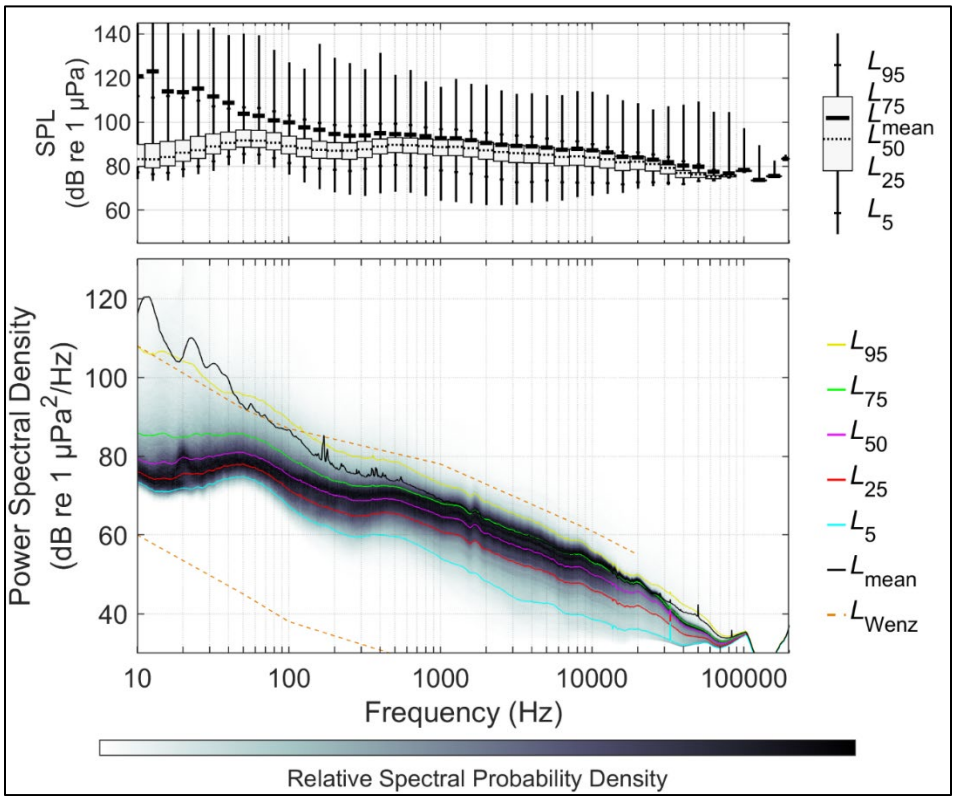

Figure 191. Distributions of spectral sound levels for the HAT data collected 24 Oct 19–26 Nov 20 based on 1-min sound averages, processed to remove the echosounder signal

A.5.4 JAX

The long-term spectral average data and percentile data for the high-frequency sampling rate (512 kHz) at JAX for the period of 13 Jan 20–12 Dec 20 are in Figure 192 and Figure 193, respectively. Flow noise and wind increase the sound level in the frequencies below 20 kHz. Figure 194 and Figure 195 show the removal of the echosounder signal from the long-term spectral average and power spectral densities, respectively. The elevation in sound energy from 100-200 Hz in the winter months is from minke whales.

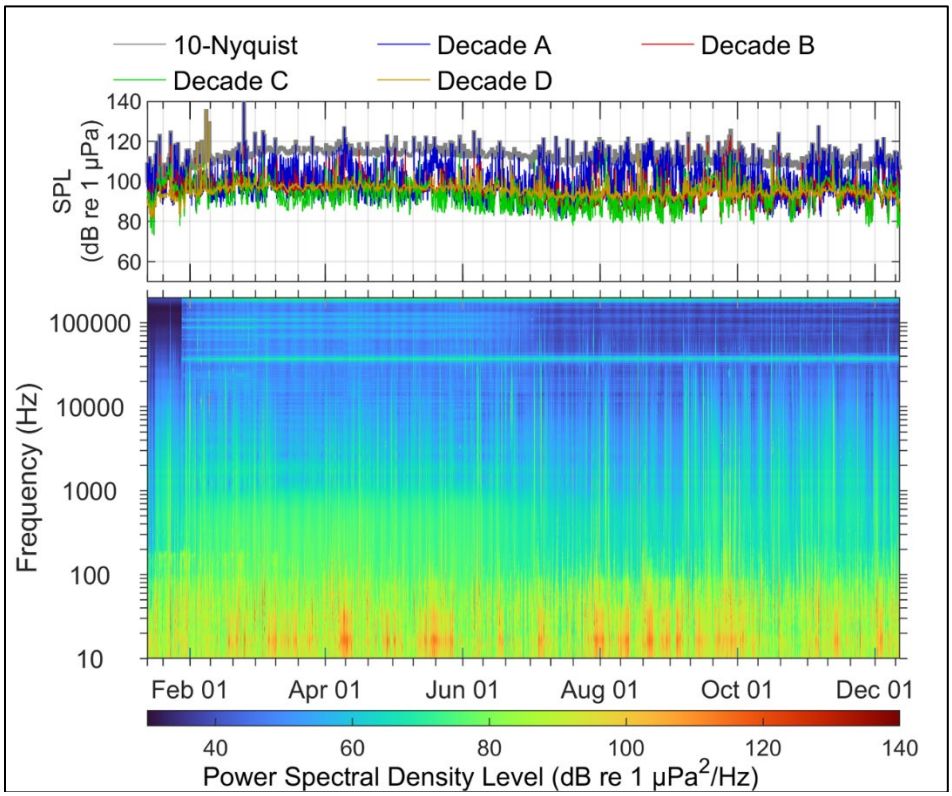

Figure 192. Long-Term Spectral Average and decade band SPL summary of acoustic data collected at BLE for the data collected 13 Jan 20–12 Dec 20

Note, bands were changed during echosounder removal process.

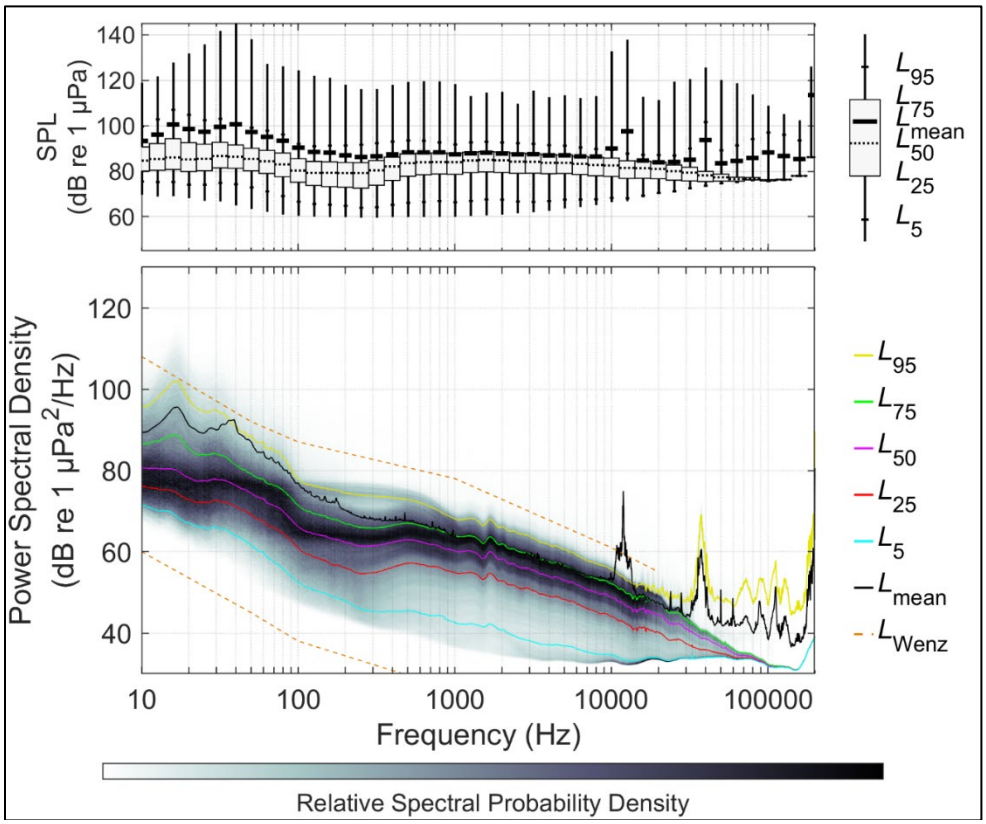

Figure 193. Distributions of spectral sound levels for the JAX data collected 13 Jan 20–12 Dec 20 based on 1-min sound averages

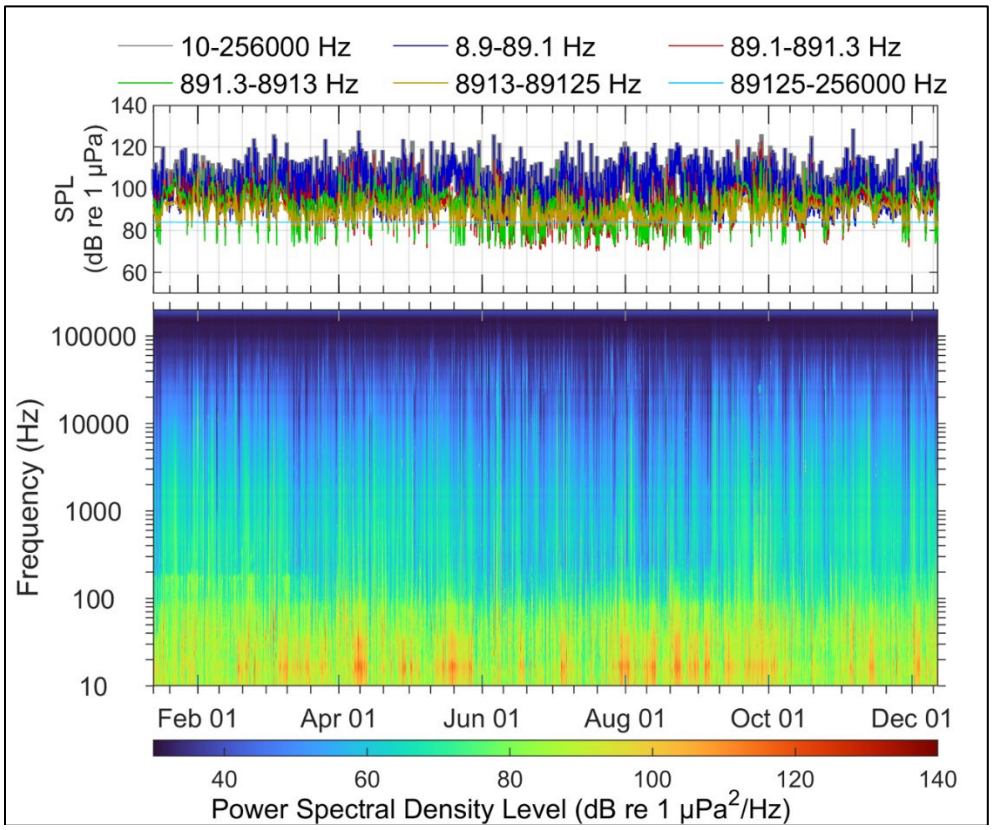

Figure 194. Long-Term Spectral Average and decade band SPL summary of acoustic data collected at BLE for the data collected 13 Jan 20–12 Dec 20, processed to remove the echosounder signature

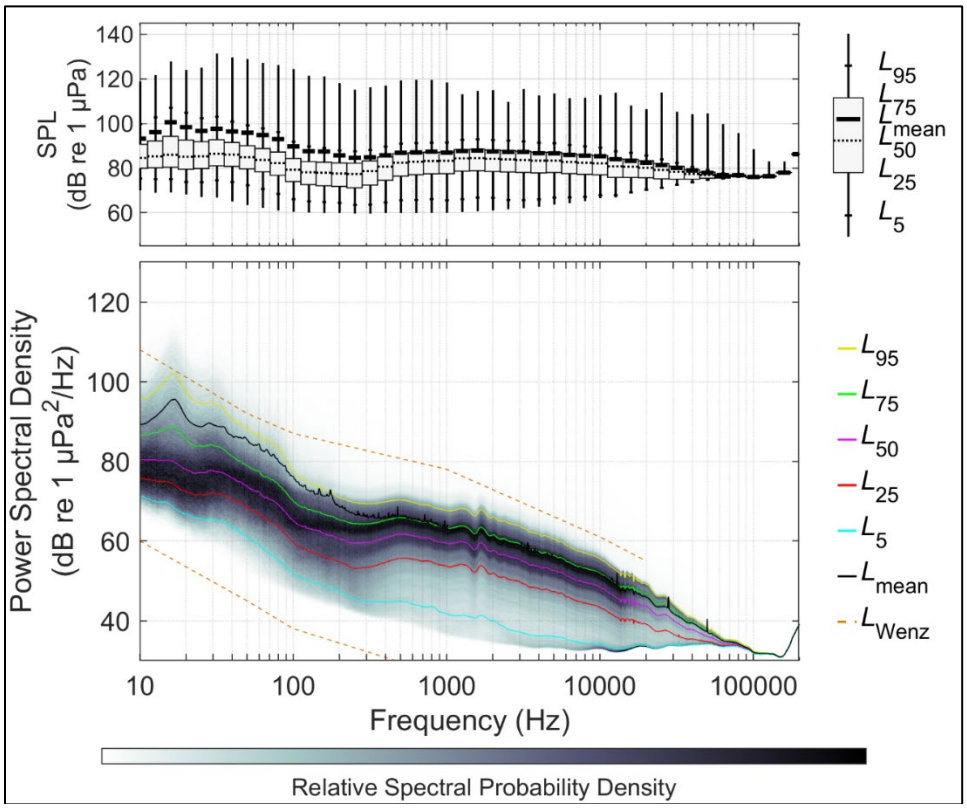

Figure 195. Distributions of spectral sound levels for the JAX data collected 13 Jan 20–12 Dec 20 based on 1-min sound averages, processed to remove the echosounder signature

A.5.5 SAV

The long-term spectral average data and percentile data for the high-frequency sampling rate (512 kHz) at SAV between 26 Oct 19–28 Nov 20 are in Figure 196 and Figure 197, respectively. The spectral figure shows the presence of minke whale sound from December to May, increasing the sound level in the100-200 Hz frequency band, while fin whales are present in the 20Hz band. Flow and wind noise also increase the sound level in the frequencies below 100 Hz and 20 kHz, respectively.

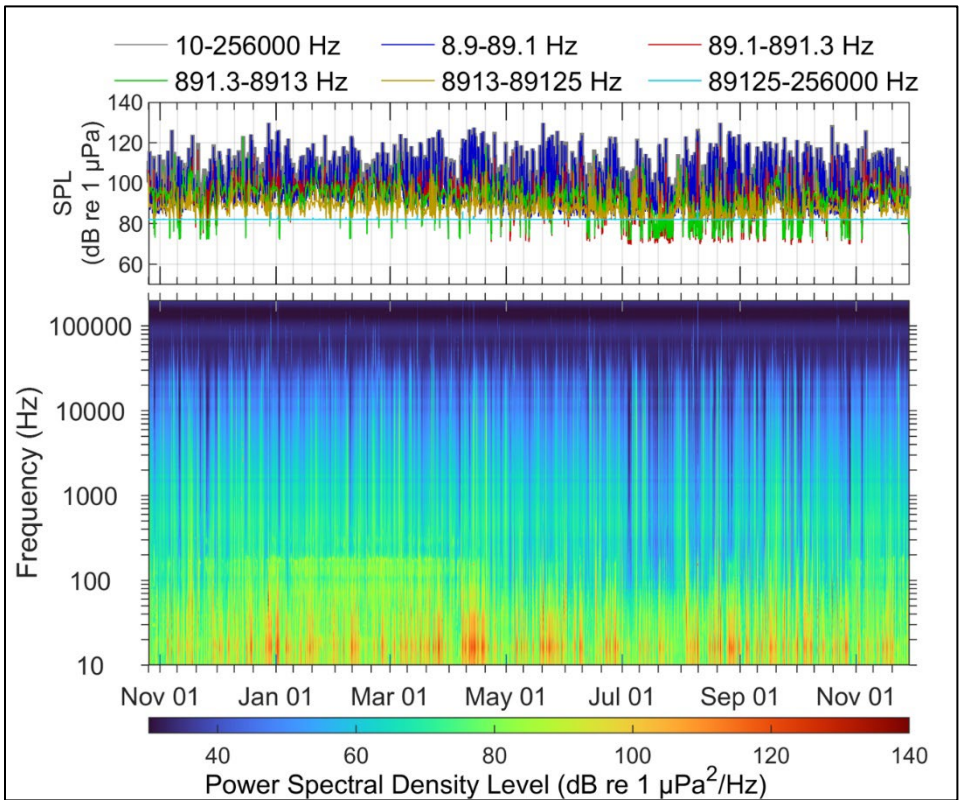

Figure 196. Long-Term Spectral Average and decade band SPL summary of acoustic data collected at SAV for the data collected 26 Oct 19–28 Nov 20

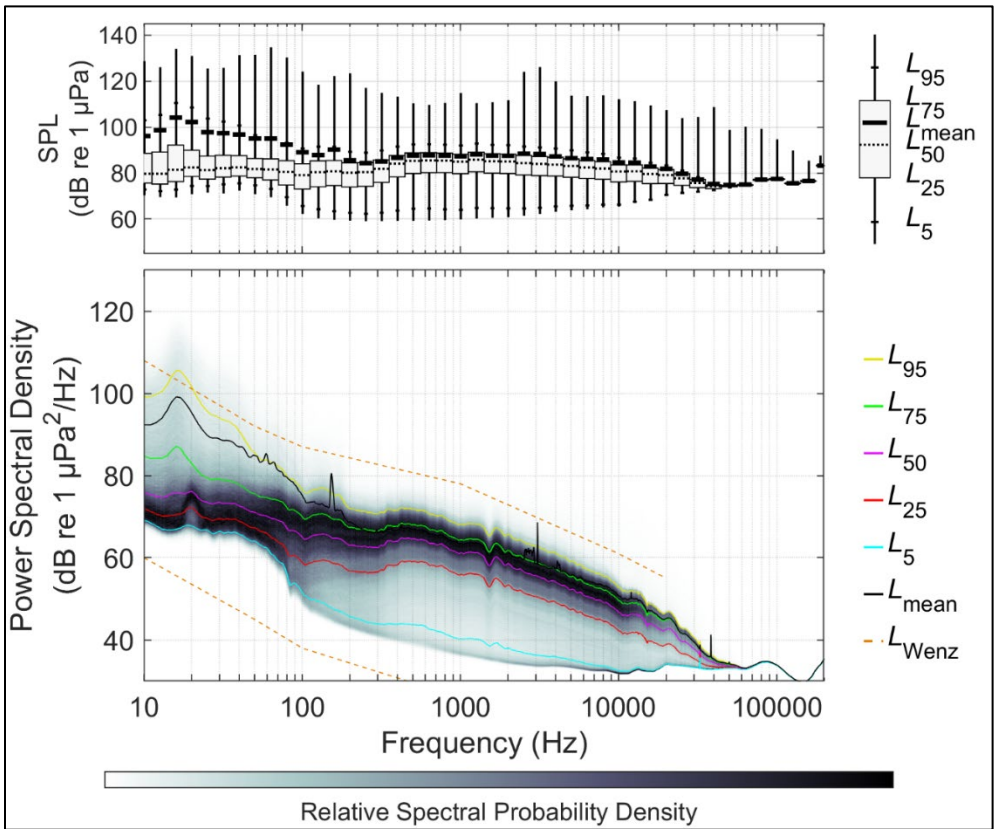

Figure 197. Distributions of spectral sound levels for the SAV data collected 26 Oct 19–28 Nov 20 based on 1-min sound averages

A.5.6 VAC

The long-term spectral average data and percentile data for the high-frequency sampling rate (512 kHz) at VAC for the period of 22 Oct 19–30 Jun 20 are in Figure 198 and Figure 199, respectively. The increased noise between 20-50 kHz is due to dolphin clicks. There is also sound level increase from November to March at 20 Hz band which shows the presence of fin whale in the area. Vessel traffic, flow and wind are other main contributors to sound level increase for the frequencies below 20 kHz. Figure 200 and Figure 201 show the removal of the echosounder signal from the long-term spectral average and power spectral densities, respectively.

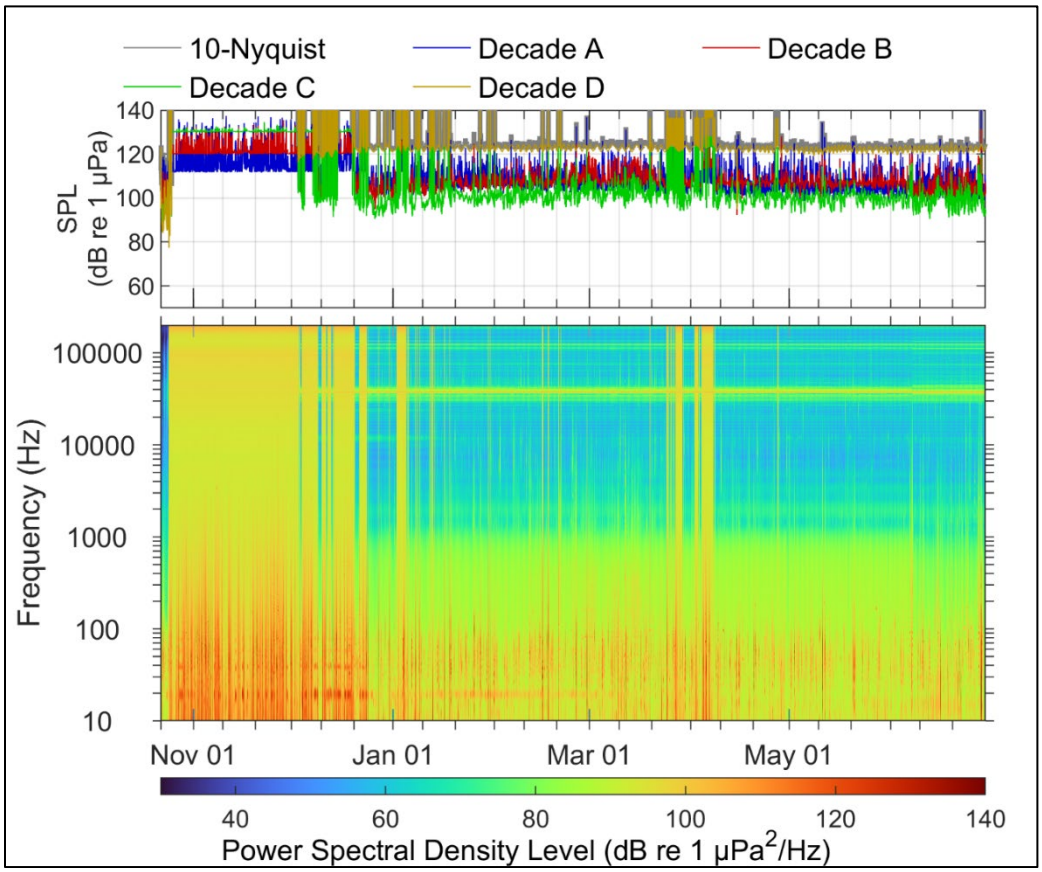

Figure 198. Long-Term Spectral Average and decade band SPL summary of acoustic data collected at VAC for the data collected 22 Oct 19–30 Jun 20

Note, bands were changed during echosounder removal process.

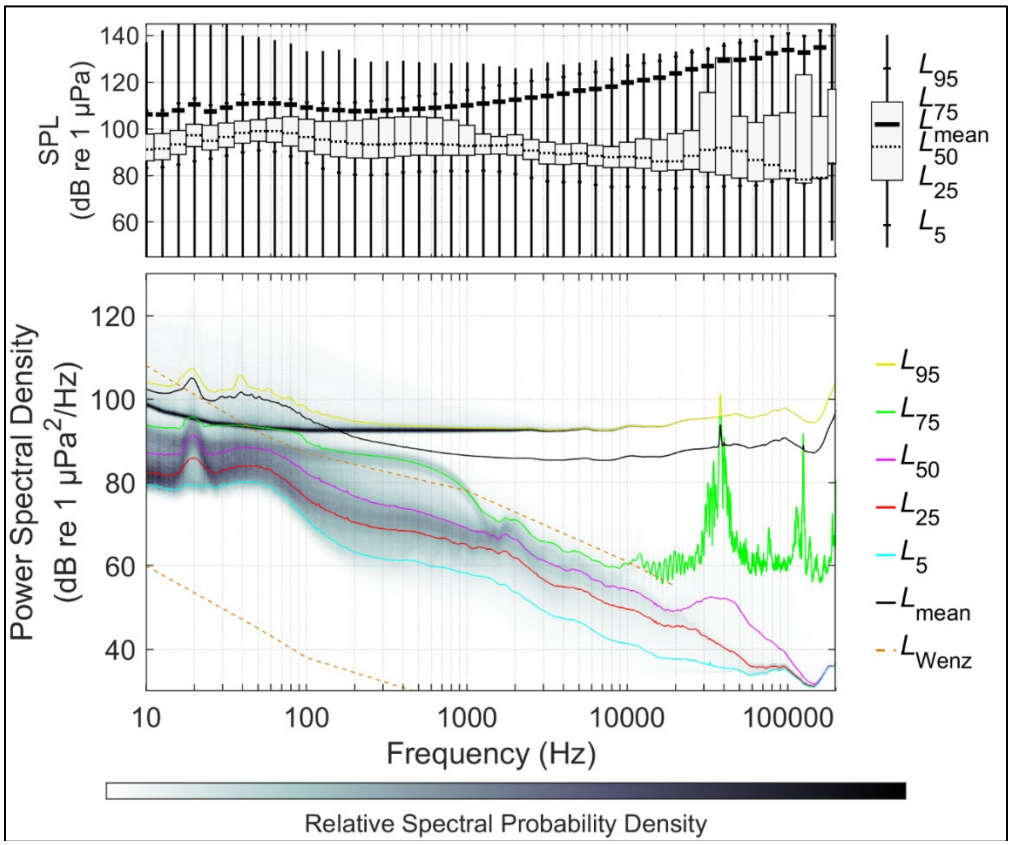

Figure 199. Distributions of spectral sound levels for the VAC data collected 22 Oct 19–30 Jun 20 based on 1-min sound averages

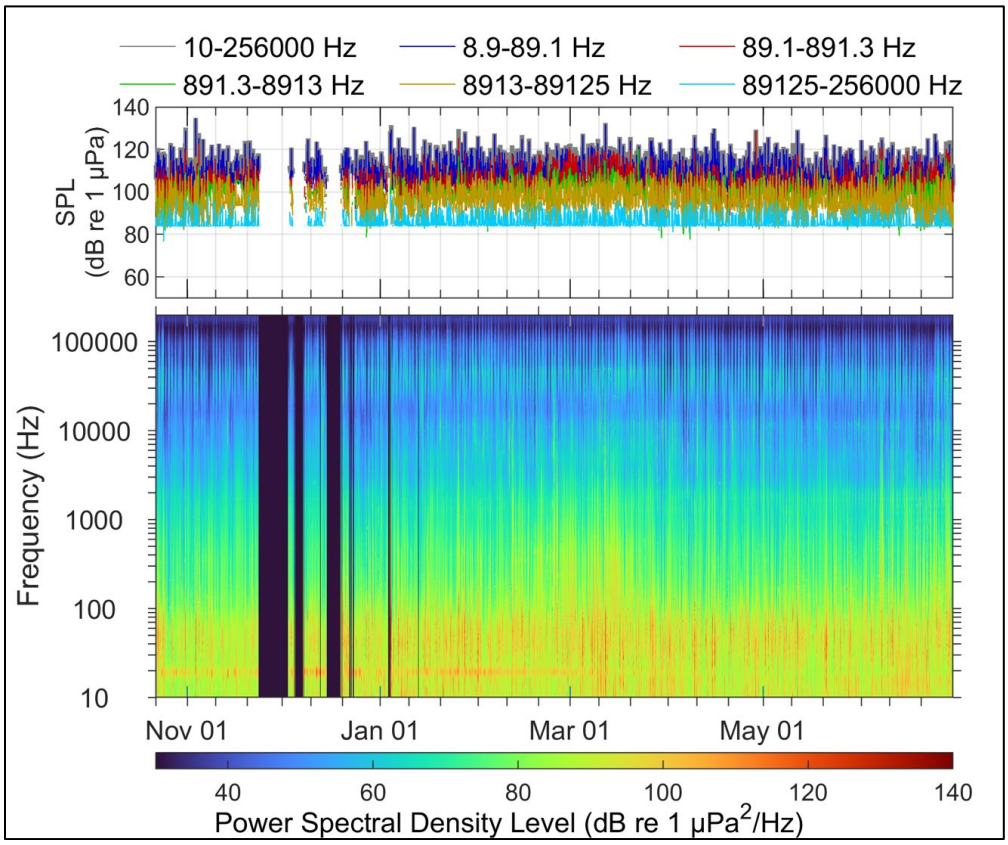

Figure 200. Long-Term Spectral Average and decade band SPL summary of acoustic data collected at VAC for the data collected 22 Oct 19–30 Jun 20, processed to remove the echosounder signature

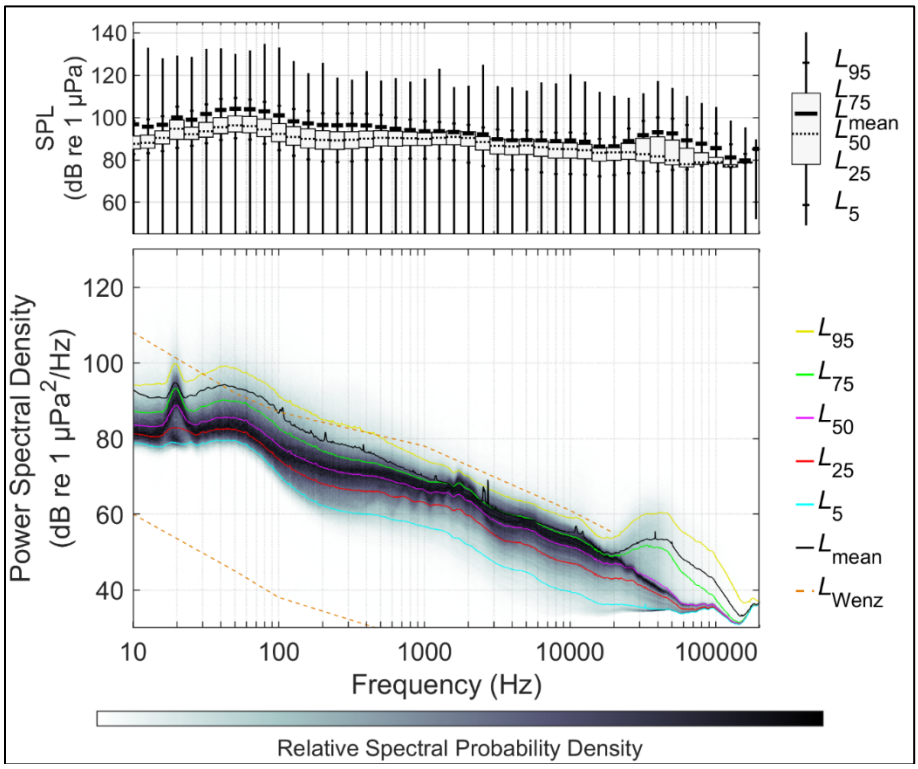

Figure 201. Distributions of spectral sound levels for the VAC data collected 22 Oct 19–30 Jun 20 based on 1-min sound averages, processed to remove the echosounder signature

A.5.7 WIL

The long-term spectral average data and percentile data for the high-frequency sampling rate (512 kHz) at WIL for the period of 25 Oct 19–27 Nov 20 are in Figure 202 and Figure 203, respectively. As is apparent in the figures below, the main sources of noise to increase the sound level are flow and wind noise. The elevation in sound energy from 100-200 Hz in the winter months is from minke whales, Fin whales are also attributable to the 20Hz peak in the winter months.

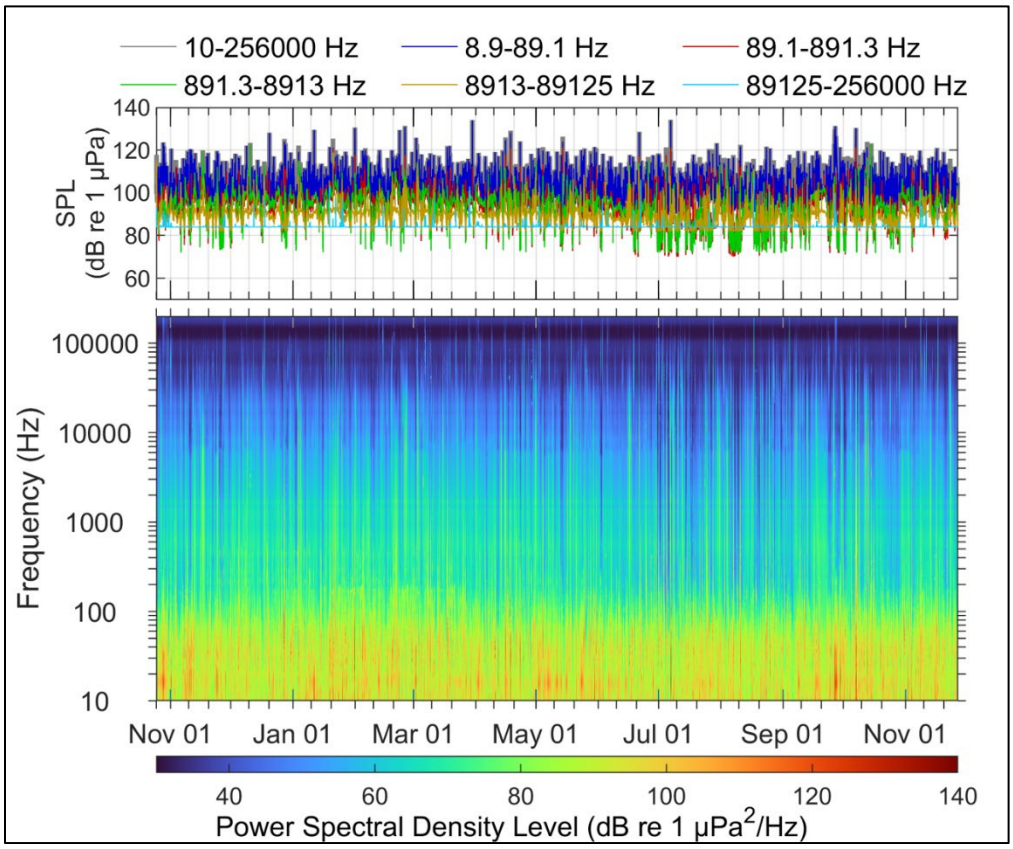

Figure 202. Long-Term Spectral Average and decade band SPL summary of acoustic data collected at WIL for the data collected 25 Oct 19–27 Nov 20

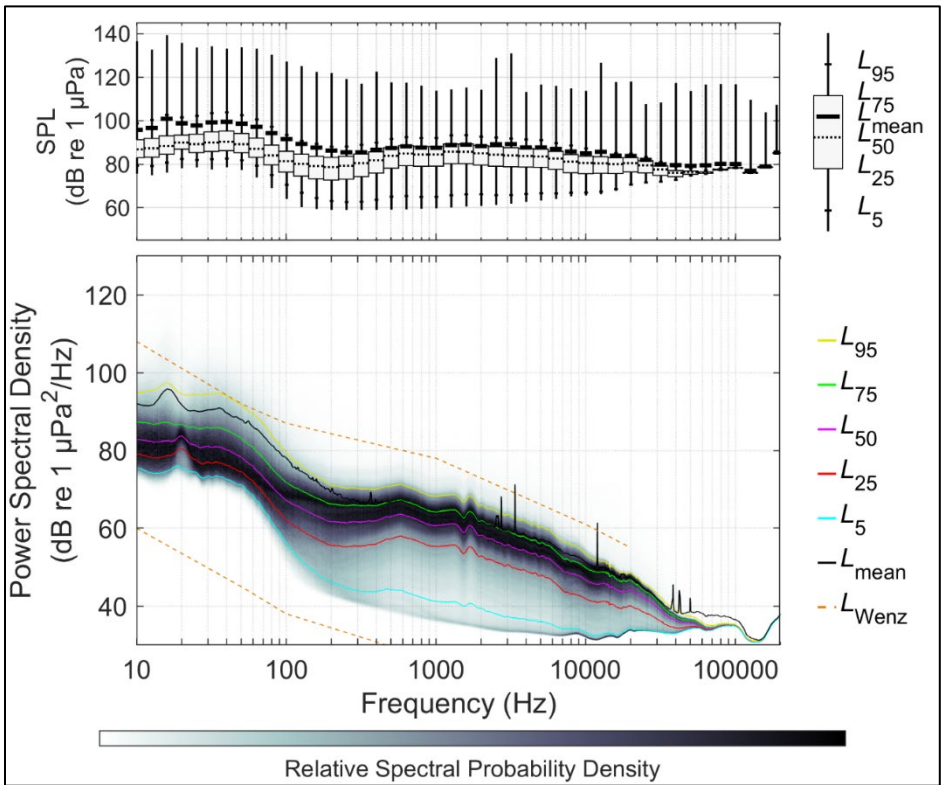

Figure 203. Distributions of spectral sound levels for the WIL data collected 25 Oct 19–27 Nov 20 based on 1-min sound averages

Appendix B. Directional Hydrophone Data Analysis

ADEON is fulfilled its objectives through deploying autonomous long-term observatories (ALTO landers) at seven locations in the Outer Continental Shelf (OCS). The ALTO landers recorded continuously for three years starting in November 2017. An important contribution of ADEON to soundscape monitoring is the collection of long-term data to explore the directionality of sounds. Two types of sensor were evaluated: 1) a GeoSpectrum Technologies Inc (GTI) M20-601 directional hydrophone (Figure 204 left) was deployed at Virginia Inter-Canyon (VAC) from December 2017 to May 2018. Four-element orthogonal hydrophone arrays were deployed at six other locations for the first deployment and at all stations for the remaining deployments. The hydrophones were separated by 50 cm (Figure 204 right).

Including directional information adds a sixth dimension to soundscape data: the direction of arrival of sounds. All soundscape data has an implicit seventh dimension: the sound's amplitude. Environmental sounds, such as wind and wave noise, are generally omnidirectional. That is, they arrive at a recorder from all sides. Human sounds and discrete biological sounds are generated by a unique source that has a location, and hence the sounds arrive from the source's direction. When multiple sources are present, their sounds can overlap in time and direction. Detection and classification algorithms allow many source types to be identified in time and frequency (and bearing), which is additional information that acoustic data users often want extracted.

New methods of presenting this complex data are required so that the data can be discussed and refined. These new methods should allow people within the soundscape community, regulators, and the lay population to understand the information these data represent. This Appendix summarizes the work conducted by JASCO:

The operating of the directional sensor system and extracting the direction of arrival from raw data.

The directogram or azigram method of visualizing short-term directional acoustic data.

A spectrogram tunnel approach to visualizing short-term directional data.

A pie chart approach for visualizing the direction of arrival of marine mammal calls over time.

Figure 204. Directional recording systems mounted on the autonomous long-term observatories (ALTO) landers that were evaluated during Atlantic Deepwater Ecosystem Observation Network (ADEON)

Left: The M20-601 directional hydrophone is the acorn-shaped black object suspended inside the steel frame. Right: Orthogonal arrays of four omnidirectional hydrophones spaced 50 cm apart (the hydrophones are inside the yellow flow shields).

B.1 Direction of Arrival Sensors and Data Analysis

B.1.1 Evaluating Autonomous Direction of Arrival Sensors

B.1.1.1 M20-601 Directional Hydrophone

The fundamental component of the M20 accelerometer (Figure 205) is a mass connected to a pair of ceramic disks. The pressure vessel that contains the ceramic disks and the mass is rigid so that the ceramic disks do not directly experience any compression or tension from a passing acoustic wave. The acoustic wave moves the entire body; however, inertia of the mass causes it to lag from the motion of the cylinder. Thus, the ceramic disks experience compression or tension that generates a change in electric charge through the piezoelectric effect (Figure 205). In the M20 two ceramic disks are used to provide mechanical support for the mass as well as to double the output response of the sensor. These disks must be carefully matched in amplitude and phase for maximum performance of the sensor. At low frequencies, the acceleration response of the sensor does not change with as the frequency of the acceleration changes. As the acceleration frequency approaches the mechanical resonance of the mass-spring system, the sensitivity increases, then decreases by 12 dB per octave above resonance. Oil is added inside the sensor to dampen the mass' movement and smooth out the resonant peak.

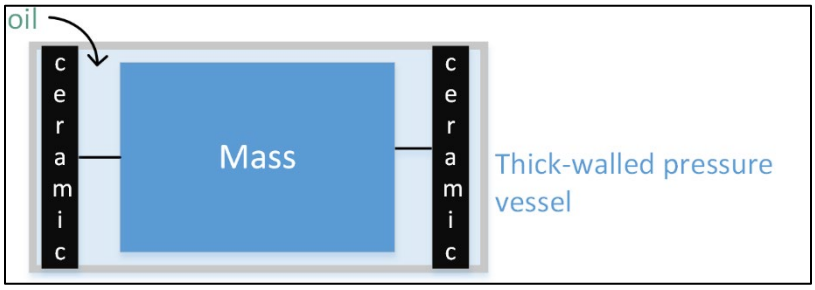

Figure 205. Fundamental structure of an M20 accelerometer sensing unit

The M20-601 is built from four of the fundamental accelerometers: two each for the X and Y axes (and none for the Z axis). The X and Y axes are mounted on a wobbler plate that is only attached to the outer shell of the sensor at its center of mass (Figure 206). This design provides the sensor with some immunity to physical movement noise. Physical rocking of the sensor will cancel for the X1 and X2 sensors as well as Y1 and Y2, but outputs from acoustic accelerations will add constructively up to a fraction of the body resonances of the sensor. For a suspended acceleration sensor to perform optimally, the body must be isolated from forces at the electro-mechanical connection point. By putting the wobbler connection point at the center of the total body mass, forces at the connection point will cause the body to rotate around the center of mass (the wobbler) rather than generating a displacement, which would be measured as an acceleration (Figure 207). This technique also relies on the body being negatively buoyant. A negatively buoyant sensor is less sensitive than a neutrally buoyant sensor according to the equation:

$$20log_{10}\left(\frac{3\rho_w}{\rho_w+2\rho_s}\right)\ (\text{dB})\ , \tag{1}$$

where ρ_w is the water density and ρ_s is the sensor density (Yeatman & Amstrong, 2011). For the M20-601, this value is approximately −4 dB, a much smaller penalty than the added mechanical noise from a neutrally buoyant sensor in realistic water conditions.

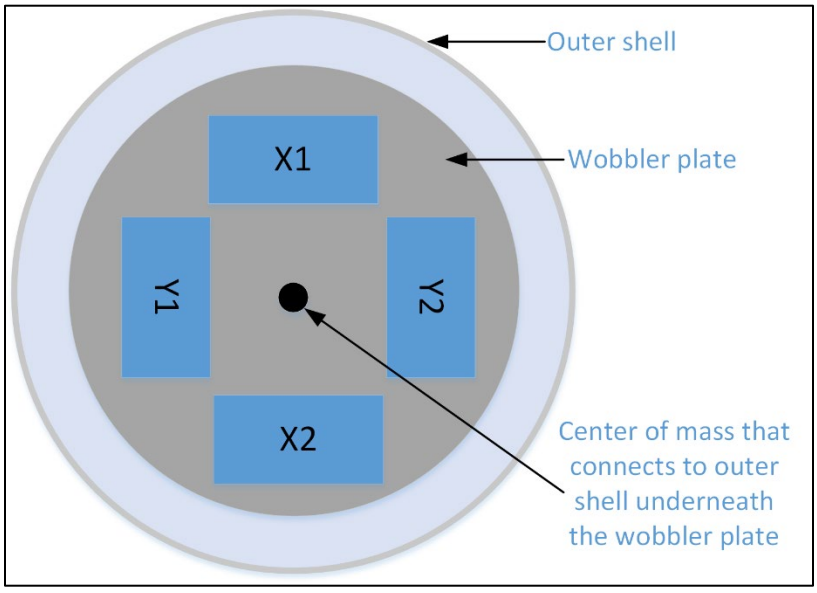

Figure 206. Sketch of the wobbler plate design that holds two X and two Y fundamental accelerometers within the M20-601 body

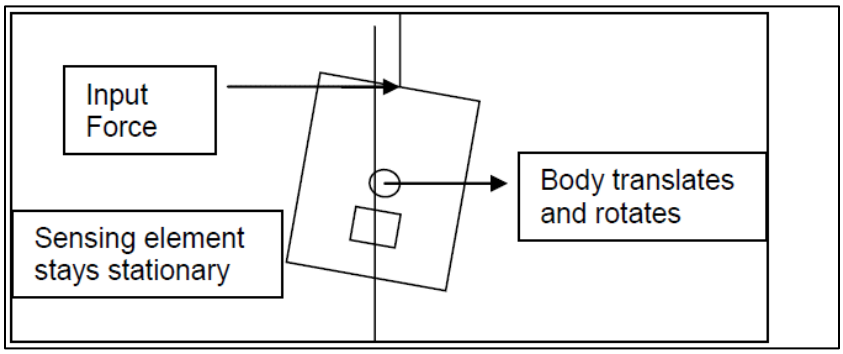

Figure 207. Acceleration balancing for particle acceleration sensors
(Figure 1, Yeatman & Amstrong, 2011)

The M20-601 includes a compass, an omni-directional hydrophone, the X and Y accelerometer sensors, and analog electronics. The first component of the electronics is a charge amplifier that converts the sensor's variable capacitance to a voltage appropriate for measuring with a standard analog-to-digital converter. The analog electronics also compensate for the frequency dependence of the accelerometer response so that the pressure sensitivity of all channels is similar in the main operational band of the sensor (~50–2000 Hz, Figure 208). The X and Y accelerometer channels are analog corrected by the compass angle, which results in three output channels: north-south, east-west, and omnidirectional. After analog corrections are completed, a frequency dependent phase shift remains between the channels that must be compensated for during analysis (Figure 209). The bearings from these sensors also needed for correcting the magnetic declination.

The M20-601 is a precision sensor whose effectiveness depends on expert design, careful machining, hand matching of components, and skilled assembly. The M20-601 design was validated by comparing the accelerometer response to a co-located calibrated hydrophone during a deep-water test in a far-field environment. To calibrate each M20 unit, the manufacturer uses a precision shaker table. No in-field calibrations were performed.

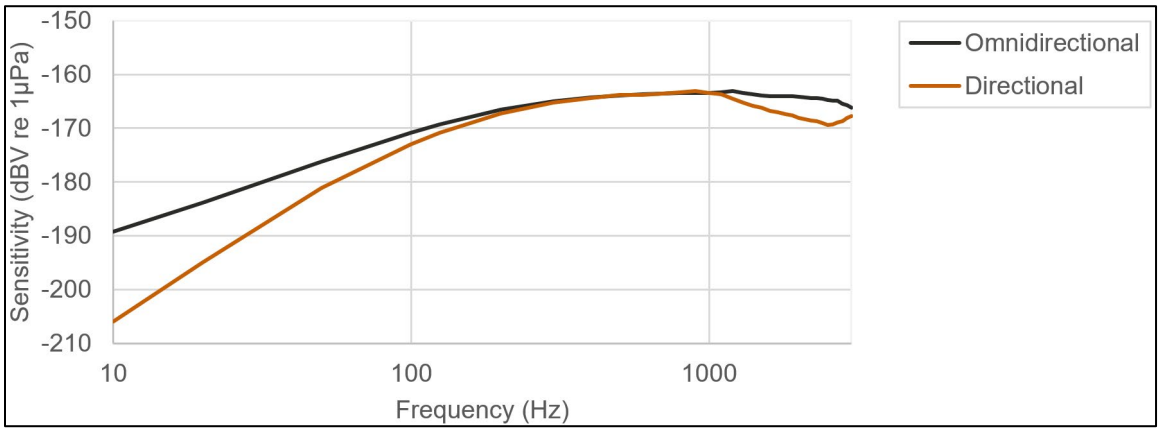

Figure 208. Pressure sensitivity of the M20-601 directional and omnidirectional channels

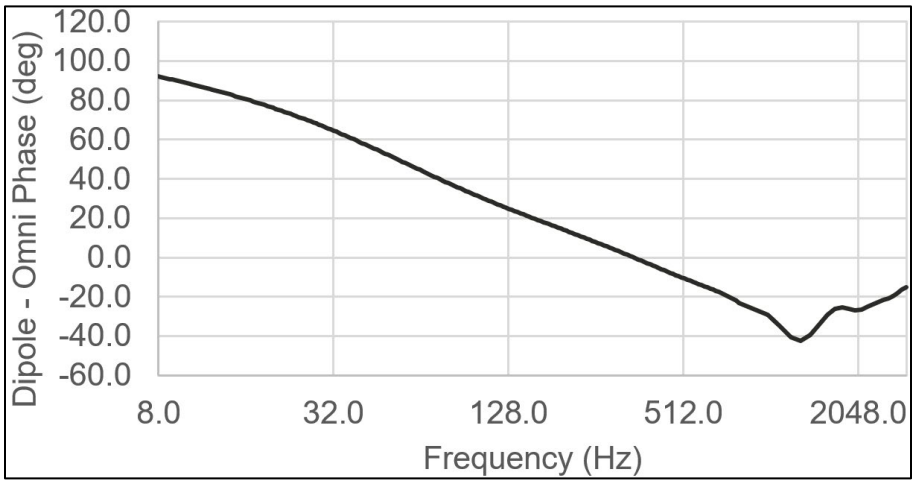

Figure 209. M20-601 directional channel phase response
Referenced to omnidirectional channel with signal from positive direction.

B.1.1.2 Orthogonal Arrays of Omnidirectional Hydrophones

In acoustics, the particle velocity, u, and the acoustic pressure, p, are related by the linearized Euler's equation:

$$\rho_{0(\partial \mathrm{u}/\partial \mathrm{t})} = -\nabla p \ . \qquad (2)$$

Here, ρ is the density of the medium, and ∇ is the spatial gradient function. The time derivative of velocity is acceleration. Therefore, the spatial gradient of pressure divided by the fluid density, yields the acceleration, which is the same quantity measured by the M20-601 accelerometers. The spatial gradient of pressure is the difference between two closely spaced hydrophones. This operation only works for frequencies where the phase difference between the hydrophones is at most λ/4. For larger differences, the phase difference is not unique, and the results are ambiguous. For the ADEON arrays, the nominal hydrophone spacing was 0.5 m (Table 23), and therefore the cut-off frequency was ~750 Hz.

The relative locations of the hydrophones are essential for accurately analyzing the direction of arrival. During deployment preparations the distances between the tips of each hydrophone pair were measured. These distances, along with the nominal hydrophone locations, were then used in a least-squares regression to find the precise hydrophone locations relative to the reference hydrophone. For simplicity and power savings, the ADEON landers with arrays of omnidirectional hydrophones did not include a compass sensor. Instead, the orientation of the arrays was determined by matching the measured bearing to the known bearing of the deployment vessel as it sailed away from the recording location.

These arrays are formed from standard omni-directional hydrophones. The hydrophones are calibrated through normal processes before deployment and on retrieval, which provides assurance of system operations.

Table 23. Locations (in centimeters) of the ADEON nominal hydrophones

Location	AMAR Channel 1	AMAR Channel 2	AMAR Channel 3	AMAR Channel 4
X	0	0	0	50
Y	0	50	0	0
Z	50	0	0	0

Hydrophone Channel 1 is the top hydrophone in Figure 204 right.

B.1.2 Determining the Direction of Arrival

B.1.2.1 M20-601: The Active Intensity Method

To determine the direction of arrival of the sounds from the M20-601 hydrophone, the method of active intensity was employed (D'Spain et al., 1991; Thode et al., 2019). Using this method, the active intensity of the sound field in direction k is computed by multiplying the pressure (p) by the velocity (v_k) in that direction:

$$I_k(f,T) = Re\left[p(f,T)v_k^*(f,T)e^{-i\emptyset(f)}\right], \quad (3)$$

where '*' denotes the complex conjugate and (f,T) indicates that the computation is performed for each frequency (f) and time bin (T) of an FFT. The equation has been extended from the version shown in Thode et al. (2019) by adding the frequency dependent phase correction $e^{-i\emptyset(f)}$.

The direction of arrival of the sound is then given by:

$$\theta(f,T) = \tan^{-1}\left[{-I_x(f,T)}\Big/{I_y(f,T)}\right] + \mu, \quad (4)$$

where μ is the magnetic declination.

Computationally, this method is relatively quick because the direction of arrival for each frequency bin output by an FFT is computed once per time slice. This method is also immune to the vertical direction of arrival angle.

B.1.3 Spatial Arrays of Hydrophones: Maximum Likelihood Estimation Beamformer

The direction of arrival for the hydrophone arrays depends on the frequencies of interest. For frequencies below the 750 Hz cut-off, analysis is performed by forming equally spaced beams in azimuth and elevation, then selecting the beam with the highest received signal level for each frequency and time. This method provides the Cramer-Rao lower bound estimate on the direction of arrival for a compact array (Urazghildiiev & Hannay, 2017). This method does not rely on having a particular geometry for the compact array; the relative positions of each sensor must be known. For ADEON, we employed a radial resolution of 10 degrees (36 beams). Vertical beams are important if the azimuthal direction for sources within ~3 water depths is desired; seven vertical beams are recommended when processing the deep water recordings for ADEON.

For frequencies above the 750 Hz cut-off, broadband direction of arrivals become ambiguous when applying a beamformer. Instead, the time delay of arrival of a transient signal on each of the hydrophones may be used to determine the direction. This method has not been applied to the ADEON data because most signals of interest analyzed to date are below 750 Hz.

B.2 Visualizing the Direction of Arrival of Broadband Data

For frequencies below the array cut-offs (~2000 Hz for the M20-601 and 750 Hz for the omnidirectional hydrophone arrays), the direction of arrival for each time-frequency bin of a spectrogram is available. Methods of providing an intuitive presentation of this data for analysts were investigated.

B.2.1 Azigrams and Directograms

Spectrograms that use an intensity gradient (e.g., grayscale) or a color gradient (e.g., jet color map) to communicate the differences in received sound levels as a function of frequency and time (Figure 210). However, it is also possible to use color to represent direction. If intensity is not included in the mapping, then the result is an azigram (Thode et al., 2019). However, by including intensity the background noise is reduced, which improves a user's understanding of the data (Figure 211). In ADEON, this type of display is referred to as a "directogram" (Miksis et al., 2018). This type of representation has also been used in airborne and naval sonar systems for several decades. Using the color-directional representation it is clear that there are least two humpbacks calling in the sample data. The color-direction-intensity was implemented using the HSV color map for direction since it "rotates" from red-to-red, and the "alpha" channel used to encode intensity.

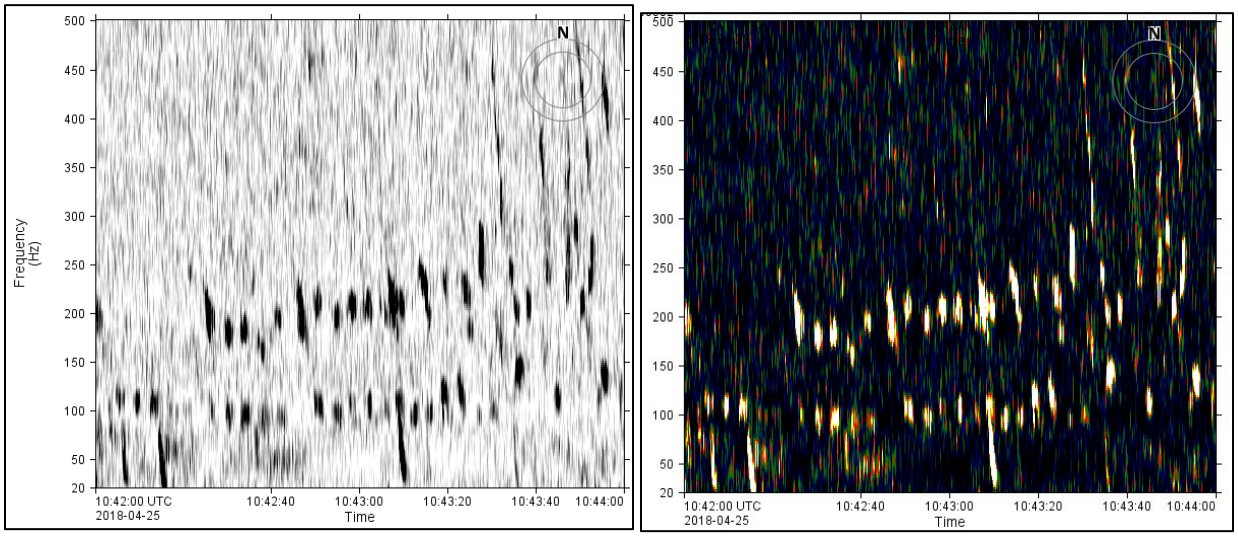

Figure 210. Two-minute spectrogram of data from VAC-2 on 25 Apr 2018 with sei and humpback whale calls
(Left) using a grayscale representation and (right) using the optimized color map developed for ADEON by Colin Ware (UNH).

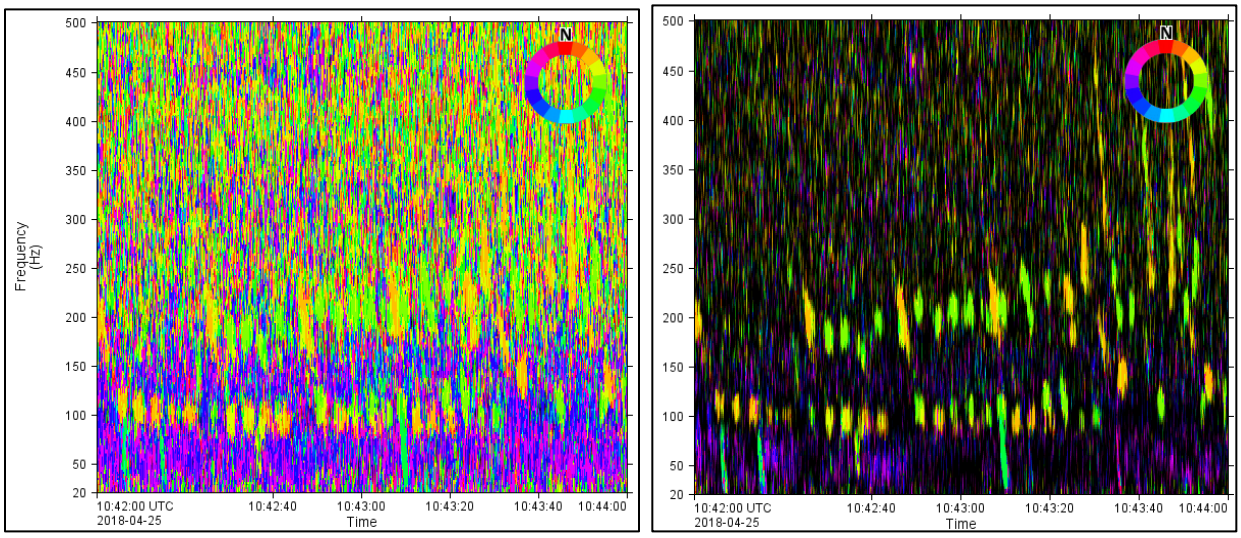

Figure 211. Azigram (left) and directogram (right) of the same two-minute spectrogram of data from VAC-2 on 25 Apr 2018 shown in

The color wheel at the top left of the figures shows how color maps to direction of arrival. (Left) Azigram representation (no intensity coding); (Right) Directogram representation that uses intensity and direction of arrival coding.

B.2.2 Tunnels

Using non-ADEON data, JASCO has collaborated with another IQOE-endorsed program, MERIDIAN at Dalhousie University, to investigate the display of directional spectrogram data using ‘tunnels’. In this format the data for a selected frequency band is summed, and total sound level is displayed for each direction of arrival. Bearing is mapped to a circle, and time is mapped to the long-axis of a tunnel with the most recent time at the top of the tunnel and historic data at the bottom (Figure 212). The tunnel is paired with a standard spectrogram to present the frequency information. The result for a vessel passage is shown in Figure 213.

While evaluating the tunnel display, we encountered a number of issues:

- Scrolling through the data in time required a too long to re-draw for many users.
- Changing frequency bands and redrawing the tunnel is difficult.
- Interpreting biological signals requires a longer time period than can be effectively displayed.
- Combing the spectrogram and tunnel in one figure was an inefficient use of screen space.

If a broadband direction of arrival display is desired in the future, we recommend using the classic ‘B-scan’ that has been used by naval sonars since the 1950s (Figure 214).

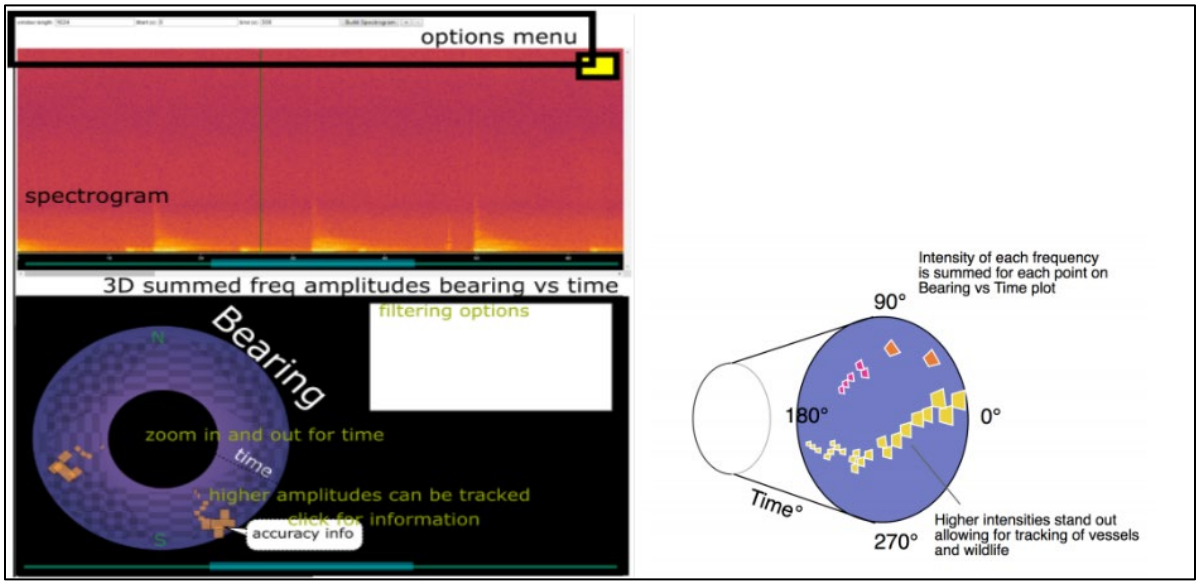

Figure 212. Conceptual schematic of the tunnel figure for broadband directions of arrival

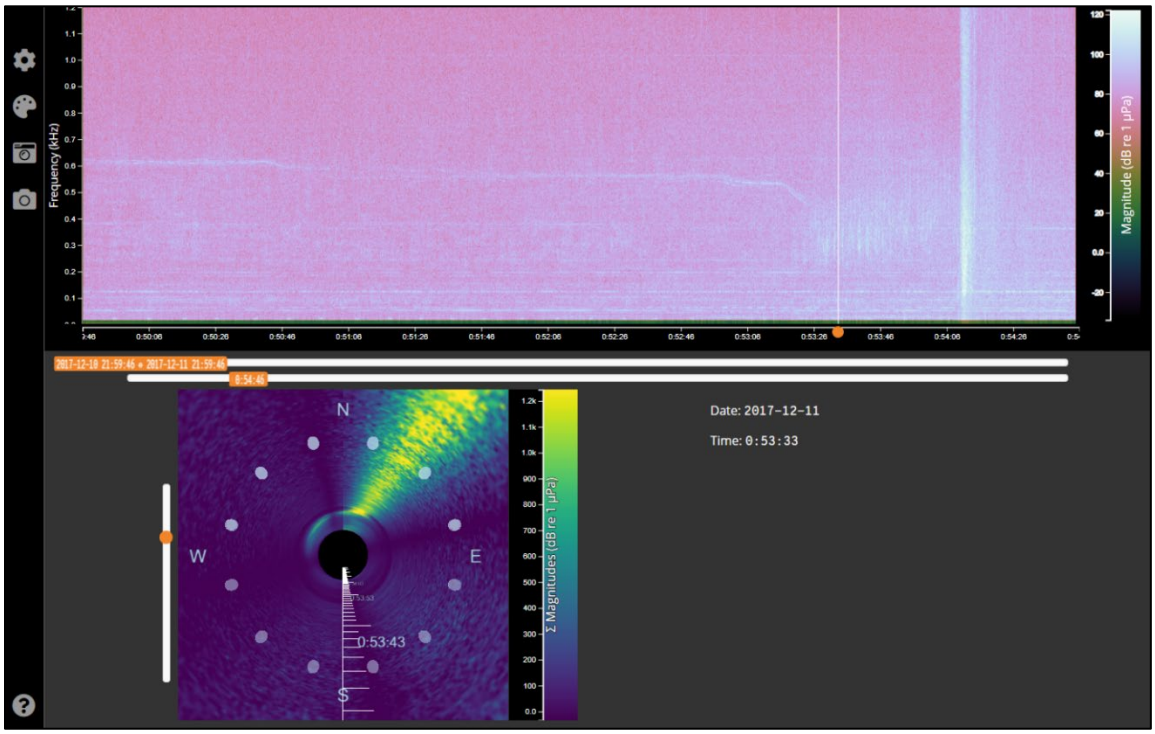

Figure 213. Tunnel diagram for a vessel passage

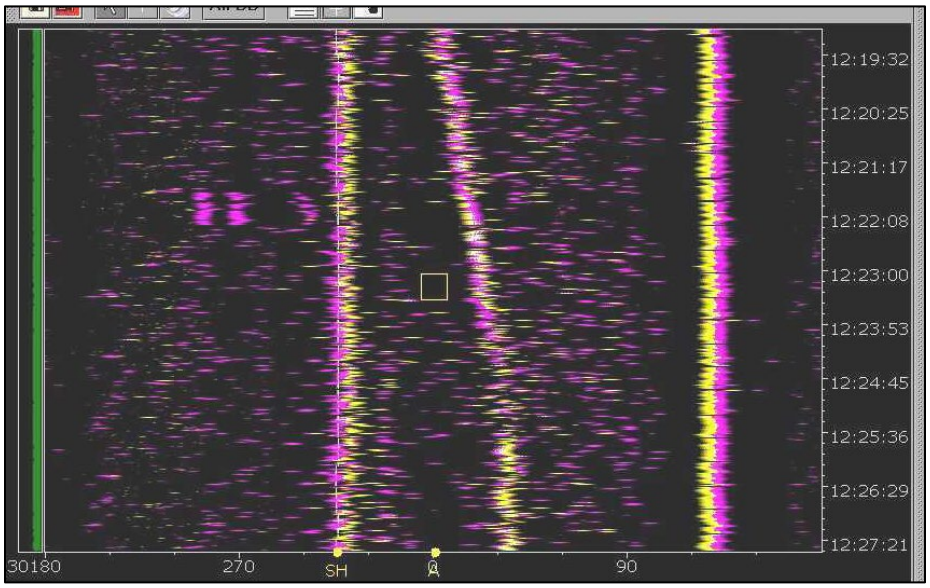

Figure 214. Example of a naval "B-scan" display

Direction of arrival is mapped to the horizontal and time to the vertical axis. The color intensity and width of each line represents the signal strength. The color is used to identify which frequency band is displayed. In this example, two bands are shown (yellow and magenta). This example is from a hull-mounted sonar; 'SH' indicates the ship's head. The line 180-degrees from ship's head is self-noise from the ship's propellers. The diagonal line is a passing merchant ship.

B.3 Validating the Directional Processing Implementation

Here, the directogram is used to demonstrate that the directional sensing and analysis is functioning properly across frequencies. Figure 215 shows the track of the R/V *Neil Armstrong* on 28 Nov 2017, with the white 'comet tail' showing the last 15 minutes of the track. On the right, the directogram shows 5 minutes of data evolving from yellow to green-yellow to green, corresponding to north-east to south-east. *Neil Armstrong* did not show any signature below 50 Hz.

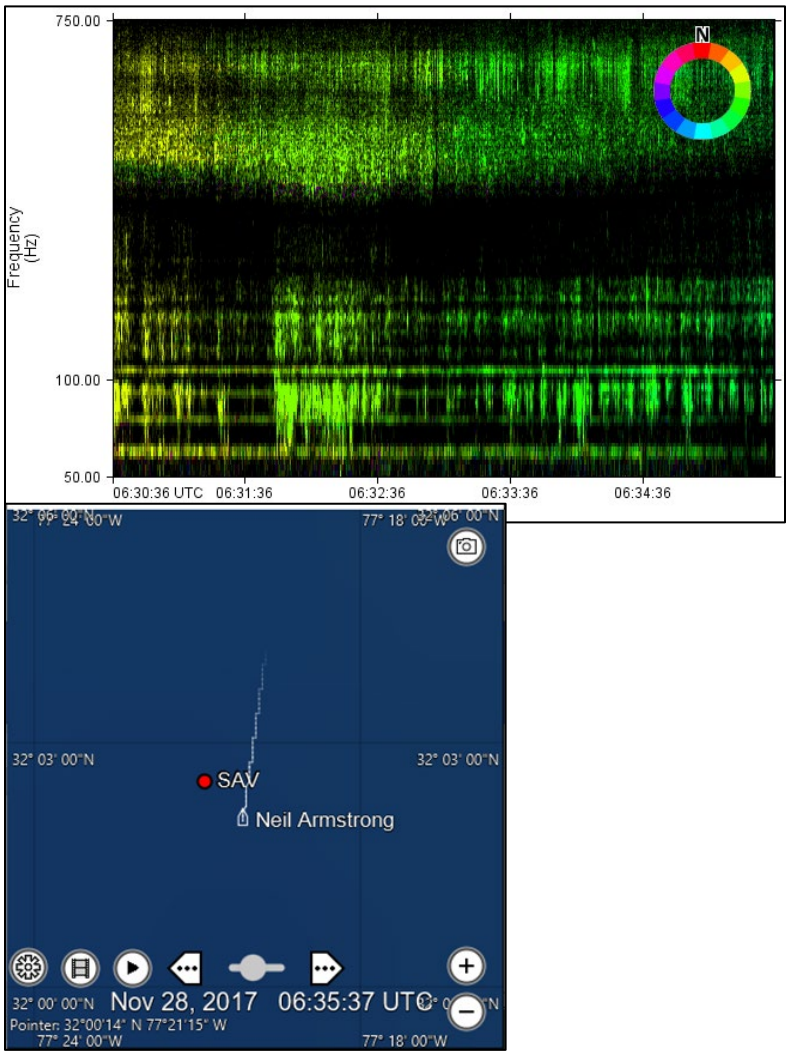

Figure 215. Example of using a directogram to validate the directional processing implementation using the passage of the deployment vessel from north-east (yellow) to south-east (green) on 28 Nov 2017 at Savannah Deep (SAV)

Track is shown in the bottom panel

B.4 Visualizing the Direction of Arrival Trends in Detections

Azigrams, directograms, B-scans, and tunnels are appropriate for displaying relatively short durations of data. However, we found that the short-term transient signals we typically try to detect are too compressed for visual identification when displayed durations are longer than 30 minutes. We desire a means of displaying and interpreting the spatial distributions of acoustic events over periods of days, weeks, and months. A display format based on pie charts was investigated for the understanding the distribution of marine mammal detections at the SAV site. This site was chosen due to the strong seasonal presence of minke whales, which provided an event type with a known temporal distribution but unknown spatial distribution.

The “events” are the number of detections per minute for different types of marine mammal vocalizations. Eleven different contour detectors were run against the recordings. The contour detectors find times and frequencies of energy in spectrograms that match defined templates for different vocalization types (Figure 216). At SAV the detections from the first recorder deployment occurred over the time period of 27 Nov 2017 to 14 Jun 2018. For each detection there is an associated bearing that was computed as the energy weighted mean bearing for all time-frequency bins that contributed to the detection (Figure 216). To present the events they were sorted by month and detector. For each month and detector the events were then summed by bearing, using 36 bins each 10 degrees wide. The resulting data were now grouped by bearing, month and direction, which made the suitable for presentation as an array of pie-charts.

Figure 217 shows the pie-chart array for three months and three detectors. The total number of detections per detector and month are shown as (N = xx) above each pie-chart. The logarithm of this value was also used to scale the diameter of the circles. The darkness of gray of each sector in the pies represents the relative number of calls detected in the bearing slice. For detector-months with fewer events, the circles are smaller and there is less variations in the slice gray-scales.

The results for the December 2017 to June 2018 SAV data set are shown in Figure 218. The peak of the minke mating chorus in January to March is easily detected from this figure. It also indicates that the calls came from two strongly preferred directions at the height of the chorus, with more variability during the early and late seasons. Detections of other species that occurred at the same time as the minke chorus arrived from other directions.

The validity of these observations depends on the correct performance of the automated detectors and bearing extraction software. During the development of this figure we discovered the importance of include vertical beams when analyzing the directions of arrival, which significantly improved the usefulness of Figure 218. Further validations of the detectors and localizers are needed to ensure that the patterns shown in the pie-chart array are reliable. The detectors as built currently are designed to reduce false alarms, which is appropriate for detecting presence, but not for use in cue-counting applications such as density estimation and the current directional distribution study. Improving the recall is an important area of improvement for our detectors.

The pie-chart array also does not provide any indication of the shorter-term occurrence of different call types. Indeed, many of the lower call count detections in Figure 218 could easily have occurred over a 4-hour period. In future work we will need to develop methods that allow an analyst to scroll through the temporal-spatial detection data.

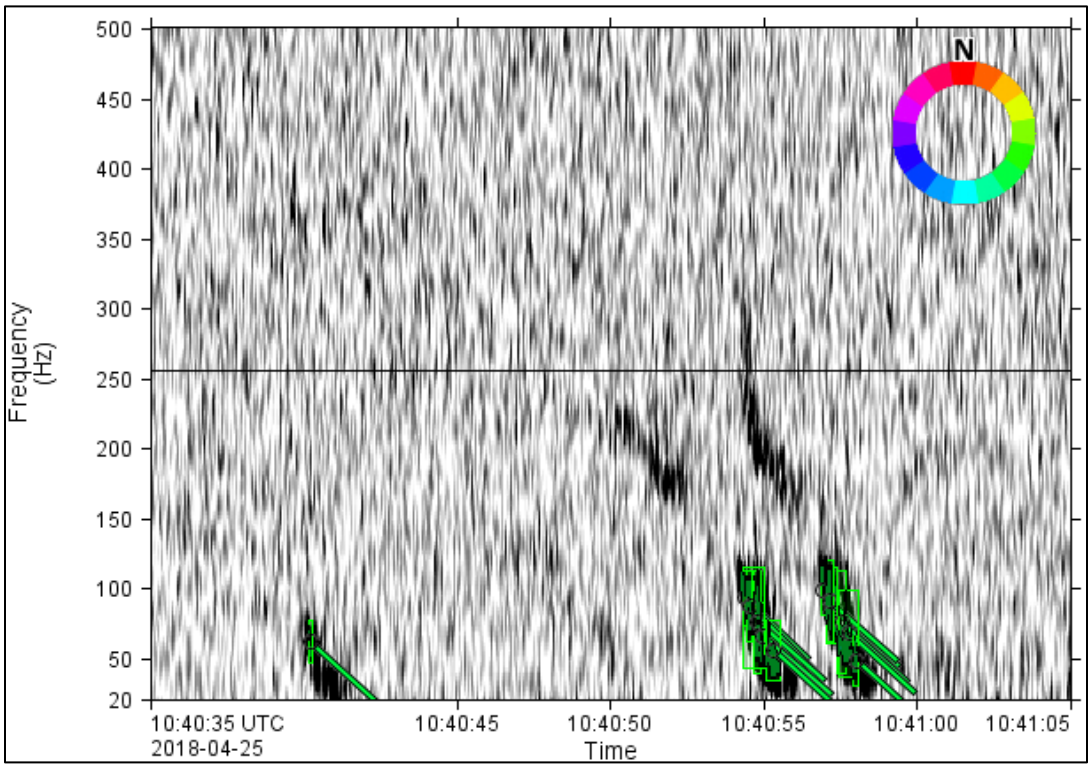

Figure 216. Examples of detected contours of sei whale calls at Virginia Inter-Canyon (VAC-2) on 25 Apr 2018

The green boxes identify the edges of the connected energy detections that comprise the contour. The lines are the detected direction of arrivals from the center of mass of the detections.

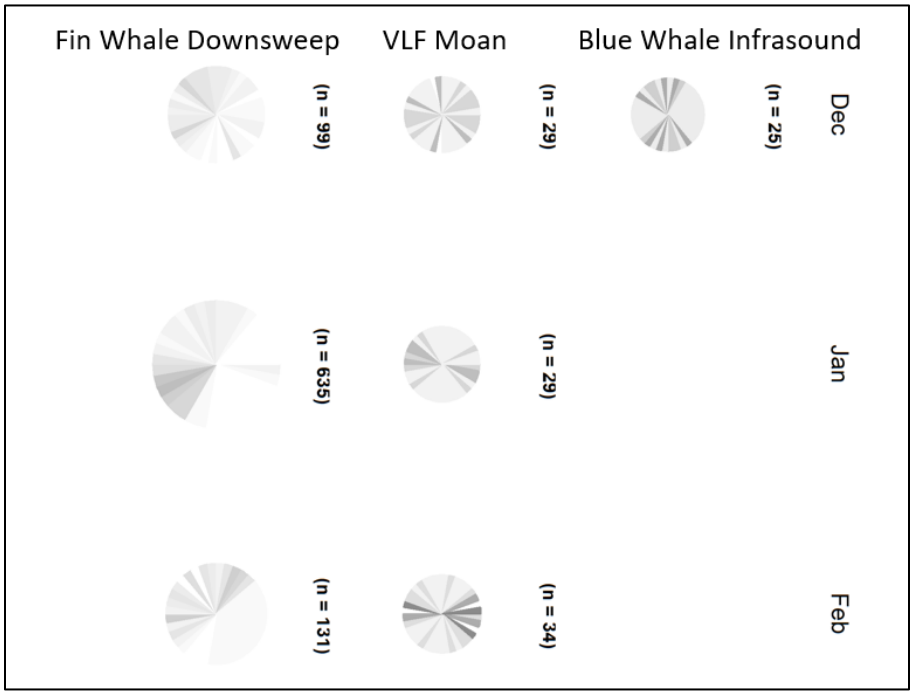

Figure 217. Pie chart presentation of long-term marine mammal event detections for VAC in Dec 17–Feb 18

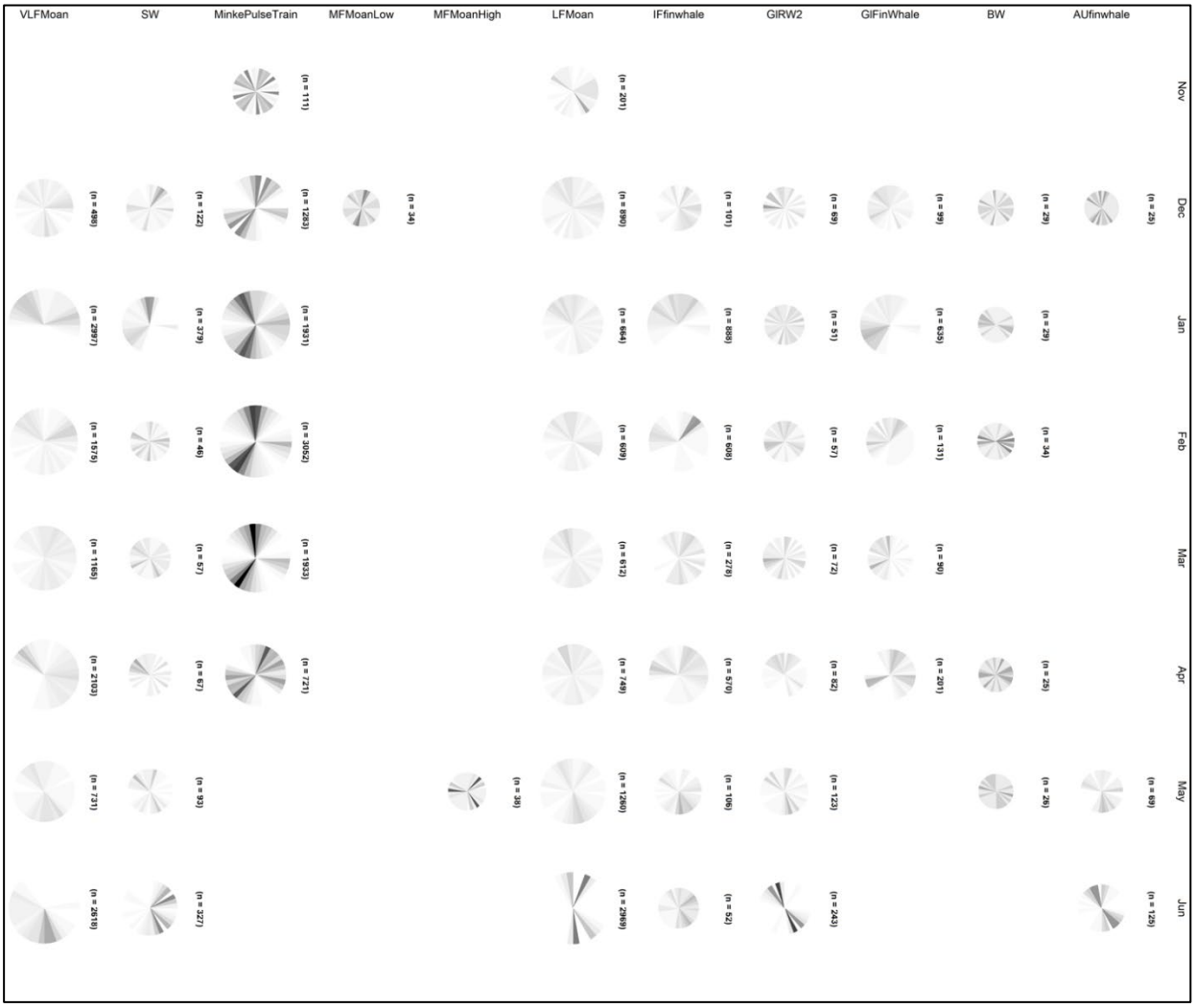

Figure 218. Pie chart array for the first set of Savannah Deep (SAV) data (December 2017 to June 2018)

Appendix C. Marine Mammal Presence in the Outer Continental Shelf

C.1 Tonal Signal Detection

Marine mammal tonal acoustic signals are detected by the following steps:

Spectrograms of the appropriate resolution for each mammal vocalization type (Table 24) that were normalized by the median value in each frequency bin for each detection window (Figure 219) were created.

- Adjacent bins were joined, and contours were created via a contour-following algorithm (Figure 219).
- A sorting algorithm determined if the contours match the definition of a marine mammal vocalization (Table 25).

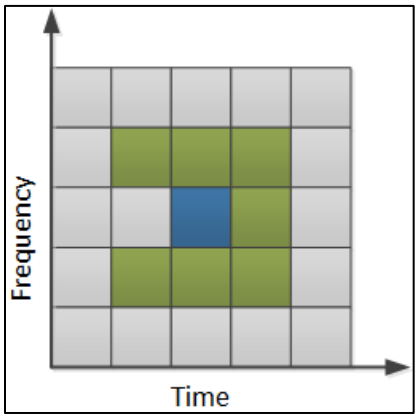

Figure 219. Illustration of the search area used to connect spectrogram bins

The blue square represents a bin of the binary spectrogram equaling 1 and the green squares represent the potential bins it could be connected to. The algorithm advances from left to right so grey cells left of the test cell need not be checked.

Table 24. Fast Fourier Transform (FFT) and detection window settings for all contour-based detectors used to detect tonal vocalizations of marine mammal species expected in the data

Detector	FFT			Detection window (s)	Detection threshold
	Resolution (Hz)	Frame length (s)	Timestep (s)		
Atl_BlueWhale_GL_IM	0.125	2	0.5	40	4
Atl_BlueWhale_IM	0.125	2	0.5	40	4
Atl_BlueWhale_IM2	0.125	2	0.5	120	4
Atl_FinWhale_130	2	0.2	0.05	5	3
Atl_FinWhale_21.2	1	0.2	0.05	5	1.7
Atl_FinWhale_21.2	1	0.2	0.05	5	4
MinkePulseTrain	8	0.1	0.025	40	3.5
N_RightWhale_Up1	4	0.128	0.032	8	2.5
N_RightWhale_Up2	4	0.128	0.032	8	3
N_RightWhale_Up3	7	0.17	0.025	10	3
SeiWhale	3.25	0.2	0.035	5	3.5
VLFMoan	2	0.2	0.05	15	4
LFMoan	2	0.25	0.05	10	3

Detector	FFT			Detection window (s)	Detection threshold
	Resolution (Hz)	Frame length (s)	Timestep (s)		
ShortLow	7	0.17	0.025	10	3
MFMoanLow	4	0.2	0.05	5	3
MFMoanHigh	8	0.125	0.05	5	3
WhistleLow	16	0.03	0.015	5	3
WhistleHigh	64	0.015	0.005	5	3

Values are based on JASCO's experience and empirical evaluation on a variety of data sets.

Table 25. A sample of vocalization sorter definitions for the tonal vocalizations of cetacean species expected in the area

Detector	Target species	Frequency (Hz)	Duration (s)	Bandwidth (B; Hz)	Other detection parameters
Atl_BlueWhale_GL_IM	Blue whales	14–22	8.00–30.00	1<B<5	minSweepRate= −500 Hz/s; minF<18 Hz 16.5<PeakF<17.5 Hz
Atl_BlueWhale_IM	Blue whales	14–22	8.00–30.00	1<B<5	minSweepRate= −500 Hz/s; minF<18 Hz 16.5<FrequencyOfPeakIntensity<18 Hz
Atl_BlueWhale_IM2	Blue whales	15–22	8.00–30.00	1<B<5	N/A
Atl_FinWhale_130	Fin whales	110–150	0.30–1.50	>6	minF<125 Hz
Atl_FinWhale_21.2	Fin whales	10–40	0.40–3.00	>6	-100<SweepRate<0 Hz/s; minF<17 Hz 20<FrequencyOfPeakIntensity<22 Hz
Atl_FinWhale_21.2	Fin whales	8–40	0.30–3.00	>6	-100<SweepRate<0 Hz/s; minF<17 Hz
MinkePulseTrain	Minke whales	50–500	0.025–0.3		0.25<PulseGap<2 s; 10<TrainLength<100 s 20 < NumberPulse < 40
N_RightWhale_Up1	Right whales	65–260	0.60–1.20	70<B<195	minF<75 Hz 30<SweepRate<290 Hz/s
N_RightWhale_Up2	Right whales	65–260	0.50–1.20	B>25	30<SweepRate<290 Hz/s
N_RightWhale_Up3	Right whales	30–400	0.50–10.00		10<SweepRate<500 Hz/s
SeiWhale	Sei whales	20–150	0.50–1.70	19<B<120	-100<SweepRate<−6 Hz/s InstantaneousBandwidth<100 Hz
VLFMoan	Blue/fin/sei whales	10–100	0.30–10.00	>10	minF<40 Hz
LFMoan	Blue/right/sei whales	40–250	0.50–10.00	>15	InstantaneousBandwidth<50 Hz
ShortLow	Fin/baleen whales	30–400	0.08–0.60	>25	N/A
MFMoanLow	Humpback whales	100–700	0.50–5.00	>50	minF<450 Hz InstantaneousBandwidth<200 Hz
MFMoanHigh	Humpback whales	500–2500	0.50–5.00	>150	minF<1500 Hz InstantaneousBandwidth<300 Hz
WhistleLow	Pilot/killer whales	1000–10000	0.50–5.00	>300	Max Instantaneous Bandwidth = 1000 Hz minF<5000 Hz
WhistleHigh	Other delphinid	4000–20000	0.30–3.00	>700	Max Instantaneous Bandwidth = 5000 Hz

N/A: Not applicable

C.2 Automated Click Detector for Odontocetes

We applied an automated click detector/classifier to detect clicks from odontocetes (Figure 220). This detector/classifier is based on the zero-crossings in the acoustic time series. Zero-crossings are the rapid oscillations of a click's pressure waveform above and below the signal's normal level (e.g., Figure 220). Clicks are detected by the following steps:

- The raw data is high-pass filtered to remove all energy below 5 kHz. This removes most energy from other sources such as shrimp, vessels, wind, and cetacean tonal calls, yet allows the energy from all marine mammal click types to pass.

- The filtered samples are summed to create a 0.334 ms rms time series. Most marine mammal clicks have a 0.1–1 ms duration.
- Possible click events are identified with a split-window normalizer that divides the ‘test’ bin of the time series by the mean of the 6 ‘window’ bins on either side of the test bin, leaving a 1-bin wide ‘notch’.
- A Teager-Kaiser energy detector identifies possible click events.
- The high-pass filtered data is searched to find the maximum peak signal within 1 ms of the detected peak.
- The high-pass filtered data is searched backwards and forwards to find the time span where the local data maxima are within 9 dB of the maximum peak. The algorithm allows for two zero-crossings to occur where the local peak is not within 9 dB of the maximum before stopping the search. This defines the time window of the detected click.
- The classification parameters are extracted. The number of zero crossings within the click, the median time separation between zero crossings, and the slope of the change in time separation between zero crossings are computed. The slope parameter helps to identify beaked whale clicks, as beaked whales can be identified by the increase in frequency (upsweep) of their clicks.
- The Mahalanobis distance between the extracted classification parameters and the templates of known click types is computed. The covariance matrices for the known click types, computed from thousands of manually identified clicks for each species, are stored in an external file. Each click is classified as a type with the minimum Mahalanobis distance, unless none of them are less than the specified distance threshold.

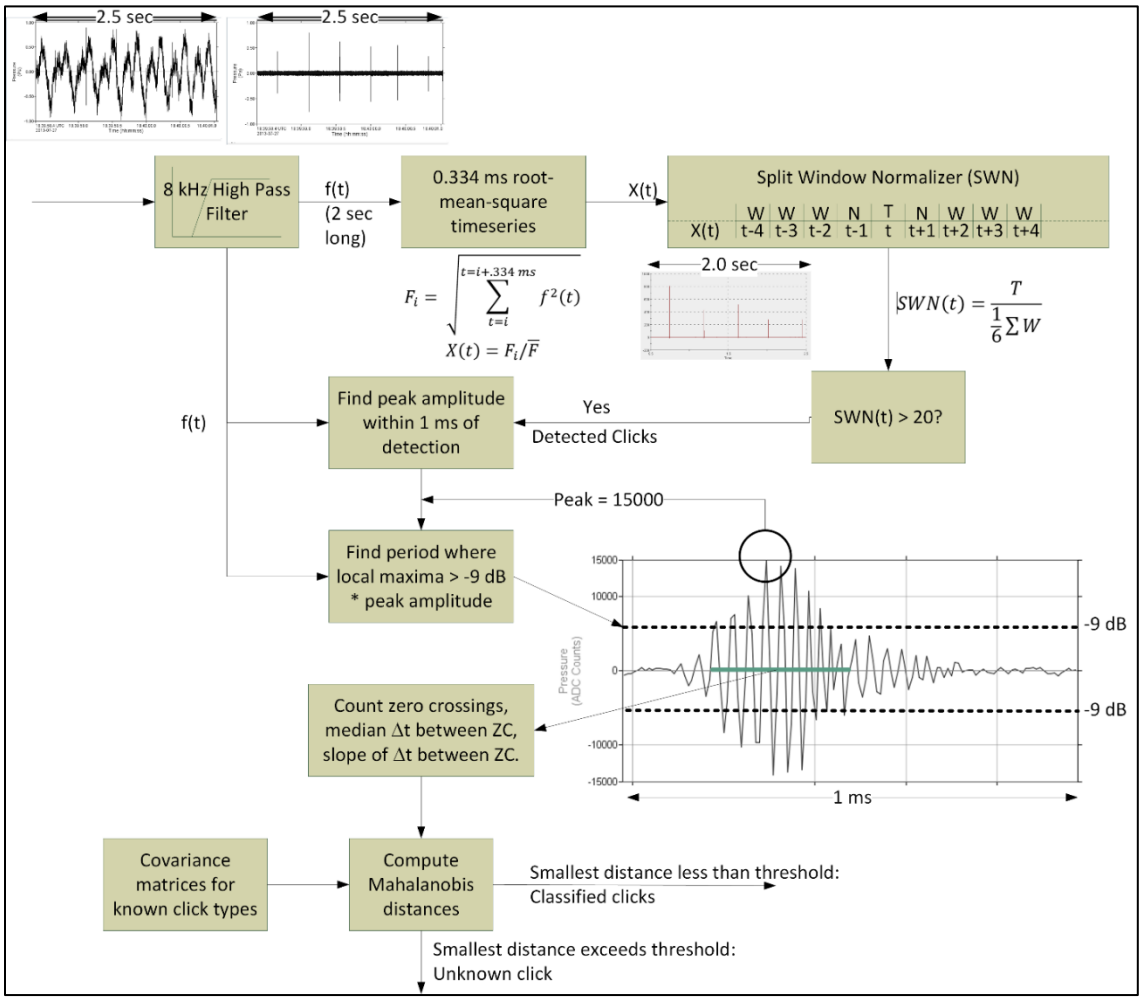

Figure 220. The click detector/classifier block diagram

Odontocete clicks occur in groups called click trains. Each species has a characteristic inter-click-interval (ICI) and number of clicks per train. The click detector includes a second stage that associates individual clicks into trains (Figure 221). The steps of the click train associator algorithm are:

- Queue clicks for *N* seconds, where *N* is twice the maximum number of clicks per train times the maximum ICI.
- Search for all clicks within the window that have Malahanobis distances less than 11 for the species of interest (this gets 99% of all clicks for the species as defined by the template).
- Create a candidate click train if:
  1. the number of clicks is greater or equal to the minimum number of clicks in a train;
  2. the maximum time between any two clicks is less than twice the maximum ICI, and
  3. the smallest Malahanobis distance for all clicks in the candidate train is less than 4.1.
- Create a new 'time-series' that has a value of 1 at the time of arrival of each clicks and zeroes everywhere else.
- Apply a Hann window to the time series then compute the cepstrum.
- A click train is classified if a peak in the cepstrum with amplitude > 5 times the standard deviation of the cepstrum occurs at a frequency between the minimum maximum ICI.

- Queue clicks for *N* seconds
- Search for all clicks within the window that have Malahanobis distances less than 10 (equal to the extent of the variance in the training data set).
- If the number of clicks is greater than or equal to 3 and dT is less than 2 * max ICI, make a new time-series at the 0.333 ms rate; where the value is 1 when the clicks occurred and 0 for all other time bins. Perform the following processing on this time series:
    1. Compute cepstrum
    2. ICI is the peak of the cepstrum with amplitude > 5 * stdev and searching for quefrency between minICI and maxICI.
    3. For each click related to the previous Ncepstrum, create a new time series and compute ICI; if we get a good match, extend the click train; find a mean ICI and variance.
- If the click features, total clicks and mean ICI match the species, output a species_click_train detection.

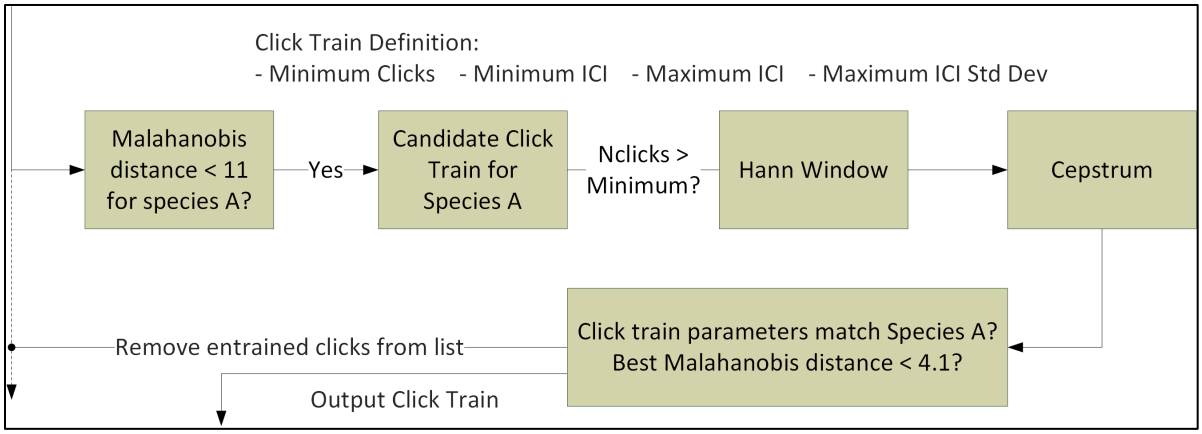

Figure 221. The click train detector/classifier block diagram

C.3 File Selection Process for Validating Detections

To standardize the file selection process, we developed an algorithm that automatically selects a sample of files for review. The selection process starts by computing the distribution of three variables that describe the detections in the full data set: the diversity of detected species per file, the number of detections per file (per species), and the temporal distribution of each species. The algorithm iteratively removes files from the data set by computing the difference between the original distribution and the distribution without each file—the file whose removal brings the new distribution closest to the original distribution is removed. The process is repeated until the sample size is reduced to N, which was set to 1 or 2% of the total duration of acoustic data. In this description, the term 'species' identifies a marine mammal detector whose performance needs to be assessed. The three variables used by the algorithm are described further below:

- **Diversity**: Select files representative of the range of species diversity (number of detected species in a file). The diversity of the full data set is log transformed to reduce the skew of the data. After being logged, the histogram bin size of the full data set is calculated using the Freedman-Diaconis rule (Freedman & Diaconis, 1981), with a maximum of 20 bins. Sample files are selected such that the distribution of diversity within the sample matches the distribution of logged diversity in the full data set.

- **Counts**: Select files representative of the range of detection counts (number of detections per file for each species). For each species, the detection counts of the full data set are log transformed to manage the skew of the data. After being logged, the histogram bin size of the full data set is calculated using the Freedman-Diaconis rule (Freedman & Diaconis, 1981), with a maximum of 20 bins. Sample files are selected such that the distribution of detection counts within the sample matches the distribution of logged detection counts in the full data set. Files with no detections are not included in the calculation for each species (0-detection count files for a species will naturally be included in files selected for other species).
- **Temporal distribution**: Select files representative of the temporal range of files containing detections for each species. The time frame of the full data set is divided into 12 equally sized bins. If the bin size is greater than 30 days, then the time frame is divided into 30-day bins. File counts per species for each bin are log transformed to reduce the skew of the data. Sample files are selected such that the distribution of files containing detections for each species within the sample matches the distribution of files containing detections for each species in the full data set.

In each iteration, we remove the file whose omission minimizes the Total Variation (υ_T). The υ_T is the sum of the following:

- Diversity Variation (υ_D),
- Count Variation (υ_C), which is the average of the per species count variations (υ_{C_s}), and
- Temporal Distribution Variation (υ_{TD}), which is the average of the per species temporal variations (υ_{TD_s}).

$$\upsilon_T = \upsilon_D + \upsilon_C + \upsilon_{TD}$$

$$\Delta = \sum_{b=1}^{B} |Pf_b - Ps_b|$$

$$\upsilon_D = \Delta_D$$

$$\upsilon_{C_s} = \Delta_{C_s}$$

$$\upsilon_C = \frac{\sum_{s=1}^{S} \upsilon_{C_s}}{S}$$

$$\upsilon_{TD_s} = \Delta_{TD_s}$$

$$\upsilon_{TD} = \frac{\sum_{s=1}^{S} \upsilon_{TD_s}}{S}$$

where Pf_b is proportion of bin ‘b’ within the full data set, Ps_b is the proportion of bin ‘b’ within subset ‘s’, Δ is difference between distributions, B is the total number of bins in the distribution, and S is the number of species. Two final constraints on the algorithm are preserving at least 10 files per species and attempting to have the files for each species at least 6 h apart.

Once the sample size has been reduced to N, the two files with the highest detection counts for each species are added back into the sample, if they were not already included. This can result in the final sample being trivially greater than N.

C.4 Detector Performance Calculation and Optimization

All files selected for manual validation were reviewed by one of two experienced analysts using JASCO's PAMlab software to determine the presence or absence of every species, regardless of whether a species was automatically detected in the file. Although the detectors classify specific signals, we validated the presence/absence of species at the file level, not the detection level. Acoustic signals were only assigned to a species if the analyst was confident in their assessment. When unsure, analysts would consult one another, peer-reviewed literature, and other experts in the field. If certainty could not be reached, the file of concern would be classified as possibly containing the species in question or containing an unknown acoustic signal. A sample of manually validated vocalizations were reviewed by a senior analyst for all stations to look for erroneous records or assign unidentified signals to a known species. Next, the validated results were compared to the raw detector results in three phases to refine the results and ensure they accurately represent the occurrence of each species in the study area.

In phase 1, the validated versus detector results were plotted as time series and critically reviewed to determine when and where automated detections should be excluded. Questionable detections that overlap with the detection period of other species were scrutinized. By restricting detections spatially and temporally where appropriate, we can maximize the reliability of the results. The following restrictions were applied to our detector results:

- If a species was automatically detected at a location, but was never manually validated, all automated detections were considered false and the species was considered absent.
- If a species was automatically detected over a specific timeframe, but manual validation revealed all detections to be falsely triggered by another sound source or species, all automated detections during that period were excluded. Any time frame restrictions employed are described in the results section.

In phase 2, the performance of the detectors was calculated based on the phase 1 restrictions and optimized for each species using a threshold, defined as the number of detections per file at and above which detections of species were considered valid.

To determine the performance of each detector and any necessary thresholds, the automated and validated results (excluding files where an analyst indicated uncertainty in species occurrence) were fed to a maximum likelihood estimation algorithm that maximizes the probability of detection and minimizes the number of false alarms using the Matthew's correlation coefficient (MCC):

$$MCC = \frac{TPxTN - FPxFN}{\sqrt{(\mathrm{TP}+\mathrm{FP})(\mathrm{TP}+\mathrm{FN})(\mathrm{TN}+\mathrm{FP})(\mathrm{TN}+\mathrm{FN})}}$$

$$P = \frac{TP}{TP + FP}; R = \frac{TP}{TP + FN}$$

where *TP* (true positive) is the number of correctly detected files, *FP* (false positive) is the number of files that are false detections, and *FN* (false negatives) is the number of files with missed detections.

Where the number of validated files was too low, and/or the overlap between manual and automated detections was too limited for the calculation of *P*, *R*, and MCC, automated detections were ignored, and only validated results were used to describe the acoustic occurrence of a species.

Appendix D. Marine Mammal Automated Detector Performance

In this section, automated detector performance metrics are provided for each species and vocalization type that was automatically detected in the acoustic data. Performance is provided for each station and cruise where there was sufficient data (sufficient *TP*s, *FP*s, and *FN*s) to calculate *P* and *R*. Automated detector results were optimized to increase the reliability of the results (Section C.4) and the automated detector performance both before and after optimization are provided. The automated detection occurrence included in figures in Section E represent the optimized or 'final' performance metrics in this section for automated detectors with a final *P* of at least 0.75.

D.1 Beaked Whales

Clicks believed to be produced by beaked whales include those of Blainville's beaked whales, Cuvier's beaked whales, and a click type that belongs to Gervais and/or True's beaked whales. Automated detector performance for Cuvier's beaked whales could not be calculated as there was too few instances where this species was manually confirmed in the acoustic data.

D.1.1 Blainville's Beaked Whales

The majority of Blainville's beaked whale clicks occurred at BLE, which was the only station with enough manually validated instances of the species to calculate automated detector performance (Table 26).

Table 26. Blainville's beaked whales: Per-file performance of the automated detector for each station and cruise

Station	Cruise	Original Automated Detector			Automated Detection Exclusion Periods	# Automated Detections per File Threshold	Final Automated Detector		
		P	R	MCC			P	R	MCC
BLE	1	0.44	0.92	0.52	None	17	0.88	0.54	0.61
	2	0.45	1.00	0.58	None	6	0.70	0.78	0.66
	3	0.29	0.93	0.42	None	26	0.70	0.55	0.57
	4	0.31	0.97	0.46	None	38	0.94	0.45	0.62

Includes the original and final automated detector Precision (P), Recall (R), and Matthew's Correlation Coefficient (MCC), and any paremeter implemented to optimized the automated detector performance including removing automated detections from certain timeframes (Automated Detection Exclusion periods) and requiring a minimum number of automated detections per file to consider the species present (# Automated Detections per File Threshold). Performance is provided only for stations and cruises where there was sufficient data (sufficient TPs, FPs, and FNs) to calculate P and R. The per-file automated detector performance is based on 1 min files sampled at 375 kHz for cruises 1 and 2 and 512 kHz for cruises 3 and 4. Performance metrics are for JASCO's automated 'NBWClick' detector.

D.1.2 Gervais and/or True's Beaked Whales

The majority of clicks matching those of the repertoire of Gervais and True's beaked whales occurred at SAV, which was the only station with enough manually validated instances of the species to calculate automated detector performance (Table 27).

Table 27. Gervais and/or True's beaked whales: Per-file performance of the automated detector for each station and cruise

Station	Cruise	Original Automated Detector			Automated Detection Exclusion Periods	# Automated Detections per File Threshold	Final Automated Detector		
		P	R	MCC			P	R	MCC
SAV	1	0.53	1.00	0.69	None	8	1.00	0.75	0.85
	2	0.20	1.00	0.43	None	4	1.00	1.00	1.00
	3	0.66	1.00	0.77	None	8	0.88	0.94	0.88
	4	0.56	0.97	0.69	None	4	0.77	0.92	0.81

Includes the original and final automated detector Precision (*P*), Recall (*R*), and Matthew's Correlation Coefficient (*MCC*), and any paremeter implemented to optimized the automated detector performance including removing automated detections from certain timeframes (Automated Detection Exclusion periods) and requiring a minimum number of automated detections per file to consider the species present (# Automated Detections per File Threshold). Performance is provided only for stations and cruises where there was sufficient data (sufficient *TP*s, *FP*s, and *FN*s) to calculate *P* and *R*. The per-file automated detector performance is based on 1 min files sampled at 375 kHz for cruises 1 and 2 and 512 kHz for cruises 3 and 4. Performance metrics are for JASCO's automated 'GervaisClick' detector.

D.2 Blue Whales

Blue whale vocalizations were infrequently manually detected and, in many instances, there was not sufficient manual detections to calculate automated detector performance. Any stations and cruises where performance could be calculated are included in Table 28.

Table 28. Blue whales: Per-file performance of the automated detector for each station and cruise

Station	Cruise	Original Automated Detector			Automated Detection Exclusion Periods	# Automated Detections per File Threshold	Final Automated Detector		
		P	R	MCC			P	R	MCC
VAC2	1	1.00	1.00	1.00	None	1	1.00	1.00	1.00
VAC	4	1.00	0.83	0.90	None	1	1.00	0.83	0.90
WIL	4	1.00	0.64	0.78	None	1	1.00	0.64	0.78
SAV	4	0.11	0.50	0.20	None	1	0.11	0.50	0.20

Includes the original and final automated detector Precision (*P*), Recall (*R*), and Matthew's Correlation Coefficient (*MCC*), and any parameter implemented to optimized the automated detector performance including removing automated detections from certain timeframes (Automated Detection Exclusion periods) and requiring a minimum number of automated detections per file to consider the species present (# Automated Detections per File Threshold). Performance is provided only for stations and cruises where there was sufficient data (sufficient *TP*s, *FP*s, and *FN*s) to calculate *P* and *R*. The per-file automated detector performance is based on 5 min files sampled at 8 kHz for VAC2, 11 min files sampled at 8 kHz for all other cruise 1 stations, 19 min files sampled at 8 kHz for cruise 2, and 9 min files sampled at 16 kHz for cruises 3 and 4. VAC2 refers to the second deployment of VAC from cruise 1. Performance metrics are for JASCO's automated 'AtlBWIMInfrasoundMoan' detector.

D.3 Delphinid Clicks

The clicks of delphinids could not be accurately differentiated across species, therefore the occurrence of these acoustic signals were considered together and the automated detector performance is provided in Table 29. Automated delphinid click detections could not be evaluated for VAC of cruise 1 because the high sampling rate data was not successfully recorded during this period.

Table 29. Delphinid clicks: Per-file performance of the automated detector for each station and cruise

Station	Cruise	Original Automated Detector			Automated Detection Exclusion Periods	# Automated Detections per File Threshold	Final Automated Detector		
		P	R	MCC			P	R	MCC
VAC	2	0.89	0.84	0.56	None	1	0.89	0.84	0.56
	3	0.91	0.88	0.48	None	1	0.91	0.88	0.48
	4	0.92	0.81	0.43	None	1	0.92	0.81	0.43
HAT	1	0.9	0.84	0.52	None	1	0.90	0.84	0.52
	2	0.85	0.91	0.69	None	2	0.94	0.91	0.79
	3	0.86	0.88	0.69	None	2	0.89	0.86	0.70
	4	0.94	0.82	0.64	None	1	0.94	0.82	0.64
WIL	1	0.8	0.8	0.52	None	5	0.94	0.71	0.59
	2	0.88	0.83	0.58	None	1	0.88	0.83	0.58
	3	0.90	0.96	0.83	None	2	0.92	0.95	0.83
	4	0.88	0.86	0.62	None	2	0.91	0.82	0.63
CHB	1	0.87	0.81	0.67	None	2	0.96	0.75	0.71
	2	0.89	0.94	0.75	None	4	1.00	0.88	0.83
	3	0.87	0.86	0.70	None	1	0.87	0.86	0.70
	4	0.89	0.84	0.65	None	1	0.89	0.84	0.65
SAV	1	0.81	0.93	0.76	None	3	0.89	0.86	0.77
	2	0.79	0.75	0.61	None	3	0.88	0.75	0.69
	3	0.86	0.92	0.82	None	2	0.90	0.89	0.84
	4	0.79	0.82	0.69	None	8	0.92	0.75	0.74
JAX	1	0.77	0.87	0.64	None	8	0.92	0.77	0.71
	2	0.89	0.89	0.78	None	2	0.96	0.89	0.85
	3	0.92	0.90	0.83	None	2	0.97	0.89	0.86
	4	0.87	0.88	0.74	None	2	0.91	0.87	0.77
BLE	1	0.69	0.92	0.65	None	57	1.00	0.63	0.70
	2	0.61	0.82	0.52	None	15	1.00	0.65	0.72
	3	0.70	0.94	0.64	None	33	0.88	0.84	0.74
	4	0.69	0.90	0.61	None	61	0.95	0.71	0.71

Includes the original and final automated detector Precision (*P*), Recall (*R*), and Matthew's Correlation Coefficient (*MCC*), and any parameter implemented to optimized the automated detector performance including removing automated detections from certain timeframes (Automated Detection Exclusion periods) and requiring a minimum number of automated detections per file to consider the species present (# Automated Detections per File Threshold). Performance is provided only for stations and cruises where there was sufficient data (sufficient *TP*s, *FP*s, and *FN*s) to calculate *P* and *R*. The per-file automated detector performance is based on 1 min files sampled at 375 kHz for cruises 1 and 2 and 512 kHz for cruises 3 and 4. Performance metrics are for JASCO's automated 'DolphinClick' detector.

D.4 Dolphin Whistles

While delphinid clicks could not be differentiated to different species, delphinid tonal vocalizations could be differentiated to some degree. Whistles with energy above 5000 Hz were believed to be produced by small dolphins and the performance of the automated high frequency dolphin whistle detector are included in Table 30.

Table 30. Dolphin whistles: Per-file performance of the automated detector for each station and cruise

Station	Cruise	Original Automated Detector			Automated Detection Exclusion Periods	# Automated Detections per File Threshold	Final Automated Detector		
		P	R	MCC			P	R	MCC
VAC	1	0.67	0.80	-0.26	None	1	0.67	0.80	-0.26
	2	0.96	0.56	0.38	None	1	0.96	0.56	0.38
	3	1.00	0.56	0.50	None	1	1.00	0.56	0.50
	4	0.91	0.54	0.40	None	1	0.91	0.54	0.40
HAT	1	0.95	0.50	0.48	None	1	0.95	0.50	0.48
	2	0.94	0.44	0.41	None	1	0.94	0.44	0.41
	3	0.96	0.47	0.48	None	1	0.96	0.47	0.48
	4	0.95	0.46	0.48	None	1	0.95	0.46	0.48
WIL	1	0.95	0.59	0.62	None	1	0.95	0.59	0.62
	2	1.00	0.67	0.70	None	1	1.00	0.67	0.70
	3	0.96	0.48	0.57	None	1	0.96	0.48	0.57
	4	0.90	0.55	0.55	None	1	0.90	0.55	0.55
CHB	1	0.92	0.48	0.56	None	1	0.92	0.48	0.56
	2	0.89	0.40	0.47	None	2	1.00	0.40	0.53
	3	0.96	0.45	0.54	None	1	0.96	0.45	0.54
	4	0.77	0.42	0.44	None	3	0.89	0.35	0.46
SAV	1	0.95	0.78	0.80	None	1	0.95	0.78	0.80
	2	0.70	0.78	0.68	None	1	0.70	0.78	0.68
	3	0.80	0.22	0.33	None	1	0.80	0.22	0.33
	4	0.93	0.49	0.61	None	1	0.93	0.49	0.61
JAX	1	0.62	0.62	0.52	None	1	0.62	0.62	0.52
	2	0.75	0.45	0.42	None	1	0.75	0.45	0.42
	3	0.77	0.34	0.42	None	1	0.77	0.34	0.42
	4	0.56	0.47	0.39	None	1	0.56	0.47	0.39
BLE	1	0.67	0.50	0.49	None	1	0.67	0.50	0.49
	2	0.90	0.75	0.78	None	1	0.90	0.75	0.78
	3	0.72	0.44	0.51	None	1	0.72	0.44	0.51
	4	0.89	0.36	0.50	None	1	0.89	0.36	0.50

Includes the original and final automated detector Precision (*P*), Recall (*R*), and Matthew's Correlation Coefficient (*MCC*), and any paremeter implemented to optimized the automated detector performance including removing automated detections from certain timeframes (Automated Detection Exclusion periods) and requiring a minimum number of automated detections per file to consider the species present (# Automated Detections per File Threshold). Performance is provided only for stations and cruises where there was sufficient data (sufficient *TP*s, *FP*s, and *FN*s) to calculate *P* and *R*. The per-file automated detector performance is based on 1 min files sampled at 375 kHz for cruises 1 and 2 and 512 kHz for cruises 3 and 4. Performance metrics are for JASCO's automated 'WhistleHigh' detector.

D.5 Dolphin Calf

The performance of the automated dolphin calf vocalization detector is provided in Table 31.

Table 31. Dolphin calf: Per-file performance of the automated detector for each station and cruise

Station	Cruise	Original Automated Detector			Automated Detection Exclusion Periods	# Automated Detections per File Threshold	Final Automated Detector		
		P	R	MCC			P	R	MCC
VAC2	1	0.33	1.00	0.57	None	2	1.00	1.00	1.00
VAC	2	0.08	0.25	-0.08	None	6	0.33	0.25	0.18
	3	0.11	0.25	0.07	None	8	1.00	0.25	0.48
	4	0.27	0.33	0.17	None	26	1.00	0.11	0.31

Station	Cruise	Original Automated Detector			Automated Detection Exclusion Periods	# Automated Detections per File Threshold	Final Automated Detector		
		P	R	MCC			P	R	MCC
HAT	1	0.78	0.50	0.55	None	1	0.78	0.50	0.55
	2	0.70	0.50	0.40	None	2	0.86	0.43	0.47
	3	0.53	0.73	0.56	None	1	0.53	0.73	0.56
	4	0.42	0.45	0.36	None	2	0.50	0.36	0.36
WIL	1	0.57	0.33	0.35	None	7	1.00	0.25	0.46
	2	0.73	0.80	0.67	None	2	1.00	0.80	0.86
	3	0.80	0.86	0.79	None	1	0.80	0.86	0.79
	4	0.82	0.82	0.79	None	1	0.82	0.82	0.79
CHB	1	0.63	0.50	0.49	None	1	0.63	0.50	0.49
	2	0.44	0.50	0.31	None	5	1.00	0.25	0.45
	3	0.73	0.89	0.78	None	2	1.00	0.67	0.80
	4	1.00	0.53	0.69	1 Feb to 1 May	1	1.00	0.53	0.69
SAV	1	0.29	0.50	0.33	None	1	0.29	0.50	0.33
	2	0.20	0.25	0.11	None	2	1.00	0.25	0.47
	3	0.29	0.67	0.39	None	2	1.00	0.33	0.57
	4	0.40	0.67	0.48	None	1	0.40	0.67	0.48
JAX	1	0.22	0.67	0.34	None	5	1.00	0.33	0.57
	2	0.43	0.43	0.30	None	1	0.43	0.43	0.30
	3	0.36	0.67	0.44	None	3	0.67	0.33	0.45
	4	0.10	0.33	0.12	None	1	0.10	0.33	0.12
BLE	4	0.10	0.50	0.19	None	4	0.50	0.50	0.49

Includes the original and final automated detector Precision (*P*), Recall (*R*), and Matthew's Correlation Coefficient (*MCC*), and any parameter implemented to optimized the automated detector performance including removing automated detections from certain timeframes (Automated Detection Exclusion periods) and requiring a minimum number of automated detections per file to consider the species present (# Automated Detections per File Threshold). Performance is provided only for stations and cruises where there was sufficient data (sufficient *TP*s, *FP*s, and *FN*s) to calculate *P* and *R*. The per-file automated detector performance is based on 5 min files sampled at 8 kHz for VAC2, 11 min files sampled at 8 kHz for all other cruise 1 stations, 19 min files sampled at 8 kHz for cruise 2, and 9 min files sampled at 16 kHz for cruises 3 and 4. VAC1 refers to the first deployment of VAC from cruise 1 and VAC2 refers to the second deployment of VAC from cruise 1. Performance metrics are for JASCO's automated 'MFMoanHigh' detector.

D.6 Pilot and Killer Whale Whistles

Whistles below 5000 Hz were attributed to either pilot or killer whales and were captured by the same automated detector. The performance of this automated low whistle detector is provided in Table 32.

Table 32. Pilot and Killer whale whistles: Per-file performance of the automated detector for each station and cruise

Station	Cruise	Original Automated Detector			Automated Detection Exclusion Periods	# Automated Detections per File Threshold	Final Automated Detector		
		P	R	MCC			P	R	MCC
VAC1	1	0.50	1.00	0.65	None	7	1.00	1.00	1.00
VAC2	1	0.79	0.48	0.48	None	1	0.79	0.48	0.48
VAC	2	0.72	0.68	0.30	None	11	0.91	0.53	0.40
	3	0.10	1.00	0.26	None	4	0.13	1.00	0.32
HAT	1	0.57	0.80	0.65	None	2	0.75	0.60	0.65
	2	0.22	1.00	0.41	None	54	1.00	0.50	0.69

Station	Cruise	Original Automated Detector			Automated Detection Exclusion Periods	# Automated Detections per File Threshold	Final Automated Detector		
		P	R	MCC			P	R	MCC
	4	0.17	0.60	0.23	None	19	0.33	0.40	0.31
WIL	1	0.60	0.86	0.68	None	1	0.60	0.86	0.68
	2	0.45	0.83	0.52	None	5	0.83	0.83	0.79
	3	0.13	1.00	0.34	Recording start to 1 Apr	10	1.00	1.00	1.00
CHB	1	1.00	0.78	0.87	Recording start to 15 Apr	1	1.00	0.78	0.87
	2	0.23	0.75	0.28	None	2	0.33	0.75	0.39
	3	0.17	1.00	0.37	None	11	0.29	0.67	0.40
	4	0.08	0.33	0.10	None	8	0.50	0.33	0.39
SAV	1	0.44	0.67	0.49	Recording start to 15 Apr	3	1.00	0.67	0.80
	2	0.17	1.00	0.34	None	3	0.50	1.00	0.68
	3	0.08	0.50	0.16	None	11	0.20	0.50	0.29
	4	0.33	0.75	0.40	None	17	1.00	0.50	0.68
BLE	1	0.67	0.71	0.60	None	4	1.00	0.43	0.61
	2	0.60	1.00	0.75	None	3	1.00	1.00	1.00
	3	0.06	1.00	0.13	None	2	0.06	1.00	0.14
	4	0.11	0.40	0.12	None	33	1.00	0.20	0.44

Includes the original and final automated detector Precision (P), Recall (R), and Matthew's Correlation Coefficient (MCC), and any paremeter implemented to optimized the automated detector performance including removing automated detections from certain timeframes (Automated Detection Exclusion periods) and requiring a minimum number of automated detections per file to consider the species present (# Automated Detections per File Threshold). Performance is provided only for stations and cruises where there was sufficient data (sufficient TPs, FPs, and FNs) to calculate P and R. The per-file automated detector performance is based on 5 min files sampled at 8 kHz for VAC2, 11 min files sampled at 8 kHz for all other cruise 1 stations, 19 min files sampled at 8 kHz for cruise 2, and 9 min files sampled at 16 kHz for cruises 3 and 4. VAC1 refers to the first deployment of VAC from cruise 1 and VAC2 refers to the second deployment of VAC from cruise 1. Performance metrics are for JASCO's automated 'WhistleLow' detector.

D.7 Fin Whales

The performance of the automated fin whale 20 Hz pulse detector is provided in Table 33.

Table 33. Fin whales: Per-file performance of the automated detector for each station and cruise

Station	Cruise	Original Automated Detector			Automated Detection Exclusion Periods	# Automated Detections per File Threshold	Final Automated Detector		
		P	R	MCC			P	R	MCC
VAC2	1	0.70	0.89	0.69	None	4	1.00	0.72	0.80
VAC	2	0.80	1.00	0.81	None	2	0.92	1.00	0.93
	3	0.76	0.89	0.73	1 May to recording end	3	0.88	0.83	0.79
	4	0.96	0.93	0.90	1 May to recording end	1	0.96	0.93	0.90
HAT	1	0.62	1.00	0.75	1 Apr to recording end	2	0.88	0.88	0.86
	2	0.71	1.00	0.82	None	4	1.00	1.00	1.00
	3	0.64	0.78	0.66	1 Apr to recording end	2	1.00	0.78	0.87
	4	0.69	0.90	0.76	1 Apr to 1 Oct	3	1.00	0.90	0.94
WIL	2	1.00	1.00	1.00	Recording start to 1 Aug	1	1.00	1.00	1.00
	3	0.86	1.00	0.90	None	2	1.00	0.89	0.93
	4	0.65	0.72	0.60	None	6	1.00	0.61	0.74
CHB	1	1.00	1.00	1.00	Recording start to 1 Jan and 15 Mar to recording end	1	1.00	1.00	1.00
	3	0.25	1.00	0.48	None	3	0.67	1.00	0.81
	4	0.18	1.00	0.41	None	4	0.67	1.00	0.81
SAV	1	0.88	0.88	0.86	Recording start to 1 Jan and 1 Mar to recording end	1	0.88	0.88	0.86
	2	0.40	0.67	0.45	None	2	0.67	0.67	0.63
	3	0.89	1.00	0.93	1 Apr to recording end	5	1.00	1.00	1.00
	4	0.55	0.86	0.65	None	5	0.83	0.71	0.75
JAX	1	0.78	0.88	0.80	15 Feb to recording end	2	1.00	0.88	0.93
	3	0.25	1.00	0.48	None	4	0.67	1.00	0.81
	4	0.40	1.00	0.61	None	6	1.00	1.00	1.00
BLE	1	0.93	1.00	0.95	1 Feb to recording end	1	0.93	1.00	0.95
	2	1.00	1.00	1.00	None	1	1.00	1.00	1.00
	3	0.67	1.00	0.80	1 Mar to recording end	5	0.86	1.00	0.92
	4	0.58	1.00	0.74	1 Apr to 1 Oct	2	0.78	1.00	0.87

Includes the original and final automated detector Precision (P), Recall (R), and Matthew's Correlation Coefficient (MCC), and any paremeter implemented to optimized the automated detector performance including removing automated detections from certain timeframes (Automated Detection Exclusion periods) and requiring a minimum number of automated detections per file to consider the species present (# Automated Detections per File Threshold). Performance is provided only for stations and cruises where there was sufficient data (sufficient TPs, FPs, and FNs) to calculate P and R. The per-file automated detector performance is based on 5 min files sampled at 8 kHz for VAC2, 11 min files sampled at 8 kHz for all other cruise 1 stations, 19 min files sampled at 8 kHz for cruise 2, and 9 min files sampled at 16 kHz for cruises 3 and 4. VAC1 refers to the first deployment of VAC from cruise 1 and VAC2 refers to the second deployment of VAC from cruise 1. Performance metrics are for JASCO's automated 'AtlFW21InfrasoundMoan' detector.

D.8 Harbor Porpoise and Kogia sp.

Clicks of harbor porpoise and Kogia sp. could not be confidently differentiated and were both identified by the same automated detector. The performance of this narrow-band high frequency automated click detector is provided in Table 34.

Table 34. Harbor porpoise or Kogia sp. clicks: Per-file performance of the automated detector for each station and cruise

Station	Cruise	Original Automated Detector			Automated Detection Exclusion Periods	# Automated Detections per File Threshold	Final Automated Detector		
		P	R	MCC			P	R	MCC
WIL	1	0.25	1.00	0.46	None	13	1.00	1.00	1.00
	3	0.31	1.00	0.51	None	8	1.00	1.00	1.00
	4	0.27	0.93	0.46	None	10	0.76	0.87	0.80
CHB	1	0.33	1.00	0.57	None	2	1.00	1.00	1.00
	3	0.09	1.00	0.28	None	9	1.00	0.67	0.81
	4	0.08	1.00	0.26	None	5	0.60	1.00	0.77
SAV	1	0.90	1.00	0.94	None	1	0.90	1.00	0.94
	3	0.63	0.95	0.74	None	4	0.95	0.90	0.91
	4	0.68	0.90	0.76	None	3	0.89	0.81	0.83
JAX	4	0.02	1.00	0.12	None	9	0.50	1.00	0.71
BLE	1	1.00	0.73	0.83	None	1	1.00	0.73	0.83
	2	1.00	0.20	0.41	None	1	1.00	0.20	0.41
	3	0.96	1.00	0.97	None	2	1.00	1.00	1.00
	4	0.79	1.00	0.87	None	4	0.98	0.98	0.97

Includes the original and final automated detector Precision (P), Recall (R), and Matthew's Correlation Coefficient (MCC), and any paremeter implemented to optimized the automated detector performance including removing automated detections from certain timeframes (Automated Detection Exclusion periods) and requiring a minimum number of automated detections per file to consider the species present (# Automated Detections per File Threshold). Performance is provided only for stations and cruises where there was sufficient data (sufficient TPs, FPs, and FNs) to calculate P and R. The per-file automated detector performance is based on 1 min files sampled at 375 kHz for cruises 1 and 2 and 512 kHz for cruises 3 and 4. Performance metrics are for JASCO's automated 'PorpoiseClick' detector.

D.9 Humpback Whales

The performance of the automated Humpback whale moan detector is provided in Table 35.

Table 35. Humpback whales: Per-file performance of the automated detector for each station and cruise

Station	Cruise	Original Automated Detector			Automated Detection Exclusion Periods	# Automated Detections per File Threshold	Final Automated Detector		
		P	R	MCC			P	R	MCC
VAC2	1	0.92	0.92	0.90	None	1	0.92	0.92	0.90
VAC	2	0.08	0.25	-0.08	None	6	0.33	0.25	0.18
	3	0.71	0.83	0.70	None	11	1.00	0.75	0.83
	4	0.60	0.60	0.47	None	8	1.00	0.47	0.62
HAT	2	0.70	0.50	0.40	None	2	0.86	0.43	0.47
	3	0.60	0.90	0.69	None	2	0.82	0.90	0.84
	4	0.35	0.75	0.45	None	17	0.83	0.63	0.70
WIL	2	0.73	0.80	0.67	None	2	1.00	0.80	0.86
	3	0.09	1.00	0.26	None	18	1.00	0.50	0.70
	4	0.05	1.00	0.21	None	10	0.33	1.00	0.57
CHB	2	0.44	0.50	0.31	None	5	1.00	0.25	0.45
SAV	2	0.20	0.25	0.11	None	2	1.00	0.25	0.47
JAX	2	0.43	0.43	0.30	None	1	0.43	0.43	0.30
BLE	3	0.06	1.00	0.21	None	5	0.25	1.00	0.49

Includes the original and final automated detector Precision (P), Recall (R), and Matthew's Correlation Coefficient (MCC), and any paremeter implemented to optimized the automated detector performance including removing automated detections from certain timeframes (Automated Detection Exclusion periods) and requiring a minimum number of automated detections per file to consider the species present (# Automated Detections per File Threshold). Performance is provided only for stations and cruises where there was sufficient data (sufficient TPs, FPs, and FNs) to calculate P and R. The per-file automated detector performance is based on 5 min files sampled at 8 kHz for VAC2, 11 min files sampled at 8 kHz for all other cruise 1 stations, 19 min files sampled at 8 kHz for cruise 2, and 9 min files sampled at 16 kHz for cruises 3 and 4. VAC1 refers to the first deployment of VAC from cruise 1 and VAC2 refers to the second deployment of VAC from cruise 1. Performance metrics are for JASCO's automated 'MFMoanLow' detector.

D.10 Minke Whales

The performance of the automated minke whale pulse train detector is provided in Table 36.

Table 36. Minke whales: Per-file performance of the automated detector for each station and cruise

Station	Cruise	Original Automated Detector			Automated Detection Exclusion Periods	# Automated Detections per File Threshold	Final Automated Detector		
		P	R	MCC			P	R	MCC
VAC	2	0.08	0.25	-0.08	None	6	0.33	0.25	0.18
HAT	2	0.70	0.50	0.40	None	2	0.86	0.43	0.47
	4	0.89	0.80	0.83	None	1	0.89	0.80	0.83
WIL	1	0.94	0.50	0.56	None	1	0.94	0.50	0.56
	2	0.73	0.80	0.67	None	2	1.00	0.80	0.86
	3	1.00	0.36	0.58	None	1	1.00	0.36	0.58
	4	0.82	0.57	0.64	None	1	0.82	0.57	0.64
CHB	2	0.44	0.50	0.31	None	5	1.00	0.25	0.45
	3	1.00	0.40	0.62	None	1	1.00	0.40	0.62
	4	1.00	0.77	0.86	None	1	1.00	0.77	0.86
SAV	1	1.00	0.47	0.57	None	1	1.00	0.47	0.57
	2	0.20	0.25	0.11	None	2	1.00	0.25	0.47
	3	0.92	0.48	0.55	None	1	0.92	0.48	0.55
	4	0.91	0.33	0.46	None	1	0.91	0.33	0.46
JAX	1	1.00	0.33	0.49	None	1	1.00	0.33	0.49
	2	0.43	0.43	0.30	None	1	0.43	0.43	0.30
	3	0.80	0.50	0.58	None	1	0.80	0.50	0.58
	4	1.00	0.60	0.74	1 Apr to 1 Nov	1	1.00	0.60	0.74
BLE	1	1.00	0.40	0.56	None	1	1.00	0.40	0.56
	3	0.91	0.67	0.74	None	2	1.00	0.60	0.71
	4	1.00	0.47	0.65	1 Jun to 1 Nov	1	1.00	0.47	0.65

Includes the original and final automated detector Precision (P), Recall (R), and Matthew's Correlation Coefficient (MCC), and any paremeter implemented to optimized the automated detector performance including removing automated detections from certain timeframes (Automated Detection Exclusion periods) and requiring a minimum number of automated detections per file to consider the species present (# Automated Detections per File Threshold). Performance is provided only for stations and cruises where there was sufficient data (sufficient TPs, FPs, and FNs) to calculate P and R. The per-file automated detector performance is based on 5 min files sampled at 8 kHz for VAC2, 11 min files sampled at 8 kHz for all other cruise 1 stations, 19 min files sampled at 8 kHz for cruise 2, and 9 min files sampled at 16 kHz for cruises 3 and 4. VAC1 refers to the first deployment of VAC from cruise 1 and VAC2 refers to

the second deployment of VAC from cruise 1. Performance metrics are for JASCO's automated 'MinkePulseTrain' detector.

D.11 Sei Whales

The performance of the automated sei whale moan detector is provided in Table 37.

Table 37. Sei whales: per-file performance of the automated detector for each station and cruise

Station	Cruise	Original Automated Detector			Automated Detection Exclusion Periods	# Automated Detections per File Threshold	Final Automated Detector		
		P	R	MCC			P	R	MCC
VAC2	1	0.31	0.67	0.37	None	7	0.67	0.33	0.43
WIL	1	0.27	0.75	0.40	None	10	1.00	0.75	0.86
	4	0.60	1.00	0.77	1 Feb to recording end	3	0.75	1.00	0.86
CHB	1	0.04	1.00	0.11	None	6	1.00	1.00	1.00
SAV	1	0.67	0.67	0.65	None	2	1.00	0.67	0.81
	3	0.25	0.75	0.37	None	4	1.00	0.50	0.69
	4	0.43	0.86	0.57	None	6	0.83	0.71	0.75
JAX	1	0.33	1.00	0.57	None	4	0.50	1.00	0.70
BLE	1	0.75	0.50	0.58	None	1	0.75	0.50	0.58
	3	1.00	1.00	1.00	None	1	1.00	1.00	1.00
	4	0.57	1.00	0.74	1 Feb to 1 Nov	1	0.57	1.00	0.74

Includes the original and final automated detector Precision (P), Recall (R), and Matthew's Correlation Coefficient (MCC), and any paremeter implemented to optimized the automated detector performance including removing automated detections from certain timeframes (Automated Detection Exclusion periods) and requiring a minimum number of automated detections per file to consider the species present (# Automated Detections per File Threshold). Performance is provided only for stations and cruises where there was sufficient data (sufficient TPs, FPs, and FNs) to calculate P and R. The per-file automated detector performance is based on 5 min files sampled at 8 kHz for VAC2, 11 min files sampled at 8 kHz for all other cruise 1 stations, 19 min files sampled at 8 kHz for cruise 2, and 9 min files sampled at 16 kHz for cruises 3 and 4. VAC1 refers to the first deployment of VAC from cruise 1 and VAC2 refers to the second deployment of VAC from cruise 1. Performance metrics are for JASCO's automated 'SWHiDownsweeps' detector.

D.12 Sperm Whales

The performance of the automated sperm whale click detector is provided in Table 38.

Table 38 Sperm whales: Per-file performance of the automated detector for each station and cruise

Station	Cruise	Original Automated Detector			Automated Detection Exclusion Periods	# Automated Detections per File Threshold	Final Automated Detector		
		P	R	MCC			P	R	MCC
VAC	3	0.58	0.65	0.47	None	2	0.63	0.59	0.47
	4	0.56	0.79	0.58	None	8	0.66	0.68	0.59
HAT	1	0.27	0.60	0.34	None	5	1.00	0.40	0.62
	2	0.15	0.67	0.24	None	1	0.15	0.67	0.24
	3	0.10	0.60	0.21	None	32	1.00	0.20	0.44
	4	0.21	0.47	0.25	None	7	0.38	0.47	0.38
WIL	2	0.25	0.67	0.35	None	6	0.67	0.67	0.64
	3	0.12	0.67	0.22	None	21	0.67	0.44	0.53

Station	Cruise	Original Automated Detector			Automated Detection Exclusion Periods	# Automated Detections per File Threshold	Final Automated Detector		
		P	R	MCC			P	R	MCC
	4	0.21	0.76	0.33	None	6	0.32	0.71	0.43
CHB	1	0.50	0.50	0.48	None	1	0.50	0.50	0.48
	3	0.11	0.29	0.14	None	2	0.20	0.29	0.21
	4	0.08	1.00	0.27	None	15	0.43	1.00	0.65
SAV	2	0.56	0.83	0.63	None	4	0.80	0.67	0.70
	3	0.09	0.29	0.09	None	1	0.09	0.29	0.09
	4	0.27	0.88	0.44	None	12	0.54	0.81	0.64
JAX	1	0.13	1.00	0.33	None	7	1.00	1.00	1.00
	2	0.13	1.00	0.33	None	1	0.13	1.00	0.33
	3	0.11	0.86	0.27	None	18	0.45	0.71	0.55
	4	0.34	0.87	0.50	None	11	0.69	0.73	0.69
BLE	2	0.88	0.78	0.79	None	1	0.88	0.78	0.79
	3	0.57	0.86	0.65	None	17	0.94	0.81	0.85
	4	0.41	0.92	0.57	None	9	0.63	0.85	0.70

Includes the original and final automated detector Precision (P), Recall (R), and Matthew's Correlation Coefficient (MCC), and any paremeter implemented to optimized the automated detector performance including removing automated detections from certain timeframes (Automated Detection Exclusion periods) and requiring a minimum number of automated detections per file to consider the species present (# Automated Detections per File Threshold). Performance is provided only for stations and cruises where there was sufficient data (sufficient TPs, FPs, and FNs) to calculate P and R. The per-file automated detector performance is based on 1 min files sampled at 375 kHz for cruises 1 and 2 and 512 kHz for cruises 3 and 4. Performance metrics are for JASCO's automated 'SpermWhaleClick' detector.

Appendix E. Marine Mammal Presence in the OCS

The marine mammal acoustic presence described here includes reference to both automated detector results and those of manual analysis. Only automated detector results with a final precision of at least 0.75 were included here. For stations and cruises where automated detector results were considered unreliable ($P < 0.75$), only manual results are provided. Readers should reference Section D when interpreting marine mammal occurrence with regards to automated detectors.

E.1 Beaked Whales

Beaked whale clicks were detected in the acoustic data in all months of the year at SAV and BLE as well as in two instances at WIL (Figure 222). Clicks from beaked whales were differentiated from those of dolphins based largely on their sloping characteristic (Baumann-Pickering et al., 2013). Effort was made to differentiate beaked whale clicks to the species level. Blainville's beaked whales, Cuvier's beaked whales, and a click type that belongs to Gervais and/or True's beaked whales were identified in the acoustic data.

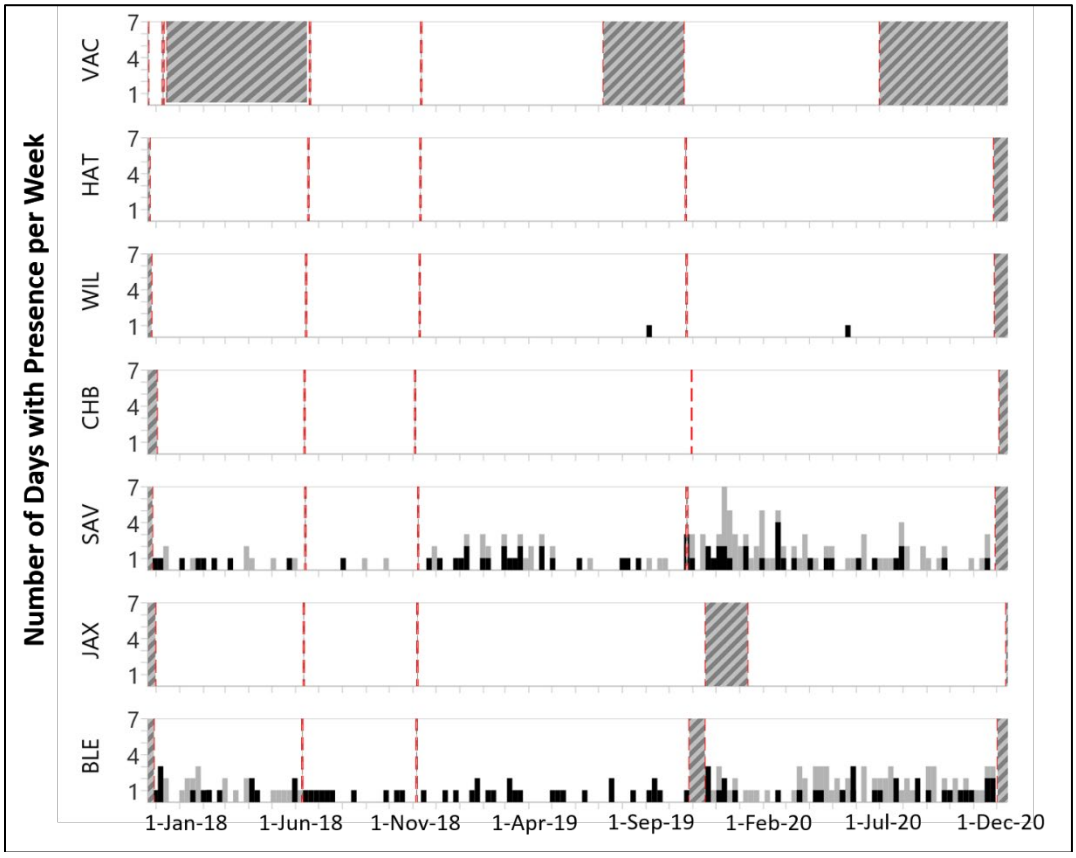

Figure 222. The number of days per week with beaked whale clicks automatically detected (grey) and manually detected (black) during the recording period at each station where hashed lines indicate periods with no acoustic data and red dashed lines indicated deployment and retrieval dates. Detections at SAV were believed to be Gervais and/or True's beaked whales, the majority of detections at BLE were believed to be Blainsville's beaked whales, and Cuvier's beaked whales were suspected on four occassions at BLE. Automatic detections for deployment periods (cruises) where the automated detector was found unreliable are not included.

E.1.1 Blainville's Beaked Whales

The majority of beaked whale detections at BLE were believed to be Blainville's beaked whales based on the frequency characteristics and inter-click-interval of the clicks (Figure 223 and Figure 224) and the species' known range overlapping with this station (Johnson et al., 2006; Baumann-Pickering et al., 2013; Stanistreet et al., 2017). Blainville's beaked whale occurrence at BLE was fairly constant across all seasons of the year, with clicks present two to three days a week (Figure 222). Outside of the regular occurrence at BLE, Blainville's beaked whale clicks were identified on 22 May 2020 at WIL (Figure 222).

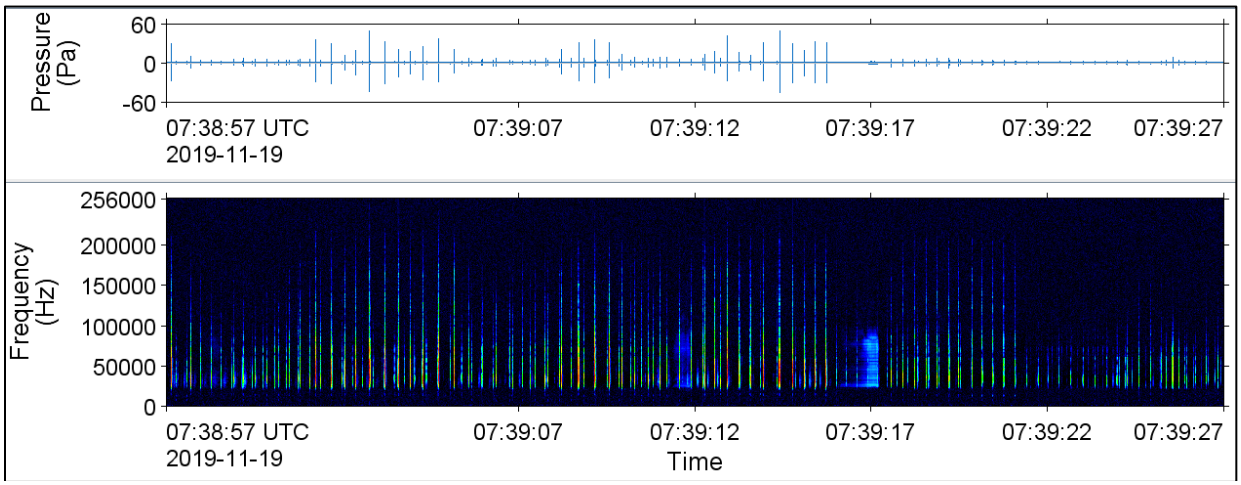

Figure 223. Zoom out: Waveform (top) and spectrogram (bottom) of Blainville's beaked whale clicks recorded at BLE on 19 Nov 2019

128 Hz frequency resolution, 0.001 s time window, 0.0005 s time step, Hamming window, normalized across time

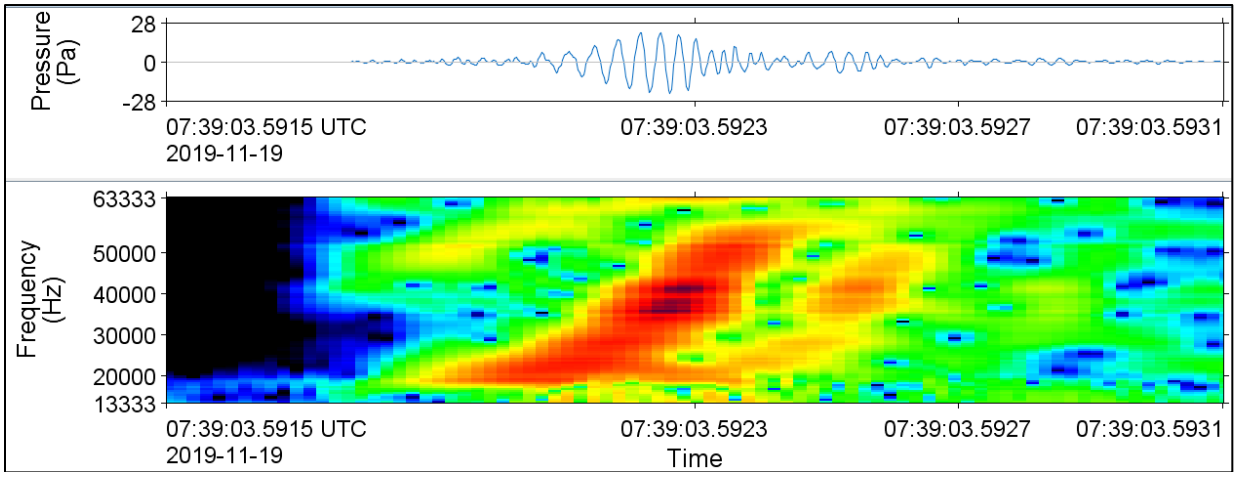

Figure 224. Zoom in: Waveform (top) and spectrogram (bottom) of a Blainville's beaked whale click recorded at BLE on 19 Nov 2019

512 Hz frequency resolution, 0.266 ms time window, 0.02 ms time step, Hamming window, normalized across time

E.1.2 Cuvier's Beaked Whales

Cuvier's beaked whale clicks were identified infrequently in the data during manual analysis and no automated detector was deemed effective at capturing these rare signals. Clicks were assigned to Cuvier's beaked whales if they resembled the characteristics described by Zimmer et al. (2005), and Gassmann et al. (2015), and if they resembled Cuvier's beaked whale clicks observed in other JASCO monitoring programs (Delarue et al., 2018; Kowarski et al., 2018). These clicks (Figures 225 and 226) were observed during manual analysis at BLE on 1 and 8 Feb 2018, 19 Jul 2018, and 28 May 2020 (Figure 222). While Cuvier's beaked whales are widely distributed globally (Macleod et al., 2005), their near-absence in the present data set is unsurprising given their preference for deep waters and shelf breaks.

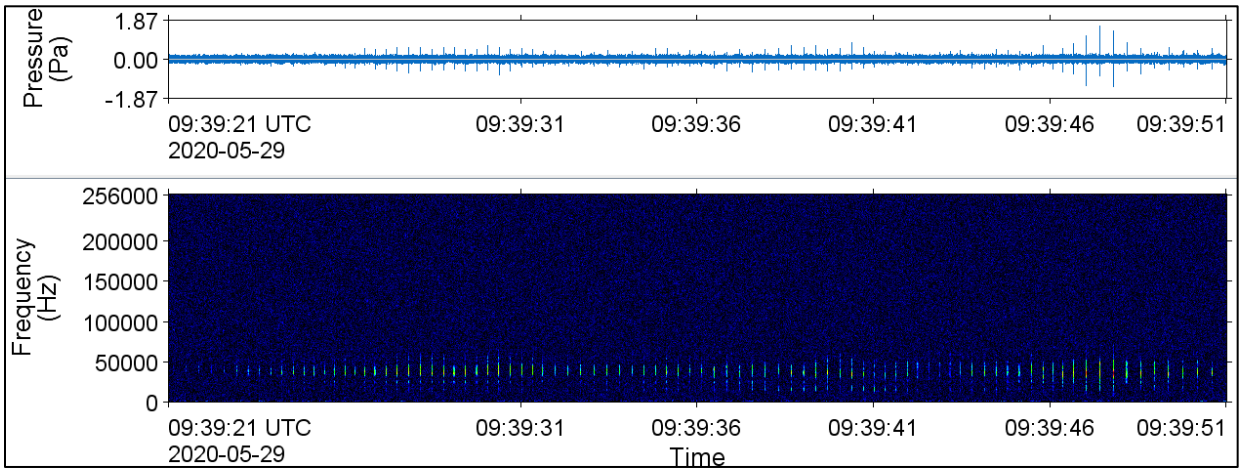

Figure 225. Zoom out: Waveform (top) and spectrogram (bottom) of Cuvier's beaked whale clicks recorded at BLE on 29 May 2020

128 Hz frequency resolution, 0.001 s time window, 0.0005 s time step, Hamming window, normalized across time

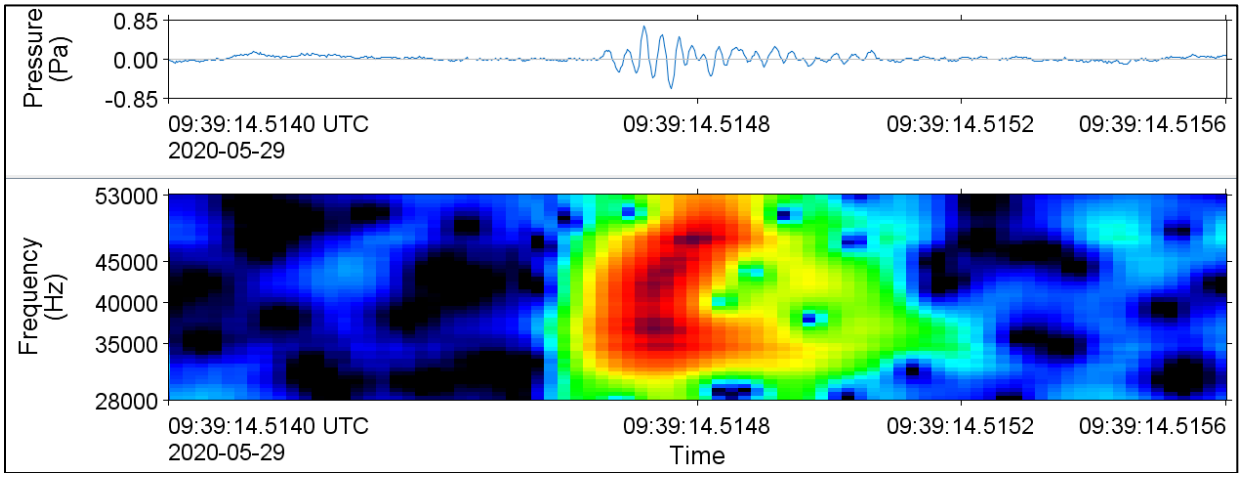

Figure 226. Zoom in: Waveform (top) and spectrogram (bottom) of a Cuvier's beaked whale click recorded at BLE on 29 May 2020

512 Hz frequency resolution, 0.266 ms time window, 0.02 ms time step, Hamming window, normalized across time

E.1.3 Gervais and/or True's Beaked Whales

Beaked whale clicks detected at SAV (Figure 222) were believed to be produced by Gervais and/or True's beaked whales based on the frequency characteristics and inter-click-intervals (Figure 227 and Figure 228) (Gillespie et al., 2009; Hildebrand et al., 2015). The click characteristics of these two species are too similar to be reliably differentiated at this time (Stanistreet et al., 2017; DeAngelis et al., 2018; Rafter et al., 2020a, 2020b). In addition to SAV, Gervais/True's beaked whale clicks were detected at WIL on 6 Sep 2019 (Figure 222).

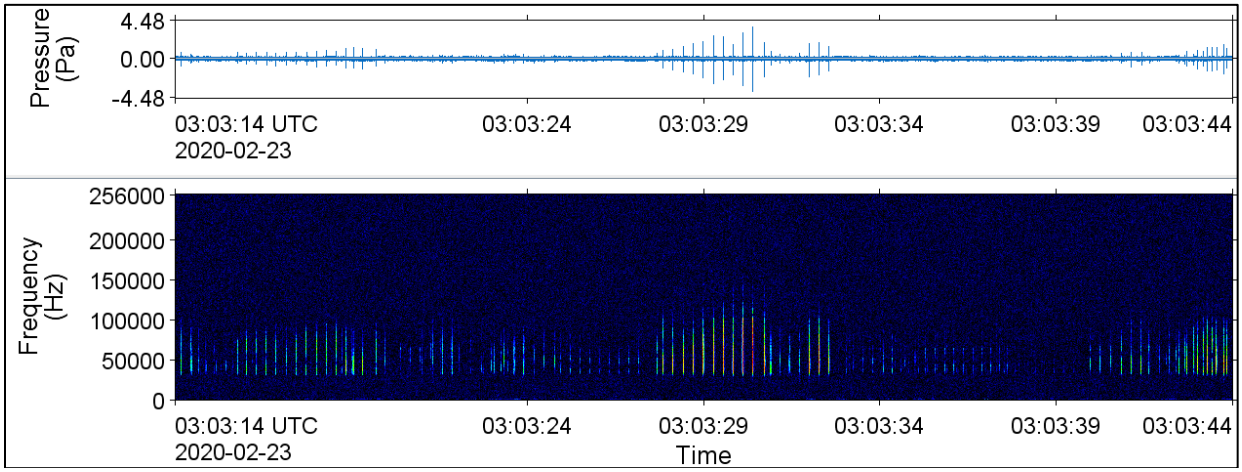

Figure 227. Zoom out: Waveform (top) and spectrogram (bottom) of Gervais/True's beaked whale clicks recorded at SAV on 23 Feb 2020

128 Hz frequency resolution, 0.001 s time window, 0.0005 s time step, Hamming window, normalized across time

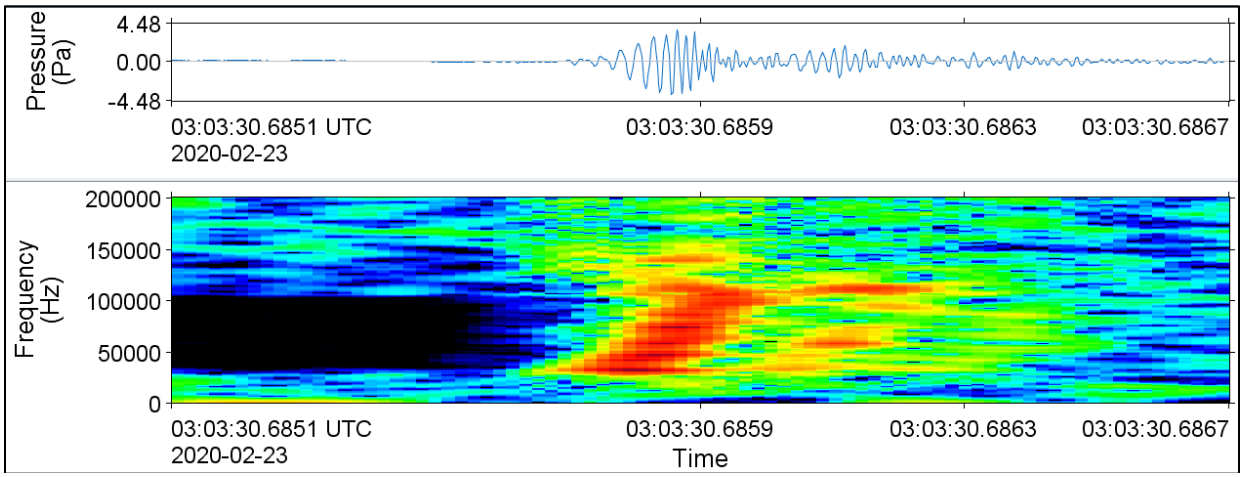

Figure 228. Zoom in: Waveform (top) and spectrogram (bottom) of a Gervais/True's beaked whale click recorded at SAV on 23 Feb 2020

512 Hz frequency resolution, 0.266 ms time window, 0.02 ms time step, Hamming window, normalized across time

E.2 Blue Whales

Blue whale vocalizations (Figure 229) (Mellinger and Clark 2003, Berchok et al. 2006) were detected sparsely through this data set (Figure 230) and were often very faint and difficult to distinguish from other ocean sounds. This species was acoustically identified at VAC, SAV, and BLE, with the highest, most regular occurrence at WIL. Blue whale vocalizations occurred primarily during the fall and winter when the males seasonally produce songs. Such a seasonal acoustic occurrence of this species has been previously reported off the eastern seaboard (Lesage et al., 2017; Davis, 2020).

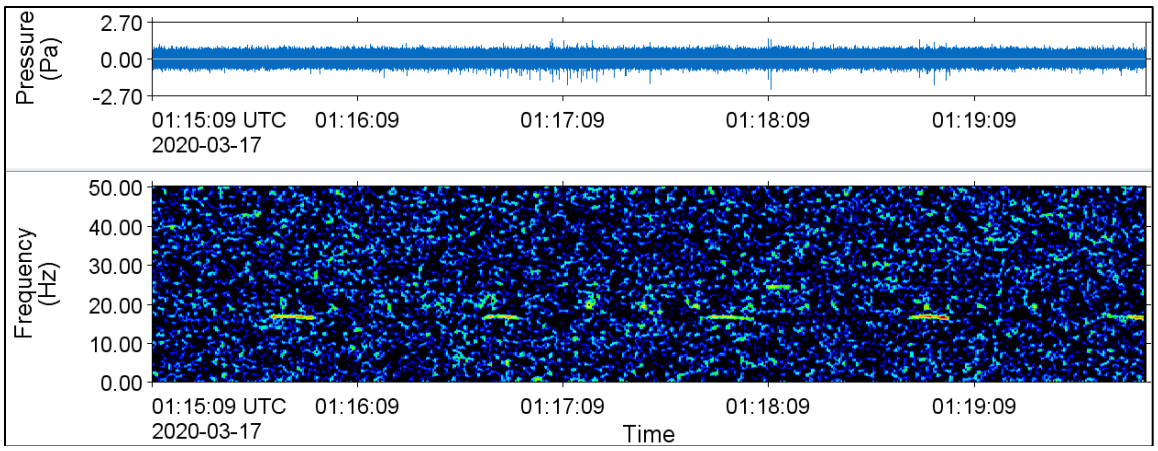

Figure 229. Waveform (top) and spectrogram (bottom) of blue whale vocalizations recorded at VAC on 17 Mar 2020

0.4 Hz frequency resolution, 2 s time window, 0.5 s time step, Hamming window, normalized across-time

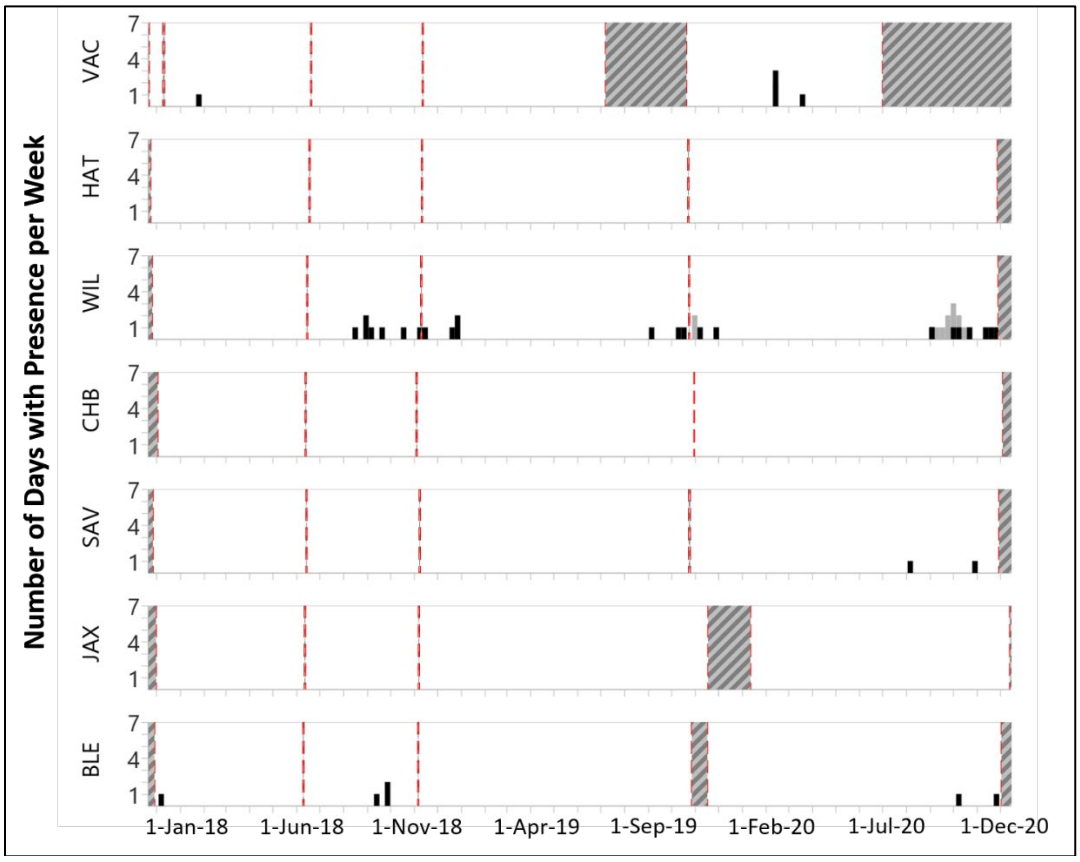

Figure 230. The number of days per week with blue whale vocalizations automatically detected
(grey) and manually detected (black) during the recording period at each station where hashed lines indicate periods with no acoustic data and red dashed lines indicated deployment and retrieval dates. Automatic detections for deployment periods (cruises) where the automated detector was found unreliable are not included.

E.3 Delphinids

Unlike most other odontocetes that are only known to produce clicks, delphinids produce both impulsive (click) and tonal (whistle) sounds that show less species-level specificity than other marine mammal signals and are therefore more difficult to distinguish acoustically (Steiner, 1981; Rendell et al., 1999; Soldevilla et al., 2008; Simões Amorim et al., 2019). The occurrence of delphinid clicks in the acoustic data is discussed before tonal signals are explored for different species groups.

Delphinid clicks are particularly difficult to differentiate across species, partially because of their directionality and the associated degradation of their spectral features when recorded at increasing angles away from the longitudinal axis of the vocalizing animal and partially because, for many species, their clicks have not been adequately characterized in the literature (Moore et al., 2008; Soldevilla et al., 2008; Eskesen et al., 2011; Hamran, 2014; Smith et al., 2016). Delphinid clicks can be distinguished from those of beaked whales, sperm whales, porpoise, and kogia sp. based on their frequency range, spectral features, and waveforms (see Figure 231 for example of typical click that was assigned to delphinids).

Delphinid clicks were regularly detected throughout the acoustic recordings at all stations (Figure 232). These acoustic signals may have been produced by any number of delphinid species, potentially multiple

at the same time as these species are known to interact. Potential species represented in Figure 232 include small dolphins such as the Atlantic spotted (*Stenella frontalis),* bottlenose (*Tursiops truncates*), clymene *(Stenella clymene)*, Fraser's *(Lagenodelphis hosei)*, pantropical spotted (*Stenella attenuata*), and/or Risso's (*Grampus griseus*) dolphin. Delphinid clicks also include those of the larger dolphins known as blackfish including false killer (*Pseudorca crassidens*), killer (*Orcinus orca*), long-finned pilot (*Globicephal melas*), and short-finned pilot (*Globicephala macrorhynchus*) whales. Based on whistle occurrence results (see Sections E.3.1 and E.3.2), it is reasonable to assume that a large proportion of delphinid clicks were produced by small dolphins, while blackfish clicks represent a smaller proportion of detections. Delphinid clicks were detected at a near daily basis at VAC, HAT, WIL, and JAX and a weekly basis at SAV and BLE (Figure 225). SAV and BLE showed evidence of a seasonal increase in days with delphinid clicks between the months of January and June (Figure 232).

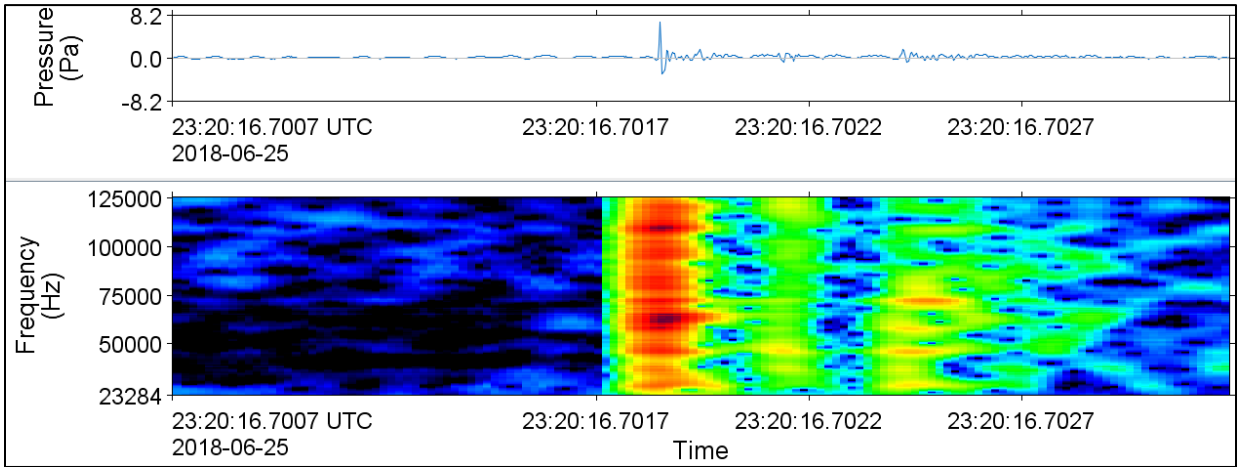

Figure 231. Waveform (top) and spectrogram (bottom) of a delphinid click recorded at VAC on 25 Jun 2018
512 Hz frequency resolution, 0.266 ms time window, 0.02 ms time step, Hamming window, normalized across time

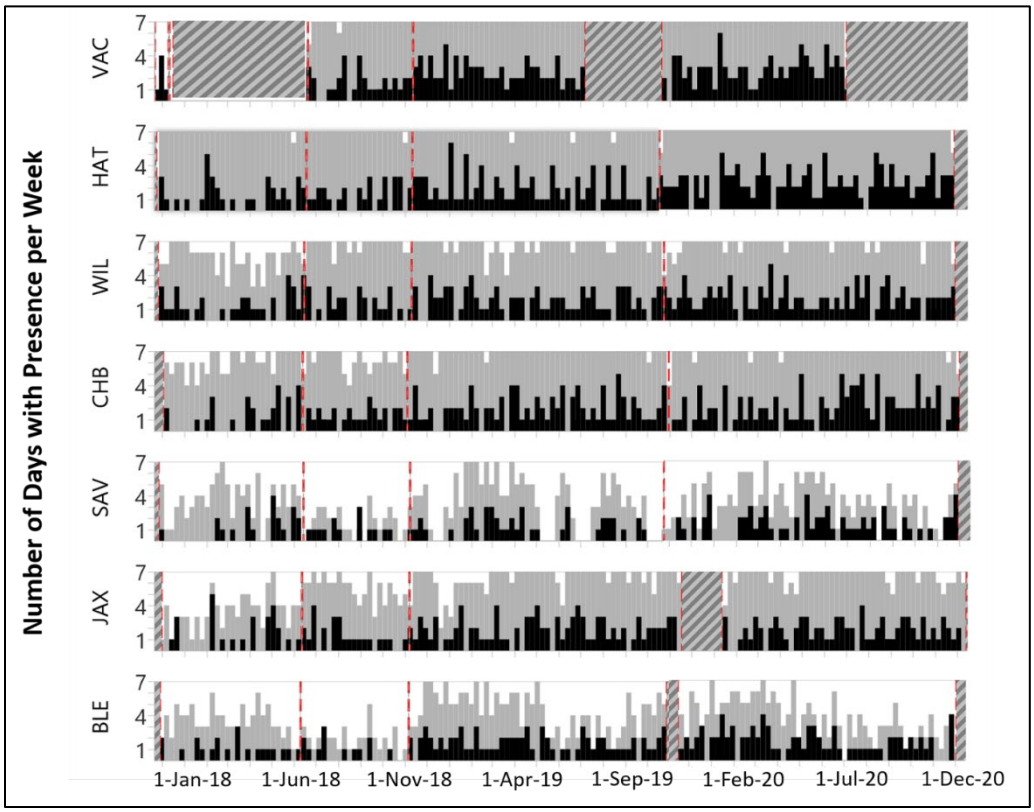

Figure 232. The number of days per week with delphinid clicks automatically detected

(grey) and manually detected (black) during the recording period at each station where hashed lines indicate periods with no acoustic data and red dashed lines indicated deployment and retrieval dates. Automatic detections for deployment periods (cruises) where the automated detector was found unreliable are not included.

E.3.1 Dolphins

Small dolphin whistles generally have energy concentrated above 5—6 kHz (Steiner, 1981; Rendell et al., 1999; Azzolin et al., 2013; Simões Amorim et al., 2019), therefore any whistles with the majority of energy between 5 and 20 kHz (e.g., Figure 233) were considered small dolphins. As with delphinid clicks (Figure 232) small dolphin whistles were present at all stations throughout the recording period (Figure 234). Dolphin whistles were most common at the more northerly recording stations with SAV and BLE having the fewest days per week with whistles consistently through the year (similarly seen in delphinid click occurrence). The whistle repertoire of some larger delphinid species including short-finned pilot whales does span above 5 kHz and therefore a portion of the whistle results here may represent larger delphinids (Rendell et al., 1999; Van Cise et al., 2018).

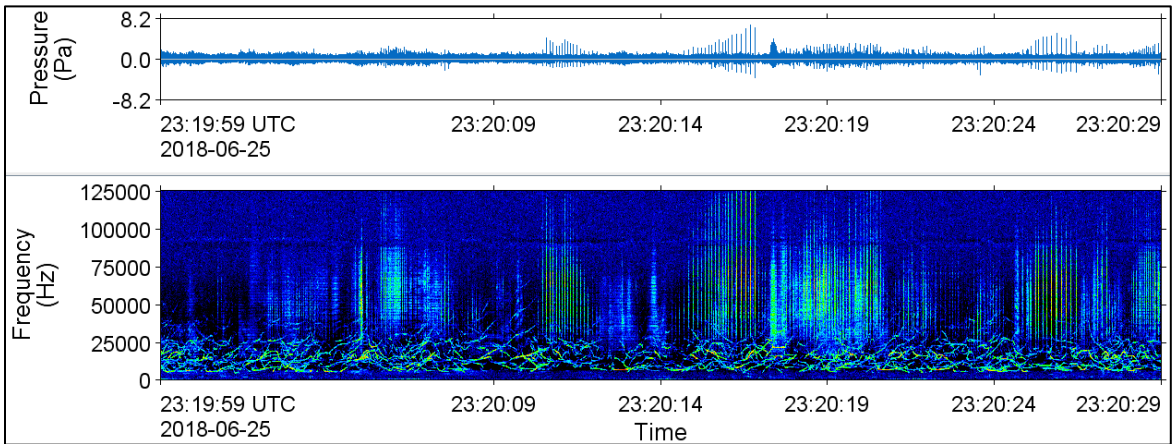

Figure 233. Zoom out: Waveform (top) and spectrogram (bottom) of dolphin clicks and whistles recorded at VAC on 25 Jun 2018

128 Hz frequency resolution, 0.001 s time window, 0.0005 s time step, Hamming window, normalized across time

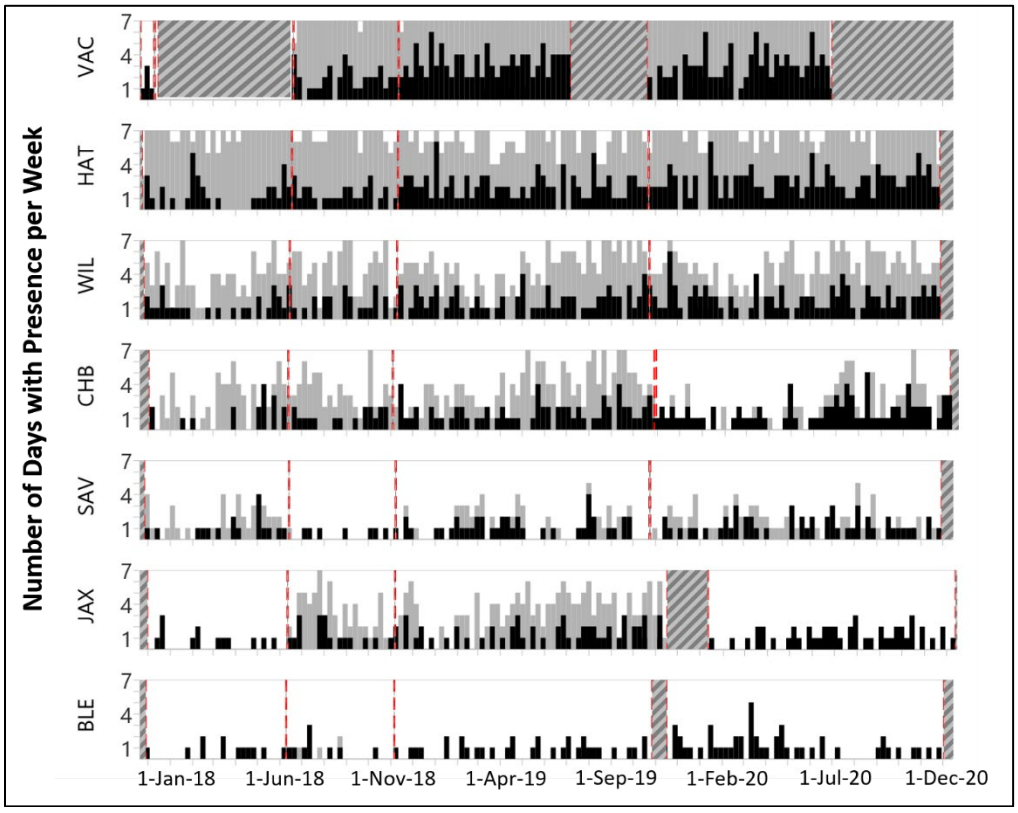

Figure 234. The number of days per week with dolphin whistles automatically detected

(grey) and manually detected (black) during the recording period at each station where hashed lines indicate periods with no acoustic data and red dashed lines indicated deployment and retrieval dates. Automatic detections for deployment periods (cruises) where the automated detector was found unreliable are not included.

Another type of vocalization observed in the acoustic data that was attributed to dolphins was the chirp and quack sequences of dolphin calves (Figure 235). These sounds almost always occurred simultaneously with dolphin whistles and previous reports suggest they are the sound of bottlenose

dolphin calves (Killebrew et al., 2001). Dolphin calf sounds were detected at all stations, though much less frequently than either delphinid clicks or dolphin whistles (Figure 236).

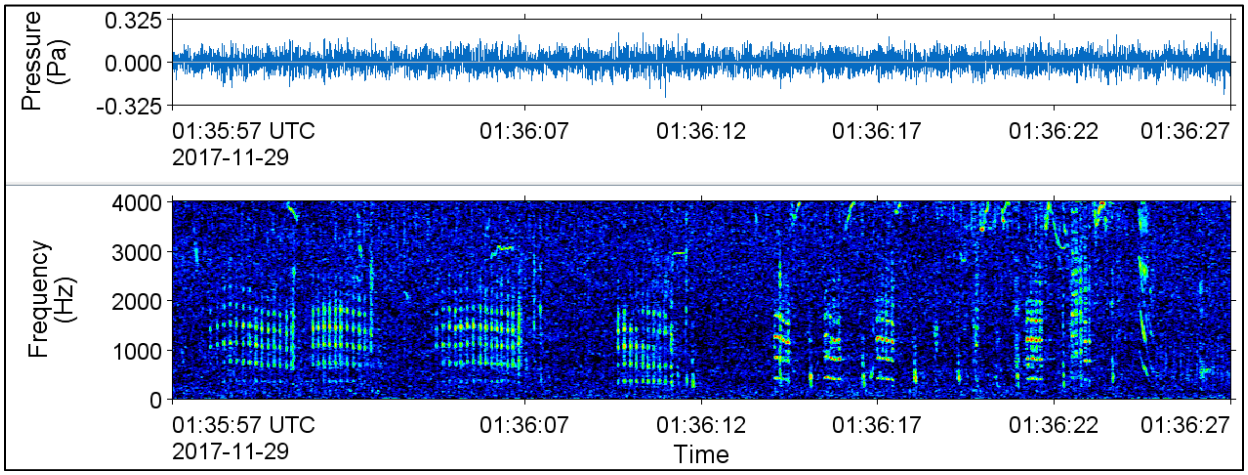

Figure 235. Waveform (top) and spectrogram (bottom) of dolphin calf vocalizations recorded at WIL on 29 Nov 2017

2 Hz frequency resolution, 0.125 s time window, 0.03125 s time step, Hamming window, normalized across-time

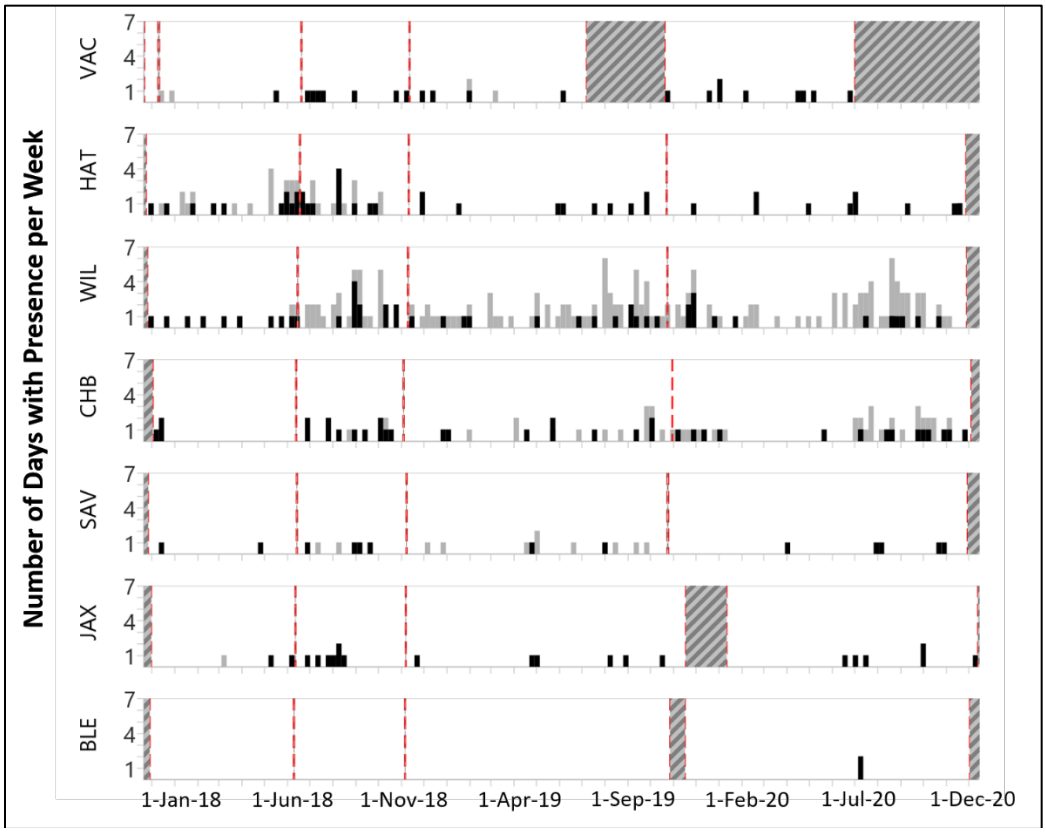

Figure 236. The number of days per week with dolphin calf vocalizations automatically detected

(grey) and manually detected (black) during the recording period at each station where hashed lines indicate periods with no acoustic data and red dashed lines indicated deployment and retrieval dates. Automatic detections for deployment periods (cruises) where the automated detector was found unreliable are not included.

E.3.2 Pilot and Killer Whales

An attempt was made to differentiate the whistles of killer and pilot whales from those of small dolphins. Pilot whale whistles can reach as low as 1.5 kHz with main energy around 3–5 kHz (Nemiroff & Whitehead, 2009; Van Cise et al., 2018) (Figure 237). Killer whale whistles can have a fundamental frequency below 1 kHz (Figure 231) (Filatova et al. 2015) (Figure 238). Therefore, whistles with the majority of energy residing under 5000 Hz were assigned to either pilot or killer whales, though some amount of error is expected when differentiating these species from each other. Indeed, the likelihood of human error in differentiating these species was so great given their similar looking/sounding signals (e.g., Figures 237 and 238) that the occurrence is presented together and represents all lower frequency whistles Figure 239). A further complication was the challenge in assigning species when whistles ranged from 4 to 8 kHz, a span that includes both small dolphins and pilot whales.

Whistles attributed to killer/pilot whales occurred throughout the recordings at all stations (Figure 239), though they were much less common than those of small dolphins (Figure 236). The majority of these whistles were thought to be produced by pilot whales with killer whales only suspected on 6 occasion at BLE (29 Nov 2018, 21 Mar 2019, 28 Mar 2019, 4 Apr 2019, 9 May 2019, 21 May 2020), one occasion at JAX (29 Nov 2018), and three occasions at WIL (28 Nov 2019, 14 May 2020, 5 Nov 2020). Long- and short- finned pilot whales overlap in distribution, but the occurrence of long-finned pilot whale whistles is likely higher at more northern stations and short-finned pilot whale whistles are expected at more southern stations.

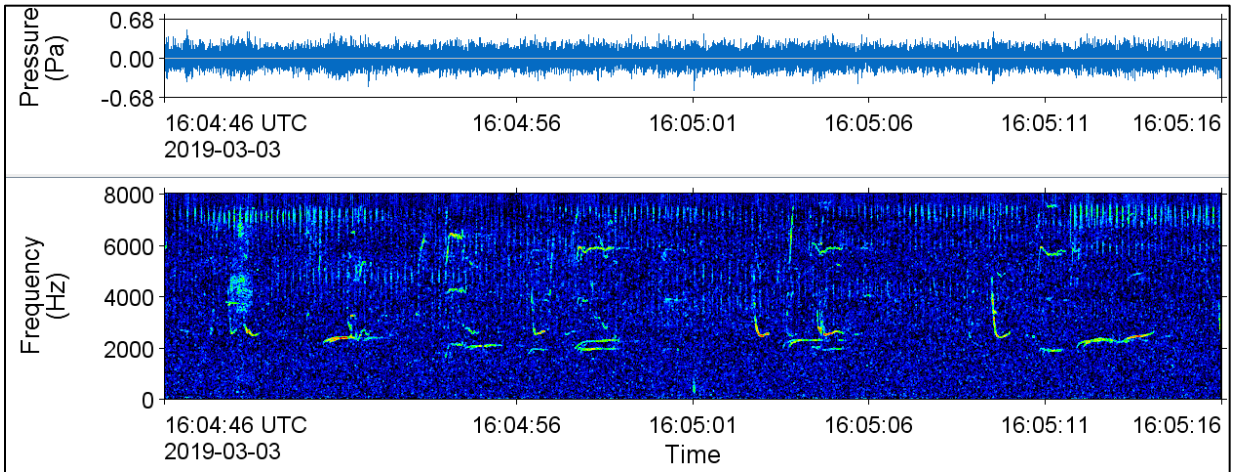

Figure 237. Waveform (top) and spectrogram (bottom) of pilot whale whistles recorded at BLE on 3 Mar 2019
4 Hz frequency resolution, 0.05 s time window, 0.01 s time step, Hamming window, normalized across time

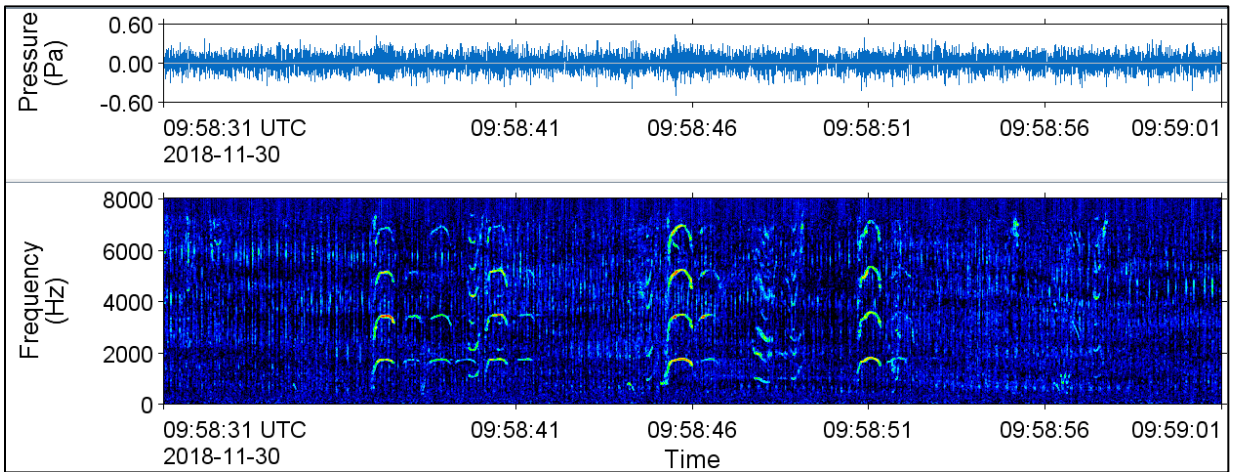

Figure 238. Waveform (top) and spectrogram (bottom) of killer whale whistles recorded at BLE on 30 Nov 2018

4 Hz frequency resolution, 0.05 s time window, 0.01 s time step, Hamming window, normalized across time

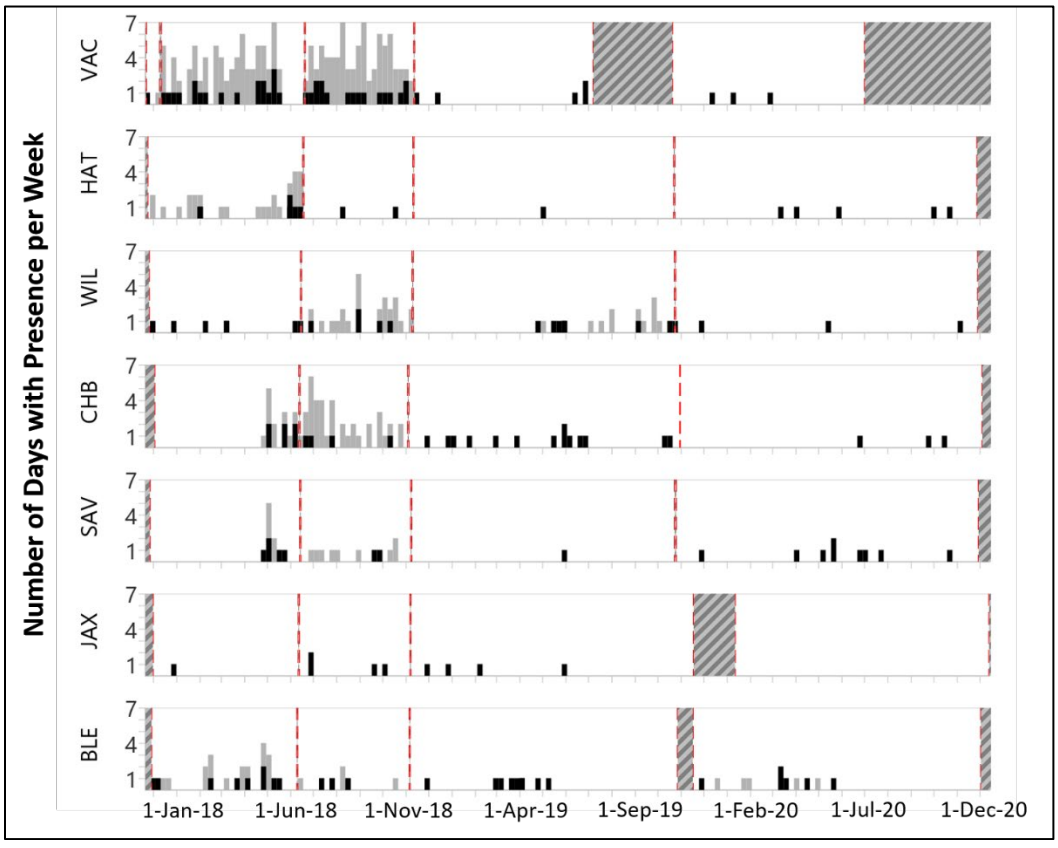

Figure 239. The number of days per week with pilot and killer whale whistles automatically detected

(grey) and manually detected (black) during the recording period at each station where hashed lines indicate periods with no acoustic data and red dashed lines indicated deployment and retrieval dates. The majority of occurrence is believed to be pilot whales with killer whales only confirmed on 6 occasion at BLE (in Nov 2018, Mar, Apr, May 2019, and May 2020), once at JAX (Nov 2018), and three times at WIL (Nov 2019, May and Nov 2020). Automatic detections for deployment periods (cruises) where the automated detector was found unreliable are not included.

E.4 Fin Whales

Fin whale vocalizations (Figure 240) (Delarue et al., 2009; Garcia et al., 2018; Miksis-Olds et al., 2019) were seasonally detected at all stations with their highest occurrence at VAC and WIL (Figure 241). The seasonal acoustic occurrence from ~August to ~March reflects the seasonal vocalizing behaviour of male fin whales and the lack of detections in the summer (noteably at VAC and WIL) may not be indicative of the species being absent, but rather a change in vocalizing behaviour to their less prolific summer non-song calls. The shorter seasonal occurrence at southern stations likely reflects the species transitting through these areas while the longer occurrence at VAC, WIL, and, to some extent, HAT (Figure 241) suggests animals remaining in, and utilizing, these areas. Davis (2020) similarly observed a seasonal acoustic occurrence of this species off the eastern seaboard.

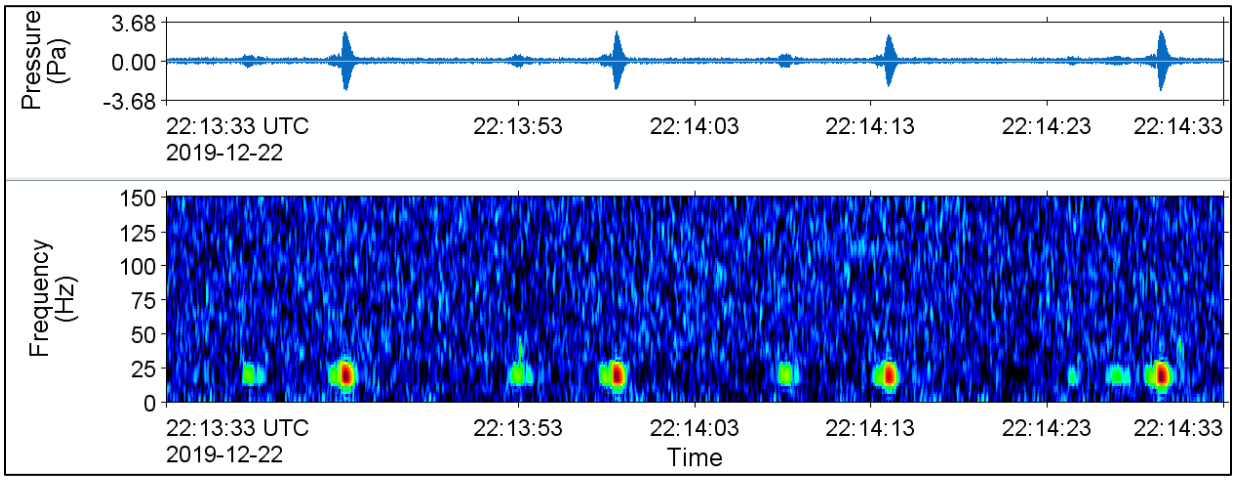

Figure 240. Waveform (top) and spectrogram (bottom) of fin whale vocalizations recorded at VAC on 22 Dec 2019

2 Hz frequency resolution, 0.125 s time window, 0.03125 s time step, Hamming window, normalized across-time

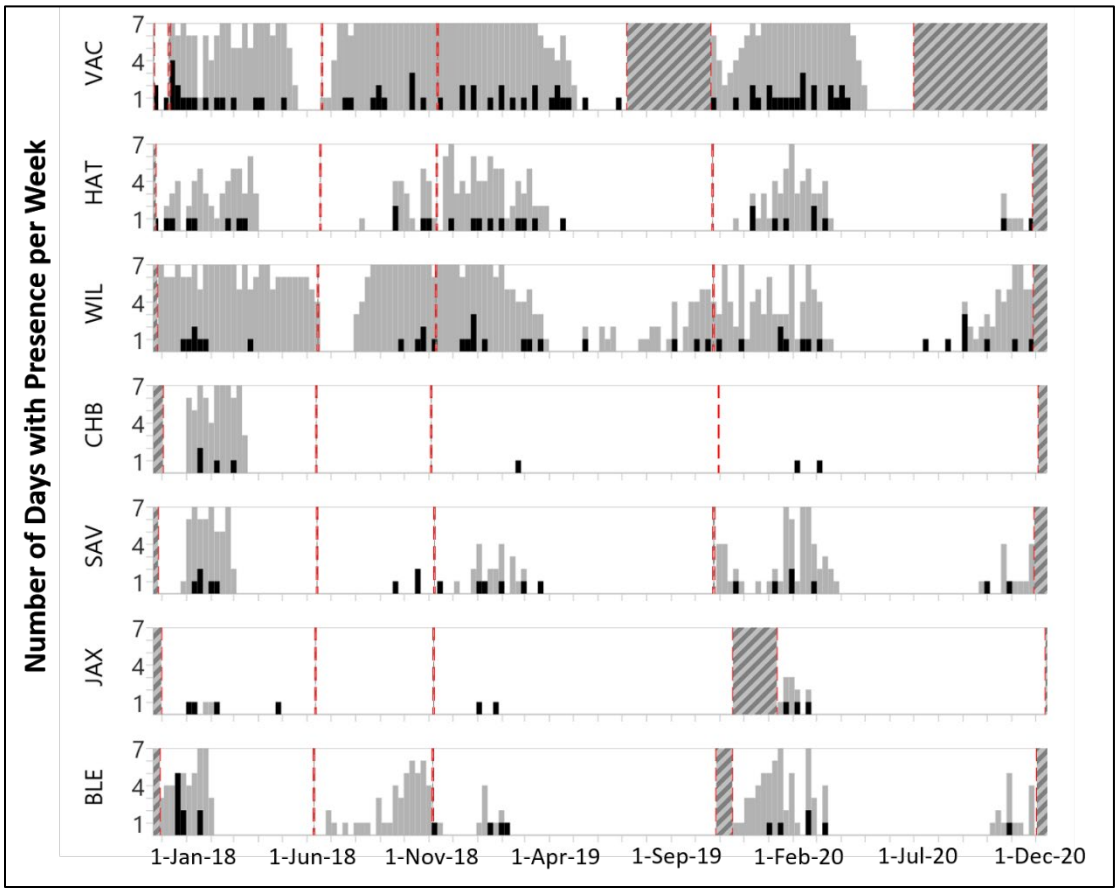

Figure 241. The number of days per week with fin whale vocalizations automatically detected

(grey) and manually detected (black) during the recording period at each station where hashed lines indicate periods with no acoustic data and red dashed lines indicated deployment and retrieval dates. Automatic detections for deployment periods (cruises) where the automated detector was found unreliable are not included.

E.5 Harbor Porpoise and Kogia sp.

Harbor porpoise clicks have a peak frequency near 125 kHz and no frequency modulated slope (Au et al., 1999). In the study area, the only other species whose clicks share similar spectral characteristics is the pygmy sperm whale (*Kogia breviceps*) and dwarf sperm whale (*Kogia sima*) (Marten, 2000; Madsen et al., 2005). Narrow-band high frequency clicks matching the characteristics of these species (Figure 242 and Figure 243) were detected at all stations except VAC and HAT (Figure 244). Given that the southern edge of harbor porpoise distribution appears to be near the mouth of Chesapeake Bay (Hayes et al., 2020) whereas Kogia sp. can occur throughout the recording area (Staudinger et al., 2014; DoN, 2016; Hodge et al., 2018; Hayes et al., 2020), it is likely that most of these detections were from Kogia sp. Kogia occurred almost daily at BLE, in most months of the year at SAV and WIL, and rarely at JAX and BLE.

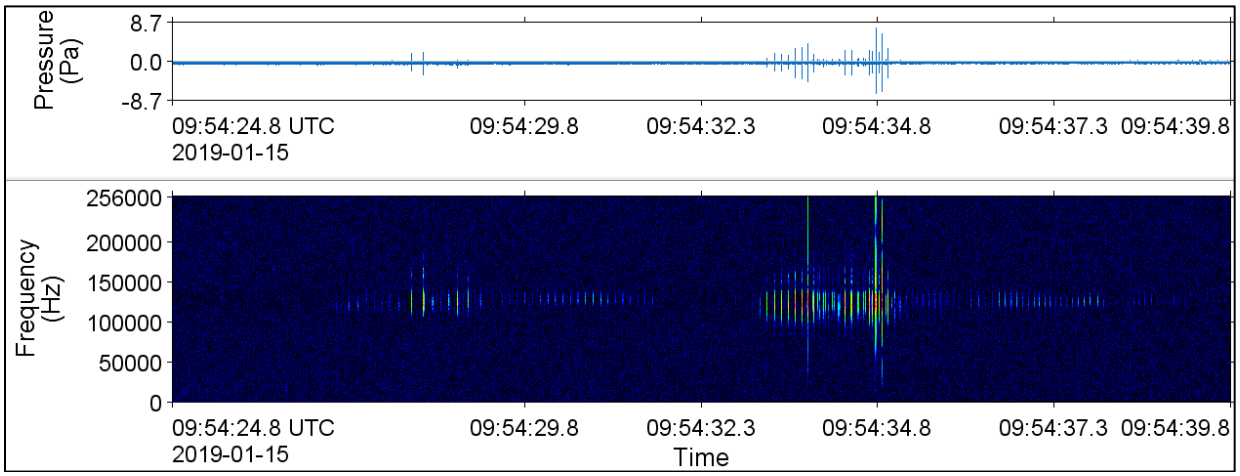

Figure 242. Zoom out: Waveform (top) and spectrogram (bottom) of porpoise-kogia clicks recorded at WIL on 15 Jan 2019

128 Hz frequency resolution, 0.001 s time window, 0.0005 s time step, Hamming window, normalized across time

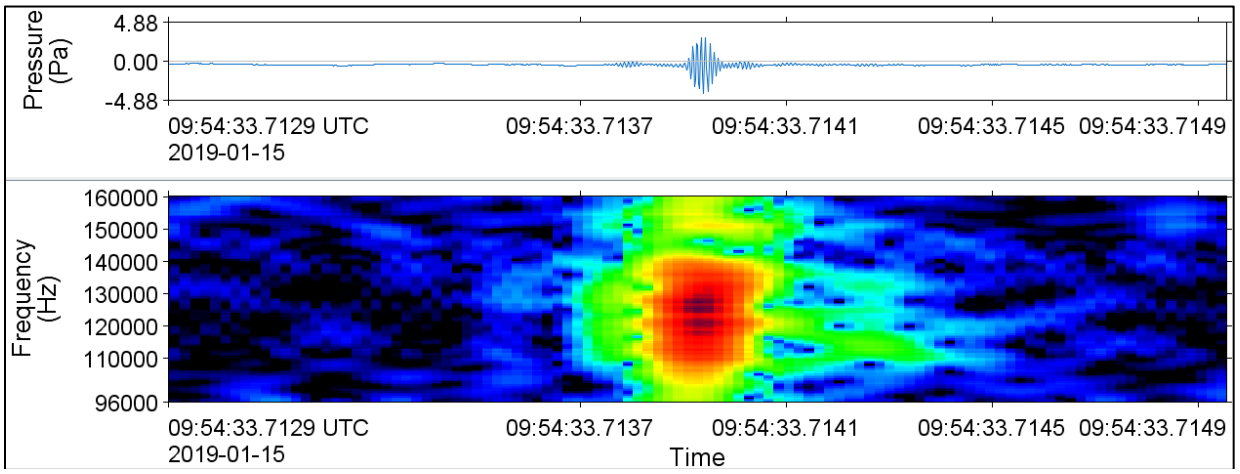

Figure 243. Zoom in: Waveform (top) and spectrogram (bottom) of a porpoise-kogia click recorded at WIL on 15 Jan 2019

512 Hz frequency resolution, 0.266 ms time window, 0.02 ms time step, Hamming window, normalized across time

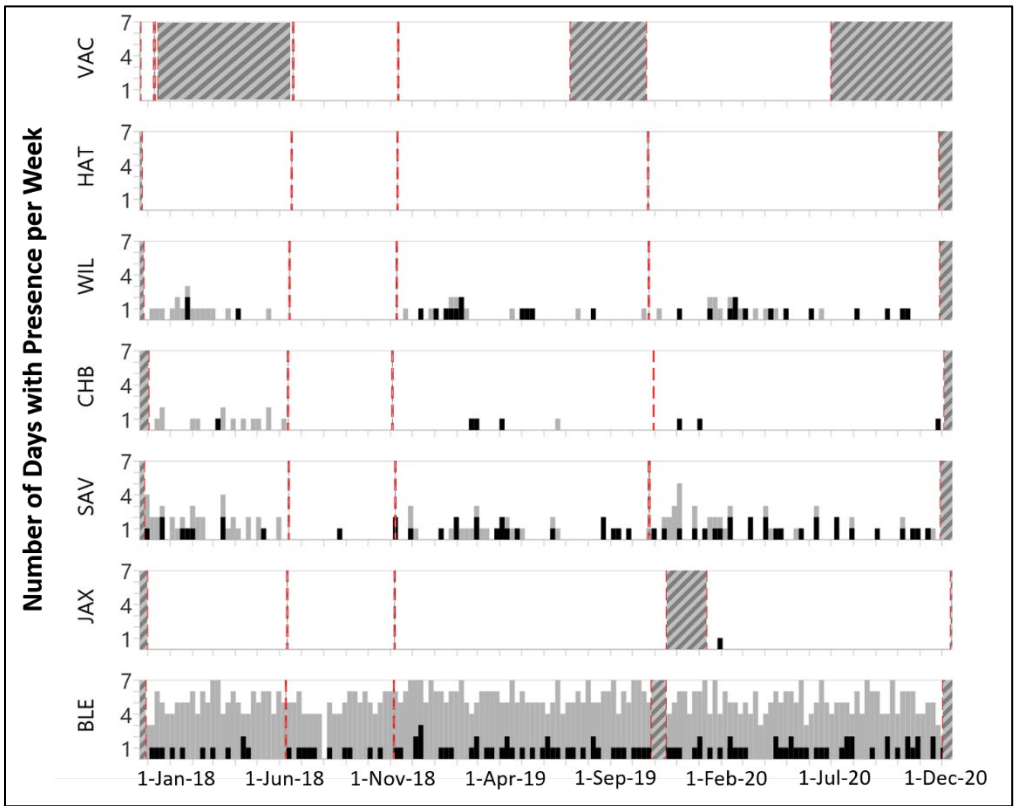

Figure 244. The number of days per week with porpoise-kogia clicks automatically detected

(Grey) and manually detected (black) during the recording period at each station where hashed lines indicate periods with no acoustic data and red dashed lines indicated deployment and retrieval dates. It is tentatively presumed that the majority of detection are from Kogia sp. Automatic detections for deployment periods (cruises) where the automated detector was found unreliable are not included.

E.6 Humpback Whales

Humpback whale vocalizations (Payne & McVay, 1971; Kowarski et al., 2019) were detected at VAC, HAT, WIL, and BLE (Figure 245). At VAC and HAT, humpback whale occurrence was seasonal, with most acoustic detections in the winter and spring (Figure 246) likely reflecting the animals moving through this area while the males produce songs during their northward migration to their feeding grounds. Similar seasonal observations of this species' acoustic occurrence have been made by Aschettino et al. (2020), and Davis et al. (2020). No summer 2020 automated detections at HAT were manually validated, therefore this may be an overestimate of the species' occurrence (Figure 246). Humpback whale acoustic detections at other stations were rare.

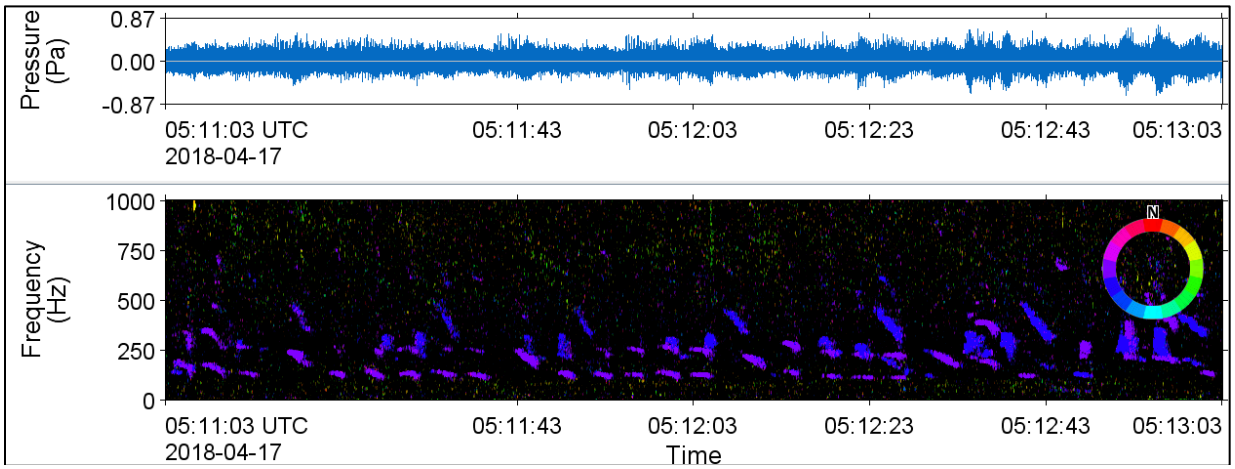

Figure 245. Waveform (top) and directogram (bottom) of humpback whale vocalizations recorded at VAC on 17 Apr 2018

2 Hz frequency resolution, 0.125 s time window, 0.03125 s time step, Hamming window, normalized across-time. Two humpback whales are singing, one from the west of the recorder (purple) and one from the westsouthwest (blue)

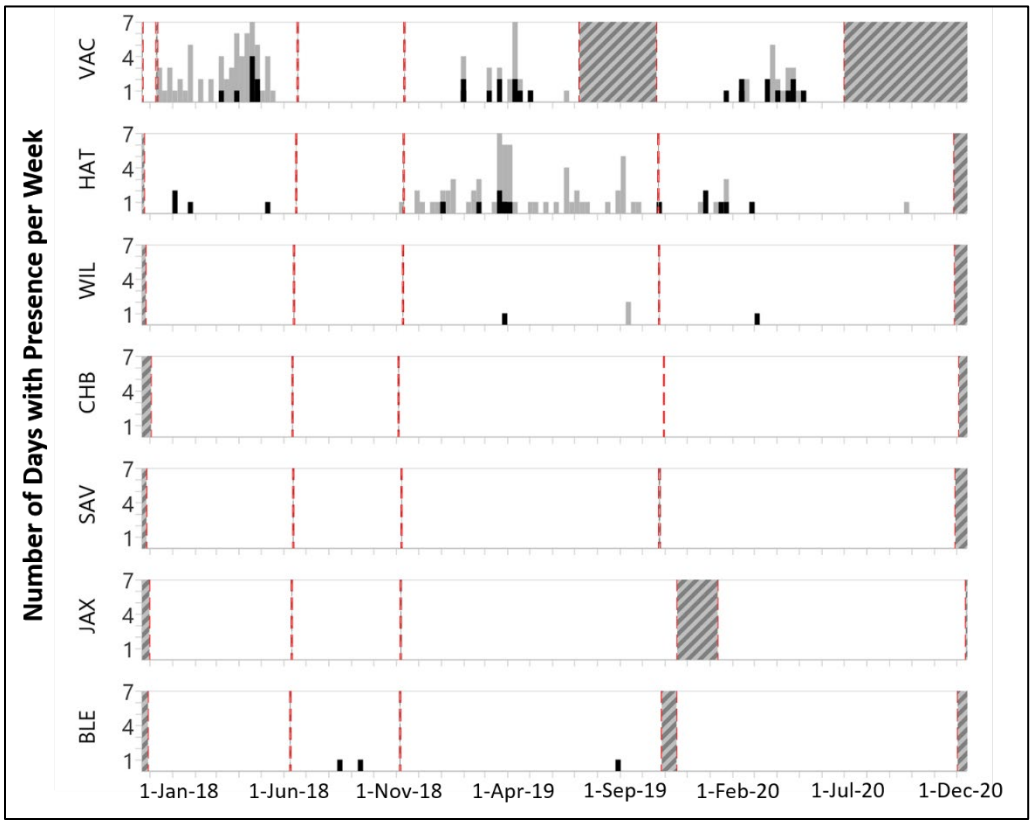

Figure 246. The number of days per week with humpback whale vocalizations automatically detected

(grey) and manually detected (black) during the recording period at each station where hashed lines indicate periods with no acoustic data and red dashed lines indicated deployment and retrieval dates. Automatic detections for deployment periods (cruises) where the automated detector was found unreliable are not included.

E.7 Minke Whales

Minke whale vocalizations (Figure 247) (Risch et al., 2014b) were detected at all stations (though rarely at VAC and HAT), with a strong seasonal trend at WIL, CHB, SAV, JAX, and BLE (Figure 248). Minke whales were seasonally acoustically present from ~February to ~June and were almost entirely absent during the summer and early fall (Figure 248). These vocalizations are believed to be a seasonal vocal display by male minke whales, therefore the trends observed here may be a combination of animals entering and leaving the area during migration and a shift vocal behavior.

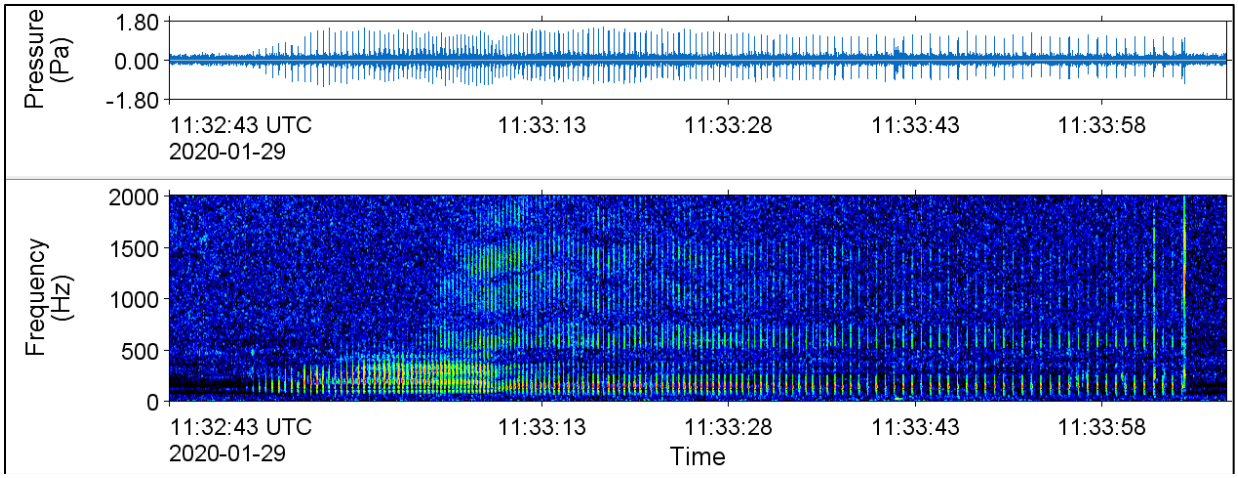

Figure 247. Waveform (top) and spectrogram (bottom) of minke whale vocalizations recorded at WIL on 29 Jan 2020

2 Hz frequency resolution, 0.125 s time window, 0.03125 s time step, Hamming window, normalized across-time

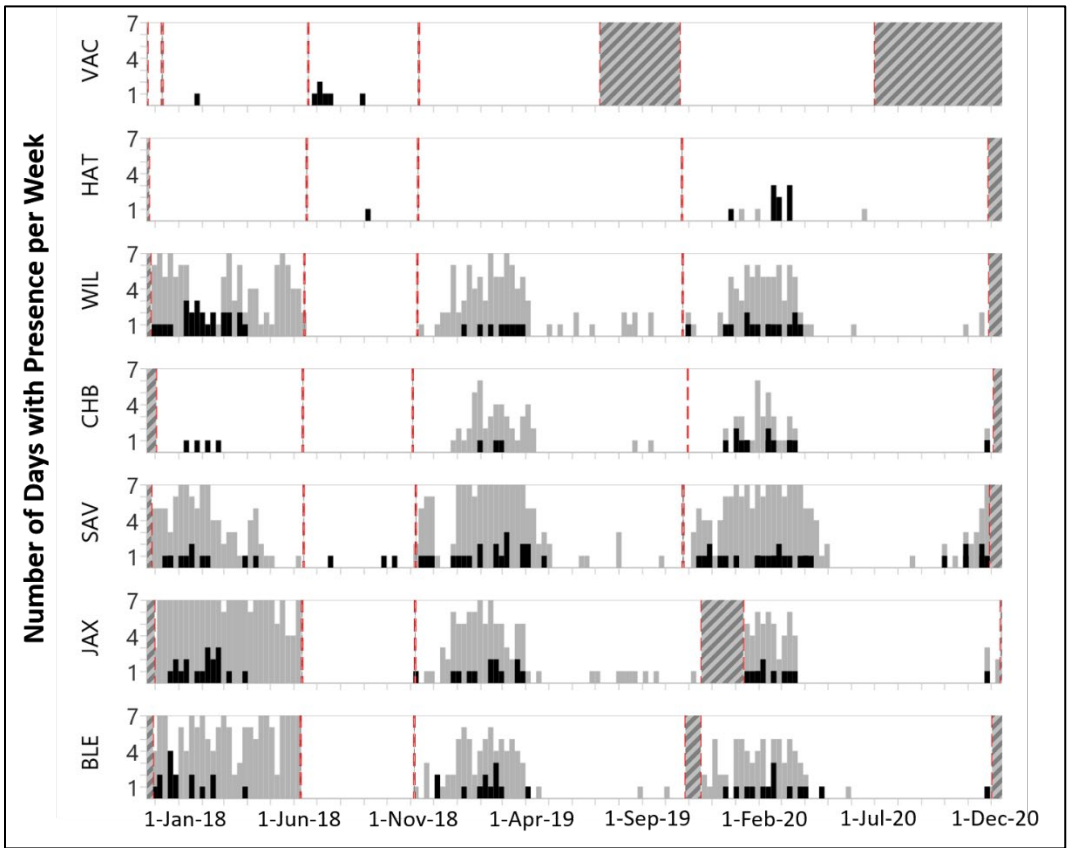

Figure 248. The number of days per week with minke whale vocalizations automatically detected

(grey) and manually detected (black) during the recording period at each station where hashed lines indicate periods with no acoustic data and red dashed lines indicated deployment and retrieval dates. Automatic detections for deployment periods (cruises) where the automated detector was found unreliable are not included.

E.8 Right whales

North Atlantic right whale vocalizations (Figure 249) (Parks et al., 2019) were detected on one occasion at HAT on 29 Jan 2018. It is unclear if this species was truly this acoustically rare in the data (the recorders were potentially too far offshore to capture the vocalizations of this coastal species) or if right whales were missed during the limited analysis, therefore this should be taken as an underestimate.

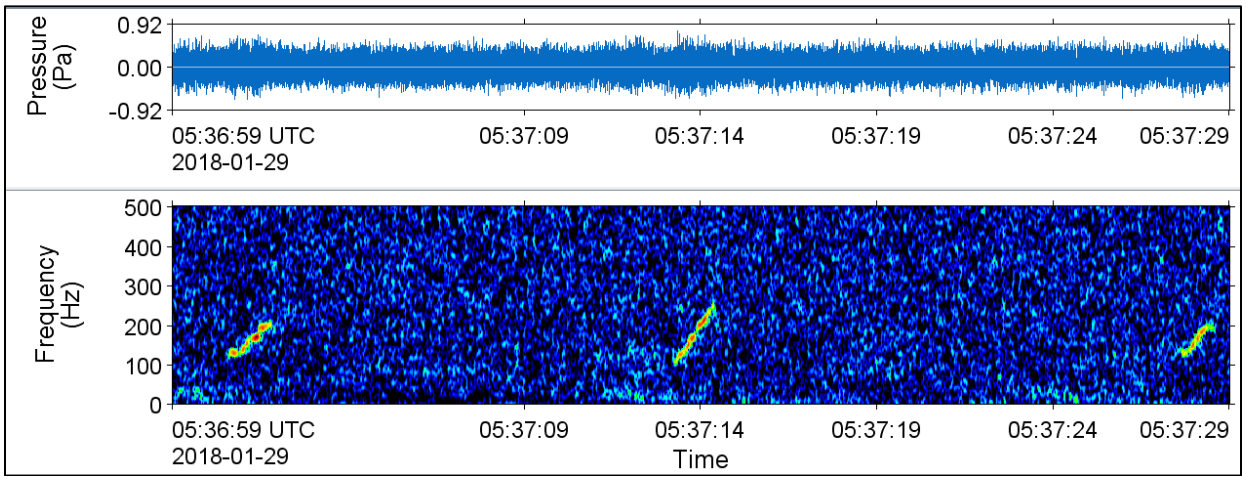

Figure 249. Waveform (top) and spectrogram (bottom) of right whale vocalizations recorded at HAT on 29 Jan 2018

2 Hz frequency resolution, 0.125 s time window, 0.03125 s time step, Hamming window, normalized across-time

E.9 Sei Whales

Sei whale vocalizations (Figure 250) (Baumgartner & Fratantoni, 2008; Nieukirk et al., 2020) were infrequently confirmed at all stations except HAT, where the species was acoustically absent (Figure 251). The species was most acoustically common at SAV and BLE, where detections at times were present on four to six days in a week (Figure 251). Manual results indicate the species primarily occurred between the months of December and March, though at VAC it was later in the year between March and June (Figure 251). Given the sparsity of sei whales confirmed in the data it is recommended that automated results be treated hesitantly until further manual validation is completed. Given the few detections, this species is likely transiting through the recording areas.

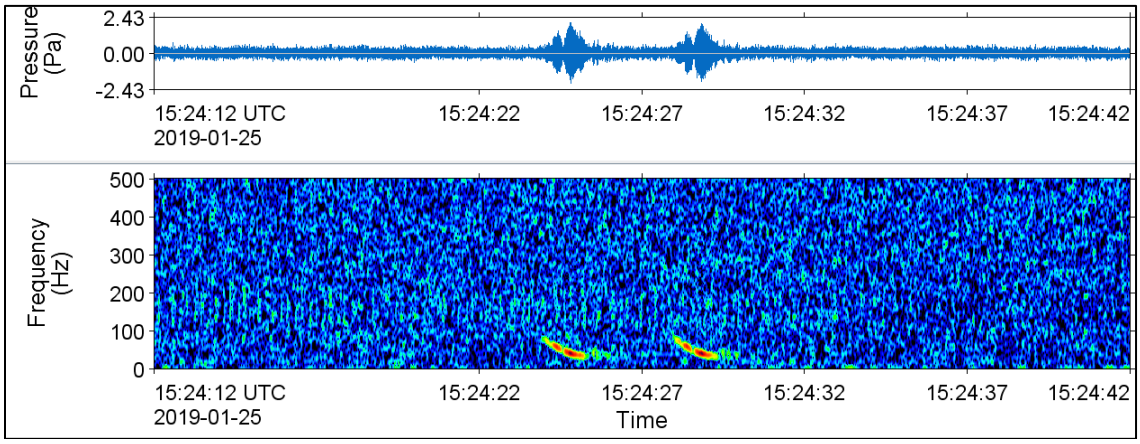

Figure 250. Waveform (top) and spectrogram (bottom) of sei whale vocalizations recorded at BLE on 25 Jan 2019

2 Hz frequency resolution, 0.125 s time window, 0.03125 s time step, Hamming window, normalized across-time

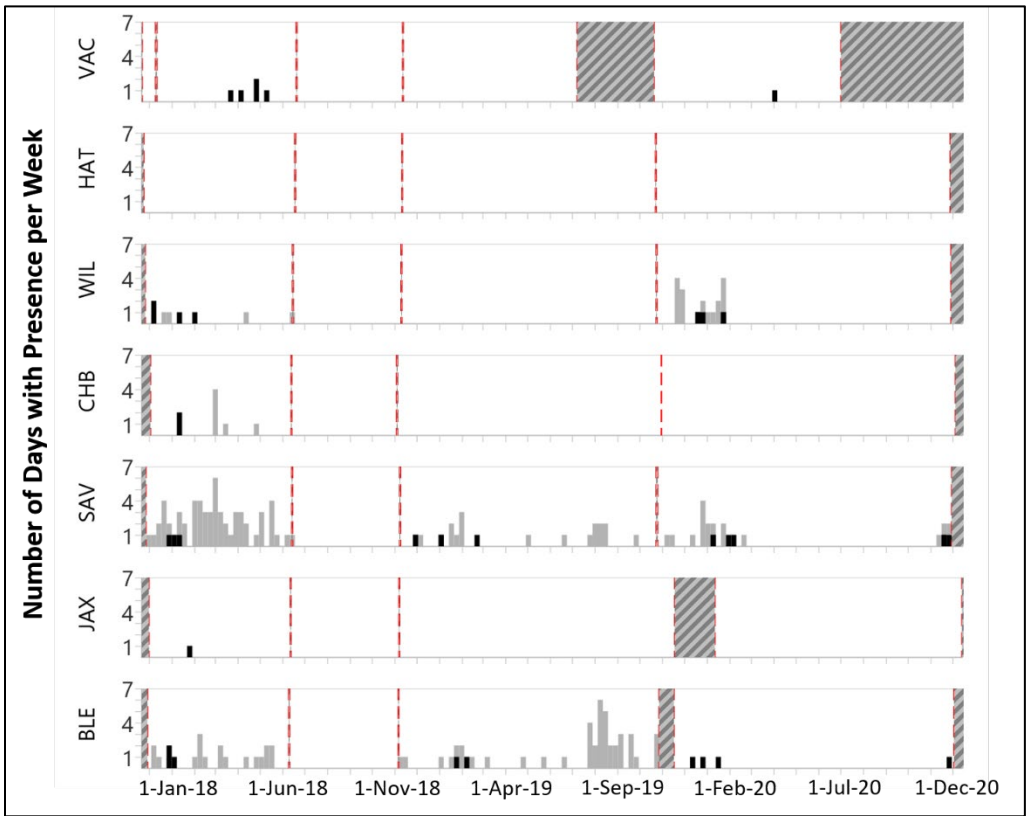

Figure 251. The number of days per week with sei whale vocalizations automatically detected

(grey) and manually detected (black) during the recording period at each station where hashed lines indicate periods with no acoustic data and red dashed lines indicated deployment and retrieval dates. Automatic detections for deployment periods (cruises) where the automated detector was found unreliable are not included.

E.10 Sperm Whales

Sperm whale clicks (Figure 252) (Madsen et al., 2002; Mathias et al., 2013) were identified throughout the recordings at all stations (Figure 253). A lack of an effective automated detector makes it difficult to ascertain seasonal trends, but VAC seems to have an increase in days with detections in the spring (Figure 253). The automated detector performed poorly because the signals were often faint and the automated detector was falsely triggered by minke whale pulse trains and vessels.

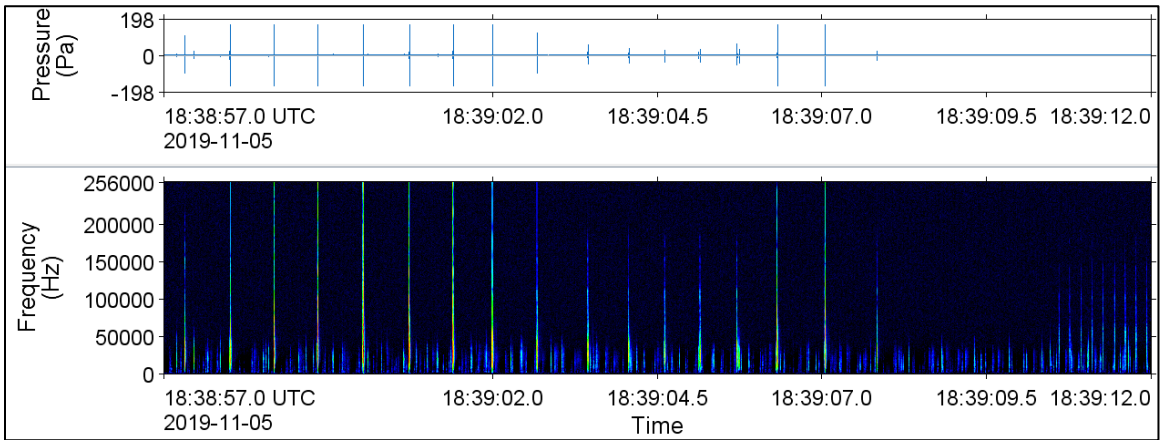

Figure 252. Waveform (top) and spectrogram (bottom) of sperm whale clicks recorded at BLE on 5 Nov 2019
128 Hz frequency resolution, 0.001 s time window, 0.0005 s time step, Hamming window, normalized across time

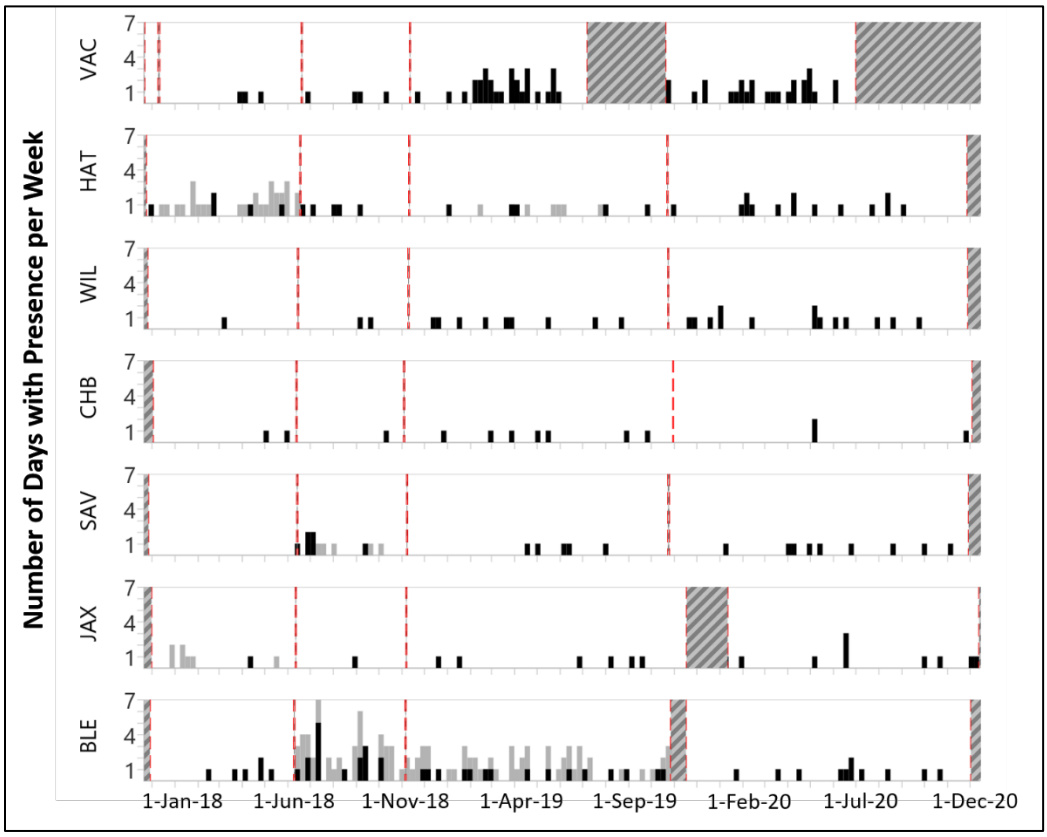

Figure 253. The number of days per week with sperm whale vocalizations automatically detected

(grey) and manually detected (black) during the recording period at each station where hashed lines indicate periods with no acoustic data and red dashed lines indicated deployment and retrieval dates. Automatic detections for deployment periods (cruises) where the automated detector was found unreliable are not included.

Department of the Interior (DOI)

The Department of the Interior protects and manages the Nation's natural resources and cultural heritage; provides scientific and other information about those resources; and honors the Nation’s trust responsibilities or special commitments to American Indians, Alaska Natives, and affiliated island communities.

BOEM
Bureau of Ocean Energy Management

Bureau of Ocean Energy Management (BOEM)

The mission of the Bureau of Ocean Energy Management is to manage development of U.S. Outer Continental Shelf energy and mineral resources in an environmentally and economically responsible way.

BOEM Environmental Studies Program

The mission of the Environmental Studies Program is to provide the information needed to predict, assess, and manage impacts from offshore energy and marine mineral exploration, development, and production activities on human, marine, and coastal environments. The proposal, selection, research, review, collaboration, production, and dissemination of each of BOEM’s Environmental Studies follows the DOI Code of Scientific and Scholarly Conduct, in support of a culture of scientific and professional integrity, as set out in the DOI Departmental Manual (305 DM 3).